DECEMBER 15, 1989

Analytical CHEMISTRY

Annual
Index
Vol.61
1989

CONSORTIUM ON AUTOMATED ANALYTICAL LABORATORY SYSTEMS

1381 A

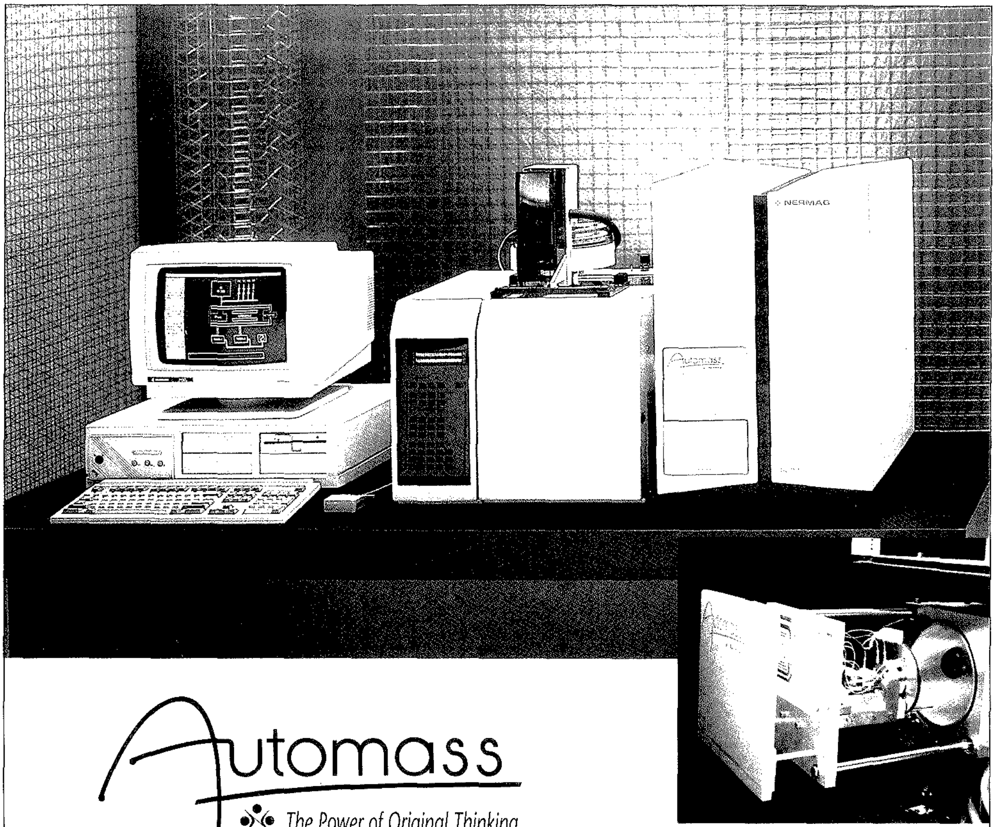

Automass

The Power of Original Thinking

When Nermag set out to develop the premier Automated Benchtop GC/MS Workstation, we were aware there was a need - *your need*, for more analytical power. Power that is simple to use, yet flexible enough to tackle the toughest problems. A true research-grade mass spectrometer was required, not a compromised mass analyzer camouflaged by glitzy game-show software.

Introducing Automass, the benchtop mass spectrometer that only Nermag could build, and the only one of its kind in the world today. The basis of Automass is a state of the art quadrupole with plug-in prefilters and an optimized Ionization Source for EI, CI, and negative ions. Our original Off Axis Ion - Photon Conversion Detector and patented Resolver electronics are enhanced by a differentially pumped vacuum system for real CI spectra.

Automass is controlled by our exclusive LUCY™ software. LUCY does window after window of instrument configuration setting, auto or manual tuning, calibration, mass spectra, chromatographic trace, and data reduction; while simultaneously examining the complete library and quantifying results. You'll Love LUCY.

Automass can flawlessly perform routine analysis all day virtually unattended, or help you tackle the most difficult analytical problem.

Automass advances Mass Spectrometry into the 90's.

Powerfully.

DELSI
NERMAG
INSTRUMENTS

France: Delsi-Nermag Instruments, 98terBlvd. Heloise, Argenteuil 9500, Tel: (1) 39.47.66.22, Fax: (1) 39.47.85.66
USA: Delsi Inc., 15701 West Hardy Rd. Houston, TX 77060, Tel: (713) 847-0811, Fax (713) 591-2132
Netherlands: Delsi instruments BV, Gebouw aetsvelt, van Houten Ind Pk 11, 1381 Weesp, Tel: (0)2940-19611
U.K.: Delsi Instruments Ltd. 33 Thrapston Rd., Brampton, Huntington, Cambs PE 18 8TE, Tel: 0480 431 609
West Germany: Delsi Instruments GmbH, Olzbachstr. 1 D-4020 Mettmann Tel: 02104/25086-87-88
Belgium: Intersmatt, 102, Av. des Volontaires, 1160 Bruxelles, Tel: 2 733.16.32

CIRCLE 32 ON READER SERVICE CARD

Capillary column for amines
Capillary column for FAME
Capillary column for naphtha
Capillary column for permanent gases
Capillary column for light hydrocarbons
Capillary column for free fatty acids
Capillary column for optical isomers
Pestic

Are you using the right chromatography column for your application?

Chrompack helps you with a full range of Tailor-made columns.
Optimized and guaranteed for a specific application field.

Tailor-made GC columns are available for:

- Amines
- C_1-C_{10} Hydrocarbons
- C_4-C_{12} Hydrocarbons
- Dioxins
- Fatty Acid Methyl Esters
- Free Fatty Acids C_2-C_{24}
- Gasoline fuels
- Glycols
- Halocarbons (EPA 624)
- PCB's
- Optical isomers
- N_2, O_2, CO, CO_2, C_1-C_3
- Permanent gases
- Pesticides
- Simulated distillation
- Triglycerides
- Volatiles in Spirits

Tailor-made HPLC columns are available for:

- Anions
- Aromatic acids
- Carbohydrates
- Cations
- Large biomolecules
- Optical isomers
- Organic acids
- Pesticides
- Petroleum products
- Polyaromatic hydrocarbons

CHROMPACK
Chrompack Inc.
1130 Route 202, Raritan NJ 08869
Tel: toll free (800) 526-3687-New Jersey (201) 722-8930
Telex 833290, Fax (201) 722-8365

Free leaflets are available for all Tailor-made columns, showing a number of specific applications. Chrompack columns are pretested and guaranteed.

FROM CHROMATOGRAPHERS – FOR CHROMATOGRAPHERS

P25336

CIRCLE 26 ON READER SERVICE CARD

SFC/SFE

Adapt your GC for supercritical fluid applications, or get a complete packed-column system with absorbance detection. Our SFC/SFE systems give you the advantages of Isco's field-proven syringe pump technology and the capability to optimize extractions and analyses with software-based pressure and density programming.

CIRCLE 75 ON READER SERVICE CARD

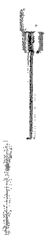

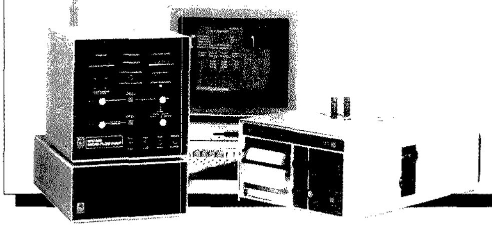

HPLC

Isco programmable chromatographs are robust, easy to maintain, and adapt readily to your changing application requirements. Unique pump and detector features provide convenient, uncluttered systems with reduced maintenance and operating costs. ChemResearch software adds PC-based data management and gradient control.
And our Foxy programmable fraction collector is the smartest choice for any automated prep HPLC.

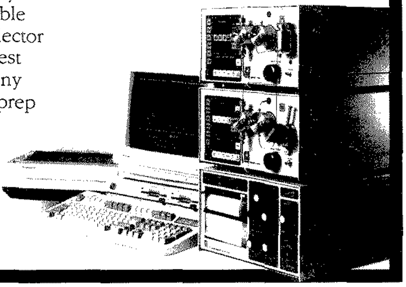

CIRCLE 76 ON READER SERVICE CARD

Capillary electrophoresis

A good detector is the key component you need to get started in HPCE, and our new CV^4 variable wavelength UV absorbance detector is the ideal foundation for a versatile, modular system. CV^4 gives you the flexibility of on-column detection at any wavelength from 190 to 360 nm with capillaries from 50 μm ID to 500 μm OD. Its exclusive optical design minimizes stray light to provide low noise and enhanced sensitivity.

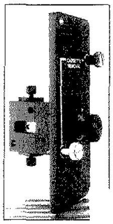

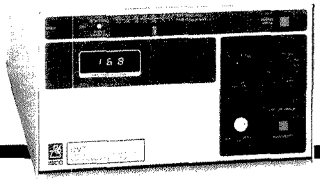

Syringe pumps for reactant feed, microbore LC, FAB

Because Isco syringe pumps feature high calibration accuracy and no detectable flow noise, they'll outperform any reciprocating pump in applications requiring high precision at very low flow rates. Three versions let you choose from pressure limits to 10,000 psi, flow rates from 0.02 μl/min to 6.7 ml/min, and capacities to 500 ml. All three pumps include interfacing for computer control.

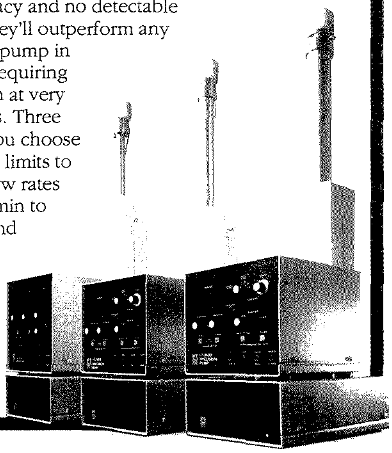

CIRCLE 77 ON READER SERVICE CARD

CIRCLE 78 ON READER SERVICE CARD

All Isco instruments carry a three-year parts and labor warranty. To find out how affordable Isco quality can be, call toll-free now.

Isco, Inc.
P.O. Box 5347
Lincoln, NE 68505

DECEMBER 15, 1989
VOLUME 61
NUMBER 24

The Audit Bureau
ANCHAM
61(24) 1353A–1392A/2689–2864 (1989)
ISSN 0003-2700

Registered in U.S. Patent and Trademark Office; Copyright 1989 by the American Chemical Society

ANALYTICAL CHEMISTRY (ISSN 0003-2700) is published semimonthly by the American Chemical Society at 1155 16th St., N.W., Washington, DC 20036. Editorial offices are located at the same ACS address (202-872-4570; FAX 202-872-6325; TDD 202-872-8733). Second-class postage paid at Washington, DC, and additional mailing offices. Postmaster: Send address changes to ANALYTICAL CHEMISTRY Member & Subscriber Services, P.O. Box 3337, Columbus, OH 43210.

Claims for missing numbers will not be allowed if loss was due to failure of notice of change of address to be received in the time specified; if claim is dated (a) North America: more than 90 days beyond issue date, (b) all other foreign: more than one year beyond issue date, or if the reason given is "missing from files."

Copyright Permission: An individual may make a single reprographic copy of an article in this publication for personal use. Reprographic copying beyond that permitted by Section 107 or 108 of the U.S. Copyright Law is allowed, provided that the appropriate per-copy fee is paid through the Copyright Clearance Center, Inc., 27 Congress St., Salem, MA 01970. For reprint permission, write Copyright Administrator, Publications Division, ACS, 1155 16th St., N.W., Washington, DC 20036.

Registered names and trademarks, etc., used in this publication, even without specific indication thereof, are not to be considered unprotected by law.

Advertising Management: Centcom, Ltd., 500 Post Rd. East, Westport, CT 06880 (203-226-7131)

1989 subscription rates include air delivery outside the U.S., Canada, and Mexico

	1 yr	2 yr
Members		
Domestic	$ 27	$ 45
Canada and Mexico	56	103
Europe	83	157
All Other Countries	120	231
Nonmembers		
Domestic	49	83
Canada and Mexico	78	141
Europe	155	280
All Other Countries	192	354

Three-year and other rates contact: Member & Subscriber Services, ACS, P.O. Box 3337, Columbus, OH 43210 (614-447-3776 or 800-333-9511).

Subscription orders by phone may be charged to VISA, MasterCard, Barclay card, Access, or American Express. Call toll free 800-ACS-5558 in the continental United States; in the Washington, DC, metropolitan area and outside the continental United States, call 202-872-8065. Mail orders for new and renewal subscriptions should be sent with payment to the Business Management Division, ACS, P.O. Box 57136, West End Station, Washington, DC 20037.

Subscription service inquiries and changes of address (Include both old and new addresses with ZIP code and *recent mailing label*) should be directed to the ACS Columbus address noted above. Please allow six weeks for change of address to become effective.

ACS membership information: Lorraine Bowlin (202-872-4567)

Single issues, current year, $7.00 except review issue and LabGuide, $12.00; **back issues and volumes and microform editions** available by single volume or back issue collection. For information or to order, call 800-ACS-5558 or write the Microform & Back Issues Office at the Washington address.

Nonmembers rates in Japan: Rates above do not apply to nonmember subscribers in Japan, who must enter subscription orders with Maruzen Company Ltd., 3–10 Nihonbashi 2-chome, Chuo-ku, Tokyo 103, Japan. Tel: (03) 272-7211.

Analytical CHEMISTRY

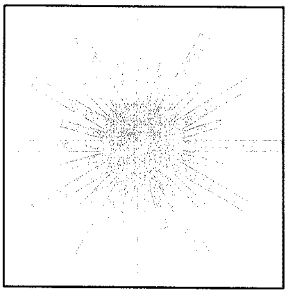

INSTRUMENTATION 1367 A

Fluorescence diagnosis and photochemical treatment of diseased tissue using lasers. In the first of a two-part series, Sune Svanberg and co-workers from the Lund Institute of Technology (Sweden) and the Lund University Hospital survey laser techniques for atomic and molecular analyses of clinical samples and describe the use of tumor-seeking agents in combination with laser radiation for malignant tumor detection and treatment

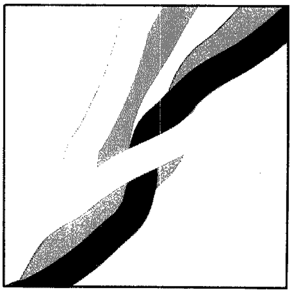

FOCUS 1381 A

***On the cover.* Consortium on Automated Analytical Laboratory Systems.** Scientists at the National Institute of Standards and Technology recently established an industry–government research consortium to accelerate the advancement of automated analytical systems, improve efficiency and data quality, and promote the transfer of analytical methods. CAALS project manager Skip Kingston of NIST's Center for Analytical Chemistry describes the consortium's philosophy and technical program

BRIEFS 1358 A

NEWS 1365 A

The **Society for Analytical Chemists** seeks applicants for two **research grants.** ▶ Researchers at Georgia Institute of Technology evaluate **method to remove volatile organic pollutants from buildings.** ▶ Lawrence Berkeley Laboratory researchers discover that cerussite is a possible material for a **new generation of scintillation detectors**

MEETINGS 1374 A

Conferences. ▶ Short courses and workshops. ▶ Call for papers

BOOKS 1376 A

Critical reviews. Books on laser microanalysis, electrophoresis, and on-line process analyzers are reviewed

NEW PRODUCTS & MANUFACTURERS' LITERATURE 1386 A

AUTHOR INDEX 2689

BRIEFS

Articles

Quantitative Imaging of Boron, Calcium, Magnesium, Potassium, and Sodium Distributions in Cultured Cells with Ion Microscopy 2690

A method for the generation of intracellular elemental concentration information from ion micrographs of cryoprepared cultured cells is detailed. Detection limits in the low- to sub-ppm dry weight range are estimated.

Walter A. Ausserer, Yong-Chien Ling, Subhash Chandra, and George H. Morrison*, Baker Laboratory of Chemistry, Cornell University, Ithaca, NY 14853-1301

Determination of Phosphorus in Zircons by Inductively Coupled Plasma Atomic Emission Spectrometry 2696

Phosphorus is determined in zircons by ICP-AES. The lowest concentration determined is 1.8 μg mL^{-1} P_2O_5. Short- and long-term precision and method precision have relative standard deviations of 1.64, 3.36, and 2.50%, respectively.

J. C. Fariñas, Departamento de Análisis Químico, Instituto de Cerámica y Vidrio, CSIC, 28500 Arganda del Rey, Madrid, Spain

Phosphine–Ozone Gas-Phase Chemiluminescence for Determination of Phosphate 2699

Gas-phase chemiluminescence generated by mixing phosphine and ozone is investigated. Phosphate is converted to phosphine by sodium tetrahydroborate.

Kitao Fujiwara*, Faculty of Integrated Arts and Sciences, Hiroshima University, Naka-ku, Hiroshima 730, Japan and **Toshie Kanchi, Shin-ichiro Tsumura, and Takahiro Kumamaru**, Department of Chemistry, Hiroshima University, Naka-ku, Hiroshima 730, Japan

Single Photon Counting Lifetime Measurements of Weak, Long-Lived Samples 2704

The origin and elimination of some systematic errors in the determination of luminescence lifetimes by the time-correlated single photon counting method are discussed.

Seth W. Snyder and J. N. Demas*, Department of Chemistry and Biophysics Program, University of Virginia, Charlottesville, VA 22901 and **B. A. DeGraff**, Department of Chemistry, James Madison University, Harrisonburg, VA 22807

Iterative Least-Squares Fit Procedures for the Identification of Organic Vapor Mixtures by Fourier Transform Infrared Spectrophotometry 2708

Programs for the qualitative and quantitative analysis of vapor mixtures are evaluated using three mixtures containing 5–11 components at approximately 2 ppm in zero air. Results are obtained using a set building method.

Xiao Hong-kui, Steven P. Levine*, and James B. D'Arcy, School of Public Health, The University of Michigan, Ann Arbor, MI 48109-2029, School of Public Health, Beijing Medical University, Beijing 100083, People's Republic of China, and Biomedical Science Department, Research Laboratories, General Motors Corporation, Warren, MI 48090

Nanogram Nitrite and Nitrate Determination in Environmental and Biological Materials by Vanadium(III) Reduction with Chemiluminescence Detection 2715

Vanadium(III) is used as a reducing reagent for the determination of nitrate (using 0.1–1.0 M HCl at 80–90 °C) and nitrite (at room temperature) in water, sediment, plant materials, and human fluids. Nanogram detection limits are achieved.

Robert S. Braman* and Steven A. Hendrix, Department of Chemistry, University of South Florida, Tampa, FL 33620

Statistical Estimation of Analytical Data Distributions and Censored Measurements 2719

By comparing analytical data to its normal cumulative probability scale, shapes of unknown data distributions are numerically defined and expected values of censored data points are estimated.

Kirk K. Nielson* and Vern C. Rogers, Rogers and Associates Engineering Corporation, P.O. Box 330, Salt Lake City, UT 84110-0330

Selective Detection of Carbon-13, Nitrogen-15, and Deuterium Labeled Metabolites by Capillary Gas Chromatography–Chemical Reaction Interface/Mass Spectrometry 2724

A chemical reaction interface MS technique selectively detects ^{13}C-, ^{15}N-, and ^{2}H-enriched phenytoin and its metabolites in urine following capillary GC at the low- to subnanogram per milliliter level.

Donald H. Chace and Fred P. Abramson*, Department of Pharmacology, The George Washington University Medical Center, Washington, D.C. 20037

---

* Corresponding author

For ground water, soil, hazardous waste,
and industrial effluent monitoring . . .

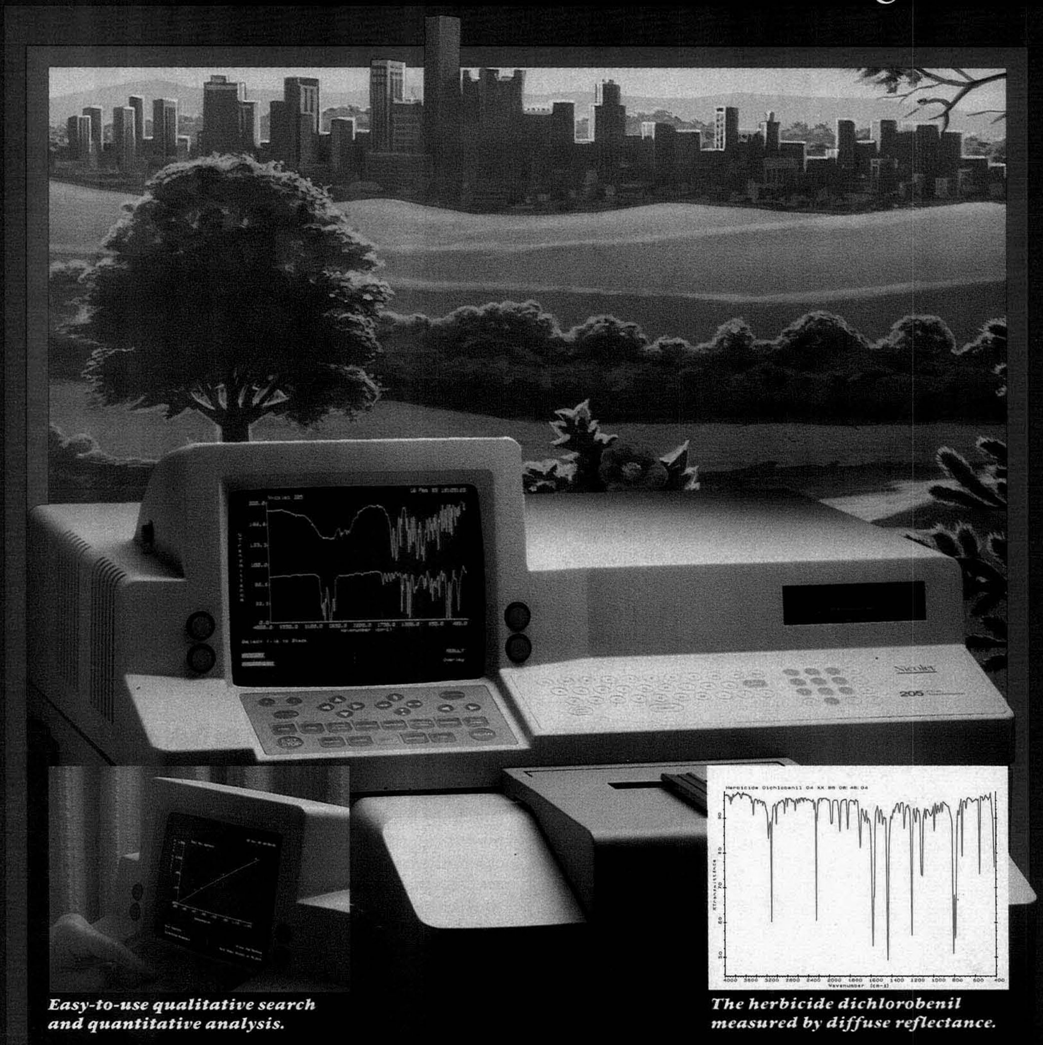

Easy-to-use qualitative search and quantitative analysis.

The herbicide dichlorobenil measured by diffuse reflectance.

You need the Nicolet 205:
The FT-IR analyzer for today and for tomorrow.

The 205 is a compact, economical FT-IR analyzer designed for automatic implementation of EPA Method 413.2, EPA Method 418.1, and ASTM Method D3921.

Some instruments stop here—but the demands for more complete analysis continually grow. The 205 gives you the added analytical power and versatile capabilities for full pollutant and material characterization, essential for future environmental and hazardous waste compliance applications.

Stay ahead with Nicolet infrared. Be prepared for Method 9073, the new RCRA* methods, and all of tomorrow's challenges.

Invest in the Model 205: The FT-IR analyzer for the future as well as today's challenges. Contact us for more information or to arrange a demonstration.

*Resource Conservation and Recovery Act

Nicolet
INSTRUMENTS OF DISCOVERY

Nicolet Analytical Instruments / 5225-1 Verona Rd. / Madison, WI 53711 / (608) 271-3333 / FAX: (608) 273-5046

CIRCLE 110 ON READER SERVICE CARD

Decomposition of Peroxyacetyl Nitrate and Peroxypropionyl Nitrate during Gas Chromatographic Determination with a Wide-Bore Capillary and Two Packed Columns 2731

For a residence time of 2 min on the GC column, 29% of PAN is decomposed on the wide-bore column, 82% on the Carbowax 400 column, and 71% on the QF-1 + diglycerol column. PPN yields similar results. The optimum column and ECD temperatures are also determined.

Nikolaos Roumelis and Sotirios Glavas*, Department of Chemistry, University of Patras, GR-26110 Patras, Greece

Deconvolution of Nonequilibrium Band Broadening Effects for Accurate Particle Size Distributions by Sedimentation Field-Flow Fractionation 2735

The distortion of particle size distribution for narrow dispersity samples attributable to nonequilibrium band broadening in sedimentation FFF is characterized. Two deconvolution techniques are applied to remove this broadening from experimental fractograms.

Mark R. Schure*, Digital Equipment Corporation, 200 Forest Street, MR01-3/T2, Marlborough, MA 01752 and **Bhajendra N. Barman and J. Calvin Giddings**, Department of Chemistry, University of Utah, Salt Lake City, UT 84112

Determination of Acrylonitrile in Stationary Source Emissions by Impinger Sampling and Gas Chromatography with Nitrogen–Phosphorus Detection 2743

Evaluation of a sampling and analytical method through both laboratory and field testing is reported. An accuracy of 4.6% and a precision of 3.3% are achieved.

James N. Fulcher, Gary B. Howe*, R.K.M. Jayanty, and Max R. Peterson, Center for Environmental Measurements, Research Triangle Institute, P.O. Box 12194, Research Triangle Park, NC 27709 and **Jimmy C. Pau, J. E. Knoll, and M. R. Midgett**, U.S. Environmental Protection Agency, Research Triangle Park, NC 27711

Separation of Cations by Open-Tubular Column Liquid Chromatography 2747

Cations are separated using open-tubular columns (9.5, 5.4, and 4.6 μm i.d.) coated with a strong and weak cation exchanger; 67–100% of the possible number of theoretical plates are obtained.

Stephan R. Müller and Wilhelm Simon*, Department of Organic Chemistry, Swiss Federal Institute of Technology (ETH), CH-8092 Zürich, Switzerland, **H. Michael Widmer and Karl Grolimund**, Central Function Research, Ciba-Geigy AG, CH-4002 Basel, Switzerland, and **Gerhard Schomburg and Peter Kolla**, Chromatography Department, Max-Planck-Institut für Kohlenforschung, D-4300 Mülheim-Ruhr, FRG

Determination of Regulatory Organic Compounds in Radioactive Waste Samples. Volatile Organics in Aqueous Liquids 2751

Volatile organic compounds are determined at μg/L levels from an aqueous matrix containing mixed fission products using remote purge and trap followed by GC/MS in a nonradioactive laboratory.

Bruce A. Tomkins*, John E. Caton, Jr., Marsha D. Edwards, Manuel E. Garcia, Robert L. Schenley, Lise J. Wachter, and Wayne H. Griest, Organic Chemistry Section, Analytical Chemistry Division, Oak Ridge National Laboratory, Oak Ridge, TN 37831-6120

Radiochemical Neutron Activation Analysis of Zinc Isotopes in Human Blood, Urine, and Feces for in Vivo Tracer Experiments 2757

The use of stable ^{70}Zn tracer for detecting Zn in humans is validated by the simultaneous use of radioactive ^{65}Zn tracer in adult volunteers. Three stable Zn isotopes are observed via neutron–irradiation products after chemical separations.

İnci G. Gökmen, Namik K. Aras, and Glen E. Gordon*, Department of Chemistry and Biochemistry, University of Maryland, College Park, MD 20742 and **Meryl E. Wastney and Robert I. Henkin**, Department of Pediatrics, Georgetown University Medical Center, Washington, DC 20007

Observation of Kinetic Heterogeneity on Highly Ordered Pyrolytic Graphite Using Electrogenerated Chemiluminescence 2763

Electron transfer involving luminol is favored at defect-rich regions of highly ordered pyrolytic graphite.

Robert J. Bowling and Richard L. McCreery*, Department of Chemistry, Ohio State University, Columbus, OH 43210 and **Christine M. Pharr and Royce C. Engstrom***, Department of Chemistry, University of South Dakota, Vermillion, SD 57069

Fumed Silica Substrates for Enhanced Fluorescence Spot Test Analysis of Benzo[*a*]pyrene–DNA Adduct Products 2766

Amorphous fumed silica enhances both the intensity and resolution of the emission, excitation, and synchronous fluorescence spectra of benzo[*a*]pyrene-*r*-7,*t*-8,9,10-tetrahydrotetrol on a filter paper substrate.

Randy W. Johnson and Tuan Vo-Dinh*, Advanced Monitoring Development Group, Health and Safety Research Division, Oak Ridge National Laboratory, Oak Ridge, TN 37831-6101

Supercritical Fluid Extraction for the Rapid Determination of Polychlorinated Dibenzo-*p*-dioxins and Dibenzofurans in Municipal Incinerator Fly Ash 2770

One-hour leaching of municipal incinerator fly ash with supercritical nitrous oxide removes more than 90% of tetrachlorodibenzo-*p*-dioxins from this matrix. Precision is better than that obtained with the Soxhlet method.

Nick Alexandrou and Janusz Pawliszyn*, Department of Chemistry, University of Waterloo, Waterloo, Ontario, Canada N2L 3G1

Thimble Glass Frit Nebulizer for Atomic Spectrometry 2777

An internally pressurized thimble glass frit nebulizer is developed as a sample introduction system for atomic spectrometry. The nebulization system consumes microliter quantities of test solution.

R. H. Clifford and Akbar Montaser*, Department of Chemistry, George Washington University, Washington, DC 20052 and **S. A. Sinex and S. G. Capar**, Division of Contaminants Chemistry, Food and Drug Administration, Washington, DC 20204

Determination of Chloride and Available Chlorine in Aqueous Samples by Flame Infrared Emission 2785

The direct determination of chloride and available chlorine in aqueous samples is achieved with detection limits of 1.59 ppm (Cl^-) and 1.61 ppm (Cl_2), average RSDs of 4.39% (Cl^-) and 1.84% (Cl_2), and an accuracy of 2.97% (Cl_2 in bleach when compared with iodometric titration).

S. W. Kubala, D. C. Tilotta, M. A. Busch, and K. W. Busch*, Department of Chemistry, Baylor University, Waco, TX 76798

Acrodisc: The Difference is Clear.

Clearly the Widest Selection.

Gelman Sciences Acrodiscs® are available in a wide variety of membrane types, with 0.2µm or 0.45µm pore sizes and 13mm or 25mm diameters.

Clearly Identified.

Acrodiscs are printed with identifying information, and are color-coded to the product packaging. Convenient tube containers allow you to see their contents at a glance.

Clearly the Best Performance.

Gelman Sciences is so certain you'll be satisfied with the performance of its Acrodisc syringe filters, every package is covered by a free-replacement guarantee. So order Gelman Sciences Acrodiscs today through your local laboratory products distributor.

CIRCLE 58 ON READER SERVICE CARD

GelmanSciences

600 S. Wagner Rd. • Ann Arbor, MI 48106-1448 • 313-665-0651

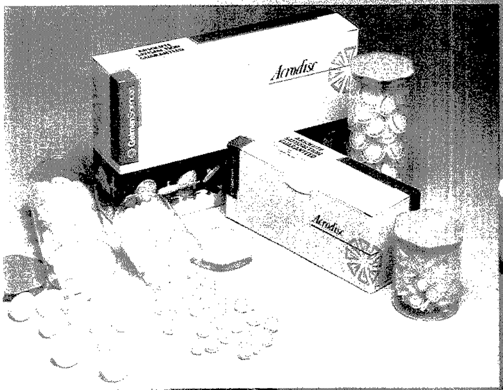

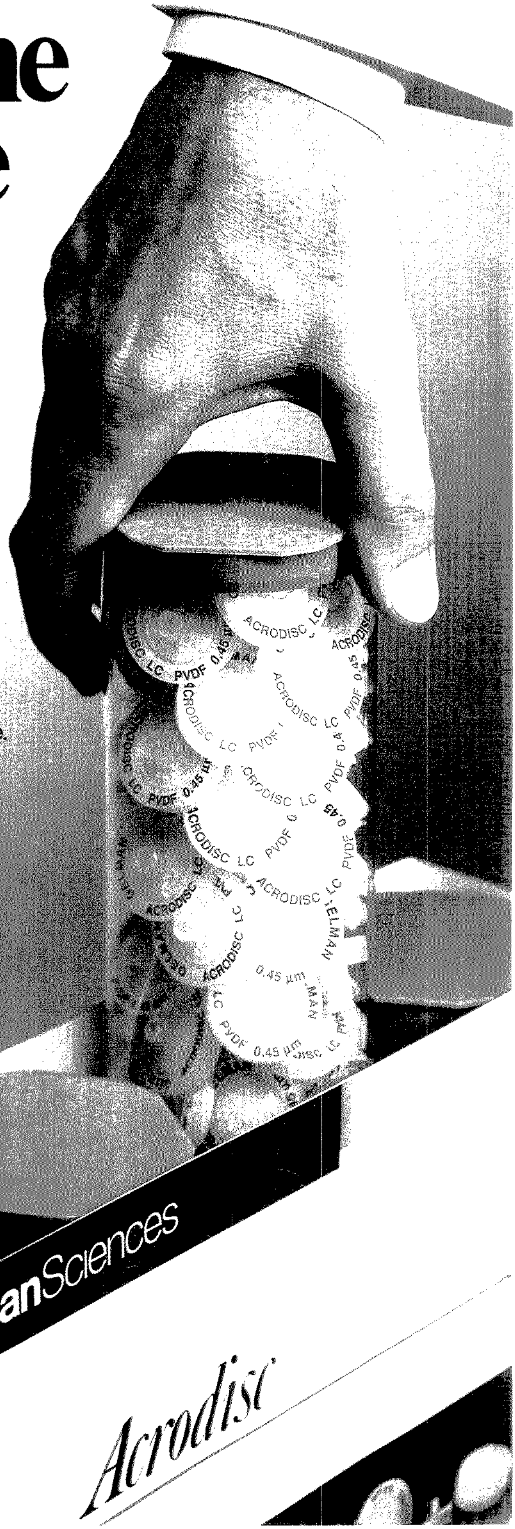

SPECIFY
WHEATON-33™
SAMPLE VIALS
...for Safekeeping

- Wheaton-33 low extractable borosilicate glass is the best protection you can provide for sensitive samples
- Wheaton-33 low extractable borosilicate glass maintains sample purity and pH
- Wheaton-33 low extractable borosilicate glass can be heat sterilized and stored at low temperature
- Wheaton-33 low extractable borosilicate glass is manufactured exclusively by Wheaton

Not all sample vials are alike. Not all sample vials provide the protection required to maintain the integrity of your valuable samples. Only Wheaton-33 sample vials are manufactured from Wheaton-33 low extractable borosilicate glass—the absolute safest protection a sample can get. [illegible]

WHEATON
1501 North Tenth Street
Millville, NJ 08332 USA
Call Toll-Free: 1-800-225-1437, Ext. 2768
TLX: 55-1295 (WHEATON US)
FAX: 1-609-825-1368

CIRCLE 177 ON READER SERVICE CARD

BRIEFS

Structural Features of Aquatic Fulvic Acids. Analytical and Preparative Reversed-Phase High-Performance Liquid Chromatography Separation with Photodiode Array Detection 2792

Characteristic repeated structural units are resolved in the hydrophilic and hydrophobic fractions of fulvic acids. The retention and UV–vis spectra of the resolved peaks are characteristic of aliphatic organic acids in the hydrophilic fraction and of conjugated aliphatic ketones and phenols in the hydrophobic fraction.

Farida Y. Saleh* and **Wenching A. Ong**, Institute of Applied Sciences and Department of Chemistry, University of North Texas, Denton, TX 76203 and **David Y. Chang**, Burlington Research, Inc., Burlington, NC 21215

Correspondence

Generation of Chemiluminescence upon Reaction of Iodine with Luminol in Reversed Micelles and Its Analytical Applicability 2800

Terufumi Fujiwara, Noriyuki Tanimoto, Jin-Jin Huang, and **Takahiro Kumamaru***, Department of Chemistry, Faculty of Science, Hiroshima University, 1-1-89 Higasisenda-machi, Naka-ku, Hiroshima 730, Japan

Technical Notes

Small-Volume Electrochemical Cell Designed for Rotating Disk Studies in Bioelectrochemistry 2803

P. N. Bartlett* and **R. G. Whitaker**, Department of Chemistry, University of Warwick, Coventry CV4 7AL, U.K.

Thin-Layer Microcell for Transmittance Fourier Transform Infrared Spectroelectrochemistry 2805

Chao-Liang Yao, Françoise J. Capdevielle, Karl M. Kadish*, and **John L. Bear***, Department of Chemistry, University of Houston, Houston, TX 77204-5641

Highly Stable Voltammetric Measurements of Phenolic Compounds at Poly(3-methylthiophene)-Coated Glassy Carbon Electrodes 2809

Joseph Wang* and **Ruiliang Li**, Department of Chemistry, New Mexico State University, Las Cruces, NM 88003

Author Index 2812

Keyword Index 2827

A-page Index 2851

Matheson has
162
Flowmeters

Matheson has choices you didn't know you had.
We are in the position of providing you with the right flowmeter for most research, analytical and process control applications.

Electronic Mass Flow Controllers and Flowmeters

...sense the mass flow of gas by measuring the differential cooling between two points. They offer precise control and/or flow indication regardless of upstream or downstream fluctuations of temperature and pressure. Meter circuitry is solid state. There are over sixty linear models ideal for use with integrators, totalizers and computer data reduction equipment.

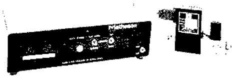

CIRCLE 100

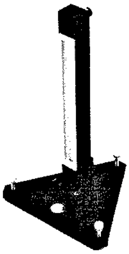

150mm Flowmeters 7600 Series

Matheson's most versatile series includes 24 models. They can be panel or bench mounted (or converted from panel to bench) with the valve on the outlet or inlet. Accuracy is 3% or 5% depending on the rate of flow. Two control valves are available including the high accuracy needle valve. This valve provides extremely accurate flow adjustment, non-reversing characteristics and excellent resolution in the low flow region for all tubes.

The TUBE CUBE® is standard.

CIRCLE 103

High Capacity Flowmeter 7700 Series

Matheson high capacity flowmeters are available in brass and stainless steel construction to solve a wide variety of flow measurement and control problems. Accuracy is ±10% of full scale with flow ranges as high as 15 CFM or 500 LPM. The glass metering element, end blocks and fittings are all enclosed in a one-piece aluminum channel frame for maximum meter protection and safety. Eight standard flow ranges are available.

CIRCLE 101

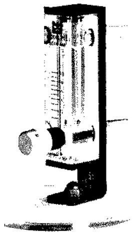

Acrylic Purge Meters 7260 Series

Accurate to 10% full scale, these economical units are used with non-corrosive gases only. Protected by an aluminum frame, the acrylic body has a direct reading scale and is capable of measuring flows up to 60 SCFH. Pressure is rated at 100 psig; temperature range is 40-150°F. Four standard ranges are available.

CIRCLE 104

150mm Multiple Tube Flowmeters 7300 and 7400 Series

These flowmeters can produce 2, 3, and 4 component gas mixtures. All mixers are supplied with a single glass float and are back-pressure compensated by mounting the control valve on the outlet side of the tube. They also permit metering of separate streams of gases. The TUBE CUBE® for safe easy replacement is standard. All units are aluminum or 316 stainless steel and can be fitted with utility valves or high accuracy valves.

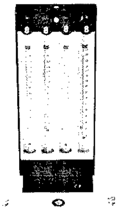

CIRCLE 102

65mm Flowmeter 7200 Series

This glass flowmeter is accurate to 5% of full scale. It has a single float and is calibrated to read directly in SLPM of air. Five standard ranges are available with direct reading scales from 0.05 to 25 SLPM maximum. Correction factors for many gases are available. Pressure to 200 psig; temperature to 250°F. The TUBE CUBE® is standard. Fittings of chromed brass or 316 stainless steel are available.

CIRCLE 105

Matheson®
Gas Products
World Leader in Specialty Gases & Equipment
30 Seaview Dr., Secaucus, N.J. 07096 1587

CARY
3
UV-Visible Spectrophotometer

WHAT'S IN A NAME?

Correct Answers

Cary UV-Vis spectrophotometers have a tradition of optical, mechanical, and photometric performance; the new Cary 1 and 3 are no exception. With excellent linearity, stability and signal-to-noise performance, the Cary's double beam design with optional dual monochromator allows you to have complete confidence in your results. No other instrument in this class delivers the same level of performance.

Application-Specific Accessories

You can mix and match a wide range of high performance accessories to fit any application. Programmable peltier heating and cooling of 6x6 cells and sippers for kinetics and DNA melting curves, solids handling devices, reflectance accessories, and a selection of samplers are available. That's just the beginning of the experimental needs that Cary accessories fill.

Unique Configurable Software

User programmability via a powerful Applications Development Language (ADL) sets the Cary on the leading edge of scientific software. Configurable to specific applications, ADL fits the most unusual requirements. From routine measurements to accessing system control functions, ADL addresses any scientific experiment with ease.

What's in a name? When the name is Cary, it's a spectrophotometer that's designed for your needs, giving you experimental flexibility and absolute integrity of analytical results. Backed by a tradition for excellence and commitment to quality, the new Cary 1 and 3 series bring to light a whole new range of analytical possibilities. For additional information, please call **(800) 231-8134**. In Canada, call **(416) 457-4130**.

CIRCLE 172 ON READER SERVICE CARD

UV-VIS
WITH A FUTURE

Analytical Chemistry Starter Grants

The Society for Analytical Chemists of Pittsburgh is soliciting applications for two $10,000 starter grants. The grants are designed to encourage innovative research by new assistant professors of analytical chemistry and to promote the training of graduate students. Analytical chemists who have accepted a U.S. college or university appointment since December 31, 1986, are eligible. For more information, contact Starter Grant Program, 300 Penn Center Boulevard, Suite 332, Pittsburgh, PA 15235 (800-825-3221). Technical inquiries should be directed to Stephen Weber (412-624-8520).

Building Bake-Off

Preliminary data collected by researchers at the Georgia Institute of Technology suggest that one method being proposed to remove volatile organic pollutants from inside new or remodeled buildings may not work. The Georgia scientists found that heating some common building materials for several days failed to "bake-out" the organic pollutants.

Volatile organics are considered a major source of indoor pollution. Builders have proposed driving out these chemicals by raising building temperatures and increasing ventilation rates for several days. Pending legislation may actually require builders to perform these "bake-outs."

The Georgia researchers evaluated the idea in four separate tests with particleboard and modular office partitions. The products were aged for several days, then baked for three to five days at 30 °C to 45 °C in an environmental chamber. "The total counts of volatile organics are about the same before and after bake out," explains Charlene Bayer, project head. She cautions that the results are preliminary and may not apply to other materials.

However, even as volatiles are driven from some building materials, carpeting and wall coverings can reabsorb the organics. The pollutants are then released over a long period of time.

Bayer recommends "aging" materials and increasing ventilation to eliminate volatile organics. Unfortunately, the Georgia researchers observed that emissions from modular office partitions only declined by one-half after four months, and it can take six months to remove noticeable odors from buildings.

A Better Way To See the Light

Following an exhaustive survey of likely candidates, researchers from the Lawrence Berkeley Laboratory (LBL) have discovered that a naturally occurring crystalline form of lead carbonate possesses superior scintillation properties. The mineral, known as cerussite, could become the ideal material for a new generation of scintillation detectors.

Substances capable of producing light when bombarded with ionizing radiation are rare. To date, fewer than 20 useful scintillation materials have been identified. Most substances dissipate ionizing energy as heat.

The discovery that cerussite is a scintillator followed the screening of more than 200 powdered materials at Brookhaven National Laboratory's National Synchrotron Light Source. Those substances that showed promise when exposed to short, intense bursts of X-rays were retested in a crystalline form. The LBL researchers collected hard-to-find crystalline samples. Cerussite, for instance, came from a mine in Tsumeb, South Africa, near the Kalahari desert.

Researchers conducting experiments with cerussite found that the lead carbonate crystal exhibited high radiation-stopping power, fast response times, and short "dead times" between responses. Cerussite could have response and rate capabilities 10 times faster than the bismuth germanium oxide detectors now used for positron emission tomography (PET) imaging. In addition, cerussite is not hygroscopic like many other commonly used scintillators.

Unfortunately, the lead mineral is generally found as tiny crystals several millimeters in size, too small for commercial detectors. Therefore, development of this discovery will hinge on whether large crystals can be grown synthetically. Says LBL biophysicist Steve Derenzo, "It would be a challenge for industry, but the rewards could be enormous."

COURTESY OF LAWRENCE BERKELEY LABORATORY

For Your Information

Mark Wrighton has been selected as the first **recipient of MIT's Ciba-Geigy professorship and research endowment.** The chair was endowed by the multinational firm with a $3 million gift that will provide both salary and research support.

The **National Institute of Standards and Technology** (NIST) has issued two **new databases for personal computers.** The first lists more than 13,000 critically evaluated X-ray photoelectron spectroscopic measurements in a format that allows searching on photoelectron and Auger lines, chemical shift, line energy, and other variables. The database covers the literature through 1985. The other release is an educational version of the DIPPR (Design Institute for Physical Property Data) Data Compilation of Pure Compounds. This special database contains evaluated data on 39 properties of 100 frequently used classroom chemicals. For information on both databases, contact the Office of Standard Reference Data, NIST, A323 Physics Bldg., Gaithersburg, MD 20899 (301-975-2208).

646 VA-Processor
Brief Operating Instructions
646 VA Processor
675 VA Sa
METROHM
SWISS MADE

Polarography with Metrohm sheds more light on trace analysis

Metals, anions, and inorganics
Selectively, simultaneously and with low detection limits down to the ppt range, you can determine many components often without solubilization, and in the presence of inert solution partners, high acid and salt concentrations or even undissolved substances.

Demanding analyses
Full keyboard, screen and printer/plotter are the components of the 646 VA Processor visible from the outside. The facility to change to any desired analytical method (DP, DC, SQW) and electrode mode (DME, HDME, SMDE, RDE) to ensure optimum determination of every substance within a polarogram speaks for the quality of the hard and software.

Automation in routine operation
The reliability of the new, unique Multi Mode Electrode (MME), of the software-controlled 675 VA Sample Changer and the options for the connection of a balance, LIMS and Dosimats for multiple standard additions make polarography suitable for everyday use in the laboratory.

Voltammetry is the economical alternative in trace analysis

Metrohm
Measurement in Chemistry
Worldwide with Metrohm

METROHM Ltd.
CH-9101 Herisau Switzerland
Phone 071 / 53 11 33
Telefax 071 / 52 11 14
Telex 88 27 12 metr ch

Brinkmann
INSTRUMENTS, INC.
Cantiague Rd., Westbury, New York 115
(516) 334-7500 (800) 645-30

CIRCLE 94 ON READER SERVICE CARD

Stefan Andersson-Engels, Jonas Johansson, and Sune Svanberg
Department of Physics
Lund Institute of Technology
P.O. Box 118
S-221 00 Lund
Sweden

Katarina Svanberg
Department of Oncology
Lund University Hospital
S-221 85 Lund
Sweden

INSTRUMENTATION

Lasers are useful in many applications in medicine and biology. Historically, most laser use has involved heat generated in the interaction of the laser beam with the tissue. Today, however, the spectroscopic aspects of this laser use are playing a more dominant role in a number of applications.

In this two-part series, Sune Svanberg and co-workers present illustrations of emerging clinical applications from cooperative work performed by the Lund Institute of Technology and the Lund University Hospital. Part I includes a survey of laser techniques for atomic and molecular analyses of samples of medical interest, spectroscopic analysis of the laser-induced plasma obtained when a high-power pulsed laser beam interacts with tissue, and the use of tumor-seeking agents in combination with laser radiation to provide new possibilities for malignant tumor detection and treatment. Part II, which will appear in the January 1, 1990, issue, describes the use of laser-induced fluorescence for tumor and plaque diagnostics. Different lasers have been used, and research efforts increasingly are being focused on excimer lasers and lasers in the IR region for the ablation of atherosclerotic plaques, cell layer by cell layer.

Laser applications in biology and medicine constitute a rapidly growing field. Soon after the introduction of the laser, this new radiation source was used in clinical investigations. Most laser use has involved heat generated in the interaction of the laser beam with the tissue (photothermal treatment) (*1*). Lasers are well known in surgery as effective cutting tools, and surgeons find them especially useful when dealing with hypervascularized tissue because of the coagulating properties of the radiation. The penetration depth of laser light into tissue is largely determined by the absorption properties of water, hemoglobin, and the skin pigment melanin. The resulting effective surgical penetration in tissue is about 0.1 mm for the CO_2 laser ($\lambda = 10.6\ \mu m$), 4 mm for the Nd:YAG laser ($\lambda = 1.06\ \mu m$), and 1 mm for the Ar^+ laser ($\lambda_1 = 488$ nm and $\lambda_2 = 515$ nm).

Short, high-energy pulses from short-wavelength excimer lasers such as ArF ($\lambda = 193$ nm), KrF ($\lambda = 248$ nm), and XeCl ($\lambda = 308$ nm) as well as from IR lasers such as the Er:YAG laser ($\lambda = 2.94\ \mu m$) and the CO_2 laser give rise to ablation and plasma formation in their interaction with tissue. The mechanism for the UV pulsed light interaction with tissue is under debate. One proposed mechanism suggests that UV pulses may disrupt the tissue through molecular bond breaking. In such a case, two or more photons are necessary to break each bond—resulting in atomic and molecular ions—and plasma emission can be detected.

The alternative mechanism suggested is absorption of light in inhomogeneously distributed chromophores. Thermal relaxation of these chromophores causes superheating of water, and microexplosions result in ablation. No plasma emission can be detected. IR light is absorbed in water, and the rapid vaporization of the water results in tissue ablation. The tissue is removed cell layer by cell layer, resulting in well-defined incisions with smooth tissue surface cuts; the surrounding tissue is not affected to any large extent. This ablative tissue interaction is use-

0003-2700/A361-1367/$01.50/0
© 1989 American Chemical Society

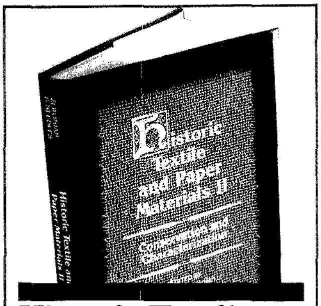

Historic Textile and Paper Materials II

Conservation and Characterization

Brand new! A summary of advances from the frontier of historic textile and paper conservation and preservation research. Compiles the most exciting work being done worldwide. Presents the perspectives of textile and paper chemists. Features discussions of some of the most promising methods and strategies in use in paper conservation today including:

- the most recent development in paper preservation
- a critical review of paper preservation methods
- the production of alkaline neutral paper
- mass deacidification processes for book preservation

Reveals previously unavailable findings, including chapters on the effects of humidity on paper aging and the use of graft polymerization to strengthen paper.

Offers information on timely issues in textile conservation, including:

- the use of thin layer chromatography to analyze dyes in historic textiles
- the effects of alkaline deacidifying agents on naturally aged textiles
- an evaluation of silk conservation techniques
- characterizing cotton nondestructively by IR spectroscopy
- heat-induced aging of linen

Historic Textile and Paper Materials II builds on the solid foundation of its precursor (ACS Advances Series No. 212) by combining a review of paper and textile preservation methods with the disclosure of the latest chemical research in the field.

S. Haig Zeronian and Howard L. Needles, *Editors*, University of California-Davis

Developed from a symposium sponsored by the Cellulose, Paper, and Textile Division of the American Chemical Society

ACS Symposium Series No. 410
254 pages (1989) Clothbound
ISBN: 0-8412-1683-5 LC: 89-38410
U.S. & Canada $54.95 Export $65.95

ORDER FROM

American Chemical Society
Distribution Office, Dept. 49
1155 Sixteenth St., N.W.
Washington, DC 20036

or CALL TOLL FREE

800-227-5558

(in Washington, D.C. 872-4363) and use your credit card!

ful in vascular surgery (*2*, *3*) and in refractive surgery of the cornea (*4*).

Although spectroscopic aspects in terms of absorption properties play a part in photothermal and photoablative treatment, they are much more important in the fields of laser photodynamic therapy and tissue diagnostics using laser-induced fluorescence (LIF). Laser interaction with tissue is reviewed in References 5 and 6. Information on different aspects of laser use in medicine are given in three topical issues of the *IEEE Journal of Quantum Electronics* (*7–9*), and a useful review of the field with special emphasis on analytical and physical chemistry is given in Reference 10. For earlier reviews of our own work, see References 11–14.

In this two-part article, we will focus on spectroscopic aspects of laser use in emerging medical applications. In Part I, tumor therapy will be discussed and fluorescence investigations aimed at tumor detection will be described, illustrating the use of both natural tissue signals and hematoporphyrin derivative (HPD) fluorescence. The spectral identification of atherosclerotic plaque in human vessels will also be illustrated. Spectral emission diagnosis in connection with tissue ablation will also be covered, with examples from plaque removal and kidney stone fracture using pulsed laser beams. In Part II, we will demonstrate how the diagnostic potential of LIF is increased by including the temporal characteristics of the fluorescence decay. The extension of point monitoring to imaging measurements will be described together with implications for practical clinical work.

Laser techniques for medical atomic and molecular analysis

Optical spectroscopic techniques such as atomic absorption and emission spectroscopy are used routinely to determine alkali ions or heavy metals (of interest from a toxicology perspective) in body fluids. Powerful laser spectroscopic techniques have been developed with greatly extended sensitivity and selectivity. In several methods, ions or electrons obtained after selective laser excitation are detected, as illustrated in Figures 1a and 1b. Such optogalvanic methods are referred to as laser-enhanced ionization (LEI) spectroscopy if flame ionization is used and if collisions play an important part in the ionization, or as resonance ionization spectroscopy (RIS) if photoionization in low-pressure samples is dominant. If a multiphoton process is used, the technique is called resonant multiphoton photoionization (REMPI). The latter techniques can be combined with mass spectrometry (resonance ionization mass spectrometry, RIMS). Laser techniques for atomic analysis are discussed in References 15–18.

Liquid chromatography (LC) and electrophoresis, in which different molecular species migrate at different rates in capillaries, are important methods for molecular analysis. The

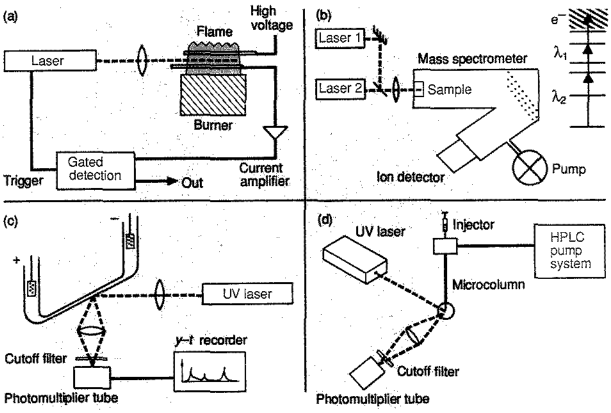

Figure 1. Principles of four laser spectroscopic techniques for the determination of elements and molecular species in body fluids.
(a) Laser-enhanced ionization (LEI) spectroscopy, (b) resonance ionization mass spectrometry (RIMS), (c) electrophoresis with laser-induced fluorescence (LIF) detection, and (d) high-performance liquid chromatography (HPLC) with LIF detection.

sensitivity of such techniques has been greatly extended by employing LIF for the detection of different molecular compounds emerging from the separative column. Additional selectivity can be obtained by analyzing the spectral distribution of the emitted fluorescence. Electrophoretic and chromatographic techniques are schematically illustrated in Figures 1c and 1d. Laser detection of LC signals is reviewed in References 19 and 20. Capillary zone electrophoresis with fluorescence detection may be used in medicine to trace small amounts of important enzymes, hormones, and peptides, as well as metabolic compounds of certain drugs (*21*, *22*). An example of a high-performance liquid chromatography (HPLC) recording using nitrogen LIF for detection is shown in Figure 2 (*23*). Two recordings for different solvents obtained with a conventional refractive index (RI) detector are shown (left and right), as well as LIF recordings of the spectral contents for individual peaks (center). The different fractions of an HPD sample exhibit fluorescence with shifts toward the red for the more aggregated forms.

Another class of medical analysis techniques using LIF is immunoassay and DNA sequencing with fluorescent tags. Such fluorescence tagging is also used in cytofluorometry and automatic cell sorting. (For a review of these aspects, see Reference 24.)

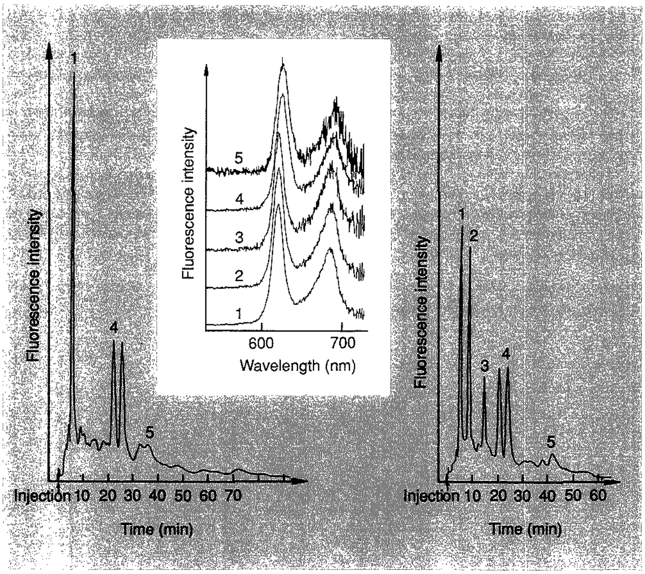

Figure 2. Chromatograms of HPD.

Left: sample suspended in 0.1 M NaOH and buffered to pH 7 with acetic acid, stirred 5 min, diluted in H_2O (2.4 times) and MeOH (5 times); flow rate: 0.7 mL/min; detection: RI at 360 nm. Right: sample suspended in H_2O, stirred 5 min, diluted in MeOH (5 times), stirred 5 min, and centrifuged; flow rate: 0.7 mL/min; detection: RI at 360 nm. Center: fluorescence spectra of peaks indicated in the left and right chromatograms obtained with 337-nm laser excitation.

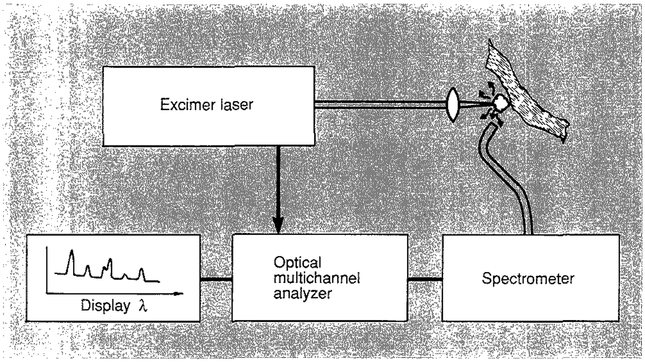

Figure 3. Experimental arrangement for spectral diagnostics of laser-induced breakdown plasma emission.

(Adapted with permission from Reference 12.)

The laser energy regime where tissue ablation occurs is distinct from the one involving nonintrusive tissue fluorescence. A hot plasma (100,000 K) can be formed, accompanied by strong light emission that can be used for tissue characterization and interactive control of the material removed. This is of particular interest in connection with the removal of atherosclerotic plaques (*25*). The early stage of the plasma ($t <$ 300 ns) is characterized by a largely structureless continuum corresponding to high electron temperatures. As the plasma cools, sharp emission lines from ions and neutral atoms occur. These phenomena can be easily studied with a time-gated optical multichannel analyzer system (shown in Figure 3). The plasma emission from a calcified human plaque is shown in Figure 4 together with the spectrum obtained when directing the same excimer laser beam onto a piece of calcium metal (*26*). Emission lines of Ca and Ca^+ can easily be recognized, and the spectra are very similar. In the tissue spectrum the sodium D line is as strong as the Ca lines and much more prominent than the corresponding sodium impurities in the calcium metal. The spectrum from normal tissue wall is much weaker and has less structure. Thus the evaporation of a calcified plaque can be stopped under computer control when the laser beam has penetrated through the calcified structure (*25*).

Another interesting medical application of a laser-produced plasma is to induce stone fracturing in biliary and urinary calculi (gallstones and kidney stones). By forming the plasma at the surface of the stone submerged in a liquid, a shock wave with extremely high local pressures can be produced that will induce fracturing of the stone into small fragments (laser lithotripsy) (*27*, *28*). For this application a flashlamp-pumped dye laser is suitable, because hundreds of millijoules per pulse can be readily transmitted through a thin fiber. For the long pulses typical for these lasers (1 μs), no damage is induced in the fiber. For a Q-switched Nd:YAG pulse with a typical length of 10 ns, pulse energies well below 100 mJ must be chosen to avoid breakdown at the fiber surface. Again, the laser-produced plasma can be spectrally analyzed and differences in stone composition detected.

The techniques of urinary stone lithotripsy with spectroscopic detection are illustrated in Figure 5. On the left, the fiber is shown in position in the ureter facing a urinary stone. On the right, an example of a urinary stone plasma spectrum is shown, as recorded in vitro (*29*). The composition of the stones has implications for the lithotripsy procedure. Gallstones are either of the lightly colored cholesterol type or of the darker bilirubinate type. The former type is much harder to fracture than the latter type. To ensure that the fiber is aimed at a stone rather than at the tissue wall, the increased backscatter of a low-power laser beam can be used. The acousto-optic signal from impinging laser pulses can also be analyzed to ensure proper tip positioning before firing high-energy pulses.

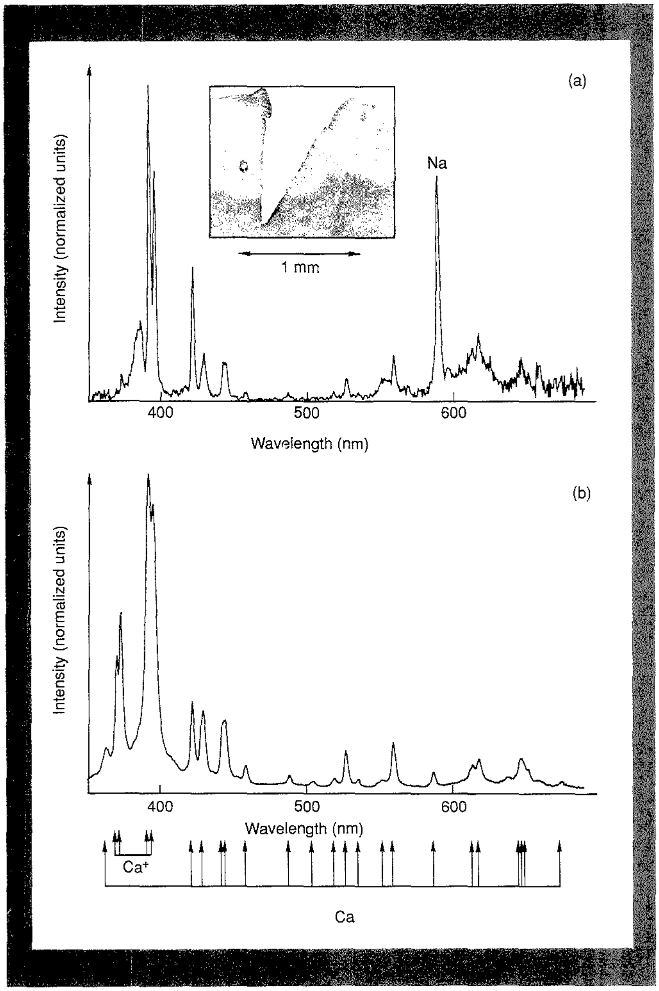

Figure 4. Laser-induced breakdown plasma spectrum for (a) a calcified plaque in an aortic wall and (b) a piece of calcium metal.

The laser source was an XeCl excimer laser working at 308 nm with 20-ns-long pulses. The spectra were obtained 500 ns after the excitation pulse. The Ca and Ca^+ lines are indicated, and the insert at the top is a tissue preparation showing the laser ablation in a plaque resulting from 100 40-mJ pulses. (Adapted with permission from Reference 26.)

HPD–photodynamic therapy

For some time, tumor-seeking agents such as HPD have been used in combination with laser radiation to localize and treat malignant tumors. Recent progress in this field is described in the literature (*14, 30–33*).

The basic principles for the HPD/laser technique are illustrated in Figure 6 (*14*). HPD is intravenously injected at a low concentration into the biological system, where the agent spreads and is subsequently cleared out of the body through natural processes. However, for reasons that remain partially unknown, the HPD molecules are selectively retained in the malignant tumor cells and in the endothelium cells in the tumor vascular system. The major absorption of HPD occurs in the Soret band, peaking at 405 nm. Fluorescence follows with a characteristic, dual-peaked distribution in the red spectral region. In tissue, the HPD fluorescence is superimposed on the natural tissue fluorescence spectrum (autofluorescence), as shown in Figure 6. The spectral fingerprint of HPD identifies the tumor and allows standard biopsy specimens to be taken at the correct location.

The excited HPD molecules can, alternatively, transfer their acquired energy to oxygen molecules in the tissue. This transfer is mediated by the long-lived triplet HPD state to which radiationless transitions can occur. Triplet HPD molecules transfer their energy to oxygen molecules that are promoted from their ground $X\,^3\Sigma_g$ state to the $^1\Delta_g$ state. Singlet molecular oxygen is known to be a strong cytotoxic agent that violently oxidizes the surrounding (tumor) tissue. The laser-induced chemical process, which is referred to as HPD–PDT (hematoporphyrin derivative–photodynamic therapy), is normally performed with laser light at 630 nm, where the HPD molecule has a minor absorption peak and where the tissue has a much better light transmission than at shorter wavelengths. Although very small light doses are needed to induce observable fluorescence, efficient therapeutic action requires much more light, and normally a dye laser pumped by an argon ion laser or a gold vapor laser (λ = 628 nm) is employed. Encouraging results have been obtained in clinical trials using HPD–PDT.

Because of the limited light penetration in tissue, only thin superficial lesions can be treated by direct surface

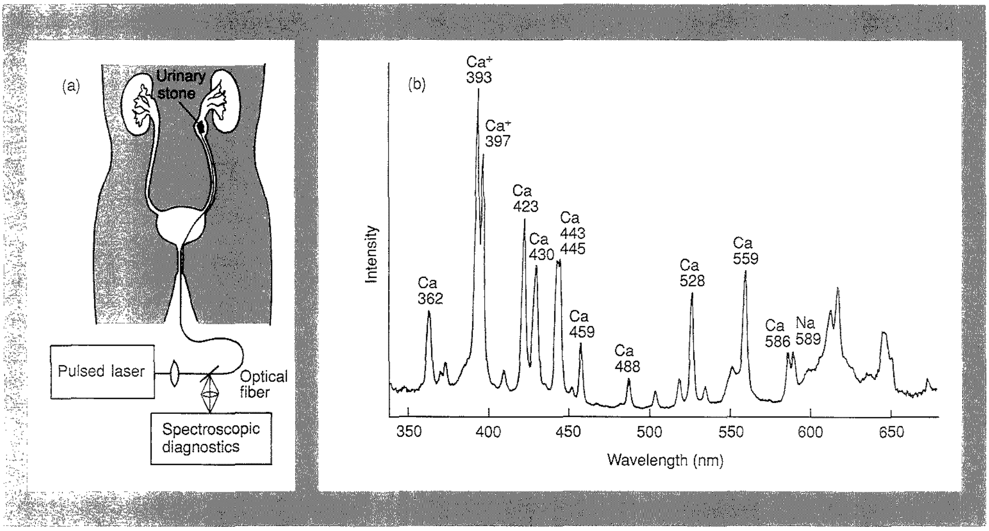

Figure 5. Principles of plasma spectroscopy in combination with laser lithotripsy.

(a) Arrangement, including excitation laser, fiber delivery system, beam splitter, and spectroscopic detection system. (b) Plasma spectrum of a urinary stone in vitro under pulsed (50 mJ, 10 ns long) Nd:YAG laser irradiation. The spectrum was recorded 500 ns after the laser pulse. (Adapted with permission from Reference 29.)

irradiation. Deeper lesions can be irradiated by implanting fiber tips in the tumor mass through the lumen of a syringe needle. Irradiation with the fiber inserted through the biopsy channel of an endoscope also substantially increases the applicability of the technique. Finally, by irradiating the tumor bed after standard surgical removal, a more radical tumor eradication can be accomplished (e.g., in brain surgery).

The result of an HPD–PDT treatment of a basiloma is shown in Figure 7 (*34*, *35*). The tumor area was uniformly irradiated by 60 mJ/cm^2 of 630-nm light. Because of the selective retention of HPD in the tumor, the necrosis (destruction of tissue) is confined to the tumor area. In the right part of Figure 7, the same area is shown three months after treatment. The only side effect of the HPD injection seems to be a hypersensitization to sunlight resulting from partial HPD retention in the skin. Therefore patients should be kept under low ambient light conditions for about four weeks.

As the name indicates, HPD as prepared from hematoporphyrin according to the Lipson procedure (*36*) is a complex mixture of monomers and dimers as well as aggregates of hematoporphyrin. Recently, the therapeutically active component was identified as dihematoporphyrin ether/ester (DHE) (*37–39*). This purified component is commercially available under

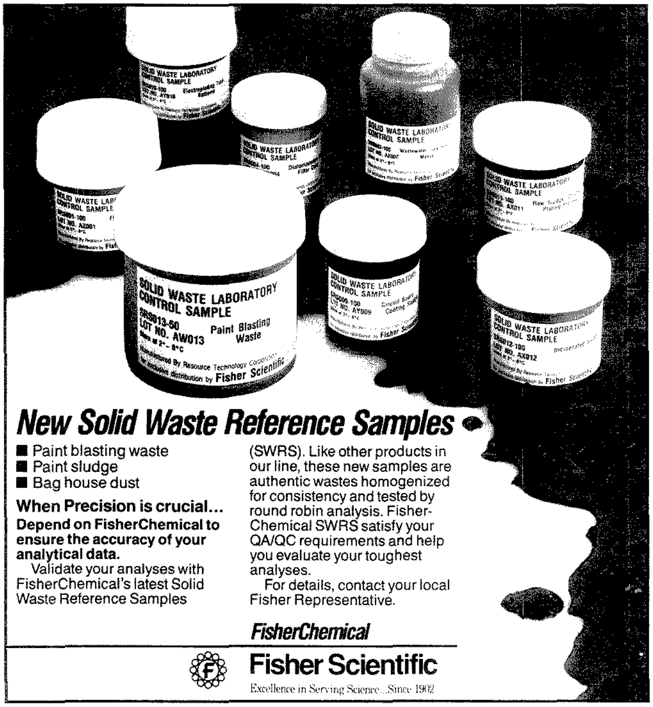
SOLID WASTE LABORATORY CONTROL SAMPLE
Paint Blasting Waste
LOT NO. AW013
Fisher Scientific

New Solid Waste Reference Samples

- Paint blasting waste
- Paint sludge
- Bag house dust

When Precision is crucial...
Depend on FisherChemical to ensure the accuracy of your analytical data.
Validate your analyses with FisherChemical's latest Solid Waste Reference Samples (SWRS). Like other products in our line, these new samples are authentic wastes homogenized for consistency and tested by round robin analysis. FisherChemical SWRS satisfy your QA/QC requirements and help you evaluate your toughest analyses.
For details, contact your local Fisher Representative.

FisherChemical
Fisher Scientific
Excellence in Serving Science...Since 1902

CIRCLE 50 ON READER SERVICE CARD

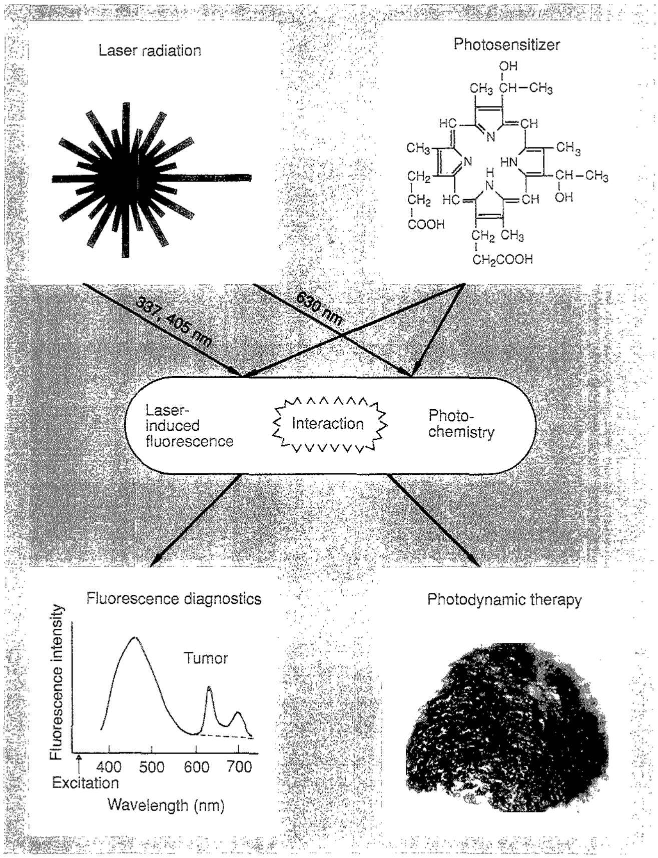

Figure 6. Schematic of the diagnostic and therapeutic use of photosensitizers in combination with laser radiation.

A tissue spectrum exhibiting the fluorescence signature of HPD is shown for excitation at 337 nm. The inserted photograph shows the necrosis of a basiloma 48 h after photodynamic therapy using 60 J/cm² and an HPD dose of 2.5 mg/kg body weight. (Adapted with permission from Reference 14.)

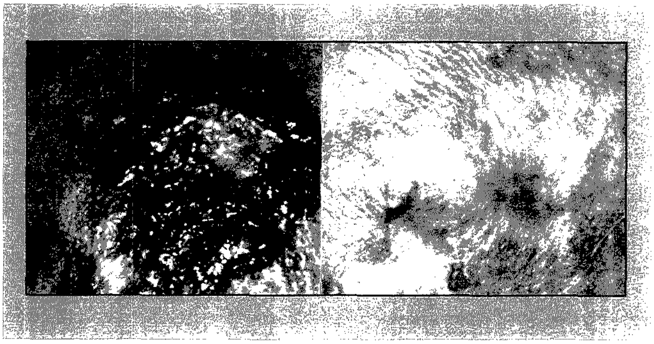

Figure 7. Photographs of basal cell carcinoma (left) 1 week and (right) 11 weeks after PDT.

the name of Photofrin II. Because monomers are known to have a much higher fluorescence yield than dimers, optimizing the conditions for therapy does not necessarily mean that tumor detection conditions are optimized. The situation is further complicated by the fact that the porphyrins transform in the living tissue after being injected.

Much research is now being devoted to the development of new and more efficient sensitizers. Apart from being photodynamically potent and strongly fluorescent, a good sensitizer should have useful absorption peaks toward the near-IR region (670–750 nm) where tissue exhibits its best transmission to achieve deep action. The classes of compounds now being investigated include phthalocyanines, chlorins, purpurins, and benzoporphyrins (*40–45*).

References

(1) Goldman, L. *The Biomedical Lasers: Technology and Clinical Applications;* Springer: Heidelberg, 1981.
(2) Grundfest, W. S.; Litvack, F.; Forrester, J. S.; Goldenberg, T.; Swan, H.J.C.; Morgenstern, L.; Fishbein, M.; McDermid, S.; Rider, D. M.; Pacala, T. J.; Laudenslager, J. B. *J. Am. Coll. Cardiol.* 1985, *5*, 929.
(3) Isner, J. M.; Steg, P. G.; Clarke, R. H. *IEEE J. Quantum Electron.* 1987, *23*, 1756.
(4) Puliafito, C. A.; Steinert, R. F.; Deutsch, T. F.; Hillenkamp, F.; Dehm, E. J.; Adler, C. M. *Opthalmol.* 1985, *92*, 741.
(5) Boulnois, J.-L. *Lasers Med. Sci.* 1985, *1*, 47.
(6) Boulnois, J.-L. In *Laser Applications in Cardiovascular Diseases;* Ginsburg, R., Ed.; Futura Publishing: New York, 1987.
(7) Alfano, R. R.; Doukas, A. G., Eds. *IEEE J. Quantum Electron.* 1984, *20*, 1342–1556.
(8) Deutsch, T. F.; Puliafito, C. A., Eds. *IEEE J. Quantum Electron.* 1987, *23*, 1701–1852.
(9) Birngruber, R.; Brueck, S.R.J.; Isner, J., Eds. *IEEE J. Quantum Electron.* 1990, *26*.
(10) Greulich, K. O.; Wolfrum, J., Eds. *Ber. Bunsen-Ges. Phys. Chem.* 1989, *93*, 233–422.
(11) Svanberg, S. *Physica Scripta* 1987, *T19*, 469.
(12) Svanberg, S. *Physica Scripta* 1989, *T26*, 90–98.
(13) Andersson-Engels, S.; Ankerst, J.; Brun, A.; Elner, Å.; Gustafson, A.; Johansson, J.; Karlsson, S.-E.; Killander, D.; Kjellén, E.; Lindstedt, E.; Montan, S.; Salford, S. G.; Simonsson, B.; Stenram, U.; Strömblad, L.-G.; Svanberg, K.; Svanberg, S. *Ber. Bunsen-Ges. Phys. Chem.* 1989, *93*, 335.
(14) Svanberg, K. Ph.D. Dissertation, Lund University Hospital, Lund, Sweden, 1989.
(15) *Analytical Laser Spectroscopy;* Omenetto, N., Ed.; John Wiley: New York, 1979.
(16) *Laser Analytical Spectrochemistry;* Letokhov, V. S., Ed.; Adam Hilger: Bristol, 1985.
(17) *Analytical Applications of Lasers;* Piepmeier, E. H., Ed.; Wiley Interscience: New York, 1986.

(18) *Principles and Applications of Resonance Ionization Spectroscopy;* Hurst, G. S.; Payne, M. G., Eds.; Adam Hilger: Bristol, 1988.
(19) Yeung, E. S. *Advances in Chromatography*, Vol. 23; Giddings, J. C.; Grushka, E.; Cazes, J.; Brown, P. R., Eds.; Decker: New York, 1984.
(20) Yeung, E. S. *Microcolumn Separations: Columns, Instrumentation and Ancillary Techniques;* Novotny, M. V.; Ishii, D., Eds.; Elsevier: Amsterdam, 1985.
(21) Gassman, E.; Kuo, J. E.; Zare, R. N. *Science* **1985,** *230,* 813.
(22) Roach, M. C.; Gozel, P. H.; Zare, R. N. *J. Chromatogr.* **1988,** *426,* 129.
(23) Johansson, J.; Johansson, E.; Andersson-Engels, S., unpublished results.
(24) Dressler, L. G.; Bartow, S. A. *Seminars in Diagnostic Pathology;* **1989,** *6,* 55.
(25) Hohla, H.; Laufer, G.; Wollenek, G.; Horvat, R.; Henke, H.-W.; Buchelt, M.; Wuzi, G.; Wolner, E. *SPIE* **1988,** *908,* 128.
(26) Andersson-Engels, S.; Gustafson, A.; Johansson, J.; Stenram, U.; Svanberg, K.; Svanberg, S. *Lasers Med. Sci.,* **1989,** *4,* 171–81.
(27) Teng, P.; Nishioka, N. S.; Anderson, R. R.; Deutsch, T. F. *Appl. Phys.* **1987,** *B42,* 73.
(28) Wondrazek, F.; Frank, F. *SPIE* **1988,** *906.*
(29) Palmqvist, C. "Laser Lithotripsy of Kidney Calculi with a Nd:YAG Laser"; Diploma paper; Lund Reports on Atomic Physics LRAP-94, 1988.
(30) *Lasers and Hematoporphyrin Derivative in Cancer;* Hayata, Y.; Dougherty, T. J., Eds.; Ikaku-Shoin: Tokyo, 1983.
(31) Dougherty, T. J. *Photochem. Photobiol.* **1984,** *45,* 879.
(32) Dougherty, T. J.; Weishaupt, K. R.; Boyle, D. G. In *Principles and Practice of Oncology;* DeVita, V. T., Jr.; Hellman, S.; Rosenberg, S. A., Eds.; J. B. Lippincott: Philadelphia, 1985; p. 2272.
(33) Manyak, M. J.; Russo, A.; Smith, P. D.; Glatstein, E. *J. Clin. Oncol.* **1988,** *6,* 380.
(34) Andersson-Engels, S.; Johansson, J.; Kjellén, E.; Killander, D.; Svaasand, L. O.; Svanberg, K.; Svanberg, S. *L.I.A. ICALEO* **1987,** *60,* 67.
(35) Andersson-Engels, S.; Johansson, J.; Kjellén, E.; Killander, D.; Olivo, M.; Svaasand, L. O.; Svanberg, K.; Svanberg, S. *SPIE* **1988,** *908,* 197.
(36) Lipson, R. L.; Baldes, E. J.; Olsen, A. M. *J. Thorac. Surg.* **1961,** *42,* 623.
(37) Dougherty, T. J. In *Porphyrins in Tumor Therapy;* Andreoni, A.; Cubeddu, R., Eds.; Alan R. Liss: New York, 1983; p. 285.
(38) Dougherty, T. J.; Potter, W. R.; Weishaupt, K. R. *Adv. Exp. Med. Biol.* **1984,** *170,* 301.
(39) Kessel, D. In *Photodynamic Therapy of Tumors and Other Diseases;* Jori, G.; Perria, C., Eds.; Librero Progresso Publishers: Padova, Italy, 1985; p. 10.
(40) Spikes, J. D. *Photochem. Photobiol.* **1986,** *43,* 691.
(41) Selman, S. H.; Kreimer-Birnbaum, M.; Chandhuri, K.; Garbo, G. H.; Seaman, D. A.; Keer, R. W.; Ben-Hur, E.; Rosenthal, I. *J. Urol.* **1986,** *136,* 141.
(42) Tralau, C. J.; MacRobert, A. J.; Coleridge-Smith, P. D.; Barr, H.; Boron, S. G. *Br. J. Cancer* **1987,** *55,* 389.
(43) Nelson, J. S.; Roberts, W. G.; Berns, M. W. *Cancer Res.* **1987,** *79,* 468.
(44) Richter, A. M.; Kelly, B.; Chow, J.; Liu, D. J.; Towers, G.H.N.; Dolphin, D.; Levy, J. G. *J. Nat. Cancer. Inst.* **1987,** *79,* 1327.
(45) Richter, A. M.; Sternberg, E.; Waterfield, E.; Dolphin, D.; Levy, J. G., unpublished work.

Katarina Svanberg (left) holds a Master's degree in economic history from Göteborg University (1970) as well as an M.D. She has been a physician at Lund University Hospital since 1983, and she recently defended a doctoral thesis in oncology and internal medicine. Her main interest is in the development of fluorescence diagnosis and photodynamic therapy.

Sune Svanberg (second from left) received his Ph.D. in physics from the University of Götenburg, Sweden, in 1972. Since 1980 he has been a professor of physics and head of the Division of Atomic Physics at Lund Institute of Technology (LTH). His research interests include laser spectroscopy of free atoms, combustion diagnostics and remote sensing using lasers, and medical applications of LIF.

Stefan Andersson-Engels (second from right) received the Master of Engineering Physics degree from LTH in 1985. Since then he has been working as a Ph.D. student in the Division of Atomic Physics, LTH, where his primary area of research is the medical application of LIF.

Jonas Johansson (right) received the Master of Engineering Physics degree from LTH in 1986. Since 1987 he has been working as a Ph.D. student in the Division of Atomic Physics, LTH. His main interest is time-resolved LIF for medical applications.

SOLID WASTE LABORATORY CONTROL SAMPLE
SRS203-225 Municipal Incinerator Ash
LOT NO. AQ203
Fisher Scientific

Introducing— TCLP Reference Sample

When reliability is crucial...

Depend on FisherChemical to ensure the accuracy of your analytical data.

Validate your analyses with FisherChemical's new TCLP sample. Like other products in our SWRS Line, this ash is an unaltered waste homogenized for consistency; stated values are achieved by round robin analysis. Rely on FisherChemical TCLP Sample to satisfy TCLP QA/QC requirements and help you evaluate your toughest analyses.

For details, contact your local Fisher Representative.

FisherChemical

Fisher Scientific

Excellence in Serving Science...Since 1902

CIRCLE 51 ON READER SERVICE CARD

MEETINGS

Conferences

For information on the following Gordon Conferences, contact Alexander M. Cruickshank, Gordon Research Center, University of Rhode Island, Kingston, RI 02881 (401-783-4011 or 3372)

■ **Gordon Research Conference on Electrochemistry.** Jan. 15–19. Ventura, CA

■ **Gordon Research Conference on Isotopes in the Physical and Life Sciences.** Jan. 22–26. Oxnard, CA

■ **Gordon Research Conference on Bioanalytical Sensors.** March 12–16. Ventura, CA

■ **12th International Conference on Cement Microscopy.** April 2–5. Vancouver, Canada. *Contact: Charles Buchanan, Jr., 409 Santee Dr., Santee, SC 29142*

■ **Oak Ridge Conference on Advanced Analytical Concepts for the Clinical Laboratory.** April 5–6. Tampa, FL. *Contact: AACC, 2029 K St., N.W., 7th Floor, Washington, DC 20006 (202-857-0717)*

■ **Royal Society of Chemistry Annual Congress.** April 9–12. Belfast, U.K. *Contact: Royal Society of Chemistry, Burlington House, London W1V 0BN, U.K.*

■ **1st International Congress on Electrophoresis, Supercomputers, and the Human Genome.** April 10–13. Tallahassee, FL. *Contact: H. Lim or R. McMullen, Florida State University, Tallahassee, FL (904-644-1010)*

■ **Meeting of the Materials Research Society.** April 16–21. San Francisco, CA. *Contact: MRS, 9800 McKnight Rd., Suite 327, Pittsburgh, PA 15237 (412-367-3003)*

■ **20th Annual Symposium on Advances in Applied Analytical Chemistry.** May 2–3. Kenner, LA. *Contact: Judy Timpa, SRRC, ARS, USDA, P.O. Box 19687, New Orleans, LA 70179 (504-286-4360)*

■ **Southeastern Safety and Health Conference and Exhibition.** May 8–10. Atlanta, GA. *Contact: Education Extension Service, Georgia Institute of Technology, Atlanta, GA 30332 (404-894-2400)*

■ **3rd International Colloquium on Centrifugal Partition Chromatography.** June 21–22. San Mateo, CA. *Contact: Eleanor Cazes, Sanki Laboratories, 106 Folcroft East Business Park, Sharon Hill, PA 19079*

■ **Techniques, Instrumentation, Data Handling: UV Spectroscopy for the '90s.** July 1–6. Yorkshire, U.K. *Contact: T. Frost, The Wellcome Foundation Ltd., Temple Hill, Dartford, Kent DA1 5AH, U.K.*

■ **Meeting on Electrochemical Techniques in Speciation Studies.** July 9–11. Liverpool, U.K. *Contact: A. E. Bottom, Kent Industrial Measurements, Ltd., Oldends Lane, Stonehouse, Glos. GL10 3TA, U.K.*

■ **2nd International Meeting on Spectroscopy Across the Spectrum—Techniques and Applications of Analytical Spectroscopy.** July 9–12. Hertford, U.K. *Contact: P. R. Brawn, Unilever Research, Colworth Laboratory, Sharnbrook, Beds. MK44 1LQ, U.K.*

■ **5th Biennial National Atomic Spectroscopy Symposium.** July 18–20. Loughborough, U.K. *Contact: J. R. Dean, Dept. of Chemical and Life Sciences, Newcastle upon Tyne Polytechnic, Ellison Bldg., Newcastle upon Tyne NE1 8ST, U.K.*

■ **43rd ACS Summer Symposium on Analytical Chemistry—Mass Spectrometry.** July 24–27. Oak Ridge, TN. *Contact: David Donohue, ORNL, Analytical Chem. Div., Bldg. 4500-S, Mail Stop 6142, Oak Ridge, TN 37831*

■ **7th International Congress of Pesticide Chemistry.** Aug. 5–10. Hamburg, F.R.G. *Contact: Secretariat, Bank Court Chambers, 2–3 Pound Way, Cowley Centre, Oxford OX4 3YF, U.K.*

■ **2nd International Symposium on Microcolumn Separation Methods.** Aug. 20–22. Uppland, Sweden. *Contact: Eva Mattsson, Swedish Chemical Society, Analytical Div., Wallingatan 26 B, S-111 24 Stockholm, Sweden*

■ **12th International Symposium on Capillary Chromatography.** Sept. 11–14. Kobe, Japan. *Contact: Kiyokatsu Jinno, School of Materials Science, Toyohashi University of Technology, Toyohashi 440, Japan*

■ **Symposium on Chemometrics with Environmental Applications.** Oct. 30–Nov. 1. Las Vegas, NV. *Contact: M. Stapanian, Lockheed Engineering & Sciences Co., 1050 E. Flamingo Rd., Las Vegas, NV 89119*

■ **7th Montreux Symposium on Liquid Chromatography/Mass Spectrometry (LC/MS; SFC/MS; CZE/MS; MS/MS).** Oct. 31–Nov. 2. Montreux, Switzerland. *Contact: M. Frei-Häusler, Postfach 46, CH-4123 Allschwil 2, Switzerland*

Short Courses and Workshops

For information on the following courses, contact University of North Carolina, OSHERC, 109 Conner Dr., Suite 1101, Chapel Hill, NC 27514 (919-962-2101)

■ **Sampling and Evaluating Airborne Asbestos Dust.** Jan. 22–26, Feb. 12–16, March 19–23, April 16–20, and June 25–29. Chapel Hill, NC

■ **Asbestos Identification by Polarized Light Microscopy.** Jan. 29–Feb. 2 and March 26–30. Chapel Hill, NC

■ **10th Annual Occupational Safety and Health Winter Institute.** Feb. 12–16. St. Petersburg, FL

For information on the following courses, contact Barbara Nowicki, Professional Analytical and Consulting Services, 409 Meade Dr., Coraopolis, PA 15108 (412-262-4222)

■ **Courses on Basics of Gas Chromatography and Thin-Layer Chromatography.** Jan. 22–25. Pittsburgh, PA

■ **Courses on Quality Assurance of Chemical Measurements and Quality Assurance of Environmental Measurements.** Jan. 29–31. Pittsburgh, PA

■ **Courses on Spectroscopy Data Interpretation: Mass, Infrared, Near-Infrared, NMR, and 2D NMR.** Feb. 21–25. Pittsburgh, PA

These events are newly listed in the JOURNAL. See back issues for other events of interest.

■ **Course on Sampling and Evaluating Airborne Asbestos Dust.** Feb. 5–9. Los Angeles, CA. *Contact: University of Southern California, Institute of Safety and Systems Management, Professional Programs, 3500 South Figueroa St., Suite 202, Los Angeles, CA 90007 (213-743-6523)*

■ **Bioseparations: Scale-Up and Design Workshop.** Feb. 27–March 2 and June 5–8. University Park, PA. *Contact: Jim Shillenn, 519 Wartik Laboratory, Pennsylvania State University, University Park, PA 16802 (800-833-5533)*

■ **Quality in the Test Laboratory.** March 13–14 and June 5–6. Warren, MI. *Contact: Macomb Community College, Advanced Center for Manufacturing Technology, 14500 Twelve Mile Rd., Warren, MI 48093 (313-445-7880)*

Call for Papers

■ **18th International Symposium on Chromatography.** Amsterdam, The Netherlands. Sept. 23–28. The symposium will cover fundamental aspects, instrumentation, new developments, and applications of chromatographic and related techniques, including LC, SFC, capillary GC, planar chromatography, field-flow fractionation, and capillary zone electrophoresis. Authors wishing to contribute oral or poster presentations should submit 400-word abstracts by Jan. 10 to Secretariat 18th ISC, RAI Organisatie Bureau Amsterdam bv, Europaplein 12, 1078 GZ Amsterdam, The Netherlands. Instructions for preparing abstracts are available from the symposium Secretariat.

■ **3rd International Meeting on Chemical Sensors.** Cleveland, OH. Sept. 24–26. The meeting will feature invited lectures and contributed paper and poster presentations dealing with chemical sensor and biosensor research and development, including sensing principles, fabrication techniques, materials, and applications. Areas of interest include electrochemical, optical, chemical, and piezoelectric sensors; enzyme sensors and immunosensors; ISFETs and CHEMFETs; biocompatibility; in vivo sensors; immobilization and fixation of biomolecules for sensor applications; and interfacial phenomena of biomolecules and biosensor elements. Prospective authors should request appropriate forms from Wen H. Ko or Chung-Chiun Liu, Electronics Design Center, Case Western Reserve University, Cleveland, OH 44106 (216-368-2934). Deadline for submission of abstracts is Jan. 31.

World Class Opportunities.

ARAMCO, the free world's largest producer and exporter of oil and gas, has the following opportunities available in Saudi Arabia.

STABLE ISOTOPE CHEMIST

Will serve as the stable Isotope Specialist with the company and will be responsible for setting up/operating/training personnel on a new stable isotope ratio mass spectrometer. Will consult with exploration geologists and provide appropriate data interpretation. BS in Chemistry, Advanced degrees preferred, with 15 years' of experience and 5 years' in stable isotope technology essential.

ELECTROCHEMISTRY CORROSION CHEMIST

Will be responsible for developing/maintaining state-of-theart electrochemical procedures and instrumentation utilized to evaluate oil field chemicals and corrosion mitigation programs. BS in Chemistry, with 8 years' experience in oil field electrochemistry and corrosion. PhD preferred, in Corrosion Electrochemistry. Additional experience will include A.C. impedance spectroscopy systems, potentiodyne, and computer controlled field potentiostats, microcomputers, high pressure compressors, and high pressure autoclaves.

ANALYTICAL INSTRUMENTATION CHEMIST

Will provide technical consulting services to refineries, gas/oil separation plants, and wet crude handling facilities in order to resolve field operational problems. BS in Chemistry advanced degrees preferred, with 10 years' experience in petroleum industry and knowledge in process chemistry essential. Additional working experience will include Perkin Elmer GC/FT-IR; fluorescence spectrometer; JEOL DX-300 gas chromatograph/mass spectrometer; Finnigan Incos 50 gas chromatograph/mass spectrometer; Phillips x-ray powder diffractometer; JEOL scanning electron microscope; Kevex energy dispersive x-ray fluorescence spectometer; and Varian HPLC.

Employment with ARAMCO will provide you with an interesting lifestyle in a multicultural environment, including comfortable family living arrangements, free medical care while in Saudi Arabia, fine schools and a broad spectrum of recreational opportunities, plus 36 calendar days of vacation annually, allowing for extensive travel. We provide an attractive compensation package which includes an expatriate premium.

For immediate consideration, please send your resume/salary history to: **ASC, Employment Dept. 06E-036-9, P.O. Box 4530, Houston, Texas 77210-4530.**

ARAMCO

BOOKS

Laser Microanalysis, On-Line Process Analyzers, and Electrophoresis

Laser Micro Analysis. Lieselotte Moenke-Blackenburg. xvi + 288 pp. John Wiley & Sons, 605 Third Ave., New York, NY 10158. 1989. $70

Reviewed by Carmen W. Huie, Department of Chemistry, State University of New York, Binghamton, NY 13901

The ability of focused laser radiation to vaporize, dissociate, excite, or ionize microquantities of matter from solid surfaces has provided the analytical chemist with a versatile method of direct chemical analysis of virtually any solid sample using either optical or mass spectrometry. Furthermore, the ability of the laser beam to be focused down to diffraction-limited spot size allows it to probe microscopic regions of the solid samples. Appropriately, the title of this book, *Laser Micro Analysis*, expresses some of the unique capabilities of this powerful analytical tool.

This book can be divided essentially into two parts. Part I deals with various fundamental aspects of laser–surface interaction and points out the major problem facing laser microanalysis, which is the lack of reproducibility in the generation of neutrals and ions from the surface. Chapters 2–4 help the reader to appreciate that laser–surface interaction and the dynamics of the laser-generated microplasma are extremely complex. By understanding these fundamental processes, a higher degree of precision and accuracy may be obtained by optimizing various laser parameters, using additional excitation sources, and ensuring proper preparation and statistical testing of sample homogeneity.

Part II is devoted to the discussion of instrumentation and application of laser microanalysis. Chapter 5 gives a comprehensive overview of laser microprobe–optical emission spectrometry, some of which is based on the author's own expertise in this area of research. Chapter 9 discusses another major topic that involves the combination of the laser microprobe and mass spectrometry (LM-MS); of particular importance is the demonstration of the potential use of LM-MS for ultratrace and microtrace analysis of specific isotopes and the speciation information provided about elements present in complex and highly heterogeneous samples. A total of 448 references are presented in these two chapters. Chapters 6 and 10 discuss the instrumentation and applications of combining the laser microprobe with inductively coupled plasma (ICP), microwave-induced plasma, direct-current plasma, and ICP-MS. These new techniques hold good promise for providing lower detection limits, wider linear dynamic range, and relative freedom from matrix effects. Chapters 7 and 8 briefly discuss the advantages and disadvantages of coupling the laser microprobe with absorption and fluorescence spectrometry, and Chapter 11 compares the analytical performances of laser microprobe techniques with various other methods of surface analysis.

> **“. . . a good introduction to the fundamentals . . . with an emphasis on the analytical applications . . . ”**

In summary, this book provides a good introduction to the fundamentals of laser–surface interactions with an emphasis on the analytical applications of the laser-generated microplasma, and it gives an excellent review of both conventional and state-of-the-art laser microprobe techniques. In particular, I can recommend this book highly to researchers who are interested in or are presently using the laser microprobe with optical emission and/or mass spectrometry for direct solid analysis. Chapters 5 and 9 provide an excellent source of references for a large number of applications. One minor criticism is that some applications presented in the various tables are not listed in the index section, which makes it difficult to locate a specific application and the corresponding references from among a large number of examples that are not presented in a specific order in each table.

On-Line Process Analyzers. Gary Nichols. 300 pp. John Wiley & Sons, 605 Third Ave., New York, NY 10158. 1988. $55

Reviewed by Robert E. Synovec, Center for Process Analytical Chemistry, Dept. of Chemistry, BG-10, University of Washington, Seattle, WA 98195

The book introduces readers to on-line process analysis by focusing primarily on existing analyzer or sensor technology. The book contains 12 well-organized chapters comprising four distinct sections: fundamental instrumentation methods, derived instrumental methods, sample systems, and process analyzer project management. The author intended to have the text integrate the multidisciplinary field of on-line process analysis into an easy-to-read introduction for anyone with a college education in the physical sciences. Toward this goal, the author has succeeded. This review will briefly describe my opinion of the scope of the book, point out certain deficiencies, and highlight the primary merits.

The author's 10 years of industrial experience have led to a coherent text that should be an excellent starting point for a scientist or technician who is interested in developing or learning about process analyzers. Nichols clearly points out that the pivotal point of on-line process analysis is the field of analytical chemistry, where the fundamental concepts and issues of on-line analysis are addressed. Unfortunately, the text is limited in that the past is focused upon, and state-of-the-art and future directions are not indicated. This deficiency is also indicated indirectly by the limited integration of pertinent references. Essentially, the numerous examples are found in commercially available instrumentation. Thus, the field of on-line process analysis is described according to what exists, with limited discussion of new concepts, new directions, or shortcomings in the current technology.

The author's discussion of existing analyzers borrows heavily from standard instrumental analysis textbooks. An example of an obvious limitation is the omission of the role and integration of fiber-optic technology into on-line process analyzers. Another disappointment is the lack of an example of an operating process analyzer with the subsequent data printout, which a process analyst would read and interpret. Essentially, the book contains only verbal discourses of various applications without any discussion of the actual data obtained by a process analyzer and how the data differ from a lab-top experiment. This would have been particularly useful for the process gas chromatography chapter, for example.

The author's experience does lead to many useful caveats concerning on-line process analyzer technology, in particular the emphasis on pinpointing process-induced effects that will limit a given application. The discussion of sample systems was quite interesting and points toward one of the major problems in implementing a process analyzer. The various examples of process analyzers and process analysis issues are integrated with fundamental principles, at least as a starting point, for a reader to begin to learn about the subject. Although much of the discussion of fundamental principles is available in more detail in other textbooks, the material is helpful in putting the process analyzer technology into proper context.

Advances in Electrophoresis, Vol. 2. A. Chrambach, M. J. Dunn, B. J. Radola, Eds. ix + 456 pp. VCH Publishers, Suite 909, 220 East 23rd St., New York, NY 10010-4606. 1989. $115

Reviewed by Robert Allen, Department of Pathology, Medical University of South Carolina, 171 Ashley Ave., Charleston, SC 29425-2645

This series would be better titled as a Review than as Advances in Electrophoresis. With the exception of Chapter 1 and parts of Chapters 4, 5, and 6 on methodological progress, one of the stated aims of the editors is not well achieved.

It would have been timely to have included a chapter on DNA electrophoretic methodology for the molecular biologist rather than to devote the entire volume to protein separation and more than one-half of the book to two-dimensional techniques.

Chapter 1 deals with the use of immobilized pH gradients in electrofocusing and covers development in the field from its initiation to the present. The authors have done an admirable job of assembling methodological hints along with theoretical aspects in a manner useful to all biologists interested in this type of separation.

Chapter 2 is concerned with the theory of electrophoretic transport and covers all aspects of electrophoresis. However, it fails to mention effects such as the increased conductance found in gels cast with ampholytes as opposed to those prepared from "empty" rehydratable gels. The review is comprehensive and well written, and it will help those entering the field to understand much of the underlying theory of electrophoresis.

The chapter on evaluation of mobility data has been extensively reviewed from the author's laboratory over the past 15 years. Unfortunately, the author provides no specific examples of the practical application of the technique, nor does he discuss various buffer systems that may be used and differential unstacking effects. He also neglects to mention that persulfate polymerization in the presence of weak base buffers can lead to formation of a discontinuous zone system. The statement of 800 base pair DNA size limitation for separation is an error by almost an order of magnitude, based on recent reports.

Chapter 4, on cultivars, is more suited to a text on quality control in horticulture. It appears that every published electrophoretic method has been reviewed, yet there is no attempt to indicate a unified approach or the problems involved in extraction of storage or other plant proteins. The suggestion of ultra-thin-layer isoelectric focusing in the future neglects the fact that this method was first described by Görg in 1979 and has been extensively used over the last 10 years. Similarly, densitometry—with the resolution and sensitivity the author suggests are required—has been available for 20 years, and programs for computerized output for at least five to seven years. The article is an excellent review

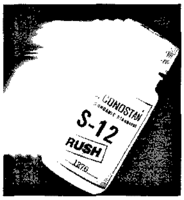

OUR STANDARD DELIVERY IS ANYTHING BUT STANDARD.

Conostan oil-based calibration standards are just a telephone call away. Standard orders are filled the day they are received, and are on the way to you within 24 hours. Orders for custom blends usually take only a day longer. Conostan orders are shipped UPS, air express, or as you designate. For service that's anything but standard, call or write for our free brochure describing the full line of single and multi-element Conostan standards for the analysis of metals in oils.

Standards to Burn
CONOSTAN®

Conostan Division
Conoco Specialty Products Inc.
P.O. Box 1267
Ponca City, OK
Phone: (405) 767-3078
Fax: (405) 767-5843

CIRCLE 28 ON READER SERVICE CARD

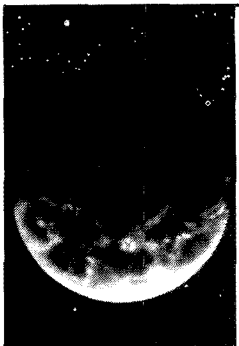

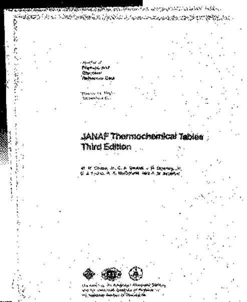

JANAF Thermochemical Tables
Third Edition

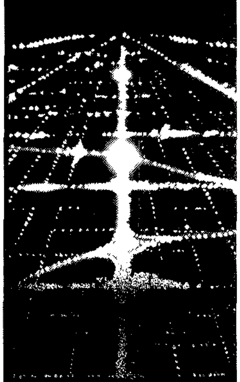

JANAF THERMOCHEMICAL TABLES

Third Edition

A Major Supplement from JOURNAL OF PHYSICAL AND CHEMICAL REFERENCE DATA

Presenting Reliable Data Utilized by Chemists, Chemical Engineers, and Materials Scientists from Around the World for Over 25 Years

JOURNAL OF PHYSICAL AND CHEMICAL REFERENCE DATA is very pleased to publish the Third Edition of the JANAF THERMOCHEMICAL TABLES.

Since the first version appeared 25 years ago, the JANAF THERMOCHEMICAL TABLES have been among the most widely used data tables in science and engineering. You'll find:

- Reliable tables of thermodynamic properties of substances of wide interest
- A highly professional approach with critical evaluations of the world's thermochemical and spectroscopic literature
- A concise and easy-to-use format

This Third Edition presents an extensive set of tables including thermodynamic properties of more than 1800 substances, expressed in SI units. The notation has been made consistent with current international recommendations.

There is no other reference source of thermodynamic data that satisfies the needs of such a broad base of users.

Order your 2-volume set of the JANAF THERMOCHEMICAL TABLES today! You'll get over 1890 pages of valuable information that is crucial to your research—in two hardback volumes.

Editors:
M.W. Chase, Jr.
National Institute of Standards and Technology
C.A. Davies
Dow Chemical U.S.A.
J.R. Downey, Jr.
Dow Chemical U.S.A.
D.J. Frurip
Dow Chemical U.S.A.
R.A. McDonald
Dow Chemical U.S.A.
A.N. Syverud
Dow Chemical U.S.A.

SUBSCRIPTION INFORMATION

The JANAF THERMOCHEMICAL TABLES, THIRD EDITION is a two-volume supplement of *Journal of Physical and Chemical Reference Data.*

1896 pages, 2 volumes, hardcover
ISBN 0-88318-473-7
Supplement Number 1 to Volume 14, 1985

U.S. & Canada	$130.00
All Other Countries	$156.00
(Postage included.)	

All orders for supplements must be prepaid.

Foreign payment must be made in U.S. currency by international money order, UNESCO coupons, U.S. bank draft, or order through your subscription agency. For rates in Japan, contact Maruzen Co., Ltd. Please allow four to six weeks for your copy to be mailed.

For more information, write **American Chemical Society**, Marketing Communications Department, 1155 Sixteenth Street, NW, Washington, DC 20036.

In a hurry? Call TOLL FREE 800-227-5558 and charge your order!

Published by the **American Chemical Society** and the **American Institute of Physics** for the **National Institute of Standards and Technology**

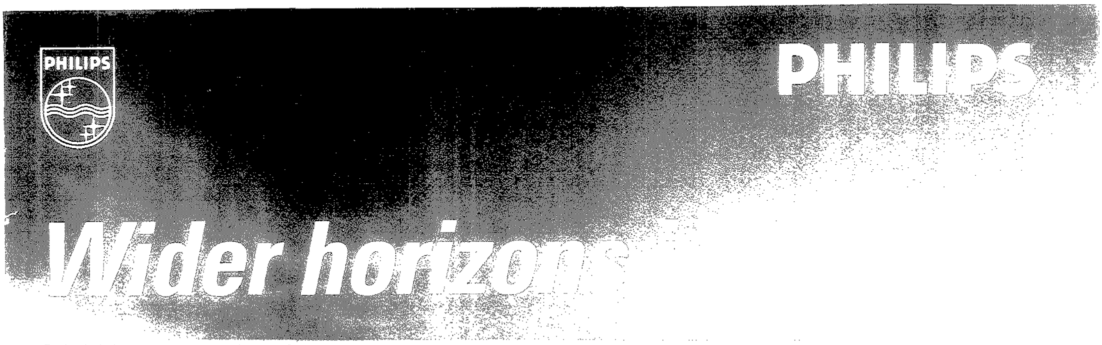

Philips Analytical

Philips Analytical offers a choice of UV/VIS instrumentation which can widen your analytical horizons.

With a wider range of UV instruments than ever before, we can offer a solution tailored to your problem:

- Choose control via keyboard or mouse
- Choose on-board or external processing
- Choose colour or monochrome graphics and hard copy
- Choose data formats including ASCII, SpectraCalc™ and Lotus 1 2 3™

Meet your requirements with a wider choice of accessories and software that includes Multicomponent, Kinetics and Quant.

With Philips UV, a solution to your problem is within your horizon.

SpectraCalc is a registered trademark of Galactic Industries. Lotus 1 2 3 is a registered trademark of Lotus Development Corporation

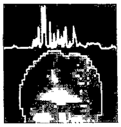

***PHILIPS ANALYTICAL** - BIGGER IDEAS FOR BETTER ANALYSIS*

For more information contact:

*Philips Scientific Analytical Division York Street, Cambridge Great Britain CB1 2PX Tel: 0223 358866 Telex: 817331 Fax: 0223 312764 or telephone direct **Austria:** (0222) 60101 – 1792 **Belgium:** (02) 525 62 75 **Denmark:** (01) 57 22 22 **Finland:** (09) 502 63 56 **France:** (1) 49 42 81 62 **Germany:** (0561) 501 384 **Italy:** (02) 64 49 12 **Netherlands:** (040) 783 901 **Norway:** (02) 68 02 00 **Spain:** (1) 404 22 00 **Sweden:** (08) 782 1591 **Switzerland:** (01) 488 22 11. **All other countries:** 44-223-358866.*

UV27a

CIRCLE 125 ON READER SERVICE CARD

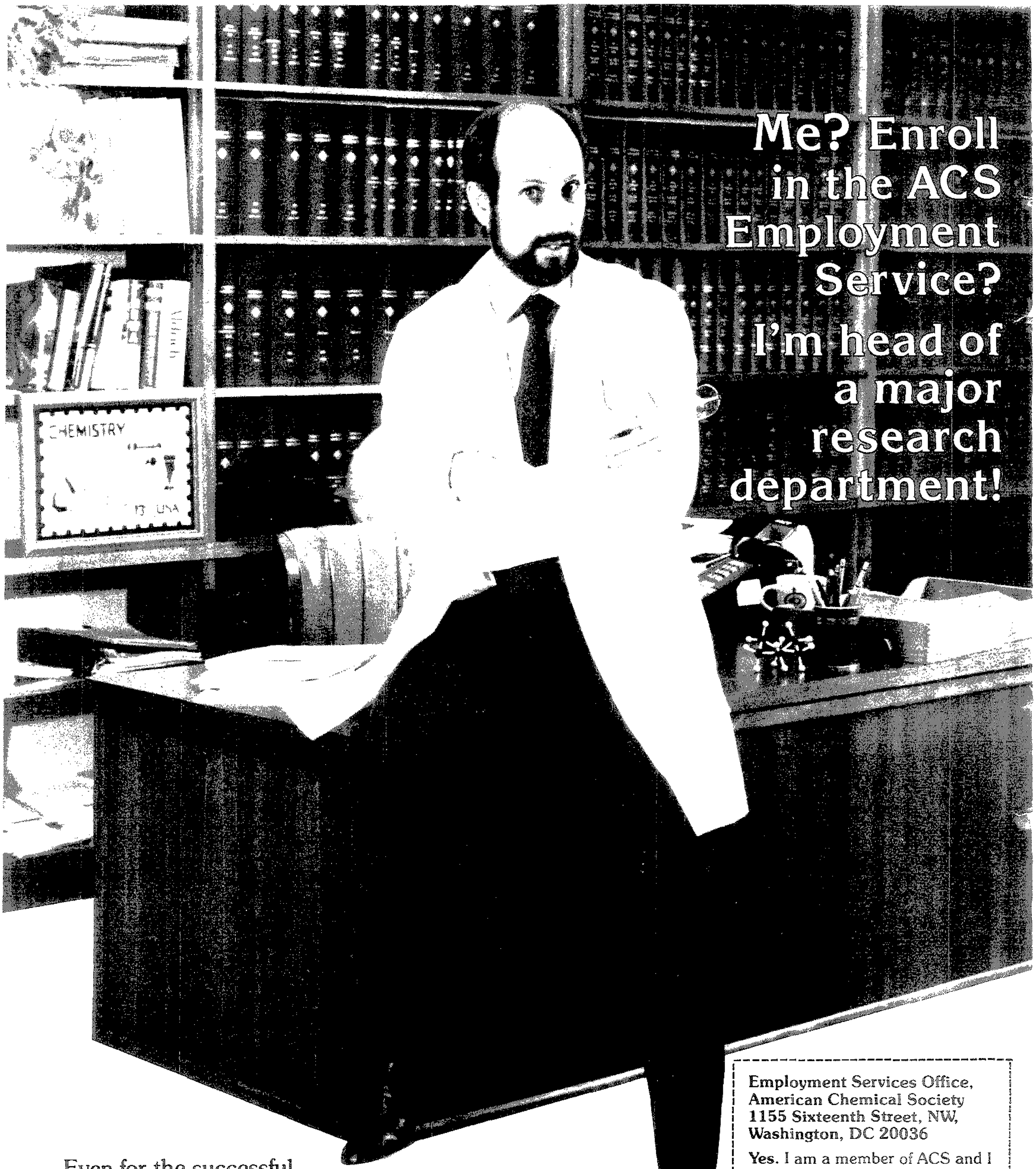
Me? Enroll in the ACS Employment Service?
I'm head of a major research department!
CHEMISTRY
USA

Even for the successful chemist or scientist in an allied field, sometimes the best way to get ahead is to make a change.

The ACS Employment Service offers the opportunity to investigate the possibilities discreetly—and at very low cost.

Our Employment Service is free to all ACS members. If you request confidentiality from current employers or other designated organizations there is a nominal charge.

For more information write, use coupon, or **CALL TOLL FREE 800-227-5558**

Employment Services Office,
American Chemical Society
1155 Sixteenth Street, NW,
Washington, DC 20036

Yes. I am a member of ACS and I would like to learn how the ACS Employment Service can help me advance my career.

Name (please print)

Membership #

Address

City

State ZIP

of the field and is otherwise informative.

Chapters 5 and 6 are both excellent reviews on the use of two-dimensional electrophoresis for the separation of plant proteins and in protein analysis in cancer research. Both of these reviews are comprehensive and provide methodological considerations of the techniques as they are best practiced in the laboratory.

Chapter 7 on the two-dimensional electrophoresis of nonhistone chromosomal proteins deals with a less familiar subject in general electrophoretic literature, but less than 5% of the work consists of literature published in the last two years. The chapter gives a good overview of fractionation procedures and provides the reader with a broad base of information.

This book will be of interest to both theoreticians and practitioners of single and multidimensional electrophoresis in the fields of protein separation.

Books Received

Trends in Analytical Chemistry, Vol. 7: Reference Edition. 402 pp. Elsevier Science Publishers, P.O. Box 882, Madison Square Station, New York, NY 10159. 1988. $200

This reference volume is a compilation of the material published in the regular monthly edition. Features, news, trends, computer articles, and others are listed by month. A subject and author index is provided, as well as a list of meetings, books, and software reviewed.

Computational Methods in the Chemical Sciences. A. F. Carley and P. H. Morgan. 337 pp. John Wiley & Sons, 605 Third Ave., New York, NY 10158. 1989. $115

This volume is part of the *Ellis Horwood Series in Chemical Information Science.* The chapters are entitled "Some Fundamental Concepts and Basic Methods," "Interpolation, Numerical Integration and Differentiation," "Solving Differential Equations," "Fitting Straight Lines and Polynomials to Experimental Data," "Optimization Methods," and "Non-Linear Least Squares Minimization." Each chapter contains several programs. The references are from the 1970s and 1980s up to 1989. An index and a program index are provided.

Spin Labeling: Theory and Applications. Lawrence J. Berliner and Jacques Reuben, Eds. xix + 650 pp. Plenum Publishers, 233 Spring St., New York, NY 10013. 1989. $95

This is volume 8 in the series *Biological Magnetic Resonance.* Chapter titles include "Inhomogenously Broadened Spin-Label Spectra," "Nitrogen-15 and Deuterium Substituted Spin Labels for Studies of Very Slow Rotational Motion," "Electron-Electron Double Resonance," "Spin-Label Oximetry," and "Magnetic Resonance Study of the Combining Site Structure of a Monoclonal Anti-Spin-Label Antibody." References are from the 1970s and 1980s through 1987. An index and a listing of the contents of other volumes are also included.

Infrared Microspectroscopy: Theory and Applications. Robert G. Messerschmidt and Matthew A. Harthcock, Eds. xv + 282 pp. Marcel Dekker, Inc., 270 Madison Ave., New York, NY 10016. 1988. $85

This is volume 6 in the series *Practical Spectroscopy.* The topics covered in the 18 chapters include imaging capabilities, polymers, polarized infrared microscopy, semiconductors, pharmaceuticals, and reflectance studies. Most of the references are from the 1980s up to 1987. An index is included.

X-ray Fluorescence Spectrometry. Ron Jenkins. x + 169 pp. John Wiley & Sons, 605 Third Ave., New York, NY 10158. 1988. $60

This is volume 99 in the series *Chemical Analysis: A Series of Monographs on Analytical Chemistry and Its Applications.* The topics covered include industrial applications, diffraction, instrumentation, sample preparation, and recent trends. The chapters average 15 pages in length. The references date to 1987, and an index is included.

An Introduction to Applications of Light Microscopy in Analysis. Diana Simpson and W. Gordon Simpson. x + 215 pp. Royal Society of Chemistry, Distribution Center, Blackhorse Rd., Letchworth, Herts SG6 1HN, England. 1988. $63

This book contains an introductory chapter, 13 applications chapters, and a concluding chapter. The applications chapters average 12 pages in length and cover such topics as mineralogy, alloys, plastics, materials, biologicals, water quality, foods, and forensics. Tables, illustrations, a bibliography, and an index are also included.

IF YOU CAN'T LIVE WITH
OUR STANDARDS,
WE'LL CHANGE THEM.

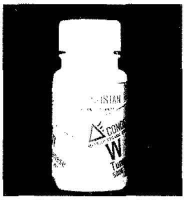

If your spectrometric analysis of metals in oils requires a blend of elements we don't routinely offer—we'll custom blend it for you. Conostan custom blending allows you to test for unusual combinations and concentrations of elements with minimal interference and repeatable results. For a complete list of Conostan single and multi-element standards, write or call for our free brochure. If you don't find what you need, we'll blend something special just for you.

Standards to Burn ®
CONOSTAN

Conostan Division
Conoco Specialty Products Inc
P.O. Box 1267
Ponca City, OK 74603
Phone: (405) 767-3078
Fax: (405) 767-5843

CIRCLE 29 ON READER SERVICE CARD

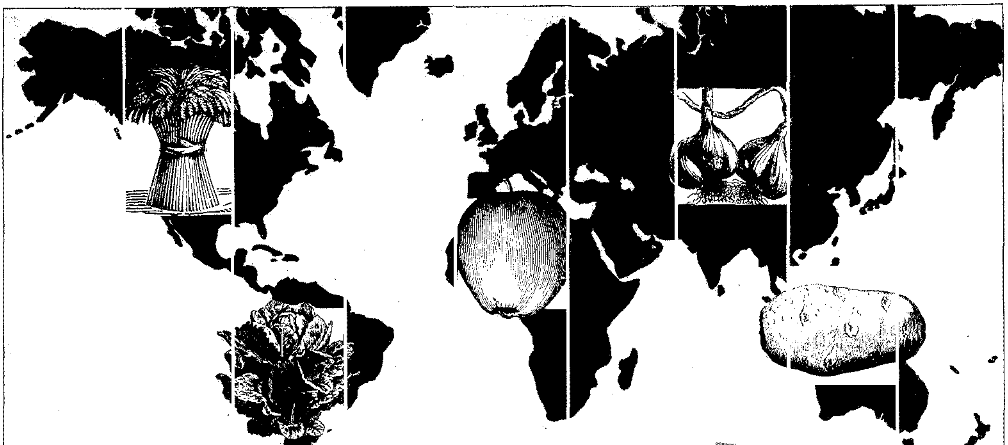

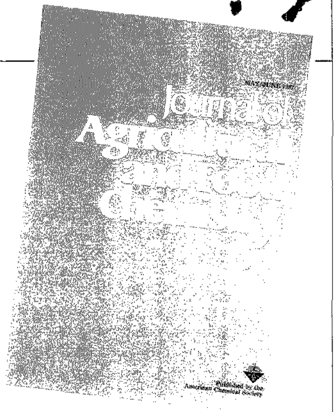
Journal of Agricultural and Food Chemistry
Published by the American Chemical Society

For the Most Current International Research in the Field . . .

Journal of Agricultural and Food Chemistry

Editor	Associate Editors	
Irvin E. Liener	G. Wayne Ivie	Marshall Phillips
Univ. of Minnesota	*U.S. Dept. of Agriculture*	*U.S. Dept. of Agriculture*

The bimonthly journal in the chemical disciplines targeted toward more efficient and economical production and greater safety of foods, feeds, fibers, and other agricultural products.

Designed to Meet Researchers' Needs . . .

The JOURNAL OF AGRICULTURAL AND FOOD CHEMISTRY keeps you up-to-date with timely, original research. You'll find reports on the chemical, biochemical, and nutritional aspects of foods and feedstuffs. More than 350 articles are published yearly on a broad range of topics such as:

☐ Woods
☐ Pesticides/Residues
☐ Fertilizers
☐ Flavor and Aroma
☐ Analytical Chemistry
☐ Pesticides/Metabolism
☐ Pesticides/Field Applications
☐ Biotechnology
☐ Toxicants
☐ Plant Nutrients and Regulators
☐ Food and Feed Processing
☐ Agricultural Products
☐ Compounds Isolated from Food Material
☐ And much more!

Subscribe to the JOURNAL OF AGRICULTURAL AND FOOD CHEMISTRY today! Join the thousands of your colleagues worldwide—who already depend on each bimonthly issue for the kind of research they can use in their day-to-day work.

JOURNAL OF AGRICULTURAL AND FOOD CHEMISTRY
Published Bimonthly. One volume per year.
Volume 37 (1989) ISSN 0021-8561

One Year Rate		U.S.	Canada and Mexico	Europe**	All Other Countries**
ACS Members*	1 year	☐ $ 25	☐ $ 33	☐ $ 45	☐ $ 49
Save 10%	2 years	☐ $ 45	☐ $ 61	☐ $ 85	☐ $ 93
Nonmembers		☐ $138	☐ $146	☐ $158	☐ $162

*Personal use only **Air service included. For nonmember rates in Japan, contact Maruzen Co., Ltd.

Editorial Advisory Board
Terry E. Acree, *Cornell Univ.*
John W. Finley, *Nabisco Brands*
Robert A. Flath, *U.S. Dept. of Agriculture*
Glenn Fuller, *U.S. Dept. of Agriculture*
R. Greenhalgh, *Chemistry and Biology Reseach Inst., Canada*
Julius J. Menn, *U.S. Dept. of Agriculture*
Steven Nagy, *Florida Dept. of Citrus*
Louis Rockland, *Chapman Center*
Gerald G. Still, *U.S. Dept. of Agriculture*
Eugene G. Teach, *ICI Americas*
Joseph Warthesen, *Univ. of Minnesota*
Willis B. Wheeler, *Univ. of Florida*

In a hurry?
Call Toll Free (800) 227-5558
and Charge Your Order! (U.S. Only)
Outside U.S. 202/872-4363
Telex: 440159 ACSP UI
89 2582 ACSPUBS
FAX: 202/872-4615

Or write:
American Chemical Society
Marketing Communications Department
1155 Sixteenth Street, NW
Washington, DC 20036 U.S.A.

Available on microfilm, microfiche, and electronically through CHEMICAL JOURNALS ONLINE on STN International.

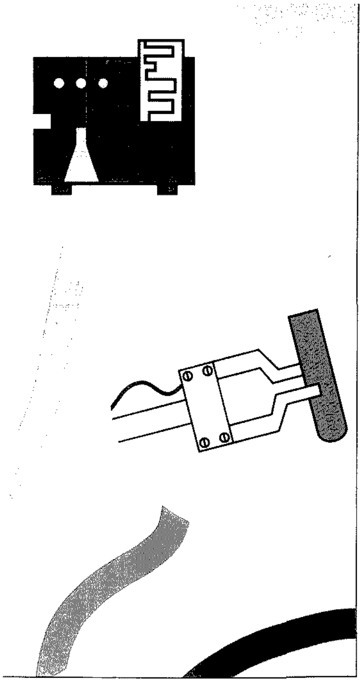

CONSORTIUM ON AUTOMATED ANALYTICAL LABORATORY SYSTEMS

H. M. (Skip) Kingston
Inorganic Analytical Research Division
Center for Analytical Chemistry
National Institute of Standards and
Technology
Gaithersburg, MD 20899

Industry and government both depend heavily on analytical laboratory measurements. Although these measurements provide critical feedback in many situations, such as product quality assurance, acceptance testing, and regulatory compliance, they are generally viewed with mixed feelings. On the positive side, industry recognizes that improvements in product and process capability often depend on advancements in analytical measurement technologies. A firm's competitiveness depends in part on the accuracy, sensitivity, reliability, and controllability of its measurements and processes. The precision and control are reflected in the quality and cost of the firm's products. On the negative side, analytical measurements are expensive because they are labor intensive, requiring high-cost personnel and expensive equipment.

Scientists at the National Institute of Standards and Technology (NIST) project that during the next decade analytical measurement capabilities will experience technical growth equal to that of the previous three decades combined. Furthermore, NIST perceives that analytical measurement tasks are ripe for automation and that development of an automated analytical laboratory offers U.S. industry opportunities for significant improvements in the quality and cost of analytical operations. To accelerate development of these benefits and to provide a broad utilization base, NIST proposes the establishment of an industry–government research Consortium on Automated Analytical Laboratory Systems (CAALS). The purpose of the consortium is to accelerate the advancement of automated analytical systems, to improve efficiency and data quality, and to promote transferability of analytical methods so that U.S.-based industry enjoys a competitive advantage in chemical measurement technology.

FOCUS

It has taken approximately nine months to form the consortium with the assistance of many industry leaders who have had significant input into the structure and proposed directions of CAALS. A committee composed of members from the Center for Analytical Chemistry and other related areas of NIST was established to guide the formation of the consortium.

Why a consortium?

Can't each firm solve these problems as it sees fit? In NIST's view, a consortium format seems best for several reasons.

- **Generic benefits.** The consortium solves a major problem for all participating firms. Variants of the same solutions need not be reinvented separately by each company via in-house programs. Needless duplication of research is avoided.
- **Standardized common interfaces.** Solutions once developed for many are more likely to be adopted as a standard for all. These solutions can provide design standards for instrument and software developers. Through technology, software, and other technical solutions, the consortium may be better able to develop common bases for instrument and software development. This standardization will help users, because they will find their equipment more compatible.
- **Affordability.** Several large U.S. and international organizations such as NIST have recognized the impact of automated analytical measurement systems on their competitiveness and have implemented internal programs to automate portions of their activities. However, most firms cannot afford to

This article not subject to U.S. Copyright
Published 1989 American Chemical Society

PURPOSE

To accelerate the advancement of automated analytical systems to improve efficiency and data quality and to promote transferability of analytical methods so that U.S.-based industry enjoys a competitive advantage in chemical measurement technology

implement such extensive in-house programs. A consortium allows small and mid-sized businesses to become involved in chemical automation research and to enjoy the benefits of a research program of this scope at modest cost. Participants from large firms benefit by leaving the generic projects to the consortium's program and by using in-house talents to pursue projects of interest to the company.

- **Broader talent pool.** The consortium will draw its talent from member companies nationwide, from other interested government agencies, and from NIST (which has the greatest diversity of analytical chemists in the world). Only qualified top talent will be encouraged (or accepted) to be part of the consortium's project teams. In addition, the consortium will develop a pool of qualified graduate students who can fill voids in employment needs in this topic area. The result will be a group of individuals whose talents offer more diversity than could be assembled by a single firm.
- **Greater product breadth.** The consortium will pursue automation technologies in many different areas of chemical analysis with the goal of developing automated laboratory systems. Through the consortium, it will be possible to pursue more projects simultaneously than could be pursued through the efforts of a single corporation.
- **Relevant participants.** The consortium format is conducive to involving diverse but relevant perspectives of various groups with vested interests in the consortium's research. These groups include users, instrumentation and software developers, regulatory agencies, and professional standard-setting organizations.

Consortium philosophy

The basic philosophy of this consortium is one of flexibility and shared decision making to evolve guidelines and functions through which the industrial community and NIST work as partners to develop automated chemical analysis technologies. NIST believes that "working shoulder to shoulder" enriches everyone involved in the research effort. Active industrial involvement focuses the research on industrial needs and accelerates the transfer of technology to member firms.

This philosophy of active involvement is reflected in the consortium design. The more a consortium member contributes to the active research of the consortium, the more benefits that member accrues. Members of the NIST consortium will share responsibility for setting the research agenda and research priorities; collaborating actively in the development of consortium technologies; sharing the intellectual property (publications and patents) developed by the consortium; and accessing and participating in research seminars, workshops, and training sessions on consortium activities and products.

The technical program

Technical guidelines have been developed to focus the efforts of the consortium. These guidelines define the scope of the consortium's research efforts within which specific projects will occur; the specifics of the research directions will be dependent on the desires of the consortium members.

By definition, an automated analytical laboratory system includes two main components: sample preparation, which is divided into analyte release and analyte separation components; and an analyte detection or identification and quantification component.

Analyte detection components have been successfully automated over the

CHEMICAL ANALYSIS SYSTEMS

ANALYTE RELEASE	ANALYTE SEPARATION	ANALYTE DETECTION
Microwave dissolution	Gas chromatography	ICP-OES elemental detection
Fusion	Liquid chromatography	Atomic absorption
Solvation	Matrix modification	ICP/MS elemental detection
Solvent extraction	Liquid–liquid extraction	Flame ionization detection
Supercritical fluid extraction		Spectroscopic detection
Solid-phase extraction		Mass spectrometry

years. Until recently, automation efforts neglected sample preparation, and errors in sample preparation were identified as a major cause of inaccurate chemical analysis. The CAALS research program will address all aspects of automating the chemical analysis system but will emphasize sample preparation. The technical program of the consortium will center on establishing definitive criteria for selecting chemical analysis components that are amenable to automation; optimizing the measurement quality of each chemical analysis system; and providing user-oriented computer programs for system selection, optimization, and control. Careful consideration will be given to the selection of the proper components for automation. Once promising components are selected, significant research and development effort will be expended to assure that they can be used effectively as components of an automated system. Examples of each of the three categories are shown in the box.

Once a set of components has been chosen, a substantial amount of additional research and development will be done to optimize the performance of each of the components with respect to the automation. In general, the concept of modular design in all aspects of the component and system operation will be followed. All hardware and software components will be modular. To the fullest extent possible, these components will be made interchangeable and compatible. The concept currently used in object programming will also be used in the hardware design to simplify the assembly of components into a system. Computer control will be implemented in a hierarchical mode in which the lowest set of software modules will interact with specific components while a higher set of computer software modules (system software) will interact with the lower set to monitor and control the overall operation of the automated chemical analysis system. Expert systems will be devised to assist the chemist in selecting the proper chemical analysis system, providing information for the implementation of recommended procedures, and evaluating analysis results.

The consortium will provide a useful service to its members by choosing practical, ubiquitous modular laboratory components for applications and testing of automated methodology. The first phase in the logical development of an automated chemical analysis system is to automate each of the selected components individually while keeping in mind the ultimate goal of a fully automated chemical analysis system. During this development, members of the consortium will be able to use the individual components in their laboratories well in advance of the complete systems. The components and systems will be replicated in the laboratories of members who wish to use the system. This phase could involve collaboration with the instrument manufacturers.

FOCUS AND OBJECTIVES

Develop and apply automated analytical techniques

Develop standard methods for automated laboratory systems, transferability, productivity

Train technical and professional staff

Build chemical analysis expertise into the operation of the laboratory system

Build quality assurance into the automated system

During the development of an analytical system, research efforts will also be directed toward advanced integration of automated systems. To accomplish this, researchers must adhere to the following guidelines.

- **Build chemical analysis expertise.** To provide a chemical analysis involving a specific material, set of analytes, and analysis error, it is necessary for any given analytical system to develop specific operational protocols. These protocols generate the data necessary to achieve intelligent instrument control. With the appropriate computer software, the system will be "smart" as well as automated. Expert systems and other forms of artificial intelligence will be used to play appropriate roles in guiding the various operations of the chemical analysis.
- **Develop standard reference methods.** These activities are necessary to replace common manual techniques, to establish their validity, and to aid in their implementation. Implementation of these automated standard methods will be accomplished with the active involvement of voluntary standards organizations, professional societies, and regulatory government agencies.
- **Build in quality assurance.** The automated analytical system will be developed so that it will monitor and adjust the procedural conditions to provide a controlled environment for high-quality chemical analysis. These methods can be used to ensure reproducibility and transferability of the results between laboratories.

CAALS workshop

On September 28, 1989, NIST held a workshop to describe CAALS to representatives of industry, government agencies, and universities. On the first day of the workshop, NIST scientists discussed areas of current expertise and described research programs that support automation efforts in inorganic, organic, gas, and particulate analysis in the Center for Analytical Chemistry. These areas include broad expertise in chemical analysis; access to experts in associated fields such as robotics, statistical engineering, and artificial intelligence; expertise in quality assurance, including the certification of reference materials; ongoing commitment to data analysis; and continuing interactions with regulatory government agencies and industry.

In addition, direct benefits to consortium members were described. These include the ability to leverage costly R&D to accelerate the development of automated systems, promote collaboration between analytical instrument users and their manufacturers, participate in any patent and copyrights generated within the consortium, and affect long-term savings by manifesting the concept of standard interfaces, modular design, and versatility in design of the fundamental building blocks of an automated chemical analysis system. Although it will be the responsibility of the consortium members in collaboration with NIST staff to set the research agenda, NIST scientists presented their concept of the first automated system for inorganic trace element analysis consisting of microwave dissolution, liquid chromatographic separation, and ICP-optical emission detection.

On the second day of the workshop, after a review of the important discussions and conclusions from the previous day, the first organizational meeting of the consortium was held. Prospective members took part in a spirited two-hour discussion of the research agenda, and a number of suggestions were made relative to the organic automated system. An extraction procedure coupled to a chromatographic separation was suggested, and it was observed that an important aspect of these analyses is the minimization of toxic waste. It was also suggested that appropriate prototype projects relate to some EPA-mandated procedure. It was agreed that more input is needed to arrive at a demonstration project that best suits the needs of CAALS members, and suggestions were received from prospective members through November 1989.

The concept of modular design and interconnectivity of subcomponents was discussed. Standardization of interfaces was a high priority, and it was decided that the subcomponents should have "open architecture" to allow for expansion and interchangeability.

A timetable of events was then established for signing charter members so that the work of the consortium can proceed expeditiously. Charter memberships will be accepted through February 1, 1990.

The next meeting of CAALS members and prospective members will be held in March 1990 in conjunction with the Pittsburgh Conference in New York City. Potential CAALS members are invited to contact NIST for further information.

Other members of the CAALS Committee who contributed their unique expertise to the development of this consortium include Harry Hertz, Director, Center for Analytical Chemistry (CAC); Barry Diamondstone, Deputy Director, CAC; James R. DeVoe, Chief, Inorganic Analytical Research Division (IARD); W. E. May, Chief, Organic Analytical Research Division (OARD); Rance A. Velapoldi, Chief, Gas and Particulate Science Division; M. R. Rubin, General Counsel, NIST; W. F. Koch, Deputy Chief, IARD; Bruce Mattson, Manager, Technology Commercialization, Office of Research and Technology Applications, NIST; R. L. Watters, Jr., Supervisory Research Chemist, IARD; W. A. MacCrehan, Research Chemist, OARD; Neomy Soffer, Guest Scientist, CAC; R. M. Colton, Robert M. Colton Associates, Consultant; and R. D. Kilmer, Center for Manufacturing Engineering, NIST.

H. M. (Skip) Kingston is a supervisory research chemist and group leader in NIST's Inorganic Analytical Research Division. He received B.S. (1973) and M.S. (1975) degrees from Indiana University of Pennsylvania and a Ph.D. in analytical chemistry from American University (1978). His research interests include methods development for trace element analysis, microwave sample preparation, laboratory robotics, and nuclear waste stability.

Mark these dates
On your slate...

The Pittsburgh Conference
March 5-9, 1990

Jacob Javits Convention Center
New York, New York

Contact us at our new location:
THE PITTSBURGH CONFERENCE
300 Penn Center Boulevard, Suite 332, Pittsburgh, PA 15235 U.S.A.
1-800-825-3221, (412) 825-3220, FAX (412) 825-3224

CIRCLE 127 ON READER SERVICE CARD

Heinrich Emanuel Merck Award for Analytical Chemistry 1990

In 1988 E. Merck, Darmstadt, has granted the Heinrich Emanuel Merck award for the first time.
The award is endowed with DM 25,000 for the promotion of new developments in Analytical Chemistry, in particular for developing new methods in classical chemistry for sample preparation in trace analysis and their application in human environment.
The next award will be granted in the scope of the European Conference on Analytical Chemistry which will take place in Vienna, August 1990.

All young chemists up to the age of 45 are required to submit an original paper to the following address; deadline will be the end of January 1990.

Herrn Prof. Dr. Günther Tölg
Institut für Spektrochemie und
Angewandte Spektroskopie
Postfach 10 13 52
Bunsen-Kirchhoff-Str. 11
D-4600 Dortmund 1

The winner of this award will be chosen by an international jury of renowned analytical chemists.

If you need more information please contact Prof. Dr. G. Tölg.

E. Merck · Frankfurter Strasse 250 · D-6100 Darmstadt 1

CIRCLE 96 ON READER SERVICE CARD

NITROGEN AND SULFUR

[illegible] TWO RESULTS

Need Nitrogen and Sulfur on the same sample? Now you you can do it! Couple the Antek Pyro-fluorescent™ Sulfur Detector with our Antek Pyro-chemiluminescent™ Nitrogen System.

Autosamplers and data acquisition/ control systems are available for automated operation.

Chromatography detectors available:
Nitrogen Specific
Sulfur Specific

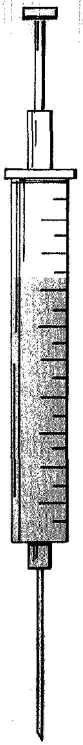

Features

- common pyroreactor for sample combustion and oxidation
- analyze gases, liquids or solids
- ppb to % range
- analysis time 30 seconds for gases and liquids. Up to 10 minutes for solids

Reduces the amount of sample prep required, the analysis time, and sample introduction by half. And, cut your instrument costs at the same time. Systems available for laboratory or process/online.

Applications

- petroleum liquids
- greases or residuals
- polymers
- biomedical samples
- coal
- foods
- engine exhaust
- water/waste water
- high purity gases (for semi-conductors, etc.)
- LPG or other hydrocarbon gases
- atmospheric gases

	Typical Results	
28.1ppm ±0.3	Water	148ppm±1
0.50ppm ±0.01	Naphtha	0.30ppm ±0.01
346ppm ±1.0	Diesel	48ppm±0.5
1.0ppm ±0.1	Butane	3.0ppm ±0.1
3.1ppm ±0.1	Propylene	1.8ppm ±0.1
0.9ppm ±0.1	Polyethylene	1.6ppm ±0.4
872ppm ±14	Coke	846ppm ±4
1.8ppm ±0.01	Fish Oil	4.1ppm ±0.4

For more information on your application or for a price quote, contact us in Houston or Dusseldorf.
In the USA, call toll free, (800) 365-2143

Patent Pending

ANTEK® INSTRUMENTS, INC.

Antek Instruments, Inc.
6005 North Freeway
Houston, Texas 77076-3998
Tel: 713/691-2265

TWX: 910-881-1792
Toll Free: 800/365-2143
FAX: 713-691-5606

Antek Instruments, GmbH
Wacholderstrasse 7
4000 Dusseldorf Angermund 31
Federal Republic of Germany

Tel: (0203) 74325/6
TLX: 8551136 ANDU D
FAX: (0203) 741545

CIRCLE 1 ON READER SERVICE CARD

NEW PRODUCTS

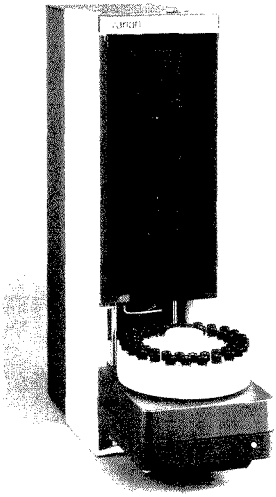

Model 8100 autosampler provides more than three 1-μL injections from 10 μL of sample. The unit does not require rinsing or priming the syringe with sample prior to injection. Varian Associates **401**

LC. Model 801 molecular size detector provides information on both the size and purity of macromolecules eluting from a chromatograph. The system uses photon correlation spectroscopy to produce a rapid readout of the diffusion coefficient, from which it calculates hydrodynamic radius and molecular weight. Oros Instruments 404

Titration. Metrohm Karl Fischer titrator Model 701, which determines the titer, drift, or sample water concentration in 30 s, features a buret resolution of 10,000 pulses and automatic drift compensation. All titration parameters can be selected via an RS 232C interface or alphanumeric display. Brinkmann Instruments 405

Concentrator. Model RC10.10 centrifugal vacuum concentrator is designed for preparation of samples prior to analysis by HPLC, TLC, GC/MS, electrophoresis, or other analytical techniques. A variety of rotors are capable of handling sample containers from 0.5 to 50 mL. Jouan 406

FT-IR. Galaxy 2020 system consists of a 2-cm^{-1}-resolution spectrometer, deuterated triglycine sulfate detector, system plotter, and IBM-compatible computer with high-resolution graphics. The software includes a 500-spectra library, interactive spectral subtraction, and a spectral math package. Mattson Instruments 407

Hydrogen. Model 8200 hydrogen generator is designed for use with gas chromatographs and sulfur monitors, and can be used for other laboratory applications requiring a source of pure hydrogen. The unit produces 99.992% pure hydrogen at a rate of 250 cc/min. Packard Instrument Co. 408

Drug abuse testing. AU5121 random access chemistry analyzer performs 16 separate analyses at a maximum throughput of 150 samples/h; AU5131 performs 12 analyses at a maximum throughput of 300 samples/h. Protocols for a variety of methods are available, including amphetamine, cocaine, methadone, opiate, phencyclidine, and barbiturates. Olympus Corp. 409

GC. P200 portable gas chromatograph system, which contains two gas chromatographs, a rechargeable carrier gas bottle, and battery pack, weighs 23 lbs. and measures 14.5 × 6 × 14 in. Each chromatograph is equipped with a thermal conductivity detector and sample injection system. Microsensor Technology 410

Carbon dioxide. Model ZFP-9 monitor determines CO_2 in ranges of 0 to 3000 ppm, 0 to 1%, 0 to 5%, and 0 to 10%. The unit, which contains a nondispersive IR detector, responds within 10 s to changing CO_2 concentrations. Automated Custom Systems 411

Photosynthesis. PNF-300 profiling natural fluorometer measures real-time underwater photosynthesis, temperature, and depth as well as surface irradiance. The system includes menu-driven software for data acquisition, display, and analysis. Biospherical Instruments 412

Software

IR/FT-IR. QuickSearch includes both spectral and chemical/physical property search features as well as a comprehensive 1125-compound spectral database with associated molecular structures. All library spectral and structural displays can be plotted. Sprouse Scientific Systems 414

Statistics. Goldspread Statistical is a Lotus-compatible software package that features spreadsheet, data management, graphics, and statistics capabilities. Up to six sets of data can be plotted simultaneously. Dynacomp 415

Manufacturers' Literature

Newsletter. *Pharmaceutical Notes*, Vol. 1, No. 1, contains information on dissolution testing and LC instrumentation. 8 pp. Waters Chromatography Division of Millipore 417

Electrochemistry. Bulletin discusses the LCEC Educational System, designed to introduce students to contemporary electrochemistry for LC detection. System components and the lab guide are described. EG&G Princeton Applied Research 418

Spectroscopy. Brochure describes cells for UV/vis/near-IR, fluorescence, and dye-laser spectroscopy. Information is provided on transmittance of cell materials, pathlength, and dimensions. Minarad Scientific 419

LC. Bibliography contains 280 references on HPLC of biomolecules using anion-exchange, cation-exchange, hydrophobic interaction, reversed-phase, and size-exclusion chromatography. SynChrom 420

For more information on listed items, circle the appropriate numbers on one of our Readers' Service Cards

Computer products. Brochure describes data acquisition hardware, software, and accessories for IBM PC-XT, PC-AT, PS/2, and Macintosh computers. Specifications are given on plug-in data acquisition boards for analog, digital, and timing input/output functions. National Instruments 421

Surface science. *Surface/Interface Bulletin*, which provides information on instruments and materials for surface and interface analysis, includes an article on adding Auger electron spectroscopy to SEMs. Surface/Interface 422

Catalogs

Chromatography. Catalog lists products for GC, HPLC, TLC, ion chromatography, biochromatography, and sample handling. A variety of chromatograms are included. Alltech 424

Software. Catalog features software for Macintosh computers, including packages for statistics, mathematics, modeling, and 3D graphics. Also described are color monitors and printers. D^2 Software 431

Evaporators. Catalog includes standard, digital, micro, and pilot plant rotary evaporators. An evaporator selection guide provides general information and highlights specific features for each of the products discussed. Buchler Instruments 426

Analytical standards. Catalog features kits that contain 14–15 individual standards within a chemical series. Alcohols, phenols, amines, hydrocarbons, ketones, aldehydes, and pesticides are included. 14 pp. PolyScience 430

Instrumentation. Catalog includes thermometers; pH, mV, temperature, and conductivity meters; water quality analyzers; electrodes; multimeters; recorders; and timers. Extech Instruments 428

Safety. Catalog features products for personal and respiratory protection, chemical storage, regulatory compliance, electrical safety, liquid/solid sampling, and asbestos control. 600 pp. Lab Safety Supply Co. 433

Immunology. Catalog lists more than 300 monoclonal and affinity-isolated polyclonal antibodies. Included are a variety of enzyme, fluorochrome, biotin, and agarose conjugates. Caltag Laboratories 429

Scientific products. Catalog includes balances, beakers, bottles, calculators, centrifuges, chromatography and electrophoresis supplies, containers, pipettors, racks, timers, and vials. PGC Scientifics 432

Laboratory equipment. Catalog lists mixers, stirrers, and heaters, including constant-run and touch-activated mixers, magnetic stirrers, hot plates, extraction heaters, and heating mantles. 16 pp. Lab-Line Instruments 425

Computer products. Catalog includes instrumentation; communication interfaces; software; and frame grabber, image processing, and computer vision products for IBM PC-XT, PC-AT, PS/2, and Apple Macintosh computers. 304 pp. MetraByte 427

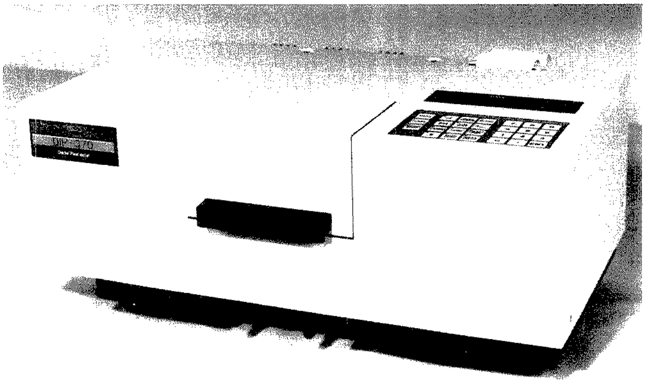

DIP-370 automatic digital polarimeter features microprocessor control, built-in printer, and multiwavelength capabilities. Optical rotations of 0.0005° can be measured. Jasco 402

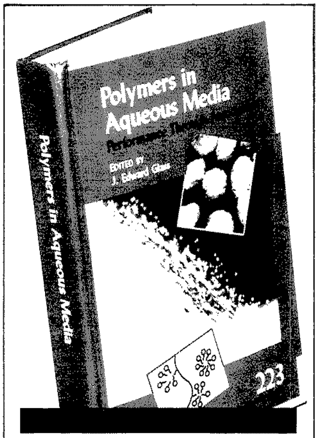
Polymers in Aqueous Media
Performance Through Association
EDITED BY J. Edward Glass
223

Polymers in Aqueous Media
Performance Through Association

This volume brings researchers up to date on a special class of polymers, those that are water soluble. Aqueous gels of varying chemical types are analyzed with respect to their properties in numerous applications. Polyelectrolyte synthesis and fundamental aspects of elongational viscosities are also discussed.

Individual chapters present discussions on topics as diverse as the structure, swelling, polarity effects, stability, and diffusion of synthetic and biopolymers; spectroscopic studies; and associative thickeners as models with commercial potential. The structures of these diverse gels are addressed through complex rheological analysis, light scattering, and novel NMR approaches.

Twenty-eight chapters are divided into six sections covering
- water-swellable polymers
- polarity effects and polymer stability
- spectroscopy
- model associative thickeners
- associative thickeners with commercial potential
- commercially related associative thickeners

This timely volume, written by leaders in the field, will be of interest to industrial and academic researchers in the area of water soluble polymers and aqueous gels.

J. Edward Glass, *Editor*, North Dakota State University
Developed from a symposium sponsored by the Division of Polymeric Materials: Science and Engineering of the American Chemical Society

Advances in Chemistry Series No. 223
361 pages (1989) Clothbound
ISBN 0-8412-1548-0 LC 89-15136
US & Canada **$99.95** Export **$119.95**

ORDER FROM

American Chemical Society
Distribution Office, Dept. 47
1155 Sixteenth St., N.W.
Washington, DC 20036
or CALL TOLL FREE

800-227-5558
(in Washington, D.C. 872-4363) and use your credit card!

Reaching Perfection in MS and SEM.
"A man's reach should exceed his grasp..."
Robert Browning

Galileo detectors for Mass Spectrometry and Electron Microscopy.

What silicon chips did for computers, Galileo high-performance detectors are doing for GC/MS, MS and SEM analysis.

Whether your projects involve environmental or pharmaceutical analysis, analysis of organic compounds or general spectroscopy applications, a Galileo detector will speed sample identification while providing accurate and precise analysis.

When research projects require frequent sample analysis over a long period of time, you'll want the latest and best technology backing you up. Galileo is the innovator in analytical instrument detectors. If you demand high performance and are concerned about down time, rapid analysis, dynamic range and cost, insist on Galileo scientific detectors. You'll wonder how you ever got along without us.

Write us and ask how to ensure that your instruments have Galileo scientific detectors.

Galileo Electro-Optics Corp.
Scientific Detector Products Group
P.O. Box 550, Dept. AA
Sturbridge, MA 01566
(508) 347-9191

GALILEO
Galileo Electro-Optics Corp.

CIRCLE 60 ON READER SERVICE CARD

LABORATORY SERVICE CENTER

Acetylthiourea • 3-Aminophthalhydrazide • p-Anisic Acid • L-Arabinose
p-Chloranil • 3,3'-Diaminobenzidine 4HCl • 1,2-Dibenzoylethylene
2,6-Dichloroindophenol, Sodium • 2,2-Dichloropropane • Diethylformamide
Diiodomethane • p-Dimethoxybenzene • Dithizone • Furfuryl Methyl Sulfide
Furoic Acid & Methyl Ester • m-Hydroxybenzoic Acid • Janus Green B
Levulinic Acid • 2-Methylcyclohexanol • Methyl Green • Neocuproine & HCl
Oxamide • Sebacic Acid • Sodium Diethyldithiocarbamate • Suberic Acid
L-Thyroxine, Na Salt • Toluidine Blue 0 • Tripalmitin • Vanillic Acid

Write for our Products List of over 3,000 chemicals

Tel: 516-273-0900 • TOLL FREE: 800-645-5566 Telefax: 516-273-0858 • Telex: 497-4275

EASTERN CHEMICAL
A Division of UNITED–GUARDIAN, INC.

P.O. Box 2500
DEPT. AC
SMITHTOWN, N.Y. 11787

Laboratory Service Center (Equipment, Materials, Services, Instruments for Leasing), Maximum space — 4 inches per advertisement. Column width, 2-3/16″; two column width, 4-9/16″. Artwork accepted. No combination of directory rates with ROP advertising. Rates based on number of inches used within 12 months from first date of first insertion. Per inch: 1″ — **\$165; 12″ — \$160; 24″ — \$155; 36″ — \$150; 48″ — \$145.**

CALL OR WRITE JANE GATENBY

ANALYTICAL CHEMISTRY
500 Post Road East
P.O. Box 231
Westport, CT 06880
203-226-7131/FAX: 203-454-9939

NMR ANALYSIS

MULTINUCLEAR LIQUID or
MULTIFIELD SOLID STATE
SPECTRAL DATA SERVICES, INC.
818 Pioneer
Champaign, IL 61820
(217) 352-7084

HELP WANTED ADS

ROP display at ROP rates. Rate based on number of insertions within contract year. Cannot be combined for frequency.

Unit	1-Ti	6-Ti	12-Ti
1″ (25 mm)	\$190	\$170	\$160
	24-Ti	48-Ti	72-Ti
	\$150	\$140	\$130

CALL OR WRITE JANE GATENBY

ANALYTICAL CHEMISTRY
500 Post Road East
P.O. Box 231
Westport, CT 06880
203-226-7131
FAX: 203-454-9939

INDEX TO ADVERTISERS IN THIS ISSUE

CIRCLE INQUIRY NO.	ADVERTISERS	PAGE NO.
1	**Antek Instruments, Inc.**	1385A
-	**Aramco** Bernard Hodes Advertising	1375A
26	***Chrompack Inc.**	1355A
28, 29	***Conostan Division/Conoco Specialty Products** Robert Lamons & Associates	1377A, 1379A
32	**Delsi/Nermag Instruments**	IFC
50, 51	***Fisher Scientific** Hawbaker Communications, Inc.	1371A, 1373A
60	***Galileo Electro-Optics Corp.** Legasse Associates Advertising Inc.	1388A
58	**Gelman Sciences**	1361A
63	***Hewlett-Packard Company** Brooks Communications	OBC
75–78	***Isco, Inc.** Farneaux Associates	1356A
100–105	***Matheson Gas Products** Kenyon Hoag Associates	1363A
96	**E. Merck**	1384A
94	***Metrohm Ltd.** Ecknauer & Schoch Werbeagentur ASW	1366A
110	***Nicolet Analytical Instruments**	1359A
125	****Philips Scientific/Analytical Division** Connors Publicity Ltd.	1378B
127	**The Pittsburgh Conference**	1384A
172	***Varian** Lanig Associates	1364A
177	***Wheaton** The Wheaton Agency	1362A

Directory section, see page 1388A.
** See ad in ACS Laboratory Guide.*
*** Company so marked has advertisement in Foreign Regional edition only.*
Advertising Management for the American Chemical Society Publications

CENTCOM, LTD

President
Thomas N. J. Koerwer
Executive Vice President *Senior Vice President*
James A. Byrne **Benjamin W. Jones**
Clay S. Holden, *Vice President*
Robert L. Voepel, *Vice President*
Joseph P. Stenza, *Production Director*

500 Post Road East
P.O. Box 231
Westport, Connecticut 06880
(Area Code 203) 226-7131
Telex No.643310
FAX: 203-454-9939

ADVERTISING SALES MANAGER
Bruce E. Poorman

ADVERTISING PRODUCTION MANAGER
Jane F. Gatenby

SALES REPRESENTATIVES

Philadelphia, PA . . . Patricia O'Donnell, CENTCOM, LTD., GSB Building, Suite 405, 1 Belmont Avenue, Bala Cynwyd, Pa. 19004. Telephone: 215-667-9666, FAX: 215-667-9353

New York, NY . . . John F. Raftery, CENTCOM, LTD., 60 East 42nd St., New York, N.Y. 10165. Telephone: 212-972-9660

Westport, CT . . . Edward M. Black, CENTCOM, LTD., 500 Post Road East, P.O. Box 231, Westport, Ct. 06880. Telephone: 203-226-7131, Telex 643310, FAX: 203-454-9939

Cleveland, OH . . . Bruce E. Poorman, John C. Guyot, CENTCOM, LTD., 325 Front St., Suite 2, Berea, Ohio 44017. Telephone: 216-234-1333, FAX: 216-234-3425

Chicago, IL . . . Michael J. Pak, CENTCOM, LTD., 540 Frontage Rd., Northfield, Ill. 60093. Telephone: 708-441-6383, FAX: 708-441-6382

Houston, TX . . . Michael J. Pak, CENTCOM, LTD. Telephone: 708-441-6383

San Francisco, CA . . . Paul M. Butts, CENTCOM, LTD., Suite 1070, 2672 Bayshore Frontage Road, Mountain View, CA 94043. Telephone: 415-969-4604

Los Angeles, CA . . . Clay S. Holden, CENTCOM, LTD., Newton Pacific Center, 3142 Pacific Coast Highway, Suite 200, Torrance, CA 90505. Telephone: 213-325-1903

Boston, MA . . . Edward M. Black, CENTCOM, LTD. Telephone: 203-226-7131

Atlanta, GA . . . John F. Raftery, CENTCOM, LTD. Telephone: 212-972-9660

Denver, CO . . . Paul M. Butts, CENTCOM, LTD. Telephone: 415-969-4604

United Kingdom

Reading, England . . . Malcolm Thiele, Technomedia Ltd., Wood Cottage, Shurlock Row, Reading RG10 OQE, Berkshire, England. Telephone: 073-434-3302, Telex #848800, FAX: 073-434-3848

Lancashire, England . . . Technomedia Ltd., c/o Meconomics Ltd., Meconomics House, 31 Old Street, Ashton Under Lyne, Lancashire, England. Telephone: 061-308-3025

Continental Europe . . . Andre Jamar, International Communications, Inc., Rue Mallar 1, 4800 Verviers, Belgium. Telephone: (087) 22-53-85, FAX: (087) 23-03-29

Tokyo, Japan . . . Sumio Oka, International Media Representatives Ltd., 2-29 Toranomon, 1-Chome Minato-ku Tokyo 105 Japan. Telephone: 502-0656, Telex #22633, FAX: 591-2530

Learn the basics of the most popular analytical technique in the world...

Basic Gas Chromatography

2nd Edition

New ACS Video Course!

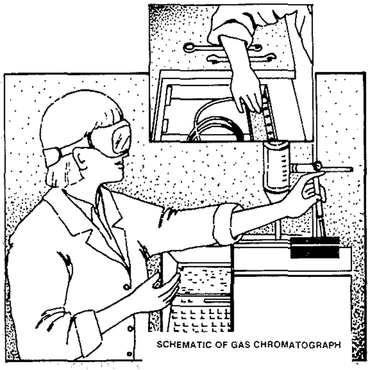

SCHEMATIC OF GAS CHROMATOGRAPH

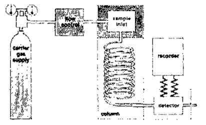

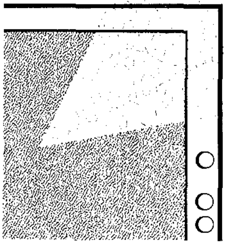

Completely updated... covers new techniques... revision of the best-selling first edition!

Targeted for anyone just beginning in GC—or for those who want to brush up their skills or get an up-to-date understanding of this technique—this newly-revised bestselling video course fully explains the fundamentals of gas chromatography. All the essentials you need to know about GC and how to use it are colorfully illustrated in this course through live-action lab demonstrations or with computer graphics. This introductory course consists of two parts, each approximately 25 minutes long, and a manual.

Part 1

Begin with a basic look at how and why GC works, including the partitioning theory. See how GC separates mixtures of gases, liquids, or solids in solution into their component parts. Learn in detail the kinds of materials that are used in both packed and capillary columns, including stationary liquid phases. Understand the difference between packed and capillary columns and why and when to use one over the other. Learn how to couple GC with other analytical techniques, such as mass spectrometry. Know the advantages and disadvantages of GC.

Part 2

Examine the equipment that is used in GC, learning in detail the components of a GC system. See in live action the system in actual use, covering everything from turning on the GC and setting the flow rate to injecting gases and liquids and installing a column. Learn the difference between isothermal analysis and temperature programming.

Course Study Guide

The approximately 100-page **Course Study Guide** covers selected details about GC in greater depth and explains more system theory than tape alone. Also, unfamiliar terms are defined, which makes the guide a useful reference for you to retain after viewing the tape.

One videotape: 50 minutes
(Catalog No. V-4000)

Author/Instructor

Harold M. McNair is Professor of Chemistry at Virginia Tech, Blacksburg, VA, and one of the ACS's most highly rated short course instructors. He has taught courses on GC and LC internationally for over 15 years.

Cost

Purchase price: $800 (US & Canada); $960 (export). One free copy of the Course Study Guide accompanies each purchase of the course. Additional guides: $30 each (US & Canada); $36 each (export). Rental price: $320 (US & Canada only).

Remember, your purchase is backed by the ACS Guarantee: if not completely satisfied, return within 15 days for a full refund or credit.

To order, complete the coupon below and mail with your payment or purchase order to **American Chemical Society, Distribution Office Dept. 09, P.O. Box 57136, West End Station, Washington, DC 20037. Or call toll-free (800) 227-5558.**

ORDER FORM

Mail to **American Chemical Society, Distribution Office Dept. 09, P.O. Box 57136, West End Station, Washington, DC 20037.**

*Please send me Basic Gas Chromatography, **2nd Edition*** (Catalog No. V-4000).

1. To **PURCHASE** this course, complete the section below:

No. Units	US & Can.	Export	No. Add'l Guides	US & Can.	Export	Total
______	$800	$960	____________	$30	$36	______

2. To **RENT** this course, complete the section below:

Preferred play date	Rental Price
______________	$320

*US and Canada only

Please specify video format: ☐ ½" VHS ☐ ¾" U-matic

Method of payment:

1) Payment enclosed (make checks payable to the ACS).
2) ☐ Purchase order enclosed PO # ______________
3) Charge my: ☐ VISA/MasterCard ☐ AMEX ☐ Diners Club/Carte Blanche

Account # ______________ Expires ______________
Name of Cardholder ______________
Signature ______________
Phone ______________
Ship to:
Name ______________
Address ______________
____
City, State, Zip ______________
Bill to:
Name ______________
Address ______________
____
City, State, Zip ______________

09

Please allow 3-4 weeks for delivery by UPS. Prices subject to change without notice. Prices quoted are in US dollars; foreign purchases must be made in US currency by international money order, UNESCO coupons or US bank draft.

Analytical
CHEMISTRY

EDITOR: **GEORGE H. MORRISON**

ASSOCIATE EDITORS: **Klaus Biemann, Georges Guiochon, Walter C. Herlihy, Robert A. Osteryoung, Edward S. Yeung**

Editorial Headquarters
1155 Sixteenth St., N.W.
Washington, DC 20036
Phone: 202-872-4570
Telefax: 202-872-6325

Managing Editor: Sharon G. Boots

Associate Editors: Louise Voress, Mary Warner

Assistant Editors: Grace K. Lee, Alan R. Newman

Editorial Assistant: Felicia Wach

Director, Operational Support: C. Michael Phillippe

Production Manager: Leroy L. Corcoran

Art Director: Alan Kahan

Designer: Amy Meyer Phifer

Production Editor: Elizabeth E. Wood

Circulation: Claud Robinson

Editorial Assistant, LabGuide: Joanne Mullican

Journals Dept., Columbus, Ohio

Associate Head: Marianne Brogan

Journals Editing Manager: Joseph E. Yurvati

Associate Editor: Rodney L. Temos

Staff Editor: Sharon K. Hatfield

Advisory Board: Bernard J. Bulkin, Michael S. Epstein, Renaat Gijbels, Peter R. Griffiths, Thomas L. Isenhour, Nobuhiko Ishibashi, James W. Jorgenson, Peter C. Jurs, Mary A. Kaiser, David L. Nelson, Lawrence A. Pachla, Ralph E. Sturgeon, George S. Wilson, Mary J. Wirth, Andrew T. Zander, Richard N. Zare
Ex Officio: Sam P. Perone

Instrumentation Advisory Panel: James B. Callis, Bruce Chase, R. Graham Cooks, L. J. Cline Love, Sanford P. Markey, Ronald E. Majors, Linda B. McGown, Gary W. Small, R. Mark Wightman

Published by the
AMERICAN CHEMICAL SOCIETY
1155 16th Street, N.W.
Washington, DC 20036

Publications Division

Director: Robert H. Marks

Journals: Charles R. Bertsch

Special Publications: Randall E. Wedin

Manuscript requirements are published in the January 1, 1989 issue, page 91. Manuscripts for publication (4 copies) should be submitted to ANALYTICAL CHEMISTRY at the ACS Washington address.

The American Chemical Society and its editors assume no responsibility for the statements and opinions advanced by contributors. Views expressed in the editorials are those of the editors and do not necessarily represent the official position of the American Chemical Society.

AUTHOR INDEX

Abramson, F. P., 2724
Alexandrou, N., 2770
Aras, N. K., 2757
Ausserer, W. A., 2690

Barman, B. N., 2735
Bartlett, P. N., 2803
Bear, J. L., 2805
Bowling, R. J., 2763
Braman, R. S., 2715
Busch, K. W., 2785
Busch, M. A., 2785

Capar, S. G., 2777
Capdevielle, F. J., 2805
Caton, J. E., Jr., 2751
Chace, D. H., 2724
Chandra, S., 2690
Chang, D. Y., 2792
Clifford, R. H., 2777

D'Arcy, J. B., 2708
DeGraff, B. A., 2704
Demas, J. N., 2704

Edwards, M. D., 2751
Engstrom, R. C., 2763

Fariñas, J. C., 2696
Fujiwara, K., 2699
Fujiwara, T., 2800
Fulcher, J. N., 2743

Garcia, M. E., 2751
Giddings, J. C., 2735
Glavas, S., 2731
Gökmen, İ. G., 2757
Gordon, G. E., 2757
Griest, W. H., 2751
Grolimund, K., 2747

Hendrix, S. A., 2715
Henkin, R. I., 2757
Howe, G. B., 2743
Huang, J.-J., 2800

Jayanty, R. K. M., 2743
Johnson, R. W., 2766

Kadish, K. M., 2805
Kanchi, T., 2699
Knoll, J. E., 2743
Kolla, P., 2747
Kubala, S. W., 2785
Kumamaru, T., 2699, 2800

Levine, S. P., 2708
Li, R., 2809
Ling, Y.-C., 2690

McCreery, R. L., 2763
Midgett, M. R., 2743
Montaser, A., 2777
Morrison, G. H., 2690
Müller, S. R., 2747

Nielson, K. K., 2719

Ong, W. A., 2792

Pau, J. C., 2743
Pawliszyn, J., 2770
Peterson, M. R., 2743
Pharr, C. M., 2763

Rogers, V. C., 2719
Roumelis, N., 2731

Saleh, F. Y., 2792
Schenley, R. L., 2751
Schomburg, G., 2747
Schure, M. R., 2735
Simon, W., 2747
Sinex, S. A., 2777
Snyder, S. W., 2704

Tanimoto, N., 2800
Tilotta, D. C., 2785
Tomkins, B. A., 2751
Tsumura, S.-i., 2699

Vo-Dinh, T., 2766

Wachter, L. J., 2751
Wang, J., 2809
Wastney, M. E., 2757
Whitaker, R. G., 2803
Widmer, H. M., 2747

Xiao, H.-k., 2708

Yao, C.-L., 2805

Quantitative Imaging of Boron, Calcium, Magnesium, Potassium, and Sodium Distributions in Cultured Cells with Ion Microscopy

Walter A. Ausserer,[1] Yong-Chien Ling,[2] Subhash Chandra, and George H. Morrison*

Baker Laboratory of Chemistry, Cornell University, Ithaca, New York 14853-1301

A method for the conversion of intensity information in ion micrographs of freeze-fractured, freeze-dried cultured cells to local dry weight elemental concentrations is presented. Homogenates generated from cultured cells are used as calibration standards. Ion microscope (IM) relative sensitivity factors for B, Ca, K, Mg, and Na with respect to the matrix element C are determined by the correlation of IM and inductively coupled plasma atomic emission spectrometry analyses of the cellular homogenates. After calibration of the IM imaging system, the relative sensitivity factors are used to determine local intracellular concentrations of B, Ca, K, Mg, and Na in cultured Swiss 3T3 fibroblasts. Intracellular B was introduced through cellular uptake of $Na_2B_{12}H_{11}SH$, a candidate therapeutic agent for boron neutron capture cancer therapy. The IM intracellular concentration results show good agreement with published electron probe X-ray microanalysis results. Estimated detection limits are in the low- to sub-parts-per-million dry weight concentration range.

INTRODUCTION

The ion microscope (IM) is a secondary ion mass spectrometer with elemental imaging capabilities (*1, 2*). The distributions of many elements in biological samples are easily measured with the IM, which produces real-time images of elemental (isotopic) distributions at a spatial resolution of less than 1.0 μm. Analytical techniques that can perform highly sensitive elemental determinations in microscopic sample regions are needed for the study of elements in animal cells, because elemental concentrations are often tightly regulated in cellular subcompartments. Although the high elemental sensitivity and good spatial resolution of the IM make it a promising tool for such studies, several analytical problems have prevented quantitative elemental imaging of biological soft tissue samples with the IM from becoming routine. First, the sample preparation method must preserve native elemental distributions within the sample. Second, corrections for the influence of local matrix effect variations on local secondary ion signals must sometimes be made (*3–5*). Additionally, a quantification microstandard in which the matrix composition closely matches that of the sample must be available.

Several recent biological IM studies have employed thin sections of animal tissue (*6–11*). As an alternative to tissue work, a cryopreparation method for cultured animal cells has been developed in our laboratory (*12*). Cultured cells provide an excellent model system for the study of diverse physiological phenomena under well-controlled experimental conditions. Briefly, cells prepared by our method are cultured on high-purity silicon wafers and rapidly frozen to immobilize diffusible intracellular ions. The frozen samples are then sandwich-fractured under liquid nitrogen and freeze-dried at −100 °C prior to analysis. During the fracturing process, the apical cell surface and the adhering cell growth medium are removed, exposing the cellular interior for microanalysis, free from contamination. Previous IM studies of cells prepared by this method (fractured cells) found that local matrix effect variations are typically undetectable, so that matrix effect correction schemes are not required (*13, 14*). The present study was undertaken to investigate the quantitative relationship between secondary ion signals and local concentrations of Na, Mg, K, Ca, and B in fractured cells.

There is widespread interest in the determination of intracellular levels of Na, Mg, K, and Ca because these are the major diffusible cations in biological systems. Our interest in the quantitative localization of intracellular B stems from recent progress in boron neutron capture therapy (BNCT), a promising strategy for the treatment of several types of human tumors (*15*). This therapy requires the selective incorporation of ^{10}B into tumor cells, with subsequent irradiation of the tumor with thermal neutrons. It is proposed that tumor cells can be selectively destroyed by the energetic products of the $^{10}B(n,\alpha)^{7}Li$ reaction. The intracellular distribution of B is important in BNCT because cell-killing efficiency is believed to depend on the proximity of the $^{10}B(n,\alpha)^{7}Li$ reaction to the genetic material of the cell.

In the present study, quantification microstandards are generated from homogenates of cultured cells. Relative sensitivity factors (RSF's) for the analytes with respect to the matrix element C are determined by correlation of IM and inductively coupled plasma atomic emission spectrometry (ICP-AES) analyses. Calibration of the IM imaging system for quantitative work is described, along with the application of imaging mode RSF's for the determination of local intracellular concentrations of B, Na, Mg, K, and Ca in cultured 3T3 fibroblasts. For B localization experiments, cells are incubated with $Na_2B_{12}H_{11}SH$, a candidate BNCT compound for the treatment of brain tumors.

EXPERIMENTAL SECTION

Sample Preparation. Quantification microstandards were prepared from cultured Swiss 3T3 mouse fibroblasts and from NRK-49F normal rat kidney fibroblasts. Swiss 3T3 cells were obtained from the laboratory of Efram Racker at Cornell University and NRK-49f cells from the American Type Culture Collection. Both cell lines were cultured in Dulbecco's modified Eagle's medium with 10% fetal bovine serum, 20 mM Hepes, 20 mM penicillin, and 100 μg/mL streptomycin (all from Gibco Laboratories). Cells were plated at a density of 1 × 10^5 cells/flask and cultured as monolayers in 150-cm^2 flasks. When confluency was approached, cells from eight flasks were detached by treatment with 0.25% trypsin in Ca- and Mg-free Dulbecco's phosphate buffered saline (Gibco), transferred to 50-mL polypropylene centrifuge tubes, collected by centrifugation at 900 rpm (Sorvall H1000B rotor) for 5 min, and drained. To remove the adhering trypsin solution, cells were twice resuspended in 30 mL of 160 mM $NH_4C_2H_3O_2$ and centrifuged as above. After thorough draining of the $NH_4C_2H_3O_2$ solution, the cell pellet was frozen

---

[1] Current address: Life Sciences Division, SRI International, 333 Ravenswood Ave., Menlo Park, CA 94025.

[2] Current address: Department of Chemistry, National Tsing Hua University, Hsinchu 30034, Taiwan, ROC.

0003-2700/89/0361-2690$01.50/0 © 1989 American Chemical Society

and finely ground with a cold mortar and pestle in a liquid nitrogen trough. The ground cellular material was transferred to a cold 1.5-mL polypropylene tube, thawed, and spiked with B from a 1 mM $Na_2B_{12}H_{11}SH$ (Callery Chemical Co.) solution. To maximize elemental homogeneity, the cellular material was twice passed through a cycle of thawing, vigorous mixing with a micropipet, rapid freezing, and regrinding. The ground cells were then lyophilized. Being a volatile salt, the $NH_4C_2H_3O_2$ is removed from the sample during lyophilization, so that the remaining cellular homogenate was composed of relatively uncontaminated cellular material (*16, 17*). The lyophilized cell homogenate was mounted for IM analysis by firmly pressing small particles of the homogenate between the polished faces of two clean 1-cm^2 silicon pieces (General Diode Corp.) with a Parr Instrument Co. Model 2811 pellet press.

The bulk of the lyophilized homogenate was analyzed by ICP-AES. Samples, approximately 15 mg dry weight, were digested to near dryness in HF cleaned quartz tubes with 0.2 mL of concentrated HNO_3 (J. T. Baker Chemical Co.), which had been double distilled and condensed in Teflon. The digestate was cooled and diluted with 0.15 mL of 37% HCl (Baker) and 2.85 mL of H_2O. Digested samples were clear and contained no visible particulate matter. As verification of the digestion and ICP-AES procedures, NBS SRM 1571 (orchard leaves) and SRM 1573 (tomato leaves) were digested and analyzed exactly as the cell homogenates.

The preparation of fractured cell monolayers has been previously described (*12*). Swiss 3T3 cells were plated onto 1-cm^2 polished silicon pieces in 5-mL culture dishes at a density of 5 × 10^4 cells/dish. The culture medium is described above. To facilitate the sandwich fracture, 30000 polystyrene beads (Duke Scientific Corp.) were added to each dish, with the bead diameter being 9.0 μm. The freezing medium was Freon-22 slush (Air Products and Chemicals, Inc.). For B localization experiments, 100 μg/mL $Na_2B_{12}H_{11}SH$ was added to the culture media 24 h after cell plating. Four days after plating, cells were frozen and freeze-fractured. Samples were freeze-dried at −100 °C for 24 h and analyzed directly on the silicon substrates.

ICP-AES Analysis. A Jarrell-Ash Model ICAP 61 Update was used for all ICP-AES measurements. A peristaltic pump operating at 2.5 mL/min introduced the samples into the spray chamber through a crossflow nebulizer. Calibration solutions were prepared in 5% HCl. Na, Mg, K, and Ca signals were calibrated from a multielement standard prepared from Na_2CO_3 and K_2CO_3 (Grade 1 Puratronic, Johnson Matthey Chemicals, Limited), 1000 ppm Mg and Mn atomic spectral standards (Baker), 99.999% Al powder, 99.999% $NH_4H_2PO_4$, 99.999% $(NH_4)_2SO_4$, 99.995% $CaCO_3$, and 99.999% Fe_2O_3 (all from Aldrich Chemical Co.). The B signal was calibrated with a multielement standard prepared from 99.999% H_3BO_3 (Aldrich), 99.999% Zn (Aldrich), and 1000 ppm Si, V, Cr, Co, Ni, Cu, As, Se, Y, Mo, Cd, and Pb atomic spectral standards (Baker). The analytical emission lines were 249.7 nm for B, 279.5 nm for Mg, 317.9 nm for Ca, 589.0 nm for Na, and 766.5 nm for K. All signals were blank and spectral interference corrected.

Ion Microanalysis. A Cameca IMS 3f secondary ion mass spectrometer with a mass filtered O_2^+ primary ion beam was used for secondary ion measurements. A primary beam diameter of 50 μm and a raster area of 250 × 250 μm were used for all experiments. Except where noted, the spectrometer was operated with 150-μm transfer optics, a 60-μm contrast aperture, a 1.8-mm field aperture, a 130-eV secondary ion energy window, and positive secondary ion detection with a pulse counting electron multiplier.

High-resolution mass scans ($m/\Delta m \approx 5000$) at nominal mass-to-charge ratios (m/z) of +10, +11, +12, +23, +24, +39, +40, and +41 were performed to check for mass interference components in the secondary ion signals from $^{10}B^+$, $^{11}B^+$, $^{12}C^+$, $^{23}Na^+$, $^{24}Mg^+$, $^{39}K^+$, $^{40}Ca^+$, and $^{41}K^+$. For these measurements, a 750-μm field aperture was used in the spectrometer. Samples of Swiss 3T3 homogenate (spiked to 1500 ppm B dry weight) and Swiss 3T3 fractured cells (incubated with 100 μg/mL $Na_2B_{12}H_{11}SH$) were analyzed at each m/z.

The energy distributions of secondary ions from Swiss 3T3 homogenate and Swiss 3T3 fractured cell samples were recorded to study the effect of the secondary ion energy window on relative ion signals. Two sets of spectra were recorded from each sample type, one with a primary ion beam of 100 nA and one with a 350-nA beam, resulting in four spectra for each m/z. The secondary ion energy window was set at ≈3 eV.

RSF Determination. RSF's for the analytes with respect to the matrix element carbon were determined by the analysis of three cell homogenate samples, two produced from Swiss 3T3 cells and one from NRK-49F's. Electron multiplier detection was used. Preliminary analyses of a Swiss 3T3 homogenate sample with primary beam currents of 100, 300, and 600 nA gave statistically identical RSF's for each analyte, so a 250-nA primary ion beam was used for all subsequent determinations. After samples were presputtered briefly to stabilize the secondary ion signals, signals at each m/z above were monitored cyclically for 1 s each for a total of 15 analysis cycles. RSF's for the relatively intense $^{23}Na^+$ and $^{39}K^+$ species were determined separately from the other analytes because of electron multiplier dynamic range considerations. In all cases, secondary ion signals were stable for the duration of the analysis. Values used for the calculation of RSF's were signals averaged over analysis cycles 6–15.

The RSF has generally been defined as

$$\mathrm{RSF}_{x/\mathrm{ref}} = (i_x/i_{\mathrm{ref}})/(C_x f_x/C_{\mathrm{ref}} f_{\mathrm{ref}}) \tag{1}$$

where i is the secondary ion intensity, C is the elemental concentration, f is the isotopic abundance, x indicates the analyte, and ref indicates the reference species (*18, 19*). The slope of a plot of i_x/i_{ref} versus $C_x f_x/C_{\mathrm{ref}} f_{\mathrm{ref}}$ is therefore $\mathrm{RSF}_{x/\mathrm{ref}}$. The RSF's for the analytes with respect to the reference matrix element carbon reported here use a modified definition

$$\mathrm{RSF}_{x/\mathrm{ref}} = (i_x/i_{\mathrm{ref}})/(f_x C_x) \tag{2}$$

so that $\mathrm{RSF}_{x/\mathrm{ref}}$ is not a true elemental RSF, but a calibration factor relating secondary ion i_x/i_{ref} ratios to C_x values determined by the ICP-AES analyses.

Ion Microscopy. Imaging experiments utilized the microchannel plate–phosphor screen detector (MCP–PS) of the Cameca IMS 3f. Images were acquired for digital image processing with a Photometrics, Ltd., Model CH220 CCD liquid-cooled camera head equipped with a Thomson-CSF TH7882CDA charge-coupled device (CCD). The CCD imager is not a video camera, but integrates images directly on the CCD chip. Image integration time is controlled by an electronic shutter. A Photometrics camera controller digitized the CCD output to 14 bits per pixel. Throughout this study, the CCD was operated in the 2 × 2 binning mode. The image processing system in our laboratory has been previously described (*20*). The ion pump for the 3f detector section was disabled during image acquisition to minimize stray ion background signal. The high sensitivity, wide dynamic range, and extremely linear response of scientific grade CCD imagers have been recently reviewed (*21–23*), and Mantus et al. (*24*) are preparing a paper that fully describes the performance of the CCD imager in ion microscopy. Single ion hits are easily detectable with this system because of its high sensitivity and very low noise level. The CCD imager exhibits near perfect response linearity over several orders of magnitude incoming light intensity and over integration times from 0.2 s to several minutes.

Imaging System Calibration. For application of the above-determined RSF's to the IM imaging system, calibration curves were constructed relating CCD pixel values to electron multiplier count rates for each m/z of interest. Curves were generated for two commonly used MCP gains, 60% (1748 V) and 70% (1956V). Gelatin films, doped with salts of the analyte elements, were deposited on 1-cm^2 silicon pieces and used as laterally homogeneous calibration standards. An IM magnification of 90× was used, so that the entire 1.35-cm-diameter ion image was centered on the 1.90-cm-diameter MCP-PS. Dark current corrected images were recorded at electron multiplier count rates of 1 × 10^3, 3 × 10^3, 1 × 10^4, and 3 × 10^4 counts/s for each m/z. In this signal range, the electron multiplier is essentially free from dead time. Calibration curves were constructed by plotting mean CCD pixel values per second (CCD_x) versus mean electron multiplier counts per pixel per second (EM_x). All curves were strongly linear and of the form

$$\mathrm{CCD}_x = y_x \mathrm{EM}_x + b_x \tag{3}$$

No dead time effects of the MCP-PS were detectable under these conditions.

Table I. Contribution of Analyte Ions to Secondary Ion Signals[a]

		% signal from analyte	
m/z	analyte	3T3 homogenate	3T3 fractured cells
10	$^{10}B^+$	>99.9	[b]
11	$^{11}B^+$	>99.9	[b]
12	$^{12}C^+$	99.8 (0.3)	>99.9
23	$^{23}Na^+$	>99.9	>99.9
24	$^{24}Mg^+$	96.9 (0.7)	98.5 (0.2)
39	$^{39}K^+$	>99.9	>99.9
40	$^{40}Ca^+$	96.9 (0.7)	97.0 (0.2)
41	$^{41}K^+$	98.6 (0.6)	99.8 (0.0)

[a] Values are reported as mean (standard deviation); $n = 3$. [b] Insufficient signal for high mass resolution spectrum.

Quantitative Imaging of Intracellular Elements. A primary ion beam of 250 nA was used for the acquisition of ion micrographs of control and $Na_2B_{12}H_{11}SH$-treated Swiss 3T3 fibroblasts. After brief sample presputtering, $^{11}B^+$, $^{12}C^+$, $^{23}Na^+$, $^{24}Mg^+$, $^{40}Ca^+$, and $^{41}K^+$ micrographs were recorded with the MCP gain fixed at 60%. Image acquisition times were 150.0 s for $^{11}B^+$, 60.0 s for $^{12}C^+$, 0.4 s for $^{23}Na^+$, 30.0 s for $^{24}Mg^+$, 30.0 s for $^{40}Ca^+$, and 3.0 s for $^{41}K^+$. $^{41}K^+$ was monitored rather than the more intense $^{39}K^+$ to avoid saturation of the CCD imager. The generation of concentration information from these images required three operations: (1) spatial registration of the analyte image and the $^{12}C^+$ reference image to permit ratioing of signals from exactly corresponding areas, (2) calculation of the mean CCD pixel values per second for identical sample features of interest in the analyte image (CCD_x) and the $^{12}C^+$ reference image (CCD_{ref}), and (3) conversion of the signal ratio CCD_x/CCD_{ref} to analyte dry weight concentration as shown below.

Rearranging eq 2 and inserting EM_x and EM_{ref} for i_x and i_{ref} produce

$$C_x = (EM_x/EM_{ref})/(f_x RSF_{x/ref}) \qquad (4)$$

Combining eq 3 and 4, one obtains

$$C_x = (CCD_x - b_x)y_{ref}/[(CCD_{ref} - b_{ref})y_x f_x RSF_{x/ref}] \qquad (5)$$

In practice, b_x and b_{ref} are negligibly small as compared to CCD_x and CCD_{ref}, so eq 5 simplifies to

$$C_x = CCD_x y_{ref}/[CCD_{ref} y_x f_x RSF_{x/ref}] \qquad (6)$$

RESULTS AND DISCUSSION

Ion Microanalysis. Table I lists the results of high-resolution mass scans for Swiss 3T3 homogenate and Swiss 3T3 fractured cell samples. Each value is the mean result of three scans. Mass scans from the homogenate and fractured cell samples are generally in close agreement, with the secondary ion signals being composed of >96% analyte ions in all cases. Although corrections for mass interference contributions to secondary ion signals can be incorporated in quantification algorithms, no corrections have been employed in this study because the contributions are relatively small.

Secondary ion energy distributions from Swiss 3T3 homogenate and Swiss 3T3 fractured cell samples are shown in Figure 1. Energy spectra from the two sample types were indistinguishable, as were spectra produced with the different primary ion beam intensities. Each curve in Figure 1 is a smoothed point-by-point average of the four spectra recorded at each m/z, where the raw spectra were scaled to 2×10^6 total counts prior to averaging. The low-energy tails were all very weak and have been omitted. The resultant curves for $^{23}Na^+$ and $^{39}K^+$ were superimposable, as were the curves for $^{24}Mg^+$ and $^{40}Ca^+$. The prominence of the high-energy spectral tail correlates with the chemical group of the element, being least prominent for the alkali metals and most prominent for $^{12}C^+$.

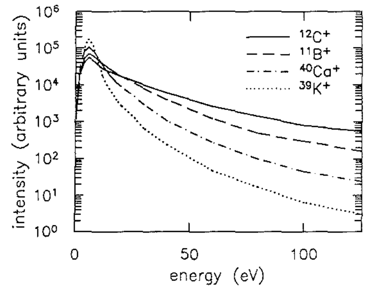

Figure 1. Secondary ion energy distributions. Each curve is a smoothed average of four spectra as described in the text, scaled to 2×10^6 total counts for ease of comparison.

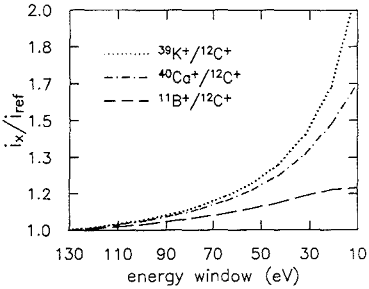

Figure 2. Variation of analyte-to-carbon ratios as the spectrometer energy window is narrowed from 130 to 10 eV. Curves were generated from the normalized data presented in Figure 1, so that a ratio of 1.0 is imposed at an energy window setting of 130 eV for each curve.

The IM secondary ion energy window is variable from 0 to 130 eV, with image resolution generally improving as the window is narrowed. Because the different analyte ions exhibit different energy distributions, decreasing the energy band-pass will attenuate the different analytical signals nonuniformly. The variation of signal ratios of $^{39}K^+$, $^{40}Ca^+$, and $^{11}B^+$ to $^{12}C^+$ as a function of energy window setting is shown in Figure 2. These curves were generated from the data plotted in Figure 1, except that the spectra were scaled to the same total counts in a 130-eV energy window centered on the spectral peak. Note that analyte-to-carbon signal ratios can increase dramatically as the energy window is narrowed. In this study, we have determined RSF's for the analytes ratioed to the matrix element C with the energy window set at 130 eV. Figure 2 demonstrates that these RSF values will be valid only when a 130-eV band-pass is used.

RSF Determination. To validate the digestion and ICP-AES procedures, NBS SRM 1571 (orchard leaves) and SRM 1573 (tomato leaves) were digested and analyzed exactly as the cell homogenates. The results are listed in Table II. Of particular interest were the B values, because loss of B during wet ashing is a well-known problem. The results in Table II indicate that significant loss of B did not occur during digestion.

Table III lists IM analyte-to-carbon ratio results (i_x/i_{ref}), ICP-AES concentration results (C_x), and calculated $RSF_{x/ref}$ values from analysis of the cell homogenate samples. As anticipated, the IM sensitivity decreases dramatically with increasing first ionization potential of the analyte. Because of imperfect elemental homogeneity, relatively large standard deviations are associated with the IM results, particularly with the higher concentration Na and K values. The $RSF_{x/ref}$ values calculated from the three samples are identical for each analyte

Table II. Analysis of NBS SRM's for Validation of ICP-AES Procedures[a]

analyte	certified composition (dry wt)	ICP-AES results (dry wt)
	NBS SRM 1571: Orchard Leaves	
B	33 (3) μg/g	31.9 (0.1) μg/g
Na	82 (6) μg/g	67 (1.3) μg/g
Mg	0.62 (0.02)%	0.678 (0.003)%
K	1.47 (0.03)%	1.64 (0.01)%
Ca	2.09 (0.03)%	2.23 (0.01)%
	NBS SRM 1573: Tomato Leaves	
K	4.46 (0.03)%	4.54 (0.02)%
Ca	3.00 (0.03)%	3.20 (0.01)%
Mg	0.7%[b]	0.731 (0.003)%
B	30 μg/g[b]	32.6 (0.2) μg/g

[a] NBS values are reported as mean (uncertainty) as defined in the NBS Standard Reference Material Catalog. ICP-AES values are reported as mean (standard deviation) for four analyses. [b] Noncertified values.

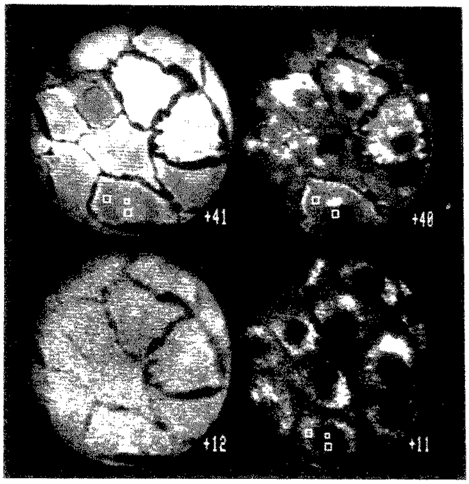

Figure 3. $^{41}K^+$, $^{40}Ca^+$, $^{12}C^+$, and $^{11}B^+$ ion micrographs from several Swiss 3T3 fibroblasts treated with 100 μg/mL $Na_2B_{12}H_{11}SH$. The three boxed areas in the lowest cell of each micrograph are included to illustrate analytical areas. In each micrograph, the lower right box denotes a cytoplasmic area, the upper right box a perinuclear area, and the upper left box a cytoplasmic area.

within statistical uncertainty.

In applying the $RSF_{x/ref}$ values for the quantification of intracellular elemental concentrations, we have assumed that the $RSF_{x/ref}$ values are not dependent on analyte concentration. To test this assumption, the three homogenate samples were spiked with B levels of 359, 682, and 1329 ppm. Statistically identical $RSF_{x/ref}$ values were calculated for each, indicating a constant B $RSF_{x/ref}$ over this concentration range. Further studies to determine linear $RSF_{x/ref}$ ranges and cell-line-to-cell-line $RSF_{x/ref}$ variability are planned in our laboratory.

Imaging System Calibration. Table IV lists typical fitting parameters for the calibration of CCD pixel values to EM count rates at MCP gains of 1748 and 1958 V (gains of 60% and 70%, respectively). All curves are strongly linear, with the slopes at 70% gain being slightly more than twice the slopes at 60% gain. Lighter ions generally generate steeper calibration curves than heavier ones. The intercept values are very small compared to the maximum allowable CCD pixel value of 16 383, a result of the low noise character of the MCP–PS–CCD image detector combination. Because of their small magnitudes, the intercept values were found to have no statistically significant impact on the image quantification results presented below; i.e. the intercept term in the CCD pixel value to EM count rate linear calibration equation can be justifiably omitted.

Three calibrations were performed over a 6-week period to monitor calibration reproducibility. Individual calibration slopes varied significantly over this period, probably because the responses of the EM and MCP-PS slowly degrade with use. For the image quantification scheme investigated here, however, variation of the analyte calibration slopes with respect to the calibration slope of $^{12}C^+$ is the relevent calibration characteristic. Ratios of analyte slopes to carbon slope from the three calibration sessions are listed in Table V. No statistical difference was found between the two MCP gains. Reproducibility of analyte-to-carbon slope ratios is quite good, with relative standard deviations ranging from 1.1% to 8.5%. In practical terms, this indicates that frequent system calibration is not critical. This is fortuitous, because completion of the calibration procedure requires several hours of data acquisition and analysis.

Quantitative Imaging of Intracellular Elements. Ion micrographs of $^{41}K^+$, $^{40}Ca^+$, $^{12}C^+$, and $^{11}B^+$ from several Swiss 3T3 fibroblasts treated with 100 μg/mL $Na_2B_{12}H_{11}SH$ are shown in Figure 3. Cell nuclei are easily discernible in the $^{40}Ca^+$ micrographs because nuclear Ca signals are low relative to cytoplasmic levels. A region adjacent to one side of the nucleus (perinuclear) exhibited markedly elevated $^{40}Ca^+$ signals in nearly all of the Swiss 3T3 fibroblasts analyzed.

Table III. Cell Homogenate Analyses: ICP-AES and IM Results with Calculated $RSF_{x/ref}$ Values[a]

		NRK1			NRK2			3T3		
analyte	f_x	i_x/i_{ref}	C_x, ppm	$RSF_{x/ref}$	i_x/i_{ref}	C_x, ppm	$RSF_{x/ref}$	i_x/i_{ref}	C_x, ppm	$RSF_{x/ref}$
$^{10}B^+$	0.20	2.4 (0.2) × 10^{-2}	359 (2)	3.4 (0.3) × 10^2	9.5 (0.9) × 10^{-2}	1329 (9)	3.6 (0.4) × 10^2	4.9 (0.5) × 10^{-2}	682 (4)	3.6 (0.4) × 10^2
$^{11}B^+$	0.80	9.0 (0.8) × 10^{-2}	359 (2)	3.1 (0.3) × 10^2	3.6 (0.3) × 10^{-1}	1329 (9)	3.4 (0.3) × 10^2	1.8 (0.2) × 10^{-1}	682 (4)	3.4 (0.4) × 10^2
$^{23}Na^+$	1.000	1.5 (0.4) × 10^2	3790 (40)	4.1 (1.1) × 10^4	1.7 (0.4) × 10^2	4220 (30)	4.1 (0.9) × 10^4	9.8 (2.3) × 10^1	2200 (20)	4.4 (1.1) × 10^4
$^{24}Mg^+$	0.7899	3.5 (0.3)	1134 (6)	3.9 (0.3) × 10^3	3.7 (0.4)	1143 (5)	4.1 (0.5) × 10^3	1.8 (0.2)	586 (3)	3.8 (0.4) × 10^3
$^{39}K^+$	0.9326	9.6 (2.4) × 10^1	2010 (90)	5.1 (1.3) × 10^4	8.9 (1.5) × 10^1	1830 (60)	5.2 (0.9) × 10^4		bdl[b]	
$^{40}Ca^+$	0.9694	7.4 (0.7) × 10^{-1}	83.6 (0.9)	9.1 (0.9) × 10^3	1.0 (0.1)	133.8 (0.1)	8.9 (1.0) × 10^3	8.8 (1.0) × 10^{-1}	98.0 (0.5)	9.3 (1.1) × 10^3
$^{41}K^+$	0.0673	6.1 (0.9)	2010 (90)	4.8 (0.7) × 10^4	6.7 (1.3)	1830 (60)	5.3 (1.0) × 10^4		bdl[b]	

[a] Values are reported as mean (standard deviation); $n = 9$ for i_x/i_{ref} entries; $n = 4$ for C_x entries. [b] bdl: signal below the ICP-AES detection limit.

Table IV. Linear Least-Squares Fitting Parameters for Typical Calibration Plots of CCD Pixel Values per Second versus EM Counts per Pixel per Second

	G_{MCP} = 1748 V			G_{MCP} = 1956 V		
analyte	slope	intercept	*r*	slope	intercept	*r*
$^{11}B^+$	69.41	−0.8919	0.99996	146.6	−2.543	0.99946
$^{12}C^+$	65.42	−0.9896	0.99996	134.6	−.5563	0.99999
$^{23}Na^+$	49.31	−0.2677	0.99995	110.8	−1.594	0.99978
$^{24}Mg^+$	51.27	−0.0628	0.99995	113.8	.0694	0.99997
$^{40}Ca^+$	42.33	0.4099	0.99993	97.30	−0.9351	0.99982
$^{41}K^+$	43.24	−0.5682	0.99998	94.16	0.3785	0.99999

Table V. Ratios of Analyte-to-Carbon Slopes from Three Calibrations of CCD Pixel Values to EM Count Rates Performed over a Six-Week Period[a]

	slope M^+/slope $^{12}C^+$	
analyte	G_{MCP} = 1748 V	G_{MCP} = 1956 V
$^{11}B^+$	1.07 (0.02)	1.08 (0.05)
$^{23}Na^+$	0.83 (0.06)	0.82 (0.01)
$^{24}Mg^+$	0.85 (0.06)	0.84 (0.01)
$^{40}Ca^+$	0.71 (0.06)	0.73 (0.02)
$^{41}K^+$	0.71 (0.05)	0.71 (0.02)

[a] Values are reported as mean (standard deviation).

Concentration data were therefore generated from three regions of each cell: nuclear, perinuclear, and cytoplasmic. These regions were identified by eye during image processing of the $^{40}Ca^+$ micrographs and delineated with boxes. After image registration, identical areas within the $^{11}B^+$, $^{12}C^+$, $^{23}Na^+$, $^{24}Mg^+$, and $^{41}K^+$ micrographs were also delineated. Boxes indicating the analytical areas are shown on a single cell in each ion micrograph in Figure 3 to illustrate this process. Dry weight analyte concentrations from similar regions in each analyzed cell were generated from eq 6. These calculations used y_x/y_{ref} values from Table V and $RSF_{x/ref}$ values of 3.3 × 10^2 for B, 4.2 × 10^4 for Na, 3.93 × 10^3 for Mg, 5.1 × 10^4 for K, and 9.1 × 10^3 for Ca.

The concentration results are listed in Table VI. Levels of K were roughly an order of magnitude higher than those of Na, in agreement with basic electrophysiology. While K, Na, and Mg exhibited reasonably homogeneous distributions, both Ca and B were distributed quite heterogeneously. It is particularly interesting to note that although both Ca and B were concentrated mainly in the cytoplasm, B levels were relatively low in the Ca-rich perinuclear region. Further studies of the uptake of boronated BNCT agents by tumor cells are in progress in our laboratory.

Because electron probe X-ray microanalysis (EPXMA) is currently the favored technique for cellular elemental microanalysis, a comparison of the IM data with published EPXMA values is warranted. A number of EPXMA studies of cultured cells have been published (e.g. ref 25–29), but most have used nonphysiological washing solutions such as $NH_4C_2H_3O_2$, NH_4NO_3, sucrose, or deionized water to remove the cellular nutrient medium. A recent study by Tvedt et al. avoided the use of washing solutions by using a perpendicular cryosectioning approach (*30*). Table VII presents comparison the EPXMA results of Tvedt et al. with our IM results. As is accepted practice in the EPXMA literature, values are reported as mmol/kg dry weight (standard error of the mean). There is good agreement between the two techniques, except that the IM Na levels are somewhat higher.

Although the IM is clearly an imaging technique with high elemental sensitivity, the estimation of detection limits for elements in the cellular matrix is problematic. Detection limits are typically defined as the concentration of an analyte that produces a signal equal to 2 or 3 times the standard deviation of the blank signal. Blanks for major physiological metals in the cellular matrix are not easily prepared. However, animal cells generally contain very little B, and so can be considered a suitable blank for the estimation of B detection limits. The standard deviation of pixel values from 20 × 20 pixel areas in three control Swiss 3T3 fibroblasts analyzed exactly as the other fibroblasts in this study averaged 15.3 pixel units (on a pixel unit scale of 0 to 16383). Raw $^{11}B^+$ signals averaging 757 pixel units were used to generate the 563 ppm cytoplasmic B level reported for $Na_2B_{12}H_{11}SH$ treated cells in Table VI. The B concentration that would give rise to a signal of 45.9 pixel units (3 times the standard deviation of the blank signal) is therefore 34 ppm dry weight. By use of the relative elemental sensitivities listed in Table III, detector calibration slopes from Table V, a 15.3 pixel unit blank standard deviation value, and an image acquisition time of 150 s, dry weight detection limit estimates of 0.36 ppm K, 0.40 ppm Na, 2.1 ppm Ca, and 4.0 ppm Mg can be calculated for the instrumental conditions used in this study. These values ignore spectral interferences and are presented only as very rough estimates. For comparison, an optimal detection limit of 1 mmol/kg dry weight is often quoted for biological EPXMA (*31*, *32*).

Several sources of uncertainty in our elemental quantification protocol should be pointed out. Our method assumes that the intracellular ^{12}C concentration is proportional to the cellular dry weight concentration at each resolvable location within the cell. Considering the moderate spatial resolving power of the IM, this is a good approximation. A second assumption is that the analyte signals are not dependent on the analyte's chemical state in the cellular matrix. This point is difficult to investigate, but the largely homogeneous IM images of K^+, Na^+, Mg^+, and C^+ obtained from fractured cells suggest an absence of significant chemical-state effects. Additionally, we have reported previously that small cytoplasmic granules may possess sputter rates differing from that of the general cytosol (*14*), so that the quantitative uncertainty associated with signals from small cytoplasmic structures is difficult to estimate. Because such structures are generally too small to be resolved by the IM, the effects of this phe-

Table VI. Dry Weight Elemental Concentration Results from Nuclear, Perinuclear, and Cytoplasmic Cellular Regions of Swiss 3T3 Fibroblasts[a]

	K, %	Na, %	Mg, %	Ca, ppm	B, ppm
			Control, *n* = 38		
nuclear	4.65 (0.9)	0.55 (0.18)	0.17 (0.02)	255 (43)	bdl[b]
perinuclear	4.09 (0.9)	0.59 (0.16)	0.15 (0.02)	455 (71)	bdl
cytoplasmic	4.44 (1.0)	0.65 (0.19)	0.18 (0.03)	355 (58)	bdl
			B Treated, *n* = 31		
nuclear	5.17 (1.3)	0.43 (0.12)	0.19 (0.03)	220 (46)	170 (40)
perinuclear	4.68 (1.1)	0.50 (0.17)	0.17 (0.03)	499 (110)	254 (60)
cytoplasmic	4.92 (1.1)	0.49 (0.12)	0.18 (0.03)	375 (89)	563 (160)

[a] Values are reported as mean (standard deviation). [b] bdl: below detection limit.

Table VII. Comparison of IM Elemental Concentration Results with X-ray Microanalysis Results of Tvedt et al.[a]

	K	Na	Mg	Ca	B
			Control, n = 38		
nuclear	1190 (38)	240 (12)	70 (1)	6.4 (0.2)	bdl
perinuclear	1150 (36)	260 (11)	62 (1)	11.4 (0.3)	bdl
cytoplasmic	1130 (43)	280 (14)	72 (2)	8.9 (0.2)	bdl
			B Treated, n = 31		
nuclear	1320 (59)	190 (9)	76 (2)	5.5 (0.2)	16 (1)
perinuclear	1200 (53)	220 (14)	69 (2)	12.4 (0.5)	23 (1)
cytoplasmic	1260 (49)	210 (10)	75 (2)	9.4 (0.4)	52 (3)
			Tvedt et al.[b]		
	1294 (37)	147 (31)	62 (3)	-1.0 (1.0)[c]	*d*

[a] Values are reported as mean mmol/kg dry weight (standard error of the mean). [b] n = 43; whole cell concentrations were reported. [c] Not significantly different from zero. [d] Not reported.

nomenon typically are not detectable.

The precision of our intracellular concentration results and their excellent agreement with values from the EPXMA literature argue that the above shortcomings are not serious, and that the IM is a reliable technique for cellular microanalysis. Strengths of the IM technique include a simple and quick sample preparation method for cultured cells, broad elemental scope, high elemental sensitivity, and the intuitive advantages of data which is output directly as real time images. The IM opens new avenues of biomedical research, because it can quantitatively image the distributions of many elements present in concentrations far below EPXMA detection limits. The capability of the IM to perform isotopic analyses additionally suggests exciting possibilities for the investigation of elemental homeostasis and transport with stable isotopes.

ACKNOWLEDGMENT

We gratefully acknowledge Ellie Kable and the Cornell Biophysics Tissue Culture Facility for culture assistance, David L. Miller and William Bauer of Idaho National Engineering Laboratory for preliminary ICP-AES studies, Mike Rutzke of the Pomology Analytical Laboratory at Cornell for the ICP-AES analyses used in this study, and David Mantus for many helpful discussions. We additionally thank K. E. Tvedt of the University of Trondheim and *Journal of Microscopy* for permission to include the EPXMA results.

LITERATURE CITED

(1) Rouberol, J. M.; Lepareur, M.; Autier, B.; Bourgot, J. M. *8th International Conference on X-Ray Optics and Microanalysis and 12th Annual Conference of the Microbeam Analysis Society*, Boston, MA, 1977; pp 133A–133D.
(2) Morrison, G. H.; Slodzian, G. *Anal. Chem.* **1975**, *47*, 932A–943A.
(3) Patkin, A. J.; Chandra, S.; Morrison, G. H. *Anal. Chem.* **1982**, *54*, 2507–2510.
(4) Burns, M. S.; File, D. M.; Deline, V.; Galle, P. *Scanning Electron Microsc.* **1986**, *IV*, 1277–1290.
(5) Brenna, J. T.; Morrison, G. H. *Anal. Chem.* **1986**, *58*, 1675–1680.
(6) Hallegot, P.; Galle, P. *Radiat. Environ. Biophys.* **1988**, *27*(1), 67–78.
(7) Schaumann, L.; Galle, P.; Thellier, M.; Wissocq, J. C. *J. Histochem. Cytochem.* **1988**, *36*(1), 37–39.
(8) Mentre, P.; Escaig, F. *J. Histochem. Cytochem.* **1988**, *36*(1), 49–54.
(9) Burns, M. S. *Soc. Neurosci. Abstr.* **1988**, *14*(1), 618.
(10) Fragu, P.; Larras-Regard, E. *Bio. Cell* **1988**, *62*(2), 145–155.
(11) Sod, E. W.; Morrison, G. H.; Crooker, A. R., submitted for publication in *J. Microsc.* (*Oxford*).
(12) Chandra, S.; Morrison, G. H.; Wollcott, C. C. *J. Microsc.* (*Oxford*) **1986**, *144*, 15–37.
(13) Chandra, S.; Ausserer, W. A.; Morrison, G. H. *J. Microsc.* (*Oxford*) **1987**, *148*, 223–239.
(14) Ausserer, W. A.; Chandra, S.; Morrison, G. H. *J. Microsc.* (*Oxford*) **1989**, *154*, 39–57.
(15) *Neutron Capture Therapy*; Hatanaka, H., Ed.; MTP: Norwell, MA, 1986.
(16) Zierold, K.; Pietruschka, F.; Schafer, D. *Microsc. Acta* **1979**, *81*(5), 361–366.
(17) Ceder, O.; Roomans, G. M.; Hosli, P. *Scanning Electron Microsc.* **1982**, *II*, 723–730.
(18) Werner, H. W. *SIA, Surf. Interface Anal.* **1980**, *2*(2), 56–74.
(19) Ramseyer, G. O.; Morrison, G. H. *Anal. Chem.* **1983**, *55*, 1963–1970.
(20) Ling, Y.-C.; Bernius, M. T.; Morrison, G. H. *J. Chem. Inf. Comput. Sci.* **1987**, *27*, 86–94.
(21) Hiraoka, Y.; Sedat, J. W.; Agard, D. A. *Science* **1987**, *238*, 36–41.
(22) Sweedler, J. V.; Bilhorn, R. B.; Epperson, P. M.; Sims, G. R.; Denton, M. B. *Anal. Chem.* **1988**, *60*, 282A–291A.
(23) Aikens, R. S.; Agard, D. A.; Sedat, J. W. In *Methods in Cell Biology, Vol. 29, Fluorescence Microscopy of Living Cells in Culture, Part B.* Wang, Y. L., Taylor, D. L., Eds.; Academic: New York, 1989; pp 291–313.
(24) Mantus, D. S.; Turner, L. K.; Morrison, G. H., paper in preparation.
(25) James-Kracke, M. R.; Sloane, B. F.; Shuman, H.; Karb, R.; Somlyo, A. P. *J. Cell Physiol.* **1980**, *103*, 313–322.
(26) Wroblewski, J.; Roomans, G. M.; Madsen, K.; Friberg, U. *Scanning Electron Microsc.* **1983**, *II*, 777–784.
(27) Wroblewski, J.; Roomans, G. M. *Scanning Electron Microsc.* **1984**, *IV*, 1875–1882.
(28) Abraham, E. H.; Donovan, C. B.; Lange, D. E. In *Microbeam Analysis* **1984**; Romig, A. D., Goldstein, J. I. Eds.; San Francisco Press: San Francisco, CA, 1984; pp 285–289.
(29) Abraham, E. H.; Breslow, J. L. Epstein, J.; Chang-Sing, P.; Lechene, C. *Am. J. Physiol.* (*Cell Physiol.*) **1985**, *17*, C154–C164.
(30) Tvedt, K. E.; Halgunset, J.; Kopstad, G.; Haugen, O. A. *J. Microsc.* (*Oxford*) **1988**, *151*(1), 49–59.
(31) Hall, T. A. *Ultramicroscopy* **1988**, *24*, 181–184.
(32) Johnson, D.; Izutsu, K.; Cantino, M.; Wong, J. *Ultramicroscopy* **1988**, *24*, 221–236.

RECEIVED for review July 21, 1989. Accepted October 2, 1989. This work was supported by grants from the National Institutes of Health, the DOE-funded PBF/BNCT Program for Cancer Treatment, and the National Science Foundation. The Cornell NIH/NSF Developmental Resource for Biophysical Imaging and Optoelectronics was used in culturing the cells.

Determination of Phosphorus in Zircons by Inductively Coupled Plasma Atomic Emission Spectrometry

J. C. Fariñas

Departamento de Análisis Químico, Instituto de Cerámica y Vidrio, CSIC, 28500 Arganda del Rey, Madrid, Spain

A method for phosphorus determination in zircons by inductively coupled plasma atomic emission spectrometry has been developed. Sample decomposition is achieved by means of Na_2CO_3 + ZnO sintering in a platinum crucible at 950 °C for 45 min and subsequent leaching with water of the attacked product. P is separated from the matrix by means of yellow molybdophosphoric acid complex formation and isobutyl acetate extraction. The analyses are performed in an aqueous phase after complex decomposition with (1 + 4) HNO_3 and evaporation of the organic extractant. The lowest quantitatively determinable concentration is 1.8 μg mL^{-1} P_2O_5. The method was tested on zircon BCS-388 with a certified P_2O_5 value of 0.12%. Short- and long-term precision and method precision reached relative standard deviations of 1.64%, 3.36%, and 2.50%, respectively. The accuracy of the method is excellent.

INTRODUCTION

Zircon ($ZrSiO_4$) is a raw material widely used in the manufacture of ceramics and glass. Its technological relevance derives fundamentally from its high refractoriness (dissociation temperature = 1676 ± 7 °C). Among its many applications the following should be mentioned as particularly important: in the ceramic and glass industry it is employed in roofs for tunnel and blast furnaces; in metal foundry it finds application in continuous casting nozzles, in blast furnace bellies, and in refractory linings for casting ladles; in the field of new and advanced ceramic materials it is the fundamental raw material for the production of zirconia (ZrO_2). The most important properties of zircon-based materials are the high thermal shock resistance and the high chemical resistance to alkali and slag attack. In addition and most essentially, zircon does not present any structural transformation below its dissociation temperature.

The impurities that are generally found in zircon comprise major fractions of Al_2O_3, Fe_2O_3, TiO_2, and HfO_2 and minor portions of MgO, MnO, NiO, Na_2O, K_2O, and P_2O_5. The presence of these impurities can have a negative impact on the aforementioned properties of these materials, degrading them considerably. Hence, accurate and reliable analytical impurity control is indispensable. For instance P_2O_5, which is found in zircons in concentrations in the order of 0.1%, is a component that must be rigorously quantified. Nevertheless, in the literature on chemical analysis of zircons (*1–9*) no phosphorus determination method is mentioned. The general literature on silicate materials, however, contains frequent references to the determination of this element. The most widely used method is spectrophotometric analysis, either through yellow molybdovanadophosphoric acid complex formation (*10*) or by means of the blue molybdophosphoric acid complex obtained from the respective yellow molybdophosphoric acid complex by reduction with either ascorbic acid (*11–17*), ferrous ammonium sulfate (*18, 19*) or tin(II) oxalate (*20*). The interference of Si, forming colored complexes analogous to those of P, has been eliminated by (a) HF attack (*10–13, 19*), (b) pH control (*18*), (c) pH control and limiting free molybdate ion concentration (*16*), (d) pH control and addition of Fe(III) in excess (*20*), and (e) tartaric acid addition (*14*).

Kuroda et al. (*21*) applied flow injection analysis (FIA) in combination with blue molybdophosphoric complex spectrophotometric detection to P determination in silicate rocks.

Riddle and Turek (*22*) described an indirect method for P determination in rocks through yellow molybdophosphoric acid complex formation, organic solvent extraction, complex decomposition, and determination of the molybdenum released in the aqueous phase by atomic absorption spectrometry.

Direct current plasma (DCP) and inductively coupled plasma atomic emission spectrometry (ICP-AES) were likewise utilized for P determination in silicates, in spite of the fact that this element possesses only scarce emission lines (*23*) which, in addition, are little sensitive, so that P is one of the elements that presents the highest detection limits in ICP (*24*). Bankston et al. (*25*) used the 214.914-nm line for P determination through DCP after solubilizing the samples by $LiBO_2$ fusion in a graphite crucible. Cook and Miles (*26*), Burman (*27*), and McLaren et al. (*28*) used the lines at 178.287, 213.618, and 214.914 nm, respectively, for P determination by ICP, solubilizing the samples with HF attack in a platinum or PTFE dish. In all cases the lines used were free of spectral interferences. However, the detection limits of this element are not reported in any of the publications mentioned.

In a previous work, Fariñas and Valle (*29*) studied impurity determination (Al, Fe, Mg, Ti, Ni, Mn, and P) in zircons by ICP. The zircon samples were dissolved by fusion in a platinum crucible of 0.2 g of zircon with 2 g of a mixture of Na_2CO_3 + $Na_2B_4O_7$; the melt was solubilized in 10% HCl and diluted to 200 mL. Although the first six elements could be accurately quantified by ICP, P resisted analysis, as P concentration was below the detection limit of any of its analytical lines. This was attributed to the considerable increase of the spectral background by the complex matrix resulting from the dissolution of the sample, together with the severe spectral interferences caused basically by Zr, rich in emission lines, as well as by other elements, such as Hf, Ti, and Cr.

The aim of this research is to develop a convenient method for reliable and accurate P determination in zircons by ICP-AES. The procedure comprises several steps, starting with a preconcentration of the element and separation of the matrix containing the solubilized P by means of Na_2CO_3 + ZnO attack, yellow molybdophosphoric acid complex formation, extraction with an organic solvent, followed by decomposition to transfer P to an aqueous acid phase, where this element is measured by ICP.

EXPERIMENTAL SECTION

Apparatus. A Jobin-Yvon Model JY-38 VHR sequential spectrometer with an ICP source was used. This is equipped with a 56-MHz radio frequency generator and a 1-m Czerny-Turner monochromator with a 3600 lines mm^{-1} grating. The output, induced, and reflected powers are 2200, 1600, and <5W, respectively. The reciprocal linear dispersion is 0.26

0003-2700/89/0361-2696$01.50/0 © 1989 American Chemical Society

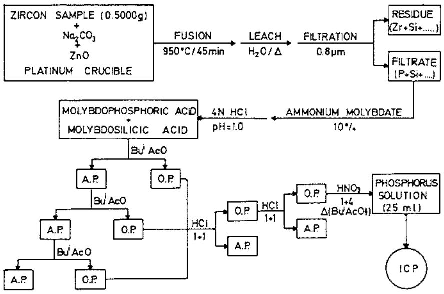

Figure 1. Schematic diagram for ICP determination of phosphorus in zircons (Bu^i AcO, isobutyl acetate; O.P., organic phase; A.P., aqueous phase).

nm mm^{-1} (first order) and the resolution is 0.0026 nm. The entrance and exit slits have a width of 30 μm and a height of 20 mm. The photomultiplier is a Hamamatsu R106. The spectral range is 170–500 nm. An Apple IIe with 64K byte memory is used for instrument control and analytical processing of intensity data. The torch is a Durr-JY/Plasmatherm, demountable, with an alumina injector and a sheathing gas tube. The sample is introduced by use of a Meinhard TR30-C2 high salt concentric glass nebulizer with a humidifier on the argon aerosol carrier inlet. The spray chamber is a coaxial Scott type. A peristaltic pump from P.S. Analytical, Ltd., set at 2.1 mL min^{-1} is used for sample delivery. The cooling, sheathing, and aerosol carrier gas flow rates are 16, 0.4, and 0.3 L min^{-1} of argon, respectively. The flow rate of the cooling water for the coils is 130 mL min^{-1}. The measurement time is 3 integrations of 400 ms step^{-1}.

Reagents. A phosphorus standard stock solution (1000 μg mL^{-1} P_2O_5) was prepared by dissolving in water 1.9174 g of KH_2PO_4 (Merck R.A.), which had been dried previously at 70 °C for 1 h, and diluting it to 1000 mL.

A solution containing 0.03% (m/v) Mo was prepared by dissolving 0.55 g of ammonium molybdate (Johnson Matthey Specpure) in water and diluting it to 100 mL.

A 10% ammonium molybdate solution was obtained by dissolving 25.00 g of $(NH_4)_6Mo_7O_{24}{\cdot}4H_2O$ (Merck R.A.) in water and diluting it to 250 mL. All reagents used were Merck R.A. products. The water was distilled and deionized (>18 MΩ).

Procedure. The general procedure used for P determination in zircons is exemplified in the scheme shown in Figure 1.

Decomposition of the Sample. A 0.5000-g portion of the zircon sample dried at 110 °C for 2 h was thouroughly mixed with 1.50 g of Na_2CO_3 and 0.50 g of ZnO in a platinum crucible, covered with a platinum cap and treated in a muffle furnace at 950 °C for 45 min. The mixture was allowed to cool slightly and then transferred to a vessel with 50 mL of hot water. The vessel was heated until all solids had been separated from the walls of the crucible. Then the mixture was heated to the boiling point and kept there for 10 min. Subsequently, the hot mix was filtered through a 0.8-μm Millipore filter and the residue washed out with three flushes of 10 mL of hot water.

Yellow Molybdophosphoric Acid Complex Formation. Once the filtrate had cooled to room temperature, 20 mL of 10% ammonium molybdate solution was added. The pH, measured by using a calibrated glass electrode, was adjusted to 1.0 by adding 4 N HCl. Subsequently, the solution was stirred for 5 min.

Extraction of the Yellow Molybdophosphoric Acid Complex. The solution was treated 3 times with 30-mL portions of isobutyl acetate in a separatory funnel, under stirring for 3 min during each treatment. The three organic portions were collected together and washed twice with 30 mL of (1 + 1) HCl.

Decomposition of the Yellow Molybdophosphoric Acid Complex. The organic fraction was poured into a vessel containing 10 mL of (1 + 4) HNO_3 and was carefully heated until isobutyl acetate evaporation was complete. The resulting nitric solution was transferred to a 25-mL volumetric flask and diluted to volume with (1 + 4) HNO_3.

Calibration and ICP Analysis. Calibration was done with two solutions containing 20 and 30 μg mL^{-1} P_2O_5 and prepared with (1 + 4) HNO_3 from the standard stock phosphorus solution. Determination of phosphorus was performed directly in the nitric solution of the sample using the P I line at 253.565 nm.

RESULTS AND DISCUSSION

Yellow molybdophosphoric acid complex formation in the presence of major quantities of Si has proved to be perfectly possible, as was shown by Riddle and Turek (*22*) with the method developed for P determination in silicates, for which these authors recommend a silicon to phosphorus ratio of ca. 400:1 or less. For zircons with a standard content of 33% SiO_2 and 0.1% P_2O_5, this ratio would then be 350:1. Similarly, the complex was formed in solutions obtained through silicates fusion with $LiBO_2$ or $Li_2B_4O_7$ (*14–16*, *20*, *25*) or with Na_2CO_3 (*18*), which means that the presence of these flux agents in the solution does not inhibit yellow molybdophosphoric acid complex formation.

To find out whether the presence of Zr in the sample solution had some effect, it was attempted, firstly, to dissolve the zircon with the aforementioned fluxes. $LiBO_2$ and $Li_2B_4O_7$ fluxing was tested in a graphite as well as in a platinum crucible by attacking the fusion product with (1 + 9) HCl or (1 + 24) HNO_3, but in no case was sample solubilization attained. Fusion with Na_2CO_3 in a platinum crucible did not succeed in dissolving the zircon. Even after HF attack in combination with a mineral acid (H_2SO_4, $HClO_4$, and HNO_3 + $HClO_4$) in a platinum dish, the sample remained unaffected by the attack in all cases. In light of these results, Na_2CO_3 + $Na_2B_4O_7$ flux was used, which had been used in a previous work by Fariñas and Valle (*29*). With this latter attack, as was mentioned in the introductory section of this paper, zircon is completely dissolved. Nevertheless, addition of a 10% ammonium molybdate solution to the sample solution produced an abundant white precipitate that could not but be attributed to the presence of Zr. This fact was effectively corroborated when adding the reagent to a Zr solution obtained through $ZrOCl_2{\cdot}8H_2O$ dissolution in water. This precipitate is soluble only in either highly acid or extremely basic media but not in the vicinity of pH = 1 where yellow molybdophosphoric acid complex formation occurs. Hence, it is absolutely necessary for P to be totally free of any presence of Zr.

P has been separated from Zr in zircons through extraction by means of Amberlite LA-1 and malonic acid (*9*) and by means of Amberlite LA-2 and chloroform (*2*, *3*). However, in both cases it is necessary to start from small fractions of the sample solution containing ca. 50 μg and 10 mg Zr, respectively, while it would be desirable to start from the largest sample amount possible, in order to obtain a solution with a maximum P concentration, to compensate for the poor ICP sensitivity of this element. For effective P separation, zircon sample was attacked with Na_2CO_3 + ZnO in platinum crucible, which actually is a sintering or solid-state reaction, since the reagents do not achieve fusion. According to Debras-Guédon (*30*) this attack, which he used for B determination in different raw materials and industrial ceramic products, completely dissolves the elements F, Cl, S, B, and P, while the major part of oxides are retained in the insoluble residue, such as SiO_2, Al_2O_3, and TiO_2. Langer and Baumann (*12*) used this attack for F determination in silicates. The authors mentioned differ, however, about the working conditions: while the former treated 0.1 g of the sample, together with 0.3 g of Na_2CO_3 and 0.1 g of ZnO at 800 °C for 30 min, the latter used 0.01, 0.44, and 0.11 g, respectively, at 800–850 °C for 15 min. In this research Debras-Guédon's conditions were used, since the Na_2CO_3 and ZnO ratio to the sample is much lower. Nevertheless, at the temperature and treatment time used by this author for the attack, the solubilized P amount, which was determined following the procedure described in the Experimental Section, was hardly detectable, which may be due to the high refractoriness of the material. It was necessary to apply the attack at 950 °C and for 45 min to achieve quantitative solubilization of P. In addition, this treatment renders the Zr almost insoluble: ICP determination of Zr yielded only 0.02% of solubilized ZrO_2, with the advantage that the problems of Zr precipitation with ammonium molybdate are avoided. The solubilized Si fraction, likewise determined by ICP, amounted to 8.8% SiO_2, which is equivalent to an Si:P ratio of ca. 95:1 and constitutes a favorable environment for yellow molybdophosphoric acid complex formation. ICP analysis of other oxides, such as Al_2O_3 and TiO_2, showed that they are entirely retained in the insoluble residue. Another additional advantage is that when the attacked product is leached with water and not with acids as in fusion, a slightly alkaline solution is obtained, which is easy to bring down to pH = 1, when adding diluted HCl. As a consequence, this zircon decomposition method was chosen, since it allows in a single operation and simultaneously both quantitative P solubilization and its separation from practically the entire amount of Zr and from the major part of the Si. However, the solution obtained with this attack cannot be injected into the plasma due to its high saline component.

P separation from the saline matrix was performed through yellow molybdophosphoric acid complex formation, following the conditions proposed by Riddle and Turek (*22*): reaction with a 10% ammonium molybdate solution and at pH = 1.0 obtained with a 4 N HCl addition. This complex can then be separated selectively from the yellow molybdosilicic acid complex, which is likewise built up, using an organic extractant depending on the pH of the solution (*31*). The most common extractants used for complex separation are diethyl ether (*31*), isobutyl acetate (*32*), n-butyl acetate (*31*), isoamyl acetate (*33*), methyl isobutyl ketone (*31*), diethyl ether–1-pentanol (5:1) (*22, 31*) or (3:1) (*32*), and chloroform–1-butanol (4:1) (*31, 34*) or (3:1) (*35*). In this work isobutyl acetate was chosen as the extractant, as it allows for quantitative extraction of the yellow molybdophosphoric acid complex at pH = 1.0. Treatment of the organic extract with a (1 + 1) HCl solution removes all excess molybdate.

The introduction of organic solutions into the plasma may cause instability problems. Hence an auxiliary gas is required (generally oxygen). In addition, it is necessary to prepare the calibration standard solutions in the respective organic medium, which is known to be laborious and messy. This is why it was preferred to decompose the complex and transfer it again to an aqueous solution, which can be done either by means of back extraction with an ammonium hydroxide–ammonium chloride buffer solution (*22, 31*) or by means of evaporation of the organic extractant in the presence of (1 + 4) HNO_3 (*36*). The former of these treatments yields an alkaline solution, which proves to be less stable in plasma and which, in addition, has a high salt content with the consequential inconvenience of having to work with a high volume end solution (100 or 200 mL). The second treatment, on the contrary, gives rise to a diluted acid solution, which permits a high concentration of the final solution (25 mL), so that this method was considered the better option for yellow molybdophosphoric acid complex decomposition.

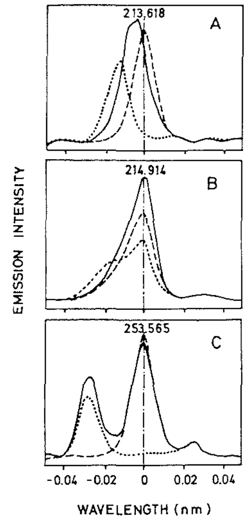

Figure 2. Wavelength scans in the vicinity of the P I 213.618 (A), 214.914 (B), and 253.565 (C) nm lines: ---, 25 $\mu g\ mL^{-1}$ P_2O_5 in (1 + 4) HNO_3; ···, 0.03% (m/v) Mo; ——, sample solution.

The final solution only contains Mo as a potential source of interferences for the emission lines of P. Possible spectral interferences were studied by means of ±0.05 nm wavelength scans in the vicinity of the most sensitive P lines (*23*) performed with the sample solution, a 25 $\mu g\ mL^{-1}$ P_2O_5 solution and a 0.03 % (m/v) Mo solution (this latter level is approximately the Mo present in the sample solution). The P I line at 213.618 nm, which is the most sensitive one, is interfered with by the Mo II line at 213.606 nm, giving rise to a peak in the sample solution corresponding to the joint contribution of P and Mo, as shown in Figure 2A. The P I line at 214.914 nm presents, as shown in Figure 2B, a Mo emission at the same wavelength, not reported in the literature. Nevertheless, the P I line at 253.565 nm is not interfered with by the unknown Mo emission at ca. 253.538 nm, as can be seen in Figure 2C. So this wavelength was chosen for analysis. It was found that, at this wavelength, the (1 + 4) HNO_3 has a depressing effect on the emission signal, whereas Mo does not exert any influence at all. To compensate for this matrix effect, the calibration standards were prepared with (1 + 4) HNO_3. The detection limit (concentration of analyte required to give a net signal equal to 3 times the standard deviation of the background) obtained experimentally is 0.36 $\mu g\ mL^{-1}$ P_2O_5. The lowest quantitatively determinable concentration is 1.8 $\mu g\ mL^{-1}$ P_2O_5, calculated as five times greater than the detection limit (*37*), which refers to a realistic value for quantitative analysis. This is equivalent to 0.009% P_2O_5 in the solid sample (starting from 0.5 g of sample and arriving at a final volume of 25 mL).

The precision and accuracy of the methodology developed were tested by analyzing zircon BCS-388 with a certified P_2O_5 value of 0.12%. Table I compiles the results obtained in short-term precision testing (10 consecutive determinations), long-term precision testing (10 determinations over 10 consecutive days), and method precision testing (10 determinations on 10 sample specimens). For each assay the mean value ($\bar{X}$), the standard deviation (s), and the relative standard deviation (RSD) are indicated. The precision and the accuracy

Table I. Phosphorus-Determination Results (% P_2O_5) in Zircon BCS-388 (Certified Value = 0.12% P_2O_5)

assay	$\bar{X}$	s	RSD
short-term precision[a]	0.122	0.002	1.64
long-term precision[b]	0.119	0.004	3.36
method precision[c]	0.120	0.003	2.50

[a] Ten consecutive determinations. [b] Ten determinations over 10 consecutive days. [c] Ten determinations on 10 sample specimens. Each determination is the mean of 10 400-ms integrations.

levels obtained from the three test series can be considered as very satisfactory.

Registry No. P, 7723-14-0; Zn, 14940-68-2.

LITERATURE CITED

(1) Sarudi, I. *Z. Anal. Chem.* **1950**, *131*, 416–423.
(2) Boix, A.; Debras-Guédon, J. *Chim. Anal.* **1971**, *53*, 459–469.
(3) Boix, A.; Debras-Guédon, J. *Bull. Soc. Fr. Céram.* **1971**, *92*, 3–14.
(4) Jaffrezic, H.; Decarreau, A.; Carbonnel, J. P.; Deschamps, N. *J. Radioanal. Chem.* **1973**, *18*, 49–53.
(5) Garg, A. N. *Radiochem. Radioanal. Lett.* **1979**, *39*, 319–328.
(6) Knyazeva, D. N.; Nikitina, I. B.; Korsakova, N. V.; Volchenkova, V. A. *Zavod. Lab.* **1982**, *48*, 16–18.
(7) Knyazeva, D. N.; Nikitina, I. B.; Korsakova, N. V.; Volchenkova, V. A. *Chem. Abstr.* **1983**, *98*, 26956q.
(8) Korte, N.; Kollenbach, M.; Donivan, S. *Anal. Chim. Acta* **1983**, *146*, 267–270.
(9) Narayanan, P.; Khopkar, S. M. *J. Liq. Chromatogr.* **1985**, *8*, 765–776.
(10) Baadsgaard, H.; Sandell, E. B. *Anal. Chim. Acta* **1954**, *11*, 183–187.
(11) Riley, J. P. *Anal. Chim. Acta* **1958**, *19*, 413–428.
(12) Langer, K.; Baumann, P. *Z. Anal. Chem.* **1975**, *277*, 359–368.
(13) Bodkin, J. B. *Analyst (London)* **1976**, *101*, 44–48.
(14) Whitehead, D.; Malik, S. A. *Analyst (London)* **1976**, *101*, 485–490.
(15) Watkins, P. J. *Analyst (London)* **1979**, *104*, 1124–1128.
(16) Iosof, V.; Neacsu, V. *Rev. Roum. Chim.* **1980**, *25*, 589–597.
(17) Kuroda, R.; Ida, I. *Fresenius' Z. Anal. Chem.* **1983**, *316*, 53–54.
(18) Chalmers, R. A. *Analyst (London)* **1953**, *78*, 32–36.
(19) Sala, J. V.; Hernandis, V.; Canals, A. *Analyst (London)* **1986**, *111*, 965–968.
(20) Ingamells, C. O. *Anal. Chem.* **1966**, *38*, 1228–1234.
(21) Kuroda, R.; Ida, I.; Oguma, K. *Mikrochim. Acta* **1984**, *I*, 377–383.
(22) Riddle, C.; Turek, A. *Anal. Chim. Acta* **1977**, *92*, 49–53.
(23) Wohlers, C. C. *ICP Inf. Newsl.* **1985**, *10*, 593–688.
(24) Winge, R. K.; Peterson, V. J.; Fassel, V. A. *Appl. Spectrosc.* **1979**, *33*, 206–219.
(25) Bankston, D. C.; Humphris, S. E.; Thompson, G. *Anal. Chem.* **1979**, *51*, 1218–1225.
(26) Cook, J. M.; Miles, D. L. *Analyst (London)* **1985**, *110*, 547–549.
(27) Burman, J. O. *ICP Inf. Newsl.* **1977**, *3*, 33–36.
(28) McLaren, J. W.; Berman, S. S.; Boyko, V. J.; Russell, D. S. *Anal. Chem.* **1981**, *53*, 1802–1806.
(29) Fariñas, J. C.; Valle, F. J. *An. Quím., Ser. B* **1987**, *83*, 310–318.
(30) Debras-Guédon, J. *Bull. Soc. Fr. Céram.* **1979**, *123*, 29–35.
(31) Simon, S. J.; Boltz, D. F. *Anal. Chem.* **1975**, *47*, 1758–1763.
(32) Tyson, J. F.; Stewart, G. D. *Anal. Proc.* **1981**, *18*, 184–187.
(33) DeSesa, M. A.; Rogers, L. B. *Anal. Chem.* **1954**, *26*, 1381–1383.
(34) Wadelin, C.; Mellon, M. G. *Anal. Chem.* **1953**, *25*, 1668–1673.
(35) Lapitskaya, E. V. *Glass Ceram.* **1982**, *39*, 521–522.
(36) Baialardo, A. M.; Coedo, A. G. *Rev. Metal. (Madrid)* **1973**, *9*, 35–38.
(37) Floyd, M. A.; Fassel, V. A.; D'Silva, A. P. *Anal. Chem.* **1980**, *52*, 2168–2173.

RECEIVED for review June 9, 1989. Accepted August 14, 1989.

Phosphine–Ozone Gas-Phase Chemiluminescence for Determination of Phosphate

Kitao Fujiwara*

Faculty of Integrated Arts and Sciences, Hiroshima University, Naka-ku, Hiroshima 730, Japan

Toshie Kanchi, Shin-ichiro Tsumura, and Takahiro Kumamaru

Department of Chemistry, Hiroshima University, Naka-ku, Hiroshima 730, Japan

Gas-phase chemiluminescence generated by mixing phosphine and ozone has been investigated. Various chambers for mixing ozone and phosphine were designed such as flashing ozone and phosphine in the opposite direction or injecting phosphine into ozone flow with the view of observing chemiluminescence: The noise power spectra in the chemiluminescence emission occurring in different chambers were given by the fast Fourier transform analysis. The color of chemiluminescence varied according to the concentration of phosphine: emission appears in the spectral range from 500 to 800 nm with peaks at 675 and 740 nm for introducing phosphine (concentration, about 15%); emission appears from 350 to 700 nm with the peaks at 530 and 675 nm for introducing phosphine (concentration, 103 ppm). For the quantitative analysis of phosphate, the sample solution was dried on the quartz boat, and then the aqueous $NaBH_4$ solution was applied to this dried phosphate and was dried again. Phosphine was generated by means of heating the dried mixture of phosphate and $NaBH_4$ at 480 °C, which was detected by the ozone gas phase chemiluminescence. The detection limit was 1 ng of P as phosphate and the linear dynamic range extends up to 5000 ng of P.

Several advantages can be counted for developing the conversion techniques of phosphate to phosphine, i.e., extension in applicable analytical method (*1*), elimination of sample matrix effects, and increase in sensitivity. In the previous papers (*2–4*), several methods have been proposed for phosphine generation, e.g., passing fine mists of aqueous solution of phosphate on a surface of heated graphite (*3*), or the solid phase reduction of phosphate by sodium tetrahydroborate (*4*). Especially, the latter method reproducibly gave the phosphine and is rather simple when compared to the former method.

In this paper, phosphine generated with the solid phase reduction of phosphate is detected by the gas-phase chemiluminescence with mixing ozone. In ref 3, we have studied the chemiluminescence detection of phosphate. However, the generation method of phosphine adopted was lacking in precision, and the detection limit was rather poor due to the low conversion efficiency. Thus, the instrumental and analytical conditions have to be reinspected for the gas-phase chemiluminescence detection of phosphine coupled with the solid-phase phosphine generation technique by sodium tetrahydroborate. The simple and high sensitive detection method of phosphate has been established.

0003-2700/89/0361-2699$01.50/0 © 1989 American Chemical Society

Table I. Summary of Instruments Used

ozone generator	Nippon Ozone Co., Type 0-3-2
spectrometer	Jasco, Type CT-25-C
multichannel detector	
PCD image sensor	Hamamatsu, Type S2304-512Q
detector	Type C2327
data processing unit	Type C2890
DMA interface	Type M2891
personal computer	NEC, PC9801 VX
printer	PC-PR201F2
scope	Trio, Type CS1577 (30 MHz)
Fourier transformation and general spectral observation	
analyzer (recorder)	Yokogawa, Type 3655E
FFT module	Yokogawa, Model 3659 20A
dc amplifier	Keithley, Type 427
dc (A/V) amplifier	NF Electronic, Type LI-76
function generator	NF Electronic, Model FG-121B
PM power source	Hamamatsu, C 488R
PM (photomultiplier)	Hamamatsu, R456
determination of phosphate	
electric furnace	Mitamura Riken, 400 W
digital thermometer	Nippo Electric, Type LM499
PM housing with electronic cooler	Hamamatsu, Type C659-A
PM	Type R649
photon counter	Type C2130
strip chart recorder	Hitachi, Model 056

It is well-known that phosphine ignites in the atmosphere and emits visible light, which is called ignis fatuus or will-o'-the-wisp (the flickering lights seen in darkness over marshland, peat bogs, and swamps) (*5*). However this luminescence was not well elucidated. As the phosphorus chemiluminescence of the room temperature, only the luminescence with oxidizing P_4 with addition of H_2O or D_2O has been previously reported by VanZee et al. (*6*). A spectroscopic characteristics of the chemiluminescence occurred by mixing phosphine and ozone or oxygen was, therefore, also give in this paper.

EXPERIMENTAL SECTION

Reagents. Phosphorous acid (H_3PO_3) of analytical grade was purchased from Wako Chemical Industries, Ltd., for producing large amounts of phosphine. A cylinder of the standard phosphine at 103 ppm diluted with helium (produced by Nippon Sanso Co., Ltd.) was used for continuous measurement of phosphine chemiluminescence.

The standard aqueous solution of phosphorus was made by dissolving potassium dihydrogen phosphate of analytical grade (Wako). Sodium tetrahydroborate used in this study was a tablet type (Nissoh Benthoron Co., Ltd.) of the grade for atomic absorption spectrometry. Selenium (SeO_2 in 0.5 mol/L HNO_3), lead ($Pb(NO_3)_2$ in 0.1 mol/L HNO_3), bismuth ($Bi(NO_3)_3$ in 0.8 mol/L HNO_3), germanium (K_2GeO_3 in 0.2 mol/L KOH), antimony ($SbCl_3$ in 2.8 mol/L HCl), arsenic (As_2O_3 in 0.05% NaCl and 0.2 mol/L HCl), and tin ($SnCl_4$ in 3 mol/L HCl) at 1000 ppm were purchased from Kanto Chemical Co., Inc., and were used for observing the effect of interferent ions.

Apparatus. Equipment used in this paper is listed in Table I.

An ozone generator was a silent discharge type operated at the applied electric voltage of 100 with flowing oxygen at the rate of 100 mL/min. The concentration of ozone was 13 g/m^3 under this condition.

Spectrometric Observation for Phosphine Chemiluminescence. To observe the chemiluminescence of phosphine at high concentration (around 10%), a spectrophotometer equipped with a photodiode array was used for simultaneous observation of wide wavelength emission. A personal computer was used for processing the multichannel signal from the photodiode array. To observe the chemiluminescence of phosphine at low concentration (less than a few hundred parts per million), the same spectrometer as employed in the above multichannel measurement was used with photomultiplier detection, where a mirror was set inside the spectrometer for switching the optical pathway from the diode array to photomultiplier. The output signal of the photomultiplier through a dc amplifier was fed into a digital analyzing recorder which has a function to perform fast Fourier transform of input signal (frequency analysis of noise in the input signal). Wavelength scanning of the spectrometer was done by a stepping motor which was controlled by a function generator.

Determination of Phosphate Ion. The method for generating phosphine from aqueous phosphate solution, which was previously reported (*4, 7*), was improved for the chemiluminescence detection. Two types of the sample vessels (boat and half cylindrical types) were examined. A boat-shaped container made of quartz was used as a sample container instead of a half cylinder of quartz tube which was adopted in the previous paper. This vessel shape is convenient when a large amount of sample solution is applied.

The generated phosphine was mixed with ozone in a chemiluminescence chamber. Various types of chambers were designed and made in our laboratory. In the case of quantitative analysis for phosphate, a photon counting system with cooling photomultiplier was adopted because of the low intensity of chemiluminescence emission. The analog output of the photon counter was recorded on a strip chart recorder.

Procedure. The recommended procedure for determination of phosphate is as follows: 10–2000 μL of phosphate solution (sample) is placed in the sample vessel and completely dried. Then, 100 μL of 6% sodium tetrahydroborate is added to this vessel and dried again at a temperature below 45 °C in an oven for 2 h. This dried mixture is inserted into a phosphine generation tube made of quartz which is heated at 480–500 °C by a cylindrical Nichrom heater whose temperature is controlled and monitored by a digital thermometer. Helium is used as the carrier gas of the generated phosphine and continuously flows in the phosphine generation tube at a flow rate of 600 mL/min. Phosphine is trapped in a U-tube cooled at liquid nitrogen temperature for 2 min. This trap is packed with a small amount of quartz wool. After collecting phosphine, the cold trap is soaked (warmed) in a water bath. Phosphine is, then, introduced into the chemiluminescence chamber and mixed with ozone, which is supplied from a generator of silent discharge type through which oxygen flows at the rate of 150 mL/min. The peak height of the chemiluminescence signal fed into a strip chart recorder is read for calculating phosphate concentration.

Caution: Phosphine is a poisonous gas. The lowest published lethal concentration for hamsters is 8 ppm (*8*). It is also explosively flammable. When using the system shown in Figure 1 for measuring chemiluminescence spectra, the operator should obey safety guides. Especially in Figure 1A, when a large amount of phosphine is collected in the trap, special caution for protecting against ignition and leaking of phosphine must be required. However, it should be noted that it the quantitative analysis of phosphate ion is not dangerous when using the system shown in Figure 4 because only a small amount of phosphate is applied and converted to phosphine. The poisonous effect of phosphine is smaller than that for arsine, which is commonly treated in atomic spectroscopy.

RESULTS AND DISCUSSION

Chemiluminescence Spectra of Phosphine. When phosphine at high concentration was exposed to air, the color of emission varied from white to red and reversed to white before termination. Sometimes, a greenish emission appears, which can be ascribed to HPO or $(PO)_2$. This fact shows that the chemiluminescence spectrum changes due to the concentration of phosphine.

Figure 1A shows the schematic diagram for observing chemiluminescence of phosphine at high concentration. Since the supply of highly concentrated phosphine is temporal, the chemiluminescence spectrum was observed with a multiwavelength detection system. In the figure, phosphine was synthesized according to the reaction

$$4H_3PO_3 \xrightarrow{\text{heat <200 °C}} PH_3 + 3H_3PO_4$$

Phosphorous acid (about 30 g) was heated in a distillation flask, which was heated in a mantle heater under temperature control. Helium flows in the flask to carry phosphine to the

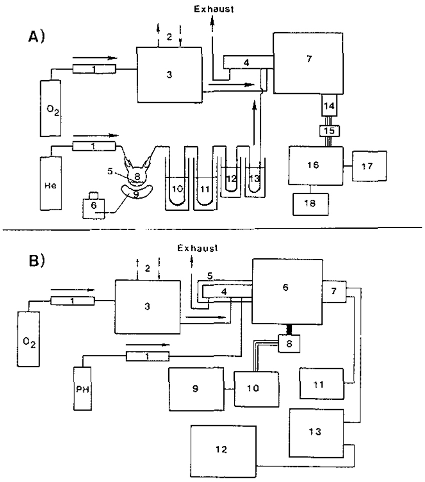

Figure 1. Schematic diagrams for spectral measurement of gas-phase chemiluminescence of phosphine. (A) System at the high concentration of phosphine (about 15%): O_2, oxygen cylinder; He, helium cylinder; (1) gas flowmeter, (2) cooling water, (3) ozone generator, (4) chemiluminescence chamber, (5) phosphorus acid, (6) slide transformers, (7) spectrometer, (8) double neck flask, (9) heater, (10) trap for eliminating water and byproducts (first trap), (11) phosphine reservoir trap (second trap), (12) trap for phosphine partitioned from the second trap (third trap), (13) trap for preventing backfire, (14) multichannel detector, (15) data treating unit (interface), (16) personal computer, (17) display, (18) printer. (B) System at the low concentration (103 ppm): O_2, oxygen cylinder; PH, phosphine cylinder; (1) gas flowmeter, (2) cooling water, (3) ozone generator, (4) chemiluminescence chamber, (5) aluminum case, (6) spectrometer, (7) photomultiplier, (8) stepping motor, (9) function generator, (10) motor controller, (11) power supply, (12) analyzing recorder, (13) dc amplifier.

trap. The first trap, cooled at dry ice/ethanol temperature, is for elimination of water and diphosphine which are byproducts of the above reaction. The second to forth traps, cooled at liquid nitrogen temperature, were for phosphine. The second trap was the reservoir of synthetic phosphine. For each chemiluminescence measurement, about 20 mg of phosphine was transferred to the third trap. The first and second traps were specially designed by Horibe (*9*). The third trap was a U-tube packed with quartz wool, and the forth, which was for protection for the second and third traps from backfire, was a simple U-tube. Because of the oxidation of a large amount of phosphine, there was a yellow and white elemental phosphorus deposit inside the chemiluminescence chamber. To prevent the window from being screened by elemental phosphorus, a type 4 chamber, shown in Figure 2, is designed and used for the measurement, where the inlet of phosphine in the chamber is distant from the window.

The upper figure of Figure 3 shows the chemiluminescence spectra measured by the above-mentioned system. A broad peak of emission appears at 670 nm with a shoulder at 740 nm. In this figure, the shoulder at 740 nm is rather small due to the reduction of figure size but reproducible in every observation. This emission looks orange, and both ozone and oxygen can make luminescence at this concentration of phosphine. The concentration of phosphine at the present condition was calculated to be about 10–15%. Due to poor sensitivity, emission other than that shown in Figure 3 could not be observed by the present system. In the upper figure of Figure 3, the background (spectral signal observed without phosphine) completely coincides with the horizontal axis of the figure.

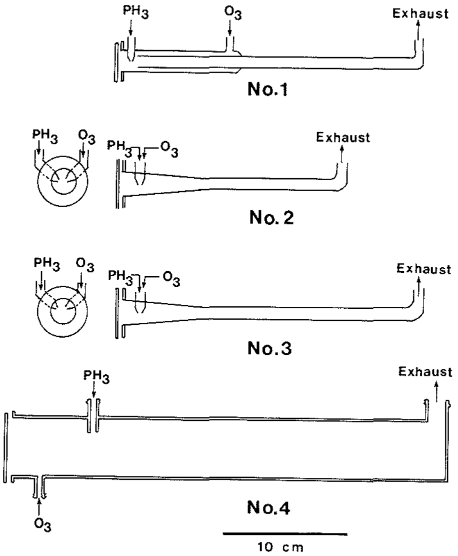

Figure 2. Schematic illustration of the chemiluminescence chamber.

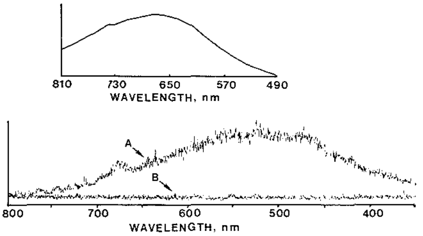

Figure 3. Chemiluminescence spectra: (upper) spectrum for high concentration of phosphine (about 15%) obtained by the system shown in Figure 1B; (lower) spectrum of low concentration of phosphine (103 ppm) obtained by the system shown in Figure 1B; (A) spectra with phosphine, (B) spectra without phosphine (background).

Figure 1B shows the measurement system of chemiluminescence for low concentrations of phosphine (less than a few hundred parts per million). Since the above-mentioned system with a photodiode array detection does not have adequate sensitivity, the regular photomultiplier detection system was adopted for low concentrations of phosphine, where phosphine at 103 ppm was continuously supplied from a cylinder. The phosphine chemiluminescence was done in the type 1 chemiluminescence chamber shown in Figure 2. The lower part of Figure 3 shows this emission spectrum. The emission obtained in this condition gives extremely broad spectra extending from 350 to 700 nm. Neither the sharp peaks in the visible region nor those due to PO at around 280 nm could observed, which appear in the chemiluminescence of P_4 observed by VanZee and Khan (*6*). The peak of emission is located at 530 nm, and some can be attributable to HPO or $(PO)_2$. When the concentration of phosphine (diluting phosphine by helium) was decreased to 20 ppm, a broad emission band between 400 and 700 was measured without any sharp peaks. It can be considered that the sharp peaks due to PO or HPO do not appear in the luminescence under atmospheric pressure like the present experiment as mentioned in the case of arsine (*10*). The small but significant peak appears at 675 nm, which is the same one as observed

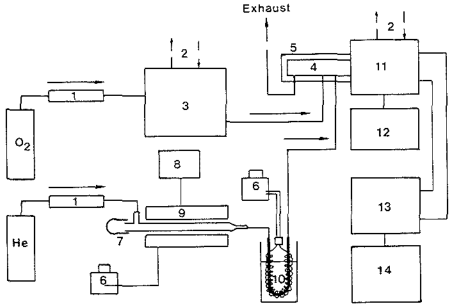

Figure 4. Schematic diagram of phosphine generation and chemiluminescence detection systems: O_2, oxygen cylinder; He, helium cylinder; (1) gas flowmeter, (2) cooling water, (3) ozone generator, (4) chemiluminescence chamber, (5) aluminum case, (6) slide transformer, (7) phosphine generation tube, (8) digital thermometer, (9) heater, (10) phosphine trap wound by a Nichrom wire which heats the trap to expel the condensed moisture, (11) photomultiplier housing (photomultiplier: Hamamatsu type R649), (12) cooling unit, (13) photon counter, (14) recorder.

at the high concentration of phosphine shown in the upper part of Figure 3.

Quantitative Analysis of Phosphate. The system illustrated in Figure 4 was constructed for phosphate determination, where peak height recorded in the strip chart recorder was measured. The chemiluminescence chambers of types 1, 2, and 3 in Figure 2 were compared in regard to the quantitative measurement. To improve the precision, the phosphine generation method mentioned in ref 4 and 7 (in which phosphine was detected by flame photometric detection–gas chromatography) was modified as follows: In the case where the volume of the phosphate solution exceeds 500 μL, the phosphate solution was dried at 50–70 °C in advance of the addition of the same volume of 6% sodium tetrahydroborate, and then the sample vessel with sodium tetrahydroborate solution was dried at 35–45 °C for about 2 h. This procedure with separated drying of sample and tetrahydroborate solutions make possible the generation of phosphine in up to 2 mL of phosphate solution in high precision. It has been confirmed that the signal intensity is independent of sample volume in its magnitude in the range between 20 μL and 2 mL. In ref 7, tetrahydroborate solution included 2–4% sodium hydroxide as the stabilizer. However, in the present case, addition of sodium hydroxide increased only the blank signal and was not required.

The dried sample and sodium tetrahydroborate were then heated at 460–480 °C under helium flow, and the generated phosphine was collected for 2 min in a U-tube that was half packed with quartz wool and cooled at liquid nitrogen temperature. In the cases where the temperature of the oven that heats the phosphine generation tube exceeds 490 °C, production efficiency of phosphine decreased. When the phosphine was purged from the trap, the trap was warmed in a water bath, which gave about a 3-fold increase in peak height than that obtained from the trap at room temperature.

The type 1 chemiluminescence chamber shown in Figure 2 provides slightly stronger emission than the type 3 chamber. The shorter chamber (type 2) gave about 40% weaker chemiluminescence emission. The flow rates of phosphine carrier (helium) giving the maximum chemiluminescence peak height were 650 and 850 mL/min for the type 1 and 3 chambers, respectively. In these helium flow rates, 150 and 100 mL/min of oxygen flow rates at the ozone generator rendered the maximum peak height of chemiluminescence for the type 1 and 3 chambers, respectively. Namely, the type 1 chamber, where phosphine was injected in the ozone, needs a higher flow rate of phosphine carrier with lower flow rate of ozone for obtaining the maximum luminescence in comparison with the case of the type 3 chamber in which the carrier and ozone directly collide with each other.

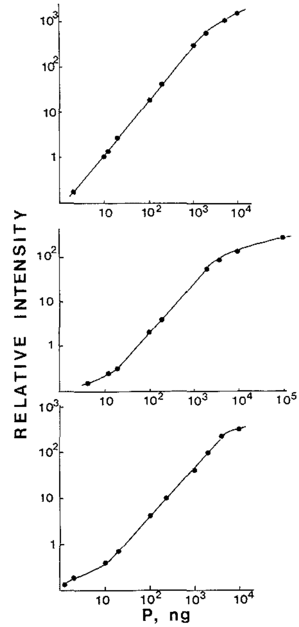

Figure 5. log–log plots of calibration curves: (upper) obtained by the no. 1 chamber in Figure 4; (middle) obtained by the no. 2 chamber in Figure 4; (bottom) obtained by the no. 3 chamber in Figure 4.

Table II. Signals Given by Diverse Ions

P	100[a]	Bi	0.11 ± 0.04
As	32 ± 4	Sb	0.07 ± 0.02
Se	0.28 ± 0.07	Sn	0.07 ± 0.03
Pb	0.14 ± 0.06	Ge	0.03 ± 0.01

[a] The signal given by phosphate ion is referred to as 100. The applied chemical form of each element is noted in Experimental Section. The applied amounts of elements are 20 μg.

Figure 5 shows log–log calibration plots obtained with using the type 1, 2, and 3 chambers. Both type 1 and 3 chambers give the same detection limits of about 1 ng, and the linear dynamic ranges are from 2 to 5000 ng for the type 1 and from 10 to 5000 ng for the type 3. The type 2 chamber shows a detection limit of 3 ng with a linear dynamic range of 50–1000 ng. The narrow dynamic range of the type 2 chamber can be explained by its short length between the entrance and exhaust gases.

Interferences. Table II shows the signal intensity when the diverse ions giving volatile hydride are applied to the present measurement, in which the signal due to 500 ng of P as phosphate ion is referred to as 100. In the table, most of elements such as Se, Pb, Bi, Sb, Sn, and Ge do not give the strong interference that As does. The present hydride generation–chemiluminescence technique is fundamentally suitable for phosphate analysis, but the selectivity against arsenic (ratio of signal intensities of P to As) is rather poor, i.e., about 3–5. In the analysis of a sample coexisting with

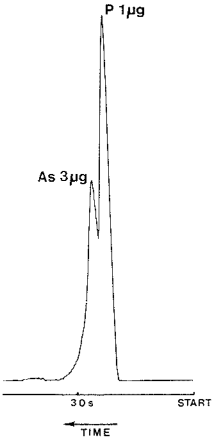

Figure 6. Transient peaks of phosphorus and arsenic when applying a mixed solution of phosphate and arsenate to the system shown in Figure 4.

arsenic, some separation methods are indispensable.

Figure 6 shows the peak separation of phosphorus (1 μg) and arsenic (5 μg), which was obtained by leaving the hydride trap at room temperature. Differential vaporization from the trap (an U-tube packed with quartz wool) at room temperature is effective for observing the coexistence of arsenic. However, an introduction of the gas chromatographic tube into the gas flow line is required for the complete separation of phosphine (bp −87 °C) and arsine (bp −55 °C) as mentioned in our previous paper (*11*). In most samples, such as natural waters, the concentration of phosphorus (phosphate) is more than 1000 times higher than that of arsenic. The interference of arsenic is, therefore, not serious in general: It should be noted that the arsenic interference in the molybdenum blue colorimetry appears at the same magnitude as the present method, which is referred to as the standard method of phosphate analysis (*12*).

Fast Fourier Transform Analysis for Noise Power Spectrum Measurement of Chemiluminescence Emission. Figure 7 shows the noise power spectra of chemiluminescence emission obtained by using the type 1 and 3 chambers (see Figure 4). Rising time of the dc amplifier inserted between the photomultiplier and the analyzing recorder was set at 0.01 s. A similar result shown in Figure 7 was also obtained by using a current input preamplifier (Model LI-76, made by NF Electronic Instruments Co., frequency response is proven within 2 kHz at the present gain), which is driven by a battery, as a substitute for the dc amplifier. A peak at 120 Hz appearing in the figure is an artifact due to the present photodetection system and not attributed to the chemiluminescence emission. It can be noted that the $1/f$ component in the emission noise due to the type 1 chamber is slightly larger than that due to the type 3 chamber. It can be considered that the mixing pattern of phosphine and ozone causes the difference in the noise frequency.

The present method is superior to the previous chemiluminescence (*3*) in terms of its simplicity, reproducibility, and sensitivity. Although arsenic interference is rather serious in comparison to atomic spectroscopy (*13*), peak deconvolution might be possible for determining phosphate with isolating from arsenic by measuring the differential vaporization. In conclusion, the type 1 chemiluminescence chamber is better than the type 2 or 3 chamber with respect to the capacity to give higher sensitivity and wider dynamic range.

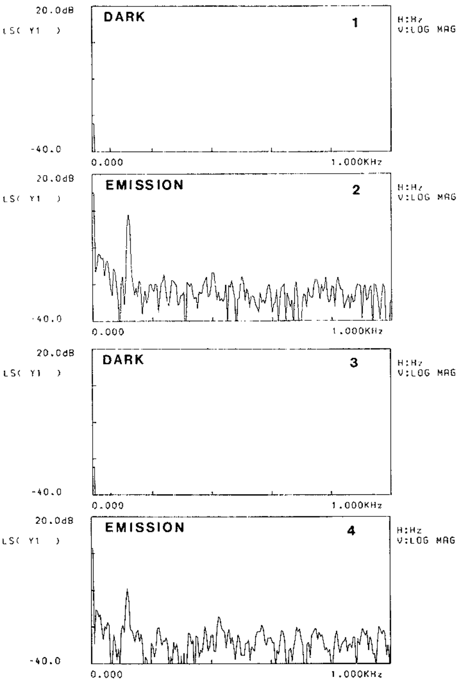

Figure 7. Noise power spectra in the chemiluminescence emissions. Spectra noted 1 and 2 were from the no. 1 chamber (Figure 2), and those noted 3 and 4 were from the no. 3 chamber (Figure 2). The ordinate of the figures is in log scale. The measurement was done by the system shown in Figure 6 with elimination of the spectrometer (direct detection of emission by the photomultiplier without the spectrometer).

ACKNOWLEDGMENT

The authors thank Hiroyuki Tsubota for his suggestions.

LITERATURE CITED

(1) Tao, H.; Miyazaki, A.; Bansho, K. *Anal. Chem.* **1986**, *58*, 202–207 and 1148–1152.
(2) Matsumoto, K.; Fuwa, K. *Bunseki Kagaku* **1981**, *20*, 188–190.
(3) Matsumoto, K.; Fujiwara, K.; Fuwa, K. *Anal. Chem.* **1983**, *55*, 1665–1668.
(4) Hashimoto, S.; Fujiwara, K.; Fuwa, K. *Anal. Chem.* **1985**, *57*, 1305–1309.
(5) Burford, J. R.; Bremner, J. M. *Soil Biol. Biochem.* **1972**, *4*, 489–495.
(6) VanZee, R. J.; Khan, A. U. *J. Chem. Phys.* **1976**, *65*, 1764–1772.
(7) Hashimoto, S.; Fujiwara, K.; Fuwa, K. *Limnol. Oceanogr.* **1987**, *32*, 729–735.
(8) *The Merck Index*, 10th ed.; Merck & Co., Inc.: Rahway, NJ, 1983; p 7221.
(9) Horibe, Y.; Shigehara, K.; Takakuwa, Y. *J. Geophys. Res.* **1973**, *78*, 2625–2629.
(10) Fraser, M. E.; Stedman, D. H.; Henderson, M. J. *Anal. Chem.* **1982**, *54*, 1200–1201.
(11) Fujiwara, K.; Watanabe, Y.; Fuwa, K.; Winefordner, J. D. *Anal. Chem.* **1982**, *54*, 125–128.
(12) *Vogel's Textbook of Quantitative Inorganic Analysis*, 4th ed.; Longman Group, Ltd.: London, 1978; pp 756–757.
(13) Fujiwara, K.; Mignardi, M. A.; Petrucci, G.; Smith, B. W.; Winefordner, J. D., submitted for publication in *Spectrosc. Lett.*

RECEIVED for review July 3, 1989. Accepted September 18, 1989. This work was supported by Grants in Aid 62540441 and 63540456 form the Ministry of Education, Science, and Culture, Japan.

2704 *Anal. Chem.* **1989**, *61*, 2704–2707

Single Photon Counting Lifetime Measurements of Weak, Long-Lived Samples

Seth W. Snyder and J. N. Demas*

Department of Chemistry and Biophysics Program, University of Virginia, Charlottesville, Virginia 22901

B. A. DeGraff

Department of Chemistry, James Madison University, Harrisonburg, Virginia 22807

The time-correlated single photon counting (SPC) lifetime technique is commonly used to investigate complex kinetics of short-lived organic species. Longer-lived luminescent transition-metal complexes in heterogeneous environments have complicated decays that require the wide dynamic range of an SPC instrument for proper analysis. As their luminescence lifetimes are 2–3 orders of magnitude longer (hundreds of nanoseconds to microseconds) than the 3–5 ns full width at half maximum flash excitation profile, it seemed that by fitting the data at times well beyond the flash spike, we could neglect the flash. We describe several significant, rarely discussed problems arising from accurately sampling lamp excitation profiles, which can invalidate lifetime determinations. D_2 and H_2 lamps with 3–5 ns wide lamp profiles have low amplitude tails that last for microseconds. These tails distort decays and make deconvolution necessary for accurate lifetime measurements in the 100 ns to microsecond range, even for single exponential decays. Additional problems arise for weak emitters, where the more intense N_2 filled lamp was required. The lamp profiles were strongly wavelength and geometry dependent, and it was difficult to obtain accurate lamp profiles needed for deconvolution. We describe these effects and their minimization or elimination.

INTRODUCTION

The time-correlated single photon counting (SPC) method is a powerful technique for measuring excited-state lifetimes, τ, in chemistry and biochemistry (*1–3*). Traditionally, SPC was used to investigate fluorescent organic molecules with τ's in the high picosecond and low nanosecond ranges. SPC's intrinsic wide dynamic range (3–4 orders of magnitude) makes it useful in treatments of complex decays (e.g. multiple exponential decays or Förster kinetics).

While the majority of τ's measured by SPC methods are in the low nanosecond range, τ values several orders of magnitude longer are amenable to measurement. Since there should be 5–10 sample τ's between flash pulses, the common 50-kHz flash rate allows measurements of τ to about 2–4 μs.

We study luminescent complexes of the platinum metals (e.g. Ru, Os, Re, and Ir), such as tris(2,2′-bipyridine)ruthenium(II) ($Ru(bpy)_3^{2+}$), in microheterogeneous environments where τ values are typically 0.1–5 μs (*4, 5*), and luminescence quantum yields are significantly smaller than for many organic compounds. In heterogeneous environments, their decays are usually multiexponential and information rich; the wide dynamic range of SPC is necessary for analysis. Here we discuss experimental pitfalls and ways to avoid them for successful application of SPC techniques to long-lived, weakly emitting metal complexes.

Specifically, flash lamps suffer from several problems: (1) Gas-phase reactions can yield long lamp afterglows; the long tails can continue to excite samples and distort the decays of even very long lived emitters. (2) The temporal dependence of the lamp profile can depend on wavelength, which makes sampling the lamp profile for deconvolutions difficult. (3) The lamp discharge is spacially inhomogeneous, which requires care in imaging and in sampling the excitation profile. We show the extent of these effects and their elimination for long-lived samples.

EXPERIMENTAL SECTION

Equipment. The SPC system was largely based on Photochemical Research Associates (PRA) components in a standard configuration (*6–9*). The lamp was a PRA 510B (5–6 kV, $^1/_2$ atm of N_2, D_2, or H_2, 43–44 kHz flash rate, and 2–3 mm electrode spacing). The sample compartment was home built. Optics were UV-grade quartz or Suprasil. A saturated $CuSO_4$ solution and a 7-54 (9863) Corning excitation filter eliminated stray visible and IR radiation from the excitation. For N_2 fills, a Corion 337-nm, 12 nm fwhw interference filter isolated the major lamp line. Sample solutions were contained in 1-cm cylindrical cuvettes at 25 ± 0.5 °C (*10*). The emission was focused into a J-Y HV-10 *f*3.5 emission monochromator (4–16 nm band-pass). The monochromator isolated specific emitting species in microheterogeneous environments, and its removal from the detection path was inconvenient. A 1-cm saturated $NaNO_2$ solution filter removed scattered UV flash lamp light for sample decays.

The flash (start) PMT signal was sent to a PRA 1718 100-MHz discriminator, which was connected to the start input of a PRA 1701 TAC. The emission was detected with a cooled Hamamatsu R928 PMT (dark counts of about 5 Hz). The sample signal stop pulse was shaped with a PRA 1716 constant fraction discriminator, delayed, and sent to the TAC stop input. Successful TAC conversions were sent to a Tracor Northern TN-7200 MCA. The MCA was calibrated with a home-built time calibrator or an Ortec 425 calibrated delay.

After transient collection, the MCA histogram was transferred to either an AT&T PC6300 or an AT-clone microcomputer with a math coprocessor. All data processing used Turbo Pascal 5 programs. Deconvolutions used either a fast phase plane (PP) method with scattered light corrections (*2, 11–13*) or a Marquardt nonlinear least squares, NLS, method adapted from the FORTRAN routines of O'Connor and Phillips (*1, 13, 14*). The NLS method included phototube time shift corrections and could fit a sum of up to four exponentials.

Samples. $Ru(bpy)_3Cl_2$ (GFS Chemical Co.) was recrystallized from methanol. Aqueous solutions (10 μM) were monitored at 600 nm. Anthracene (Aldrich, puriss 99.9%) was recrystallized from methanol. Fresh solutions (10 μM) in B&J spectroscopic grade cyclohexane were monitored at 400 nm. Water was doubly distilled from alkaline $KMnO_4$. $D(t)$'s were collected to about 10 000 counts peak. Deoxygenation was by purging with solvent-saturated N_2 for at least 20 min. $E(t)$'s were collected by scattering off of a starch solution or from a Suprasil rod.

RESULTS AND DISCUSSION

Flash Tail Effects. As our sample τ's were orders of magnitude longer than the width of $E(t)$, we expected that $E(t)$ would approximate a delta function and τ information could be extracted without deconvolution. However, because of lamp afterglow, deconvolution was always necessary.

For oxygen-free $Ru(bpy)_3^{2+}$ solutions, a well-characterized single exponential decay, linear least squares (LLS) fits to ln

0003-2700/89/0361-2704$01.50/0 © 1989 American Chemical Society

Table I. Unsuccessful SPC Fits of $Ru(bpy)_3Cl_2$[a]

purge gas[b]	τ, ns	χ_r^2	fit method[c]	conditions
N_2	689	2.42	LLS	fit range 100–500[d]
N_2	714	1.12	LLS	fit range 250–500
N_2	734	0.886	LLS	fit range 350–500
air	324	6.49	NLS	flash collected from Suprasil rod scatter
N_2	588	1.43	NLS	flash iris adjusted between flash and sample
air	373	1.66	PP	flash iris adjusted between flash and sample
air	371	1.56	PP	flash collected at λ = 384 nm

[a] All measurements were made with a N_2-filled flash lamp, a flash profile collected off of a starch scattering solution, at λ = 337 nm, unless otherwise noted. [b] Purge gas is indicated for all solutions. [c] Fit methods are: LLS, linear least squares; NLS, nonlinear least squares deconvolution; PP, phase plane deconvolution. [d] Data channel fit range on a 2-μs decay of a 512-channel file. Flash peak was in channel 37.

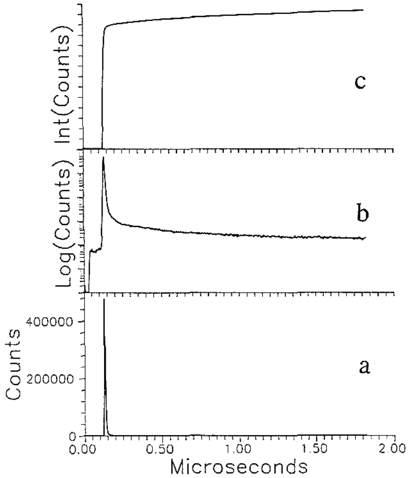

Figure 1. (a) Flash profile for a N_2-filled lamp collected at 337 nm off of a starch scattering solution collected under the conditions outlined in the experimental section. (b) The logarithmic plot of the same flash profile, revealing the long-lived tail. (c) The integration of the flash profile.

($D(t)$) versus t yielded unacceptable results. The first three entries of Table I illustrate the failure of LLS fits. The observed τ's were 650–750 ns even if fitting started more than a microsecond after the 3–6 ns wide D_2 or N_2 flash pulses; the accepted τ is 584–600 ns (*15*). Also, the χ_r^2's for fitting over the entire decay were statistically unacceptable, and the weighted residuals plots showed strong systematic biases. As we will show, this failure arises from a low-amplitude, but not negligible, tail on $E(t)$.

$E(t)$ (Figure 1) shows a very long low-amplitude tail. Figure 1c shows the integral of $E(t)$. The tail amplitude is orders of magnitude less intense than the peak but accounts for a significant fraction of the integrated flash intensity—about 10% in Figure 1.

The tail appears to be a lamp afterglow that lasts the entire period between flash pulses and contributes 10–20% of the total emitted photons with all fill gases investigated, although each had a different profile. With 10–20% of the sample excitation occurring during the decay, deconvolution is necessary even for microsecond lived samples.

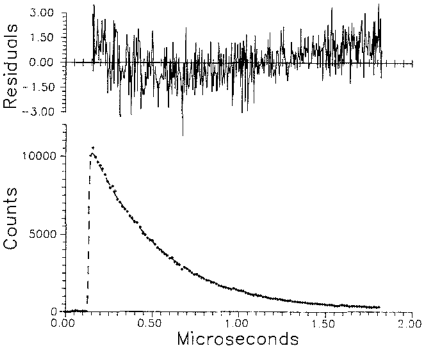

Figure 2. An unsuccessful fit of $Ru(bpy)_3^{2+}$ in an air-purged solution: (•) data with only every fourth point plotted; (– –) calculated best fit. The flash profile was collected at a different lamp iris setting than for the decay. τ = 362.9 ns, τ_r^2 = 1.56. The weighted error residuals for the fit is shown above the data.

Low Light Effects. Our samples are largely weak, red emitters, and we needed an emission monochromator. This necessitated using a N_2 fill gas, which is about 50 times brighter than D_2 (*9*). However, this configuration yielded deconvolution problems that were traced to spacial and wavelength sampling of the time dependence of $E(t)$. These effects are present whether filters or a monochromator are used to isolate the emission.

The last entries of Table I show the results of several unsuccessful deconvolutions arising from geometry and wavelength effects. Figure 2 shows a poor fit that arose from the adjustment of the flash lamp iris between measuring $E(t)$ and $D(t)$. While the fit to $D(t)$ in Figure 2a appears reasonable, the weighted residuals plot (Figure 2b) is unacceptable. Further, both χ_r^2 and the calculated τ's depend strongly on the region fit. Also, PP and NLS deconvolutions gave different τ's, and the scatter coefficient of the PP method and the time shift parameter of the NLS method were physically unreasonable.

There was little doubt that the measurement was at fault and that a single exponential model is in fact correct. The literature and our own laser measurements indicate that the $Ru(bpy)_3^{2+}$ decay is a single exponential, and extensive purification of the complex did not correct the problem.

The most likely source of the difficulty is that the observed $E(t)$ is not the true one. An upward curved residuals plot ($Y_{expt} > Y_{calc}$) at longer times can arise if the observed $E(t)$ falls below the true $E(t)$, and downward curvature if the observed $E(t)$ is too large. To adjust for these errors, the fitting parameters are skewed by the different modeling methods to best adjust for the incorrect $E(t)$. We now show that this interpretation is correct and that the incorrect $E(t)$ arose from wavelength effects in the lamp and the sampling of the excitation beam.

Wavelength Effects. The different lines of the N_2 spectrum have different temporal $E(t)$'s. For determining $E(t)$, we set the monochromator to the most intense 337-nm line, but the remaining lines contributed significant sample excitation intensity. Our samples absorbed differently at the different excitation lines. The "effective" $E(t)$ needed in deconvolutions is then the sums of the $E(t)$'s from each line weighted by the fraction of each line absorbed by the sample. Since the emission monochromator samples only one wavelength at a time, it is virtually impossible to get a good "effective" $E(t)$. We even tried measuring $E(t)$'s at different wavelengths and generating an intensity weighted average of the different curves; while the results were better, the χ_r^2's and residuals plots were still unacceptable.

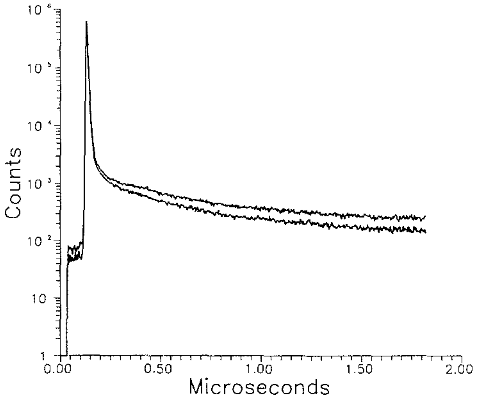

Figure 3. Logarithm of $E(t)$ for a N_2-filled lamp (337 nm) at different lamp iris settings. The differences in the tail caused the problems in deconvolution in Figure 2. The larger tail corresponds to the larger aperture.

Table II. Successful SPC Fits[a]

sample	purge gas	τ, ns	χ_r^2	fit method[b]
$Ru(bpy)_3Cl_2$	air	363.50 ± 0.35	1.1481	NLS
$Ru(bpy)_3Cl_2$	air	362.71	1.165	PP
$Ru(bpy)_3Cl_2$	N_2	580.05 ± 0.73	1.087	NLS
$Ru(bpy)_3Cl_2$	N_2	579.23	1.165	PP
$Ru(bpy)_3Cl_2$[c]	air	354.5 ± 0.67	1.069	NLS
anthracene	air	4.143 ± 0.022[d]	1.023	NLS
anthracene	air	4.136[d]	1.044	PP
anthracene	N_2	5.135 ± 0.020[e]	1.087	NLS
anthracene	N_2	5.053[e]	1.360	PP

[a] All measurements were made with a N_2-filled flash lamp, a flash profile collected off of a starch scattering solution, at $\lambda = 337$ nm, unless otherwise noted: $[Ru(bpy)_3Cl_2] = 10\ \mu M$; [anthracene] $= 10\ \mu M$. [b] Fit methods are: NLS, nonlinear least squares deconvolution; PP, phase plane deconvolution. [c] $[Ru(bpy)_3Cl_2] = 100\ \mu M$. D_2 filled lamp. [d] In air-saturated cyclohexane, anthracene has a reported lifetime of 4.10 ns (*17*). [e] In N_2-saturated cyclohexane, anthracene has a reported lifetime of 5.23 ns (*17*).

Table III. Deconvolution of Multiexponential Decays of $Ru(bpy)_3Cl_2$[a]

purge gas	weighting factor	τ, ns	χ_r^2	Durbin–Watson	fit type[b]
O_2	6.417 ± 0.011	157.21 ± 0.17	1.114	1.81	Single
O_2	6.452	157.05	1.169		PP
air	3.246 ± 0.004	363.50 ± 0.35	1.148	1.85	Single
air	3.256	362.71	1.165		PP
N_2	1.854 ± 0.0025	580.05 ± 0.73	1.087	1.98	Single
N_2	1.859	579.23	1.098		PP
O_2	6.339 ± 0.046	152.51 ± 1.19	1.150	1.91	Double
air	3.410 ± 0.056	359.03 ± 1.80			
O_2	6.438 ± 0.016	156.19 ± 0.72	1.161	1.86	Double
N_2	1.865 ± 0.017	578.93 ± 2.64			
air	3.285 ± 0.003	359.94 ± 0.28	1.205	1.92	Double
N_2	1.858 ± 0.002	585.35 ± 0.47			
O_2	6.63 ± 0.23	156.1 ± 3.15	1.237	1.92	Triple
air	3.17 ± 0.57	377.5 ± 31.1			
N_2	1.80 ± 0.65	575.1 ± 35.0			

[a] The O_2, air, and N_2 decay profiles were mathematically added together to simulate a triple exponential decay of known lifetimes and weighting factors with real instrument response. [b] The fit methods are as follows: PP, phase plane; Single, Double, Triple, single, double, and triple exponential nonlinear least squares, respectively.

The only way that we found to obtain good $E(t)$'s was to restrict the excitation to the single intense 337-nm line with an interference filter. The observed $E(t)$ measured by setting the monochromator to 337 nm then is the "effective" $E(t)$ once geometric effects are eliminated.

Geometric Effects. To measure $E(t)$, we originally scattered excitation into the emission monochromator from a fluorescence-free Suprasil rod. The count rate for $E(t)$ was matched to $D(t)$ by moving the rod to scatter a similar amount. This procedure yielded erratic deconvolutions. We found that the problem arose from the strong dependence of $E(t)$ on the sampled portion of the excitation beam. Slight differences in rod position gave different $E(t)$'s and good or poor deconvolutions depending on whether a good $E(t)$ resulted. Different $E(t)$'s were easily detectable by comparing scattering from the bright central beam to the surrounding halo; the peak/tail ratios were quite different. Since the primary intense peak shape was less affected, this sampling problem would be less noticeable for short-lived species. Geometric effects have been observed in phase-resolved measurements (*16*).

The commonly recommended procedure of using a starch scattering solution to sample $E(t)$ should have corrected the sampling problem. If the optical density and geometry are similar for the sample and the starch solution, then the detector samples $E(t)$ and $D(t)$ similarly and errors cancel out.

As we discovered, the problem is more complex. Our samples were generally much weaker than the scatter signal, and we attenuated the scattered beam to match the $E(t)$ and $D(t)$ count rates. Initially, we used the convenient procedure of varying the iris diameter on the PRA lamp's collection lens to reduce $E(t)$. While it seemed reasonable that the lens sampling of the arc image would be very similar for different iris openings, deconvolution failures proved this assumption wrong (Figure 3). The measured $E(t)$ varies strongly with iris setting and is worse with the largest iris. This is understandable since the larger iris collects more of the long-lived halo. Thus, a suitable $E(t)$ for deconvolution had to be obtained at the same iris setting as was used to collect $D(t)$. Acceptable ways to attenuate $E(t)$ were to insert neutral density filters in the optical train or adjust the emission monochromator slit height.

Successful Deconvolution. Using these procedures, we were able to successfully and routinely deconvolute. For example, we repeated the experiments for deaerated and air-saturated $Ru(bpy)_3^{2+}$. The fits and residuals were all excellent with fitting starting at the flash peak. Table II summarizes several successful single exponential fits using both the PP and NLS methods. Experiments were done by using both N_2 and D_2 filled flash lamps with $Ru(bpy)_3^{2+}$ and anthracene samples. In contrast to the data taken using incorrect sampling, the same τ's are obtained by both the NLS and the PP methods, the scatter or time shift factors were all reasonable, the χ_r^2's were acceptable, and the residuals plots showed no bias. All values agreed well with the literature.

Table III and Figure 4 demonstrate the use of our instrument and methodology for deconvoluting double and triple exponential decays. The double and triple decays were generated by adding two or three separate data files for oxygen-, air-, and nitrogen-saturated solutions. This allows verifying the accuracy of parameter extraction of multiexponentials. The extracted parameters for the two- and three-component systems should match those for the single-component samples that went into the summation. In all cases the agreement is excellent; as expected precision as estimated by the NLS

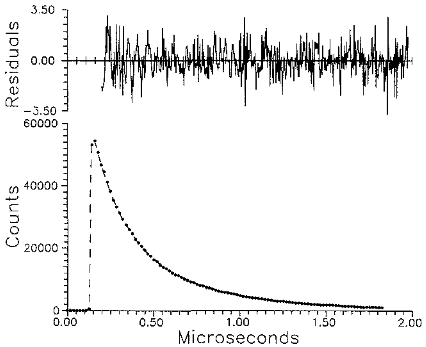

Figure 4. Triple exponential decay (*) and fit (– –) of $D(t)$ composed of three decays of $Ru(bpy)_3^{2+}$ in air-, O_2-, and N_2-purged solutions. The results are summarized in Table III. The weighted error residuals for the fit are shown above the data.

algorithm falls rapidly with increasing numbers of exponentials.

An alternative approach to eliminating problems in the spacial sampling of $E(t)$ is to replace the starch with a reference emitter of known τ; from the reference decay and τ, $E(t)$ is derived. This $E(t)$ is then used in subsequent deconvolutions with $D(t)$ (*6–8*). This method is most useful where color effects are present, but they are not a problem with long-lived emitters and an R928 PMT. The calculation of $E(t)$ is generally a derivative method that introduces noise onto $E(t)$ and degrades the quality of the results. Further the reference flurophore does not solve the problem of the varying time dependences with wavelength in broad-band excitation; the reference in general has a different spectrum than the unknown and, thus, samples the regions differently. Therefore, in the absence of color effects, maximum precision for complex decays will be obtained by avoiding the use of a reference emitter.

CONCLUSIONS

Special precautions are necessary to successfully apply SPC techniques to long-lived, weakly emitting materials. When flash lamp excitation is used, deconvolution is required for all time scales, even for τ's orders of magnitude longer than the 3–6 ns fwhm excitation flash width. More subtle effects arise from the dependences of $E(t)$ with monitoring geometry and excitation wavelength.

These results are especially germane for those analyzing complex kinetics. Only by careful minimization of instrumental distortions will extracted parameters have meaning in complex decays. In the presence of small instrumental distortions, multiple decays can be fit, but the χ_r^2's and weighted residual plots are no longer good criteria of a satisfactory model and erroneous parameters may be accepted as correct. Using the above described sampling techniques, we have successfully extracted complex decay parameters for double, triple, and even quadruple exponential decays spanning the nanosecond to microsecond range. Satisfactory χ_r^2's and residual plots, as well as chemically meaningful parameters, are obtained.

ACKNOWLEDGMENT

We thank Roger Morris, Marvin Grubb, and P. T. Rieger for their technical assistance.

LITERATURE CITED

(1) O'Connor, D. V.; Phillips D. *Time-correlated Single Photon Counting*; Academic Press: New York, 1984.
(2) Demas, J. N. *Excited State Lifetime Measurements*; Academic Press: New York, 1983.
(3) Lakowicz, J. R. *Principles of Fluorescence Spectroscopy*; Plenum Press: New York, 1983.
(4) Snyder, S. W.; Raines, D. E.; Rieger, P. T.; Demas, J. N.; DeGraff, B. A. *Langmuir* **1985**, *1*, 548–552.
(5) Snyder, S. W.; Buell, S. L.; Demas, J. N.; DeGraff, B. A. *J. Phys. Chem.* **1989**, *93*, 5265–5271.
(6) Barrow, D. A.; Lentz, B. R. *J. Biochem. Biophys. Methods* **1983**, *7*, 217.
(7) Lakowicz, J. R.; Cherek, H.; Balter, A. *J. Biochem. Biophys. Methods* **1981**, *5*, 131.
(8) Carraway, E. R.; Hauenstein, Jr., B. L.; Demas, J. N.; DeGraff B. A. *Anal. Chem.* **1985**, *57*, 2304–2308.
(9) *Single Photon Counting Manuals*; Photochemical *Research* Associates: Oak Ridge, TN.
(10) Buell, S. L.; Demas, J. N. *Anal. Chem.* **1982**, *54*, 1214–1215.
(11) Greer, J. M.; Reed, F. W.; Demas J. N. *Anal. Chem.* **1981**, *53*, 710.
(12) Love, J. C.; Demas, J. N. *Anal. Chem.* **1984**, *56*, 82–85.
(13) Marquardt, D. W. *J. Soc. Ind. Appl. Math.* **1963**, *11*, 431.
(14) Bevington, P. R. *Data Reduction and Error Analysis for the Physical Sciences*; McGraw-Hill: New York, 1969.
(15) Lin, C.-T.; Bottcher, W.; Chou, M.; Creutz, C.; Sutin, N. *J. Am. Chem. Soc.* **1976**, *98*, 6536.
(16) Jameson, D. M.; Gratton, E.; Hall, R. D. *Appl. Spectrosc. Rev.* **1984**, *20*, 55–106.
(17) Lampert, R. A.; Chewter, L. A.; Phillips, D.; O'Connor, D. V.; Roberts, A. J.; Meech, S. R. *Anal. Chem.* **1983**, *55*, 68–73.

RECEIVED for review July 10, 1989. Accepted September 20, 1989. The single photon counting equipment was purchased in part with a grant from the donors of the Petroleum Research Fund, administered by the American Chemical Society. We gratefully acknowledge the support of the National Science Foundation (CHE 86-00012 and 88-17809).

Iterative Least-Squares Fit Procedures for the Identification of Organic Vapor Mixtures by Fourier Transform Infrared Spectrophotometry

Xiao Hong-kui,[1,2] Steven P. Levine,*[,1] and James B. D'Arcy[1,3]

School of Public Health, The University of Michigan, Ann Arbor, Michigan 48109-2029, School of Public Health, Beijing Medical University, Beijing 100083, Peoples' Republic of China, and Biomedical Science Department, Research Laboratories, General Motors Corporation, Warren, Michigan 48090

Least-squares fitting (LSF) was applied to the qualitative analysis of IR spectra based on comparing standard reference spectra with the sample mixture spectrum. Identification of compounds in the sample was made by judging the fit level of the spectrum of each compound with the sample spectrum. An iterative procedure was developed to eliminate compounds with the worst fit levels in order to approach an optimal fit for the sample spectrum. The qualitative analysis results obtained from the optimal fit were further used for quantitative analysis.

INTRODUCTION

Recently, much attention has been focused on computerized processing of infrared (IR) spectral information for qualitative and quantitative analysis of mixtures. A number of programs have been developed to assist the chemist in the identification and quantitation of unknown compounds. Many approaches to automated spectral interpretation have been developed such as pattern recognition, factor analysis, hierarchical clustering, and expert systems (*1–18*). Summaries of recent literature in this and related subjects are available in symposium proceedings (*19*, *20*).

Most of these systems make decisions principally based on information of peak position, uniqueness, and intensity for structural elucidation of compounds in the condensed phase. However, the IR spectra of compounds present in the vapor phase at trace concentrations are different from those in the condensed phase. This is due to a lack of effects from changes in hydrogen bonding, the dielectric constant of the medium, and nonpolar solvent–solute interactions.

Many of the systems for interpretation of condensed-phase IR spectra cannot be readily applied to gas or vapor systems. A successful application of an expert system to the interpretation of the IR spectra of pure compounds in the vapor phase was accomplished with PAIRS (*14*). A computerized interpretation system, MIXIR, has also been developed, which shows promise for application to the interpretation of the IR spectra of vapors (*21*). This system is in the early stages of development of testing on such spectra.

In the workplace, the concentration of most toxic organic compounds may be below one-tenth the occupational exposure limit, frequently expressed as the threshold limit value (TLV) or the permissible exposure limit (PEL) (*22*). When the concentrations of organic vapors are as low as 1 ppm, and the composition of the sample is complex, spectral peaks may be overlapped. In this circumstance, it is extremely difficult to interpret IR spectra by using computerized techniques that depend on picking peaks. This is due to low peak intensities, "chemical noise", and electronic noise (*23–27*).

In this context, "chemical noise" may be considered to consist of components of the vapor-phase mixture that are outside the reference library, and of little or no interest to the analyst. For example, in the workplace, this may include low concentrations of low molecular weight hydrocarbon gases, along with oxides of sulfur and nitrogen. Because of the problems associated with noise, overlap of spectral features, and low peak intensities, no computerized software is currently available for the qualitative interpretation of the IR spectra of mixtures of gases and vapors in low concentration.

In this study, least-squares fitting (LSF), sometimes called classical least squares (CLS), was applied to the qualitative analysis of IR spectra based on comparing standard reference spectra with the sample mixture spectrum. Identification of compounds in the samples was made by judging the fit level of the spectrum of each compound with the sample spectrum. An iterative procedure was developed, and manually applied, to eliminate compounds not meeting predetermined worst-fit criteria. The qualitative analysis results thereby obtained from the optimal fit were further used for quantitative analysis using LSF.

For traditional quantitative applications, where the identities of the components of the mixture are known, LSF approaches have been used with good success (*23–27*). As expected, Warner and co-workers found that the results of an analysis using LSF can be strongly affected by not including all components in samples. They reported the results obtained when using nonnegative least squares and linear programming for unknown samples (*28*). Haaland and Easterling approached the problem of quantitation of components in a mixture by selecting spectral regions that yield the best fit for reference spectra and then combining the results from all spectral regions in a statistically efficient manner. These methods were first reported in a seminal paper by Haaland (*29*) and then in later publications (*30*, *31*). Later, they applied partial-least-squares (PLS) methods for quantitative IR spectroscopy (*32*).

In this paper we present the results obtained when using a commercially available version of the LSF program developed by Haaland (*29–31*) for the qualitative and quantitative IR spectral analysis of trace organic vapors in impurity- and moisture-free air. Interpretation of data is presented that yields optimal approaches to the analysis of samples of unknown composition and concentration.

EXPERIMENTAL SECTION

Samples. Three air mixture samples containing five to 11 compounds in zero air were provided by T. Pritchett, U.S. Environmental Protection Agency (EPA). The concentration of compounds was verified by EPA using gas chromatography (GC). Forty-seven reference standard vapor IV spectra were acquired as a reference library with the use of GC-certified gas cylinders (Scott Specialty Gas Co.).

Hardware. A Nicolet 20 SXB Fourier transform infrared spectrometer was used with a liquid nitrogen cooled HgCdTe–InSb sandwich detector and 10-m Hanst gas cell. Interferograms were

---

* Author to whom correspondence should be addressed.
[1] The University of Michigan.
[2] Beijing Medical University.
[3] General Motors Corp.

0003-2700/89/0361-2708$01.50/0 © 1989 American Chemical Society

collected to yield spectra of from 0.5 to 8.0 cm^{-1} resolution through deresolution of the 0.5-cm^{-1} interferograms by the method described in previous papers (*23–27*).

Software. For the detailed theory of LSF software, see papers by Haaland et al. (*29–31*). Detailed discussions of the application of LSF software to quantitative analysis of trace gases in ambient air have also been published (*23–27*).

METHODS

The least-squares fitting method III, which assumes a linear base line over the width of the peak, was adopted for this study. With method III, more than one peak, and therefore more than one base line, can be present within a window. From ref 29, the best fit in a least-squares sense is obtained by minimizing the expression $\sum_i[A_{si} - kA_{ri}]^2$, where A_{si} is the sample absorbance at frequency i, A_{ri} is the reference absorbance at frequency i, and k is the ratio of sample and reference concentrations.

The error variance, σ^2, is estimated from

$$\sigma^2 = \frac{\sum_i(A_{si} - \hat{k}A_{ri})^2}{n - 1}$$

where n is the total number of observations.

For large n (typically $n > 400$) a 95% confidence interval on the true concentration in the sample is $\hat{C}_s \pm 1.96[\mathrm{SE}(\hat{C}_s)]$, where

$$\mathrm{SE}(C_s) = \frac{\hat{\sigma}C_r}{(\sum A_{ri}^2)^{1/2}}$$

and C_s is the least-squares estimate of the sample concentration, C_r is the known concentration of the reference, and $\mathrm{SE}(C_s)$ is the standard error of the estimated concentration (*29*).

The reference spectra in a selected region were fitted with the sample spectra. The lack of spectral fit was expressed in terms of an estimated error variance. If the concentrations of the reference spectra are known, concentration errors could be expressed as the standard error of the estimated concentration, or as the 95% confidence interval of the estimated concentration.

The infrared spectral interpretation procedure described herein is designed to report the presence of each compound chosen from a reference library of compounds on the basis of a comparison of the reported concentration and 1.96 times the standard error, which was used to calculate the 95% confidence interval.

Two methods of data analysis were evaluated in this study. The first method attempted to eliminate compounds from the library of compounds by analyzing the spectra in one group of 47 compounds, or in groups of 16. The second method attempted to build a set of possible compounds by fitting the reference spectra one at a time to the sample spectrum.

Method I (Set Reduction Method (SRM)). First, in order to provide a point of comparison for all iterative procedures, the Nicolet LSF software was altered to allow the use of a reference set of up to 48 compounds, rather than the 16 compounds that are normally the maximum allowed by the software. This method is referred to as SRM-47, since 47 compounds were used in this study. After the first iteration, all positives are kept for the second iteration. At this point, this method becomes the same as the SRM detailed immediately below.

Secondly, in order to institute the iterative LSF set reduction approach using the commercially available version of the Nicolet LSF software, the library had to be divided into subsets of 16 compounds each from the library of 47 compounds. To accomplish this, the reference standard spectra were divided into three categories: aliphatic hydrocarbons, aromatic compounds, and oxygenated compounds. The IR window for each compound was then selected. The window can be either a narrow window chosen specifically for that compound or a "general" window covering the fingerprint and/or the C–H stretch region(s). If sufficiently wide windows are chosen, the results may, in some circumstances, be approximated by the use of a "general" window, since the overlapping windows merge into a single region for LSF analysis.

Sample spectra were then analyzed by the LSF program, which yielded the concentration and a value of 1.96 times the standard error, which was used to calculate the 95% confidence interval for each compound. Judgment was made by the manual comparison of each compound's concentration and 95% confidence interval. *Those compounds whose reported 95% confidence interval did not include a concentration of zero were kept* and combined to form a new data set for the next LSF analysis. The remaining compounds were eliminated.

This procedure was repeated until no further compounds were eliminated, and the standard error for each analyte stayed essentially constant. This took between three and four iterations. All compounds remaining were then reported as positive identifications.

Method II (Set Building Method (SBM)). A specific IR window was selected for each compound. Compounds were then entered, one reference standard spectrum at a time, into the LSF program file for analyzing the sample spectrum. This procedure was repeated with each compound in the library (a 47-compound library in this example). Compounds were reported as not present according to the same criteria as in method I. In the case in which only one compound would be reported as present, analysis of the data would have stopped at this point.

In cases in which more than one compound was reported as being present when the SBM was used, then the compounds selected formed a set of reference spectra for the ILSF analysis of the sample using the SRM. Compounds were then eliminated by iteration using method I.

Both of the ILSF methods were performed manually, with data from each cycle of the LSF software reentered by hand.

Quantitative Analysis. For both the SRM and the SBM, the iterative LSF (ILSF) analysis yielded results that are considered to be quantitative when the final iteration was completed. Data obtained by using the ILSF methods were compared to that obtained when the spectra of known compounds were entered as reference spectra into the LSF program file for quantitative analysis.

RESULTS AND DISCUSSION

For each step of the investigation, results are shown only for an illustrative fraction of the complete data set. This is done to conserve space, since a full reporting of the data would not add to the information content of the results or the generalizability of the conclusions. The full data set is available upon request.

Assumptions in the Use of ILSF Methods. When one is using ILSF methods, it is important to understand the assumptions implicit in the use of the estimated concentration and its relationship to the 95% confidence interval as a critical value on which to base decisions of the presence or absence of compounds in the spectrum of a mixture (*33*). (The relationship of the standard error to the 95% confidence interval is explained in the Methods section.) These assumptions are (1) spectral errors are normally distributed for the sample spectra; (2) there are no errors or noise in either the reference spectra or the concentrations of the reference spectra; (3) there are no model errors (Beer's law is followed, the method III linear base-line assumption across each peak is correct, and temperature, pressure, and pressure broadening must be

Table I. Summary of Qualitative Results Obtained for Samples I–III by Using the Set Reduction Methods (SRM) and the Set Building Method (SBM)

	sample I iteration				sample II iteration				sample III iteration				mean of final iteratn[b]
	1st	2nd	3rd	4th	1st	2nd	3rd	4th	1st	2nd	3rd	4th	
					SRM-General Windows[a]								
true pos	6	6	6	c	5	5	5	4	8	7	7	c	
false pos	8	1	1		12	3	1	1	10	3	3		
true neg	33	40	40		30	39	41	41	26	33	33		
false neg	0	0	0		0	0	0	1	3	4	4		
sensitivity[d]	100	100	100		100	100	100	80	73	64	64		81
specificity[e]	80	98	98		71	91	98	98	72	92	92		96
					SRM-47								
true pos	5	5	5	c	5	5	5	5	10	10	10	10	
false pos	11	6	5		21	11	6	2	22	6	4	3	
true neg	30	35	36		21	31	36	40	14	30	32	33	
false neg	1	1	1		0	0	0	0	1	1	1	1	
sensitivity	83	83	83		100	100	100	100	91	91	91	91	91
specificity	73	85	88		50	74	86	95	61	83	89	92	92
					SRM-Specific Windows								
true pos	6	6	6	c	5	5	5	5	8	8	8	8	
false pos	8	1	1		16	4	2	2	9	7	3	3	
true neg	33	40	40		26	38	40	40	27	29	32	32	
false neg	0	0	0		0	0	0	0	3	3	3	3	
sensitivity	100	100	100		100	100	100	100	73	73	73	73	91
specificity	80	98	98		62	90	95	95	75	80	89	89	94
					SBM-Specific Windows								
true pos	6	6	6	6	5	5	5	5	9	9	9	9	
false pos	15	7	0	0	11	3	1	1	15	5	2	2	
true neg	26	34	41	41	31	39	41	41	21	31	34	34	
false neg	0	0	0	0	0	0	0	0	2	2	2	2	
sensitivity	100	100	100	100	100	100	100	100	82	82	82	82	94
specificity	63	83	100	100	74	93	98	98	58	86	94	94	97

[a] 650–1350 cm^{-1} for fingerprint, 2900–3200 cm^{-1} for C–H stretch region. [b] Mean values were based on the results of the final iteration. [c] When two iterations yield identical results, no further iterations were performed. [d] The percentage of compounds actually present in the mixtures and identified as such. [e] The percentage of compounds actually not present in the mixtures and identified as such.

constant); (4) if analysis is performed by using specific frequency windows for each analyte, and these windows, in the case of overlap, are pooled by LSF, spectral error variance is constant in all bands pooled; (5) there are no components of the mixture not initially included in the set of reference spectra. Thus, for actual samples of mixtures, the confidence interval will be underestimated (*33*).

Protocol Designation. Four separate protocols were performed for each of the three samples using the library of 47 spectra. The tests included (1) ILSF set reduction method starting with up to 48 compounds in a single iteration and with the use of broad, or "general", frequency windows (SRM-47), (2) ILSF set reduction method starting with three sets of 16 compounds and with the use of broad, or "general", frequency windows (SRM-G), (3) ILSF set reduction method starting with three sets of 16 compounds and with windows optimized, or "specific", for each component (SRM-S), and (4) ILSF set building method with windows optimized, or "specific", for each component (SBM-S).

In method SRM-47 and SRM-G, broad windows were used, encompassing both 2900–3200 cm^{-1} for the C–H stretch region and 650–1350 cm^{-1} for the fingerprint region. In the other two methods, all windows were in the fingerprint region between 650 and 1350 cm^{-1}, except for hexane and cyclopentane, for which peaks in the C–H stretch region (2900–3200 cm^{-1}) were used.

Sensitivity and Specificity. In this text and in Tables I and II, nomenclature is used in which the terms "sensitivity" and "specificity" are defined in a manner consistent with use in the health sciences and with use in a prior publication in this journal (*16, 17*). "Sensitivity" is a measure of true positive results and is defined as the percentage of compounds actually present in the mixture and identified as such. For example, in Table I, for the results obtained for sample III by using the SRM-general method

$$\text{sensitivity} = \frac{\text{true positives (7)}}{[\text{true positives (7)} + \text{false negatives (4)}]} = 64\%$$

Similarly, "specificity" is a measure of true negative results and is defined as the percentage of compounds actually not present in the mixture and identified as such. In the same example as above

$$\text{specificity} = \frac{\text{true negatives (33)}}{[\text{true negatives (33)} + \text{false positives (3)}]} = 92\%$$

Comparison of Results. The data show that, for the six-component mixture in sample I, results were approximately equivalent for the SRM-general and SRM-specific tests, but improved to the point that there were neither false positives nor false negatives with the SBM-specific approach. The SRM-47 method produced results that had lower sensitivity and specificity than that of the other methods.

For the five-component mixture in sample II, the SBM-specific results were equivalent in specificity to the SRM-general results, but better than those obtained with the SRM-specific and SRM-47 approaches. For sensitivity, the SBM, SRM-47, and SRM-specific methods were equivalent and were better than the SRM-general results.

For the 11-component mixture in sample III, the SBM-specific was better than either of the SRM results in both sensitivity and specificity, except for the high sensitivity achieved with the SRM-47 method.

Table II. Qualitative Analysis of Three Samples Using the Set Building Method with Specific Windows (SBM-S)

		sample I iteration				sample II iteration				sample III iteration			
	window, cm^{-1}	1st	2nd	3rd	4th	1st	2nd	3rd	4th	1st	2nd	3rd	4th
acetaldehyde	1029–1189	TN[a]				FP[b]	TN			FP	TN		
butyl acetate	990–1330	FP	TN			TN				FP	TN		
2-ethoxyethyl acetate	1011–1310	TN				TN				FP	TN		
ethyl acetate	1000–1145	FP	TN			TN				TP	TP	TP	TP
n-butyl alcohol	880–1150	TN				TN				TN			
ethoxyethanol	970–1310	FP	TN			TN				FP	TN		
1-propanol	924–1155	FP	FP	TN		TN				FP	TN		
2-propanol	1031–1200	FP	TN			TN				TP	TP	TP	TP
ethyl ether	976–1240	TN				TN				TP	TP	TP	TP
bis(chloroethyl) ether	1077–1273	TN				TN				FP	TN		
ethylene oxide	764– 954	TN				TN				TN			
1,4-dioxane	832–1177	TN				TN				TN			
tetrahydrofuran	840–1144	TP[c]	TP	TP	TP	FP	FP	TN		FP	FP	FP	FP
propylene oxide	700–1197	TN				TN				FP	FP	TN	
acetone	1160–1260	TN				TN				TN			
methyl ethyl ketone	872–1241	TN				TN				TN			
methyl propyl ketone	866–1257	TN				TN				TN			
methyl amyl ketone	1087–1255	TN				TN				TN			
methyl isobutyl ketone	896–1312	TN				TN				TN			
cyclopentane	2802–3052	FP	TN			TN				TP	TP	TP	TP
hexane	2799–3025	FP	TN			FP	FP	FP		FP	TN		
benzene	620–1075	TP	TP	TP	TP	FP	FP	TN		TN			
ethylbenzene	1152–1291	TP	TP	TP	TP	TN				TP	TP	TP	TP
styrene	878–1032	FP	TN			FP	FP	FP	FP	FN[d]			
toluene	996–1143	FP	FP	TN		TP	TP	TP	TP	FP	FP	FP	FP
m-xylene	958–1165	FP	FP	TN		TN				TN			
o-xylene	840–1190	TN				TN				TN			
p-xylene	961–1161	TN				FP	TN			TN			
carbon tetrachloride	712– 841	TN				TN				TP	TP	TP	TP
chloroform	1188–1250	TN				TN				TN			
methylene chloride	1219–1309	TP	TP	TP	TP	TN				TN			
vinyl chloride	819–1066	TN				TP	TP	TP	TP	TN			
3-chloropropene	850–1126	TN				FP	TN			FN			
1,1-dichloroethane	670–1324	TP	TP	TP	TP	TN				TP	TP	TP	TP
1,2-dichloroethane	1180–1340	FP	FP	TN		TN				FP	FP	TN	
1,1-dichloroethylene	1040–1173	TN				FP	TN			FP	FP	TN	
1,1,1-trichloroethane	981–1138	TP	TP	TP	TP	FP	TN			FP	TN		
1,1,2-trichloroethane	866– 983	FP	TN			FP	TN			TP	TP	TP	TP
trichloroethylene	754– 973	TN				TP	TP	TP	TP	FP	TN		
tetrachloroethylene	734– 942	FP	FP	TN		TP	TP	TP	TP	TN			
chlorobenzene	994–1148	FP	FP	TN		TP	TP	TP	TP	TN			
o-chlorotoluene	710–1161	FP	FP	TN		TN				TN			
Freon-11	809–1066	TN				FP	TN			TP	TP	TP	TP
acetonitrile	862–1120	TN				FP	TN			TN			
acrylonitrile	862–1046	TN				TN				FP	TN		
dimethyl disulfide	917–1347	TN				TN				TN			
pyridine	958–1245	TN				TN				TN			
sensitivity[e]		100	100	100	100	100	100	100	100	82	82	82	82
specificity		63	83	100	100	74	93	98	98	58	86	94	94

[a] TN: true negative. [b] FP: false positive. [c] TP: true positive. [d] FN: false negative. [e] See Table I.

In sample III, cyclopentane is present. Both cyclopentane and *n*-hexane are present in the library of reference spectra used in this study. Cyclopentane was detected by the SBM on the first iteration, as was *n*-hexane. By the second iteration, *n*-hexane was eliminated. (This is illustrated in Tables II and III.) This is because, on the first iteration using the SBM, the hexane spectrum is matched with the sample spectrum. Since the sample spectrum contained cyclopentane, the peaks of the sample spectrum in the C–H stretch region contained features similar to that of the spectrum of hexane. At this point, since the LSF file of the sample did not yet contain cyclopentane as a known constituent, the false positive result was given for hexane.

However, in the second iteration, cyclopentane had been added to the reference file set with hexane, and the LSF result showed that the peaks in the C–H stretching region were attributed to cyclopentane. Therefore, the remaining spectral features did not fit that of hexane. At this point, the 95% standard error for the fit of the cyclopentane was reduced from 0.29 to 0.12, thereby indicating an improved fit. This performance was paralleled by that of the two SRM tests in which *n*-hexane was rejected in the second iteration when general windows were used and in the third iteration when specific windows were used. (These data are not shown, but are available upon request.)

Note that in these methods, when the results of two successive iterations are identical, no further iterations are performed. This does not mean that the results are more accurate when the convergence rate is higher. While this may be the case, it has not been systematically investigated.

In most cases, the SRM-specific results were better than those obtained by using the SRM-general method. This is because the use of a wide frequency window for all compounds in many cases includes "no information" regions that will, at the concentrations studied here, contain significant noise and/or cause the base lines to be improperly drawn for peaks used for the identification and quantitation of target analytes. The linear base-line assumption will be more accurate over

Table III. Results of Analyses of Samples I–III Using the Set Building Method with Specific Windows

	1st iteration		2nd iteration		3rd iteration		4th iteration	
	concn[a]	SE[b]	concn	SE	concn	SE	concn	SE
Sample I								
tetrahydrofuran	5.96	0.28	3.17	0.27	1.20	0.32	2.25	0.38
1,1-dichloroethane	4.28	0.65	3.01	0.41	2.34	0.40	2.45	0.40
benzene	4.47	0.92	6.32	0.42	6.49	0.35	6.31	0.32
ethylbenzene	5.70	0.27	2.63	0.54	2.89	0.11	2.65	0.07
methylene chloride	2.02	0.18	2.23	0.30	2.11	0.31	2.33	0.23
1,1,1-trichloroethane	3.52	1.96	2.57	0.10	2.79	0.26	2.68	0.12
Sample II								
vinyl chloride	11.03	2.37	2.46	0.09	2.44	0.08	2.52	0.08
trichloroethylene	2.07	0.54	2.82	0.36	2.72	0.20	2.71	0.02
toluene	13.06	2.92	2.88	0.26	2.29	0.17	2.27	0.14
chlorobenzene	2.36	0.11	2.61	0.08	2.46	0.06	2.43	0.06
tetrachloroethylene	2.27	0.27	2.45	0.02	2.39	0.02	2.39	0.02
styrene (FP)[c]	6.91	2.48	2.29	0.07	0.17	0.07	0.19	0.07
Sample III[f]								
Freon-11[d]	12.12	0.25	9.03	2.65	4.19	0.06		
cyclopentane	2.98	0.29	1.46	0.12	1.30	0.08		
1,1,2-trichloroethane	5.62	0.74	5.04	2.34	1.44	0.19		
ethylbenzene	11.35	0.62	4.57	0.83	5.67	0.97		
2-propanol	6.25	2.63	4.87	0.59	1.98	0.50		
styrene (FN)[e]	0.67	0.88						
3-chloropropene (FN)	−2.14	3.03						
carbon tetrachloride	1.34	0.23	1.59	0.31	1.66	0.05		
ethyl ether	1.86	0.39	3.30	0.29	2.76	0.15		
1,1-dichloroethane	1.19	1.12	2.05	1.07	0.98	0.32		
ethyl acetate	1.54	0.85	2.20	1.14	1.34	0.06		
tetrahydrofuran (FP)	4.20	2.23	8.92	2.19	0.42	0.27		
toluene (FP)	31.12	14.90	4.35	0.31	0.80	0.49		

[a] Concentration (ppm (v/v)) in zero air. [b] 1.96 × standard error. Calculate the confidence interval as shown in the Methods section. [c] False positive (indicated concentration > standard error). [d] The concentration of Freon-11 was not certified with a certified gas cylinder standard. [e] False negative (concentration is negative, or < standard error). [f] No improvement in results obtained after third iteration.

a narrower spectral range. However, in cases in which the frequency window is chosen poorly, results obtained with the specific window methods may degrade. (This will be discussed below.)

The data shown in Table I also demonstrates that the SBM was almost always better than or equivalent to the SRM methods in sensitivity and specificity. This is illustrated by reference to the mean value of the sensitivity and specificity, obtained from the final iteration for each method.

In some cases, the results obtained for specific analytes vary with each method. For example, as can be seen from Tables II and III, styrene is reported as a false negative in sample III by all methods except for the SRM-47 method. The SRM-47 method correctly identifies styrene, as well as 2-propanol and ethyl ether, but then Freon-11 is missed. These changes in results are, undoubtedly in large part, due to the interaction between changes in spectral windows, base-line assumptions, and the ILSF method chosen. These factors are the subject of continuing investigations.

The operation of the SBM is further illustrated in Table II, in which each of the iterations for each of the samples is shown. For example, for sample I, styrene is reported as a positive in the first iteration, but is correctly identified as a true negative by the second iteration. In contrast to that, for sample III, styrene is incorrrectly identified as a negative in the first iteration. Succeeding iterations do not contain styrene in the sample set.

As an illustration of the complexity of the spectra of the mixtures used for this investigation, Figure 1 shows the spectra of the mixture and its components, as well as of 2-ethoxyethyl acetate, which is the false positive result for sample I obtained by using SRM-G and SRM-S.

Confidence Interval and Number of Iterations. The 95% confidence interval of the concentration results obtained from LSF is the critical value in the ILSF qualitative analysis. Based on the comparison between the concentration and its confidence interval, expressed in the tables in terms of 1.96 times the standard error, the lack of fit of standard reference spectra to the sample spectrum was calculated. With this information, a judgment was made of whether or not each compound existed in the sample.

As shown in Table III, by reference to the results obtained for sample III, the value of the standard error strongly affects the positive or negative classification of each target analyte. When the SRM-specific method is used (results not shown), ethyl ether is classified as being a false negative. This is because the 95% confidence interval includes zero, and the reported result is therefore "not present" for ethyl ether. If a value of the confidence interval of less than 95% had been used, ethyl ether would have been accurately reported as present. However, as shown in Table II, ethyl ether is reported as a true positive when one uses the SBM.

Similarly, for sample III in Table II, the styrene is reported as "not present". Once again, had the standard error been set at, for example, 90% rather than 95%, the confidence interval would not have included zero, and the compound would have been reported as present.

However, in that situation, the false positive results might have increased as well. Therefore, these is always the risk of losing sensitivity while improving specificity.

Spectral Regions. In the mixtures used for this study, it is rare to find a compound that has spectral features that are completely resolved from those of other compounds. However, in the gas phase under conditions of ambient temperature and pressure, the peaks neither shift nor change shape. Therefore, the selection of optimal frequency windows becomes important.

Frequency regions chosen for each compound for use with the SBM are given in Table II. However, this may be somewhat misleading since the LSF program will combine

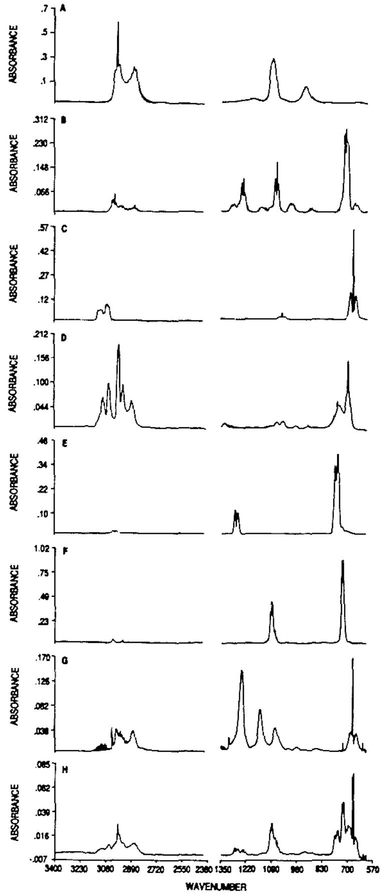

Figure 1. Portions of the infrared spectra of standard reference compounds and sample I (600–1350 cm^{-1}, 2400–3300 cm^{-1}). All the standard reference spectra selected are based on the results of iterative least-squares set reduction method-specific. Traces: (A) 100 ppm tetrahydrofuran, (B) 50 ppm 1,1-dichloroethane, (C) 49.1 ppm benzene, (D) 51.2 ppm ethylbenzene, (E) 49.1 ppm methylene chloride, (F) 49.6 ppm 1,1,1-trichloroethane, (G) 10.6 ppm 2-ethoxyethyl acetate, (H) sample mixture I.

Table IV. Comparison of Results Obtained for the Analysis of Sample I Using FTIR and GC Methods

	concentration,[a] ppm					
	FTIR					
	SRM-G	SRM-S	SBM-S	SRM-47[b]	LSF	GC[c]
tetrahydrofuran	2.92	2.32	2.30	FN[d]	2.30	2.3
1,1-dichloroethane	1.51	2.33	2.57	2.00	2.57	3.46
benzene	4.04	2.34	2.27	1.14	2.27	2.30
ethylbenzene	4.35	2.60	2.65	2.87	2.65	2.11
methylene chloride	1.60	2.38	2.44	2.34	2.44	2.40
1,1,1-trichloroethane	0.30	2.70	2.70	2.89	2.70	2.47

[a] Data for SRM-G, SRM-S, and SBM-S were obtained from the final iteration of each method. Reference spectra for the LSF column were based on the results obtained by GC analysis. [b] The sensitivity of SRM-47 for all samples was 91% (Table I). This example should not be interpreted to imply that the use of SRM-47 results in a greater incidence of FN results. [c] GC results are not certified. These results are shown for comparison purposes only. [d] False negative. Compound was identified by the GC method, but not by this FTIR method, and was included in the reference set for LSF analysis.

Table V. Effect of Windows on the Results Obtained by FTIR for Sample I

	window, cm^{-1}, and concentration, ppm				
compound	window I	concn	window II	concn	GC results
tetrahydrofuran	840–1144	2.22	840–1144	2.30	2.3
1,1-dichloroethane	670–1324	1.71	670–1324	2.57	3.46
benzene	*620–1075*	6.11	*2650–3200*	2.27	2.30
ethylbenzene	*1152–1291*	3.76	*2650–3200*	2.65	2.11
methylene chloride	1219–1309	2.48	1219–1309	2.44	2.40
1,1,1-trichloroethane	981–1138	2.71	981–1138	2.70	2.47

overlapping windows in each iteration. The spectral region thus used will vary for each mixture depending on the degree of overlap of the individual windows.

Selection of appropriate IR frequency windows for LSF was discussed at length by previous authors (*23–27*). However, the most optimal IR window for each compound selected for one mixture may not be appropriate for other mixtures (*26*). As further evidence of this, sample I was analyzed by using a set of reference spectra consisting only of the compounds known to be present in the sample. No iteration was performed.

When sample I was analyzed by LSF using either specific windows within the fingerprint region or the entire fingerprint region, both benzene and ethyl benzene were reported at concentrations significantly greater than those reported by GC analysis (Tables IV and V).

These results were improved significantly when alternate windows in the C–H stretching region were used for these two analytes. This is shown in Table V. Illustration is also given in Figure 1, in which the spectra are shown in both the fingerprint and the C–H stretch regions for sample I and for the components of the sample.

Results may also have been improved if windows had been used for these analytes in both the fingerprint and C–H regions simultaneously. However, this was not tested.

For the 2-propanol in sample III, which has strong C–H stretching peaks, after its IR window was changed from the fingerprint region to the C–H region, the results were unchanged (actual data not shown). The results given for benzene, ethyl benzene, and 2-propanol indicate that, for those compounds which have strong peaks in the C–H stretching region and weak peaks in the fingerprint region, the results may be improved by selecting an IR window for LSF analysis in the C–H stretch region. This, in some cases, would also avoid the complicated overlapped peak envelopes in the fingerprint region of the spectra of certain mixtures.

Noniterative Procedure. Table IV summarizes the quantitative aspects of the LSF-based methods used for the analysis of these samples. Data is shown only for sample I. The data column labeled "LSF" shows the results of analysis where only those compounds known to be present from the GC results were included from the beginning in the LSF data set, and no iteration was performed.

These data indicate that results obtained by using the LSF, SRM-47, SRM-specific, and SBM-specific methods are in good agreement with the results of GC analysis of the samples. The results obtained by using the SRM-general method are not as accurate. Note that no information is available certifying the absolute accuracy of the GC results, so these data are given for comparison purposes only. Therefore, it is clear that, for the compounds and mixtures, at the concentrations evaluated in this study, LSF-based methods are usable for the quantitation of complex mixtures of unknown composition of traces of organic vapor in zero air.

Resolution. Previous studies have shown that, for analysis of trace concentrations of vapors in ambient air, 2-cm^{-1} resolution was adequate (*23–27*). It is important that a resolution be chosen that can both provide the required information and not require the use of excessive computer time and/or higher performance instruments. This is because the ultimate application of this research is to real-time and/or portable Fourier transform infrared (FTIR) systems for occupational health use (*22*).

The effect of resolution on quantitative aspects of the analysis of this data set was studied for all three sample mixtures. There was no demonstrable difference in accuracy when the resolution was varied from 0.5 to 4 cm^{-1}. Thus, 2-cm^{-1} resolution was used in this study.

Analysis Time. Consideration of time of data analysis is important. For these samples, the average computation time, including printing of results, was 4 h for the SRM-47 method, but only 1 h for each of the other methods. Actual computational time for the SBM is less than for the SRM because a higher fraction of the total time is taken by the SBM for printing of intermediate results. Since this will not be a factor in the fully automated software, it is estimated that the SBM will be faster than the SRM by approximately a factor of 2.

It is recognized that the Nicolet 1280 computer is not ideal for this type of analysis. Indeed, a DEC VAX system is generally recommended for such applications. However, we are automating this approach with a 20-MHz PC-DOS 80386-387 system. With this system, we expect computational time to be decreased by a factor of almost 2 orders of magnitude when compared to that required by the Nicolet system.

CONCLUSIONS

Iterative least-squares fit (ILSF) methods based on a commercially available version of the LSF program written by Haaland were developed for qualitative and quantitative analysis of complex mixtures of vapors at trace concentrations. These programs were evaluated for three mixtures containing five to 11 components at approximately 2 ppm in zero air. The results indicate that the ILSF method is very promising as a tool for the interpretation of IR spectra of mixtures.

Generally, performance of the ILSF methods, as measured by "sensitivity" and "specificity", were in the following order: set building method-specific, better than set reduction method-47, approximately equal to set reduction method-specific, better than set reduction method-general. Both qualitative and quantitative results were improved by using specific frequency windows for each compound and by using the set building method rather than the set reduction method.

The standard error after LSF for each compound played an important role in qualitative analysis. The "sensitivity" and "specificity" obtained by each method for each component will be, in part, a function of the set point chosen for the percentage value of the standard error, and thereby for the size of the confidence interval. In general, for a given method, specificity can only be improved at the expense of sensitivity (and vice versa). Investigation is under way into the idea of a programmable confidence interval set point for each iteration.

Work is continuing in this study. Efforts are centered on fully automating the ILSF procedures, on testing the effects of false positive and false negative components on accuracy, on specifying the presence of certain compounds and compound classes, on investigating approaches to base-line problems, and on testing these procedures on sample mixtures in ambient air.

ACKNOWLEDGMENT

The authors thank Ying Li-shi, whose invaluable contributions to the SRM and use of LSF for this application are central to the success of this work. The efforts of Tom Pritchett, U.S. EPA-ERT, are greatly appreciated for supplying the three sample mixtures used in this study. In addition, we thank Dan Sparks and Bill Herget at Nicolet Analytical Instrument Company for valuable guidance, and Mary Weed for artwork.

LITERATURE CITED

(1) Antoon, M. K.; D'esposito, L.; Koenig, J. L. *Appl. Spectrosc.* **1979**, *33*, 351.
(2) Varmuza, K. *Anal. Chim. Acta* **1980**, *122*, 227.
(3) Frankel, D. S. *Anal. Chem.* **1984**, *56*, 1011.
(4) Brown, C. W.; Lynch, P. F.; Obremski, R. J.; Lavery, D. S. *Anal. Chem.* **1982**, *54*, 1472.
(5) Moldoveanu, S.; Rapson, C. A. *Anal. Chem.* **1987**, *59*, 1207–1212.
(6) Fuller, M. P.; Ritter, G. L.; Draper, C. S. *Appl. Spectrosc.* **1988**, *42*, 217.
(7) Zupan, J. *Anal. Chim. Acta* **1978**, *103*, 273–288.
(8) Zupan, J.; Munk, M. E. *Anal. Chem.* **1983**, *55*, 2137–2142.
(9) Zupan, J.; Munk, M. E. *Anal. Chem.* **1985**, *57*, 1609–1616.
(10) Zupan, J.; Munk, M. E. *Anal. Chem.* **1986**, *58*, 3219–3225.
(11) Woodruff, H. B.; Smith, G. M. *Anal. Chem.* **1980**, *52*, 2321.
(12) Woodruff, H. B.; Smith, G. M. *Anal. Chim. Acta* **1981**, *133*, 545–553.
(13) Tomellini, S. A.; Saperstein, D. D.; Stevenson, J. M.; Smith, G. M.; Woodruff, H. B. *Anal. Chem.* **1981**, *53*, 2367–2369.
(14) Tomellini, S. A.; Stevenson, J. M.; Woodruff, H. B. *Anal. Chem.* **1984**, *56*, 67–70.
(15) Tomellini, S. A.; Hartwick, R. A.; Stevenson, J. M.; Woodruff, H. B. *Anal. Chim. Acta* **1984**, *162*, 227–240.
(16) Puskar, M. A.; Levine, S. P.; Lowry, S. R. *Anal. Chem.* **1986**, *58*, 1156–1162.
(17) Puskar, M. A.; Levine, S. P.; Lowry, S. R. *Anal. Chem.* **1986**, *58*, 1981–1989.
(18) Ying, L. S.; Levine, S. P.; Tomellini, S. A.; Lowry, S. R. *Anal. Chem.* **1987**, *59*, 2197.
(19) Eighth International Conference on Computers in Chemical Research and Education, June 15–20, 1987, Beijing, Peoples Republic of China; *Anal. Chim. Acta* (Special Issue) **1988**, *210*, 1–224.
(20) Second Hidden Peak Symposium on Computer-Enhanced Analytical Spectroscopy, June 1–3, 1988, Snowbird, UT. Proceedings to be published by Plenum Press.
(21) Tomellini, S.; Wythoff, B. *Anal. Chim. Acta*, in press.
(22) Air Contaminants—Permissible Exposure Limits. 29 Code of Federal Regulations, Part 1910.1000, U.S. Dept. of Labor (OSHA) Document 3112, 1989.
(23) Strang, C. R.; Levine, S. P.; Herget, W. F. *Am. Ind. Hyg. Assoc. J.* **1989**, *50*, 70–77.
(24) Strang, C. R.; Levine, S. P. *Am. Ind. Hyg. Assoc. J.* **1989**, *50*, 78–83.
(25) Ying, L.-S.; Levine, S. P.; Strang, C. R. *Am. Ind. Hyg. Assoc. J.* **1989**, *50*, 354–359.
(26) Ying, L.-S.; Levine, S. P. *Am. Ind. Hyg. Assoc. J.* **1989**, *50*, 360–365.
(27) Ying, L.-S.; Levine, S. P. *Anal. Chem.* **1989**, *61*, 677–683.
(28) Warner, I. M.; Davidson, E. R.; Christian, G. D. *Anal. Chem.* **1977**, *49*, 2155–2159.
(29) Haaland, D. M.; Easterling, R. G. *Appl. Spectrosc.* **1980**, *34*, 539–548.
(30) Haaland, D. M.; Easterling, R. G. *Appl. Spectrosc.* **1982**, *36*, 665–673.
(31) Haaland, D. M., Easterling, R. G.; Vopicka, D. A. *Appl. Spectrosc.* **1985**, *39*, 73.
(32) Haaland, D. M.; Thomas, E. V. *Anal. Chem.* **1988**, *60*, 1193.
(33) Haaland, D. M., Sandia Laboratories, Albuquerque, NM, personal communication, March 1989.

RECEIVED for review March 27, 1989. Revised manuscript received August 14, 1989. Accepted September 29, 1989. The authors thank the U.S. EPA Environmental Response Team (EPA-ERT) (Research Contract 68-03-3255 and related contracts) and the Centers for Disease Control (CDC-NIOSH) (Research Grant 1-R01-02404) for their generous support.

Anal. Chem. **1989**, *61*, 2715–2718

Nanogram Nitrite and Nitrate Determination in Environmental and Biological Materials by Vanadium(III) Reduction with Chemiluminescence Detection

Robert S. Braman* and Steven A. Hendrix

Department of Chemistry, University of South Florida, Tampa, Florida 33620

Nitrite in environmental water samples is reduced at room temperature to nitric oxide in acidic medium containing vanadium(III). Nitrate is also rapidly reduced after heating to 80–90 °C. Nitric oxide is removed from the reaction solution by scrubbing with helium carrier gas and is detected by means of a chemiluminescence NO_x analyzer. Nanogram detection limits are obtained. The method has the advantage of not requiring highly acidic solutions for nitrate reduction and has been applied to the analysis of a variety of environmental waters, sediment, plant materials, and human urine and blood serum.

INTRODUCTION

The chemiluminescence detector-based method for trace nitrites and nitrates in aqueous samples was first reported by Cox (*1*) and was later applied to analyses of seawater by Garside (*2, 3*). Because of the sensitive nature of the detector, it was possible to analyze samples containing nanomolar concentrations or nanogram amounts of nitrite and nitrate ions. The chemiluminescence analysis method, then, is of importance in environmental analyses, chemical oceanography, and other applications where trace nitrite and nitrate data are needed. Parts-per-billion concentrations can be analyzed with milliliter sample volumes while parts-per-million and higher concentrations can also be determined by using microliter range sample sizes or by dilution.

The earlier methods (*1, 2*) used an acetic acid–potassium iodide mixture at room temperature for nitrite reduction to nitric oxide. Ferrous ammonium sulfate with ammonium molybdate in hot, approximately 50% concentrated sulfuric acid, was used for reduction of nitrate plus nitrite. Nitrate was determined as the difference between analyses of the same sample by the two methods. Extensive trapping of the analyte carrier gas was needed to prevent introduction of acidic gases into the NO_x detector.

REDUCTION METHODS

We have studied the use of vanadium(III) as a reductant for nitrate and find that it has substantial advantages. It is more reactive as a reducing agent than iron(II)–molybdate and can be used at far lower acidities. As was found, sequential, multiple large volume water samples (10–100 mL) can be analyzed by using the same reduction solution, a feature not achieved by the iron(II)–molybdate reduction method which requires fresh, blanked reduction solution for each sample of substantial volume. Addition of large water samples reduces the acidity of the iron(II)–molybdate reagent to the point that it no longer reduces nitrates.

Vanadium(II) was mentioned as a possible reducing agent in the initial work by Cox (*1*), making reference to work by Hassan and Zaki (*4*) who reported that it reduces nitrate to nitric oxide. As will be shown, our work indicates that this is incorrect. Vanadium(III), not vanadium(II), reduces nitrate to nitric oxide. The earlier work (*4*) did not verify the presence of vanadium(II) in the reducing agent nor the presence of NO as the gas evolved.

Our work agrees with that of Ellis and Vogel (*5*) who report reduction of nitrates to ammonium ion by carefully prepared vanadium(II) in hot acidic solutions protected from air oxygen.

The stronger reducing agents such as chromium(II) (*6*) and alkaline titanium(III) (*7*) apparently also reduce nitrates to ammonium ion. In our work, solutions containing vanadium(II) mixed with vanadium(III) did not produce NO from nitrates or nitrites.

Use of vanadium(III) as the nitrate reducing agent is examined here and applied to the analysis of a variety of environmental samples and human fluids. Comparison is made to the acidic iron(II)–molybdate reduction method (*1–3*).

EXPERIMENTAL SECTION

Apparatus. Solutions being analyzed for nitrites or nitrates by reduction reactions producing NO were degassed by using helium which was then passed into a Bendix Model 8101 chemiluminescence analyzer. The apparatus arrangement used is shown in Figure 1. The analyzer inboard flow rate was controlled by a micrometering valve set to approximately 200 mL/min. The helium degassing flow rate was set at approximately 120 mL/min, while oxygen make-up gas to the "T" was set at 100 mL/min. A single bubbler containing 1–2 M NaOH at room temperature was used to remove any acidic gases from the inboard flow into the detector. The "T" system avoids the problem of matching the flow of the analysis stream from the reaction chamber to the inboard flow demanded by the detector.

Cold trapping is not necessary in this apparatus arrangement because the mix of dry make-up gas with the saturated carrier gas produces a relative humidity near 60%. Chemiluminescent analyzers were originally designed for use in continuous analyses of ambient air and so can accommodate high-humidity air. The detector was used in the NO only mode. The output signal was recorded by means of a Linear Instruments, Inc., Model 252A integrating recorder.

Several sizes of reaction chambers were used in the development of the method ranging in size from a 50-mL microimpinger to a 300-mL round-bottomed flask. Flasks in the 50–100-mL range gave the most rapid responses. Volumes of reducing reagent needed varied from 20 to 50 mL depending upon the amount necessary to cover the bubbler frit.

Reducing Reagents. Solutions of vanadium(III) approximately 0.10 M, also 1–2 M in HCl, were produced by reduction of acidic 0.10 M solutions of vanadyl sulfate using a Jones reductor. Generally, the solution developed a pink-purple color during this step indicating the presence of vanadium(II). Redox titration of the reduced solution using standard cerium(IV) confirmed that approximately 10–90% of the vanadium present was vanadium(II) depending upon the contact time of the vanadium solution with the reductor. Figure 2A is a typical titration of a reduced vanadium sample. The vanadium(II) was converted to vanadium(III) by bubbling air or oxygen through the solution. Figure 2B gives the titration curve for the vanadium(III) solution thus prepared. The absence of vanadium(II) in the solution can be determined by measuring the solution potential with the stronger reducing vanadium(II/III) couple having a potential of $E° = -0.256$ V versus standard hydrogen electrode and the weaker reducing vanadium(III/IV) couple having a solution potential of $E° = +0.359$ V versus standard hydrogen electrode or, more simply, by determining the response of the system to nitrate. Solutions containing vanadium(II) did not produce NO from nitrite or nitrate standards added using the analysis procedure.

0003-2700/89/0361-2715$01.50/0 © 1989 American Chemical Society

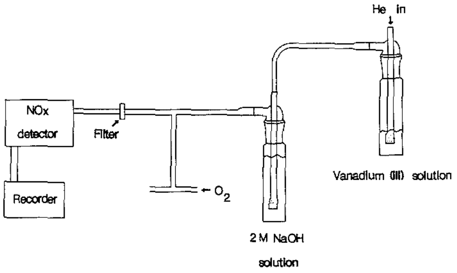

Figure 1. Apparatus arrangement.

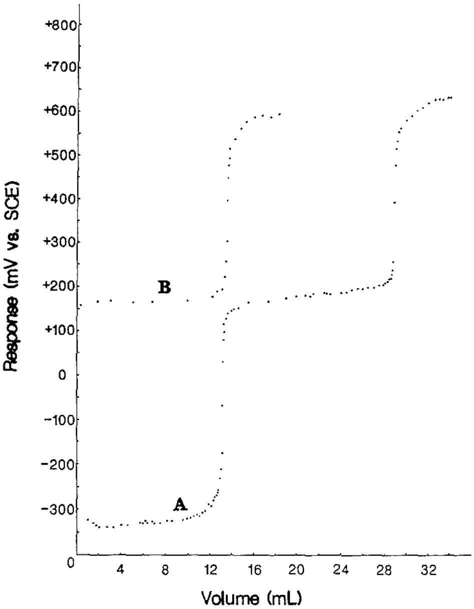

Figure 2. Potentiometric titration of (A) $VOSO_4$ solution after passage through a Jones reductor and (B) vanadium(II) solution after exposure to oxygen.

Vanadium(II) is reported to reduce nitrates to ammonia (*7*) in earlier work using this as a reducing agent for titrimetric analysis of nitrates. Acidic solutions of vanadium(IV) did not reduce nitrate to NO, consequently, vanadium(III) is the active reducing agent.

Prepared solutions of vanadium(III) appeared to maintain their reducing character over at least several months. The initial potentiometric assay was 0.0704 M versus 0.0654 M 7 months later.

The acidic reducing agents used by Cox (*1*) and Garside (*2*) were also prepared in order to compare the two methods. These were concentrated sulfuric acid, 4% ferrous ammonium sulfate, and 2% ammonium molybdate. To 5 mL of sample was added 5 mL of concentrated sulfuric acid, 2 mL of 4% ferrous ammonium sulfate, and 2 mL of 2% ammonium molybdate. This solution was degassed in a hot water bath at 80–90 °C. Successive samples of microliter range amounts can be analyzed by using the hot acidic iron(II)-molybdate reductant. If larger water volumes are to be analyzed, i.e. 5–10 mL, then new blank reagent solutions must be used for each sample to avoid loss of response by decrease in acidity through dilution.

Procedure—Nitrites. Nitrites are rapidly reduced to NO at room temperature by the vanadium(III) reagent. Nitrates are only very slowly reduced at room temperature. Consequently, nitrite samples are added to the degassed reducing solution at room temperature and are then degassed until all is removed. A series of samples can be analyzed by using the same vanadium(III) solution despite dilution of the vanadium(III) as the samples are added.

Procedure—Nitrite + Nitrate. Nitrates are rapidly reduced by vanadium(III) at 80–95 °C. Consequently, the vanadium(III) reagent is added to a reaction flask and heated to this temperature range until the residual nitrate is removed. Samples are then added to the blank solution and the NO signal is recorded. Since nitrites are also reduced, this analysis gives nitrites + nitrates.

Procedure—Nitrite and Nitrate. Nitrites can be separately determined at room temperature and the results subtracted from the analysis of nitrite + nitrate. Alternatively, a hot degassed vanadium(III) solution can be cooled to room temperature and the sample added. This analysis gives nitrite only. The solution is then placed in the hot water bath with no helium carrier gas flowing for 2 min and is then degassed while heating to obtain the nitrate signal. The vanadium(III) solution can then be cooled in an ice bath to be ready for the next sample. This temperature cycling procedure provides for direct analysis of both nitrite and nitrate in the same sample.

Procedure—Sediment Analysis. Samples of essentially 98% calcium carbonate ocean sediments were analyzed directly for nitrite + nitrate. In this case, the vanadium(III) reagent was prepared in 4 M HCl to allow for depletion of the acid by reaction with carbonates during analysis. Sediment samples of 100–300 mg were weighed and added to the blanked, hot reducing solution directly through the top of the reaction flask. The apparatus was immediately reassembled and the analysis performed. The carbonate dissolved quickly with no significant change in response time. The carbon dioxide produced did not give a signal in the NO_x detector with most probably being removed by the NaOH bubbler trap. Some 34 sediment samples were analyzed in sequence utilizing the same vanadium(III) reductor solution. Nitrate calibrations performed following these analyses showed no degradation in response.

Procedure—Human Fluids, Leaves, and Tobacco. Urine and serum responded in a manner similar to that of other fluids. Since nitrite and nitrate samples are in the parts-per-million concentration range, samples of 10–100 μL can be injected directly into a blanked, hot vanadium(III) reduction solution or into a blanked room temperature vanadium(III) solution.

Plant leaves were simply dipped into the reduction solution and then removed. The apparatus was then reassembled and degassed for analysis. A single dipping was sufficient to remove 90% of the surface nitrate present on a leaf.

Tobacco samples in the 1–5 mg range were added directly to the reducing solution for analysis. Alternatively, samples were weighed and soaked in water in a 100-mL volumetric flask and small volumes of the solution injected or pipetted into the reaction flask for analysis.

RESULTS AND DISCUSSION

Vanadium(III) Concentration Study. The effect of vanadium(III) concentration on the reduction of nitrate was determined by analyzing standard nitrate samples over a range of vanadium(III) concentrations produced simply by diluting the starting 0.066 M reduction solution with deionized water. Results indicate that reduction occurs at a reasonable rate (4–5 min/analysis) down to approximately 0.001 M vanadium(III). A similar response effect was obtained for nitrite at room temperature. Table I gives the results for these sets of analyses.

Temperature Effect Study. The effect of temperature on the rate of nitrate reduction was determined by analysis of a series of standards at varying water bath temperatures, the results of which are given in Table II. The indication is that water bath temperature should be approximately 85–95 °C for rapid reaction. Under these conditions analyses require 2–5 min per sample. Typical responses for nitrite + nitrate at varying water bath temperatures are shown in Figure 3. Nitrite reacts at room temperature and equally well at the elevated temperatures.

Table I. Effect of Vanadium(III) Reductor Solution Concentration on Nitrite and Nitrate Response[a]

$[V^{3+}]$, M	NO_2^--N, ng	NO_3^--N, ng	time[b]
0.063	77.13	72.22	1.5, 1.5
0.043	74.71	76.54	1.6, 1.6
0.0315	73.56	77.10	1.6, 2.0
0.0210	89.14	77.10	2.1, 1.6
0.0145	79.49	84.69	2.1, 2.7
0.00741	73.49	75.42	1.6, 3.2
0.00394	75.16	64.71	2.0, 3.9
0.00091	78.05	83.42	2.2, 6.2
	$N = 8$	$N = 8$	
	77.59 ± 5.14	76.41 ± 6.26	

[a] 10-μL injections of 8.00 ppm standard solution. [b] In minutes, measured base line to base line; NO_2^-, NO_3^-.

Table II. Effect of Water Bath Temperature on Nitrate Reduction

water bath temp, °C	response time[a]	water bath temp, °C	response time[a]
60	7.7	85	3.0
66	7.8	90	2.4
71	6.5	98	2.1
79	4.2		

[a] In minutes, measured base line to base line, 10-μL injections of 8.00 ppm standard nitrate solution.

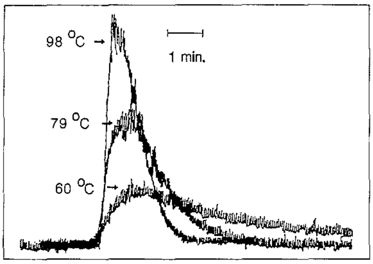

Figure 3. Effect of water bath temperature on $NO_3^- + NO_2^-$ response time.

Table III. Effect of Vanadium(III) Reductor Solution Acidity on NO_3^- and NO_2^- Response[a]

pH	$[V^{3+}]$[b]	NO_3^--N, ppm	NO_2^--N, ppm
0.6	0.033	8.41 ± 0.30	8.01 ± 0.05
1.0	0.031	5.27 ± 1.23	8.49 ± 0.17
2.0	0.030		7.79 ± 0.11
3.0	0.029		6.39 ± 0.15

[a] Average of duplicate 8.00 ppm standard NO_3^- injections, hot, and 8.00 ppm standard NO_2^- injections, cold. [b] After dilution with 2 M NaOH.

Table IV.

a. Determination of $NO_3^- + NO_2^-$ as Nitrogen in Hillsborough River Water

total solution vol, mL	$NO_3^- + NO_2^-$-N, ppm	time[a]
70	0.13	4.5
90	0.13	4.1
110	0.13	4.3
130	0.13	3.9
150	0.13	4.0
170	0.13	4.0
190	0.12	4.0
210	0.12	3.4
230	0.10	3.2
250	0.11	3.0

b. Determination of NO_2^- as Nitrogen in Tampa Bay Seawater

total solution vol, mL	NO_2^--N, ppb	time[a]
75	1.56	6.0
100	1.65	5.6
125	1.69	5.2
150	1.68	5.0
175	1.57	4.4
200	1.56	4.2
225	1.77	4.0
250	1.73	3.6
275	1.69	3.4
300	1.66	3.4

[a] In minutes, measured base line to base line.

Vanadium(III) Acidity Effect Study. The acidity of the vanadium(III) reductor solution was adjusted to several different values by addition of 2 M NaOH. The solution was then used to analyze standard nitrite and nitrate solutions in order to determine the effect on response. Nitrite standards were analyzed by use of room temperature vanadium(III) solution while the nitrate standards were analyzed by use of hot vanadium(III) solution. The results, given in Table III, indicate that nitrate response diminishes beginning at approximately pH 1 and disappears altogether at pH 2 and higher. Nitrite response begins to diminish at approximately pH 2. Adjusting the vanadium(III) reductor solution to pH 0.6 required the addition of approximately 20 mL of 2 M NaOH doubling the initial vanadium(III) solution volume. This and further additions of 2 M NaOH did not reduce the vanadium(III) concentration to the point where its activity was significantly decreased. Nitrate and nitrite response can be restored by the addition of HCl to the reductor solution.

Interferences. The possibility of nitro-organic compounds producing a positive nitrite or nitrate response was investigated by analyzing several of these compounds using the nitrite + nitrate procedure. *N*-Nitrosodimethylamine, 1-nitrosopyrrolidine, 4-nitrosophenol, 2-nitrosotoluene, and nitrobenzene produced no detectable response. Also, no degradation of sample materials (i.e. vegetation or human fluids) to produce volatile organic compounds or other gases detectable by the NO_x analyzer was observed.

Response Curves and Detection Limits. The response curves for nitrite and nitrate are the same within statistical variation. Two curves obtained by using the same reduction solution are

$$NO_3^- \text{ as N (ng)} = 7.997(x) - 0.075$$
$$S_b = \pm 0.048,\ S_r = \pm 0.514\ (N = 4)$$

$$NO_2^- \text{ as N (ng)} = 7.598(x) + 0.549$$
$$S_b = \pm 0.181,\ S_r = \pm 2.130\ (N = 4)$$

where (x) is the integrator count per response, S_b is the standard deviation of the slope, and S_r is the standard deviation of the residuals.

A lower detection limit of 2–3 ng of nitrate or nitrite-nitrogen was found.

Sequential Analyses of Large Water Samples. Two sets of sequential analyses were performed to further determine the effect of dilution on analysis response. The possibility of analyzing, in sequence, a series of large volume water samples was demonstrated by using 20-mL samples of Hillsborough River water (Tampa, FL). The nitrite + nitrate procedure was used. A 300-mL reaction flask was used starting with 50 mL of 0.0645 M vanadium(III). Ten samples were

Table V. Comparison of the Iron(II) Molybdate Method and the Vanadium(III) Method in Analysis of Various Environmental Samples

	iron(II) molybdate[b]		vanadium(III)[b]	
sample[a]	$NO_3^- + NO_2^-$	NO_2^-	$NO_3^- + NO_2^-$	NO_2^-
A	9.5	2.3	9.2	2.5
B	808.6	10.6	774.7	13.0
C	2.4	0.1	2.3	0.2
D	735.8	6.6	725.5	9.1

[a] Samples: (A) 2-mL samples from Tampa Bay; (B) 2-mL samples from USF golf course pond; (C) 4-mL samples from Lake Carroll, Tampa, FL; (D) 4-mL samples from Hillsborough River, Tampa, FL. [b] μg/L as N, average of two to three samples.

Table VI. $NO_3^- + NO_2^-$ in Various Samples

	response
human blood serum[a]	17.4 ± 0.3 ng (N = 2)
human urine[b]	146.0 ± 15.0 ng (N = 2)
domestic beer[c]	52.1 ± 3.6 ng (N = 2)
imported cigarette[d]	0.056 ± 0.002% (N = 3)
domestic cigarette[e]	1.30 ± 0.03% (N = 3)
sediment[f]	0.13 ± 0.03 ppm (N = 4)
nondairy cream[g]	0.75 ± 0.07 ppm (N = 2)
corn flake[h]	0.26 ppm (N = 1)

[a] 25-μL injections, as N. [b] 6-μL injections, as N. [c] 20-μL injections, as N. [d,e] Microliter injections of solution containing whole cigarette, minus filter, weighed and placed in 100-mL volumetric flask, expressed as % KNO_3. [f] Wet sample basis. [g] 25-μL injections, as N. [h] 115-mg sample, as N.

analyzed by using the original reduction solution. Table IVa gives the analysis data and response times. A similar series of ten analyses was performed using 25-mL samples of seawater from an area near the mouth of Tampa Bay. In this case, the nitrite-only procedure was used. Table IVb gives the results and response times for these analyses. Note that even with the addition of up to 250 mL of sample solution to the original 50 mL of vanadium(III) reagent in the reaction flask, no decrease in response or increase in analysis time is observed.

An interesting aspect of the analyses obtained by using the vanadium(III) method was that the response times decreased with added sample volume. This was likely due to the decrease in headspace volume of the analysis chamber with the addition of samples and the simultaneous decrease in the time required to sweep out the NO produced.

Comparison of Vanadium(III) to Iron(II)–Molybdate Method. Several different sources of environmental waters were analyzed using the two reduction methods. Results are given in Table V. Note that the vanadium(III) method and the iron(II)–molybdate method give equivalent results.

Sediment, Vegetation, Tobacco Leaf, and Human Fluid Analyses. This series of analyses was done to demonstrate the range of sample types that can be examined for nitrite and nitrate using the vanadium(III) reduction method. Table VI gives results of some of the various analyses. All responses were typical in shape for nitrate responses in hot vanadium(III) reduction solutions. Figure 4 shows some of these responses for the different samples. Since in all of these cases only small samples were involved, many sequential analyses are possible without changing the vanadium(III) reducing solution. The response of nitrate standards before and after many sample analyses was the same in all cases.

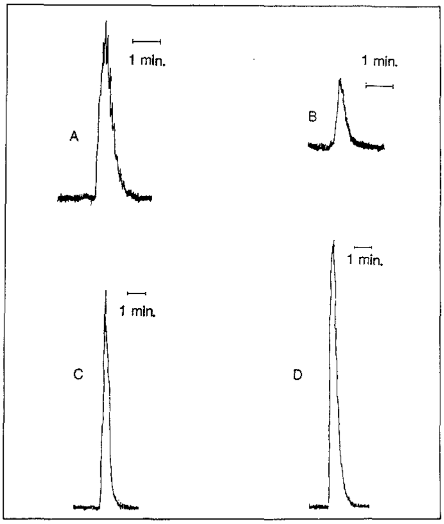

Figure 4. $NO_3^- + NO_2^-$ in various samples: (A) human blood serum, 25 μL, 2.12 ppm; (B) mangrove leaf, 14 ng/leaf; (C) domestic beer, 20 μL, 2.70 ppm; (D) human urine, 10 μL, 10.30 ppm.

CONCLUSIONS

The vanadium(III) reduction method is shown here to be applicable to the analysis of a variety of sample types. the reduction reagent is active at low concentrations and at moderate (down to 0.1 M) acid concentrations. A series of water samples can be analyzed sequentially, even at 20 mL per sample, if very low concentrations are encountered without loss of response. The response time was as rapid as 1 min per sample when a small headspace volume was used in the reaction flask. For most analysis conditions, the response time was 2–4 min per sample. Modifications of the technique provide for nitrite analysis only, nitrite + nitrate, or nitrite and nitrate in the same sample using temperature cycling.

The apparatus arrangement needed is much simpler than that reported for the iron(II)–molybdate method. The response and range of uses are superior to those of the earlier methods largely because of the milder acidity conditions needed for analyses.

Analysis of human fluids and plant materials demonstrates the range of applications to analysis of complex materials. Since only small amounts of sample are needed in urine or serum analysis, the technique can be used for the analysis of a large number of samples sequentially without the necessity of sample prereduction or other preparation. This makes the vanadium(III) method superior to many other trace nitrate methods.

LITERATURE CITED

(1) Cox, R. D. *Anal. Chem.* **1980**, *52*, 332–335.
(2) Garside, C. *Marine Chem.* **1982**, *11*, 159–167.
(3) Garside, C. *Deep-Sea Res.* **1985**, *32*, 723–732.
(4) Hassan, S. S. M.; Zaki, M. T. M. *Z. Anal. Chem.* **1976**, *282*, 138.
(5) Ellis, C. M.; Vogel, A. I. *Analyst (London)* **1956**, *81*, 693–703.
(6) Lingane, J. J.; Pecsok, R. L. *Anal. Chem.* **1949**, *21*, 622–625.
(7) Cresser, M. C. *Analyst (London)* **1977**, *102*, 99–103.

RECEIVED for review September 19, 1989. Accepted September 27, 1989.

Anal. Chem. 1989, 61, 2719–2724

Statistical Estimation of Analytical Data Distributions and Censored Measurements

Kirk K. Nielson* and Vern C. Rogers

Rogers and Associates Engineering Corporation, P.O. Box 330, Salt Lake City, Utah 84110-0330

A numerical method was developed for estimating the shapes of unknown distributions of analytical data and for estimating the expected values of censored data points. The method is based conceptually on the normal probability plot. Data are ordered and then transformed by using a power function to achieve approximate linearity with respect to a computed normal cumulative probability scale. The exponent used in the power transformation is an index of the distribution shape, which covers a continuum on which normality is defined as $d = 1$ and log normality is defined as $d = 0$. Expected transformed values of censored points are computed from a straight line fitted to the transformed, accepted data, and these are then back-transformed to the original distribution. The method gives improved characterization of analytical data distributions, particularly in the distribution extremities. It also avoids the biases from improper handling of censored data arising from measurements near the analytical detection limit. Illustrative applications were computed for atmospheric SO_2 data and for mineral concentrations in hamburgers.

INTRODUCTION

In environmental surveillance of chemical compounds, trace elements, and radionuclides, analytical measurements often span very wide ranges, but still may represent a single population. To represent the population by its measured parameters, a central value (mean, median, etc.) and distribution width (standard deviation, range, etc.) generally are sought for simplicity and convenience in statistical analyses. Two common causes of subjective bias in representing the population are the choice of distribution attributed to it and the method of dealing with censored data points. The distribution often is simply assumed to be normal or log-normal, even though it may have an intermediate or alternative shape. Even when distributions are analyzed by using normal or log-normal probability plots, their shapes still are usually assessed subjectively for linearity and for approximation to normality or log normality. While the biases resulting from inaccurate distribution assumptions affect both central value and width estimates, they can be particularly misleading when one is making decisions about confidence intervals or compliance with prescribed limits.

The problem of censored data points also is common in environmental surveillance, where vanishingly small concentrations frequently lead to observations that are less than the analytical limit of detection (LD). As concentrations approach zero, the combined measurement uncertainties in samples and blanks can even cause a fraction of observations to be negative. Although there are numerical definitions of the appropriate LD for data acceptability (*1–4*), there is less consistency in reporting and interpretation of the lower, censored measurements. They variously are ignored or reported as zero, as <LD, as the numerical LD, or as the measured values. Reporting the numerical LD and the total number of measurements is particularly important.

To interpret the resulting left-censored distributions, special methods are required to avoid biased estimates of the central value and width of the distribution. Although the lower limit of the data range usually is ignored, several numerical and graphical methods have been reported (*5–10*) to estimate the means and standard deviations of censored distributions. The numerical methods sometimes are limited by their allowable fraction of censoring, assumed distribution shape (normal, log-normal, etc.), computational complexity, use of lookup tables, and difficulty in being understood by the nonstatistician. Graphical methods involving probability plotting are easier to understand and provide more insight into the data distribution, but may lack numerical precision, accuracy, and convenience.

This paper describes a least-squares regression method, related to probability plotting, to estimate numerically the shape of an unknown distribution and the expected values of censored data points. These can serve in turn to compute unbiased statistics such as medians, confidence intervals, ranges, and proximity to normality, log-normality, or other distribution shapes. The method assumes that the analytical data come from a single population and that they are transformable to a normal distribution. It requires a constant point of censor (LD) for all observations, so that all censored values are known to be less than the lowest accepted (noncensored) value. The method is well-suited to interactive use on personal computers, where the nature of the data distribution can be visually examined and interpreted. Although the distribution shape need not be known, the precision of censored value estimates is greatly increased if it is known. The method is evaluated empirically by using fixed and random distribution shapes, with varying fractions of censoring. It is applied here to environmental and trace-element observations.

THEORY

The use of probability plots to examine the normality or log normality of data distributions is described in many statistics textbooks. In some cases (*8, 9, 11*), straight lines have been drawn or fitted to the cumulative probability plots to define the median (intercept at the $p = 0.5$ point) and standard deviation (slope), even if some of the data points are censored. Figure 1 illustrates such a case. The ability to obtain an unbiased median and standard deviation despite censoring depends on knowledge of the total number of observations, n, from which the probability plotting position, p_i, for each point is computed. To compute p_i, the accepted data first are ordered by numerical value. The sequence number, i, for each point then is used in computing p_i as

$$p_i = (i - 0.5)/n \tag{1}$$

An alternative function to eq 1 for computing the probability plotting position also has been used (*12*) for better consistency with certain theoretical considerations:

$$p_i = i/(n + 1) \tag{2}$$

In empirical comparisons, only eq 1 defined probability positions such that the slope of a straight-line normal prob-

0003-2700/89/0361-2719$01.50/0 © 1989 American Chemical Society

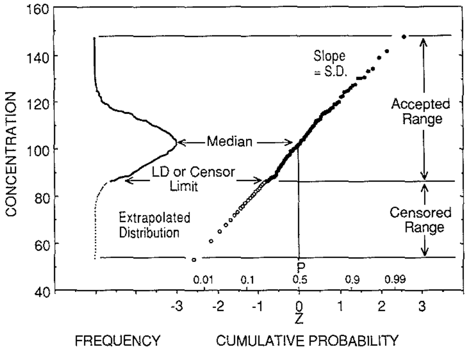

Figure 1. Comparison of a censored normal distribution frequency plot to its cumulative probability plot.

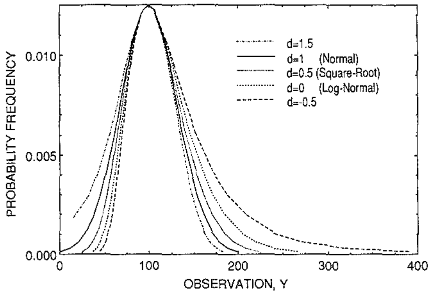

Figure 2. Comparison of the shapes of five frequency distributions, each composed of 500 points with median = 100 and standard deviation = 32.

ability plot was equal to the standard deviation of the numbers being plotted. Therefore eq 1 was used throughout this work for computing probability plotting positions.

The linear reduced variate scale, *z*, shown in Figure 1 in standard deviation units, is related to the cumulative probability scale by the areas under the standard normal distribution curve, as tabulated in standard statistics tables and texts. The slope must be defined in terms of the linear (*z*) scale in order to directly define the standard deviation of the plotted distribution. For generating the probability plots on a computer and for least-squares fitting of the probability distribution, the transformation of probability fractions to the reduced variate scale utilizes the relation (*13*)

$$z_i = t_i - \frac{a_0 + a_1 t_i + a_2 t_i^2}{1 + b_1 t_i + b_2 t_i^2 + b_3 t_i^3} \qquad (3)$$

where

$$t_i = [\ln (1/p_i^2)]^{1/2} \qquad 0 < p_i \leq 0.5$$

$$a_0 = 2.515517 \qquad b_1 = 1.432788$$

$$a_1 = 0.802853 \qquad b_2 = 0.189269$$

$$a_2 = 0.010328 \qquad b_3 = 0.001308$$

Plotting data points versus their *z* values defined by eq 3 yields a straight line for normally distributed data, and thus also for the logarithms of log-normally distributed data. Skewness causes curvature in a normal probability plot, and the degree of curvature is consistent with the deviation from the normal distribution and with the approximation of an alternative distribution. For example, normal and log-normal distributions are compared with the intermediate square-root distribution and with more negatively and positively skewed distributions in Figure 2, and their corresponding normal probability plots are illustrated in Figure 3. These graphs also illustrate the continuum of possible distributions that may represent natural systems, on which the normal and log-normal shapes represent two discrete points. A numerical classification of the distributions in Figures 2 and 3 can be written as a distribution index, *d*, which is the exponent that can be used to transform the given data, Y_i, to a normally distributed equivalent, $Y_{ni} = Y_i^d$. To preserve the median, $\bar{Y}$, and nominal width of the original data distribution, the transformation

$$Y_{ni} = \bar{Y}\{1 + [(Y_i/\bar{Y})^d - 1]/d\} \qquad (4)$$

is found empirically to yield an equivalent normalized transformed data set. The distribution indices, *d*, describe a continuous set of distributions except for a discontinuity at $d = 0$, which corresponds to the log-normal transformation. Distributions defined by $|d| \leq 0.001$ approach log normality. The transformations provided by various values of *d* are compared graphically in Figure 4 to further illustrate the continuum of distributions described by eq 4.

The distribution index is useful in numerically defining unknown data distributions, but more importantly, it provides a basis to transform data to normal distributions and thereby obtain unbiased estimates of distribution parameters and censored values. The method for obtaining the unbiased estimates involves first finding the distribution index, and then transforming the data to a normal distribution by using eq 4. Unbiased confidence intervals, censored values, and other parameters then are computed from the transformed data, after which each is back-transformed to the original distribution by using the inverse of eq 4.

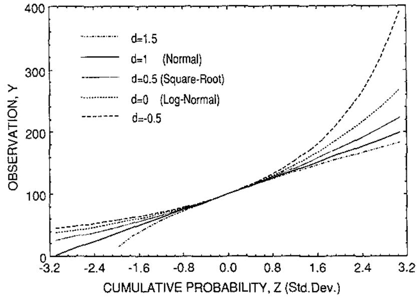

Figure 3. Comparison of the normal cumulative probability plots of five distributions, each composed of 500 points with median = 100 and standard deviation = 32.

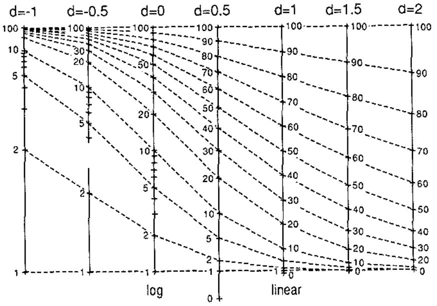

Figure 4. Comparison of plotting scales for seven different frequency distributions. Equivalent points are connected by the dashed lines.

To compute the index, d, of an unknown distribution, the reduced variates for the data set first are defined by using eq 1 and 3. The value of d then is sought that transforms the data to yield a straight cumulative probability plot (solid line, Figure 3). The value of d is iteratively estimated from trial values, d_j, which are tested by trial transformations of the original data using eq 4. The normality of each transformed distribution is measured by fitting the transformed data by least squares to a quadratic function of the reduced variate

$$Y_{ni} = c_0 + c_1 z_i + c_2 z_i^2 \tag{5}$$

to estimate its curvature. The fitting coefficients define the transformed distribution median as c_0, its relative width as c_1/c_0, and its relative curvature as c_2/c_1.

The curvature obtained with each trial index is used to improve further estimates of d_j until a near-zero curvature (normal distribution) is obtained. Initial trial values of $d_1 = 1$ and $d_2 = -0.5$ are used to define corresponding curvatures c_2/c_1 according to eq 4 and 5. Each successive trial index, d_j, is computed from a least-squares fit of all preceding values and their associated curvatures, $(c_2/c_1)_j$, to the quadratic function

$$d_j = f_0 + f_1(c_2/c_1)_j + f_2(c_2/c_1)_j^2 \tag{6}$$

where f_0, f_1, and f_2 are the fitting coefficients. The next trial index is computed from eq 6, for zero curvature, as $d_j = f_0$. This approach converges to within 1% of the final value of d in about six iterations and to within about 0.1% in nine iterations.

It should be noted that although the least-squares fitting of eq 5 to experimental data utilizes conventional methods (*14*), the conventional statistics describing goodness of fit (i.e., the correlation coefficient, r; standard error of the estimate, s_{yx}) cannot be interpreted or used in the usual way owing to the ordering of the observations prior to fitting. These statistics indicate much lower, nonrandom variation. However, they still can be used as a relative index of fitting precision.

Unbiased estimates of confidence intervals and censored values are made on data that have been transformed to a normal distribution by using the distribution index d in eq 4. Confidence intervals are computed from eq 5, using eq 3 to obtain the reduced variates z_j from the desired probability fractions. The resulting confidence intervals then are transformed back to the original distribution by using the inverse of eq 4. Censored values similarly are computed from a fit of all accepted transformed values to eq 5, defining c_0, c_1, and c_2. The reduced variate of each censored point is computed from eq 1 and 3 and is used in eq 5 to estimate the transform of the expected value of the censored point. The expected values finally are transformed back to their original distribution by using the inverse of eq 4. Unbiased estimates of other statistics can be computed similarly from the normal-transformed data and then back-transformed to the original distribution. Any negative extrapolated values of Y_{ni} are undefined in the reverse transformation from eq 4, but are considered to be zero for defining the distribution shape.

NUMERICAL EVALUATION OF UNCERTAINTIES

The accuracy of defining the distribution index, d, was evaluated by testing the method defined by eq 1 and 3–6 on known distributions with varying indices of $d = -0.5$ to $d = +1.5$. The computed values of d consistently were within less than 0.01% of the known value. To evaluate the precision of the distribution indices, a computer program was written to generate random normal distributions with prescribed medians, $\bar{Y}$, and standard deviations, s_Y. The random distributions were generated on a microVax II computer using random numbers, R_i (a unit rectangular variate), generated by the microVMS operating system, with the normal distribution approximation (*15*)

$$Y_i = \bar{Y} + s_Y[(\sum_{j=1}^{k} R_{ij}) - k/2]/(k/12)^{1/2} \tag{7}$$

A value of $k = 48$ was used in eq 7, as a trade-off between computational speed and bias of the resulting normal distributions. Higher order summations in eq 7 did not alter significantly the resulting distributions.

The program transformed the normal distributions by using the inverse of eq 4, and in the case of the log-normal distribution, an approximate value of $d = 0.0001$ was used. It then ordered the data and computed its cumulative probability variate, z_i, using eq 1 and 3. For evaluating distribution indices, d, the program iteratively used eq 4–6 as described above. Through repetition of this process for many known random distributions, a mean and standard deviation of d were computed for normal, log-normal, and other distribution shapes. The means corresponded to the known transform values used in generating the distributions. The standard deviations of the distribution indices, s_d, were dependent on the number of points in the random distributions, on their widths, and on the fraction of data points that were censored, f_c, but not on the distribution shape. log–log plots of s_d versus the number of data points were approximately linear for values of $s_d \leq 1$, indicating an exponential decrease in the uncertainty of the estimated value of d with the number of points in the distribution. Increased relative widths of the distributions, expressed as $s_Y/\bar{Y}$, lowered s_d as the inverse of the relative width, and censoring of the low end of the distribution raised s_d linearly. From empirical combinations of the fitting parameters of s_d for 10–500 data points, $s_Y/\bar{Y}$ ranging from 0.1 to 1.0, and f_c ranging from 0 to 0.7 (at $s_Y/\bar{Y} = 0.5$), the standard deviation of d was found to vary approximately as

$$s_d = (1.3 + 11f_c)n^{-0.58}\bar{Y}/s_Y \tag{8}$$

From this relation, it can be observed that an unknown distribution cannot be distinguished confidently to be normal ($d = 1$), as opposed to log-normal ($d = 0$), if the number of points is small ($n \approx 10$) and the width is narrow ($s_Y/\bar{Y} \leq 0.5$). However, it can be characterized with increasingly greater confidence as the number of points is increased and as its width is increased.

The precision of estimating the expected values of censored data points also was evaluated by using random normal distributions defined by eq 7. Only normal distributions were used because other distributions can be transformed to become normal. Censoring was accomplished for each distribution after ordering of its randomly chosen values by removing all values below a prescribed LD. The remaining values then were fitted by least squares either to a straight line or to a quadratic as in eq 5, and the expected values of the censored points were computed from the fitted function. The straight-line function was used to simulate cases in which the distribution is previously known to have a given shape, either normal or one that can be transformed to become normal. It thus yields uncertainties that are smallest, since random variations in the numerical distributions are forced to conform to the prescribed shape. The quadratic curve was used to simulate cases in which the distribution shape is unknown, and hence any random curvature in the numerical distributions can be interpreted as possible curvature in the cumulative probability plot. Hence extrapolations of expected censored values may have a wider range of variation due to random curvature in the uncensored portion of the data. Resulting distributions were averaged over repeated trials to establish the mean expected values and their variability.

The mean values and their confidence intervals for the 100-point distribution 100 ± 10 are illustrated in Figure 5 for

Table I. Standard Deviations of the Expected Minima of Distributions with Varying Censored Fractions, f_c, Assuming Known and Unknown Distribution Shapes[a]

		known distribution shape[b]					unknown distribution shape[c]				
n[d]	$f_c = 0$	$f_c = 0.1$	$f_c = 0.3$	$f_c = 0.5$	$f_c = 0.7$	$f_c = 0.9$	$f_c = 0.1$	$f_c = 0.3$	$f_c = 0.5$	$f_c = 0.7$	$f_c = 0.9$
10	6.0	5.3	6.8	9.6	16	–[e]	8.0	14	25	53	–[e]
20	4.9	4.2	5.6	7.8	11	–[e]	5.9	11	18	40	–[e]
50	4.4	3.1	4.1	5.4	8.0	17	5.5	10	17	27	113
100	3.8	2.5	3.5	4.4	6.5	14	4.3	8.9	15	24	61
200	3.4	1.6	2.2	3.0	4.7	11	3.4	7.0	13	22	51
500	2.5	1.3	1.8	2.3	3.3	7.0	2.9	5.7	8.7	15	34
1000	3.6	1.0	1.3	1.9	2.7	4.8	2.7	4.4	6.9	12	29

[a] Normal distribution, 100 ± 10. [b] Linear fit to normal probability plot. [c] Quadratic fit to normal probability plot. [d] Number of points in the distribution (100 distributions averaged for n = 10, 20, 50; 50 distributions averaged for n = 100, 200; 30 distributions averaged for n = 500; 20 distributions averaged for n = 1000). [e] Insufficient data for fitting.

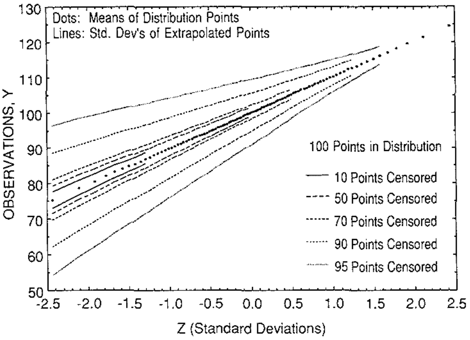

Figure 5. Mean expected values (dots) and 1σ confidence intervals for the normal distribution 100 ± 10 with five different fractions of censoring.

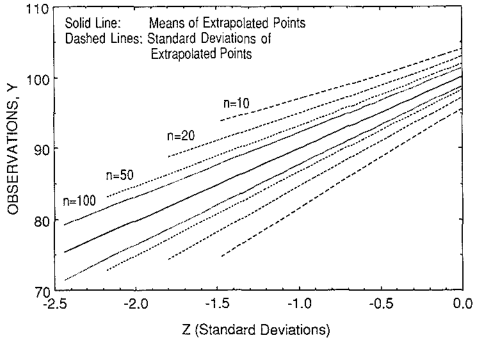

Figure 6. Mean expected values (solid line) and 1σ confidence intervals for the half-censored normal distribution 100 ± 10, containing varying numbers of data points.

varying fractions of censoring and a linear (known) distribution shape. The confidence intervals increase in magnitude with the fraction of points censored and with distance from the median. Figure 6 illustrates the corresponding variations of the half-censored 100 ± 10 distribution when it contains varying numbers of data points. The widths of the confidence intervals decrease as the number of data points is increased. In both cases, the confidence intervals vary nearly linearly with z, in contrast to the confidence intervals about uncensored distributions, which exhibit greater curvature near the extremes of the distribution.

The precision of computing expected values of censored points for unknown distributions (quadratic fit) is compared

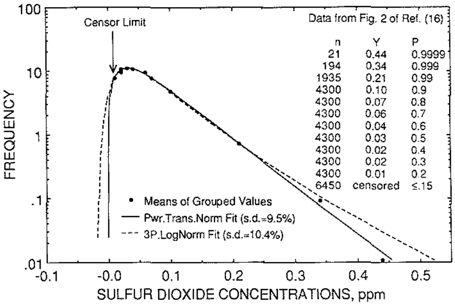

Data from Fig. 2 of Ref. (16)

n	Y	P
21	0.44	0.9999
194	0.34	0.999
1935	0.21	0.99
4300	0.10	0.9
4300	0.07	0.8
4300	0.06	0.7
4300	0.04	0.6
4300	0.03	0.5
4300	0.02	0.4
4300	0.02	0.3
4300	0.01	0.2
6450	censored	≤.15

Figure 7. Comparison of three-parameter log-normal (0.0245 ppm offset) and power-transformed normal (d = 0.301) distribution fits to grouped atmospheric sulfur dioxide data.

with that for known distributions (linear fit) in Table I for the lowest values (minima) of the 100 ± 10 distribution. The uncertainties of the minima are relatively small in either case until censoring becomes severe. For example, the uncertainty in Table I of 4.4 for a 100-point distribution with 50% censoring indicates that the lowest value for this distribution (approximately 75, as shown in Figure 5) is uncertain by less than 6%. The corresponding uncertainty of 15 for the unknown distribution in Table I indicates the same minimum value is uncertain by about 20% if the distribution shape is unknown. The uncertainties of the minimum points in the known distribution are even smaller with f_c = 0.1 than for the uncensored distribution due to the averaging caused by computing the expected values from the fitted line. Uncertainties for the unknown shape, computed from the fitted quadratic, show a similar trend only for the 1000-point case. These are consistently greater than values from the linear fit because of random curvature in the distributions being averaged.

EXAMPLE APPLICATIONS

The statistical methods presented here for estimating distribution shapes and censored values are applied to two test data sets that illustrate their use, characteristic results, and interpretation. One application was to published environmental air quality monitoring data that had been previously analyzed by fitting to a three-parameter log-normal distribution (*16*). Although the previous analysis was itself a great improvement over earlier log-normal analyses (*17*), the present analysis gave slightly better fit overall, and significantly improved fit in the distribution extremities.

A set of 43 000 SO_2 measurements, represented by 11 grouped data points in Figure 2 of ref 16, was distributed over symmetric frequency intervals to obtain the weighting values, n_i, shown in Figure 7. The resulting data then were fitted by weighted least squares to the reported three-parameter

Table II. Measured Parameters and Fitted Distribution Statistics for Mineral Concentrations in 112 Hamburger Samples

	measd param			power-transformed fit param				log-normal fit param	
elem	LD^a	n > LD^b	mean^c ± SD	distribn index^d	rel fit^e uncert, %	median^c	slope^c	median^c	slope^c
Al	110	92	163 ± 37	0.6 ± 0.7	1.7	147	44	146	41
Si	50	36	79 ± 39	−0.1 ± 0.5	8.9	37	21	35	23
P	40	112	1920 ± 350	0.6 ± 0.5	1.9	1900	350	1880	350
S	30	112	2100 ± 280	1.8 ± 0.6	2.9	2120	270	2080	290
Cl	100	112	11800 ± 1800	−2.3 ± 0.7	1.9	11400	1400	11700	1600
K	60	112	3190 ± 780	−1.6 ± 0.5	1.9	3030	540	3120	620
Ca	30	112	1490 ± 450	1.2 ± 0.3	12.3	1500	430	1420	450
Mn	2	109	4.3 ± 1.2	0.1 ± 0.4	3.0	4.1	1.1	4.1	1.1
Fe	2	112	45 ± 8	0.2 ± 0.5	1.3	45	8	44	8
Cu	0.8	46	1.3 ± 0.5	−0.1 ± 0.8	5.3	0.7	0.4	0.7	0.4
Zn	0.8	112	34 ± 9	0.2 ± 0.3	2.5	32	9	32	9
Br	0.6	112	30 ± 11	1.1 ± 0.2	18.9	30	11	28	12
Rb	0.6	112	3.7 ± 2.3	−0.5 ± 0.2	7.4	3.1	1.3	3.3	1.4
Sr	1	112	5.4 ± 2.3	−0.9 ± 0.3	14.1	4.8	1.6	5.0	1.8

[a] 2σ analytical limit of detection based on X-ray peak counting statistics. [b] Number of measured values above the LD. [c] Concentrations and standard deviations in ppm dry weight. [d] Computed from eq 4–6 and 8. [e] Computed as $\{\sum[(Y - Y_{\text{fit}})/Y]^2/(n-1)\}^{0.5}$.

log-normal distribution and to a normal distribution that was transformed by using the distribution index $d = 0.301$ in eq 4. The distribution index was determined iteratively by using eq 4–6, with the same point weighting indicated in Figure 7.

The computed distribution index indicates the data actually have a distribution shape that is intermediate between log-normal ($d = 0$) and normal ($d = 1$). Although the offset used in the three-parameter log-normal analysis (*16*) facilitates a quasi-log-normal fit to the data with similar medians (0.032 for 3P log versus 0.031 for power-transformed normal), the resulting fit, shown in Figure 7, is considerably different in the extremities of the distribution. At the low end, the negative values suggested by the three-parameter log fit are reduced by the power-transformed fit, and at the high end, the maximum values are predicted to be lower by the power-transformed fit. If data as in Figure 7 were used to estimate compliance with an SO_2 standard of 0.4 ppm, the three-parameter log-normal distribution would indicate noncompliance about 3 times as often as the power-transformed normal distribution.

In an application to the analysis of mineral concentrations in fast foods, the method was used to estimate distribution shapes and censored data ranges. X-ray fluorescence analyses of 14 minerals in 112 commercially obtained hamburger samples yielded the means and standard deviations presented in Table II for all measurements above the LD. The distribution indices given in Table II were computed for each element by subjecting these data to the distribution analyses defined by eq 4–6. Censored values of Al, Si, Mn, and Cu were computed from fits to the power-transformed data, and the resulting fitted values were transformed back to the original data distributions. The computed minimum values in these distributions were 49, 10, 1.9, and 0.2 ppm for Al, Si, Mn, and Cu, respectively.

The wide variation in distribution indices for different elements in Table II results from the different modes of occurrence of the minerals and the different populations to which they belong. Bromine and calcium are approximately normally distributed ($d \approx 1$), whereas Si, Mn, Fe, Cu, and Zn are nearly log-normally distributed ($d \approx 0$). Distributions of Cl, K, Rb, and Sr are skewed positively even more than a log-normal distribution, and S is skewed negatively from a normal distribution. The distributions of Al and P are intermediate between normal and log-normal distributions.

For comparison with the arithmetic means and standard deviations, the fitted intercepts (medians) and slopes (standard deviations) of the data also are presented in Table II. For the 10 elements with ranges above the LD, the fitted median values are similar to the means, and the fitted slopes are similar or slightly less then the standard deviations. For the four elements with ranges partly below the LD, the fitted medians are lower than the means due to inclusion of additional data points on the low end of the distribution. Their fitted slopes are generally slightly lower due to the improved distribution fit, despite a contribution toward higher values from the additional points at the low end of the distributions. The fitting uncertainties indicate very high values for several elements (Si, Ca, Br, Sr). Visual examination of their cumulative probability plots indicates significant nonlinear structure that results from more than one population. Thus the high fitting uncertainties are explained, and the single-population representation for these elements is not appropriate.

For comparison with the power-transformed medians and slopes (standard deviations), corresponding log-normal distribution fit parameters also are presented in Table II. For the 10 completely measured distributions, the median of the log-normal fit (geometric mean) is lower than the power-transformed median when the distribution index is positive ($d \geq 0.2$) and higher when the distribution index is negative ($d \leq -0.2$). Slopes are similar to or exceed the power-transformed slopes, indicating unexplained curvature (skewness) in the log-normal fits. These comparisons illustrate the improvement obtained when single-population distribution shapes are defined numerically instead of by an assumed shape. Due to the relatively narrow widths of all these distributions, however, the log-normal parameters also give reasonable values in many cases. This is consistent with the uncertainty relationship in eq 8, that distinctions between distribution shapes become increasingly important for distributions that are wide and that are defined by large numbers of data points.

LITERATURE CITED

(1) Currie, L. A. *Anal. Chem.* **1968**, *40*, 586–593.
(2) ACS Committee on Environmental Improvement. *Anal. Chem.* **1980**, *52*, 2242–2249.
(3) Long, G. L.; Winefordner, J. D. *Anal. Chem.* **1983**, *55*, 712A–724A.
(4) ACS Committee on Environmental Improvement. *Anal. Chem.* **1983**, *55*, 2210–2218.
(5) Cohen, A. C. *Technometrics* **1959**, *1*, 217–237.
(6) Sarhan, A. E.; Greenberg, B. G. *Contributions to Order Statistics*; Wiley & Sons: New York, 1962.
(7) Harter, H. L.; Moore, A. H. *Biometrika* **1966**, *53*, 205–213.
(8) Corley, J. P.; Denham, D. H.; Michels, D. E.; Olsen, A. R.; Waite, D. A. *A Guide for Environmental Radiological Surveillance at ERDA Installations*; Report ERDA-77-24, Battelle Pacific Northwest Laboratory, 1977.

(9) Miller, M. L.; Fix, J. J.; Bramson, P. E. *Radiochemical Analyses of Soil and Vegetation Samples Taken from the Hanford Environs, 1971–1976*, Report BNWL-2249, Battelle Pacific Northwest Laboratory, 1977.
(10) Gilbert, R. O.; Kinnison, R. R. *Health Phys.* **1981**, *40*, 377–390.
(11) Toy, A. J.; Lindeken, C. L. *The Implications of Sampling from a Log-Normal Population*; Report UCRL-76936, University of California, Lawrence Livermore Laboratory, 1975.
(12) Gumbel, E. J. *Statistical Theory of Extreme Values and Some Practical Applications*; Applied Mathematics Series 33; National Bureau of Standards: Washington, DC, 1954.
(13) Abramowitz, M.; Stegun, I. A. *Handbook of Mathematical Functions*; Applied Mathematics Series 55; National Bureau of Standards: Washington, DC, 1970; p 933.
(14) Dixon, W. J.; Massey, F. J. *Introduction to Statistical Analysis*; McGraw-Hill: New York, 1969.
(15) Hastings, N. A. J.; Peacock, J. B. *Statistical Distributions*; John Wiley & Sons: New York, 1975; p 100.
(16) Ott, W. R.; Mage, D. T. *Comput. Ops. Res.* **1976**, *3*, 209–216.
(17) Mage, D. T.; Ott, W. R. *J. Air Pollut. Control Assoc.* **1978**, *28*, 797–798.

RECEIVED for review July 11, 1989. Accepted October 3, 1989. This work was partially funded by NIH Grants 1R43-CA38519 and 9R44-DK38751.

Selective Detection of Carbon-13, Nitrogen-15, and Deuterium Labeled Metabolites by Capillary Gas Chromatography–Chemical Reaction Interface/Mass Spectrometry

Donald H. Chace and Fred P. Abramson*

Department of Pharmacology, The George Washington University Medical Center, Washington, D.C. 20037

We have applied a new chemical reaction interface/mass spectrometer technique (CRIMS) to the selective detection of ^{13}C-, ^{15}N-, and ^{2}H-labeled phenytoin and its metabolites in urine following separation by capillary gas chromatography. The microwave-powered chemical reaction interface converts materials from their original forms into small molecules whose mass spectra serve to identify and quantify the nuclides that make up each analyte. The presence of each element is followed by monitoring the isotopic variants of CO_2, NO, or H_2 that are produced by the chemical reaction interface. Chromatograms showing only enriched ^{13}C and ^{15}N were produced by subtracting the abundance of naturally occurring isotopes from the observed M + 1 signal. A selective chromatogram of ^{2}H (D) was obtained by measuring HD at m/z 3.0219 with a resolution of 2000. Metabolites representing less than 1.5% of the total labeled compounds could be identified in the chromatogram. Detection limits from urine of 380 pg/mL of a ^{15}N-labeled metabolite, 7 ng/mL of a ^{13}C-labeled metabolite, and 16 ng/mL of a deuterium labeled metabolite were determined at a signal to noise ratio of 2. Depending on the isotope examined, a linear dynamic range of 250–1000 was observed using CRIMS. To identify many of these labeled peaks (metabolites), the chromatographic analysis was repeated with the chemical reaction interface turned off and mass spectra obtained at the retention times found in the CRIMS experiment. CRIMS is a new analytical method that appears to be particularly useful for metabolism studies.

INTRODUCTION

The stable isotopes ^{13}C, ^{15}N, and ^{2}H (D) are utilized often in biochemical and pharmacological applications (*1*), particularly in the study of xenobiotic biotransformation (*2*). Incorporation of a stable isotope is intended to make a drug and its labeled metabolites unique. Numerous mass spectrometric methods have been utilized in their detection. The most common of these methods has been the twin ion or ion cluster GC/MS technique for the detection and structural identification of drug metabolites in complex biological samples (*2*, *3*). In such a method, the mass spectrum of each chromatographic peak is examined for a characteristic ion pair or cluster, such as M^+ and $[M + 3]^+$. However, these techniques are tedious, structure dependent, and therefore lack generality. Due to the large number of chromatographic peaks in biological matrices, labeled compounds in low amounts may not be detected due to interference of overlapping mass spectra from other compounds. In contrast, radiolabels, i.e. ^{14}C or ^{3}H, have been used in metabolism studies because their methods of detection are not structure dependent. The presence of a radiolabel in a chromatogram, whether gas, liquid, or thin layer, directs the analyst to further investigation of the fractions containing the label, thereby greatly simplyfing the investigation. We wished to develop a method that detected stable isotopes in a structure-independent manner similar to the way radiolabels are used. The goals for this method were to preserve the high chromatographic resolution characteristic of capillary columns while being sensitive, highly selective, versatile, and reliable. To this end, we used a chemical reaction interface/mass spectrometer technique (CRIMS) to detect the most commonly used isotopes, ^{13}C, ^{15}N, and D.

Markey and Abramson (*4*, *5*) developed the chemical reaction interface, a microwave-powered device that completely decomposed a complex molecule to its elements in the presence of helium. The addition of a reactant gas, for example, oxygen, formed stable oxidation products (CO_2, SO_2, H_2O, etc.) which reflected the elemental composition of the original analyte and which were detected by a conventional quadrupole mass spectrometer. This technique is different from inductively coupled plasma mass spectrometry which attempts to directly sample the components in the plasma. CRIMS is different in that the inlet of the MS is some distance downstream from the microwave cavity. This allows time for reactive intermediates to form stable products, a process which is enabled by the presence of a reactant gas, otherwise pyrolysis and only partial conversion to volatile products would

0003-2700/89/0361-2724$01.50/0 © 1989 American Chemical Society

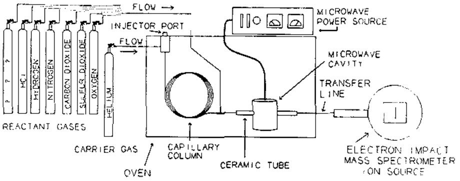

Figure 1. Schematic of capillary gas chromatograph–chemical reaction interface/mass spectrometer.

result. The general characteristics of this process, although greatly simplified, are illustrated in eq 1.

$$\mathrm{ABCD} + 4\mathrm{X} \rightarrow \begin{array}{c} \mathrm{C} \\ {}^{\mathrm{A}}_{\mathrm{X}}\mathrm{X} \quad \mathrm{B}^{\mathrm{X}}_{\mathrm{X}} \\ \mathrm{D} \end{array} \rightarrow \mathrm{AX} + \mathrm{BX} + \mathrm{CX} + \mathrm{DX} \tag{1}$$

Any complex molecule composed of elements represented by the letters, A, B, C, and D, is mixed with an excess of reactant gas, X, in a stream of helium. In the high-energy region of the chemical reaction interface, the molecules are decomposed completely. The stable products that represent the elemental composition of the original analyte are detected by the mass spectrometer. For example, element B can be monitored with a characteristic mass from BX. The combination of capillary gas chromatograph (GC) and a chemical reaction interface/mass spectrometer (GC–CRIMS) allows the analyst to selectively detect stable isotope labeled substances as they elute (*6*).

Heppner (*7*) described a microwave-induced plasma/gas chromatograph–mass spectrometer (MIP/GC–MS) method which was mechanically different but similar in principle to CRIMS. A high-energy plasma coverted compounds eluting from a gas chromatograph to stable molecules in the presence of hydrogen. CH_4, C_2H_2, C_2H_4, and C_2H_6 were products of carbon, HCN was formed from nitrogen, and CO and H_2O were products of oxygen. These were detected by a mass spectrometer and used to calculate the elemental C/O and C/N ratios of analytes. Other methods that detect ^{13}C- or ^{15}N-labeled compounds in a structure-independent way use a mass spectrometer following gas chromatography and combustion in a cupric oxide furnace (*8–10*). The combination of a direct introduction probe with CRIMS was applied in this laboratory to the analysis of sulfur in a variety of proteins (*11*).

We have expanded and generalized our earlier detection scheme (*4, 5*) and now report the ability of GC–CRIMS to selectively detect compounds labeled with ^{13}C, ^{15}N, and D in a biological matrix. We have established the utility of CRIMS by identifying major and minor metabolites of phenytoin, a drug whose metabolic profile has been well investigated (*12–15*).

EXPERIMENTAL SECTION

Apparatus. A schematic of the capillary gas chromatograph–chemical reaction interface/mass spectrometer is shown in Figure 1. The microwave power is transmitted by a Bowman cavity of a design previously reported (*4–6*). The cavity, which is placed inside the gas chromatograph column oven, is powered by a 100-W, 2450-MZh Opthos (Rockville, MD) Model MPG-4 microwave supply and operates at approximately 70 W of forward power and reflected power of 15 W or less. A Varian Model 3300 gas chromatograph equipped with a Varian Model 1075 split/splitless injector was used with a 30-m DB-5, 0.25 mm i.d., 0.25-μm film thickness, capillary column (J & W). This capillary column was connected to a $^1/_{16}$ in. stainless steel Swagelok "T" using Vespel/graphite ferrules. The remaining ends of the "T" were connected to a reactant gas supply using a $^1/_{16}$ in. o.d., 0.01 in. i.d. stainless steel tube and to a 4 in. piece of $^1/_4$ in. o.d., 0.125 in. i.d. ceramic tube (Scientific Instrument Services) using Swagelok hardware and 5% Vespel/graphite ferrules (Alltech Associates). The tip of the column traverses the stainless steel "T" and extends approximately $^1/_4$ in. into the ceramic tube which passes through the microwave cavity. The chemical reaction interface was connected to the mass spectrometer using a 14 in. section of 0.53 mm i.d., deactivated, uncoated fused silica tubing (J & W) housed in a heated (250 °C), $^1/_4$ in. o.d. stainless steel tube. The flow of reactant gas was adjusted with a Granville-Phillips Series 203 variable leak. A Telsa coil (vacuum leak detector, Fisher Scientific) was occasionally required to initiate the microwave plasma.

Ultrapure carrier grade helium (Air Products) was fitted with a high-purity stainless steel regulator (Matheson) and was operated at a pressure of 38–40 psi, producing a helium flow of 1–2 mL/min. A standard grade of SO_2 available from most manufacturers contains greater than 1% air. This was undesirable so we obtained a higher purity sulfur dioxide (Matheson) prepared in part by preevacuation of the cylinder prior to addition of the gas. The air content present in this tank was less than 1%. Carrier grade hydrogen was also obtained and connected to a high-purity brass regulator with a stainless steel diaphragm. To avoid actual and virtual leaks, all GC flow controls were bypassed and the carrier and reactant gas lines and regulators were preevacuated prior to use in order to remove air and contaminants.

Du Pont 21-491 and Du Pont 21-492 mass spectrometers were used. The 21-491 was pumped by 3-in. NRC diffusion pumps at the source housing and the analyzer. The 21-492 was pumped at the source housing by a 6-in. NRC diffusion pump and a 2-in. CVC diffusion pump at the analyzer. The mass spectrometers were equipped with Analytical Specialities (St. Louis, MO) Model 667 power supplies, which had a maximum output of 5000 V for acceleration and ±500 V for the electric sector with rapid voltage switching and settling times of less than 5 ms which allowed multiple ion recording. This device is also available from Vacumetrics (Ventura, CA). The power supply was controlled by a Teknivent data acquisition interface, and accompanying software, and an IBM XT Model 286 computer.

For all studies, the settling times of the mass spectrometers were 1, 1, and 5 ms for mass changes of 0.1, 1, and >1 amu, respectively. For the linearity and reproducibility studies of ^{15}N, five samples for each mass were needed to capture the peak apex due to instability of the magnet power supply of the Du Pont 21-491 MS. Each mass was integrated for 5 ms and averaged 3 times, which yielded acquisition time of 100 ms per mass. The selected ^{15}N chromatograms presented were obtained on the Du Point 21-492 which has superior magnet stability so that only three samples surrounding each mass were needed. Each sample surrounding each mass was integrated for 4 ms, and averaged 10 times yielding an acquisition time of 151 ms per mass. For all ^{13}C analyses, the Du Pont 21-491 required three samples surrounding each mass which were acquired with an integration time of 17 ms and averaged 4 times resulting in an acquisition time of 212 ms per mass. At the 2000 resolution used for HD, the Du Pont 21-492 required five samples, each integrated for 16 ms and averaged 5 times giving an acquisition time of 410 ms.

Materials and Methods. A male beagle dog was placed in a metabolic cage 24 h prior to administration of labeled phenytoin during which time urine was collected, filtered, and frozen until analyzed. All of the isotopes used in this study were checked for purity by using HPLC and for isotopic purity by GC/MS and/or GC–CRIMS. The determined atom percent incorporation for all isotopes were essentially equivalent to the values listed by the manufacturer. For ethyl-d_5-primidone, the area of the single HPLC peak detected at the appropriate retention time was 50% of that from an equal weight of pharmaceutical primidone.

Fifty milligrams of [2-^{13}C, 1,3-$^{15}N_2$]- (99 atom %, Cambridge Isotopes), [2,4,5-$^{13}C_3$]- (90 atom %, Cambridge Isotopes), or [ring-d_{10}] (99 atom %, MSD Isotopes) phenytoin was prepared for intravenous injection by dissolving 50 mg of the drug in 2 mL of a solution which contained 40% propylene glycol, 10% ethanol, and 50% deionized distilled water adjusted to pH 12.5 with 14 N NaOH. The phenytoin solution was drawn through a Milex-GS 0.22-μm filter unit into a 3-mL syringe. The labeled phenytoin was administered through a Y-tube into a saline solution, which was flowing at a rate of 1 mL/min. The phenytoin solution was injected intravenously into the dog over a period of 2 min. Urine was collected for 48 h following the injection of labeled phenytoin, filtered, and frozen until analysis.

Five micrograms of [2-^{13}C-, 1,3-$^{15}N_2$]phenobarbital (99 atom %, Cambridge Isotopes) or 2.5 μg of [ethyl-d_5] primidone (98 atom %, KOR Isotopes) was added as an internal standard to a 1% aliquot (12–20 mL) of the total volume of urine collected. The pH of the urine was adjusted to 4.7 with 0.2 M acetate buffer and was enzymatically hydrolyzed by 100 000 Fishman units of β-D-glucuronidase {EC 3.2.1.31} and 800 000 Roy units of sulfatase {EC 3.1.6.1} isolated from Helix Pomatia (Boehringer, Mannheim) for 20 h at 37 °C. This hydrolysate was added to a 4.5 in. by $^1/_4$ in. column containing XAD-2 resin (Alltech Associates), rinsed with 30 mL of distilled water and sequentially eluted with 20 mL of a 3:1 chloroform–2-propanol (v:v) mixture followed by 20 mL of methanol. All solvents were Optima grade (Fisher Scientific). The total combined organic eluate was dried at 50 °C under a stream of nitrogen.

The samples were derivatized by extractive alkylation. Ethylation was chosen in preference to methylation in order to detect metabolites which underwent methylation, a common biochemical pathway (*16*). The reaction was carried out by addition of 3 mL of 0.2 M *tert*-butylammonium hydroxide (TBAH, Fisher Scientific) in 0.15 M NaOH to the dry residue. This was followed by addition of 3 mL of 3:1 (v:v) methylene chloride–ethyl iodide (Sigma) and shaken in a 50 °C water bath for 20 h. After removal of the aqueous layer, the organic layer was dried at 80 °C under a stream of nitrogen. A 1 mg/mL silver nitrate solution in 0.1 N hydrochloric acid was heated in a boiling water bath and a 2-mL aliquot was added to the dry residue in order to remove TBA salts. The derivatives were extracted with 1 mL of toluene and dried in a conical reaction vial under a stream of nitrogen. Following this half of the derivatization, the dried samples were acylated by using 50 μg of trifluoroacetylimidazole (TFAI, Alltech Associates). Unreacted TFAI was removed under a gentle stream of nitrogen and the residue reconstituted in 100 μL of toluene. One microliter of this mixture was injected by splitless injection. The injector temperature was 265 °C and the column was 80 °C. The chromatograph was programmed to 130 °C at 50 °C/min at the start of the run and then at 10, 4, and 3 °C/min to 160, 220, and 250 °C, respectively. The analysis began at 5 min into the column temperature program when the solvent had eluted.

Operation of the Chemical Reaction Interface. The pressure in the chemical reaction interface and the quantity of helium are important parameters for successful operation. The quantity of helium required to sustain the plasma was 1–2 mL/min. Our instrumentation has no provision for measuring the pressure either in the reaction interface or in the ion source. We adjusted the pressure in the chemical reaction interface by monitoring the indicated helium pressure in the source housing. Using a Penning ionization gauge (CVC), a pressure of approximately 3×10^{-5} Torr for the Du Pont 21-492 mass spectrometer or 1×10^{-4} Torr for the Du Pont 21-491 mass was measured. In addition to the carrier gas flow, the pressure in the chemical reaction interface was also dependent upon the length and inside diameter of the transfer line. The day to day operation of the chemical reaction interface is very reproducible once these parameters are optimized.

GC–CRIMS Using SO_2 or H_2. Only a small amount of SO_2 was optimal since a change of greater than 5% (the readability of the Penning gauge) pressure was not observed with either mass spectrometer. We do not have direct knowledge of the actual reaction interface pressures. Grossly, the quantity of SO_2 added was determined by the glow from the chemical reaction interface which changed from a pale peach color, which was characteristic of helium, to a pale blue tint. A lavender hue indicates the presence of excessive nitrogen, usually from a leak, but also from less than ideally pure SO_2. The quantity of SO_2 added to the chemical reaction interface was optimized by monitoring the isotopes of SO_2 at m/z 65 or 66 since SO_2 at m/z 64 was always off scale. If a decrease of more than 20% of the ion signal representing SO_2 was observed for 500 ng or less material on column, then more reactant gas is added until only a small decrease was noted.

As with SO_2, a pressure change of greater than 5% as measured in the source housing was not detected upon addition of H_2 to the chemical reaction interface. The quantity of H_2 was grossly determined by the appearance of a pale red plasma in the chemical reaction interface. The quantity of H_2 added to the chemical reaction interface was optimized by monitoring H_3^+ at m/z 3.0235. If any decrease of the ion signal representing H_2 (i.e. H_3^+) was observed for 500 ng or less material on column, then more reactant gas was added.

Too much reactant gas lowers the energy level of the plasma, thus preventing complete dissociation of the analytes. Compounds present at greater than 1 μg on column should be avoided as they may alter the chemical reaction interface chemistry causing erroneous results (loss of selectivity) or malfunction (soot formation, quenching of plasma).

Selective Detection of Specific Isotopes. The choice of SO_2 as a reactant gas was based upon several considerations. Initially, oxygen was selected due to simplicity of products anticipated. However, the destructive characteristics of this gas on filament materials led us to consider alternative sources of oxygen atoms. The spectrum of SO_2 as a reactant gas indicates O_2, SO, and SO_3 are created by the chemical reaction interface. Also, SO_2 was found to be more effective than O_2 as a reactant gas because NO was produced in greater quantity, thus improving our sensitivity. It should be noted that NO is not an inert product. A chromatogram of NO at m/z 30 contains both positive deflections and negative deflections (data not shown). The positive deflections are associated with the presence of nitrogen in an analyte. Negative deflections are associated with large amounts of a nitrogen-free substance in the chromatographic effluent, similar to the decrease in m/z 65 or 66 noted previously. It is important to use high-purity reactant gases and to have a leak-free GC and CRI system in order to decrease the base-line quantity of NO produced by the chemical reaction interface. A large air leak raises the nitrogen background at m/z 30 and m/z 31 and results in decreased ability to detect enriched ^{15}N-labeled metabolites.

Selective detection of ^{13}C was achieved by using SO_2 as the reactant gas and monitoring $^{12}CO_2$ at m/z 44 and $^{13}CO_2$ at m/z 45. We define enriched as the measured isotope minus its natural abundance. Since the isotopic contribution of $^{13}C^{16}O_2$ and $^{12}C^{17}O^{16}O$ at m/z 45 from unenriched material is 1.19%, a chromatogram showing only ^{13}C-enriched substances can be generated by using eq 2.

$$\text{enriched } m/z\ 45 = \text{measured } m/z\ 45 - [0.0119 \times \text{measured } m/z\ 44] \quad (2)$$

To improve the dynamic range of our data system, the output of the ion signal at m/z 45 was fed into an amplifier with approximately a 10-fold higher gain. If the ion intensity of m/z 44 is greater than the dynamic range of the data system, eq 2 will not properly correct for the natural abundance of ^{13}C. Although CO at m/z 28 was a more abundant product than CO_2 using SO_2, it was not chosen because of interference from N_2 at the same mass.

Selective detection of ^{15}N was achieved by monitoring ^{14}NO at m/z 30 and ^{15}NO at m/z 31. Since the isotopic contribution of $^{15}N^{16}O$ and $^{14}N^{17}O$ at m/z 31 from unenriched material is 0.403%, a chromatogram showing only ^{15}N-enriched substances can be generated by using eq 3.

$$\text{enriched } m/z\ 31 = \text{measured } m/z\ 31 - [0.00403 \times \text{measured } m/z\ 30] \quad (3)$$

Selective detection of deuterium was achieved by using H_2 as the reactant gas and monitoring HD at m/z 3.0219 with a resolution of 2000. A high repeller voltage was used to minimize the production of H_3^+. A calculation such as eq 2 or 3 could not be generated from D because H_2 was the reactant gas and thus m/z 2 was always off-scale. However, the low natural abundance of deuterium (0.015%) means that HD is inherently selective. A reactant gas other than hydrogen might be preferable in order to generate isotope ratio data, but the sensitivity for deuterium was best with H_2. Although H_2 and HD were produced using nitrogen as the reactant gas, the sensitivity and chromatography were poorer.

In the chromatogram for each isotope the sensitivity of CRIMS was evaluated from the ratio of the area of the smallest detectable peak to the area of the internal standard, which is present at a known concentration. For ^{13}C, the concentration of the internal standard, [2-^{13}C]-, [1,3-$^{15}N_2$]phenobarbital, was divided by 3 to adjust for its one ^{13}C atom compared to the three in phenytoin. Likewise, for D, the internal standard concentration was divided by 2 in order to correct for labeled D present in ethyl-d_5-primidone as compared to phenytoin, and no correction was necessary for ^{15}N analysis since both the internal standard and phenytoin have two labeled nitrogens. In these estimations, it was assumed that the metabolites retained the same number of enriched atoms as phenytoin. Mass spectrometric examination of these metabolites showed that this assumption was true except for ring-modified deuterated phenytoin.

Linearity and Reproducibility. The linearity and reproducibility for the detection of each isotope were tested by the serial dilution of urine collected after the administration of each isotope with control urine. These diluted urines were processed and analyzed in the manner described above. The samples from each isotope study were analyzed on three separate days. The ratio of area under the largest labeled peak in the chromatogram of enriched isotope (retention time (r.t.) = 22.7 min.) to the internal standard was calculated. This ratio was plotted against the calculated dilution. The data collected from each of three separate days was pooled and a regression analysis performed by using a weighting of $1/y^2$.

RESULTS AND DISCUSSION

The microwave plasma provides sufficient energy to chemically convert all of the molecules that enter it; however, it is not necessary to know or account for the chemical structures of all the intermediates. It should be noted that we have no reason to believe that CRIMS chemistry depends upon a particular design of microwave cavity, although the useful operating parameters may vary. We have shown *(4–6)* that, in the presence of an excess of reactant gas such as oxygen or hydrogen, the nature of the products produced by the chemical reaction interface is characteristic of the reactant gas chosen and is reproducible. In general, gases that contain oxygen, i.e. O_2, SO_2, and CO_2, produce oxidation products such as CO and CO_2 from carbon, NO and NO_2 from nitrogen, and H_2O from hydrogen for molecules containing these elements. Use of hydrogen as a reactant gas results in fundamentally different chemical reaction interface products; i.e. carbon is converted to CH_4 and C_2H_2, nitrogen to HCN, NH_3, and $(CN)_2$, and oxygen to H_2O. Other reactant gases that have been examined include nitrogen and HCl. Manipulation of a desired product by choice of the reactant gas to suit a particular elemental/isotopic analysis makes CRIMS a versatile method.

Since all of the elements in the plasma appear to be in equilibrium, contaminated reactant or carrier gases, leaks in the chromatographic system, or too large a sample can change the products produced in the chemical reaction interface. Because septa are being punctured, air leaks are unavoidable, but we use longer columns (e.g. 30 m) rather than shorter columns and their necessarily higher head pressure to limit septum leakage. To minimize the background levels of N_2 and O_2, we preevacuate all gas lines and regulators, remove unnecessary GC flow regulators and use high-purity reactant and carrier gases.

The characteristic high chromatographic resolution obtained by using a capillary column was exhibited by symmetric peaks with widths at half height of approximately 6 s. This high resolution was preserved by CRIMS because the volume of the ceramic tube, 0.82 cm^3, is under subatmospheric pressure which produces a low apparent dead volume. The helium flow required to optimize the chemical reaction interface was 1–2 mL/min, which is a typical value for 0.25 mm i.d. capillary columns.

^{13}C Detection. Carbon-containing molecules were converted to $^{12}CO_2$ at m/z 44 and $^{13}CO_2$ at m/z 45 by the chemical reaction interface using SO_2 as the reactant gas. These particular products of carbon were chosen because they were abundantly produced by the chemical reaction interface, the background at m/z 44 and 45 was small, and other CRI products produced under optimum condition did not interfere with detection at these masses.

If samples sizes of greater than 1 μg on column are present, the chemical reaction interface chemistry is altered so that another ion at m/z 44 is produced, i.e. CS which is either itself a product or a fragment of CS_2. Because the natural abundance of $^{13}C^{32}S$ and $^{12}C^{33}S$ at m/z 45 is greater than the natural abundance of $^{13}C^{16}O_2$ and $^{12}C^{17}O^{16}O$ at m/z 45, the net enriched calculation (eq 2) does not correct for the natural contribution of m/z 45 from m/z 44. This produces a peak that could be confused with ^{13}C. However, under proper operation, this is not a problem as this false signal is associated with particularly large chromatographic peaks (1 μg or more on column) in the analysis which are readily noted as significant dips in what are generally constant signals from the reactant gas or one of its background products such as NO.

Figure 2A shows a nonselective chromatogram which is produced by monitoring $^{12}CO_2$ at m/z 44, similar to what would be obtained by a flame ionization gas chromatographic detector. A chromatogram of $^{13}CO_2$ at m/z 45 is shown in Figure 2B. This chromatogram is generally nonselective due to the natural abundance of ^{13}C, although highly enriched ^{13}C compounds are readily apparent. Since the isotopic contribution to M + 1 from M for CO_2 is known, the use of eq 2 generates a chromatogram of enriched ^{13}C, Figure 2C, which now selectively detects that ^{13}C which is present at amounts above the natural abundance. Each positive deflection in this derived chromatogram represents a compound that is labeled to some extent with ^{13}C. The high level of selectivity of the analysis has been demonstrated *(6)* in a chromatogram of enriched ^{13}C for urine collected from the dog prior to drug administration. Despite the presence of more than 125 peaks (as shown in Figure 2A), nothing was detected other than [2-^{13}C-1,3-$^{15}N_2$]phenobarbital, the internal standard (333 ng/mL of urine).

^{15}N Detection. Nitrogen-containing molecules are converted substantially to NO when SO_2 is used as the reactant gas. The presence of ^{15}N-enriched substances is determined using eq 3. As shown previously *(6)*, this procedure eliminated most chromatographic peaks and provided an isotope-selective chromatogram.

Deuterium Detection. Deuterium-containing molecules are converted to HD when hydrogen is used as the reactant gas. A resolution of 2000 was obtained by using the Du Pont 21-492 mass spectrometer to separate HD (m/z 3.0219) from H_3^+ (m/z 3.0235). H_3^+ was formed in the mass spectrometer source from H_2. Its formation could be reduced to a constant level but not eliminated. Signal to background, but not selectivity, was impaired when lower resolution was used. The higher resolution is needed to eliminate the contribution of the H_3^+ background to HD detection. The selectivity provided by a chromatogram of HD at m/z 3.0219 of urine from a dog administered [ring-$^2H_{10}$]phenytoin has been demonstrated previously *(6)*.

Figure 3 expands the time scale between 25 and 30 min as well as the y axis in order to demonstrate selectivity. In this region of the chromatogram, minor metabolites elute. This figure shows overlays of Figure 2A, which is a chromatogram of $^{12}CO_2$ representing nonselective detection, with the calculated chromatograms showing enriched ^{13}C, ^{15}N, and D for treated and control urine. The high selectivity and sensitivity of each isotopic analysis using CRIMS result in detection of minor ^{13}C-, ^{15}N-, and D-labeled compounds which could not be completely resolved from other urine components in the nonselective chromatogram. For example, only the leading shoulder of the peak at r.t. 26.9 min is enriched with ^{13}C, ^{15}N,

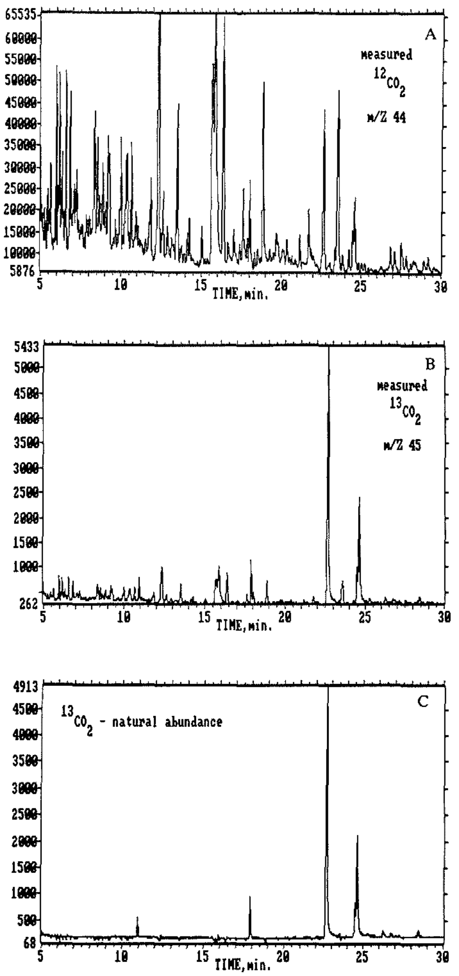

Figure 2. CRIMS capillary gas chromatograms of a derivatized extract of urine from a dog receiving 50 mg of [2,4,5-$^{13}C_3$]phenytoin. The internal standard [1,3-$^{15}N_2$, 2-^{13}C]phenobarbital (r.t. 11 min), is at a concentration of 333 ng/mL in urine. The *y* axis represents ion intensity and the *x* axis represents time. Panel A: Nonselective chromatogram obtained by monitoring $^{12}CO_2$ at *m/z* 44. Panel B: Nonselective chromatogram of ^{13}C obtained by monitoring $^{13}CO_2$ at *m/z* 45. Panel C: Selective chromatogram showing enriched ^{13}C using eq 2. Adapted from ref 6 with permission of the publisher.

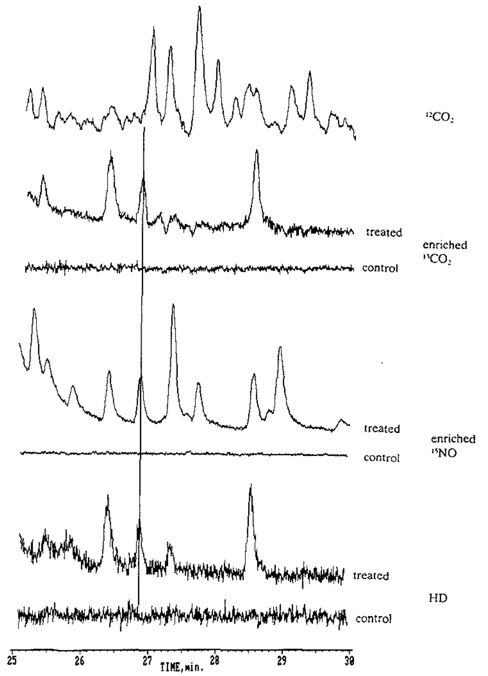

Figure 3. *x*-axis expansion and overlays of nonselective carbon chromatogram from Figure 2 and calculated chromatograms from control and treated urine for each isotope. Note the ability of CRIMS to detect an enriched peak for each isotope at r.t. = 26.75 min which in the nonselective chromatogram is the small shoulder of the peak at r.t. 26.9 min.

or D. While in the chromatograms presented in Figure 2, the apparent resolution is low because of the limitations in plotting the time axis, a true representation of the chromatography is present in Figure 3 in which the *x*-axis expansion was made. Each peak eluting between 25 and 30 min represents less than 1.5% of the total enriched isotope present in the chromatogram. The peak at r.t. = 25.3 min in the calculated ^{13}C chromatogram reflects a concentration of 16 ng/mL in urine. The signal to noise ratio for this peak is 4.5, indicating that a metabolite present at a lower concentration may be detected. The small shoulder at r.t. = 28.7 min in the calculated ^{15}N chromatogram represents a concentration of 770 pg/mL in urine. The signal to noise ratio for this peak was 4, indicating somewhat lower concentrations of metabolites may be detected. In the HD chromatogram, a concentration of 16 ng/mL in urine was detected at r.t. = 27.3 min. The signal to noise ratio was 2, indicating that a metabolite present at a lower concentration may not be detected.

Linearity and Reproducibility. To evaluate the linearity of ^{13}C analysis, a plot of the ratio of metabolite (r.t. 22.7 min) to the internal standard, ^{13}C-labeled phenobarbital (r.t. 11 min) against the calculated dilution was generated over a range of 250-fold. These data are shown in Figure 4A. The intraday variation of slopes was 7%. The correlation coefficient of the entire data set was 0.87 with an average coefficient of variation (CV) of 34%. These data indicate that detection of ^{13}C is linear but the precision is poor.

As with carbon, urine containing ^{15}N-labeled metabolites was diluted and analyzed on three separate days. The linearity of ^{15}N analysis was determined by a plot of the ratio of the metabolite at r.t. = 22.7 min to the internal standard, ^{15}N-labeled phenobarbital (r.t. 11 min) against the calculated dilution which was up to 1000-fold. These data are shown in Figure 4B. The intraday variation of the slope was 20%. The correlation coefficient of the entire data set was 0.72 with an average CV of 43%. These data indicate ^{15}N analysis is somewhat less linear and less precise than ^{13}C.

Once again, urine containing D-labeled metabolites was diluted 250-fold and analyzed on three separate days. The linearity of deuterium analysis was determined by a plot of the ratio of the metabolite at r.t. = 22.7 min to the internal standard, [D_5]pyrimidone (r.t. 14.3 min) against the calculated dilution. These data are presented in Figure 4C. The intraday variation of the slope was 7%. The correlation coefficient of the entire data set was 0.95 with an average CV of 16%. These

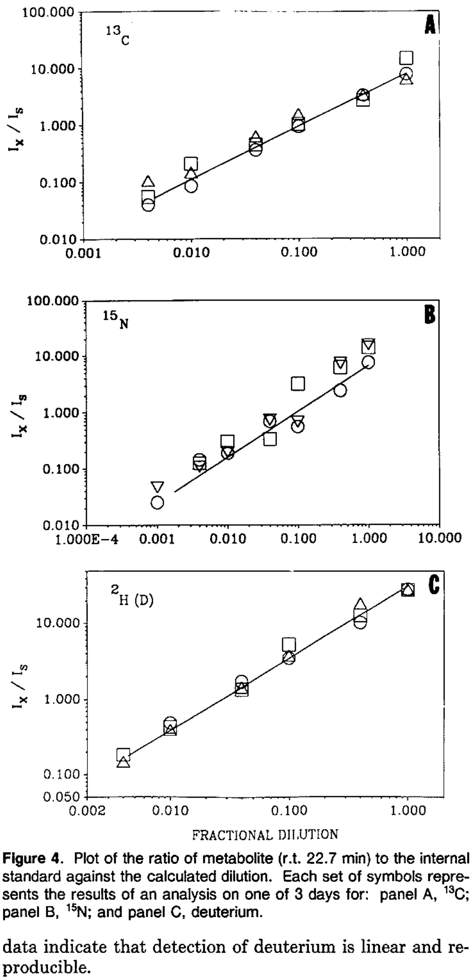

Figure 4. Plot of the ratio of metabolite (r.t. 22.7 min) to the internal standard against the calculated dilution. Each set of symbols represents the results of an analysis on one of 3 days for: panel A, ^{13}C; panel B, ^{15}N; and panel C, deuterium.

data indicate that detection of deuterium is linear and reproducible.

Identification of Labeled Unknowns. Each chromatogram presented shows that the chemical reaction interface selectively detects the commonly used isotopes, ^{13}C, ^{15}N, and D. Phenytoin metabolites that retain the label are easily detected by using the chromatogram of enriched isotope and their retention times can be recorded. This method is analogous to detection of a radiolabel which locates a substance regardless of its specific chemical form. While not structurally informative, CRIMS directs the analyst to more definitive studies such as conventional mass spectrometry. A unique and powerful advantage of CRIMS is that the method of label-selective detection uses the same instrument and gas chromatographic conditions by which conventional GC/MS identification can be obtained. Each labeled peak may be identified with conventional scanning GC/MS by turning off the power of the chemical reaction interface, reinjecting the sample, and obtaining spectra at the retention times of the labeled materials found by using CRIMS.

For each type of stable isotope label, metabolites representing less than 1.5% of the drug-related compounds in urine were detectable by using 1% aliquots of urine. Over 20 peaks were detected in the ^{15}N net enriched chromatogram; nine or more labeled peaks were found with ^{13}C or D. More sensitive detection was realized for ^{15}N-labeled metabolites because of the low natural abundance of ^{15}N, the presence of fewer nitrogen-containing substances in the urine extract as compared to carbon, and the relatively clear masses at *m/z* 30 and 31. Fewer metabolites were found by using ^{13}C because of its higher natural abundance and the greater number of endogenous compounds in urine, which give a high background and low signal to noise ratio in the net enriched chromatogram. Another contribution to the lower limit of detection was the necessarily limited integration time to keep *m/z* 44 on scale. A longer integration time at *m/z* 45 relative to *m/z* 44 would improve our signal to noise ratio and likely improve sensitivity. Deuterium detection was similar to ^{13}C. The higher resolution at which HD was monitored reduced sensitivity but enabled HD to be a mass channel of unambiguous composition, thus reducing the background and allowing a longer integration time.

In CRIMS, the number of labeled atoms present in a molecule is linearly related to its detection, i.e. three ^{15}N atoms present in a metabolite rather than one increases the apparent detection limits by 3. In standard GC/MS techniques, the number of labeled atoms is not linearly related to its detection due to natural isotope cluster abundances. For example, detection of a trilabeled compound at M + 3 as compared to a monolabeled compound at M + 1 results in a much greater than 3-fold increase in sensitivity. Furthermore, many compounds may not have an M^+ or useful masses to do cluster identification at all.

A comparison of the enriched isotope chromatograms shown in Figure 3 reveals that many peaks representing enriched metabolites were common to all three isotopes. This demonstrates the versatility of CRIMS, where studies do not have to be limited by the choice of stable isotope.

Using full scan spectra at the retention times determined by CRIMS, we have identified much of the metabolic profile of phenytoin which has been reported in the literature (*12*–15). The compounds include phenytoin (r.t. 18 min), *m*-hydroxyphenytoin (r.t. 22.7 min), *p*-hydroxyphenytoin (r.t. 24.7 min), catecholphenytoin (r.t. 27.3 min), and *O*-methylcatecholphenytoin (r.t. 26.8).

CONCLUSIONS

The data presented are the first applications of GC–CRIMS for stable isotope analyses in drug metabolism. This method detects the presence of ^{13}C, ^{15}N, and D in a compound-independent manner and is seemingly perfect in its selectivity. Detecting the enriched isotope in a calculated chromatogram directs the analyst to further identification by MS. The ability to identify each labeled peak by simply by turning off the chemical reaction interface power and repeating the chromatographic analysis makes CRIMS particularly versatile. The device does not need to be disassembled for each type of application of GC–MS or GC–CRIMS and provides the high resolving power of capillary chromatography. Another special ability of CRIMS is to identify more than one label in an analysis. For example, ^{13}C and ^{15}N can be detected by monitoring CO_2 and NO simultaneously.

We believe CRIMS provides a powerful tool in the qualitative investigation of the metabolism of labeled molecules, although we did not demonstrate the precision of CRIMS for ^{15}N and ^{13}C detection sufficient for high-quality quantification. The cause of poor precision was the result of magnet instability in our mass spectrometers at the time the experiments were carried out. More recent (unpublished) results have shown that the precision of CRIMS for all of the isotopes investigated has improved to 3–6% when a mass spectrometer with better stability was used. Phenytoin was chosen as the model drug because its metabolism has been well characterized and we wanted to demonstrate the ability of CRIMS to assist in the determination of metabolic profile by comparing our results with several studies in the literature. We believe that the analysis of this substance and its metabolites in urine, using only a simple purification and derivatization scheme, is a very stringent test of the method. With this approach we have demonstrated that CRIMS provides sensitive, selective, and reproducible results. GC–CRIMS should simplify the search for the metabolites of a substance whose profile is unknown by providing direction to the analyst. Furthermore, the ability to detect subnanogram per milliliter quantities of labeled metabolites in complex matrices may result in the detection of new metabolites of drugs whose profiles have been previously only partly characterized.

ACKNOWLEDGMENT

The authors wish to acknowledge and express appreciation for the technical assistance and advice of Dr. S. P. Markey of the National Institutes of Health and the advice of Drs. Katherine Kennedy and Mehdi Moini of the George Washington University Medical Center. We also thank Dr. Ed White of the National Institute of Standards and Technology for his gift of ethyl-d_5-primidone. We want to recognize the technical expertise of Bill Fraiser (Analytical Specialties) in the design and installation of the high-voltage power supplies and the improvement of other electronic and magnetic components of our Du Pont mass spectrometers.

LITERATURE CITED

(1) Baillie, T. A. *Pharmacol. Rev.* **1981**, *33*, 81.
(2) VandenHeuvel, W. J. A. *J. Clin. Pharmacol.* **1986**, *26*, 427.
(3) Baillie, T. A.; Rettenmeier, A. W. *J. Clin. Pharmacol.* **1986**, *26*, 481.
(4) Markey, S. P.; Abramson, F. P. *Anal. Chem.* **1982**, *54*, 2375.
(5) Markey, S. P.; Abramson, F. P. In *Synthesis and Applications of Isotopically Labeled Compounds. Proceedings of an International Symposium, Kansas City, MO, U.S.A., 1982*; Duncan, W. P., Susan, A. B., Eds.; Elsevier: Amsterdam, 1983; p 291.
(6) Chace, D. H.; Abramson, F. P., In *Synthesis and Applications of Isotopically Labelled Compounds. Proceedings of the Third International Symposium, Innsbruck, Austria, 1988*; Baillie, T. A., Jones, J. R., Eds.; Elsevier: Amsterdam, 1989; pp 253–258.
(7) Heppner, R. A. *Anal. Chem.* **1983**, *55*, 2170.
(8) Matthews, D. E.; Hayes, J. M. *Anal. Chem.* **1978**, *50*, 1465.
(9) Preston, T.; Owens, N. J. P. *Biomed. Environ. Mass. Spectrom.* **1985**, *12*, 510.
(10) Nakagawa, A.; Kitagawa, A.; Asami, M.; Nakamura, K.; Schoeller, D.; Slater, R.; Minagawa, M.; Kaplan, I. R. *Biomed. Environ. Mass Spectrom.* **1985**, *12*, 502.
(11) Abramson, F. P.; Markey, S. P. *Biomed. Environ. Mass Spectrom.* **1986**, *13*, 411.
(12) Maynert, E. W. *J. Pharmacol. Exp. Ther.* **1960**, *130*, 275.
(13) Glazko, A. J. *Drug Metab. Dispos.* **1973**, *1*, 711.
(14) Langenhove, A.; Costello, C. E.; Biller, J. E.; Biemann, K.; Browne, T. R. *Biomed. Environ. Mass. Spectrom.* **1980**, *7*, 577.
(15) Mihda, K. K.; Hindmarsh, K. W.; McGilveray, I. J.; Cooper, J. K. *J. Pharm. Sci.* **1977**, *66*, 1596.
(16) Borchardt, R. T. In *Enzymatic Basis of Detoxication*; Jacoby, W. B., Ed.; 1980; Vol. II, 43.

RECEIVED for review April 19, 1989. Accepted September 12, 1989. This research was in partial fulfillment of the degree of Doctor of Philosophy in Pharmacology from the Graduate School of Arts and Sciences of The George Washington University for D.H.C. Preliminary reports of this work were presented at the following meetings: Third International Symposium on the Synthesis and Applications of Isotopically Labelled Compounds, July 1988, Innsbruck, Austria; 36th American Society of Mass Spectrometry Conference on Mass Spectrometry and Allied Topics, June 1988, San Francisco, CA; International Symposium on Applied Mass Spectrometry in the Health Sciences, September 1987, Barcelona, Spain; Symposium on Accuracy in Trace Analysis—Accomplishments, Goals, and Challenges, September 1987, Gaithersburg, MD. The authors acknowledge the financial support of this research by the United States Public Health Service under Grant NIH-GM36143.

Anal. Chem. **1989**, *61*, 2731–2734

Decomposition of Peroxyacetyl Nitrate and Peroxypropionyl Nitrate during Gas Chromatographic Determination with a Wide-Bore Capillary and Two Packed Columns

Nikolaos Roumelis and Sotirios Glavas*

Department of Chemistry, University of Patras, GR-26110 Patras, Greece

A fused silica cross-linked methyl silicone 0.53-mm column was used for the analysis of PAN and PPN. Relative to $CHCl_3$ this column exhibited a 37% PAN destruction on the column when the retention time, t_R, increased from 0.72 to 3.10 min. In comparison, the PAN destruction observed on packed columns filled with two most often used packing materials was found to be 99% for the 5% Carbowax 400 on a Chromosorb W column, with a t_R increase from 1.16 to 4.54 min, and 81% for the 4.8% QF-1 + 0.18% diglycerol on a Chromosorb G column, with a t_R increase from 0.62 to 2.72 min. On the basis of first-order kinetics for PAN destruction on the column, we have calculated a destruction of 29% on the wide-bore, 82% on the Carbowax 400, and 71% on the QF-1 + diglycerol column for the same residence time of 2.0 min on all columns. Clearly, the wide-bore column is a better choice for the analysis of these two air pollutants. In addition the effect of the temperature of the column and the detector on the PAN destruction was studied, with best results obtained at 30 and 45 °C, respectively. Similar results were obtained for the higher PAN homologue peroxypropionyl nitrate.

INTRODUCTION

For the determination of peroxyacetyl nitrate (PAN) in ambient air as well as in laboratory studies, gas chromatography with electron capture detection is used almost exclusively. A review of the literature reveals that packed columns are usually used with the stationary phases 5–10% Carbowax 400 (*1–5*), 10% Carbowax 600 (*6–8*), and 4.8% QF-1 + 0.18% diglycerol (*9–11*). These columns are usually made of glass in various lengths, although the use of Teflon tubing has also been reported (*5*). Since the thermal decomposition of PAN is given, low temperatures of the injection port, the oven, and the detector are used, which vary from 17 °C in the oven up to 80 °C in the detector (*4, 8*).

In an earlier study of ours (*12*) PAN was separated on a 60-cm-long quartz column filled with 4.8% QF-1 + 0.18% diglycerol on Chromosorb G and then converted to NO on a Mo converter. The resulting NO was detected from its chemiluminescence with ozone. Using this system and on the basis of first-order kinetics for PAN destruction on the column, we obtained a preliminary evaluation of PAN destruction of 25% for a t_R of 2.1 min relative to zero retention time.

These indications and the known instability of PAN prompted us to examine the use of a fused silica wide-bore column, which inherently is more inert than the packed columns. For the evaluation of a 5-m-long HP-1 cross-linked methyl silicone 0.53-mm wide-bore column and for its comparison with two of the more widely used packed columns, namely the 5% Carbowax 400 on 80/100 Chromosorb W-AW-DMCS and 4.8% QF-1 + 0.18 diglycerol on 80/100 Chromosorb G-AW-DMCS, we used an electron capture detector (ECD). Since an ECD is extremely sensitive to flow variations, we studied the PAN destruction relative to chloroform, a stable electron-capturing substance.

We found that peroxypropionyl nitrate (PPN), the next higher PAN homologue, behaved similarly to PAN, and results for PPN are also presented.

In addition to column choice, operating parameters such as oven and detector temperature, as well as carrier gas flow rate, were also studied for each of the above columns used. We finally determined the detection limits attained by each column.

EXPERIMENTAL SECTION

All mixtures of PAN and $CHCl_3$ as well as PPN–$CHCl_3$ mixtures were prepared at room temperature in a 4.5-L glass flask, equipped with two septa ports and a Teflon stopcock and connected to a vacuum line provided with Teflon stopcocks. From the anhydrides of acetic and propionic acids, the corresponding peroxyacids were synthesized according to the method of Nielsen et al. (*13*), and next the procedure of Gaffney et al. (*14*) was followed for the preparation of pure liquid PAN and PPN. PAN and PPN were kept in different small vials at −10 °C, and only one portion per vial was removed when needed after thawing. Freshly prepared PAN and PPN were used in all cases, and thus the peaks of their thermal decomposition products, methyl nitrate and ethyl nitrate, respectively, were insignificant. Carlo Erba chromatographic grade $CHCl_3$, distilled at 61 °C to remove the ethanol, was used. PAN, PPN, and $CHCl_3$ were introduced into the 4.5-L flask along with the air or nitrogen matrix, making typical mixing ratios of 120 ppb PAN, 120 ppb PPN, and 1200 ppb $CHCl_3$. For the study of PAN and PPN destruction on the column, as well as for the study of the effect of column and detector temperature, nitrogen 4.5 was the matrix atmosphere at 1000 mbar in order to avoid possible integration errors of $CHCl_3$, which elutes a little earlier than PAN and thus could interfere with the air peak. The experiments for the detection limit were carried out in air to emulate atmospheric conditions.

All analyses were carried out with a Hewlett-Packard 5890A gas chromatograph equipped with a ^{63}Ni electron capture detector, operated in the constant current variable frequency mode. The integrator used was a HP Model 3396 A.

The columns used in this comparison were (1) a HP-1 5-m-long fused silica cross-linked methyl silicone gum, 0.53-mm i.d., 2.65-μm film thickness; (2) a 45-cm-long glass column, 2-mm i.d., filled with 5% Carbowax 400 on Chromosorb W-AW-DMCS (80/100 mesh); and (3) a 45-cm-long glass column, 2-mm i.d., filled with 4.8% QF-1 and 0.18% diglycerol on Chromosorb G-AW-DMCS (80/100 mesh). The carrier and the makeup gas were 10% CH_4/Ar. In some experiments with the wide-bore column, helium was also used as carrier gas, with CH_4/Ar being the makeup gas. Except for an increased resolution between PAN and $CHCl_3$, He yielded the same results as those obtained with the 10% CH_4/Ar carrier gas, as will be presented later. A 0.5-mL sample for the capillary column and 1 mL for the packed columns were manually injected into the GC by using appropriate gastight syringes equipped with Teflon plungers. Each point represents the average of four repetitions. The precision of the manual injections was ±5%. The injector temperature was always set at 30 °C except for the varying column temperature experiments.

RESULTS AND DISCUSSION

All results reported below for PAN were corrected by a factor of 1.5 ± 0.5% per hour to account for the thermal PAN

0003-2700/89/0361-2731$01.50/0 © 1989 American Chemical Society

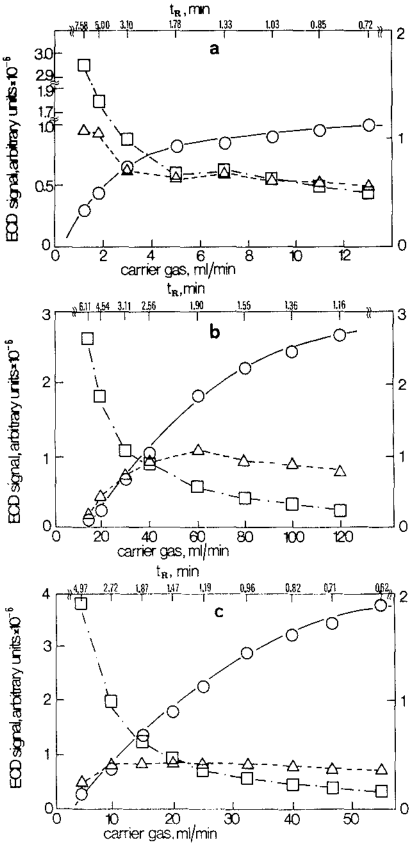

Figure 1. Absolute PAN and $CHCl_3$ ECD signals as well as their ratios vs retention time for (a) wide-bore, (b) 5% Carbowax 400, and (c) 4.8% QF-1 + 0.18% diglycerol columns. Key: △, PAN; □, $CHCl_3$; ○, PAN/$CHCl_3$.

decomposition in the 4.5-L flask. Similarly, PPN values were corrected by 2.0 ± 1% per hour. $CHCl_3$ did not exhibit any significant variation. In all experiments better than base-line resolution was attained between PAN and $CHCl_3$ with typical values of $R \geq 2$, and thus no errors were introduced in the measurement of the peak area counts with the integrator.

PAN and PPN Destruction on the Column. To evaluate the PAN and PPN destruction on the three different columns, the oven and detector were kept at 30 °C. The residence time of PAN on the column, as indicated by its retention time, was varied by changing the carrier gas flow rate.

The experiments with the wide-bore column were carried out both at constant carrier/makeup gas ratios while the carrier gas flow rate was varied, and at varied carrier gas flow rates while the total flow of carrier plus makeup gas was held constant. We assume that the change in response of the ECD due to the change of the flow rate of the carrier gas (and makeup gas) follows the same pattern for PAN, PPN, and $CHCl_3$. Figure 1 shows the absolute PAN signal, as well as the $CHCl_3$ area counts, plotted as a function of the carrier gas flow rate and the retention time of PAN for the packed columns used, whereas the wide-bore experiments are plotted vs carrier gas flow rate at a constant carrier to makeup gas ratio.

Two factors determined the shape of the obtained curves of PAN and $CHCl_3$ vs carrier gas flow rate and therefore vs retention time of PAN. The first factor was the effect of carrier gas (and makeup gas) flow rate on the response of the ECD. We had expected a larger ECD signal at lower flow rates, and this was indeed the case at all times for $CHCl_3$. The second factor was destruction of the analyte on the GC column. In the case of $CHCl_3$ the second factor did not seem to be operative, or if it was, it was overwhelmed by the increased sensitivity of the ECD, due to the decrease of the flow rate; thus, overall, the signal became larger as the flow rate of the carrier gas was lowered. In the case of PAN, however, and only for the packed columns, the destruction on the column overwhelmed the expected higher sensitivity at lower flow rates; thus the absolute PAN signal decreased. These two opposing factors reached an optimum of PAN signal, which for the QF-1 column occurred at 20 mL/min and for the Carbowax 400 column at 55 mL/min, corresponding to retention times of 1.50 and 2.00 min, respectively. Unlike the form of the curves for the packed columns, the PAN curve with the wide-bore column showed PAN values increasing with decreasing flow rates.

A more quantitative evaluation of this phenomenon was possible if one considered the PAN/$CHCl_3$ area count ratios, rather than the absolute PAN values, assuming that $CHCl_3$ is not destroyed on the column. Using PAN/$CHCl_3$ ratios removes the factor of the carrier gas flow rate on the response of the ECD. These PAN/$CHCl_3$ area count ratios for the three columns vs carrier gas flow rate are also plotted in Figure 1. By use of the values of the PAN/$CHCl_3$ area count ratios for the capillary column that correspond to a $4.3t_R$ increase, from 0.72 to 3.10 min, the PAN destruction on the column was calculated to be 35%. Similarly, for the Carbowax column and for a $3.9t_R$ increase, the PAN destruction was 91%, and for the QF-1 column and for a $4.4t_R$ increase, the value was 81%. When He is used as the carrier gas, the same flow rates are used as for the CH_4/Ar carrier gas, and the total carrier plus makeup gas is kept constant at 62 mL/min, the PAN destruction on the wide-bore column for the same as above $4.3t_R$ increase was calculated to be 38%, in reasonable agreement with the earlier result of 35%.

Similar results were obtained for PPN. On the wide-bore column and with a t_R increase of 4.9 times, PPN decreased by 46%; whereas on the Carbowax column and for a $4.1t_R$ increase, PPN decreased by 95%; and on the QF-1 column and for a $4.1t_R$ increase, PPN decreased by 70%.

Alternatively, it was possible to determine the PAN destruction on each column and thus compare the columns used, at a specific retention time relative to zero retention time. If PAN were destroyed on the column via first-order kinetics, then a plot of ln $[PAN]_t/[PAN]_0$ vs time should yield a straight line. $[PAN]_t$ is the amount of PAN that arrives at the detector after retention time t, and $[PAN]_0$ is the amount of injected PAN. This ln $[PAN]_t/[PAN]_0$ vs time (t) plot is equivalent to a plot of ln PAN/$CHCl_3$ vs time, where PAN/$CHCl_3$ is the determined area count ratio. As seen in Figure 2A, good linear fits were obtained for all three columns. From the slopes of these plots the PAN destruction for a residence time of 2 min on each column was calculated to be 29%, 82%, and 71% on the wide-bore, the Carbowax, and the QF-1 columns, respectively. However, a more realistic figure of necessary corrections of PAN destruction on the column could be given when t_R values obtained under optimum operating conditions (maximum absolute PAN signal) were used, as seen in Figure 1. For the capillary column t_R was chosen at 1.33 min; for the Carbowax, 2.00 min; and for the QF-1 column, 1.50 min. The corresponding PAN destruction percentages were then 20%, 82%, and 61%, respectively.

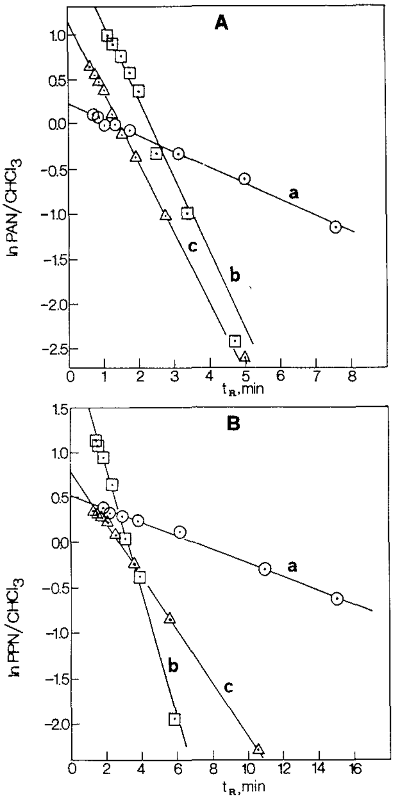

Figure 2. First-order plots of (A) PAN and (B) PPN destruction on the column for (a) wide-bore, (b) 5% Carbowax 400, and (c) 4.8% QF-1 + 0.18% diglycerol columns.

Similarly, PPN destruction on the column followed first-order kinetics, as seen in Figure 2B. From the slopes of the straight lines and taking a residence time of 3.0 min on all columns, the PPN destruction on the column was 23%, 87%, and 58% for the wide-bore, Carbowax, and QF-1 columns, respectively.

Effect of Column Temperature. Since the PAN thermal sensitivity is known, the oven temperatures reported in the literature are always low, ranging from 17 to 33 °C. To evaluate this factor more quantitatively, we conducted experiments at oven temperatures of 30, 40, and 50 °C, maintaining however the retention time of PAN at all three temperatures constant as much as possible (less than 1.5% variation) by varying the carrier flow rate. Thus we avoided the factor of PAN destruction on the column presented earlier. Simultaneously to exclude the effect of carrier gas flow rate on the ECD sensitivity, chloroform was used as a reference compound. The ratios of PAN/$CHCl_3$ absolute area counts obtained for the three different columns are presented in Figure 3. From these PAN/$CHCl_3$ ratios, the PAN destruction at 50 relative to 30 °C was calculated to be 48% on the wide-bore column with CH_4/Ar and 53% with He carrier gas, 95% on the 5% Carbowax 400 column, and 79% on the QF-1 column. Although the phenomenon is purely thermal and similar results for all columns should be expected, this was not found to be the case. Possibly the higher reactivity of the packed columns compared to that of the capillary column differentiated an otherwise purely thermal effect.

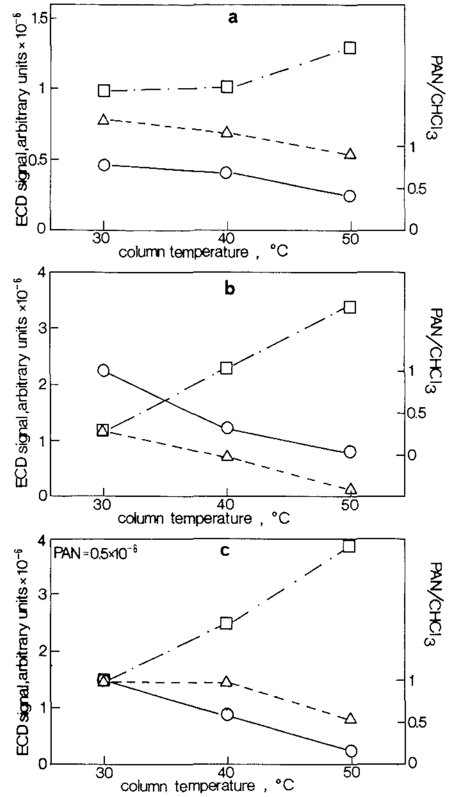

Figure 3. Plots of absolute PAN and $CHCl_3$ ECD signals and their ratios vs column temperature, under constant retention time of (a) 1.30 min for the wide-bore, (b) 1.90 min for the 5% Carbowax 400, and (c) 1.27 min for the 4.8% QF-1 + 0.18% diglycerol columns. Key: △, PAN; □, $CHCl_3$; ○, PAN/$CHCl_3$.

The results obtained with PPN, for the same variation of column temperature from 30 to 50 °C, were 56% on the methyl silicone wide-bore column with CH_4/Ar and 62% with He carrier gas, 96% PPN destruction on the Carbowax column, and 85% on the QF-1 column.

All experiments reported in this section were carried out at both injector and detector temperatures for all columns set at 60 °C, because the GC oven temperature determines the minimum temperature of the injection port and the detector.

Effect of Detector Temperature. Unlike the universally accepted low oven temperatures for PAN analysis, the detector temperature selected by workers in this field varies greatly from 30 (*5*) to 80 °C (*8*). In our experiments the oven temperature was constant at 30 °C; the carrier gas flow rate was at the previously determined optimum conditions for the packed columns, and for the capillary column the rates were 7 mL/min carrier gas and 55 mL/min makeup gas. The detector temperature was varied from 30 to 80 °C. Chloroform was used again as reference, and we assumed that it responded to the ECD the same way as PAN did. As the temperature of the detector increased from 30 to 45 °C the PAN destruction was less than ~10% for all three columns. As the detector temperature increased, however, to 80 °C, the PAN destruction reached 41–46% for all columns used, again as

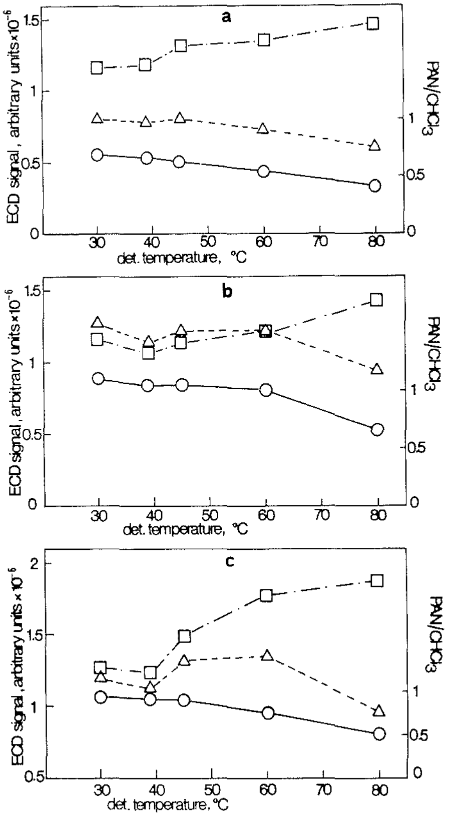

Figure 4. Plots of absolute PAN and $CHCl_3$ ECD signals and their ratios vs detector temperature under constant column temperature at 30 °C: (a) wide-bore; (b) 5% Carbowax 400; (c) 4.8% QF-1 + 0.18% diglycerol columns. Key: △, PAN; □, $CHCl_3$; ○, PAN/$CHCl_3$.

obtained from the ratio of PAN/$CHCl_3$ at 80 °C, in relation to the PAN/$CHCl_3$ ratio at a detector temperature of 30 °C. For an analyst who is interested in obtaining the maximum absolute PAN signal, the choice temperature should be 45 °C, as seen in Figure 4, since that is where the maximum absolute PAN signal appears to be. In addition, at this temperature the detector is maintained with less condensation while the standing current remains approximately the same as at 30 °C.

Similar results were obtained for PPN. The PPN destruction at a detector temperature of 80 vs 30 °C, obtained from the respective PPN/$CHCl_3$ area count ratios, was for all columns 38–47%.

Detection Limits. The three most important parameters that determine the detection limit, that is, the absolute PAN signal—namely column and detector temperature and carrier gas flow rate—were examined above. Thus for the determination of the detection limits using all three columns, the oven temperature was set at 30 °C and that of the detector at 45 °C. The results reported below were not corrected for the up to 10% destruction on the detector due to its setting at 45 vs 30 °C. The carrier flow rates were set at the optimum conditions mentioned earlier. In addition to the above, the resolution of the PAN peak from the earlier peaks, that is, the air peak, was a significant factor in achieving the lowest detection limit. This pertained mainly to the QF-1 and the capillary columns because with the Carbowax column PAN was much better resolved from the air peak. The detection limits obtained for a 1-mL sample injected were 0.06 ppb PAN for the wide-bore, 0.16 ppb for the Carbowax, and 0.12 ppb for the QF-1 column. These detection limits were established by repeated evacuations of a sample containing initially 20 ppb PAN in air, following addition of pure air up to 1000 mbar. It was assumed that the detector responded linearly within this range of 20–0.06 ppb. The calibration of the ECD was carried out by injecting 2 mL of the 20 ppb PAN containing sample into a GC-NO_x chemiluminescence detector, which in turn was easily calibrated with standard NO, as discussed in more detail elsewhere (*11*). Since overloading is a matter of concern with the wide-bore columns, linearity in the response of the ECD was observed for up to 3-mL PAN samples injected.

Conclusions. Because of the inherent inertness of the fused silica column, the PAN and PPN destruction on this column was significantly less than with the packed ones. The results of this work suggest that a correction should be applied to the PAN and PPN values obtained with GC due to the compounds' destruction on the analytical column. The greater the retention times of PAN and PPN, the greater is this correction. With the ease and low cost of packed to wide-bore conversion, it is surprising that the use of wide-bore columns for PAN and PPN analysis has not been reported in the literature. After the submission of this paper, correspondence (*15*) was published on the use of capillary columns for the analysis of PAN and PPN.

ACKNOWLEDGMENT

We thank U. Schurath of the University of Bonn for helpful discussions.

LITERATURE CITED

(1) Stephens, E. R.; Price, M. A. *J. Chem. Educ.* **1973**, *50*, 351–354.
(2) Taner, R. L.; Miguel, A. H.; Andrade, J. B.; Gaffney, J. S.; Streit, G. E. *Environ. Sci. Technol.* **1988**, *22*, 1026–1034.
(3) Mayrahn, H.; Helas, G.; Warneck, P. *J. Atmos. Chem.* **1987**, *5*, 405–415.
(4) Rudolph, J.; Vierkorn-Rudolph, B.; Meixner, F. X. *J. Geophys. Res.* **1987**, *92*, 6653–6661.
(5) Grosjean, D.; Fung, K.; Collins, J.; Harrison, J.; Breitungs, E. *Anal. Chem.* **1984**, *56*, 569–573.
(6) Holdren, M. W.; Spicer, C. W. *Environ. Sci. Technol.* **1984**, *18*, 113–116.
(7) Lonneman, W. A.; Bufalini, J. J.; Namie, G. R. *Environ. Sci. Technol.* **1982**, *16*, 655–660.
(8) Peake, E.; Sandhu, H. S. *Can. J. Chem.* **1983**, *61*, 927–935.
(9) Tsalkani, N.; Perros, P.; Toupance, G. *J. Atmos. Chem.* **1987**, *5*, 291–299.
(10) Nieboer, H.; van Ham, J. *Atmos. Environ.* **1976**, *10*, 115–120.
(11) Tsani-Bazaca, E.; Glavas, S.; Güsten, H. *Atmos. Environ.* **1988**, *22*, 2283–2286.
(12) Schurath, U.; Kortman, U.; Glavas, S. *Proceedings of 3rd European Symposium on Physico-Chemical Behaviour of Atmospheric Pollutants*; Versino, B., Ott, H., Eds.; Varese, D. Reidel: Dordrecht, Holland, 1984; pp 27–37.
(13) Nielsen, T.; Hansen, A. M.; Thomsen, E. L. *Atmos. Environ.* **1982**, *16*, 2447–2450.
(14) Gaffney, J. S.; Fajer, R.; Senum, G. I. *Atmos. Environ.* **1984**, *18*, 215–218.
(15) Roberts, J. M.; Fajer, R. W.; Springston, S. R. *Anal. Chem.* **1989**, *61*, 771–772.

RECEIVED for review May 3, 1989. Accepted September 15, 1989. This work was financially supported by the European Economic Community under Contract EV4V-0070-D(B). N. Roumelis also thanks the Hellenic Refineries of Aspropyrgos for a fellowship.

Deconvolution of Nonequilibrium Band Broadening Effects for Accurate Particle Size Distributions by Sedimentation Field-Flow Fractionation

Mark R. Schure*[,1]

Digital Equipment Corporation, 200 Forest Street, MR01-3/T2, Marlborough, Massachusetts 01752

Bhajendra N. Barman and J. Calvin Giddings

Department of Chemistry, University of Utah, Salt Lake City, Utah 84112

Two different deconvolution methods, Fourier and iterative, are applied to experimental fractograms from sedimentation field-flow fractionation in order to obtain accurate particle size distributions by removing nonequilibrium band broadening. These methods are compared in effectiveness and ease of application. The iterative method, although slower, is generally superior by virtue of its ability to remove variable levels of zone broadening from different parts of the fractogram as required by FFF theory. The conditions under which deconvolution is useful for the removal of nonequilibrium band broadening effects are examined. Deconvolution is particularly recommended for the resolution enhancement of small particles eluting at low retention and for fractograms obtained under high-speed conditions.

INTRODUCTION

Field-flow fractionation (FFF) is a relatively new analytical methodology applicable to the separation of particles, polymers, and macromolecules in solution (*1*, *2*). Recent efforts have shown that sedimentation FFF is particularly effective for the separation of a wide variety of particulate species (*1–3*). Because of the simple correspondence between experiment and theory, the particle size distribution is readily calculated from experimental fractograms (*4–7*).

An accurate particle size distribution is essential but often difficult to achieve for detailed particle characterization. Sedimentation FFF is an effective method for this purpose because of its high selectivity and resolution, but even here a number of distortions may exist in the experimental fractograms leading to inaccuracies in the acquired particle size distributions. One distortion, unrelated to the FFF process as such, is due to light scattering rather than simple absorption when detection is based on light attenuation. The resulting signal is a complex function of the particle size when the particle size is in the vicinity of the wavelength of light used in the detector. Using the theory of Mie scattering (*8*), both Kirkland et al. (*3*) and Yang et al. (*5*) have demonstrated that correction to the light scattering intensity as a function of particle size can yield a compensated size distribution and thus largely eliminate this distortion.

A more universal distortion (not dependent on a specific detector type) is due to zone broadening mechanisms in FFF that lead to the artificial broadening of the size distribution curves obtained. These broadening mechanisms include the nonequilibrium effect (*9–11*) and extracolumn effects such as detector and injector dead volumes and flow irregularities in the channel. In other elution techniques such as size-exclusion chromatography (SEC), many numerical methods have been devised to correct for these distortions. However, due to the theoretical intractability of the SEC process, standards must be used to quantitate nonequilibrium and extracolumn broadening. Unfortunately, the polydispersities of the polymer standards needed for SEC are generally not well characterized (*12*).

Traditionally, polydispersity estimates in sedimentation FFF are obtained from the intercept of an H (plate height) versus $\langle v \rangle$ (linear velocity) plot. This method has the advantage that it does not rely on a quantitative nonequilibrium theory. However, this method provides an estimate of the upper limit of the sample polydispersity since all other zone broadenings that are not dependent on a linear flow velocity and sample polydispersity are assumed to be negligible. Two other shortcomings with this method are (a) multiple experiments are necessary, and (b) this method works well for well-separated Gaussian peaks of narrow dispersity only, since inaccuracies in the estimation of apparent H are possible when fused peaks are present or if the sample is broad. In the latter case, earlier eluting components will experience more band spreading than the later eluting components.

In FFF the contribution of nonequilibrium, the dominant mechanism of zone broadening, has been well characterized and verified in a series of papers (*4*, *11*, *13*, *14*). The nonequilibrium broadening can be obtained readily from theory due to the open channel design used in FFF separations.

In principle, one could simply obtain the particle size distribution from an experimental fractogram and subtract out the contribution due to nonequilibrium broadening using theory. This approach will work for well-separated Gaussian peaks of narrow dispersity. As will be demonstrated in this paper, it is much more convenient to use a formal convolution theory that does not require well separated Gaussian zones so that any zone shape could be incorporated for the reliable estimation of the true particle size distribution.

In order to examine the deconvolution of nonequilibrium band broadening in sedimentation FFF at a fundamental level, simple experimental fractograms of well-characterized samples using constant field and low flow conditions will be used. The effectiveness of deconvolution procedures will be tested on the fractograms obtained at different field and/or flow conditions. By such choice, we are able to minimize the complications arising from field or flow programming, steric effects (important for >0.5-μM particles), and lift forces (significant for large particles and high flow conditions).

We will examine the extent of nonequilibrium distortion and evaluate two methods for the removal of nonequilibrium zone broadening from particle size distributions in this paper. A light scattering correction will also be applied to gain an

---

* Author to whom correspondence should be addressed.

[1] Present address: Rohm and Haas Co., Computer Applications Research, 727 Norristown Rd., Spring House, PA 19477.

0003-2700/89/0361-2735$01.50/0 © 1989 American Chemical Society

improved accuracy in particle size distributions by sedimentation FFF. Although we will focus on experimental fractograms taken from sedimentation FFF, this methodology may be used for other FFF techniques as well.

THEORY

While the theory of sedimentation FFF has been previously presented (*4, 11, 13, 14*), a few essential elements will be given here for continuity of treatment.

The basic retention equation common to most FFF methods relates R, the retention ratio, to the dimensionless mean layer thickness λ by (*4*)

$$R = 6\lambda[\coth(1/2\lambda) - 2\lambda] \tag{1}$$

The retention ratio is simply the ratio of the column void time t° to the mean retention time t_r of the component of interest. For high levels of retention ($t_r \gg t^\circ$) the following approximation is valid:

$$R = 6\lambda \tag{2}$$

For sedimentation FFF, λ is expressed in terms of the particle diameter d and particle density ρ_s by

$$\lambda = \frac{6kT}{\pi d^3 G w |\rho_s - \rho|} \tag{3}$$

where k is Boltzmann's constant, T is temperature in K, G is the acceleration due to the spinning of the channel, and w and ρ are the channel thickness and carrier density, respectively. For nonspherical particles, d is the effective spherical diameter.

The zone broadening of narrow particle distributions is measured by plate height H and can be cast in the simple form

$$H = \frac{2D}{R\langle v\rangle} + \frac{\chi w^2 \langle v\rangle}{D} + \sum_k H_k + H_p \tag{4}$$

where D is the diffusion coefficient of the particles and $\langle v\rangle$ is the average linear velocity of the fluid. The first term of eq 4 is the plate height contribution due to longitudinal diffusion. The second term is the plate height contribution due to nonequilibrium, in which χ is the λ-dependent nonequilibrium coefficient (*11*). The third term is the sum of instrumental contributions from injection, detection, system dead volumes, and flow irregularities (*15–17*). The fourth term, H_p, is the contribution of particle size polydispersity to the plate height. The value of H_p is obtained from (*13*)

$$H_p = 9L\left(\frac{\mathrm{d}\ln R}{\mathrm{d}\ln\lambda}\right)^2\left(\frac{\sigma_d}{d}\right)^2 \tag{5}$$

where σ_d is the standard deviation of the particle size distribution and L is the channel length. Equation 5 can be reduced to a still simpler form (*13*) in the limit of $\lambda \to 0$

$$H_p = 9L(\sigma_d/d)^2 \tag{6}$$

Note that H_p, unlike the other H terms, represents the width of the particle size distribution (σ_d/d) and as such approaches zero for monodisperse samples. It does not, therefore, represent an intrinsic band broadening process in the system.

The observed plate height may be obtained from an experimental fractogram by using the relationship

$$H = \frac{\sigma_t^2}{t_r^2}L \tag{7}$$

where σ_t^2 is the variance of a peak in time units.

Apparent Polydispersity. One of the goals of sedimentation FFF theory is to provide a simple method for the evaluation of particle polydispersity for samples of narrow size distribution. For this purpose, system band broadening must be subtracted from the experimental fractogram. It is useful in this regard to examine the "apparent" polydispersity that would be assigned to a monodisperse particle population if the system band broadening was attributed to a finite polydispersity. Thus we imagine an experiment with monodisperse particles in which the system zone broadening mechanisms act to artificially broaden the otherwise infinitely narrow peak, said broadening then being calculated as though it were a polydispersity effect. Toward this end we set plate height due to polydispersity, H_p from eq 5, equal to the nonequilibrium plate height contribution given in eq 4. (We will neglect the contributions of longitudinal diffusion, which is generally negligible in sedimentation FFF, and also the extracolumn contributions, $\sum H_k$.) This yields

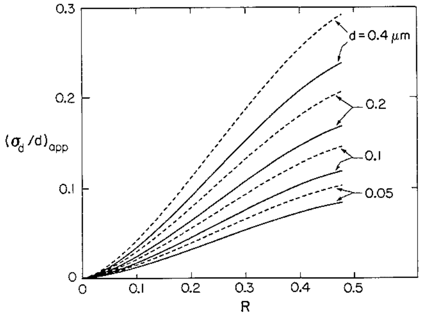

Figure 1. Apparent polydispersity as a function of retention ratio R. Conditions are L = 90 cm, T = 296 K, η = 1 cP, w = 0.0127 cm, breadth b = 2.0 cm. Solid lines represent $\langle v\rangle$ = 0.656 cm/s (flow rate = 1 mL/min). Dashed lines correspond to $\langle v\rangle$ = 0.984 cm/s (1.5 mL/min).

$$\frac{\chi w^2\langle v\rangle}{D} = 9L\left(\frac{\mathrm{d}\ln R}{\mathrm{d}\ln\lambda}\right)^2\left(\frac{\sigma_d}{d}\right)^2 \tag{8}$$

By substituting the Stokes–Einstein equation

$$D = kT/3\pi\eta d \tag{9}$$

into eq 8 for D (where η is the solution viscosity) and rearranging, we obtain

$$\left(\frac{\sigma_d}{d}\right)_{app} = w\frac{\mathrm{d}\ln\lambda}{\mathrm{d}\ln R}\left(\frac{\pi\chi\eta\langle v\rangle d}{3kTL}\right)^{1/2} \tag{10}$$

The ratio $(\sigma_d/d)_{app}$ calculated in this way is referred to here as *apparent polydispersity* and is evaluated in Figure 1 for four particle sizes and two flow rates. The χ and d ln λ/d ln R quantities are calculated via computer methods; the formula for χ is given as eq 26 in ref 11. Figure 1 shows that the apparent polydispersity is predicted to be quite large when particles elute in less than 5 column volumes ($R > 0.2$) at a typical flow rate of 1.0–1.5 mL/min; however, the apparent polydispersity rapidly diminishes for even the larger particles at higher retention levels ($R < 0.2$).

The curves shown in Figure 1 would normally be realized by changing the field strength so as to vary λ (and hence R) in eq 10. By substitution of the approximations $\chi = 24\lambda^3$ and d ln λ/d ln R = 1 (both valid for small R) into eq 10 and use of the definition of λ given in eq 3, the apparent polydispersity is given approximately as

$$\left(\frac{\sigma_d}{d}\right)_{app} \simeq \frac{24kT}{\pi d^4(G|\Delta\rho|)^{3/2}}\left(\frac{3\eta\langle v\rangle}{Lw}\right)^{1/2} \tag{11}$$

Examination of this equation shows that at constant field

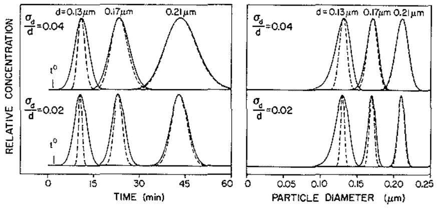

Figure 2. Artificial fractograms in time and size domains showing peaks with (outer peak) and without (inner peak) nonequilibrium zone broadening: top peaks, $\sigma_d/d = 0.04$; bottom peaks, $\sigma_d/d = 0.02$. Conditions are the same as given in Figure 1 with $G = 1510$ g and $\langle v \rangle = 0.656$ cm/s. Void time $t^\circ = 2.29$ min. R values (left to right) are 0.210, 0.098, 0.0529.

strength G the apparent polydispersity decreases as d^{-4}; larger particles have a much lower apparent polydispersity than small particles in a constant field experiment.

Both eq 10 and 11 indicate that apparent polydispersity will increase with flow velocity. Therefore, the removal of nonequilibrium band broadening becomes increasingly important if the fractograms are obtained under high-speed conditions.

We now examine some representative cases where the actual polydispersity is varied in an attempt to elucidate the effect of apparent polydispersity. For a slightly polydisperse sample the system band broadening will further expand the peak width arising solely from the size distribution. To evaluate this additional effect, artificial fractograms are created with a computer. First, a size distribution is established and the fractogram with no broadening is calculated directly from the size distribution by using eq 1 and 3. Next the elution time fractogram is broadened with nonequilibrium effects using the convolution relationship given in the next section. The "broadened" size distribution is then calculated directly from the broadened elution time fractogram.

The results of these calculations for three particle sizes under constant field conditions and two polydispersities are given in Figure 2 for both the time-based fractogram and the resulting particle size distribution. As can be seen from Figure 2 the more retained, larger particles show little increase in polydispersity. However, the smallest particles shown in Figure 2 have an apparent polydispersity approximately twice that of the true polydispersity. These results suggest that deconvolution can be advantageous for small particles eluting early in the fractogram where the polydispersity may otherwise be largely overestimated.

Zone Broadening as a Convolution Process. Zone broadening may be modeled as a convolution process in the time domain in which the elution curve, represented by response $F(t)$, may be expressed as

$$F(t) = \int_{-\infty}^{\infty} G(t,t')W(t')\, \mathrm{d}t' \qquad (12)$$

where $W(t')$ is the ideal elution response curve that would be obtained for the sample with no zone broadening mechanisms present and $G(t,t')$ is the response due purely to all the mechanisms of zone broadening except polydispersity. In this treatment t is time and t' is a dummy time variable. Equation 12 may be written in a shortened form

$$F(t) = G(t,t')*W(t') \qquad (13)$$

where the asterisk (*) operator denotes a convolution process. The time (t) domain is used because G is known to be close to Gaussian shape (*18*) when expressed in the time rather than in the retention ratio (R) domain.

For the case of Gaussian zone broadening, eq 13 may be written explicitly in discrete form as

$$F(t_i) = A_0 \sum_{j=1}^{N} W(t_j)\, \frac{\exp\left[-(t_i - t_j)^2/2\sigma_{t_j}^{\,2}\right]}{\sigma_{t_j}} \qquad (14)$$

where $F(t_i)$ is the amplitude (concentration) of a fractogram at time t_i, N is the number of data points in the discrete fractogram, A_0 is a normalization factor, $W(t_j)$ is the ideal fractogram, and $\sigma_{t_j}^{\,2}$ is the broadening function variance for a monodisperse particle population ($H_p = 0$) obtained by combining eq 4 and 7

$$\sigma_{t_j}^{\,2} = \frac{\left[\dfrac{2D_j}{R_j\langle v\rangle} + \dfrac{\chi_j w^2\langle v\rangle}{D_j} + \sum_k H_k\right]}{L}\, t_j^{\,2} \qquad (15)$$

The problem requiring solution is to obtain W for a given F (from the experimental fractogram), utilizing the G term obtained from theory as written above. This problem, known commonly as an inverse problem, has been extensively studied in chromatography and spectroscopy. A variety of numerical methods have been used in the solution of the inverse problem including Fourier transform methods (*19*, *20*), the singular-value decomposition method (*21*), an iterative solution method (*22*–*25*), and the Kalman filter approach (*26*). Some of these approaches are summarized in a recent book by Jansson (*24*). In this paper we will compare the Fourier transform and iterative relaxation methods; details of each method are given below. The technique of fractogram deconvolution for one type of iterative relaxation method was recently presented for sedimentation FFF (*22*) and thermal FFF (*23*).

DATA ANALYSIS

The data used in this paper were taken from original strip chart recordings and carefully digitized with a hand-held digitizing tablet connected to the computer system described below. About 150 points were obtained across each fractogram. The data were then numerically interpolated to produce equispaced data and simultaneously smoothed by using a polynomial least-squares algorithm (*27*) with subsequent production of 1000 data points.

The presence of noise in the fractograms is a serious problem with the iterative deconvolution but not with the Fourier method since in the latter case most noise shows up at frequencies higher than the selected cut-off frequency (see later). However, if a noisy fractogram is used, it must be carefully prefiltered before the iterative deconvolution method is attempted.

The initial data treatment is the same for both deconvolution procedures. First the experimental conditions of channel length, thickness, breadth, void volume, field strength, flow rate, particle density, and refractive indices are entered from a disk file along with the data stored as time–detector amplitude pairs. Next, optional digital filtering (*28*–*30*) and base-line correction are performed. The retention ratio R is then calculated for all data by dividing the channel volume by the retention volume at each time value. By use of a recently devised algorithm (*31*), the λ value at each data point is calculated from each R value when $R < 1.0$. Note that the standard FFF theory used here is a long-time asymptotic theory (*18*), where the highest R value for a zone center is unity. Following these procedures the particle diameter and broadening parameter σ_{t_j} are calculated for each data point. An array of extinction cross sections used in the light scattering correction is then calculated for each data point (particle diameter) from the refractive indices of the particle-carrier system by using a computer program given in ref 32; details of the light scattering correction will be given below. The specific method of deconvolution is then begun. Upon completion of the deconvolution step the particle size distribution is analyzed via moment analysis using interactive graphics to manually establish the limits of integration. All computer programs used in this study are written in FORTRAN-77 and were run on a VAXlab/GPX computer (Digital Equipment Corp., Maynard, MA) utilizing the VAXlab software library for graphics and signal processing.

Fourier Deconvolution. The W term in eq 13 may be recovered by means of the following treatment. Taking the Fourier transform of both sides of eq 13 yields

$$F(f) = G(f) \cdot W(f) \qquad (16)$$

where f refers to the frequency domain. Note that taking the Fourier transform of a convolution pair yields an ordinary product in the frequency domain (*33, 34*). Equation 16 can be rearranged and inverse transformed

$$W(t) = \mathbf{F}^{-1}[W(f)] = \mathbf{F}^{-1}\left[\frac{F(f)}{G(f)}\right] \qquad (17)$$

The G term may be explicitly written in both the time and frequency domains if a Gaussian form is used for the broadening function

$$G(t,t') = \frac{1}{(2\pi)^{1/2}\sigma_t} \exp[-(t - t')^2/2\sigma_t^2] \qquad (18)$$

and

$$G(f) = \exp[-2f^2\pi^2\sigma_t^2] \qquad (19)$$

In eq 19 it is assumed that the dummy variable t' is zero in eq 18, which is the appropriate centering for deconvolution (*20*) of the broadening function. In addition, eq 19 does not include a normalization constant which is ultimately absorbed into the A_0 term in eq 14 (*20*).

There are both advantages and disadvantages in using the Fourier deconvolution technique for FFF. The primary advantage is speed; deconvolution can be accomplished at a speed approximately 2 orders of magnitude faster than that attainable with the iterative method. A corresponding disadvantage is that only one unique σ_t may be specified in the broadening function, i.e., $G(f)$ is independent of time. For our purposes, we choose σ_t at the point of highest amplitude in the fractogram. This approach should work well for moderately narrow distributions.

Another disadvantage of the Fourier deconvolution method is that the $G(f)$ term falls to zero much more rapidly than does $F(f)$, in which case the quotient in eq 17 takes on very large values at high frequencies. This situation can be bypassed if $F(f)/G(f)$ is constrained to be a constant after an arbitrary number of terms of the quotient. The constant is chosen by inspection of the power spectrum of $F(f)$ which can be estimated by the product $F(f)F^*(f)$, where $F^*(f)$ is the complex conjugate of $F(f)$; the constant is that value which lies on the noise threshold. This will be shown in more detail in the results section.

Iterative Relaxation Method. This method is described in detail elsewhere (*24*). We will provide the essential elements here as they pertain to zone broadening. We can approximate the solution of eq 12 by the iterative expression

$$W^{(k+1)}(t_i) = W^{(k)}(t_i) + r[W^{(k)}(t_i)]\{F(t_i) - [G*W^{(k)}]|_{t_i}\} \qquad (20)$$

where the superscript indicates the iteration number and $r[W^{(k)}(t_i)]$ is the relaxation parameter. For practical purposes, this treatment proceeds by scaling all $F(t_i)$ values between 0 and 1.

Although a number of different functional forms exist for the relaxation parameter (*24*), we have used

$$r[W^{(k)}(t_i)] = r_0 W^{(k)}(t_i)[1 - W^{(k)}(t_i)] \qquad (21)$$

with r_0 equal to 2 for the iterative deconvolution results shown in this paper (*24*). For the first iteration where $k = 1$, the function $W^1(t_i)$ is set equal to $F(t_i)$; hence each successive iteration should cause $W^{(k+1)}(t_i)$ to be less broad as convergence is approached. Convergence is reached when the root-mean-squared (RMS) error changes by less than 1×10^{-4}. The RMS error is calculated by summing the square of the quantity in braces ({}) in eq 20 over all t_i values, dividing by the number of such values, and taking the square root of this quotient. Typically 40 to 50 iteractions are required for convergence to be reached.

Light Scattering Correction and Scale Change. The detectors most commonly used in sedimentation FFF are commercial liquid chromatographic detectors that monitor UV light attenuation in a small cell at 254 nm. Because the size of particles that commonly elute from sedimentation FFF channels is the same order as the wavelength of the light used in the detector cell, the primary response of the detector results from light scattering. Due to the particle size dependence of the detector signal, compensation must be applied to obtain a response proportional to particle concentration over the particle size range of study.

When the concentration of particles is sufficiently low that secondary scattering is minimized, the following relationship holds (*8*)

$$\tau = \sigma_{\text{ext}}(d)\, b\, n_{\text{v}} \qquad (22)$$

where τ is the detector response (turbidity) due to n_{v} particles per unit volume, each with extinction cross section $\sigma_{\text{ext}}(d)$, in a detector cell with path length b. The extinction cross section is the sum of the scattering component $\sigma_{\text{sca}}(d)$ and the absorption component $\sigma_{\text{abs}}(d)$ (*8, 32*).

The scattering correction is applied in different ways to the two methods of deconvolution described above. In the case of the Fourier method the deconvolved time domain fractogram is converted to a relative number concentration distribution as a function of particle diameter by a simple change in abscissa, as given by eq 1 and 3. The relative number concentration is then corrected for scattering by dividing by $\sigma_{\text{ext}}(d)$. This method is also used for the undeconvolved fractograms. In the case of the iterative method the convolution of $G*W^{(k)}$ in eq 20 in multiplied by $\sigma_{\text{ext}}(d)$ at each iteration; hence $W^{(k)}$ is proportional to n_{v} given in eq 22. This allows for the easy mathematical construction of the experimental (turbidity-based) fractogram. When convergence is reached, $W^{(k)}$ in the time domain is converted to a relative number concentration distribution as a function of particle diameter by the abscissa change mentioned above.

Finally, the number concentration distributions n_{v} vs d from both deconvolution methods can be cast into the differential form, $\delta n/\delta d$ (where δ is the differential operator), by applying the following treatment. Let δn be the number of particles that elute between retention volume V_{r} and $V_{\text{r}} + \delta V_{\text{r}}$. Then

$$\delta n = n_{\text{v}}\, \delta V_{\text{r}} \qquad (23)$$

The quantity δn will also be equal to the number of particles eluted between particle diameter $d + \delta d$, provided that δV_{r} corresponds to the particle diameter increment δd. Hence

$$\delta n = n_{\text{d}}\, \delta d \qquad (24)$$

where n_{d} is the number concentration of particles per unit diameter. Combining the two equations above yields

$$\frac{\delta n}{\delta d} = n_{\text{v}} \frac{\delta V_{\text{r}}}{\delta d} \qquad (25)$$

The quantity $\delta V_{\text{r}}/\delta d$ is calculated by curve fitting local data of V_{r} (from t_{r}), d pairs and numerically differentiating. We have chosen to use the quantity $\delta n/\delta d$ for all of the particle size distributions given in this paper.

Table I. Experiment Summary[a]

experiment	flow rate, mL/min	field strength, gravities	sonication	injection volume, μL
A (PMMA)	1.13	57.6	no	40
B (PMMA)	1.73	42.8	yes	20
C (PMMA)	1.23	42.8	yes	15
D (PMMA)	0.440	42.8	yes	14
E (polystyrene)	1.46	61.6	no	15
F (polystyrene)	0.640	61.6	no	15
G (polystyrene)	0.369	61.6	no	18

[a] PMMA: $|\Delta\rho|$ = 0.21 g/mL, sample RI = 1.485 (real), 0.0 (imaginary). Polystyrene: $|\Delta\rho|$ = 0.051 g/mL, sample RI = 1.7685 (real), 0.69 (imaginary). For both samples the carrier (water) has RI = 1.3702 (real), 0.0 (imaginary).

EXPERIMENTAL SECTION

Two samples are used in this study. The first sample is a poly(methyl methacrylate) (PMMA) latex (Seradyn, Indianapolis, IN) having various degrees of aggregation of single spherical particles; the primary singlet size is approximately 0.213 μm and the density is 1.21 g/mL. The extent of aggregation of particles into doublets, triplets, and higher order aggregates can be varied by sonication. The second sample is a mixture of two polystyrene latex standards (Seradyn) with nominal diameters of 0.327 and 0.551 μm and density 1.05 g/mL.

All data were obtained by using a laboratory-built apparatus with construction features similar to those of the Model S101 SdFFF Colloid/Particle Fractionator (FFFractionation, Inc., Salt Lake City, UT). The system has a channel length (tip to tip) of 90.5 cm, thickness 0.0254 cm, breadth 2.00 cm, radius of rotation 15.3 cm, dead volume 0.1 mL, and void volume 4.50 mL. The carrier used in all experiments was water containing 0.05% (w/v) sodium dodecyl sulfate and 0.01% (w/v) sodium azide.

RESULTS AND DISCUSSION

Four fractograms of the PMMA samples are shown in Figure 3; the conditions used for separation are given in Table I. Note that the fractograms clearly display the extensive particle aggregation; the successive peaks represent single particles, doublets, triplets, etc. (35). The broad undefined peak to the right of fractogram A in Figure 3 represents the sum of higher-order aggregates. By sonication of the sample prior to injection, the larger aggregates are broken up as shown by the disappearance of this broad peak in fractograms B through D of Figure 3. Note also that as the flow rate is decreased from fractogram B through D, which are run under identical field strength, both the run time and the resolution increase dramatically.

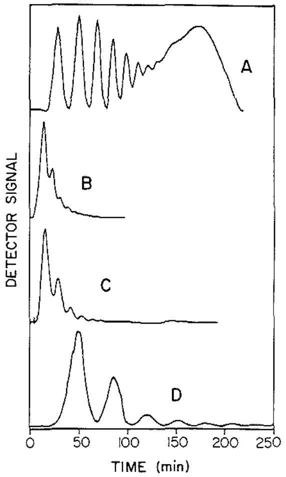

Figure 3. Experimental PMMA fractograms. Experimental conditions for A, B, C, and D are given in Table I.

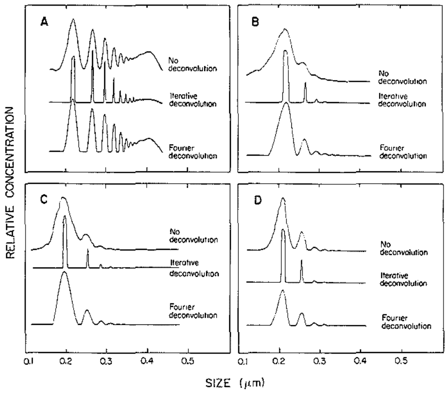

Figure 4. Particle size distributions of experiments A through D with and without deconvolution. Light scattering correction and scale change are used in all distributions.

Both the Fourier and the iterative relaxation deconvolution methods were applied to the fractograms in Figure 3 in an attempt to remove the contribution of nonequilibrium zone broadening. The results of these deconvolutions are shown in Figure 4 for the Fourier method and the iterative relaxation method along with the size distributions obtained from the fractograms prior to deconvolution. These figures show that a large increase in resolution is offered by deconvolution, the iterative relaxation method producing the largest increase. For experiment B where the high flow rate leads to strong peak overlap, deconvolution offers essentially base-line resolution in the size distribution.

The effective particle sizes that are produced from the deconvolution methods are given in Table II along with the

Table II. Mean Particle Diameters (in μm) from the PMMA Experiments

	experiment[a]						
peak no.	A	B	C	D	$\bar{d}^c$	% RSD[c]	d_n^b
1	0.218, 0.218, 0.220	0.215, 0.217, 0.217	0.200, 0.200, 0.200	0.209, 0.210, 0.209	0.211	3.6	0.213 (1)
2	0.267, 0.267, 0.266	0.258, 0.263, 0.266	0.249, 0.252, 0.254	0.255, 0.257, 0.256	0.259	2.5	0.268 (2)
3	0.297, 0.297, 0.297	0.289, 0.292, 0.293	0.285, 0.287, 0.286	0.288, 0.288, 0.287	0.291	1.6	0.307 (3)
4	0.320, 0.320, 0.320	0.314, 0.314, 0.315	0.310, 0.310, 0.311	0.313, 0.313, 0.313	0.314	1.2	0.338 (4)
5	0.336, 0.335, 0.335	0.332, 0.332, 0.332	0.330, 0.329, 0.329	0.332, 0.332, 0.331	0.332	0.69	0.364 (5)
6	0.347, 0.350, 0.349	0.346, 0.346, 0.346	0.347, 0.347, 0.347	0.348, 0.348, 0.348	0.347	0.36	0.387 (6)
7	0.361, 0.360, 0.360						0.407 (7)

[a] First number: no deconvolution, second number: Fourier deconvolution, third number: iterative deconvolution. [b] Calculated particle diameter based on number (n) of aggregated singlets. [c] Calculated from the 12 particle diameters.

Table III. The σ_d Values (in nm) Estimated from the PMMA Experiments

	experiment[a]				$\bar{\sigma}_d$ per method between fractograms B, C, and D	% RSD per method between fractograms B, C, and D
peak	A	B	C	D		
1	11.7, 7.79, 2.63	28.9, 13.5, 3.79	20.3, 12.3, 2.69	13.9, 9.18, 2.78	21.0, 11.6, 3.09	35.8, 19.1, 19.8
2	7.24, 4.92, 1.26	*b*, 6.60, 1.67	9.47, 6.65, 1.35	6.92, 5.08, 1.76	8.2, 6.11, 1.59	22.0, 14.6, 13.5
3	4.88, 3.18, 1.18	*b*, 5.62, 2.53	6.26, 4.10, 1.54	5.45, 3.92, 3.02	5.86, 4.55, 2.36	9.78, 20.5, 31.9
4	3.91, 2.51, 0.916	*b*, 4.87, 3.23	5.11, 3.79, 1.89	4.03, 2.83, 2.92	4.57, 3.83, 2.68	16.7, 26.6, 26.2
5	3.62, 2.32, 1.39	*b*, 3.50, 3.49	4.20, 2.35, 2.25	3.31, 2.35, 2.74	3.76, 2.73, 2.82	16.8, 24.3, 22.1

[a] First number, no deconvolution; second number, Fourier deconvolution; third number, iterative deconvolution. [b] Peak quantitation is unreliable due to fused peaks.

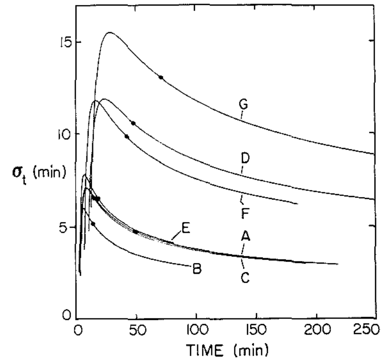

Figure 5. The broadening parameter σ_t for all fractograms from eq 15. The solid circles indicate values of σ_t used in the Fourier deconvolution for each fractogram.

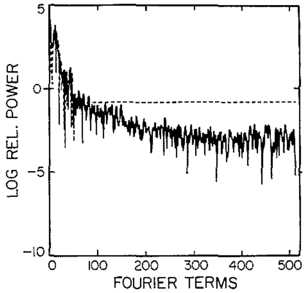

Figure 6. The logarithm of the power spectrum of the time domain data for fractogram A (——) and the Fourier deconvolved time domain (- - -).

particle sizes obtained without deconvolution. Also given in Table II is the theoretical particle diameter d_n, equal to the effective particle diameter for doublets ($n = 2$), triplets ($n = 3$), and higher order aggregates. Assuming that each singlet particle contributes a volume of $\pi d_1^3/6$ to the aggregate, the volume equivalent (effective) diameter of the aggregate is $d_n = n^{1/3}d_1$ where d_1 is the diameter of the singlet particle. Assuming that d_1 is 0.213 μm (SEM analysis yields $d_1 = 0.213 \pm 0.013$ μM), good agreement between experiment and the calculated d_n is found for the effective doublet and triplet diameters d_2 and d_3. The higher order aggregates show increasing departures in effective diameter; the onset of steric and hydrodynamic effects for the relatively elongated aggregates are most likely responsible for this observed behavior (*35–37*). Other sources of error must be considered here such as the light scattering and diffusivities, which are based on the explicit assumption of spherical particles; the deviation of these quantities for aggregated particles requires further investigation.

As shown in Table II, deconvolution by both methods yields mean effective particle diameters that are very close to the diameters obtained without deconvolution. This suggests that deconvolution offers little gain (or distortion) for the determination of the mean effective particle diameter. However, observation of Table III and Figure 4 shows that deconvolution offers a large gain in removing the nonequilibrium zone broadening contribution, which is useful when accurate polydispersity (size distribution) quantitation is desired.

Table III along with Figure 4 shows that a smaller degree of effective band broadening is removed by the Fourier method as compared to the iterative method. There are two reasons for the differences in the two approaches. First, as mentioned previously, one unique σ_t must be used for Fourier deconvolution. As shown in Figure 5, σ_t varies for each fractogram over a large range so that one region of the fractogram may be accurately deconvolved and another not. One observes the appearance of oscillations in regions of overdeconvolution (more broadness is removed than is physically allowed). To compensate for these oscillations, the power spectrum is held constant, as shown in Figure 6, in the frequency region of oscillation. Occasionally the base line will become slightly negative with this approach. In those cases the negative segments are set equal to zero. Although this scheme is functional, the fidelity of deconvolution is questionable because of the substantial change of σ_t over the fractogram.

The relative accuracy of the two deconvolution methods is difficult to judge without absolute polydispersity values. Some approximate polydispersities are available from previous sedimentation FFF results. These values, obtained from plate height versus flow velocity plots, are as follows (*35, 37*). For singlets, doublets, and triplets the calculated σ_d values are 4.9 ± 1.9 nm, 3.8 ± 2.3 nm, and 3.1 ± 1.5 nm, respectively. Comparing these values with those from Table III (3.09, 1.59, and 2.36 nm) for the iterative method, it can be seen that the mean σ_d values from plate height measurements are higher than those from the iterative deconvolution (but comparable in terms of the statistical significance). However, they are smaller than the σ_d values obtained by using the Fourier method of deconvolution (11.6, 6.11, and 4.55 nm). Because of the reasonably close agreement of the iterative method and plate height σ_d values, it appears that the iterative method is superior in performance to the Fourier method.

An indirect criterion of the effectiveness and accuracy of deconvolution is provided by comparison of the resolution and peak areas obtained for different particle populations, such as those shown in Figure 4. For all four experiments (A, B, C, and D), the resolution between successive peaks should be identical even though the experimental conditions vary. Figure 4 shows that the resolution between successive peaks obtained by the iterative method is comparable in the four experiments. The Fourier method provides similar levels of

Table IV. Mean Particle Diameters (in μm) from the Polystyrene Experiments

peak no.	experiment[a] E	F	G	$\bar{d}$[b]	% RSD[b]
1	0.180, 0.201, 0.192	0.170, 0.200, 0.185	0.164, 0.163, 0.175	0.181	8.0
2	0.327, 0.329, 0.328	0.326, 0.325, 0.327	0.322, 0.322, 0.320	0.325	0.95
3	0.483, 0.484, 0.484	0.489, 0.489, 0.489	0.493, 0.493, 0.490	0.488	0.77

[a] First number, no deconvolution; second number, Fourier deconvolution; third number, iterative deconvolution. [b] Calculated from the nine particle diameters.

Table V. The σ_d Values (in nm) Estimated from the Polystyrene Experiments

peak	experiment[a] E	F	G	$\bar{\sigma}_d$ per method between fractograms	% RSD per method between fractograms
1	22.6, 28.9, 11.9	20.5, 20.1, 9.87	30.9, 30.7, 14.0	24.7, 26.6, 11.9	22.3, 21.3, 17.3
2	35.3, 23.9, 5.75	30.0, 19.4, 4.33	25.7, 24.8, 5.15	30.3, 22.7, 5.08	15.8, 12.7, 14.0
3	10.6, 7.26, 2.87	8.03, 5.08, 2.10	8.75, 6.85, 3.42	9.13, 6.40, 2.80	14.5, 18.1, 23.7

[a] First number, no deconvolution; second number, Fourier deconvolution; third number, iterative deconvolution.

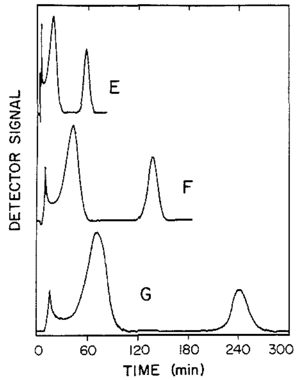

Figure 7. Experimental fractograms for polystyrene latex mixture. Conditions are given in Table I.

resolution in experiments A, C, and D, but a lesser resolution is found for experiment B, which is the most challenging of the experiments because of its greater degree of band broadening arising from high flow conditions.

We note in addition that the relative heights and areas of the successive peaks after deconvolution should be identical in experiments B, C, and D (but not A). Both deconvolution methods perform satisfactorily in this regard noting that the results, as given in Figure 4, are presented with arbitrary concentration scales.

The raw fractograms from three experiments obtained by using the polystyrene mixture are shown in Figure 7. The first peak in these fractograms is due to a small-sized impurity (nominal diameter 0.225 μm) that was known to be present with the larger particle fractions of the mixture. Also present in the first peak is the void response.

The results of deconvolution of the particle size distributions for the polystyrene samples are shown in Figure 8. As can be seen from this figure, the variation in results between the two deconvolution methods is quite pronounced although good agreement is again found between the methods with respect to the mean diameter of the component particles as shown in Table IV. Similar to Table III for the PMMA experiments, the tabulated σ_d values for the polystyrene experiments are given in Table V. Again, the iterative relaxation method reduces the broadening beyond that achieved by the Fourier deconvolution method.

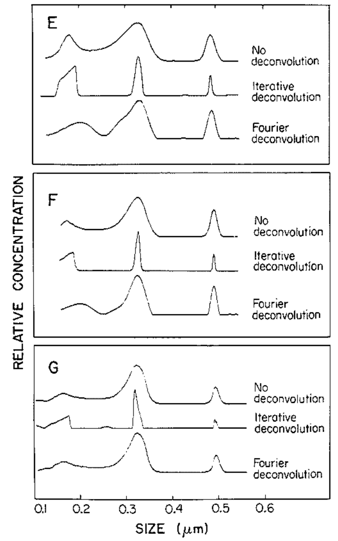

Figure 8. Particle size distributions of experiments E, F, and G with and without deconvolution. Light scattering correction and scale change are used in all distributions.

The accuracy of the deconvolution methods may be compared with the results from microscopic observations and plate height measurements. The 0.327-μm polystyrene standard was subject to characterization by the supplier where 231 particles were measured by transmission electron microscopy (TEM) (*38*). The particle sizes were obtained by reference to a grid; results of computer analysis gave a standard deviation σ_d of 7.61 nm. This compares with the resulting mean σ_d for three experiments of 5.08 nm using iterative deconvolution. Although not shown here, the particle size histogram from TEM analysis is very jagged, indicating a distinct undersampling of the particle population. The plate height measurements provided a σ_d value of 21.8 ± 6.2 nm for the 0.327-μm polystyrene standard, which bears considerable uncertainty. This value is slightly less but comparable to 22.7 nm obtained by the Fourier deconvolution method. For the 0.551-μm polystyrene standard, the σ_d value of 8.8 ± 1.5 nm obtained by plate height measurements is again comparable to 6.4 nm obtained by the Fourier deconvolution method. In this case, the iterative deconvolution method provided a much lower σ_d value of 2.8 nm.

Although the iterative method of deconvolution appears to be the method of choice for deconvolution of sedimentation FFF fractograms, this method puts stringent requirements on the theory of retention and of zone broadening. This may explain some of the variability seen in σ_d between experiments. This may also explain some of the rather odd peak shapes found when the iterative method is used in the low retention regions of the fractograms. Some of the squareness of these earlier peaks may be reduced by applying filtering on each iteration to $W^{(k+1)}(t_i)$; however, this causes additional broadness as measured by σ_d. Other sources of distortion may include detector nonlinearity and the error from strip chart recorder transcription.

As the results presented here indicate, significant reduction in the experimentally determined σ_d value can be realized with deconvolution. The iterative relaxation method appears to perform much better than the Fourier method except for its increased computation time, typically a few minutes when the G broadening matrix is stored in computer memory as a banded array with sparsity removed. In addition, the iterative relaxation method utilizes the theoretical relationships more effectively because there are very few assumptions made regarding σ_{tj}.

Although we have shown here the results of particle size distributions using deconvolution for samples where each peak has a relatively narrow distribution, thus maximally challenging the deconvolution process, deconvolution has been applied to a variety of experimental fractograms. For the case of a wide size distribution such as found for a safflower oil emulsion (*6*), deconvolution carried out under conditions of high resolution offers little enhancement because the intrinsic broadness of the size distribution is large compared to the nonequilibrium broadening. This is consistent with the theoretical results given in Figure 2. However, experiments with polydisperse samples can be carried out at high flow conditions where significant nonequilibrium band broadening will occur, and it should be possible for the resolution (accuracy) to be recovered by deconvolution. It remains for future work to explore the extent to which accuracy and separation speed can be optimized.

The results of deconvolution presented here have been performed on constant field fractograms. Field programming, which has been utilized with great success in sedimentation field-flow fractionation, is a prime candidate for the deconvolution technique because there is an inherent loss of resolution as the field strength is decreased. In this respect it may be anticipated that experiments (programmed or nonprogrammed) can be carried out in shorter time and the resolution restored mathematically, as demonstrated for experiment B. Also flow programming may be useful in this regard with resolution restored by means of deconvolution. The accuracy of deconvolution from programmed field experiments needs to be examined in extending the deconvolution methodology because secondary relaxation effects (*39–41*), which complicate the retention theory for programmed-field operation, may be difficult to incoporate into a programmed-field zone broadening theory (*42, 43*). Some aspects of deconvolution for programmed runs will be presented in a subsequent paper.

The deconvolution techniques place a tremendous burden on the accuracy of theory as the retention ratio approaches unity. In a recent paper (*18*) it is suggested that large deviations from standard retention theory exist near the void peak ($R = 1$); this is unfortunate since this region can benefit greatly from resolution enhancement. Although empirical equations can be produced for retention and zone broadening in this region, it is preferable to design experiments such that the first peak elutes after four channel volumes. This may be impractical, however, for very broad particle dispersions. As shown in this paper, the iterative relaxation method of deconvolution tends to perform poorly in the region near the void peak. In this regard it may be desirable to limit the retention ratio range over which deconvolution is applied.

Finally, we note that sedimentation FFF with deconvolution may be useful for very high accuracy in particle size determination. With deconvolution, the sedimentation FFF technique may yield an accuracy that approaches or exceeds that of electron microscopy as a particle sizing technique. Due to the large number of particles that need to be counted for statistical accuracy, the possible disturbances caused by removing particles from their normal environment, and the possibility of particle shrinkage in the electron beam, sedimentation FFF may assume a complementary role for the accurate determination of colloid particle size distributions.

ACKNOWLEDGMENT

The authors thank Seradyn for the PMMA and polystyrene samples used in this study and are grateful to P. Stephen Williams for helpful discussions.

NOMENCLATURE

A_0, detector signal normalization constant
b, detector path length
D, diffusion coefficient
d, particle diameter
$\mathbf{F}^{-1}$, inverse Fourier transform operator
$F(f)$, detector signal in frequency domain
$F^*(f)$, complex conjugate of $F(f)$
$F(t)$, detector signal in time domain
G, field strength (acceleration)
$G(f)$, detector signal in frequency domain due only to nonequilibrium zone broadening
$G(t)$, $G(t,t')$, detector signal in time domain due only to nonequilibrium zone broadening
H, total plate height
H_k, plate height from instrumental contributions
H_p, plate height due to polydispersity
k, Boltzmann's constant
L, channel length
n, n_v, n_d, number concentrations
R, retention ratio
r_0, relaxation constant
$r[W^{(k)}(t_i)]$, relaxation parameter
T, absolute temperature
t, t_i, t_j, t', time
t_r, retention time
t^0, void time
$\langle v \rangle$, average flow velocity
V_r, retention volume
$W(f)$, detector signal without zone broadening in frequency domain
$W(t)$, detector signal without zone broadening in time domain
w, channel thickness
η, viscosity
λ, dimensionless layer thickness
ρ, density of carrier liquid
ρ_s, density of sample particles
σ_t, σ_{t_j}, standard deviation of Gaussian peaks in time domain
σ_d, standard deviation of particle size distributions
$(\sigma_d/d)_{app}$, apparent polydispersity
σ_{ext}, extinction coefficient
χ, nonequilibrium parameter
τ, turbidity

LITERATURE CITED

(1) Giddings, J. C. *Chem. Eng. News* **1988**, *66*, 34–45.
(2) Caldwell, K. D. *Anal. Chem.* **1988**, *60*, 959A–971A.
(3) Kirkland, J. J.; Rementer, S. W.; Yau, W. W. *Anal. Chem.* **1981**, *53*, 1730–1736.
(4) Giddings, J. C.; Karaiskakis, G.; Caldwell, K. D.; Myers, M. N. *J. Colloid Interface Sci.* **1983**, *92*, 66–80.

(5) Yang, F.-S.; Caldwell, K. D.; Giddings, J. C. *J. Colloid Interface Sci.* **1983**, *92*, 81–90.
(6) Yang, F.-S.; Caldwell, K. D.; Myers, M. N.; Giddings, J. C. *J. Colloid Interface Sci.* **1983**, *93*, 115–125.
(7) Yau, W. W.; Kirkland, J. J. *Sep. Sci. Technol.* **1981**, *16*, 577–605.
(8) Kerker, M. *The Scattering of Light*; Academic Press: New York, 1969.
(9) Giddings, J. C. *J. Chem. Educ.* **1973**, *50*, 667–669.
(10) Giddings, J. C. *J. Chem. Phys.* **1968**, *49*, 81–85.
(11) Giddings, J. C.; Yoon, Y. H.; Caldwell, K. D.; Myers, M. N.; Hovingh, M. E. *Sep. Sci.* **1975**, *10*, 447–460.
(12) Schimpf, M. E.; Myers, M. N.; Giddings, J. C. *J. Appl. Polym. Sci.* **1987**, *33*, 117–135.
(13) Giddings, J. C.; Yang, F. J. F.; Myers, M. N. *Anal. Chem.* **1974**, *46*, 1917–1924.
(14) Karaiskakis, G.; Myers, M. N.; Caldwell, K. D.; Giddings, J. C. *Anal. Chem.* **1981**, *53*, 1314–1317.
(15) Giddings, J. C.; Schure, M. R.; Myers, M. N.; Velez, G. R. *Anal. Chem.* **1984**, *56*, 2099–2104.
(16) Giddings, J. C.; Schure, M. R. *Chem. Eng. Sci.* **1987**, *42*, 1471–1479.
(17) Williams, P. S.; Giddings, S. B.; Giddings, J. C. *Anal. Chem.* **1986**, *58*, 2397–2403.
(18) Schure, M. R. *Anal. Chem.* **1988**, *60*, 1109–1119.
(19) Tung, L. H. *J. Appl. Polym. Sci.* **1969**, *13*, 775–784.
(20) Kirmse, D. W.; Westerberg, A. W. *Anal. Chem.* **1971**, *43*, 1035–1039.
(21) Rosen, E. M.; Provder, T. *Sep. Sci.* **1970**, *5*, 485–521.
(22) Jahnová, V.; Matulik, F.; Janca, J. *Anal. Chem.* **1987**, *59*, 1039–1043.
(23) Schimpf, M. E.; Williams, P. S.; Giddings, J. C. *J. Appl. Polym. Sci.* **1989**, *37*, 2059–2076.
(24) Jansson, P. A. *Deconvolution with Applications in Spectroscopy*; Academic Press: New York, 1984.
(25) Ishige, T.; Hamielec, A. E. *J. Appl. Polym. Sci.* **1971**, *15*, 1607–1622.
(26) Alba, D.; Meira, G. R. *J. Liq. Chromatogr.* **1984**, *7*, 2833–2862.
(27) Bevington, P. R. *Data Reduction and Error Analysis for the Physical Sciences*; McGraw-Hill: New York, 1969.
(28) Savitsky, A.; Golay, M. J. E. *Anal. Chem.* **1964**, *36*, 1627–1639.
(29) Steinier, J.; Termonia, Y.; Deltour, J. *Anal. Chem.* **1972**, *44*, 1906–1909.
(30) Madden, H. H. *Anal. Chem.* **1978**, *50*, 1383–1386.
(31) Schure, M. R. *Sep. Sci. Technol.* **1987**, *12*, 2403–2411.
(32) Bohren, C. F.; Huffman, D. R. *Absorption and Scattering of Light by Small Particles*; Wiley: New York, 1983; Appendix A.
(33) Bracewell, R. N. *The Fourier Transform and Its Application*; McGraw-Hill: New York, 1978.
(34) Brigham, E. O. *The Fast Fourier Transform*; Prentice-Hall: Englewood Cliffs, NJ, 1974; Chapter 9.
(35) Jones, H. K.; Barman, B. N.; Giddings, J. C. *J. Chromatogr.* **1988**, *455*, 1–15.
(36) Gajdos, L. J.; Brenner, H. *Sep. Sci. Technol.* **1978**, *13*, 215–240.
(37) Giddings, J. C.; Barman, B. N.; Li, H. *J. Colloid Interface Sci.*, in press.
(38) Bangs, L., private communication.
(39) Yau, W. W.; Kirkland, J. J. *Anal. Chem.* **1984**, *56*, 1461–1466.
(40) Giddings, J. C. *Anal. Chem.* **1986**, *58*, 735–740.
(41) Hansen, M. E.; Giddings, J. C.; Schure, M. R.; Beckett, R. *Anal. Chem.* **1988**, *60*, 1434–1442.
(42) Giddings, J. C.; Williams, P. S.; Beckett, R. *Anal. Chem.* **1987**, *59*, 28–37.
(43) Williams, P. S.; Giddings, J. C. *Anal. Chem.* **1987**, *59*, 2038–2044.

RECEIVED for review April 21, 1989. Accepted September 15, 1989. Part of this study was presented at the 190th meeting of the American Chemical Society, Chicago, IL, September 1985. This work was supported by Grant CHE-8800675 from the National Science Foundation.

Determination of Acrylonitrile in Stationary Source Emissions by Impinger Sampling and Gas Chromatography with Nitrogen–Phosphorus Detection

James N. Fulcher, Gary B. Howe,* R. K. M. Jayanty, and Max R. Peterson

Center for Environmental Measurements, Research Triangle Institute, P.O. Box 12194,
Research Triangle Park, North Carolina 27709

Jimmy C. Pau, J. E. Knoll, and M. R. Midgett

U.S. Environmental Protection Agency, Research Triangle Park, North Carolina 27711

Acrylonitrile (AN) has been identified as a suspected carcinogen and may be regulated in the future as a hazardous air pollutant under Section 112 of the Clean Air Act. A method for sampling and analysis of AN in stationary source emissions has been developed and evaluated through both laboratory and field testing. In this method, a midget impinger containing methanol followed by a back-up sorbent tube containing activated charcoal is used to trap AN vapor. Analysis is performed by capillary column gas chromatography with a nitrogen–phosphorus detector (NPD). The percentage accuracy of the method is 4.6% based on laboratory tests covering the range of 10.6–1038 ppm AN and 0–40% moisture by volume at 100 °C. The precision of the method in laboratory tests, expressed as a pooled relative standard deviation, was 3.3%. The precision of the method in field tests at two different sites was 1.9% and 2.4% (pooled relative standard deviation), respectively. The instrumental limit of detection for acrylonitrile in methanol was determined to be 0.051 ng/μL.

INTRODUCTION

The U.S. Environmental Protection Agency (USEPA), Research Triangle Park, NC, has a program to evaluate and standardize source testing methods for hazardous pollutants in anticipation of future regulations. The Research Triangle Institute (RTI) was recently contracted by the USEPA to develop and evaluate a sampling and analysis method for acrylonitrile (AN) emissions from stationary sources. A test method based on National Institute for Occupational Safety and Health (NIOSH) Method 1604 (*1*) was developed earlier by another EPA contractor (*2*). This method used charcoal tubes to adsorb the compound during sampling, followed by solvent desorption and gas chromatographic analysis with flame ionization detection (GC/FID). Hydrocarbon interference and the presence of water vapor in the source have been detrimental to the effectiveness of the method, reflected primarily in poor accuracy at low concentrations of AN. Poor accuracy and recovery at low levels of acrylonitrile on charcoal have also been documented in other work (*3*). In the present study, two modifications were investigated. The first was the use of an impinger to remove most of the water from the sample stream before it reaches the charcoal tube. The second modification was the use of a nitrogen–phosphorus detector (NPD), rather than an FID, in the analysis of the samples. The NPD was chosen for this study because it responds selectively to nitrogen- and phosphorus-containing compounds

0003-2700/89/0361-2743$01.50/0 © 1989 American Chemical Society

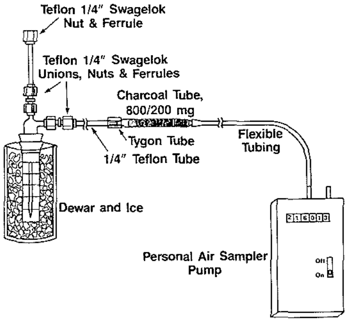

Figure 1. Acrylonitrile sampling apparatus.

(4). Generally, a very weak response is obtained with compounds that do not contain these elements. The new method was evaluated initially in the laboratory to determine the precision, accuracy, and detection limits. After the laboratory evaluation, the method was tested in the field at two different sites. The first field test was conducted at an acrylic fiber manufacturing plant (site A) where AN was used as a raw material. The second test was performed at an AN manufacturing facility (site B). Samples were collected over a two-day period at each location.

This paper describes the development of this method in both laboratory and field studies. Further details of the evaluation are contained in a project report (5).

EXPERIMENTAL SECTION

Apparatus. Test mixtures of acrylonitrile in dry or humidified nitrogen were produced for use in the present study. These mixtures were generated with a dynamic dilution system consisting of a pressurized stainless steel sphere of AN in dry nitrogen (100–3000 ppm), a heated glass mixing bulb, a heated glass sampling manifold, and mass flow control of diluent nitrogen and AN in nitrogen gas flows. When required, a three-neck flask containing organic-free water and housed in a heating mantle was used to humidify the diluent nitrogen.

The pressurized sphere of AN vapor in nitrogen was produced at RTI using a gas standard preparation system. This system consists of a six-port rotary valve fitted with a calibrated volume stainless steel loop for injecting pure AN liquid, a high-precision bourdon-tube vacuum/pressure gauge (Heise Model CMM), a vacuum pump, and a high-pressure cylinder of clean, dry nitrogen. The accuracy of this system in producing gas standards has been established previously and is described in a separate publication (6).

Sampling apparatus consisted of a 25-mL midget impinger, a coconut charcoal tube with an 800-mg front section and a 200-mg back section, and a low flow air sampling pump (SKC Model 222-3). A schematic of the acrylonitrile sampling train is shown in Figure 1. The sampling trains were connected to the sampling manifold during laboratory testing with $^1/_4$ in. o.d. Teflon tubing. During field testing a site A, $^1/_8$ in. o.d. stainless steel tubing was used as a sample probe for each sampling train. A stainless steel manifold was used at site B and sample trains were connected to the manifold with $^1/_4$ in. o.d. Teflon tubing.

Samples were analyzed with a Hewlett-Packard Model 5880A gas chromatograph equipped with a nitrogen-phosphorus detector and a split/splitless capillary injector. Laboratory samples and site A samples were injected onto a 30 m × 0.25 mm i.d. DB-WAX fused silica capillary column (0.5-μm film thickness). Site B field test samples were injected onto a 30 m × 0.55 mm i.d. DB-WAX fused silica capillary column (1.0-μm film thickness).

Procedure. Tests of the precision and accuracy of the proposed method were performed in the laboratory by using test mixtures generated with the dynamic dilution system. The mixtures ranged in acrylonitrile concentration from 10.8 to 1038 ppm and in water vapor concentration from 0 to 40% by volume at 100 °C. During a given test, concentrated acrylonitrile in dry nitrogen from a pressurized canister was metered into a spherical 1-L glass mixing bulb located in a heated enclosure. Diluent nitrogen was metered into the bulb simultaneously, and the concentration of AN in the dilution system manifold was calculated from the two flow rates and the concentration of the gas in the source canister. For some tests, water vapor was introduced to the test mixture by passing the diluent nitrogen through a heated flask containing organic-free water. The water vapor concentration was calculated from two gas flow rates and the water temperature.

During each test, three samples were collected simultaneously from the glass manifold. Each sampling train consisted of an impinger containing 25 mL of chromatographic grade methanol, a charcoal tube, and a sampling pump in series. The impingers were placed in Dewar flasks containing ice water. Prior to sampling, the dilution system was allowed to equilibrate. Following this, sampling was carried out for 1 h at a nominal rate of 50 mL/min. Flow rates were measured with a soap-film flowmeter before and after each test. After sampling, the charcoal tubes were removed and capped, and the impinger solutions were transferred to glass storage vials with several solvent rinses.

Before analysis, 5 μL of valeronitrile was added as an internal standard to each impinger solution. Charcoal tubes were desorbed with 10 mL of 2% formic acid in methanol. The desorbing solutions were also spiked with the valeronitrile internal standard. Samples were analyzed by gas chromatography with nitrogen–phosphorus detection. Helium carrier gas was supplied at a flow rate of 1.3 mL/min (measured at 60 °C column temperature). Detector hydrogen and air were supplied at 6.5 and 85 mL/min, respectively. A helium flow of 30 mL/min was used for carrier make-up gas. The detector temperature was 240 °C and the injector temperature was 250 °C. Injections of 1-μL sample aliquots were performed with a split ratio of 60:1. The column temperature program was 60 °C for 3 minutes, 5 °C/min to 100 °C, 100 °C for 1 min. Detector linearity was evaluated for acrylonitrile over a range of concentrations (10–3840 ppm) and was found to be excellent (log area vs log concentration yielded a slope of 1.006 and a correlation coefficient of 0.99992).

The instrumental limit of detection (LOD) was determined by using the single sample method (7). A solution of AN at a concentration of approximately twice the estimated limit of quantitation (obtained from literature values) was analyzed nine consecutive times. The standard deviation of the detector response was then multiplied by 3 to obtain the response at the LOD. The LOD was calculated by applying the detector calibration factor to this response.

The procedure for sample collection and analysis during field testing was similar to that of the laboratory evaluation. Six sampling runs were performed on each of two days at site A with four samples collected in parallel during each run. Source gas containing acrylonitrile vapor was introduced into each sample train through a $^1/_8$ in. o.d. stainless steel probe inserted through the wall of an exhaust vent on the plant roof. After sampling, impinger solutions and charcoal tubes were stored on ice during return to the laboratory for analysis. Each impinger sample was analyzed as described previously and one charcoal tube was selected at random from each run for analysis.

At site B, source gas effluent from a wet scrubber was pumped to a stainless steel sampling manifold to which four sampling trains were connected. Seven sampling runs were performed on the first day and six on the second day. Sample analysis procedures were identical with those used for Site A field samples except that a wide-bore capillary column was used to increase injection volume capacity and allow measurement of the lower concentrations. Chromatographic conditions were the same as those used with the narrow bore column except for a helium carrier gas flow rate of 5.6 mL/min and the use of a split/splitless injection technique. The splitless period was 1.2 s and the injector liner was purged during the split mode with 120 mL/min of helium.

RESULTS AND DISCUSSION

Accuracy and Precision Tests. The results of laboratory tests to determine the accuracy and precision of the proposed method are shown in Table I. The measured acrylonitrile concentrations are based on calculations from the impinger

Table I. Accuracy and Precision Test Results

run no.	H_2O vapor concn, %	true AN concn, ppm	measured AN concn, ppm imp A	imp B	imp C	% accuracy	% RSD
1	0	10.8	9.72	9.72	9.94	−9.3	1.3
2	0	1000	980	980	990	−1.7	0.6
3	30	10.7	9.95	10.0	10.2	−6.1	1.3
4	20	10.6	10.1	10.2	10.3	−3.8	1.0
5	30	10.7	9.63	9.63	9.74	−9.7	0.7
6	33	10.9	10.4	11.6	10.9	0.6	5.5
7	32	107	107	125	108	5.9	8.9
8	32	101	104	103	106	3.3	1.5
9	32	98.6	104	102	104	4.8	1.1
10	40	513	508	503	503	−1.6	0.6
11	32	1038	996	986	1007	−4.0	1.0

Table II. Site A Field Test Results

run no.	AN Source Concn, ppm imp A	imp B	imp C	imp D	mean	std dev	% RSD
1	105	112	111	107	109	3.3	3.04
2	108	108	112	108	109	2.0	1.83
3	109	109	111	109	110	1.0	0.91
4	109		111	109	110	1.5	1.39
5	111	109	111	110	110	1.0	0.87
6	110	113	114	110	112	2.1	1.84
7	84.0	82.8	85.7	82.5	83.8	1.4	1.73
8	83.8	85.1	87.4	86.9	85.8	1.7	1.93
9	83.2	83.5	85.4	81.7	83.4	1.5	1.82
10	84.3	80.2	85.1	84.4	83.5	2.2	2.67
11	74.9	73.8	76.8	74.1	74.9	1.3	1.80
12	102	102	104	101	102	1.3	1.23

Table III. Site B Field Test Results

run no.	AN source concn, ppm imp A	imp B	imp C	imp D	mean	std dev	% RSD
1	23.2	22.5	23.5	23.3	23.1	0.46	2.0
2[a]	15.7	17.5		20.6			
3[a]	26.3	19.3	25.9	25.7			
4	28.3	27.0	28.2	27.8	27.8	0.58	2.1
5	28.0	26.5	26.0	26.7	26.8	0.86	3.2
6	27.4	26.3	26.9	27.2	27.0	0.46	1.7
7	33.6	30.6	32.7	33.6	32.6	1.40	4.3
8	32.9	31.5	32.9	32.3	32.4	0.65	2.0
9	38.2	38.1	38.6	38.5	38.4	0.27	0.7
10	43.5	44.9	41.5	41.3	42.8	1.74	4.1
11	42.4	41.0	42.4	41.4	41.8	0.71	1.7
12	44.1	43.4	43.6	43.4	43.6	0.30	0.7
13	46.6	46.0	46.6	46.0	46.3	0.32	0.7

[a] Results discarded due to problems with sampling manifold flow during sample collection.

solution analysis and sample gas volume collected. Analysis of the desorbed charcoal tube samples showed insignificant (less than 1%) breakthrough of the impingers. The percentage accuracy of the mean concentration is shown for each run. The overall average percentage accuracy is 4.6%.

The relative standard deviation of the triplicate samples ranged from 0.6 to 8.9%. The overall method precision, expressed as the pooled relative standard deviation, is 3.3%.

To test the effect of moisture on precision and accuracy, logarithmic transformations were carried out, and means, standard deviations, and deviations from the prepared values were calculated. Linear regression of the standard deviations on the means showed that the standard deviations were not level dependent (calculated t statistic, 0.32; critical value, 2.62). Linear regression of the deviations from the prepared values on the H_2O concentrations failed to show any correlation (calculated t statistic, 1.27; critical value, 2.62). Application of the Bartlett test (*8*) to the standard deviations showed that the variances were not homogeneous (calculated χ^2 statistic, 3.09; critical value, 16.9). The pooled standard deviation calculated from the remaining data was 0.0086, which corresponds to a coefficient of variation of 0.9%. The lack of correlation of the deviations with moisture content and the constancy of the variances are indications that moisture did not affect the measurements significantly.

A test of the mean of the transformed deviations yielded a t-statistic value of 7.49, which when compared with the critical value, 2.20, indicated that the mean was significant at the 95% confidence level. It corresponded to a negative bias of 2.2%.

Limit of Detection. The average concentration of acrylonitrile determined for a low concentration solution of acrylonitrile in methanol based on nine injections was 0.459 ng/μL with a standard deviation of 0.017 ng/μL. The limit of detection is then 0.051 ng/μL which is equivalent to 0.192 ppm in air for a 3-L air sample with AN collected in 25 mL of methanol.

Site A Field Test. The results of analyzing impinger samples from site A are shown in Table II. Excellent method precision was achieved with the highest relative standard deviation of 3.04% occurring in run no. 1. Linear regression of the standard deviations versus the means showed that the values were not level dependent. Application of the Bartlett test showed that the standard deviations were homogeneous; therefore, it was possible to calculate a pooled standard deviation that was more representative of the data than the standard deviation of any single run (*6*). This value was 1.8 ppm (1.9% relative standard deviation).

Concentrations determined from analysis of one charcoal tube from each sampling run were 1% or less of the total concentration measured. This agrees well with the results obtained in the laboratory evaluation.

Site B Field Test. Results of the analysis of impinger samples from site B are shown in Table III. Excellent precision was again achieved with the highest percent relative standard deviation at 4.3% for run no. 7. Application of the statistical methods cited above showed that the standard deviations in Table III were also homogenous; the pooled standard deviation was 0.84 ppm (2.4% relative standard deviation).

Concentrations determined from analyzing charcoal tubes from selected runs were again less than 1% of the total concentration.

Stability Study. A study of acrylonitrile stability in methanol was performed by preparing and analyzing four solutions containing AN at levels near that observed in the site A field test samples. Two of the solutions contained 36 ppm of 4-methoxyphenol as an inhibitor to AN polymerization. Each solution was analyzed immediately after preparation, after 2 days, and then after 2 weeks. The study results are shown in Table IV. The data indicate that AN in

Table IV. Acrylonitrile in Methanol Stability Study Results

solvent	measured acrylonitrile concn, ng/μL		
	initial	2 days	2 weeks
methanol	33.7	34.1	34.7
methanol	33.4	34.6	34.5
methanol with inhibitor	33.9	34.4	33.8
methanol with inhibitor	34.3	34.4	34.9

methanol at about 35 ng/μL, either with or without inhibitor, is stable for at least two weeks.

CONCLUSIONS

A simple, inexpensive, and accurate method for the determination of AN emission from stationary sources has been developed. The method has demonstrated a high level of precision that appears to be unaffected by moisture levels as high as 40% by volume at 100 °C and is applicable over a wide range of AN concentrations (10-1000 ppm). Acrylonitrile in methanol either with or without inhibitor was found to be stable for at least two weeks.

There are two major advantages of this new method. First, acrylonitrile is trapped in methanol contained in an impinger instead of a charcoal tube, avoiding the problems with poor trapping efficiency and low analytical recovery of acrylonitrile sampled with charcoal. The backup charcoal tube specified in this new method is used only as an indicator of impinger breakthrough and could possibly be omitted or substituted with another impinger. Second, the specificity of the NPD avoids the problem of hydrocarbon interference with detection by FID.

LITERATURE CITED

(1) Acrylonitrile, Method 1604 (2/15/84). In *NIOSH Manual of Analytical Methods*, 3rd ed.; Eller, P. M., Ed.; Vol. 1. DHHS (NIOSH) Publ. 84-100; U.S. Department of Health and Human Services: Washington, DC, 1984.
(2) Bernstiel, T. J.; Daly, M. D.; Nunn, A. B., III; Reckner, L. R. Evaluation of Charcoal Tube Adsorption for Measurement of Acrylonitrile Emissions from Stationary Sources. USEPA Contract No. 68-02-3405. Scott Environmental Technology, Inc.
(3) Gagnon, Y.; Posner, J. Recovery of Acrylonitrile from Charcoal Tubes at Low Levels. *Am. Ind. Hyg. Assoc. J.* **1979**, *40*, 923–925.
(4) Cooper, S. W.; Jayanty, R. K. M.; Knoll, J. E.; Midgett, M. R. Determination of Selected Nitrogen-Containing Hazardous Pollutants in Complex Matrices by Gas Chromatography with a Nitrogen-Phosphorous Detector. *J. Chromatogr. Sci.* **1986**, *24*, 204–209.
(5) Fulcher, J. N.; Howe, G. B.; Jayanty, R. K. M.; Peterson, M. R. Development and Validation of a Test Method for Acrylonitrile Emissions. US EPA Contract Nos. 68-02-4125 and 68-02-4442. Research Triangle Institute.
(6) Howe, G. B.; Albritton, J. R.; Tompkins, S. B.; Jayanty, R. K. M.; Decker, C. E. Stability of Parts-Per-Million Organic Cylinder Gases and Results of Source Test Audits. USEPA Contract No. 68-02-4550. Research Triangle Institute.
(7) *Quality Assurance of Chemical Measurements*, 2nd printing; Taylor, J. K., Ed.; Lewis Publishers, Inc.: Chelsea, MI, 1987; p 81.
(8) Duncan, A. J. *Quality Control and Industrial Statistics*, 3rd ed.; Richard D. Irwin, Inc.: Homewood, IL, 1965; p 642.

RECEIVED for review June 30, 1989. Accepted September 29, 1989. Although the research described in this article has been funded wholly or in part by the United States Environmental Protection Agency through Contract nos. 68-02-4125 and 68-02-4442 to Research Triangle Institute, it has not been subjected to Agency review and therefore does not necessarily reflect the views of the Agency and no official endorsement should be inferred.

Anal. Chem. **1989,** *61,* 2747–2750

Separation of Cations by Open-Tubular Column Liquid Chromatography

Stephan R. Müller and Wilhelm Simon*

Department of Organic Chemistry, Swiss Federal Institute of Technology (ETH), CH-8092 Zürich, Switzerland

H. Michael Widmer and Karl Grolimund

Central Function Research, Ciba-Geigy AG, CH-4002 Basel, Switzerland

Gerhard Schomburg and Peter Kolla

Chromatography Department, Max-Planck-Institut für Kohlenforschung, D-4300 Mülheim-Ruhr, FRG

The band broadening in open-tubular column liquid chromatography with capillaries of 9.5, 5.4, and 4.6 μm inner diameter coated with poly(butadienesulfonic acid) or poly(butadiene–maleic acid) is measured and compared with results from the Golay equation. For a capillary column of 9.5 μm i.d./0.58 m length, coated with the strong cation exchanger, 210 000 and 47 100 theoretical plates for $k' = 0$ and $k' = 1.65$, respectively, at the optimal flow rates were obtained. These values correspond to about 99% and 67%, respectively, of the theoretical ones. For the capillary column of 4.6 μm i.d./0.90 m length, coated with the weak cation exchanger, 680 000 and 246 000 theoretical plates for $k' = 0$ and $k' = 0.16$, respectively, were obtained at the optimal flow rates. These values correspond to about 100% and 89%, respectively, of the theoretical ones. For both capillary columns about 91–100% of the theoretical plate numbers were obtained at higher flow rates ($3 \cdot \nu_{\mathrm{opt}}$). Separations of alkali-metal/ammonium ions within 6 min and of the alkali-metal ions within 3 min with detected quantities in the 10^{-15} mol range (9.5 μm i.d. capillary), as well as of ammonium, alkali, and alkaline-earth metal ions in 4 min (4.6 μm i.d. capillary) with quantities of 0.2 to 20 × 10^{-15} mol were achieved.

INTRODUCTION

To realize acceptable analysis times in high-resolution open-tubular column liquid chromatography, column diameters ≤10 μm have to be used (*1–3*). For such separation systems, both the injection and detection processes frequently are limiting factors to the resolution power of the chromatographic system (*4*). On-column electrochemical detectors are of special interest to obtain small detection volumes and fast response (*5–13*). Utilizing a pressure pulse-driven stopped-flow injection system (*8*) and an on-column potentiometric detector (*7*), 10^6 theoretical plates were obtained for nonretained components in 220 s with a column of 1.30 m length and 3.5 μm inner diameter (i.d.) (*7*). This corresponds to a loss of 25% in the theoretically possible number of theoretical plates (*7*). There are very few reports quantitating the loss of resolution in realistic liquid chromatographic separations in open-tubular columns of a diameter ≤10 μm (*13–21*). Here we report on the chromatographic resolution observed in the separation of cations utilizing capillaries of 9.5, 5.4, and 4.6 μm i.d. taking theoretically care of the diffusion of components in the stationary phase (*14–16*).

EXPERIMENTAL SECTION

Chromatographic System. The chromatographic system used has been described previously (*5–8*). It consists of the components shown in Figure 1: A constant flow high precision pump, Model P-500 (≤40 bar, Pharmacia Fine Chemicals AG, Uppsala, Sweden), for the pressure pulse and rinsing procedure, a helium cylinder (≤200 bar, PanGas, Zürich, Switzerland) and a high-pressure autoclave equipped with a Teflon liner (≤200 bar, 0.75 L, Berghof GmbH, Eningen, FRG) for the elution process, a titanium tube (1 m, Pharmacia Fine Chemicals AG, Uppsala, Sweden) and three VICI switching valves, Model C6W, with electric actuators (switching time <200 ms, Valco Instruments Co., Inc., Houston, TX) as a stopped-flow injection system (*8*) now controlled by a TTLout Apple II+ (Apple Computer, Inc., Cupertino, CA) system, and a piezoresistant pressure gauge (Model EDR 212, Haenni Messgeräte, Jegensdorf, Switzerland).

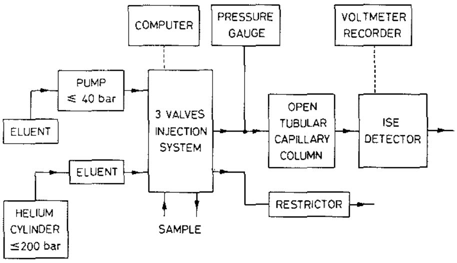

Figure 1. Schematic diagram of the open-tubular column liquid chromatograph.

Detector. The detector cell and the position control system for the microelectrode and the fused silica capillary columns used were described previously (*6*). To reduce the noise, a reference electrode of the free-flowing free-diffusion liquid-junction type was used (*22*). The cell assembly was the following:

$$\underbrace{\mathrm{Hg};\ \mathrm{Hg_2Cl_2},\ \mathrm{KCl(satd.)}|3\ \mathrm{M\ KCl}}_{\text{reference electrode}}|\text{mobile phase}|$$

$$\text{mobile phase, sample components}\ \underbrace{|\text{membrane}|3\ \mathrm{M\ KCl,\ AgCl;\ Ag}}_{\text{ion-selective microelectrode}}$$

The membrane contained 3% (w/w) potassium tetrakis(4-chlorophenyl)borate in 2,3-dimethylnitrobenzene (both Fluka Chemie AG, Buchs, Switzerland). The potential difference between the ion-selective microelectrode and reference electrode was measured as described earlier (*23*) and recorded (Kontron, W+W Recorder Model 314). The peak widths and the retention times were measured manually from the chromatograms.

Capillaries. The inner diameters of the fused silica capillary columns of nominally 10 (one batch) and 5 μm i.d. (two batches; Polymicro Technologies, Phoenix, AZ) were measured by the method described by Guthrie et al. (*24*). The results were 9.5, 5.4, and 4.6 μm i.d., respectively.

Stationary Phases, Prepolymers. As stationary phases two prepolymers were used: The strong cation exchanger poly(bu-

0003-2700/89/0361-2747$01.50/0 © 1989 American Chemical Society

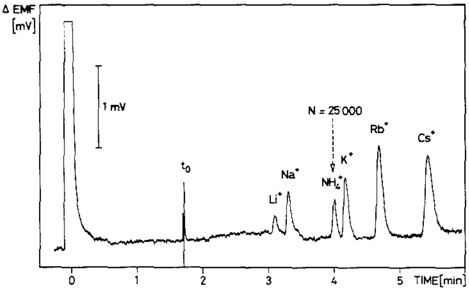

Figure 2. Separation of 75 pL of alkali metal/ammonium ions (15–500 μmol L^{-1}) in a 9.5 μm i.d. open-tubular column (0.58 m) coated with a strong cation exchanger (poly(butadienesulfonic acid); $d_f \approx 0.1$ μm), 1.4 mM formic acid (43 nL min^{-1}) as a mobile phase, and an ion-selective microelectrode as detector.

tadienesulfonic acid) was synthesized at the Max-Planck-Institut für Kohlenforschung, Mülheim-Ruhr, FRG (*25, 26*). The weak cation exchanger poly(butadiene–maleic acid) (Polysciences, Inc., Warrington, PA, 42% solids in water) was first diluted with water (1:3) and then refluxed during 3 h. The water was then evaporated under vacuum and the rest was dried during 15 h at room temperature and 1.3×10^{-5} bar. With this method a complete hydrolysis of possibly existing poly(butadiene–maleic anhydride) is obtained. This procedure was necessary because the poly(butadiene–maleic acid) is produced from the anhydride. Both prepolymers can easily be cross linked with a radical starter and have also been used to coat silica gel for cation exchange chromatography (*25–27*).

Coating of the Open-Tubular Capillary Columns. A static coating procedure was used. All fused silica capillary columns were first rinsed with HF/HNO_3 (2.26% (v/v)/2.15% (v/v)) and then with 1% (w/v) HCl for 10 min each. The obtained hydroxylated surface offers good adhesion for the relatively polar prepolymers and leads to homogeneous films. Subsequently the capillary columns were washed with distilled water and methanol and were finally filled with a solution of the prepolymer and 5% (w/w) (relative to the prepolymer) dicumyl peroxide (Peroxid-Chemie GmbH, Hoellriegelskreuth, FRG) in methanol. The prepolymer concentrations were as follows: 4% (w/v) of poly(butadienesulfonic acid) for the 9.5 μm i.d. capillary column, 7.5% (w/v) and 8.5% (w/v) of poly(butadiene–maleic acid) for the 5.4 and 4.6 μm i.d. capillary columns, respectively. One end of each of the filled capillary columns is dipped into Woods Metall (Fluka Chemie AG, Buchs, Switzerland) at 80 °C, then cooled so that the capillary columns were sealed. Later the capillary columns were put into a desiccator, which is evacuated to 1.3×10^{-5} bar. Six weeks later they were removed from the desiccator and the prepolymer is cross linked in a gas chromatograph with a slow flow of helium (3 bar) during 2 h at 160 °C. This way a calculated (assumed density of the prepolymer, 1 g/mL) film thickness of 0.1 μm was obtained.

Chemicals. The chromatograms were obtained by using formic acid, tartaric acid, or tartaric acid and 2,6-pyridinedicarboxylic acid (Fluka AG, Buchs, Switzerland) and doubly quartz distilled water as mobile phase. To regenerate the 9.5 μm i.d. capillary column, 0.1 M hydrochloric acid (E. Merck, Darmstadt, FRG) was used. The ammonium, alkali, and alkaline-earth metal chlorides, amino acids, nucleosides/bases, and neurotransmitters were from E. Merck, Darmstadt, FRG, or Fluka AG, Buchs, Switzerland.

RESULTS AND DISCUSSION

The previously described strong cation exchanger poly(butadienesulfonic acid) (*25, 26*) was used to successfully coat (*28*) fused silica columns of 9.5 μm bore and 0.58 m length. Figure 2 shows a separation of alkali metal/ammonium ions. For NH_4^+, 25000 theoretical plates at a capacity ratio k' of 1.4 are obtained. Depending on the history of the column (loading of the cation exchanger with alkaline-earth metal cations), variable k' values may be obtained for the same cation under apparently identical experimental conditions.

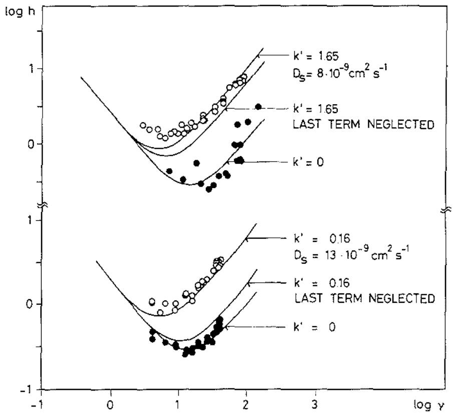

Figure 3. Reduced plate height as a function of the reduced linear velocity. (Top) For a sample of 75 pL of water (●, $k' = 0$) and ammonium chloride (O, $k' = 1.65$; 30 μmol L^{-1}) in a 9.5 μm i.d. open-tubular column (0.58 m) coated with a strong cation exchanger (poly(butadienesulfonic acid); $d_f \approx 0.1$ μm), 1.4 mM formic acid as a mobile phase and an ion-selective microelectrode as detector. (Bottom) For a sample of 10 pL water (●, $k' = 0$) and potassium chloride (O, $k' = 0.16$; 25 μmol L^{-1}) in a 4.6 μm i.d. open-tubular column (0.90 m) coated with a weak cation exchanger (poly(butadiene–maleic acid); $d_f \approx 0.1$ μm), 2.0 mM tartaric acid as a mobile phase, and an ion-selective microelectrode as detector.

In Figure 3 (top) the reduced plate height h as a function of the reduced linear velocity ν is given for a nonretained ($k' = 0$, water) and a retained ($k' = 1.65$, NH_4^+) component for the 9.5 μm i.d. column. The plate heights for a nonretained component were obtained by injecting a sample of water. In contrast to the signal at $t = 0$ in Figure 2 this water injection leads to a fully symmetrical elution profile. The curves in Figure 3 were calculated by using the Golay equation (*29*)

$$h = \frac{2}{\nu} + \frac{1 + 6k' + 11k'^2}{96(1 + k')^2}\nu + \frac{2k'}{3(1 + k')^2}\left(\frac{d_f}{d_c}\right)^2\frac{D_m}{D_s}\nu$$

where d_c is open-tubular column inner diameter, d_f is the film thickness of stationary phase, D_m (NH_4^+, 1.6×10^{-5} cm^2 s^{-1} (*30*)) and D_s are the mean diffusion coefficients of the components in the mobile and stationary phase, respectively. To obtain the diffusion coefficients in the stationary phase, D_s was computed from the Golay equation for each pair of experimentally determined values h and ν, utilizing the known parameters k', d_c, d_f, and D_m. Numbers thus obtained for D_s were between (2 and 16) $\times 10^{-9}$ cm^2 s^{-1} so that a mean of 8×10^{-9} cm^2 s^{-1} was used. Since D_s was therefore adjusted to 8×10^{-9} cm^2 s^{-1} to calculate the top curve in Figure 3, the correlation between experimental and predicted data may look trivial. The diffusion coefficient is however the only parameter adjusted to a set of 29 experimental values and the resulting diffusion coefficient is realistic. It is in the same range as for plasticized PVC membranes with 0.4 wt % PVC (*31*) and other reported diffusion coefficients for stationary phases (immobilized silicon rubber) in open-tubular columns (*16*). The data in the table and Figure 3 suggest that there are no major extracolumn contributions to signal broadening at least at high flow rates. The volumes of the sample injected were 75 and 10 pL for the columns of 9.5 and 4.6 μm i.d., respectively. These values correspond to approximately half and one-third of the values that can be tolerated according to the calculation presented by Knox and Gilbert (*1*) (see also ref 8). For re-

Table I. Parameters for Two Open-Tubular Columns with a d_f of 0.1 μm and a D_m of 1.6 × 10^{-5} cm² s⁻¹ (*30*)

operation conditions/parameters		number of theoretical plates		
		Golay eq	expt	% of theory
L = 0.58 m; 9.5 μm i.d.; D_s = 8 × 10^{-9} cm² s⁻¹				
k' = 0	ν_{opt} = 13.86	211 500	210 000	~99
	ν = 87.83	65 100	61 000	~94
k' = 1.65	ν_{opt} = 4.58	69 900	47 100	~67
	ν = 33.28	18 900	19 000	~100
L = 0.90 m; 4.6 μm i.d.; D_s = 13 × 10^{-9} cm² s⁻¹				
k' = 0	ν_{opt} = 13.86	678 000	680 000	~100
	ν = 40.82	413 000	376 000	~91
k' = 0.16	ν_{opt} = 5.61	275 000	246 000	~89
	ν = 40.82	74 100	72 700	~98

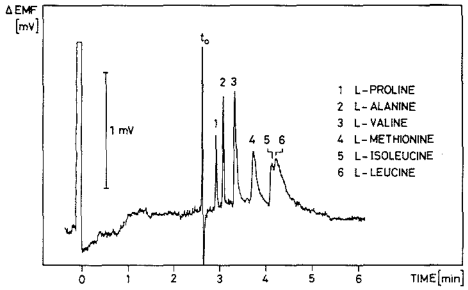

Figure 4. Separation of 75 pL of amino acids (20–110 μmol L⁻¹) in a 9.5 μm i.d. open-tubular column (0.58 m) coated with a strong cation exchanger (poly(butadienesulfonic acid): $d_f \approx$ 0.1 μm), 0.6 mM formic acid (15.4 nL min⁻¹) as a mobile phase, and an ion-selective microelectrode as detector.

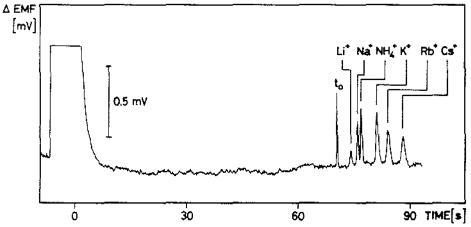

Figure 5. Separation of 15 pL of alkali metal/ammonium ions (12–1300 μmol L⁻¹) in a 4.6 μm i.d. open-tubular column (0.90 m) coated with a weak cation exchanger (poly(butadiene-maleic acid), $d_f \approx$ 0.1 μm), 2.0 mM tartaric acid (12.7 nL min⁻¹) as a mobile phase, and an ion-selective microelectrode as detector.

tained components (k' = 1.65, NH_4^+) and the optimal flow rate (ν = 4.58) a loss of 33% in the number of theoretical plates is obtained. At higher flow rates (ν = 33.28, k' = 1.65) 100% of the possible number of theoretical plates were obtained.

As discussed in detail earlier, neither the sample injection (*8*) nor the detection (*7*) or the positioning error of the detector at the exit end of the open tubular column (*6*) contribute by more than about 15% to the loss in the number of theoretical plates for the experimental parameters used here. We have no convincing explanation for the better adherence to the theoretical efficiency at higher mobile phase flow rates shown in Figure 3 (top) and Table I.

Since the signals in Figure 2 are rather symmetrical, it does not indicate an overloading of the column. Assuming an injected sample volume of 75 pL, which can be calculated from the product of pressure and time (*8*), the elution profile for Cs^+ corresponds to about 10^{-15} mol.

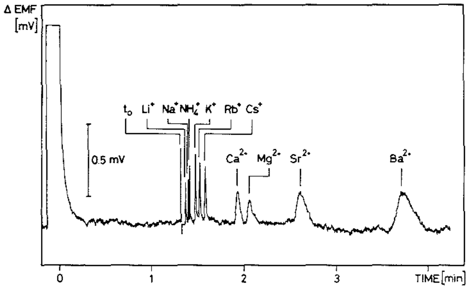

Figure 6. Separation of 15 pL of alkali, ammonium, and alkaline-earth metal ions (12–1300 μmol L⁻¹) in a 4.6 μm i.d. open-tubular column (0.90 m) coated with a weak cation exchanger (poly(butadiene–maleic acid), $d_f \approx$ 0.1 μm), 2.0 mM tartaric acid, 0.4 mM 2,6-pyridinedicarboxylic acid (11.4 nL min⁻¹) as a mobile phase, and an ion-selective microelectrode as detector.

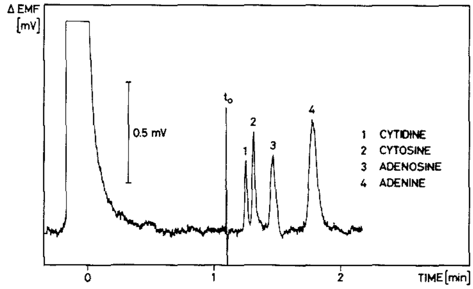

Figure 7. Separation of 15 pL of nucleosides/bases (70–300 μmol L⁻¹ in 5 mM HCl) in a 4.6 μm i.d. open-tubular column (0.90 m) coated with a weak cation exchanger (poly(butadiene–maleic acid), $d_f \approx$ 0.1 μm), 2.0 mM tartaric acid (13.4 nL min⁻¹) as a mobile phase, and an ion-selective microelectrode as detector.

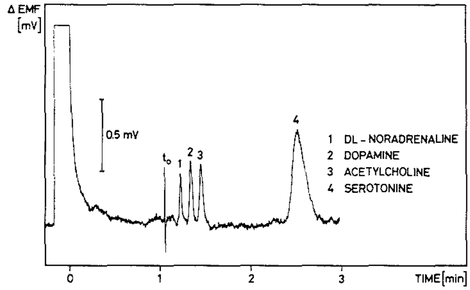

Figure 8. Separation of 10 pL of neurotransmitters (240–1370 μmol L⁻¹ in 5 mM HCl) in a 4.6 μm i.d. open-tubular column (0.90 m) coated with a weak cation exchanger (poly(butadiene–maleic acid), $d_f \approx$ 0.1 μm), 2.0 mM tartaric acid (13.4 nL min⁻¹) as a mobile phase, and an ion-selective microelectrode as detector.

Figure 4 shows further cation separations. Six different amino acids can be separated within 4.3 min by the same capillary column and detected with an ion-selective microelectrode. The amounts detected are in the range of (1.5–8.3) × 10^{-15} mol.

The commercially available prepolymer poly(butadiene–maleic acid) was used to coat two different fused silica capillary columns (5.4 μm i.d., 0.62 m length; 4.6 μm i.d., 0.90 m length) with a weak cation exchanger. With the 5.4 μm i.d. column a separation of ammonium, alkali, and alkaline-earth metal ions in 7 min was obtained. In Figures 5–8 different rather fast separations of cations with the 4.6 μm i.d. capillary column are presented. The amounts of eluted sample were in the range of (0.2–20) × 10^{-15} mol.

Figure 5 and 6 corroborate the fastest so far reported separations of ammonium, alkali, and alkaline-earth metal ions. Because of the complexation by 2,6-pyridinedicarboxylic acid, an addition of this complexation agent changes the sequence of elution of alkaline-earth metal cations (see also ref 32). In comparison with commercially available systems (Dionex Corp., Sunnyvale, CA, IonPac Fast Cation I and IonPac Fast Cation II (*33*)) ours is 6 times faster (Figure 6).

Figure 3 (bottom) gives a comparison of experimentally obtained plate heights with those calculated by the Golay equation for the 4.6 μm i.d. column. The calculated diffusion coefficents of components in the stationary phase are between (5 and 25) × 10^{-9} cm^2 s^{-1} for ammonium and alkali-metal ions. The curve representing the reduced plate height as a function of the reduced linear velocity (Figure 3 (bottom): potassium ion; $D_m = 1.6 \times 10^{-5}$ cm^2 s^{-1} (*30*); $D_s = 13 \times 10^{-9}$ cm^2 s^{-1} (mean), only parameter adjusted to a set of 24 experimental data) is in good agreement with the prediction by the Golay equation. A loss of 11% only in the number of theoretical plates is obtained at the optimal flow rate ($k' = 0.16$, $\nu = 5.61$, Table I). There are no obvious extracolumn contributions to signal broadening (see Table I ($k' = 0$) and Figure 3).

In a comparison of experimentally obtained numbers of theoretical plates with those calculated by the Golay equation, van Berkel et al. (*16*) (capillary column: 5 μm i.d., 1 m length, $d_f = 0.028$ μm (PS-255)) and Folestad et al. (*14*) (capillary column: 11.7 μm i.d., 1.97 m length, $d_f = 0.15$ μm (PS-255)) also reported a loss in theoretical plates of 20% and 7% for 9-methylanthracene ($k' = 0.8$; $D_s = (0.5\text{–}2.7) \times 10^{-9}$ cm^2 s^{-1}) and 9-cyanoanthracene ($k' = 0.16$; $D_s = (0.01\text{–}0.22) \times 10^{-9}$ cm^2 s^{-1}), respectively.

In contrast Dluzneski (*19*) reports a chromatogram for which we calculate a loss of 90.5% and 93.9% in the number of theoretical plates for riboflavin ($k' = 0$, $N = 82\,000$) and perylene ($k' = 0.47$, $N = 43\,000$), respectively, in an open-tubular capillary column of 1.7 μm i.d. (0.65 m length) neglecting the third term in the Golay equation.

The 9.5 and 4.6 μm i.d. capillary columns have been in operation for 10 and 5 months, respectively, and both are still performing well.

LITERATURE CITED

(1) Knox, J. H.; Gilbert, M. T. *J. Chromatogr.* **1979**, *186*, 405.
(2) Knox, J. H. *J. Chromatogr. Sci.* **1980**, *18*, 453.
(3) Yang, F. J. *J. Chromatogr. Sci.* **1982**, *20*, 241.
(4) Novotny, M. V. *J. Chromatogr. Libr.* **1985**, *30*, 19.
(5) Manz, A.; Simon, W. *Chromatogr. Sci.* **1983**, *21*, 326.
(6) Manz, A.; Simon, W. *Mikrochim. Acta* **1986**, *I*, 147.
(7) Manz, A.; Simon, W. *Anal. Chem.* **1987**, *59*, 74.
(8) Manz, A.; Simon, W. *J. Chromatogr.* **1987**, *387*, 187.
(9) Knecht, L. A.; Guthrie, E. J.; Jorgenson, J. W. *Anal. Chem.* **1984**, *56*, 479.
(10) Novotny, M. V. *Anal. Chem.* **1988**, *60*, 500A.
(11) White, J. G.; St. Claire, R. L., III; Jorgenson, J. W. *Anal. Chem.* **1986**, *58*, 293.
(12) White, J. G.; Jorgenson, J. W. *Anal. Chem.* **1986**, *58*, 2992.
(13) St. Claire, R. L., III; Jorgenson, J. W. *J. Chromatogr. Sci.* **1985**, *23*, 186.
(14) Folestad, S.; Josefsson, B.; Larsson, M. *J. Chromatogr.* **1987**, *391*, 347.
(15) Folestad, S.; Larsson, M. *J. Chromatogr.* **1987**, *394*, 455.
(16) Berkel van O.; Poppe H.; Kraak, J. C. *Chromatographia* **1987**, *24*, 739.
(17) Poppe, H.; Kraak, J. C.; van Berkel-Geldof, O.; Tock, P. P. H. *Proc. Int. Symp. Capillary Chromatogr., 9th* **1988**, 345.
(18) van Berkel-Geldof, O.; Kraak, J. C.; Poppe, H. *Proc. Int. Symp. Capillary Chromatogr., 9th* **1988**, 427.
(19) Dluzneski, P. R. Column Fabrication and Luminescence Detection in Open-Tubular Liquid Chromatography. Dissertation, The University of North Carolina at Chapel Hill, 1987; p 101.
(20) Dluzneski, P. R.; Jorgenson, J. W. *J. High Resolut. Chromatogr. Chromatogr. Commun.* **1988**, *11*, 332.
(21) Tock, P. P. H.; Stegeman, G.; Peerboom, R.; Poppe, H.; Kraak, J. C.; Unger, K. K. *Chromatographia* **1987**, *24*, 617.
(22) Dohner, R. E.; Wegmann, D.; Morf, W. E.; Simon, W. *Anal. Chem.* **1986**, *58*, 2585.
(23) Lanter, F.; Erne, D.; Ammann, D.; Simon, W. *Anal. Chem.* **1980**, *52*, 2400.
(24) Guthrie, E. J.; Jorgenson, J. W.; Knecht,. L. A.; Bush, S. G. *J. High Resolut. Chromatogr. Chromatogr. Commun.* **1983**, *6*, 566.
(25) Kolla, P.; Köhler, J.; Schomburg, G. Paper presented at the 9th Königsteiner Chromatographie-Tage, Bad Soden, October 1987, p 87.
(26) Kolla, P. Polymerbeschichtetes Kieselgel als stationäre Phase für die HPLC mit Kationenaustauscheigenschaften. Dissertation, Universität des Saarlandes, FRG, 1988.
(27) Kolla, P.; Köhler, J.; Schomburg, G. *Chromatographia* **1987**, *23*, 465.
(28) Schomburg, G.; Kolla, P.; Roeder, W.; Ruffing, F.-J.; Müller, St. R.; Simon, W. *Proc. Int. Symp. Capillary Chromatogr., 9th* **1988**, 373.
(29) Golay, M. J. E. In *Gas Chromatography*; Desty, D. H., Ed.; Butterworths: London, 1958; p 36.
(30) *Électrochimie*; Milazzo G., Ed.; Dunod: Paris, 1969; p 370.
(31) Oesch, U.; Simon, W. *Anal. Chem.* **1980**, *52*, 692.
(32) Kondratjonok, B.; Schwedt, G. *Fresenius' Z. Anal. Chem.* **1988**, *332*, 333.
(33) *IonPac Columns, The Polymeric Advantage*; Dionex Corp.: Sunnyvale, CA, 1988; p 13.

RECEIVED for review June 26, 1989. Accepted September 12, 1989.

Anal. Chem. 1989, 61, 2751-2756

Determination of Regulatory Organic Compounds in Radioactive Waste Samples. Volatile Organics in Aqueous Liquids

Bruce A. Tomkins,* John E. Caton, Jr., Marsha D. Edwards, Manuel E. Garcia,[1] Robert L. Schenley, Lise J. Wachter, and Wayne H. Griest

Organic Chemistry Section, Analytical Chemistry Division, Oak Ridge National Laboratory, Oak Ridge, Tennessee 37831-6120

Regulatory target volatile organic compounds may be identified and quantitated in radioactive aqueous samples containing mixed fission products by using a modified version of the Environmental Protection Agency (EPA) purge-and-trap procedure for nonradioactive samples. The volatile organic species are sparged in a glovebox (radioactive zone) and collected on a three-stage sorption trap (nonradioactive zone). Because the trap is not contaminated in this procedure, it may be taken to a nonradioactive analytical laboratory and analyzed by gas chromatography/mass spectrometry. Recoveries of three surrogate and five matrix spike standards are comparable to those achieved for nonradioactive aqueous samples using the conventional EPA method. The concentrations of 10 frequently occurring volatile species are presented for aqueous samples drawn from six nuclear waste storage tanks.

The U.S. Environmental Protection Agency (EPA)-mandated closure and decommissioning of Department of Energy nuclear waste storage tanks requires the chemical characterization of highly radioactive aqueous liquids to determine their regulatory status and to select appropriate treatments and disposal. Included in this characterization is the determination of regulatory volatiles, which are organic compounds that can be removed from an aqueous sample with an inert sparge gas.

The EPA has produced an extensive volume of tested methods for *nonradioactive* wastes in its Solid Waste Manual 846 (*1*) and lists the regulatory organic compounds in its Appendix VIII (*2*). EPA SW-846 Method 5030, "Purge and Trap" (*1*), describes the purging of regulatory volatile organic compounds from aqueous samples onto solid sorbent traps for determination by gas chromatography/mass spectrometry (GC/MS), Method 8240 (*1*). The direct application of these procedures to the characterization of radioactive wastes would result in the contamination of expensive instrumentation and the potential exposure of laboratory staff to unsafe levels of radiation.

This paper describes modifications to Methods 5030 and 8240 that allow the purge and trap step to be performed safely in a remote glovebox and permit the final determination to be performed in a nonradioactive GC/MS laboratory. The performance of the modified procedure, based upon surrogate standards, matrix spikes, and blanks, is comparable to that achieved for nonradioactive groundwater by the two aforementioned EPA methods.

EXPERIMENTAL SECTION

Sample Collection. The aqueous radioactive waste samples were collected as described in detail elsewhere (*3*). Briefly, a small vacuum pump was used to draw the sample from a particular depth in the waste tank into a precleaned 250-mL wide-mouth jar (I-Chem, Hayward, CA). Approximately 15–25 mL of headspace was left in the jar. All samples were screened and tagged in the field for α and β/γ radiation before transferring to a lead pig and shipping to the analytical laboratory.

Caution: The samples described in this work are highly radioactive, contain substantial quantities of radiotoxic materials, and are extremely hazardous. Only laboratories that possess appropriate equipment and can ensure the safety of its chemical operators should attempt the operations described in the Experimental Section.

Sparging Equipment. The collection of volatiles was performed with equipment custom-made at the Oak Ridge National Laboratory and arranged as shown in Figure 1. A special Teflon sampling head, detailed in Figure 2 and equipped with a Teflon-faced silicone rubber septum, screwed snugly onto a 40-mL volatile organics analysis (VOA) vial (Shamrock Glass, Co., Seaford, DE, part no. 6-06K). These vials were precleaned according to EPA standard protocols (*4, 5*) and were used as received. The head provided a 10/32 screw port for a reusable "Fingertight" fitting, manufactured by Upchurch Scientific (Oak Harbor, WA). A length of capillary Teflon ($^1/_{16}$ in. o.d. × 0.3 mm i.d.) passed through the fitting into the 40-mL vial. The other end of the tubing was connected to a $^1/_{16}$ in. to $^1/_8$ in. male bulkhead fitting mounted on the glovebox wall, as shown in Figure 1. The head provided an additional port for a $^1/_8$ in. to $^1/_8$ in. Swagelok union. One end of the union was screwed into the sampling head; the other was connected to $^1/_8$ in. o.d. Teflon tubing, which in turn was connected to a bulkhead union in the glovebox wall. The sampling head was supplied with nitrogen sparge gas (30 mL/min) through a needle valve and a $^1/_8$ in. o.d. copper line connected to a $^1/_8$ in. bulkhead union.

Traps designed for EPA Method 624 (*4*) (Supelco, Inc., Bellefonte, PA, part no. 2-0293) were used for collecting volatiles. These traps, which were baked at 215 °C with a helium (99.996% purity) purge (30 mL/min) overnight before use, were 30.5 × 0.33 cm o.d. and contained 1 cm of 3% SP-2100, 15 cm of Tenax GC, and 8 cm of grade 15 silica gel. One end of the trap was connected to a $^1/_8$ in. bulkhead union on the outside of the glovebox, as shown in Figure 1; the other was connected to a ball rotameter. The gas flow rate was monitored continuously throughout an experiment.

Surrogates and Spikes. The contents of an ampule of Purgeables Surrogate Standard Mix-CLP (Supelco, catalog no. 4-8876), containing 250 μg each of 1,2-dichloroethane-d_4, toluene-d_8, and 4-bromofluorobenzene, was diluted to 10 mL with Purge & Trap methanol (Baxter Healthcare, Corp., Burdick & Jackson Division, Muskegon, MI). This diluted surrogate standard solution (final concentration 25 μg/mL) was transferred immediately with no headspace to 1.5-mL amber screw-cap vials. New standards were prepared weekly.

A matrix spike stock solution containing ca. 10 mg/mL each of toluene, benzene, 1,1-dichloroethylene, chlorobenzene, and trichloroethylene (all from Supelco) was prepared in Purge & Trap methanol. A 25-μL aliquot was diluted with Purge & Trap methanol to 10 mL, then transferred to 1.5-mL amber screwcap vials in the same manner as the surrogates. The diluted matrix spike solution (final concentration 25 μg/mL) was also prepared weekly.

A test mixture containing 25 μg/mL each of the regulatory volatile organic target compounds from the Contract Laboratory Program Purgeable Mixture A (200 μg/mL of each of 13 com-

---

* To whom correspondence should be addressed.

[1] Present address: Environmental Compliance Division, Oak Ridge National Laboratory, Oak Ridge, TN 37831-6222.

0003-2700/89/0361-2751$01.50/0 © 1989 American Chemical Society

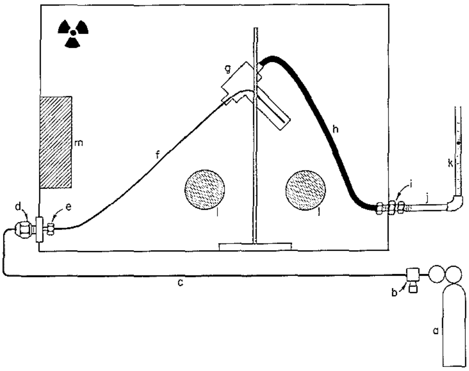

Figure 1. Layout of volatile organics sampling equipment in and around the glovebox: (a) nitrogen cylinder with two-stage regulator; (b) needle valve; (c) ${}^{1}/_{8}$ in. o.d. copper line; (d) and (e) ${}^{1}/_{8}$ to ${}^{1}/_{16}$ in. bulkhead union mounted in the glovebox wall; (f) capillary tubing ${}^{1}/_{16}$ in. o.d. × 0.3 mm i.d.; (g) Teflon sampling head and 40-mL VOA vial detailed in Figure 2; (h) ${}^{1}/_{8}$ in. o.d. Teflon tubing; (i) ${}^{1}/_{8}$ in. to ${}^{1}/_{8}$ in. bulkhead union mounted in the glovebox wall; (j) EPA Method 624 three-stage trap for volatiles; (k) flow rotameter. The two glove ports (1) and bag-in/bag-out port (m) are fixed features of the glovebox.

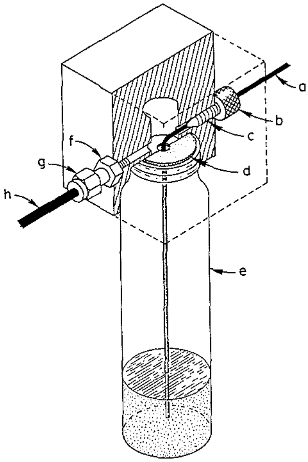

Figure 2. Teflon sampling head used for the collection of volatile organics: (a) capillary Teflon tubing ${}^{1}/_{16}$ in. o.d. × 0.3 mm i.d.; (b) fingertight fitting; (c) 10/32 screw port; (d) Teflon-faced rubber septum with hole; (e) 40-mL VOA vial; (f) Swagelok ${}^{1}/_{8}$ to ${}^{1}/_{8}$ in. union fitting; (g) ${}^{1}/_{8}$ in. Swagelok nut; (h) ${}^{1}/_{8}$ in. o.d. Teflon tubing. Details are given in text.

ponents), Purgeable Mixture B (200 μg/mL of each of 11 components), and Hazardous Substances List (HSL) Volatile Standard Mix (2000 μg/mL of each of eight components) (Supelco, catalog no. 4-8851, 4-8852, and 4-8920, respectively) was prepared in Purge & Trap methanol. A 0.8-mL total volume contained 100 μL each of purgeable A and B and 10 μL of the HSL volatiles mix and was used to test the recovery of selected purgeables using the glovebox procedure.

A supplementary standard solution containing 250 μg/mL each of the following compounds listed in EPA Appendix VIII (*2*) was prepared in Purge and Trap grade methanol (Baxter): 1,2,3-trichloropropane; dibromomethane; *trans*-1,4-dichloro-2-butene; fluorotrichloromethane; methacrylonitrile; methyl methacrylate; acrylonitrile; iodomethane; 2-picoline; and pyridine. These materials were purchased from either the Aldrich Chemical Co. (Milwaukee, WI) or Chem Service, Inc. (West Chester, PA), in 95% or greater purity and were used as received. A 1-mL volume of this standard was diluted to 10 mL (final concentration 25 μg/mL) with Purge & Trap methanol and then transferred immediately to 1.5-mL amber screw-cap vials without headspace. This diluted standard solution was used for only one set of recovery studies; hence, there was no need to replace it routinely.

Sparging System Test Procedure. The sampling head, VOA vial, trap, and ball rotameter were assembled as shown in Figure 1. Nitrogen (99.997% purity) was passed briefly through the system, usually for less than 1 min, to ensure that there was free gas flow through both the sampling head and the trap. A gas flow of approximately 20 mL/min, manually observed on the flow rotameter, was sufficient to "pass test".

Sparging Procedure for Volatile Organics Present in Radioactive Waste Tank Liquids. Immediately following (and using exactly the same pieces as) the sparging system test procedure, the liquid contents of the 250-mL jar were sampled in the glovebox for volatile organics. In this procedure, the "blank" sample was distilled water that was spiked as described below. The "matrix spike" and "matrix spike duplicate" were radioactive aqueous samples taken from the 250-mL jar and spiked as described below. The following steps were executed sequentially within 30 s:

(a) The jar was opened and a 5-mL aliquot was transferred to the VOA vial with a calibrated variable-volume 5-mL-capacity pipettor (Pipetman, Rainin Instrument Co., Woburn, MA).

(b) A 25-μL-capacity syringe (Hamilton Co., Reno, NV) was rinsed, and 10 μL of the Purgeables Surrogate Standard was added to the sample (all samples, matrix spikes, matrix spike duplicates, and blanks).

(c) A second 25-μL-capacity syringe (Hamilton) was rinsed, and 10 μL of the Matrix Spike were added to the sample (matrix spike and matrix spike duplicate samples only).

(d) The VOA vial was screwed into the sampling head.

The sample was then sparged for 11 min at 30 mL/min with nitrogen. At the end of the sampling period, the trap was disconnected from the glovebox wall, sealed, checked for radioactivity with standard probe and smear techniques, and transferred to a noncontaminated laboratory for quantitation of volatile organics by GC/MS (described below).

A second 5-mL aliquot was drawn from each sample bottle and treated as described above, thereby forming the "backup" sample.

GC/MS Quantitation of Volatiles. The volatiles were analyzed by use of a procedure based upon EPA Method 8240 (*1*); however, modifications were introduced to allow the volatile analytes to be desorbed directly from a Method 624 stainless steel trap. The volatiles present on an adsorbent trap were first thermally desorbed in a tube furnace held at 182 °C while helium passed through the trap at 35 mL/min for 11 min. The effluent stream was bubbled through 5 mL of laboratory distilled water held in a conventional purge and trap vessel in a Model LSC-2 Tekmar liquid sample concentrator (Tekmar Co., Cincinnati, OH). The water contained exactly 250 ng each of bromochloromethane, 1-chloro-2-bromopropane, and 1,4-dichlorobutane from a Purgeables Internal Standard Mix-CLP (Supelco, part no. 4-8835). The volatile compounds thermally desorbed from the Method 624 trap and the internal standards in the water were collected in the internal trap of the Tekmar apparatus. The components were then desorbed from the internal trap by heating to 110 °C with a helium flow of 30 mL/min for 4 min and were swept onto the head of a 200 × 0.64 cm o.d. (6.6 ft × ${}^{1}/_{4}$ in. o.d.) glass column packed with Carbopack B coated with 1% SP-1000 (Supelco) located in a Hewlett-Packard Model 5995 GC/MS. The oven temperature was programmed from 45 °C (hold for 3 min) to 180 °C (hold for 45 min) at a rate of 8 °C/min. The analytes were detected by the mass spectrometer, which operated at 70-eV ionization potential, mass range 35–260 amu, and a scan time of 0.24 scan/s.

Method calibration was performed according to the EPA Contract Laboratory Program (CLP) procedure (*7*), using five standards (20, 50, 100, 150, and 200 μg/L) containing the analytes present in Purgeable Mix A, Purgeable Mix B, and the Hazardous Substances List Mix described earlier. The calibration curves, which were linear as defined by EPA methods described in SW-846 or the CLP (*1, 7*), were checked daily with a single check standard. If the daily calibration check showed significant drift, as defined by the EPA methods, the instrument was immediately recalibrated. The detection limits were typically 5–10 μg/L, as defined by the EPA methods. Analyte concentrations exceeding 200 μg/L are considered estimates only and are flagged (*7*) with the "E" qualifier.

Method Performance Evaluation. Method performance was evaluated through the use of surrogate standards, matrix spikes and matrix spike duplicates, water blanks, and trip blanks, as well as the evaluation of individual compound recoveries by using the mixtures of purgeable organic compound standards and the diluted supplemental standard. A matrix spike and matrix spike duplicate accompanied every lot of samples prepared on a given day. A blank sample, consisting of 5 mL of Burdick & Jackson Distilled in Glass water was also prepared daily. The trip blank was a trap that was carried into the radiochemical laboratory and accompanied each group of sample, matrix spike and matrix spike duplicate, and blank traps to the GC/MS laboratory, but it was not spiked in the radiochemical laboratory, nor was it subjected to the collection of volatiles described above. In general, a blank, matrix spike, and matrix spike duplicate accompanied every three to six radioactive waste samples. Surrogate standards were added to each sample and water blank, as described previously. Each blank, matrix spike, and matrix spike duplicate was subjected to the identical analytical procedure described above in "Sparging Procedure for Volatile Organics Present in Radioactive Waste Tank Liquids".

The recoveries of the regulatory target volatile organic compounds, as well as the components of the supplemental standards selected from Appendix VIII (*2*), were evaluated by spiking a 5-mL Distilled in Glass water sample with 10 μL of the appropriate standard solution in the glovebox and then proceeding with the usual sparging conditions. Each recovery was evaluated in triplicate.

RESULTS AND DISCUSSION

The aqueous radioactive waste samples analyzed in this study have been stored in underground waste storage tanks with headspace for up to 40 years. The major radionuclides present were the usual products of uranium fission, viz. ^{137}Cs and ^{90}Sr, exhibiting activity up to 6×10^5 and 1×10^4 Bq/mL, respectively. Other radionuclides, such as ^{60}Co, ^{233}U, and ^{3}H, were commonly observed, but at hundredfold less activities.

A number of inorganic anions and cations were also observed in the aqueous waste samples. The pH of each sample ranged between 0.5 and 13, with the great majority exceeding 8. Nitrate and sulfate were the dominant anions with concentrations up to 31 000 and 83 000 mg/L, respectively. The concentrations of sodium and potassium have not yet been measured but are expected to range from milligrams per liter to grams per liter. The major cation measured was uranium (up to 4000 mg/L). Lower concentrations of 10 pollutant metals specified in the Resource Conservation and Recovery Act of 1976 were occasionally observed, particularly chromium and mercury.

The very high radiation fields and small tank access ports limited access to the tank contents, and the high specific activity of the tanks precluded the collection of samples using the standard EPA protocols. Compromise procedures had to be utilized, as described in detail elsewhere (*3*). Briefly, the radioactive liquid was pumped from the tank into a 250-mL wide-mouth jar to a level approximately 1 cm from its lip (ca. 15–25 mL headspace). The jar was then sealed and placed in a lead pig. In all cases, a single 250-mL sample was drawn from each tank and depth specified. Because several analytical groups shared each sample, the sampling of the jar liquid contents for the analysis of regulatory target volatile organic compounds was always performed first, usually within 2 days of receipt of sample. This arrangement also satisfied regulatory holding time requirements for aqueous samples analyzed for volatiles. EPA SW-846 specifies a holding time of 14 days from time of receipt (*1*), while the CLP protocol specifies 10 days (*7*).

Even small aliquots of these samples were sufficiently radioactive to preclude chemical manipulations on the open bench or even a radiochemical hood (*6*), and sample preparation had to be conducted in a contained area such as a glovebox. The glovebox also provided an important additional advantage based on its previous usage: It contained a controlled atmosphere which did not contain traces of common volatile organic solvents. The aqueous tank samples occasionally foamed upon sparging; hence a very small and narrow sparging vessel, such as that described in EPA Method 5030, was inappropriate. The sparging vessel must be sufficiently large and wide to permit the foam to rise and disperse naturally to minimize the equipment contaminated.

The custom-designed sampling head and 40-mL VOA vial are designed to replace the expensive volatile sparger usually employed with conventional purge-and-trap equipment. The precleaned VOA vials are inexpensive and are discarded after each use. The head itself has been reused over 200 times with no observable degradation in purging efficiency. It is, of course, possible for the head to become accidentally contaminated. In that case, this inexpensive piece and its related components may also be discarded without significantly increasing the cost of a series of analyses. The dimensions of the 40-mL VOA vial are quite different than those specified in EPA Method 5030, resulting in a smaller liquid sample depth (1 cm) and total volume (40 mL) than that approved for a 5-mL sample (3 cm and 15 mL, respectively). On the other hand, the recovery of most regulatory target volatile organic compounds does not appear to be adversely affected by the additional dead volume (see discussion below). Furthermore, even when some of the waste samples foamed during sparging, the connecting tubing and sorbent trap did not become contaminated.

The major disadvantage of the new sampling head is that the sample and appropriate spikes must be added to an open vessel. The addition of these liquids to the VOA vial, usually within approximately 15 s, was therefore achieved as quickly and as smoothly as possible to minimize the inevitable losses of volatile analytes. The heavy, bulky latex gloves with cotton liners used in radiochemical glovebox work compounded the problem; handling the delicate 25-μL glass syringes became a cumbersome, unwieldy operation. In spite of the obvious physical disadvantages, an experienced operator can usually minimize the loss of surrogates, matrix spikes, and sample volatiles by rapid and smooth manipulations, thereby achieving a respectable recovery for each.

The ultimate goal of the sample preparation is to transfer the regulatory target organic volatiles quantitatively to a sorbent trap, which remains noncontaminated, and may be analyzed in a nonradioactive GC/MS laboratory. During the course of this work, over 200 traps were examined by health physicists for α and β/γ radioactive contamination using both probe and smear techniques before transfer to such a laboratory; radioactive contamination was never detected.

In the present procedure, the Purgeable Surrogate Standard compounds are added to every waste sample or blank before purging in the glovebox. The Purgeables Internal Standard Mix-CLP is added to the water in the purge-and-trap vessel of the Tekmar apparatus just prior to desorbing the Method 624 trap through the Tekmar vessel and onto the internal trap of the Tekmar. This latter step occurs just prior to thermal desorption of the internal trap in the Tekmar apparatus and subsequent GC/MS quantitation of volatiles. This practice is at variance to the single-stage procedure described in EPA Method 5030, in which both surrogates and internal standards are added to the sample at the same time. The analysis of volatiles in aqueous radioactive samples requires a two-step procedure conducted at two completely separate locations.

The quantitation of the Purgeable Surrogate Standard compounds allows a calculation of the recovery of these materials taken through the entire procedure (glovebox, purge-and-trap, and thermal desorption purge-and-trap GC/MS), while that of the Purgeables Internal Standard Mix compounds allows a calculation of the recovery of the materials taken only through the Tekmar purging vessel and internal trap, then delivered to the GC/MS. The present method therefore allows a thorough evaluation of recovery and permits problems in recovery to be pinpointed to the purge-and-trap step either in the glovebox or prior to GC/MS. In practice, the response factors determined by using only the purge-and-trap instrument associated with the GC/MS were evaluated daily with a 50 μg/L standard mixture containing all of the test volatile organic compounds. The response factors of these compounds always agreed with those observed from the original five-point calibration curve, within the limits dictated by EPA SW-846. On that basis, the recovery of volatile organics from the purging vessel and internal trap of the conventional Tekmar apparatus to the GC/MS may be taken as unity. Variations in recovery values for individual analytes are therefore properly attributed to the performance of the remote purge-and-trap operation performed in the glovebox.

The three volatile surrogate standards were recovered in reasonable yield both from the aqueous radioactive waste tank samples and from water blanks prepared inside the glovebox. By use of a database of 65 waste tank samples, the recoveries (mean ± standard deviation, %) of toluene-d_8, bromofluorobenzene, and 1,2-dichloroethane-d_4 were 89 ± 17, 59 ± 15, and 81 ± 11, respectively. Both the average and precision of the recoveries are acceptable at the 50 μg/L level in this hostile matrix. The mean values observed were similar to the Quality Control Acceptance Limits specified by EPA Method 8240 for groundwater samples, viz. 88–110% for toluene-d_8, 86–115% for bromofluorobenzene, and 76–114% for 1,2-dichloroethane-d_4 (*1*). The recoveries (same conventions) of the surrogates from seven water blanks for toluene-d_8, bromofluorobenzene, and 1,2-dichloroethane-d_4 were 91 ± 11, 61 ± 12, and 86 ± 13, respectively. Data from the remaining four blanks were discarded because of a technical laboratory error. The exact reasons for the reduced recoveries of bromofluorobenzene compared with those expected from the EPA Quality Control Acceptance Limits for both blank and real samples are unknown. We suggest that this surrogate has the highest boiling point (and is therefore the least volatile) of the three surrogates, and the sparging conditions employed may not be vigorous enough to transfer it quantitatively to the sorbent trap.

The recoveries of the five matrix spike compounds were evaluated by using ten pairs of matrix spikes and corresponding matrix spike duplicates. The agreement between the recovery of any given compound for a given sample pair was typically within about 10%. The recoveries of the spike compounds were as follows (mean ± standard deviation in %, *n* number of samples): 1,1-dichloroethene (105 ± 18, 20); trichloroethene (87 ± 14, 20); benzene (89 ± 15, 19); toluene (81 ± 20, 15); and chlorobenzene (67 ± 13, 19). Some of the raw data values were deleted from the evaluation because they either exceeded 150% recovery (one for benzene, two for toluene, one for chlorobenzene) or they were inexplicably zero when all other matrix spike compounds were recovered at reasonable levels (two for toluene, comprising one pair). The recoveries of all five matrix spike compounds generally fell within the ranges specified (*7*) for groundwater analyses by the U.S. EPA Contract Laboratory Program, which are typically between 70% and 130%. SW-846 does not list Quality Control Acceptance Limits for matrix spikes.

Table I. Comparison of Supplementary Volatile Organic Compound Standard Analyses with Purge and Trap in the Glovebox and the GC/MS Lab

	concentration,[a] μg/L		
		determined w/P&T in	
compound	actual	glovebox	GC/MS lab
CLP Purgeable Mixture A, B, and Hazardous Substances List[b]			
methylene chloride	50	137 ± 5.8B	53B
acetone	50	56 ± 15B	37B
carbon disulfide	50	96 ± 3.6	63
1,1-dichloroethene	50	70 ± 1.7	52
1,1-dichloroethane	50	57 ± 1.5	50
1,2-dichloroethene (total)	50	54 ± 2.5	50
chloroform	50	56 ± 2.5	48
1,2-dichloroethane	50	43 ± 2.5	50
2-butanone[c]	50	12 ± 1.7	43
1,1,1-trichloroethane	50	49 ± 1.5	48
carbon tetrachloride	50	53 ± 1.5	50
vinyl acetate	50	20 ± 1.6	18
bromodichloromethane	50	43 ± 2.1	49
1,2-dichloropropane	50	50 ± 1.5	54
cis-1,3-dichloropropene	50	36 ± 4.0	50
trichloroethene	50	53 ± 1.5	56
dibromochloromethane	50	38 ± 4.5	54
1,1,2-trichloroethane	50	37 ± 3.1	54
benzene	50	51 ± 1.5	50
trans-1,3-dichloropropene	50	41 ± 3.1	49
bromoform	50	23 ± 4.6	5
4-methyl-2-pentanone[d]	50	13 ± 2.1	52
2-hexanone	50	9 ± 1.0	40
tetrachloroethene	50	44 ± 3.5	56
1,1,2,2-tetrachloroethane	50	19 ± 5.1	56
toluene	50	49 ± 1.0	50
chlorobenzene	50	43 ± 3.5	51
ethylbenzene	50	37 ± 4.6	48
styrene	50	33 ± 5.7	42
xylenes (total)	50	35 ± 2.5	47
Appendix VIII Supplementary Standards[b]			
1,2,3-trichloropropane	55	11[e]	21
dibromomethane	50	ND	ND
1,2-dibromoethane	50	12 ± 0.6	14
trans-1,4-dichloro-2-butene	51	6[e]	10
fluorotrichloromethane	60	43 ± 3.6	40
methacrylonitrile	50	ND	ND
methyl methacrylate	50	ND	8
acrylonitrile	50	ND	ND
iodomethane	50	33 ± 4.7	28
2-picoline	50	ND	ND
pyridine	51	ND	ND
Alcohol/Ketone Standards[f]			
methyl alcohol	20000	ND	ND
ethyl alcohol	22600	5600	ND
acetone	21900	9100	4700
isopropyl alcohol	21700	ND	ND
allyl alcohol	19900	ND	ND
2-butanone[c]	20500	1000	6200
isobutyl alcohol	20500	ND	ND
n-butyl alcohol	20800	ND	ND
4-methyl-2-pentanone[d]	21800	1600	3700

[a] ND, not detected; B, also detected in blank. [b] Average ± standard deviation for $n = 3$ in glovebox preparation; single preparation in GC/MS lab. [c] Also named methyl ethyl ketone. [d] Also named methyl isobutyl ketone. [e] Detected in two samples, average listed. [f] Average of duplicate preparation in glovebox; single preparation in GC/MS lab.

Eleven water blanks were evaluated during this study. The most common contaminant was methylene chloride, which was present in all samples except one at concentrations less than 20 μg/L. In the remaining blank, the unusually high concentration of methylene chloride, 880 μg/L, was attributed to storage of the trap in the analytical laboratory while awaiting GC/MS analysis. When traps were analyzed

Table II. Concentrations of Regulatory Target Volatile Organic Compounds in Selected Radioactive Aqueous Waste Tank Samples

		concentration, μg/L									
tank	sample no.	acetone[a]	chloroform[a]	toluene[a]	methylene chloride[a]	methyl isobutyl ketone	total xylenes	benzene	methyl ethyl ketone	tetrachloroethene	trichloroethene
T-4	044	400[b]	170	78	12	11	<5	7	<5	<5	<5
	045	200[b]	160	98	14	10	170	10	<5	<5	3
	111	72	120	60	12	<5	36	7	<5	<5	<5
T-2	038	20	300[b]	12	1000[b]	<5	<5	3	<5	<5	<5
	039	22	400[b]	7	800[b]	<5	<5	<5	<5	<5	<5
	112	17	300[b]	8	900[b]	<5	<5	<5	<5	<5	<5
TH-4	055	22	6	4	8	<5	<5	3	<5	<5	<5
	056	600[b]	11	18	8	3000[b]	<5	149	85	<5	<5
	057A[c]	71	7	21	7	400[b]	10	115	<5	<5	<5
	057B[c]	54	5	23	6	200[b]	22	118	<5	<5	<5
	116	150	<5	13	6	300[b]	<5	10	<5	<5	5
	117	16	4	79	200[b]	9	<5	21	<5	<5	<5
W-6	077	67	5	6	9	<5	<5	<5	<5	47	13
	078	44	9	10	8	9	<5	2	<5	158	24
	079	111	3	10	7	91	<5	10	75	500[b]	82
W-4	022	<5	<5	13	10	<5	<5	<5	<5	<5	<5
	023	55	<5	14	10	1000[b]	<5	3	<5	<5	49
	119	<5	<5	46	10	3	<5	2	<5	<5	14
W10	094A[c]	<5	<5	12	13	<5	<5	6	<5	21	27
	094B[c]	<5	<5	<5	19	<5	<5	38	<5	<5	<5
	095	97	16	26	12	23	<5	22	<5	48	81

[a] Detected in the blank, usually at levels below 20 μg/L. [b] Estimate only; value exceeds highest calibrated standard value. [c] Field sampling duplicates.

promptly, usually within 48 h, the analytical blank remained below 20 μg/L. Acetone was not observed in two blanks, but it was present in eight blanks at levels less than 40 μg/L and in one at 150 μg/L. Toluene was also not detected in two blanks, but it occurred in eight blanks at levels less than 20 μg/L, but in one at 43 μg/L. Seven other volatiles were detected in less than five blanks at concentrations generally less than 20 μg/L: bromodichloromethane, benzene, 4-methyl-2-pentanone, tetrachloroethene, trichloroethene, total xylenes, and carbon tetrachloride. In general, the blank levels for the volatiles were deemed low enough, and the number of contaminant species few enough, for further work to proceed; however, the quantitative data for these compounds in waste samples were flagged with a "B" qualifier, signifying that the analyte had also been detected in the blank with that set of samples.

Table I shows the recovery of the contract laboratory program (CLP) test volatile analytes taken from purgeables A and B and the HSL mixtures when performed both in the glovebox and by using the standard EPA Methods 5030/8240 procedure. In general, the species that are immiscible with water were recovered at 75% or better at the 50 μg/L level using either the glovebox or EPA Method 5030 equipment. Species that are freely miscible with water were invariably recovered less efficiently from the glovebox than with the more standard procedure. These species included acetone (some analyte contributed by the normal blank level), 4-methyl-2-pentanone, 2-butanone, and 2-hexanone.

Table I also shows the recoveries of various supplementary standards from appendix VIII. The same trends were observed as for the CLP compounds described above. Several of these compounds (e.g., pyridine and acrylonitrile) are not recovered well even using the conventional purge and trap methodology, and special analytical procedures (*1*) are required. These compounds were included in this study to determine if their presence could be detected in waste samples. The remote purge-and-trap performed as well as the conventional method, but neither collected all of the test compounds.

The exact reasons for the losses of the water-immiscible analytes are not known. However, we postulate that the losses of the water-soluble analytes are caused by insufficient sparging in the glovebox apparatus. As a further test, a standard containing 20 mg/L (the maximum concentration observed in some waste samples) of water-soluble analytes was also tested on both apparatus, as shown in Table I. Both 2-butanone and 4-methyl-2-pentanone were recovered less efficiently by the present method than by the standard procedure; ethyl alcohol and acetone were recovered more efficiently in the glovebox; and the remaining analytes were not observed by using either method.

While the recoveries of certain analytes could probably by improved by increasing the gas flow going into the glovebox apparatus, and therefore increasing the degree of agitation, such a change could prove most detrimental if the sample itself began to foam (some did). Gentle sparging within the 40-mL VOA vial permitted the foam to disperse easily before reaching—and contaminating—the Teflon sampling head and the associated tubing. More vigorous sparging unquestionably would have contaminated the sparging apparatus, and possibly the glovebox itself. For these reasons, we elected to leave the gas flow unchanged but to note the problems with water-miscible analytes, and to supplement measurements of these species at milligram per liter concentrations with a direct injection aqueous gas chromatographic analysis patterned after EPA Method 8015, "Nonhalogenated Volatile Organics" (*1*).

Table II reports the concentrations of the ten most commonly observed regulatory target volatile organic compounds in six representative waste tanks. In four of these tanks, the most concentrated species were one or more of the analytes which had been observed routinely in the blanks, viz. acetone, chloroform, toluene, and methylene chloride. Concentrations of these four materials should not be considered significant unless they exceed the blank level, which was approximately 20 $\mu g/L$. The remaining six analytes were not detected routinely in the blanks; concentration levels are therefore significant if they exceeded the normal reporting level for each compound, which is typically 5–10 $\mu g/L$. In several cases, the observed concentration exceeded the highest calibration standard concentration, which was 200 $\mu g/L$. In such cases, the value displayed in Table II is an estimate, and is so designated.

Several conclusions may be drawn from Table II. First, the liquid present in most of the radioactive liquid storage tanks is certainly not homogeneous. Tank T-2 appears to be the only vessel whose contents may be reasonably uniform; all of the other tank wastes display significant differences with changing sampling depth. Second, the contaminants observed are either common laboratory solvents or industrial degreasers. Third, the sampling procedure employed does permit reproducible samples to be obtained at a given depth. Two pairs of samples were drawn sequentially from the same level in tanks TH-4 and W-10 and may be considered field duplicates within the usual errors of sampling. In both cases, the agreement between the field duplicates for a given tank was quite reasonable, particularly when both the trace level of analyte and the properties of the sample matrix are considered.

The performance of this modified EPA methodology, as defined by surrogate standards, matrix spikes, blanks, and field duplicate samples, shows that volatile organic compounds present in highly radioactive samples can be determined confidently by using remote purge-and-trap technology followed by GC/MS analysis in a nonradioactive analytical laboratory.

ACKNOWLEDGMENT

The authors express their appreciation to the staff of the High Radiation Level Analytical Laboratory, Oak Ridge National Laboratory, for providing the radiochemical characterization and inorganic analysis data presented in this paper. The authors also acknowledge Ms. Nancy R. Sweat-Pope and Mr. William F. Fox, health physicists and members of the Environmental Compliance Division, Oak Ridge National Laboratory, for their advice concerning the proper handling of both the radioactive waste samples and the sampling traps which were discussed in this work. Ms. Linda L. Kaiser, Mr. Christopher B. Scott, and their co-workers designed and executed the sampling plan described in this paper.

LITERATURE CITED

(1) *Test Methods for Evaluating Solid Waste. Volume 1B, Laboratory Manual Physical/Chemical Methods*; SW 846, Third Edition, United States Environmental Protection Agency, Office of Solid Waste and Emergency Response: Washington, DC, November 1986.

(2) Hazardous Constituents. In *40 Code of Federal Regulations, Part 261, Appendix VIII*, Office of the Federal Register, National Archives and Records Administration: Washington, DC, 1987; pp 408–417.

(3) Autrey, J. W.; Costanzo, D. A.; Griest, W. H.; Kaiser, L. L.; Keller, J. M.; Nix, C. E.; and Tomkins, B. A. Sampling and Analysis of the Inactive Waste Storage Tank Contents at ORNL; ORNL/RAP-53; Environmental and Health Protection Division, Oak Ridge National Laboratory: Oak Ridge, TN, August 1989.

(4) Guidelines Establishing Test Procedure for the Analysis of Pollutants: Method 624—Purgeables. In *40 Code of Federal Regulations, Part 136, Appendix A, Method 624*; Office of the Federal Register, National Archives and Records Administration: Washington, DC, 1988; pp 432–446.

(5) National Primary Drinking Water Regulations. Analysis of Trihalomethanes: Part I—The Analysis of Trihalomethanes in Drinking Water by the Purge and Trap Method. In *40 Code of Federal Regulations, Part 141, Subpart C, Appendix* C; 1988, Office of the Federal Register, National Archives and Records Administration: Washington, DC, 1988; pp 549–556.

(6) Operating Guide for Radiochemical Laboratories at Various Activity Levels: Procedure No. A-7. In *Procedures and Practices for Radiation Protection*: *Health Physics Manual*, Oak Ridge National Laboratory: Oak Ridge, TN, July 1, 1987.

(7) *USEPA Contract Laboratory Program*: *Statement of Work for Organic Analysis*, *Multi-Media*, *Multi-Concentration*, *S. O. W. 787*; Oak Ridge National Laboratory: Oak Ridge, TN, 1987.

RECEIVED for review June 27, 1989. Accepted October 6, 1989. Oak Ridge National Laboratory is operated by Martin Marietta Energy Systems, Inc., under Contract No. DE-AC05-84OR21400 with the U.S. Department of Energy.

Anal. Chem. **1989**, *61*, 2757–2763

Radiochemical Neutron Activation Analysis of Zinc Isotopes in Human Blood, Urine, and Feces for in Vivo Tracer Experiments

İnci G. Gökmen,[1] Namik K. Aras,[1] and Glen E. Gordon*

Department of Chemistry and Biochemistry, University of Maryland, College Park, Maryland 20742

Meryl E. Wastney and Robert I. Henkin[2]

Department of Pediatrics, Georgetown University Medical Center, Washington, D.C. 20007

Enriched stable isotopes are being increasingly used for study of trace element nutrition in humans who cannot be studied by use of in vivo radioactive tracers (e.g., subjects under age 18 and pregnant women). Zinc metabolism in these subjects can be evaluated by administration of Zn enriched to 65% in the minor isotope, ^{70}Zn (0.6% natural abundance). The enhanced ^{70}Zn is detected later in red blood cells, plasma, urine, and feces by measuring ^{70}Zn/^{64}Zn or ^{70}Zn/^{68}Zn ratios. Stable isotope concentrations are measured by neutron activation of the samples and observation of their products: 244-day ^{65}Zn, 14-h ^{69m}Zn, and 4-h ^{71m}Zn. Zinc-65 can be observed in these samples without chemical separations 3 weeks after irradiations, but large amounts of ^{24}Na and other short-lived species preclude direct observation of the short-lived Zn activities. Preirradiation chemistry was developed to remove most interferences, the major steps being to place the sample on Chelex resin, elute alkali metals and alkaline earths from it, and irradiate the resin containing the Zn. γ-Rays of ^{69m}Zn can be observed on the irradiated resin, but additional precipitation and solvent extraction steps are needed to remove ^{56}Mn and ^{64}Cu for clear observation of ^{71m}Zn and ^{65}Zn within hours after irradiation. Yields for pre- and postirradiation separations are typically 85% and 70%, respectively. The stable isotope tracer method was validated by simultaneous in vivo tracing with radioactive ^{65}Zn in four subjects.

Marginal Zn deficiency in humans has been reported to be common throughout the world, including the United States (*1*). High nutritional requirements for Zn are found in growing children, pregnant women, and preterm infants and some postoperative patients, the last two groups often being fed by total parenteral nutrition. With present nutritional practices, each of these groups may be at risk of deficiency. Radioactive nuclides have been helpful in understanding several aspects of human nutrition and metabolism (*2–4*), but they cannot be used to study pregnant women, subjects under age 18, and postoperative patients from whom informed consent cannot be obtained. An alternate approach for obtaining information about Zn metabolism is stable isotope tracing (*5, 6*). Zinc enriched to about 65% in ^{70}Zn, a minor isotope with 0.62% natural abundance, is administered to subjects. Samples of blood, urine, and feces are collected at several times after administration. The appearance of the tracer is observed as an enhanced ratio of ^{70}Zn/^{64}Zn or ^{70}Zn/^{68}Zn (*5–11*). Our objective was to develop a method for observing the enhanced Zn ratios and to validate the stable isotope method by simultaneous use of radioactive ^{65}Zn tracer.

Table I. Nuclear Properties of Isotopes of Zinc and Interfering Elements That Lead to Observable Radioactive Species after Chelex Separation and Neutron Irradiation

target nuclide	abundance,[a,b] %	thermal neutron cross section,[a] b	product	energy of major γ-ray,[a] keV
^{64}Zn	48.6 (15.84)	0.78	244-day ^{65}Zn	1115.5
^{68}Zn	18.8 (8.38)	0.072	13.8-h ^{69m}Zn	438.7
			56-min ^{69}Zn	weak
^{70}Zn	0.62 (65.51)	0.008	3.9-h ^{71m}Zn	386.3
		0.09	2.4-min ^{71}Zn	512
^{23}Na	100	0.10	15-h ^{24}Na	1368.5
^{37}Cl	24.2	0.43	37.2-min ^{38}Cl	1642
^{41}K	6.73	1.46	12.4-h ^{42}K	1525
^{55}Mn	100	13.3	2.6-h ^{56}Mn	847, 1811
^{63}Cu	69.2	4.4	12.7-h ^{64}Cu	1346

[a] Reference 13. [b] Numbers in parentheses are the percent abundances in Zn enriched in ^{70}Zn; ref 14.

METHOD

The isotopes ^{64}Zn, ^{68}Zn, and ^{70}Zn can be observed by mass spectrometry (*9–11*) or, as in this work, by neutron activation analysis (NAA) to observe 244-day ^{65}Zn, 14-h ^{69m}Zn, and 4-h ^{71m}Zn, respectively, whose nuclear properties are listed in Table I. Zinc-65 can be observed by instrumental NAA from γ-ray spectra taken three weeks after irradiation (*12*), but half-lives of ^{71m}Zn and ^{69m}Zn are so short that their radiations are obscured by the enormous activities of 15-h ^{24}Na, 35-h ^{82}Br, 37-min ^{38}Cl, and other short-lived species. Thus, it was necessary to develop a separation procedure to remove interfering activities.

Postirradiation separation is desirable for avoiding contamination, but levels of ^{24}Na and other short-lived species are so high in activated biological samples that it is impractical to work with them quickly enough to observe ^{71m}Zn. Thus, we developed a radiochemical NAA procedure involving a minimum of preirradiation separation to remove most interfering species, followed by postirradiation chemistry for further cleanup. With the use of high-purity chemicals one can achieve acceptably low blank values so that the preirradiation chemistry does not contaminate the Zn samples with Zn of natural isotopic abundances.

EXPERIMENTAL SECTION

Preparation of Tracer. We tested the stable isotope method by simultaneously performing radioactive tracer studies in adult volunteers using ^{65}Zn. The radioactive and stable tracers were administered simultaneously to ensure that all conditions were identical. Preparation of ^{65}Zn tracer by neutron irradiation of the enriched ^{70}Zn tracer ensures that the chemical forms of the

---

[1] Current address: Department of Chemistry, Middle East Technical University, Ankara, Turkey.

[2] Current address: Center for Molecular Nutrition and Sensory Disorders, Washington, D.C. 20016.

0003-2700/89/0361-2757$01.50/0 © 1989 American Chemical Society

two tracers are identical. Other advantages were that no purchase of carrier-free ^{65}Zn was required and the ^{65}Zn in the collected samples could be used for chemical-yield determinations. Calculations indicated that ^{65}Zn in vivo tracer would cause insignificant interference with ^{65}Zn produced in NAA.

Zinc enriched to 65.5% ^{70}Zn was obtained as ZnO from the Stable Isotopes Division, Oak Ridge National Laboratory. Isotopic compositions of natural and ^{70}Zn-enriched Zn are listed in Table I. Enriched ZnO was irradiated at the National Bureau of Standards (NBS) reactor for 8 h at a flux of 5×10^{13} n/(cm^2 s) together with two standards, each of which contained 161 μg of Zn. The tracer was allowed to decay for 2 weeks, dissolved by addition of 0.5 mL of Ultrex HCl, and diluted to 100 mL with addition of high-purity water from NBS. The acidity was adjusted to pH 7 with addition of concentrated NH_4OH. The Zn concentration was determined by comparing γ-ray spectra of three 100-μL subsamples with that of a Zn standard. The concentration of the tracer solution was found to be 181 ± 14 μg/mL.

The activity of the solution was determined with a Ge(Li) detector whose efficiency was calibrated with NBS radioactivity standard, SRM 4216E (*15*). It was found that 11.0 mL of the prepared solution contained 2.02 ± 0.04 μCi of ^{65}Zn γ activity as a tracer. As the 1115-keV γ-ray is emitted in only 51% of decays (*13*), the total activity is 3.96 ± 0.07 μCi. The mass of Zn in each 11.0-mL portion administered to subjects was 1.99 ± 0.16 mg.

Administration of Tracers and Sample Collection. Tracers were administered orally, after an overnight fast, to four normal volunteers. Samples of blood, urine, and feces were then taken from the subjects, and NaI spectra were taken by external counting over the thigh and liver areas and whole body to monitor in vivo ^{65}Zn as described previously (*16*, *17*).

Blood. Samples were collected at about 30-min intervals for the first 2 h of the study, then at 3, 5, 24, and 72 h after administration, and then weekly, as previously described (*17*), although not all of the samples collected were analyzed for stable Zn isotopes. Blood samples were taken from a vein in the antecubital fossa by using a stainless steel needle and Leur-Lok top 30-mL plastic disposable syringes. Aliquots (10 mL) were placed into three tubes for the following procedures: (1) For ^{70}Zn measurements, 10 mL of blood was added to an acid-cleaned polystyrene tube to which 0.1 mL of 0.1% sodium citrate solution was originally added prior to blood collection to prevent clotting (later increased to 0.4 mL, as some clotting was observed). Blood samples were centrifuged at 3000 rpm for 10 min. Plasma for the ^{70}Zn study was transferred to acid-cleaned polystyrene tubes by using acid-cleaned 1-mL plastic pipets. The remaining red blood cells (RBC) were washed three times with Zn-free NaCl, and ^{70}Zn was measured as described below. (2) For ^{65}Zn measurements, 10 mL of blood was placed in a 16 × 100 mm glass tube with 14 mg of disodium ethylenediaminetetraacetic acid as anticoagulant and centrifuged at 3000 rpm for 10 min. Plasma for the ^{65}Zn study was transferred to glass tubes, the RBC were washed three times with Zn-free NaCl, and ^{65}Zn was assayed by γ-ray spectrometry (*18*). (3) For independent measurement of total Zn concentrations, the third aliquot of blood was placed into a metal-free glass tube containing 10 μL of heparin (1:1000) with low Zn. After the blood was centrifuged at 3000 rpm for 10 min, plasma was transferred to polystyrene tubes and Zn determined by flame aspiration atomic absorption spectrophotometry (AAS) (*18*).

Urine. Entire samples were collected over consecutive 24-h periods for the first 7 days of the study and then at weekly intervals. Samples were collected in plastic-lined cardboard containers, weighed, and assayed for ^{65}Zn by placing the container on a NaI detector (*18*). Aliquots (10 mL) were transferred into acid-cleaned 4-dram polyvials with 10-mL acid-cleaned polystyrene plastic pipets for stable Zn measurements.

Feces. Entire samples were collected daily in polyethylene bags for the first 7 days after isotope administration, placed in tin containers, and assayed for ^{65}Zn activity by methods previously described (*18*).

Sample Preparation. Plasma, RBC, and 10-mL urine subsamples were assayed for ^{65}Zn activity to be used for yield determination of preirradiation separations. All collected plasma (2.0–2.7 mL) and weighed portions of RBC that correspond to 0.4–1.9 mL were transferred into Teflon containers of Parr acid digestion bombs (*19*) and digested with 2.0 mL of NBS HNO_3 at 130 °C for 1 h.

Fecal samples were weighed, frozen in polybags by immersion in liquid nitrogen, and placed on preweighed plastic weighing dishes. They were freeze-dried from 15 to 24 h and transferred to clean polybags. Later they were homogenized in Teflon ball mills (*20*), which were placed on a motor-driven shaker (3–4 min). Homogeneity of samples was checked by assaying ^{65}Zn activity of four subsamples (200–300 mg) taken from the same sample, and 5% variation was found. From each fecal sample, 200–300-mg subsamples were placed inside polybags and assayed for ^{65}Zn activity and acid-digested under the same conditions as for blood and urine samples (2.0 mL of NBS HNO_3 at 130 °C for 1 h in an acid digestion bomb).

Chelex Separation. Chelex-100 resin is frequently used as a preconcentration medium for trace elements in estuarine and seawater samples (*21–29*) and has also been used for biological and environmental matrices (*30*, *31*). Decontamination factors of $\geq 10^7$, $\geq 10^5$, and $\geq 10^3$ were obtained for Na, Cl, and Br, respectively, by using Chelex-100 as a preirradiation separation medium for NAA determinations (*28*, *29*). The procedure developed by Kingston (*27*) for transition-metal analysis of high-salinity waters using Chelex-100 was used with some modifications (*32*).

Chelex-100 resin, 200–400 mesh size, in Na form, was purchased from Bio-Rad Laboratories. Polypropylene columns with porous polyethylene resin supports (QS-Q), 12-mL extension funnels (QS-R), and bottom closures (QS-B) were obtained from Isolab. Nitric acid, acetic acid, and the water used to prepare the reagents were NBS high-purity reagents prepared by sub-boiling distillation (*33*). Ammonium hydroxide was prepared by bubbling filtered NH_3(g) through high-purity water until saturation was achieved (*34*).

All bottles and beakers were made from FEP (fluorinated ethylene propylene) Teflon and the pipets from polypropylene. These were cleaned by keeping them 1 week in 1:4 HCl and another week in 1:4 HNO_3 and rinsing twice with water. Dilute reagents of 2.5 M HNO_3 and 2.0 M NH_4OH were prepared by dilutions of concentrated solutions. They were prepared in polypropylene volumetric flasks and transferred and stored in FEP Teflon bottles. Ammonium acetate buffers, 1 and 8 M, were prepared by mixing known volumes of glacial acetic acid and saturated NH_4OH and diluting them to appropriate volumes. The acidity of the buffers was adjusted to pH 5.1–5.4 by slow addition of NH_4OH or CH_3COOH.

The Chelex-100 separation scheme was performed in a Class 100 clean room. About 400 mg of dried Chelex-100 was mixed with 10 mL of water and the slurry transferred into a plastic column. After the water level dropped to the top of the resin, three 5-mL portions of 2.5 M HNO_3 were added to the column to elute trace elements from the resin. The resin was washed with two 5-mL portions of water to remove excess acid and converted to NH_4^+ form by addition of two 5-mL portions of 2.0 M NH_4OH. After the last few drops were checked for basicity, the residual NH_4OH was removed with two 5-mL portions of water. The NH_4^+ form of Chelex-100 is more effective than the H^+ form in retaining the transition-metal elements.

Digested plasma, RBC, fecal samples, and 10-mL urine subsamples were transferred into Teflon beakers with 10-mL water rinses. Acidity was adjusted to pH 5.2–5.7 by slow addition of 2.0 M NH_4OH to maximize transition-metal binding and minimize binding of alkali metals and alkaline earths. A few drops of 8 M NH_4COOCH_3 were added to buffer the system. A small volume of sample solution was poured into the column and more solution added after the Chelex completed its shrinkage. After the sample had passed through the resin, the resin was washed with two 5-mL portions of water. Then alkali and alkaline-earth elements were removed by washing the resin with five 10-mL portions of 1.0 M NH_4COOCH_3 solution.

The resin was dried at 50 °C in the plastic columns in an oven in the clean room. The resin shrinks upon drying and becomes about a 1-cm-long solid mass, which can easily be transferred to a polybag. The polybag was heat-sealed and placed inside another bag, and all samples were assayed for ^{65}Zn activity. The comparison of this assay with the one obtained before Chelex separation gives the chemical yield, *Y*.

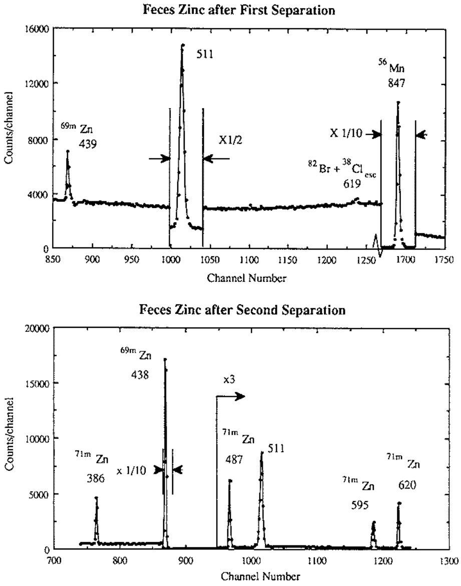

Figure 1. Portion of γ-ray spectrum of freeze-dried, Chelex-separated feces, observed on the irradiated resin for (top) 23 min after 1-h neutron irradiation and 2-h cooling and (bottom) 1 h after 1-h irradiation and postirradiation chemistry.

Irradiation. Urine, plasma, and RBC samples were irradiated 3 h and feces samples (which contained more Zn) for only 0.5–1 h at a flux of 5×10^{13} n/(cm^2 s). Usually six samples of plasma, urine, or cells or 8–10 fecal samples were irradiated together with two Zn standards and two Co-flux monitors in the same plastic pneumatic tube sample carrier ("rabbit").

Postirradiation Separation. The Chelex procedure removes many activities with very large decontamination factors, including alkali metals; however, Mn and Cu remain on the resin, and they have more favorable activation properties than Zn does (Table I) and must be removed by postirradiation separation to observe the three Zn isotopes clearly.

After irradiated samples decayed for about 30 min, bags were changed and γ-ray spectra were collected at 20–25 cm from the detectors (count 1). As the samples contained high levels of interfering activities, it was not possible to collect the γ-ray spectra with the samples closer to the detectors. Counting time was 30 min for fecal samples and 3 h for other matrices. The only Zn line observable in this count was the 438-keV γ-ray of ^{69m}Zn. The magnitude of its peak area relative to that of the same line in a Zn standard irradiated simultaneously with the sample was used to determine the mass of Zn on the resin, T.

As Chelex resin becomes hard upon drying after the first separation, it was crushed inside of the bag and transferred to a beaker to which 5 mL of 2.5 M HNO_3 was added. The slurry was then poured into a polypropylene column. After the resin settled and the level of solution dropped to the top of it, three 5-mL portions of 2.5 M HNO_3 were added. The eluent was collected in a large test tube containing 10 mg of Mn and 1 mg each of Zn and Cu carriers and about 100 mg of $KBrO_3$ as an oxidant. The tube was heated over a Bunsen burner with swirling until a dark brown MnO_2 precipitate formed (*35*). The test tube was centrifuged and the solution transferred into a clean tube. The Mn precipitation was repeated by addition of 10 mg of Mn carrier and 100 mg of $KBrO_3$ to remove remaining Mn.

Copper was also eluted with Zn and Mn from the resin with 2.5 M HNO_3. Copper-64 has two γ-rays, a weak one at 1346 keV and strong annihilation radiation at 511 keV (*13*). The former was not observable in the presence of 1811-keV γ-rays of ^{56}Mn. Originally, we thought that ^{24}Na was responsible for the peak at 511 keV, but removal of ^{24}Na did not remove the 511-keV peak, so we suspected Cu.

Copper was removed by dithizone extraction (*36*). Although extraction with dithizone might carry some Zn, extraction at pH 1 was suggested to eliminate Cu interference from Zn (*37*). After MnO_2 was precipitated twice, the acidity of the solution was adjusted to pH ≤ 1 with concentrated HNO_3. Then the solution was transferred into a 125-mL separatory funnel, and 30 mL of 1% dithizone in $CHCl_3$ was added. The separatory funnel was shaken for 2 or 3 min and the $CHCl_3$ layer discarded. The remaining solution was made basic by addition of 5 mL of concentrated NH_4OH. The contents of the funnel were mixed, and Zn was extracted by addition of 0.2% dithizone in $CHCl_3$. Two 30-mL portions of the reagent were usually sufficient to obtain a green endpoint of extraction. The $CHCl_3$ phase was transferred into a clean separatory funnel, and Zn was back-extracted into 30 mL of 1.0 M H_2SO_4 solution.

To avoid spectrometry of a large liquid volume, the Zn was precipitated as $ZnHg(SCN)_4$ (*37*). One milliliter of Zn carrier (10 mg of Zn/mL) was added to the back-extracted solution (30 mL of 1.0 M H_2SO_4) that contained Zn, and 5 mL of NH_4SCN–$HgCl_2$ reagent was added. The reagent was prepared by dissolving 64 g of NH_4SCN and 54 g of $HgCl_2$ in 1 L of H_2O and filtering any precipitate formed. After addition of reagent, the solution was cooled under running water and stirred with a glass rod. The precipitate was filtered on a 2.4-cm-diameter Whatman glass-fiber filter.

The filter was sealed in a polybag, and the γ-ray spectrum was collected at 3–5 cm from the detector (count 2). All γ-rays of the three Zn isotopes were observed during this count. Portions of the spectra of the same fecal sample obtained after irradiation following Chelex separation and after postirradiation removal of Mn and Cu are shown in Figure 1.

After spectra of the samples were collected, those of the standards were taken for 0.5–1 h at 3–5 cm from the detectors (same positions as in count 2 above). Spectra were stored on disks and later analyzed with a program that allowed peak fitting to be done manually. The program fitted peaks produced by the species of interest (^{24}Na, ^{38}Cl, ^{56}Mn, ^{64}Cu, ^{82}Br, ^{65}Zn, ^{69m}Zn, and ^{71m}Zn). Each peak was displayed on the cathode-ray tube with 25 channels on both sides of the peak. The net peak area was found by subtracting the background counts from the total area. The program performed decay corrections and compared the decay-corrected count rates with corresponding count rates of the standards.

Blanks. Zinc concentrations in materials were measured by instrumental neutron activation analysis (INAA) to determine the blank levels. Where feasible, e.g., plastic bags irradiated with samples, blank levels were subtracted from total Zn values to obtain net values for the samples. The total procedure blank was determined by running ultrapure or Chelex-cleaned water through the entire procedure and activating the Chelex resin. In the case of blood samples, saline solution was used to simulate blood and put through the procedure, including drawing it through the same type of needles as those use for blood collection. The procedure blank was about 0.12 μg of Zn except for blood samples. For the latter, the sodium citrate anticoagulant adds 0.02–0.08 μg of Zn for 0.1–0.4 mL of the solution added, raising the total blank to 0.14–0.20 μg. The use of the stainless steel needle caused no significant increase in the Zn blank levels.

Observation of Stable Tracer. The objective of the experiments is that of determining the fraction, F, of the stable tracer present in each of the pools under study. From the spectra such as that shown in the lower panel of Figure 1, we obtain the areas of peaks of γ-rays from the three Zn isotopes for the samples and a normal Zn standard irradiated simultaneously. From ratios of the appropriate peak areas in the sample and standard spectra, corrected for decay between counting periods, we obtain the enrichment factor of the enriched isotope with respect to nonenriched isotopes, ^{64}Zn or ^{68}Zn:

$$\mathrm{EF}_{68} = (^{70}\mathrm{Zn}/^{68}\mathrm{Zn})_{\mathrm{spl}}/(^{70}\mathrm{Zn}/^{68}\mathrm{Zn})_{\mathrm{std}} \qquad (1)$$

with a similar relationship for ^{64}Zn. To a good approximation, the EF value for a sample is given by

$$\mathrm{EF}_{68} = 1 + (FnA_{70}^{*})/(PA_{70}) \qquad (2)$$

Table II. Comparison of Zinc Concentrations in Various Biological Matrices As Measured by NAA and AAS

			Zn concentration, μg/mL		
sample type	subject[a]	yield, %	NAA[b]	AAS[b]	literature
plasma	CL (9)	74 ± 5	1.13 ± 0.23	0.89 ± 0.13	0.8–1.1[c,d]
	BE (9)	73 ± 11	0.93 ± 0.08	0.86 ± 0.04	0.86–1.16[d,e]
	JN (9)	97 ± 4	0.80 ± 0.28	0.71 ± 0.06	
	ZC (7)	97 ± 5	0.66 ± 0.10	0.76 ± 0.06	
RBC	CL (9)	85 ± 20	10.5 ± 2.3		9.2–12.8[d,e]
	BE (6)	68 ± 31	10.8 ± 2.1		11.5[f]
	JN (7)	90 ± 8	9.2 ± 2.3		
	ZC (8)	91 ± 10	10.9 ± 2.0		
urine	CL (7)	78 ± 15	0.39 ± 0.16	0.31 ± 0.05	0.4–0.6[c]
	BE (7)	70 ± 13	1.05 ± 0.41	0.89 ± 0.17	0.33–0.66[c,e]
	JN (7)	75 ± 17	0.23 ± 0.05	0.28 ± 0.06	
	ZC (7)	79 ± 15	0.18 ± 0.16	0.16 ± 0.05	

			Zn concentration, μg/g		
sample type	subject	yield, %	NAA[b]	AAS[b]	literature
feces	CL (7)	94 ± 6	0.51 ± 0.09		0.45[g]
	BE (6)	94 ± 5	0.54 ± 0.07		
	JN (5)	95 ± 3	0.45 ± 0.20		
	ZC (5)	93 ± 4	0.60 ± 0.06		

[a] Subjects CL and BE are males and JN and ZC are females. Numbers in parentheses are the numbers of samples. [b] Zinc concentrations are given as the average of the number of samples analyzed plus or minus the standard deviation for both techniques. Only Zn concentrations for 24-h urine samples are given in the table. [c] Reference 38. [d] The interval represents a range of means from many studies. [e] Reference 39. [f] Reference 40. [g] Reference 41.

Table III. Total Daily Zinc Excreted via Urine and Feces

		Zn, mg/day		
pool	subject	NAA	AAS	literature
urine[a]	CL	0.47 ± 0.14	0.46 ± 0.08	0.04–1.25[b,c]
	BE	1.18 ± 0.48	0.88 ± 0.18	0.33–0.66[c,d]
	JN	0.26 ± 0.04	0.28 ± 0.04	0.45[e]
	ZC	0.33 ± 0.08	0.39 ± 0.12	
feces	CL	13.4 ± 2.6		10–15[c,f]
	BE	14.1 ± 2.9		8–12[e]
	JN	11.2 ± 6.3		
	ZC[g]	23.3 ± 11.9		

[a] Only 24-h urine results are used. [b] Reference 42. [c] Ranges of mean values from various large studies. [d] Reference 39. Calculated from Zn concentrations in urine assuming the average person excretes 1.2 L daily of specific gravity 1.015. [e] Reference 38. Typical averages for Western populations. [f] Reference 43. [g] Subject ZC was taking a 15-mg Zn supplement daily.

where A_{70} and $A_{70}{}^*$ are the isotopic abundances in natural Zn and of Zn enriched in ^{70}Zn, respectively; n is the mass of Zn tracer administered; and P is the mass of Zn in the pool in question. (The simple equations ignore ^{70}Zn contributed by natural zinc and the fact that the chemical atomic mass of the enriched Zn is about 5% greater than that of normal Zn. The P and F values were calculated by using the rigorous equations.) Rearrangement of eq 2 yields F:

$$F\ (\%) = 100(\mathrm{EF} - 1)PA_{70}/nA_{70}{}^* \qquad (3)$$

Inserting the values $A_{70} = 0.62\%$ and $A_{70}{}^* = 65.5\%$ and $n = 1.99$ mg, we obtain the equation specific to our experimental design:

$$F\ (\%) = 0.476(\mathrm{EF} - 1)P \qquad (4)$$

The mass of Zn (in milligrams) in the pool, P, is given by

$$P = 1000TM/(mY) \qquad (5)$$

where T is the mass of Zn on the Chelex resin after irradiation (in micrograms), as determined from the ^{69m}Zn in count 1, M is the total mass (or volume) of the pool, m is the mass (or volume) of the sample taken for analysis, and Y is the chemical yield of the preirradiation chemistry. For feces and urine, M is the total sample collected and m is that of the subsample analyzed. For blood samples, M was calculated by using the body hematocrit. Zinc concentrations were measured in all types of samples by neutron activation analysis (NAA) and, independently, in plasma and urine, via AAS. Note that the measurement of F requires two independent measurements: the value of EF from the ratios of peak areas in spectra displaying γ-rays of irradiation products of the three Zn isotopes (or which could be obtained from mass spectra of the stable isotopes) relative to the same ratios for natural Zn and the total Zn in the subsample of the pool, which can be measured by NAA, AAS, or any other appropriate chemical method. The chemical yield of the postirradiation separation does not enter into the calculation of F, but it influences the counting rates and, thus, the statistical uncertainties of peak areas in the spectra collected to determine the EF values (count 2). Yields for postirradiation chemistry averaged about 70%, as determined from the ^{69m}Zn count rates in count 1 and count 2 after correction for the different geometries with the Zn standard irradiated with the sample.

RESULTS

Results of the chemical analyses of the four types of samples in the four subjects are listed in Table II. For the samples analyzed by both AAS and INAA, there is good agreement of results between methods (as shown by paired t-tests) except for urine samples for subject BE. There is also good agreement with Zn concentrations from the literature. Our values tend to be toward the low end of the ranges from the literature, as expected, as the literature includes older measurements that may not have excluded contamination as well as those in recent studies.

In Table III we list the average amounts of Zn excreted per day in urine and feces for each subject, calculated from the concentrations in Table II and the masses of urine and feces collected per day. There was considerable fluctuation from sample to sample. With the possible exception of subject BE, the daily values for Zn via urine are within the ranges of previous values. The amount of Zn excreted via feces is almost constant for subjects CL and BE, but large fluctuations are observed for subjects JN and ZC. One reason for this fluctuation is unavailability of daily feces samples. Except for subject ZC, who was taking 15-mg Zn supplements daily, the total fecal Zn amounts are comparable with literature values.

In Table IV, we have summarized the major sources of errors in the determination of the fraction F of tracer Zn appearing in the various fractions. Note that there are two

Table IV. Major Sources of Error in Determination of Fractions of Enriched ^{70}Zn in Body Pools

pool	av mass of Zn on resin (T), μg	av error in T, %	av error in yield, %	av Zn in pool (P), mg	expected error in P, %	av EF	av error in EF, %	error in F at half max, %	
								^{70}Zn	^{65}Zn
plasma	1.6	12	18	2.8	24	2.29	9	18	10
RBC	7.6	5	14	23	20	1.29	4.5	23	10
urine	3.4	8	17	0.5/day	19	1.61	6	18	8
feces	79	3.4	3	18/day	6	1.78	6.6	14	7

distinct parts to the measurement of F, the mass of Zn in the pool, P, and the enrichment factor, EF, of the enriched isotope relative to the nonenriched isotopes. The major contributions to the error in P over which we have control are the uncertainties in the yield, Y, the average error ranging from 19% for urine to 3% for feces, and in the determination of Zn on the Chelex resin. There was considerable redundancy in the experiments, because we could observe irradiation products of three isotopes of Zn, whereas only two are required for observation of the enrichment. As count rates of ^{69m}Zn 438-keV γ-rays in the final spectra were much greater than those of the ^{65}Zn 1115-keV γ-rays, the former yielded greater accuracy, so all EF values quoted in the tables are based on ^{69m}Zn rates. The EF values based on ^{65}Zn count rates generally agreed with those based on ^{69m}Zn, but uncertainties of the latter are much smaller.

An uncertainty over which we had no control was that of total blood volumes, which were calculated from the subjects' body weights as V (mL) = 71.4 × body weight (kg) for males and 65.0 × body weight (kg) for females (*14*). The calculated blood volumes were divided into RBC and plasma by using the body hematocrits (packed cell volumes) obtained from the measured hematocrits multiplied by a factor of 0.874 to correct for trapped plasma and the lower hematocrits of small vessels from which the blood was collected (*17*). Obviously it would have been preferable to have obtained experimental values of the blood volumes, but that was not possible along with the many other measurements being done. We have arbitrarily assigned errors of 10% to the total volumes of the RBC and plasma pools.

If one ignores small errors in the terms included in the constant, 0.476, in eq 4, the expected error in F is given by

$$(\sigma_F/F)^2 = \{(\sigma_P/P)^2 + [\sigma_{\mathrm{EF}}/(\mathrm{EF} - 1)]^2\}^{1/2} \tag{6}$$

Thus, errors in P contribute in the usual way, but those in EF are greatly magnified by (EF − 1) in the denominator when EF is only slightly greater than unity. In Table IV are listed average EF values over all samples of each kind collected, which show why errors are often large when averaged over all samples collected. The average error in F over all samples is almost meaningless because the error is infinite when no tracer is present, i.e., EF = 1.00, but drops sharply with increasing F, asymptotically approaching a constant value. Thus, in Table IV, we have listed the percent error in F at half of the maximum F value for the particular pool, which is a representative value, for both the stable and the radioactive tracer. The accuracy for the radioactive tracer is better than for the stable tracer, as the former is determined almost entirely by counting statistics in the samples from the various pools.

Measurements of F in each pool present unique problems, as illustrated by the plots of F vs time for subject JN in Figure 2. Zinc in plasma rises quickly to a maximum of F = 4–6% at about 2 h and quickly falls to ~1% or less by a few hours later. The Zn concentration is quite low and the sample size is limited, so errors in both P and EF are often large. On the other hand, the average EF is the highest among the pools investigated (see Table IV), which tends to reduce the errors. The Zn concentration in RBC is about 10-fold greater and F is much greater after a few hours, but greater normal concentrations of Zn in RBC cause the EF values to be generally lower than for plasma, thus magnifying the contribution of errors in EF to those of F, the result being that overall expected errors for RBC are somewhat greater than those for plasma. Because of the much greater concentration of Zn and the generally greater F values for RBC, plasma must not be contaminated by RBC. This was not a problem in the samples reported, as the standard deviations of Zn concentrations in plasma from three of the four subjects were less than the expected error of measurement. One plasma sample from JN yielded a Zn concentration about twice as great as the average for the subject, suggesting possible contamination.

Quantities of urine samples are virtually unlimited, but the Zn concentration is low and little of the tracer appears in the pool. The easiest pool for these experiments is feces, as the sample size is unlimited and major portions of the tracer are present in it, much of it being unabsorbed Zn. The errors are rather high because the large natural concentration of Zn in feces causes the EF to be rather low except when the large pulse of mostly unabsorbed Zn tracer is present.

Procedure blanks for all samples are about 0.12 μg, with an additional 0.02–0.08 μg for blood samples, depending on the amount of sodium citrate used as the anticoagulant. Appropriate blank values were subtracted prior to calculation of Zn concentrations and total masses of Zn in the pools. It was not necessary to correct EF values for the blanks, as the values are insensitive to blanks that, being natural Zn, contain very little ^{70}Zn.

The objective of the experiment was the validation of stable isotope tracing of Zn in human nutrition studies by comparison with results of simultaneous tracing with in vivo radioactive ^{65}Zn, as shown for subject JN in Figure 2. Paired t-tests of ^{65}Zn and ^{70}Zn data of all tissues of each subject showed no significant differences between the tracers except for fecal data of one subject (CL, $p < 0.05$). Detailed kinetic analyses of the tracer data of the four subjects are given in ref 44.

DISCUSSION

The radiochemical procedure developed allowed us to observe γ-ray spectra of irradiation products of ^{64}Zn, ^{68}Zn, and ^{70}Zn free of serious contamination soon enough after irradiation to obtain good statistics for the peak areas needed to calculate the enrichment factors of ratios of ^{70}Zn/^{68}Zn and ^{70}Zn/^{64}Zn relative to those of natural Zn. Furthermore, within the limits of error of results based on the stable and radioactive Zn tracers, the use of Zn stable isotope tracers was verified for four subjects. An important aspect of the design of the experiment was the fact that the ^{65}Zn activity of the in vivo tracer was low enough in samples collected that it did not interfere with determination of ^{64}Zn levels in the samples via the ^{64}Zn(n,γ)^{65}Zn reaction. This allowed us to validate the stable isotope method against the radioactive tracer *in the same subjects at the same time*, eliminating uncertainties that would have arisen had the stable and radioactive tracer experiments been done at different times.

The experimental design could be improved. The largest uncertainties in determining masses of Zn in the pools are those of the chemical yield, which arises from the use of in

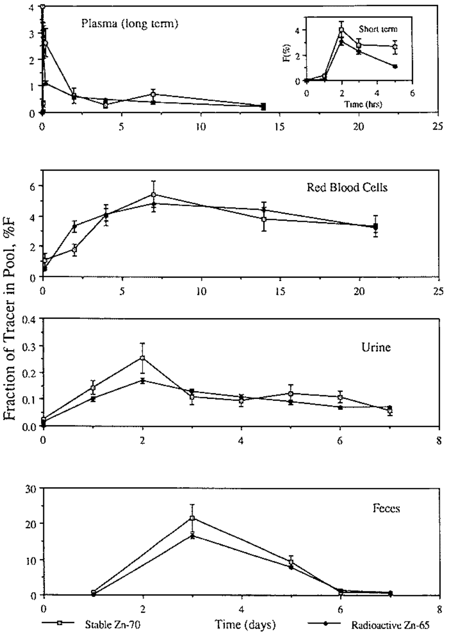

Figure 2. Fraction of the ^{65}Zn and ^{70}Zn tracers appearing in the four pools vs time. The data are those for subject JN. Closed circles represent the data obtained with ^{65}Zn and open circles are those from the ^{70}Zn tracer. Note that different time scales are used for the various pools. Uncertainties represent expected standard deviations from analysis of errors in the various steps of the experiments.

vivo ^{65}Zn tracer to determine the yield. The low activity of ^{65}Zn in samples taken from the body caused large statistical errors in the count rate of the 1115-keV γ-ray peak in the spectra. One cannot increase the exposure of subjects to ^{65}Zn radiations just to improve the accuracy of yield determinations. The determination of the mass of Zn on the Chelex resin has large uncertainity because of the high activity from contaminants on the irradiated resin, which makes it necessary to place the sample far from the detector for the initial count.

As determination of the fraction of the tracer, F, in each pool is separable into the determination of the mass of Zn in the pool, P, and that of the enrichment factor, EF, of the enriched isotope, Zn in the pool could be determined either chemically, e.g., by AAS, or by activation of a portion of each sample separately from the determination of EF. As activation analysis could be done using long-lived ^{65}Zn, no chemical separation would be needed, as one could wait for interfering radiations to decay before taking spectra. This would eliminate substantial errors in chemical yields and greatly reduce the error in P resulting from errors in T.

The other problem in our experiments, which caused a loss of some samples, was the unreliability of sodium citrate as an anticoagulant. As blanks caused by Zn of natural isotopic abundances introduce very little of the enriched isotope, one can use heparin. Various commercial heparins differ greatly in their Zn levels, so one has to test various supplies to find those of acceptably low Zn levels, which we have since identified.

ACKNOWLEDGMENT

We thank the subjects for their cooperation, without which this work could not have been done. We gratefully acknowledge the help of the staff of the National Institute of Standards and Technology reactor facility during irradiations, and Roger Aamodt and Warren Rumble of the National Institutes of Health for help with in vivo radiation counting. We thank Sally Harrison for her advice on treatment of the experimental data.

LITERATURE CITED

(1) Prasad, A. S. *Nutr. Today* **1981**, March/April, 4–11.
(2) Foster, D. M.; Aamodt, R. L.; Henkin, R. I.; Berman, M. *Am. J. Physiol.* **1979**, *237*, R340–R349.
(3) Babcock, A. K.; Henkin, R. I.; Aamodt, R. L.; Foster, D. M.; Berman, M. *Metabolism* **1982**, *31*, 335–347.
(4) Wastney, M. E.; Aamodt, R. L.; Rumble, W. F.; Henkin, R. I. *Am. J. Physiol.* **1986**, *251*, R398–R408.
(5) Gordon, G. E.; Gökmen, İ. G.; Aras, N. K.; Henkin, R. I. *J. Radioanal. Chem.* **1982**, *70*, 146–161.
(6) Janghorbani, M. T.; Ting, B. T. G.; Istfan, N. W.; Young, V. R. *Am. J. Clin. Nutr.* **1981**, *34*, 581–591.
(7) Janghorbani, M. T.; Young, V. R. *Am. J. Clin. Nutr.* **1980**, *33*, 2021–2030.
(8) Ehrenkranz, R. A.; Ackerman, B. A.; Nelli, C. M.; Janghorbani, M. T. *Am. J. Clin. Nutr.* **1984**, *40*, 72–81.
(9) Janghorbani, M. T.; Young, V. R.; Gramlich, J. W.; Machian, L. A. *Clin. Chim. Acta* **1981**, *114*, 163–171.
(10) Jackson, M. J.; Giugliano, R.; Oliveira, E. F.; Shrimpton, R.; Swainbank, I. G. *Brit. J. Nutr.* **1988**, *59*, 193–203.
(11) Turnland, J. R. *Biol. Trace Elem. Res.* **1987**, *12*, 247–257.
(12) Gökmen, İ. G.; Gordon, G. E.; Aras, N. K. *J. Radioanal. Chem.* **1987**, *113*, 453–459.
(13) Lederer, C. M.; Shirley, V. S.; Browne, E.; Dairiki, J. M.; Doebler, R. E. *Table of Isotopes*, 7th ed.; Wiley-Interscience: New York, 1978.
(14) Stable Isotope Certificates; Oak Ridge National Laboratory, Oak Ridge, TN, 1981.
(15) National Bureau of Standards Certificate of Analysis, Standard Reference Material SRM 4216E, 1977.
(16) Aamodt, R. L.; Rumble, W. F.; Johnston, G. S.; Markley, E. J.; Henkin, R. I. *Am. J. Clin. Nutr.* **1981**, *34*, 2648–2652.
(17) Aamodt, R. L.; Rumble, W. F.; Babcock, A. K.; Foster, D. M.; Henkin, R. I. *Metabolism* **1982**, *31*, 326–334.
(18) Aamodt, R. L.; Rumble, W. F.; Johnston, G. S.; Foster, D. M.; Henkin, R. I. *Am. J. Clin. Nutr.* **1979**, *32*, 559–569.
(19) *Acid Digestion Bombs Bulletin 4745*; Parr Instrument Co., 1981.
(20) Zeisler, R.; Langland, J. K.; Harrison, S. H. *Anal. Chem.* **1983**, *55*, 2431–2434.
(21) Riley, J. P.; Taylor, D. *Anal. Chim. Acta* **1968**, *40*, 479–485.
(22) Leyden, D. E.; Patterson, T. A.; Alberts, J. J. *Anal. Chem.* **1975**, *47*, 733–735.
(23) Riley, J. P.; Shirrow, G. *Chemical Oceanography*; Academic Press: New York, 1975; Vol. 1, 2.
(24) Bruland, K. W.; Franks, R. P.; Knauer, G. A.; Martin, J. H. *Anal. Chim. Acta* **1979**, *105*, 233–245.
(25) Lee, C.; Kim, N. B.; Lee, I. C.; Chung, K. S. *Talanta* **1977**, *24*, 241–245.
(26) Kingston, H. M.; Barnes, I. L.; Brady, T. J.; Rains, T. C.; Champ, M. A. *Anal. Chem.* **1978**, *50*, 2064–2070.
(27) Kingston, H. M. "Interagency Energy-Environment R&D Program Report"; U.S. Environmental Protection Agency Report EPA-600/7-79-174, 1979.
(28) Greenberg, R. R.; Kingston, H. M. *J. Radioanal. Chem.* **1982**, *71*, 147–167.
(29) Greenberg, R. R.; Kingston, H. M. *Anal. Chem.* **1983**, *55*, 1160–1165.
(30) Agarwal, M.; Bennett, R. B.; Stumpf, I. G.; D'Auria, J. M. *Anal. Chem.* **1975**, *47*, 924–927.
(31) Kingston, H. M.; Pella, P. A. *Anal. Chem.* **1981**, *53*, 223–227.
(32) Gökmen, İ. G.; Aras, N. K.; Gordon, G. E.; Henkin, R. I. In *Trace Element Analytical Chemistry in Medicine and Biology*; Bratter, P., Schramel, P., Eds.; Walter deGruyter: Berlin, 1984; Vol. 3, pp 513–519.
(33) Kuehner, E. C.; Alvarez, R.; Paulsen, P. J.; Murphy, T. J. *Anal. Chem.* **1972**, *44*, 2050–2056.
(34) Moody, J. R. National Bureau of Standards, personal communication, 1982.
(35) *Radiochemistry of Manganese*; Schuman, R. P., Ed.; National Academy of Sciences/National Research Council, Nuclear Science Series, NAS-NS-3018, 1971.
(36) Dyer, F. F.; Ledicotte, G. W. *Radiochemistry of Copper*; National Academy of Sciences/National Research Council, Nuclear Science Series, NAS-NS-3027, 1961.
(37) *Radiochemistry of Zinc*; Hicks, H. G., Ed.; National Academy of Sciences/National Research Council, Nuclear Science Series, NAS-NS-3015, 1960.
(38) Iyengar, G. V. *Biol. Trace Elem. Res.* **1987**, *12*, 263–295.
(39) Versieck, J. *Trace Elements in Human Body Fluids and Tissues*. In *CRC Crit. Rev. Clin. Lab. Sci.* **1985**, *22*, 97–184.
(40) Iyengar, V.; Woittiez, J. *Clin. Chem.* **1988**, *34*, 474–481.
(41) Snyder, W. S., et al. "Report of the Task Group on the Reference Man"; International Committee on Radiation Protection Publication No. 23, 1975.
(42) Iyengar, G. V.; Kollmer, W. E.; Bowen, H. J. M. *The Elemental Composition of Human Tissues and Body Fluids*; Verlag Chemie: Weinheim, FRG, 1978.
(43) National Research Council, National Academy of Sciences, Subcommittee on Zinc. *Zinc*; University Park Press: Baltimore, MD, 1979.

(44) Wastney, M. E.; Gökmen, İ. G.; Aamodt, R. L.; Rumble, W. F.; Henkin, R. I.; Gordon, G. E., submitted for publication in *Am. J. Physiol.*

RECEIVED for review July 17, 1989. Accepted September 14, 1989. This work was supported in part by the U.S. Department of Agriculture's Human Nutrition Program under Grant No. 59-2241-0-1-472-0. Portions of the work reported here were included in the Ph.D. dissertation of İ. G. Gökmen, submitted in partial fulfillment of requirements for the Ph.D. degree at the University of Maryland, College Park.

Observation of Kinetic Heterogeneity on Highly Ordered Pyrolytic Graphite Using Electrogenerated Chemiluminescence

Robert J. Bowling and Richard L. McCreery*

Department of Chemistry, Ohio State University, Columbus, Ohio 43210

Christine M. Pharr and Royce C. Engstrom*

Department of Chemistry, University of South Dakota, Vermillion, South Dakota 57069

Kinetic heterogeneity on highly ordered pyrolytic graphite (HOPG) electrodes was characterized by using electrogenerated chemiluminescence imaging. The reaction of luminol in alkaline peroxide was used with a sensitive microscope-based imaging system to monitor the course of electron transfer at various regions on the HOPG surface. The ability to image with temporal resolution provided for the construction of local voltammograms, so that estimates of kinetic differences between basal plane and defect-rich HOPG could be obtained. Electrochemical pretreatment of basal plane HOPG produced a surface electrochemically similar to a defect-rich surface.

INTRODUCTION

The complex surface structure of glassy carbon (GC) electrodes has resulted in numerous attempts to understand its relationship to heterogeneous electron transfer. A variety of analytical techniques has been used to characterize carbon electrode surfaces, often accompanied by pretreatment procedures designed to generate reproducible electrochemical behavior. Attempts have been made to correlate the existence of catalytic moieties such as oxygen functional groups or the effects of surface cleaning with the observed electron transfer rate (*1–13*). Unfortunately, it is difficult to deconvolute the effects of surface cleanliness, electrocatalytic functional groups, and carbon microstructure on $k°$ for a given redox system. For example, the dependence of electroactivity on surface oxygen content remains unclear. X-ray photoelectron spectroscopy (XPS) on polished GC showed an increase in the oxygen to carbon ratio (O/C) from 0.084 to 0.22 upon electrochemical activation (*11*). An increase in O/C to 0.221 upon oxygen plasma activation has also been reported (*13*) for GC. However, vacuum heat treatment (*8*) and intense laser pulses (*3–5*) reduce the surface oxygen content to 0.06 and 0.04, respectively, while activating the electrode toward electron transfer. While it is likely that surface oxygen may have an important role in the electroactivity of certain specific redox system such as hydrazine (*10*), it is difficult to assess its importance until better ways of controlling the other aforementioned variables are devised.

This work is an attempt to understand the role of carbon microstructure on the heterogeneous electron transfer kinetics at highly ordered pyrolytic graphite (HOPG). The advantage of using HOPG as an electrode for this work is its atomically clean surface as measured by scanning tunneling microscopy (*14*) and XPS (*13*). HOPG also has a well-defined layered structure with microcrystallite sizes on the order of 1 or 2 μm (*15*), making it well-suited for studies of heterogeneous electron transfer at edge versus basal plane carbon. Previous reports on HOPG have shown that increases in $k°$ for ferrocyanide and dopamine correlate with an increase in edge-plane carbon as measured by Raman spectroscopy (*16–19*).

In this work, the technique of electrogenerated chemiluminescence (ECL) imaging has been used to characterize the HOPG surface. In ECL imaging, the light from an electrochemically initiated ECL reaction is collected and used as a representation of the local current density on an electrode surface. ECL imaging has previously been used to study the distribution of electrochemical activity on heterogeneous electrodes (*20, 21*) and to characterize nonuniform current density on disk electrodes due to diffusional mass transfer (*22, 23*). In the present work, the potential dependence of the ECL reaction of luminol in alkaline peroxide has been used to obtain microscopically local kinetic information on HOPG electrodes in an attempt to correlate the presence of edge plane carbon with heterogeneous electron transfer kinetics. An imaging system consisting of an optical microscope, a low-lag vidicon camera with a microchannel plate intensifier, and an image-processing computer was used to acquire ECL images with spatial resolution in the submicrometer range and temporal resolution of $^1/_{30}$th of a second. The temporal resolution allowed collection of light intensity from local regions of the electrode surface during the course of a potential scan, providing a correlation between electrochemical behavior and physical microstructure of the surface.

EXPERIMENTAL SECTION

Apparatus. The HOPG electrode was mounted in a holder as described previously (*16, 17*) and was placed on the stage of a Zeiss Standard 16 microscope (Thornwood, NY). The electrode surface was immersed in a solution containing 2 mM luminol, 5 mM hydrogen peroxide, and 0.5 M sodium borate, adjusted to pH 10.5 and placed with the surface facing upward for viewing through the microscope. A platinum wire auxiliary and a saturated calomel reference electrode were used. The microscope was operated with either a 25× or 63× Plan Neofluar objective and a 10× ocular.

The imaging system was a Hamamatsu Argus 100 video intensified microscopy system (Photonics Microscopy, Oak Brook, IL). The camera, consisting of a low-lag vidicon with a micro-

© 1989 American Chemical Society

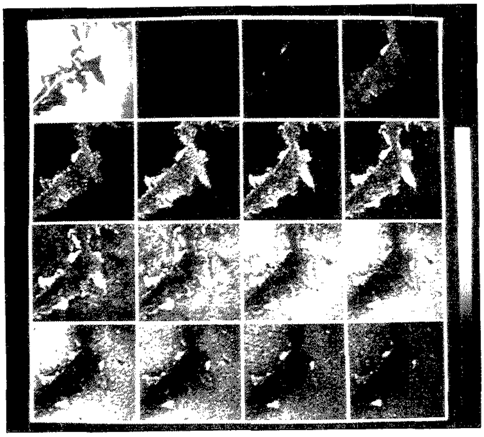

Figure 1. ECL images of scratched HOPG surface during a potential scan. First panel was taken with external illumination with no applied potential, showing the defect created by mechanical scratching. Remaining panels are ECL images collected at 50-mV increments, with panel 2 taken at 0.25 V. Each panel in the figure represents a viewing area 400 μm on a side. See text for details of solution conditions.

channel plate intensifier (*24*), was mounted on the microscope. The microscope and camera were housed in a dark-box which was in turn mounted on a vibrationally damped table (Newport Stabletop, Fountain Valley, CA). Signals from the camera were recorded by an image-processing computer, which displayed images on a monitor. Software treatment of the images will be described in the appropriate sections under Results and Discussion. Photographs shown in this paper were taken from the monitor screen with a 35-mm camera and Kodak Tri-max black and white film (Rochester, NY).

Reagents. Luminol (5-amino-2,3-dihydro-1,4-phthalazinedione) was obtained from Eastman Kodak (Rochester, NY). All other chemicals were reagent grade. Solutions were prepared in water purified on a Sybron Barnsted Nanopure system (Boston, MA). HOPG was a gift from Arthur Moore (Union Carbide, Parma, OH).

Procedure. A fresh basal plane surface of HOPG was exposed before each experiment by removal of the old surface with adhesive tape. Exposure of edge plane carbon was achieved by creating a defect in the basal plane surface with a razor edge, or with a clean, broken tip of a pasteur pipet. In those experiments involving electrochemical pretreatment (ECP), the electrode potential was held at 2.0 V in 0.1 M KNO_3 for specified periods of time, as described previously (*12, 13*) prior to obtaining ECL images.

RESULTS AND DISCUSSION

Electrochemical Activity of Defects. Previous Raman spectroscopic studies have indicated that electron transfer in the ferrocyanide and dopamine systems is facilitated at edge orientation relative to basal plane orientation (*16–18*). The importance of edge orientation to luminol electrochemistry was determined by deliberately creating defects in the basal plane structure through mechanically scratching its surface. The first panel in Figure 1 is an optical micrograph of the scratched region taken under external illumination at 63×. The dark, irregularly shaped feature is the scratch region, while the brighter, relatively homogeneous background is undisturbed basal plane. The remaining panels of Figure 1 represent a time-sequence of images captured during a potential-scan experiment in the presence of luminol. The potential scan was from 0.20 to 0.95 V at a rate of 50 mV/s. Images were captured at 1-s intervals, so each panel represents a 50-mV increment in applied potential. The results show clearly that the defect region generates ECL intensity at less positive potentials than the surrounding region, indicating that electron-transfer kinetics of the luminol system are substantially more favorable in the defect-rich region. The decay of current at potentials beyond the peak, as expected from classical potential sweep voltammetry, is observed by a decrease in light intensity at more positive potentials. Such a decay will be observed when the defect region is large relative to $(Dt)^{1/2}$.

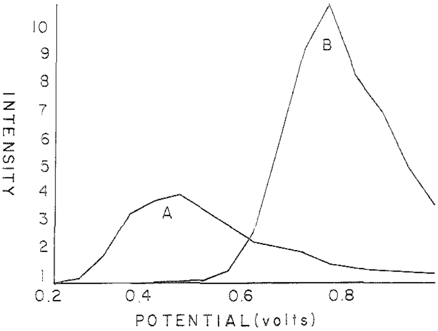

Figure 2. ECL intensity–potential profiles taken from Figure 1 from (a) the scratch region and (b) the undisturbed HOPG region. Scan rate was 10 mV/s.

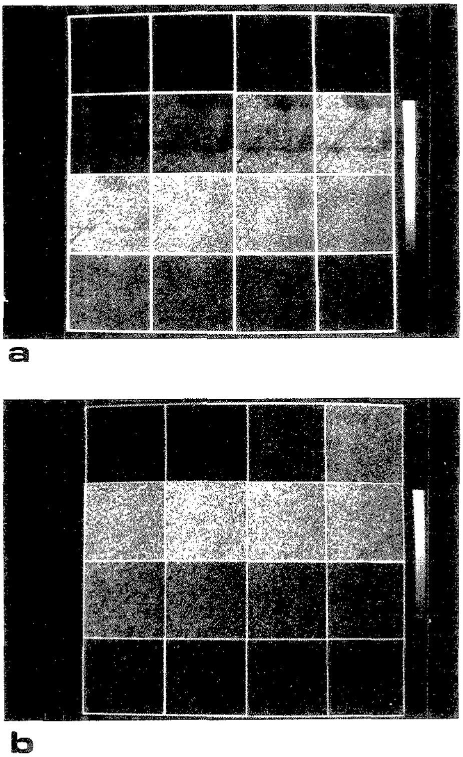

Figure 3. ECL images during a potential scan of (a) fresh HOPG surface and (b) HOPG surface after electrochemical pretreatment (see text for details). Conditions are given in Figure 1.

A more quantitative comparison of electron-transfer facility can be made by constructing ECL intensity–potential curves

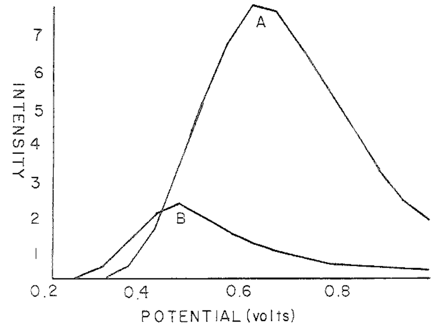

Figure 4. ECL intensity–potential profiles from Figure 3 of (a) the fresh surface and (b) the pretreated surface. Scan rate was 10 mV/s.

for the two regions. Such curves can be likened to a local voltammogram, since ECL intensity is proportional to local current density. Thus, local current–potential relationships can be obtained and related to local structural effects. A square area defined to be 10 μm on a side was selected both inside the scratch region and on the undisturbed surrounding region. The total intensity within the square regions was obtained from each ECL frame in Figure 1. Those intensities were plotted against applied potential in Figure 2. The current–potential curve for the scratch region peaks out at approximately 0.45 V whereas the surrounding basal plane peaks at approximately 0.78 V. The transfer coefficient for the luminol system has been estimated to be approximately 0.36 from previous work (*23, 25*). By use of that value and classical Butler–Volmer kinetics, the standard heterogeneous rate constant in the defect region is over 100 times that of the undisturbed basal plane. The decreased peak intensity within the defect region as compared to the surrounding undisturbed region may result from decreased mass transfer to the scratch, which lies below the level of the surrounding region.

Electrochemical Treatment of HOPG. A fresh surface of HOPG was subjected to electrochemical pretreatment by application of +2.0 V for 2 min, followed by −0.1 V for 30 s. Through the microscope, the surface was observed to undergo considerable cracking during both the positive and negative phases of the pretreatment. Time-sequenced ECL images taken at 50-mV increments during a potential scan of HOPG from 0.200 to 0.995 V before and after such treatments are shown in Figure 3. The intensity–potential behavior between 0.200 and 1.00 V is plotted in Figure 4, showing that the pretreated surface behaves similarly to the defect region described in the preceding section. The peak potential for the pretreated surface is 0.45 V, which is similar to that described above for the mechanical defect region.

It should be pointed out that while the intensity–potential profile of the pretreated surface shifts to less positive values, the absolute peak intensity on the pretreated surface is significantly lower than on either the undisturbed basal plane or the mechanical defect area. The decrease in intensity seems to become more severe the longer the electrode is made to undergo ECL. It is suspected that some specific interaction between luminol and the oxidized HOPG surface occurs, interfering with either the electron-transfer or the light-emitting mechanism of luminol. For example, electrochemical pretreatment of GC has been shown to produce a layer of graphite oxide (*26*) that could specifically interact with luminol.

Additional insight into the relationship between defects and electron-transfer kinetics can be found by high-resolution imaging of the pretreated surface. Figure 5A shows the pretreated surface under external illumination at 630×, making visible the details of the cracking referred to above. An ECL image of that same surface, taken at an applied potential of 0.35 V, is shown in Figure 5B. At that applied potential, which is on the rising portion of the luminol oxidation wave, subtle differences in electron-transfer kinetics should be most evident. The ECL image has undergone

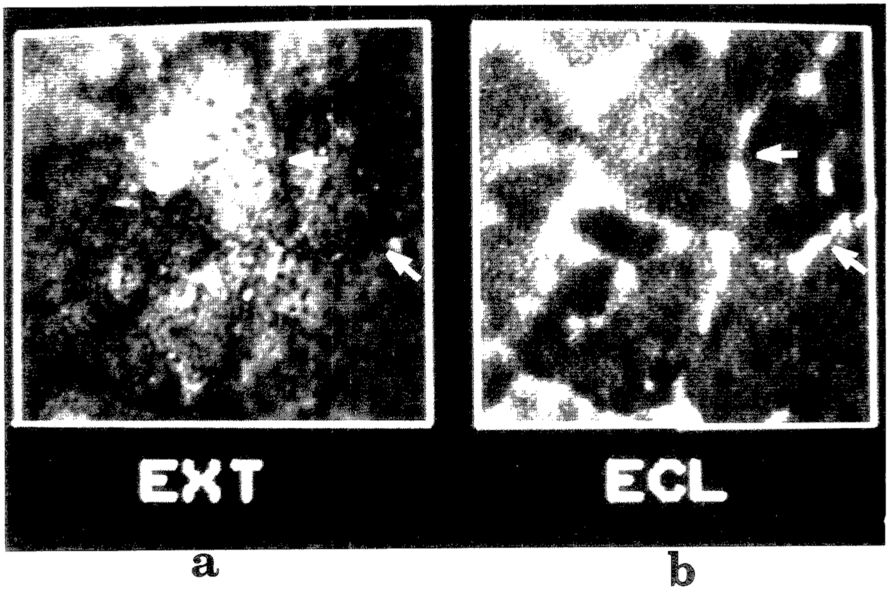

Figure 5. High magnification (630×) images of electrochemically pretreated HOPG shown (a) under external illumination and (b) undergoing ECL at 0.35 V. Each image represents a viewing area 160 μm on a side. Images have been contrast-enhanced (see text).

contrast enhancement through the application of a sigmoid-shaped look-up table, in which high-intensity regions are further intensified and low-intensity regions are deemphasized. The contrast enhancement makes it possible to observe a correlation between microscopic cracks and ECL intensity. For example, the arrows in Figure 5 point to cracks on the externally illuminated image and corresponding regions of high intensity on the ECL image.

CONCLUSION

Results presented here give direct evidence that the electron-transfer kinetics of luminol oxidation are enhanced at regions rich in defects over undisturbed basal plane HOPG. Quantitatively, the electron-transfer rate constant differs between the two regions by over 2 orders of magnitude. Electrochemical pretreatment produces a surface that is visibly rich in defects and that behaves electrochemically in a manner similar to a surface possessing obvious mechanical defects. The correlation between defects and electron transfer activity on electrochemically pretreated surfaces reinforces the conclusion that activation during oxidation/reduction pretreatment is due to fracturing of the graphite lattice and formation of edge plane defects, rather than being due to oxide formation (*18*). At least for the current case of luminol, it is unnecessary to invoke surface oxides to explain enhanced activity.

Registry No. KNO_3, 7757-79-1; graphite, 7782-42-5; luminol, 521-31-3.

LITERATURE CITED

(1) Evans, J. F.; Kuwana, T. *Anal. Chem.* **1977**, *49*, 1632.
(2) Elliot, C. M.; Murray, R. W. *Anal. Chem.* **1988**, *250*, 173.
(3) Stulik, K.; Brabcova, D. *J. Electroanal. Chem.* **1988**, *250*, 173.
(4) Poon, M.; McCreery, R. L. *Anal. Chem.* **1986**, *58*, 2745.
(5) Hershenhart, E.; McCreery, R. L.; Knight, R. D. *Anal. Chem.* **1979**, *51*, 358.
(6) Hu, I.-F.; Karweik, D. H.; Kuwana, T. *J. Electroanal. Chem.* **1985**, *188*, 59.
(7) Stutts, K. J.; Kovach, M.; Kuhr, W. G.; Wightman, R. M. *Anal. Chem.* **1983**, *55*, 1632.
(8) Fagan, D. T.; Hu, I.-F.; Kuwana, T. *Anal. Chem.* **1985**, *57*, 2759.
(9) Hu, I.-F.; Kuwana, T. *Anal. Chem.* **1986**, *58*, 3235.
(10) Engstrom, R. C. *Anal. Chem.* **1982**, *54*, 2310.
(11) Engstrom, R. C.; Strasser, V. A. *Anal. Chem.* **1984**, *56*, 136.
(12) Wang, J.; Hutchins, L. O. *Anal. Chim. Acta* **1985**, *167*, 325.
(13) Evans, J. F.; Kuwana, T. *Anal. Chem.* **1979**, *51*, 358.
(14) Park, S.; Quate, C. F. *Appl. Phys. Lett.* **1986**, *48*, 112.
(15) Koenig, J. L.; Tuinstra, F. *J. Chem. Phys.* **1970**, *53*, 1126.
(16) Bowling, R. J.; Packard, R. T.; McCreery, R. L. *J. Electrochem. Soc.* **1988**, *60*, 1459.
(17) Bowling, R. J.; Packard, R. T.; McCreery, R. L. *J. Am. Chem. Soc.* **1989**, *111*, 1217.
(18) Bowling, R. J.; Packard, R. T.; McCreery, R. L. *Langmuir* **1989**, *5*, 683.
(19) McQuillan, A. J.; Hester, R. F. *J. Raman Spectrosc.* **1984**, *15*, 1, 15.
(20) Engstrom, R. C.; Johnson, K. W.; DesJarlais, S. *Anal. Chem.* **1987**, *59*, 670.
(21) Petersen, S. L.; Weisshaar, D. E.; Tallman, D. E.; Schulze, R. K.; Evans, J. F.; DesJarlais, S.; Engstrom, R. C. *Anal. Chem.* **1988**, *60*, 2358.
(22) Engstrom, R. C.; Pharr, C. M.; Koppang, M. D. *J. Electroanal. Chem.* **1987**, *221*, 251.
(23) Engstrom, R. C.; Pharr, C. M.; Tople, R. A.; Unzelman, P. L., in press.
(24) Wick, R. A. *Appl. Opt.* **1987**, *26*, 3210.
(25) Haapakka, K. E.; Kankare, J. J. *Anal. Chim. Acta* **1982**, *138*, 263.
(26) Kepley, L. J.; Bard, A. J. *Anal. Chem.* **1988**, *60*, 1459.

RECEIVED for review June 16, 1989. Accepted September 25, 1989. This work was supported by the Air Force Office of Scientific Research (R.L.M.) and the National Science Foundation, Grant No. CHE-8703018 (R.C.E.). C.M.P. was the recipient of a Sigma Xi Grant-In-Aid of Research.

Fumed Silica Substrates for Enhanced Fluorescence Spot Test Analysis of Benzo[*a*]pyrene–DNA Adduct Products

Randy W. Johnson and Tuan Vo-Dinh*

Advanced Monitoring Development Group, Health and Safety Research Division, Oak Ridge National Laboratory, Oak Ridge, Tennessee 37831-6101

Amorphous fumed silica has been found to enhance both the intensity and resolution of the emission, excitation, and synchronous fluorescence spectra of benzo[a]pyrene-*r*-7,*t*-8,9,10-tetrahydrotetrol (BPT) on a filter paper substrate. Experimental parameters including the type and concentration of fumed silica were investigated as well as the method of application. The use of fumed silica as an enhancing agent in luminescence detection of polynuclear aromatic hydrocarbons is attractive since the procedure is simple, rapid, and cost-effective, and therefore suitable for routine analysis.

INTRODUCTION

Polynuclear aromatic (PNA) compounds are generally recognized as potential carcinogens and mutagens. The process is believed to be initiated by conversion of these compounds via chemical or metabolic activation into highly reactive electrophiles which undergo attack by nucleophilic centers in DNA (*1, 2*). The formation of complexes between electrophiles and specific sites in DNA may lead to induction of mutation and consequently other manifestations of genetic alterations. Benzo[*a*]pyrene and (BP) has often been investigated as the model compound for the carcinogenic PNAs. It is metabolized to a number of oxiranes, phenols, and quinones (*3–5*). The ultimate carcinogenic product of BP is believed to be BP-7,8-dihydrodiol 9,10-epoxide (BPDE) which binds to DNA (*6*). Methods for the measurement of BPDE–DNA complexes are therefore important for biomonitoring of human exposure to genotoxic PNA chemicals.

The highly fluorescent aromatic nucleus of the PNA molecule has allowed the detection of BPDE–DNA adducts by luminescence. Extremely sensitive assays are required due to the low levels of environmental exposure, which lead to low levels of adduct formation. Radioactive methods such as the ^{32}P postlabeling technique can detect DNA adducts of PNA at extremely low levels (*7*). Nonradioactive techniques such as surface-enhanced Raman scattering (SERS) spectrometry (*8*), fluorescence line-narrowing (FLN) spectroscopy (*9*), room temperature phosphorimetry (RTP) (*10*), and fluorometric detection for liquid chromatography (*11*) have been utilized

---

* Author to whom correspondence should be addressed.

0003-2700/89/0361-2766$01.50/0 © 1989 American Chemical Society

to detect minute amounts of BPDE–DNA adducts. The synchronous luminescence (SL) technique has been used for the selective characterization of mixtures of different PNAs (*12–14*). The SL technique involves scanning excitation and emission synchronously with a fixed wavelength difference ($\Delta\lambda$). A signal is seen only when $\Delta\lambda$ matches the interval between one absorption and one emission band; in many cases, a single peak is observed. Since DNA quenches the fluorescence of the covalently bound BPDE, acid hydrolysis induced removal of the pyrenyl moieties from the DNA as tetrols is generally required with each of these luminescence assays with the exception of the FLN, SERS, and RTP techniques. In this paper we report a simple technique for increasing the sensitivity of fluorescence detection for the benzo[*a*]pyrene tetrol (BPT) derivative.

In previous studies, sensitized luminescence by energy transfer has been extensively investigated (*15–19*) for improving the sensitivity of luminescence analysis. In this work we now report the development of a simple method for fluorescence enhancement of a PNA compound (BPT) on filter paper by a substance with no intrinsic fluorescence—fumed silica. There have been many diverse applications of silica and its derivatives in analytical spectroscopy. The use of silica and its derivatives as absorbants of analyte compounds has been widely documented (*20–25*). A C_{18}-derivative chromatographic silica was used to preconcentrate pyrene from methanol–water solutions (*26*). The hydrophobic interactions between the PNA and the silica surface largely determine the amount of preconcentration. Utilizing a sensitive laser fluorometric system, Kirsch and co-workers (*27*) were able to achieve a detection limit of approximately 8000 molecules of Rhodamine 6G adsorbed onto the surface of small silica spheres. They point out two major advantages: (1) there is no solvent fluorescence or Raman scatter and (2) the particles are viewed from a stationary position. Cellulose substrates generally have highly reflective surfaces and can produce scattered light. Front surface illumination/detection geometry used with a solid surface can produce higher levels of scattered light than do solution measurements where a right-angle geometry is used.

In this paper we report the effectiveness of fumed silica as a fluorescence enhancer on a paper support utilizing the biologically important compound BPT as a model. Experimental factors such as the type and concentration of fumed silica and method of application are discussed in detail. The results indicate that fumed silica induces an efficient enhancement of the fluorescence emission signals from BPT on a filter-paper background and is therefore potentially useful for the luminescence detection of PNA–DNA adducts.

EXPERIMENTAL SECTION

Instrumentation. All fluorescence spectra were obtained with a Perkin-Elmer 650-40 luminescence spectrometer equipped with a 150-W xenon lamp excitation source and an R928 Hamamatsu photomultiplier tube. An IBM-XT personal computer was linked to the spectrophotometer through a RS-232 interface and appropriate software was written to control the spectrophotometer, collect and process the data, and display the results in graphic forms. Special laboratory-constructed sample holders were used. These interchangeable, finger-type sample holders allow frontal excitation and right-angle detection (*28*).

Procedure. Two different procedures were investigated to obtain enhanced fluorescence. In the first method, equal volumes of 1×10^{-5} M benzo[*a*]pyrene-*r*-7,*t*-8,9,10-tetrahydrotetrol (BPT) in ethanol and 10% (w/w) aqueous suspensions of fumed silica were combined and thoroughly mixed. With a Gilson micropipet, 2.5 mL of this solution was applied to filter paper (within the sample holder) and allowed to dry for approximately 2 min prior to measurement. In another procedure, fumed silica or analyte solution was applied to the filter paper first and upon drying the BPT solution was spotted onto the pretreated paper substrate.

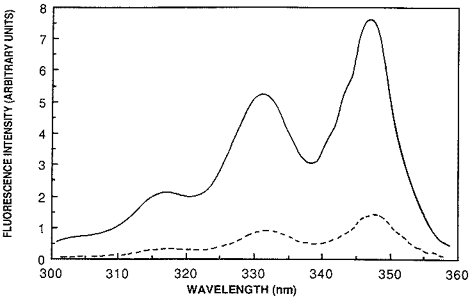

Figure 1. Excitation scan of 1×10^{-5} M ethanolic BPT mixed with an equal volume of aqueous 10% (w/w) grade LM 190 fumed silica (—) compared to the excitation scan of 1×10^{-5} M BPT mixed with an equal volume of water (- - -) on filter-paper substrate.

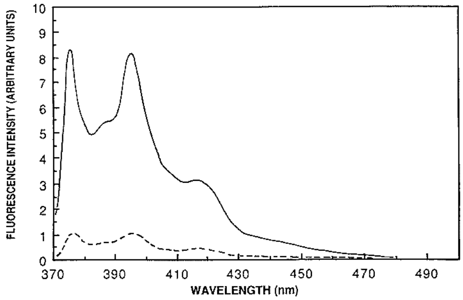

Figure 2. Emission scan of 1×10^{-5} M ethanolic BPT mixed with an equal volume of aqueous 10% (w/w) grade LM-130 fumed silica (—) compared to the emission scan of 1×10^{-5} M BPT mixed with an equal volume of water (- - -) on filter-paper substrate.

In either case, the fluorescence of BPT without sensitizer was measured for comparison. Appropriate background spectra were obtained and subtracted for all measurements. For excitation measurements, the emission wavelength was set at 380 nm; for emission measurements, the excitation wavelength was set at 349 nm. For synchronous luminescence analyses, $\Delta\lambda$ was set at 17 nm. Spectral resolutions were set at 1.5 nm for excitation, emission, and synchronous scans.

Materials. Amorphous fumed silica (grades EH-5, LM-130, L-90, and M-5) was graciously provided by the CABOT Corp. BPT was acquired from the National Institues of Health Repository. Spectral-grade ethanol was purchased from Warner Graham Co., and distilled water was purchased from American Scientific Products. Grade 2043A filter paper from Scheicher and Schuell, Inc., was used for all measurements.

RESULTS AND DISCUSSION

Enhanced Fluorescence Spectra. The experimental parameters investigated in luminescence enhancement by fumed silica included both the type and concentration of the fumed silica as well as the method of application. The effect of these parameters on the fluorescence of BPT was determined.

Figures 1, 2, and 3 show the excitation, emission, and synchronous spectra of ethanolic 1×10^{-5} M BPT premixed with an equal volume of aqueous 10% grade LM-130 fumed silica (final BPT concentration 4×10^{-9} g) prior to application onto filter paper. For comparison, spectra obtained with BPT on paper substrate without fumed silica are also shown (dashed curve). It was observed that premixing the sample with fumed silica significantly enhanced the fluorescence of BPT by almost 1 order of magnitude. In all cases, the signal has been increased ~5 times. The limit of detection for BPT

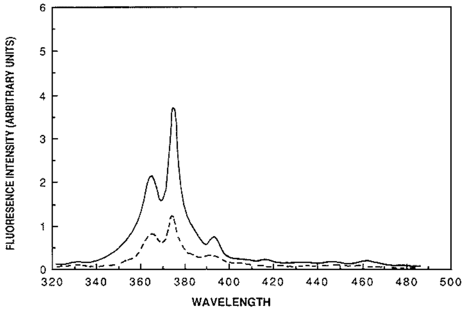

Figure 3. Synchronous scan of 1 × 10^{-5} M ethanoic BPT mixed with an equal volume of aqueous 10% (w/w) grade LM-130 fumed silica (—) compared to the emission scan of 1 × 10^{-5} M BPT mixed with an equal volume of water (---) on filter-paper substrate. $\Delta\lambda$ as set to 17 nm.

Table I. Fluorescence Intensity as a Function of Fumed Silica Size[a]

fumed silica type[b]	surface area,[b] m^2/g	nominal particle diameter,[b] μm	fluorescence intensity,[c] arbitrary units
L-90	100 ± 15	0.027	5.95 ± 0.86
LM-130	160 ± 15	0.017	9.24 ± 0.45
M-5	200 ± 25	0.014	9.59 ± 0.72
EH-5	380 ± 30	0.007	8.60 ± 1.84

[a] Fumed silica materials were suspended in aqueous solution to give 10% solutions and were premixed with equal volumes of 1 × 10^{-5} M ethanolic BPT solution prior to application onto filter paper. [b] Data supplied by vendor. [c] Measured at 380 nm with λ_{ex} = 349 nm.

is 2 pg. The dynamic range is approximately 2–3 orders of magnitude. The relative standard deviation of the measurement technique is approximately 10%. Figure 3 also illustrates the utility of the SL technique. While the emission and excitation spectral profiles of BPT are relatively broad, the synchronous spectrum exhibits narrower bandwidths, thereby simplifying detection of BPT in a mixture of PNA or other compounds with significant emission overlap. The synchronous spectra also show the presence of a small impurity, as indicated by the peak at 395 nm. It is noteworthy from Figures 1 and 2 that besides the intensity enhancement, the spectral characteristics of BPT in the presence of fumed silica are very similar to those in the absence of fumed silica. The lack of significant structure alteration in the fluorescence excitation (Figure 1) and emission (Figure 2) spectra indicates that spectral changes due to absorption onto fumed silica are minimal for the excited singlet and ground state.

The different commercially available grades of fumed silica vary according to surface areas and nominal particle diameters. For the grades used in this study, the surface areas ranged from 100 to 380 m^2/g and nominal particle diameters from 0.007 to 0.027 mm (Table I). Figure 4 depicts the fluorescence intensity of 1 × 10^{-5} M BPT measured at 380 nm (λ_{ex} = 349 nm) when premixed with equal volumes of 10% (w/w) of each of the four grades of fumed silica utilized in this study. Grade L-90 with the largest particle diameter (0.027 μm) and smallest surface area (100 m^2/g) gives the weakest fluorescence signal, while the other grades give statistically equivalent signals. It is interesting to note that in previous investigations of silver-coated fumed silica as a substrate for surface-enhanced Raman scattering (SERS), Grade L-90 with the largest particle diameter provided the maximum SERS intensity while the smaller silica sizes gave weaker signals (*29*).

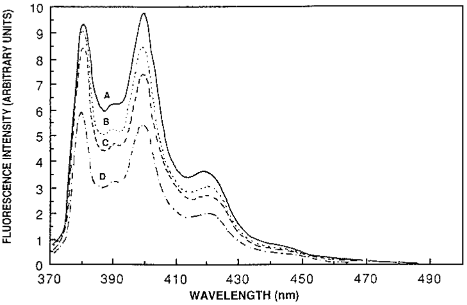

Figure 4. Comparison of the emission spectral intensities of 1 × 10^{-5} M BPT premixed with equal volumes of 10% solutions of different grades of fumed silica: curve A, grade M-5; curve B, grade EH-5; curve C, grade LM-130; curve D, grade L-90. Excitation wavelength was set to 349 nm.

Table II. Fluorescence Intensity as a Function of Fumed Silica Concentration[a]

% fumed silica	fluorescence intensity,[b] arbitrary units LM-130[c]	 EH-5[d]
1	2.21	2.53
2	2.03	2.17
3	1.88	1.80
4	1.87	1.70
5	2.44	1.72
6	1.84	1.90
7	2.62	1.42
8	2.10	1.73
9	2.37	1.92
10	2.10	1.69

[a] Fumed silica materials were suspended in aqueous solution to give 5% solutions and applied to filter paper. Upon drying, 2.5 μL of 5 × 10^{-6} M ethanolic BPT was applied to the same spot. [b] Measured at 380 nm with λ_{ex} = 349 nm. [c] Relative standard deviation = ± 9.8%. [d] Relative standard deviation = ± 11.8%.

The fluorescence intensity of 5 × 10^{-6} M BPT (applied on top of dried silica spot) with different concentrations of grades LM-130 and EH-5 fumed silica was measured at 380 nm (λ_{ex} = 349 nm). The concentrations ranged from 1% to 10% (w/w). Use of higher concentrations was prohibited due to aggregate formation of fumed silica particles. While Alak and Vo-Dinh (*29*) found an optimum concentration of 3% for SERS enhancement, the fluorescence signals from 1% to 10% on paper varied by only 10–12% and no clear pattern was observed (Table II).

Effect of Sample Preparation and Delivery. While the nominal particle size of the fumed silica (as indicated by grade) and the concentration (from 1% to 10%) appeared to play minor roles in fluorescence enhancement of BPT, the method of sample preparation and delivery seemed to be a key factor. Figure 5 shows the emission spectra of 1 × 10^{-5} M BPT premixed with equal volumes of grade LM-130 fumed silica prior to application (curve A), application of fumed silica to the filter paper substrate prior to BPT (curve B), and application of of BPT to the paper substrate prior to fumed silica (curve C). For comparison, the emission spectra obtained with BPT on paper substrate without fumed silica is shown (curve D). Premixing equal volumes of enhancing agent and analyte solution gave the best enhancement of the BPT fluorescence signal, followed by application of analyte onto previously applied enhancing agent. Application of fumed silica onto analyte gave a comparatively small enhancement of fluorescence signal. The two most effective methods, premixing of

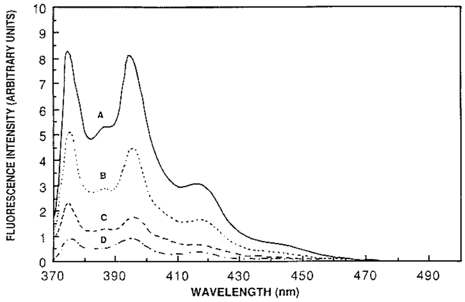

Figure 5. Comparison of the emission spectral intensities produced by different sample application methods: curve A, 1×10^{-5} M ethanolic BPT premixed with 10% (w/w) aqueous grade LM-130 fumed silica; curve B, 5% (w/w) aqueous fumed silica applied first to filter paper with 5×10^{-6} M BPT spotted on top; curve 5×10^{-6} BPT applied to filter paper first with aqueous fumed silica on top; curve D, 5×10^{-6} M BPT solution applied without fumed silica. Excitation wavelength was set to 349 nm.

analyte and enhancing agent solution and application of fumed silica preceding analyte application both allow the agent to have extensive contact with the paper. When the fumed silica is applied onto the analyte, incident light is prevented from fully reaching the BPT, thus weaker fluorescence enhancement is observed.

Fumed silica has no intrinsic fluorescence of its own; therefore, it is not functioning in the same manner by which anthracene or naphthalene enhances luminescence: that is, a transfer of excitation energy. While further investigation is underway to more fully explain the phenomena, several possibilities exist. As a manifestation of the chromatographic effect as noted in preconcentration studies (*26*), the fluorescence enhancement might be due to improved adsorption of the BPT onto the surface treated with fumed silica. Fumed silica can also retain more BPT molecules onto the surface. The microstructure of fumed silica particles might also induce surface-enhanced mechanisms in fluorescence emission. This latter possibility is under current investigation.

The use of amorphous fumed silica as a luminescence sensitizing enhancing in this type of analysis is attractive for several reasons. One of the problems related to analysis of complex mixtures by the sensitized (energy transfer) technique is that not all compounds will be sensitized. The degree of sensitization is determined by the amount of spectral overlap between analyte and sensitizer. Since fumed silica is inducing an increase in fluorescence signal in another manner, spectral overlap between sensitizers and analyte molecules is not required and the applicability of the technique is more general. The potential exists therefore for the resolution of minute quantities within a multicomponent mixture of PNA compounds. As demonstrated, fumed silica enhances both intensity and resolution of luminescence on filter paper. It is inert and gives no interfering fluorescence emission. Very small amounts of sample are required (4×10^{-9} g final concentration on paper). The procedure is simple, fast, and cost-effective and therefore suitable for routine analyses. Fumed silica is an inexpensive, easy-to-handle material. We have demonstrated the application of fumed silica enhancement of fluorescence for BPT and are currently investigating its utility for the detection of a number of PNAs. This technique also has potential for other analytical applications where detection of minute concentrations is required, such as DNA sequencing utilizing fluorophores (*30*).

ACKNOWLEDGMENT

The authors acknowledge the assistance of G. H. Miller for preliminary fluorescence measurements. The computer software was written by Mr. Peter St. Wecker.

Registry No. BPT, 61490-68-4; silica, 7631-86-9.

LITERATURE CITED

(1) Heidelberger, C. *Annu. Rev. Bicchem.* **1975**, *44*, 79.
(2) Jerina, D. M.; Daly, J. W. *Science* **1974**, *185*, 573.
(3) Nemoto, N.; Gelboin, H. *Arch. Biochem. Biophys.* **1975**, *170*, 739.
(4) Nemoto, N.; Gelboin, H. V. *Biochem. Pharmacol.* **1976**, *25*, 1221.
(5) Nemoto, N.; Takayama, S.; Gelboin, H. V. *Biochem. Pharmacol.* **1977**, *25*, 1825.
(6) Levin, W.; Wood, A. W.; Yagi, H.; Jerina, D. M.; Conney, A. H. *Proc. Natl. Acad. Sci. U.S.A.* **1976**, *73*, 3867.
(7) Gupta, R. C.; Reddy, M. V.; Randerath, K. *Carcinogenesis* **1982**, *3*, 1081.
(8) Vo-Dinh, T.; Uziel, M.; Morrison, A. L., *Appl. Spectrosc.* **1987**, *41*, 605.
(9) Sanders, M. J.; Cooper, R. S.; Small, G. J.; Heisig, V.; Jeffrey, A. M. *Anal. Chem.* **1985**, *57*, 1148.
(10) Vo-Dinh, T.; Uziel, M. *Anal. Chem.* **1987**, *59*, 1093.
(11) Rahn, R. O.; Chang, S. S.; Holland, J. M.; Shugart, L. R. *Biochem. Biophys. Res. Commun.* **1982**, *109*, 262.
(12) Vo-Dinh, T. *Anal. Chem.* **1978**, *50*, 396.
(13) Vo-Dinh, T. In *Modern Fluorescence Spectroscopy*; Wehry, E. L., Ed.; Plenum Press: New York, 1981.
(14) Vo-Dinh, T. *Appl. Spectrosc.* **1982**, *36*, 576.
(15) Frenkel, J. *Phys. Z. Sowjetunion* **1936**, *9*, 158.
(16) Forster, T. *Discuss. Faraday Soc.* **1959**, *27*, 7.
(17) Powell, R. C.; Soos, Z. G. *J. Lumin.* **1975**, *11*, 1.
(18) Hornyak, I. *J. Lumin.* **1972**, *5*, 132.
(19) Hornyak, I. *J. Lumin.* **1975/1976**, *11*, 241.
(20) Watanabe, H.; Goto, K.; Taguchi, S.; McLaren, J. W.; Berman, S. S.; Russell, D. S. *Anal. Chem.* **1981**, *53*, 738.
(21) Taguchi, S.; Yai, T.; Shimada, Y.; Goto, K. *Talanta* **1983**, *30*, 169.
(22) Uden, P. C.; Parees, D. M.; Walters, F. H. *Anal. Chem.* **1975**, *8*, 795.
(23) Ryan, D. K.; Weber, J. H. *Talanta* **1985**, *32*, 859.
(24) Jezorek, J. R.; Faltynski, K. H.; Blackburn, L. G.; Henderson, P. J.; Medina, H. D. *Talanta* **1985**, *32*, 763.
(25) Leydon, D. E.; Luttrell, G. H. *Anal. Chem.* **1975**, *47*, 1612.
(26) Carr, J. W.; Harris, J. M. *Anal. Chem.* **1988**, *60*, 698.
(27) Kirsh, B.; Voigtman, E.; Winefordner, J. D. *Anal. Chem.* **1985**, *57*, 2008.
(28) Vo-Dinh, T.; Walden, G.; Winefordner, J. D. *Anal. Chem.* **1977**, *49*, 1126.
(29) Alak, A. M.; Vo-Dinh, T. *Anal. Chem.* **1989**, *61*, 656–660.
(30) Smith, L. M.; Sanders, J. Z.; Kaiser, R. J.; Hughes, P.; Dodd, C.; Connell, C. R.; Heiner, C.; Kent S. B. H.; Hood, L. E.; *Nature* **1986**, *321*, 674.

RECEIVED for review May 16, 1989. Accepted September 5, 1989. This work was sponsored by the Laboratory Director's R&D Fund and Office of Health and Environmental Research, U.S. Department of Energy, under Contract DE-AC05-84OR21400 with Martin Marietta Energy Systems, Inc. This research was also supported in part by an appointment of R.W.J. to the postgraduate Research Training Program under Contract No. DE-AC05-76OR00033 between the U.S. Department of Energy and the Oak Ridge Associated Universities.

Supercritical Fluid Extraction for the Rapid Determination of Polychlorinated Dibenzo-*p*-dioxins and Dibenzofurans in Municipal Incinerator Fly Ash

Nick Alexandrou and Janusz Pawliszyn*

Department of Chemistry, University of Waterloo, Waterloo, Ontario, Canada N2L 3G1

The use of supercritical fluids yields rapid and quantitative extraction of polychlorinated dibenzo-*p*-dioxins and dibenzofurans from municipal incinerator fly ash. One hour of leaching with nitrous oxide at 400 atm and 40 °C removes over 90% of tetrachlorodibenzo-*p*-dioxins from this matrix compared to 20 h of extraction time for the Soxhlet method. Extraction time can be even shorter when higher pressures are applied. Pure carbon dioxide does not extract dioxins and therefore can be used effectively in the cleanup step to remove weakly absorbed organic material. However, this nonpolar fluid is able to remove quantitatively polychlorinated dioxins and furans when 10% of benzene is added to the fluid. Isolation of these pollutants can also be ensured by destroying the fly ash matrix by etching with acid first and then removing the released organics with carbon dioxide. The dramatically different extraction properties of nitrous oxide and carbon dioxide fluids, structurally similar molecules, are discussed. The extraction rate appears to be limited by kinetics of desorption rather than solubilities. The supercritical fluid extraction process was conducted with an inexpensive fluid delivery system based on a high-pressure vessel.

INTRODUCTION

Incinerators are used in large cities throughout the world to deal with the problem of waste. As the trash is burned, inorganic compounds in the combustion zone of the incinerator form small particulate matter known as fly ash. Thousands of tons of fly ash are produced in this process and require disposal. The fly ash composition consists of approximately 75–90% inorganic matter. In addition, some 600 organic compounds are present, among them hydrocarbons, polycyclic aromatic hydrocarbons, and polychlorinated organics. For example, polychlorinated dibenzo-*p*-dioxins (PCDD) and polychlorinated dibenzofurans are two of the groups present and known to be highly toxic (*1*). There are 75 isomers present in PCDD and 135 in PCDF. The major compound of concern is 2,3,7,8-tetrachlorodibenzo-*p*-dioxin (TCDD), which is the most toxic and has shown carcinogenic effects in animals. Between 1 and 2% of the fly ash escapes into the atmosphere through the stack emission. However, most of it is isolated by an electrostatic precipitator and is disposed of by either dumping it or burying it in landfill sites. This poses a threat to our soil and water supply. For instance, dioxins have been found in fish tissue and pulp and paper effluents.

The first step in chromatographic analysis of environmental samples, such as fly ash, involves separating the organic components of interest from the matrix. This process is achieved traditionally by using liquid extractions. Solid samples such as fly ash are leached with an organic solvent in a Soxhlet apparatus. Methods based on solvent extraction are often time-consuming, due to small diffusivities in the liquids, and are very expensive since they require high-purity organic solvents and waste disposal fees. In addition to the long extraction times and usually high toxicity of the organic liquid, these extraction processes are highly nonselective. Therefore, sequential chromatographic techniques must often be used to separate complex mixtures after extraction (*2*). This significantly increases the time and cost of overall chromatographic analysis of environmental samples. For example, analysis of polychlorinated dibenzo-*p*-dioxins and dibenzofurans often take days to complete. A promising technique, which can significantly increase speed and simplify the isolation process, is supercritical fluid extraction (SFE).

Supercritical fluid extraction processes are well accepted by chemical engineers (*3–7*). This method exploits the properties of the gas at temperatures and pressures near the critical point. It combines both distillation and extraction in a single process since both vapor pressure and phase separation are involved. In the food industry, the nontoxic properties of supercritical carbon dioxide and low extraction temperatures have been recognized (*8*). The speed, selectivity and low energy cost of supercritical fluid extraction have allowed many important industrial applications such as coal extraction (*9*) and the regeneration of activated carbon beds used in wastewater treatment (*10*).

The interesting properties of supercritical extraction can contribute significantly to an increase in analytical separations performance. The first descriptions of such a process were published in 1976 (*11*), where solvent-free microanalytical supercritical extraction was followed by thin-layer chromatography. However, more numerous applications of this method were not reported until quite recently. Most of these analytical investigations were focused on samples similar to those already explored in engineering applications such as determination of caffeine from coffee (*12*), the extraction of oils from natural products (*13*), and the removal of pesticide residue from plant sources (*14*) or organic pollutants from environmental sorbents, such as Tenex-GC (*15*), XAD resins (*16*), and polyurethane foam (*16, 17*). Only a limited number of studies have been done on direct extraction of environmental solids such as fly ash (*18*), river sediment (*18, 20*), urban dust (*18–20*), and diesel exhaust particulates (*15*). Isolation of organic pollutants from these solids is often difficult since in many cases they are strongly bound to the matrix. For example, it is proposed that polychlorinated dibenzo-*p*-dioxins and dibenzofurans are produced during the formation of municipal incinerator fly ash (*21*).

In this paper we discuss application of the supercritical fluid extraction method to the recovery and the analysis of these important pollutants present in the municipal incinerator fly ash.

EXPERIMENTAL SECTION

Distilled in Glass Grade solvents (benzene, methanol, hexane, and dichloromethane) used in this study were purchased from BDH Chemicals, Toronto, Ontario. The liquified, bone-dry carbon dioxide, nitrous oxide, helium, and nitrogen were acquired from Inter City Welding, Kitchener, Ontario. The fly ash was supplied

0003-2700/89/0361-2770$01.50/0 © 1989 American Chemical Society

by the Ontario Ministry of the Environment from an electrostatic precipitator of a municipal incinerator in Toronto, Ontario. ^{13}C labeled 2,3,7,8-tetrachlorodibenzo-*p*-dioxin was obtained from Cambridge Isotope Laboratories (Woburn, MA).

All glassware, vials, and extraction vessels were washed with Sparkleen laboratory detergent in an ultrasonic agitation bath for 1 h. They were dried at 100 °C for 30 min followed by 2 h at 220 °C in a Fisher Isotemp Model 350 oven. The appropriate solvent was used in rinsing the glassware prior to its use. The stainless steel tubing was cleaned, under vacuum, using dichloromethane. The tubing, with nitrogen flowing through it, was then dried in the oven at 210 °C for 2 h.

The fly ash to be extracted was sieved to 150 μm. Approximately 10-g samples were Soxhlet extracted with benzene (300 mL) for 40, 20, 6, and 2 h. Coarse porosity glass fritted extraction thimbles were used in the extractions. The solutions were reduced in volume by rotary evaporation (Buchi Rotovapor-R), transferred to a 25-mL pear flask for further concentration and then concentrated, in a vial, to 500 μL by a gentle stream of nitrogen. The samples were stored in a refrigerator to prevent evaporation and for future analysis with gas chromatography (GC) and gas chromatography/mass spectrometry (GC/MS).

High-pressure vessels were used to supply supercritical fluid for extraction. These vessels were constructed of stainless steel in the Science Machine Shop at the University of Waterloo (*22*) or were purchased (High Pressure Equipment Co., Erie, PA, Model OC-2). Their volumes are about 200 mL and the vessels are made to withstand pressures in excess of 20 000 psi. The vessel is equipped with a safety valve that contains a disk which ruptures at 7000 psi. This type of safeguard is extremely important to protect the operator in the case of manual and/or electronic temperature control failure. The 0.25 in. i.d. copper tubing coil is soldered to the outside surface of the vessel. This system is used to pass liquid nitrogen just before filling it up with high-density liquid fluid. Liquid nitrogen is supplied from a pressurized stainless steel thermos. The vessel is heated with the beaded heater (Cole, Palmer Chicago, IL). The pressure is monitored electronically by a pressure transducer (Model AB, Data Instruments, Lexington, MA). The temperature in the high-pressure vessel and extraction vessel is monitored with thermistors (Radio Shack, Barrie, Ontario). The pressure and temperature in the extraction system are controlled electronically (*22*). Switching the heater on and off is done with the help of a solid-state relay (Model EOM-1DA42-3/32, Potter and Brumfield, Princeton, IN). Operation of the high-pressure fluid source based on the heated pressure vessel consists of two steps. In the first step, the high-pressure container is cooled to below the critical temperature of the fluid (for CO_2, t_c is 32 °C), using a source of coolant (liquid nitrogen). The vessel is then filled with liquid fluid from a high-pressure cylinder. In the next step, the vessel is heated, which significantly increases the pressure in the vessel. Supercritical fluid at a well-regulated pressure is then supplied to the extraction vessel.

Refilling of the high-pressure vessel takes about 25 min. The fully charged vessel (cooled to −15 °C) is able to provide fluid for 5 h of continuous supercritical extraction at 400 atm. If an uninterrupted supply of the supercritical fluid is required, then two vessels can be used simultaneously, one operating while the other is being serviced.

It should be emphasized that the fluid density in the extraction vessel and therefore the solubility (extraction) properties are independent from that which exist in a high-pressure container. Only the extraction pressure is determined by the conditions in the larger volume vessel. The extraction temperature, which determines density of the fluids, is regulated independently by using a heater attached to the extraction vessel.

The extraction vessels, capacity 0.8 g of fly ash, were constructed of Swagelok 316 stainless steel fittings and 5 cm 1/4 SS tubing. the $^{1}/_{16}$ in. stainless steel tubing leading from the extraction vessel was connected to a Swagelok zero dead volume connector. A fused silica capillary, 20 cm × 20 μm, was connected to the zero dead volume connector and was used as a restrictor to maintain the pressure in the system. The capillary was directed into a 1.5-mL vial with septum and vent containing approximately 1.0 mL of hexane. A measured flow rate of approximately 120 mL/min of the depressurized gas was obtained at 400 atm. The samples were concentrated to 100 μL by directing a gentle stream of nitrogen into the vial. These samples were also stored in a refrigerator to prevent evaporation and for future GC and GC/MS analysis.

Two methods were used to extract aliphatic hydrocarbons from fly ash. With the use of a disposable pipet 5% (by volume) hexane was added to the high-pressure vessel while being cooled. The high-pressure vessel was filled with CO_2. The fly ash in the extraction vessel was extracted for 1 h at 80 °C and 400 atm for the removal of the hydrocarbons. Hydrocarbons were also extracted with CO_2 at 325 atm for 2 h and 40 °C. The extraction of the PCDDs/PCDFs was accomplished in three different ways. Benzene (10% by volume) was added to the CO_2 in the high-pressure vessels. A pressure of 400 atm was used to extract the PCDDs/PCDFs at 60 °C for 2 h. Secondly, nitrous oxide (with no modifier) was used as the supercritical fluid. The temperature of the extraction was 40 °C for 2 h at an extraction pressure of 400 atm. The fly ash was treated with 1 N HCl to break down the matrix and facilitate the ease of the extraction of the PCDDs/PCDFs. The fly ash was then stirred for 2 h in 1 N HCl, centrifuged, washed with a copious amount of distilled water, and air-dried. CO_2 was used to extract it at 400 atm for 2 h and 40 °C. This fly ash was also extracted with nitrous oxide at 400 atm for 2 h and 40 °C. In the above SFE procedure, approximately 0.5 g of fly ash was extracted.

A Varian 3500 capillary gas chromatograph, equipped with an on-column capillary injector, an electron capture detector (ECD), flame ionization detector (FID), and 30 m × 0.25 μm fused silica capillary column (DB-5) (J & W Scientific, California) was used for chromatogaphic analysis. Nitrogen, with a flow rate of 1.2 mL/min, was used as the carrier gas. The temperature program consisted of an initial oven temperature of 65 °C for 1 min, programmed to 230 °C at 15 °C/min, held there for 1 min, programmed to 300 °C at 3 °C/min, and held there for 30 min. The ECD temperature was 325 °C. The temperature program of the on-column injector consisted of an initial temperature of 65 °C, held for 1 min., programmed to a final temperature of 300 °C at 100 °C/min, and held for 60 min. The on-column injections consisted of a 1-μL solvent plug along with a 1-μL sample. The gas chromatograph was interphased with INTEL 386 computer (EMJ Data Systems, Guelph, Ontario, Canada) using Lab-Master DMA data acquisition card (Scientific Solutions, Columbus, OH) and ASYST software (ASYST Software Technologies, Inc.).

Quantitation of the extracted polychlorinated dibenzo-*p*-dioxins and dibenzofuranas (PCDDs/PCDFs) was achieved with a Hewlett-Packard HP5890 GC/MSD system. An ionization voltage of 70 eV and ion source temperature of 300 °C were used. Before each set of analysis, the instrument was tuned with the compound perfluorotributylamine (PFTBA). This compound was used since it is stable and produces fragments throughout the entire mass range. Three such peaks at *m/z* 264.00, 413.95, and 501.95 were used since they are close to the ion masses of the PCDDs and PCDFs. Since the mass of the PCDDs and the PCDFs are known, selected ion monitoring (SIM) was used. SIM of the $(M - COCl)^+$, M^+, and $(M + 2)^+$ ions for the TCDD/TCDF through to the H_7CDD/H_7CDF were used for identification. The $(M - COCl)^+$, $(M + 2)^+$, and the $(M + 4)^+$ ions were monitored for the OCDD/OCDF. M denotes the parent molecule. To ensure correct identification and quantitation of PCDDs and PCDFs, a standard mixture of these compounds was injected before a new set of unknowns was analyzed. The capillary column and temperature program were identical with the ones used for GC/ECD analysis. The helium carrier gas flow rate was 2.0 mL/min.

The analysis of fly ash in most cases was performed in triplicate extractions. In some cases where the variance is discussed in the text, a series of six samples were analyzed.

RESULTS AND DISCUSSION

Table I shows Soxhlet extracton data of polychlorinated dibenzo-*p*-dioxins and dibenzofurans from municipal incinerator fly ash as a function of leaching time. Benzene was used as solvent since it gives the highest extraction efficiency and recoveries of dioxins from this matrix (*23*). The pollutants of interest are divided into groups containing the same number of chlorines in the single molecule. For example, T_4CDD stands for tetrachlorodibenzo-*p*-dioxins to which the most

Table I. Extraction Data of Polychlorinated Dibenzo-*p*-dioxins and Dibenzofurans from Municipal Incinerator Fly Ash Using Soxhlet Extraction with Benzene[a]

PCDD	40 h	20 h		6 h		2 h		GC/MS analysis
PCDF	$\bar{x}$	$\bar{x}$	s, %	$\bar{x}$	s, %	$\bar{x}$	s, %	s, %
T_4CDD	107	90	13	64	19	52	6	4
P_5CDD	139	135	30	83	18	63	19	4
H_6CDD	87	87	6	51	10	41	2	3
H_7CDD	77	79	6	48	8	38	5	4
O_8CDD	18	20	35	12	8	11	1	2
T_4CDF	42	44	18	29	17	24	13	1
P_5CDF	159	155	10	99	10	41	1	4
H_6CDF	119	124	2	84	4	56	7	3
H_7CDF	140	151	20	94	12	77	5	3
O_8CDF	16	19	16	5	40	31	33	3

[a] The units are in ng/g of fly ash. Estimated standard deviations are expressed in percent of mean $\bar{x}$.

toxic 2,3,7,8-tetrachlorodibenzo-*p*-dioxin congener belongs and T_4CDF stands for tetrachlorodibenzofurans.

Results in Table I indicate that only about 50% of dioxins and furans are removed from the matrix in the first 2 h of extraction. In order to complete the extraction, the process should continue for 20 h. Results corresponding to 40 h are not statistically different compared to a 20-h leaching time. Also complete recoveries (93 ± 13%) of ^{13}C labeled tetrachlorodibenzodioxin standard were observed after 20 h of leaching time.

Soxhlet extraction results are characterized by large standard deviation, approaching in some cases 35% of total value. This poor precision is not associated with GC/MS analysis since the standard deviation in this case is only a small percentage, as would be expected (see Table I). One source of variance might be generated by the variation in sample or injection size. However, this source will affect all components to the same degree. Therefore, estimated standard deviation should be similar for all components. Analysis of variance (ANOVA) (*24*) performed on sets of data does not show any correlation between the sample number and results being consistently high or low. Another source of variance might be high inhomogeneity of fly ash. However, this is not supported by the supercritical fluid extraction results using the same fly ash where the estimated standard deviations are significantly smaller (see Table II).

Another source of variance might be associated with a number of fillings within the same period of time. However, a special effort was made to ensure the uniform condition of the Soxhlet leaching process, including the number of fillings. The relative variance associated with this effect should be independent of the extraction time. However, the relative variance in Table I increased with time of the extraction. This trend is particularly visible when comparing 2-h with 6-h results. There are two possible explanations for this large standard deviation. Aggragation of the small fly ash particles occurs during the extraction process which limits access of the solvent to the solid matrix. This aggregation process increases with time. The fly ash cake becomes progressively more dense with the time of extraction. This random process traps a portion of organics present in the fly ash. The mechanical stirring can break down these aggregates and release the pollutants. The stirring process is very inconvenient considering toxic benzene fumes and long extraction times. In addition, the Soxhlet extraction process is performed at temperatures close to the boiling point of the solvent, in our studies about 80 °C. At these elevated temperatures the synthesis of additional amounts of polychlorinated dioxins and furans on active sites located on fly ash matrix is possible. The other major concern when applying Soxhlet extraction is the use of toxic solvents. The replacement of benzene with other less toxic solvents results in lower extraction efficiencies (*23*).

Considering the serious limitations of Soxhlet extraction in the analysis of dioxins in fly ash (toxic solvents, long extraction times, high extraction temperatures, and poor precision), we decided to apply supercritical fluids in this application. Table II summarizes the results obtained. The extraction efficiencies are expressed relative to 20-h Soxhlet extraction results.

Initially, we explored the application of the most common and least expensive fluid, carbon dioxide. Our initial results with this solvent were very discouraging. No significant amount of dioxins were extracted by the pure solvent even at 400 atm (see Table II). Only a small amount of furans were found in the extraction mixture. The negative result could be due to poor solubility of dioxins and furans in carbon dioxide. However, we were able to quantitatively extract a standard of heptachlorodibenzo-*p*-dioxin and ^{13}C labeled tetrachlorodibenzo-*p*-dioxin from an empty extractor tube and also when it was deposited directly onto fly ash. These results indicate that the solubility is not a limiting factor but rather that the pollutants of interest are strongly absorbed onto the matrix and cannot be removed with carbon dioxide at 400 atm. In order to release them, it is necessary to use a stronger solvent which is able to break this specific interaction. This observation emphasizes the differences between the engineering applications of the supercritical fluid extraction where

Table II. Extraction Data of Polychlorinated Dibenzo-*p*-dioxins and Dibenzofurans from Municipal Incinerator Fly Ash Using Supercritical Fluid Extraction with Different Fluids at 400 atm[a]

PCDD	CO_2 40 °C	CO_2 + 10% benzene 60 °C 2 h		CO_2 + 10% toluene 60 °C	CO_2 acid-treated fly ash 40 °C		N_2O 40 °C 2 h	
PCDF	2 h $\bar{x}$	$\bar{x}$	s, %	2 h $\bar{x}$	$\bar{x}$	s, %	$\bar{x}$	s, %
T_4CDD		117	12	49	96	25	98	7
P_5CDD		96	13	54	90	4	83	8
H_6CDD		96	11	57	87	8	81	2
H_7CDD		78	7	91	83	3	74	1
O_8CDD		75	6	35	75	17	81	6
T_4CDF	19	88	5	53	92	5	83	5
P_5CDF	9	97	5	48	114	5	87	1
H_6CDF	19	97	5	54	111	7	88	4
H_7CDF		79	48	65	100	17	89	4
O_8CDF		94	6	16	65	18	91	6

[a] The units are in percent of extraction compared to 20 h of Soxhlet extraction. Estimated standard deviation s is expressed in percent of $\bar{x}$.

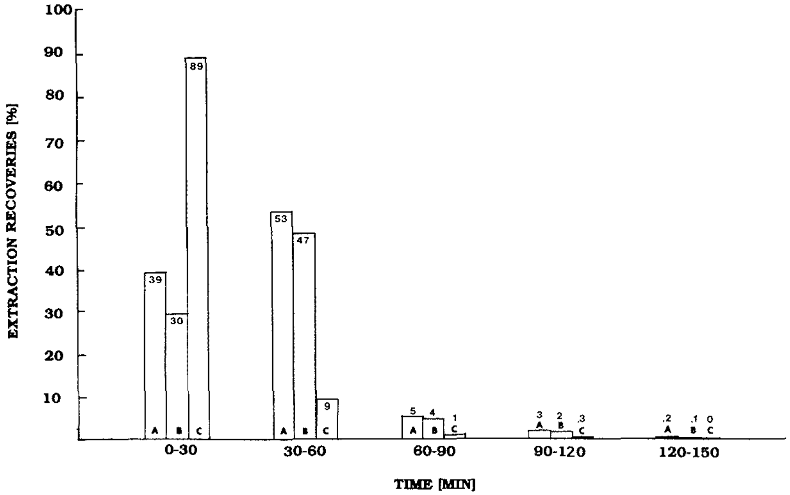

Figure 1. Extraction rates of octachlorodibenzo-*p*-dioxins/octachlorodibenzofuran from (O_8CDD/O_8CDF) municipal incinerator fly ash using various methods of supercritical fluid extraction: (a) dynamic method at 400 atm with nitrous oxide of untreated fly ash; (b) dynamic method at 400 atm with carbon dioxide of acid treated fly ash; (c) static method with nitrous oxide at 400 atm for 2 h followed by dynamic leaching of pollutants with the fluid. (See details in text.) Recoveries are given in percentage of total amount extracted with nitrous oxide.

relatively large amounts of the product is dissolved in the fluid and transferred to the collection vessel, and the trace analysis applications where minute quantities of specifically adsorbed material are needed to be removed quantitatively from the matrix. In order to achieve the engineering goal, it is, in most cases, sufficient to ensure that the material of interest is soluble in the supercritical fluid, while to ensure quantitative removal of pollutants, it is necessary to use a strong solvent that will remove organic components from the matrix.

It was shown that the addition of a polar modifier, such as methanol, to the supercritical solvent, can increase the recovery of polar compounds adsorbed on environmental sorbents (*15*). However, even 10% concentration of methanol by volume did not improve the recovery rates compared to pure carbon dioxide. In the next step, we used benzene as the modifier. As discussed above, benzene is a solvent of choice for Soxhlet extraction. Indeed, addition of 10% of benzene to the fluid produced over 95% recovery of toxins compared to 20-h Soxhlet extraction (see Table II). The time of extraction was only 2 h but still a significant amount (about 4 mL) of toxic benzene was used in this process. Our efforts in replacing this toxic solvent with toluene, or partially with methanol, resulted in lower recoveries (see Table II). The amount of benzene used can be reduced to about 0.5 mL if it is placed directly into the extractor together with the fly ash sample prior to analysis. This approach is more convenient since it does not require preparation of the supercritical fluid mixture containing 10% benzene. The extraction of fly ash/benzene mixture is performed with pure carbon dioxide.

At this point we decided to try a different approach. Since the polychlorinated dibenzo-*p*-dioxins and dibenzofurans are dissolved in carbon dioxide, they can be removed by this fluid if the pollutants are released from the matrix. One way to achieve this goal would be to destroy the fly ash matrix by exposing it to a strong acid. The results related to this analysis are shown in Table II. Removal of dioxins in this way is quantitative in most cases, approaching 90% recoveries. In the procedure, we added small quantitites of 1 N hydrochloric acid to the sample before separating solids with the help of centrifuge. If filtering was used in place of centrifuging, the recoveries were significantly lower indicating that small particles together with adsorbed dioxins were trapped in the filter paper. The results obtained are very encouraging considering that no organic solvent was used in this process. However, this procedure requires an extra step involving acid etching, which significantly increases the cost and time of overall analysis. Also, precision of the results is poor as indicated by the high estimated standard deviation of the experimental results and is comparable to Soxhlet extraction values. This variance can be associated with highly inhomogeneous material produced after etching of municipal incinerator fly ash. This situation could be significantly improved if a proper sampling procedure is developed.

In our final attempt we used a different fluid, nitrous oxide, which has been reported to extract polyaromatic hydrocarbons with higher efficiency from various matrixes (*20*). Although its molecular structure is similar to carbon dioxide, N_2O has a small dipole moment and weak basic properties (*25*). This small molecular difference between N_2O and CO_2 produced a dramatically different outcome in extraction results. As Table II shows, the extraction efficiencies at 400 atm are close to 100% for tetrachlorodibenzo-*p*-dioxins and approach 90% for all others. This result is substantially different compared to extraction with carbon dioxide when no significant removal of the toxins were observed. In addition, precision of the results is significantly better and is close to that expected for GC/MS analysis. Estimated standard deviations are in a few percent range. They are similar to values from Table I corresponding to precision of chromatographic analysis. A strong relationship between type of solvent and extraction efficiencies was already observed for Soxhlet extraction of furan samples (*23*).

Time of supercritical fluid extraction with N_2O was 2 h, one-tenth of that for the Soxhlet method; however, it is still quite significant. Therefore, in the next step of our investigations we looked at the dynamics of extraction process. Figure 1a shows the amount of sample removed from the matrix at five 30-min time intervals. It is clearly visible that extraction rates are initially high for the first two periods and then fall dramatically in the last three. Figure 1A shows only the results related to octachlorodibenzo-*p*-dioxins/dibenzofurans, but very similar results were obtained for other congeners. About 90% of pollutants were removed in the first hour and less than 10% in the second hour. Therfore, the extraction time of municipal incinerator fly ash can be reduced to 60 min without significant loss in efficiency. Extraction for an additional 30 min beyond second hour does not produce removal of additional dioxins and furans. Even the increase in density of N_2O by elevating pressure to 450 atm did not remove additional toxins. Reextraction of fly ash with benzene in 20-h Soxhlet extraction did not remove a significant amount of toxins. Therefore, we concluded that the extraction was complete after 2 h. Two-hour extraction produced above 85% recoveries of ^{13}C-labeled dioxin standards. We also investigated the possible loss of analytes to the atmosphere through aerosol formation (*26*). However, our studies involving a double trap did not reveal the presence of the dioxins or furans in the gas flow from the collection vial.

Figure 1B provides information related to the removal of dioxins and furans from acid-treated fly ash matrix with carbon dioxide. Again the removal of most of these pollutants occurs in the first hour. The efficiencies are somewhat smaller compared to extraction with nitrous oxide, probably due to incomplete destruction of the fly ash matrix by the acid. This result is consistent with data reported in Table II for O_8CDD/O_8CDF. This indicates that solubilities of chlorinated dioxins and furans are not dramatically different in supercritical CO_2 and N_2O (Figure 1A,B). Therefore, the unique capability of nitrous oxide to remove these pollutants must be associated with its strong, specific interaction with matrix or adsorbed molecules, which allows its release.

Figure 1C shows static extraction results compared to the dynamic method used in most of the experiments described in this paper. In this approach, the fused silica capillary restrictor is first sealed. The extractor with the fly ash sample is then pressurized with nitrous oxide to 400 atm for 2 h. Then, the capillary is broken open and the appropriate fractions are collected. In this process over 90% of dioxins and furans have been removed from the fly ash in the first half hour after the restrictor was open. Over 60% of the toxins eluted from the extractor in the first 10 min. It must be remembered, however, that the total extraction time, including the initial static period, is over 2 h. However, this experiment clearly indicates that the solubilities of dioxins and furans are not a limiting factor in the removal of these pollutants from fly ash since the fluid can carry much larger amounts of these compounds than dynamic extraction results would indicate (Figure 1A,B). Rather, dynamics of mass transport from the surface of the fly to the bulk of the fluid is likely responsible for slow extraction of the toxins. This process consists of three distinct steps. The first one involves the desorption of pollutants from the surface followed by solvation of the material in the fluid and diffusion of it to the bulk of the solvent.

Careful analysis of results from Figure 1 support the notion of slow extraction dynamics. Amounts of the toxins extracted in the first half hour period using nitrous oxide (Figure 1A) and carbon dioxide (Figure 1B) are lower compared to the second period. This can be explained by the slow desorption of the pollutants from the surface. Therefore, it takes time to build up the high concentration of the toxins in the fluid. In fact, the fraction collected within the first few minutes after beginning the extraction process does not contain significant amounts of the pollutants. This effect is not observed for a static approach (Figure 1C) since the sample is allowed to be exposed to the fluid for a period of 2 h prior to the leaching procedure.

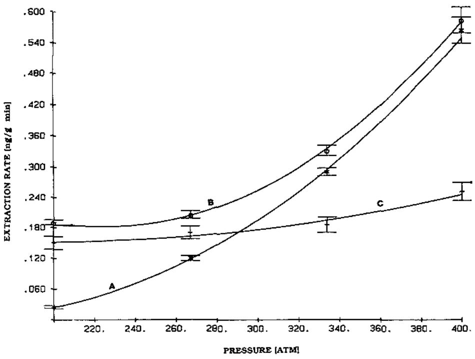

Figure 2. Extraction rates vs pressure for various extraction conditions: (a) nitrous oxide and untreated fly ash; (b) nitrous oxide and acid-treated fly ash; (c) carbon dioxide and acid-treated fly ash. Extraction rates correspond to the amount of O_8CDD/O_8CDF removed in the first 30 min of leaching at given pressure.

In order to better understand the factors involved in extraction dynamics, let us consider the interface between the fly ash surface and the fluid. It is expected that the supercritical fluid solvent molecules form a thin layer of condensed liquid at the solid surface (*27*). The properties of the layer will determine the dynamics of the extraction process. The density, thickness, and elution strength of this liquid increase with pressure. Therefore, we investigated the rates of extraction as a function of pressure. Figure 2 summarizes the results obtained. Figure 2A corresponds to the extraction of untreated fly ash with nitrous oxide while parts B and C of Figure 2 correspond to acid-treated matrix leached with N_2O and CO_2, respectively. Extraction rates of dioxins and furans from acid-treated fly ash increase gradually with pressure when carbon dioxide is used. The change is more significant for nitrous oxide. The most dramatic changes are observed when untreated fly ash is extracted with this fluid. An interesting feature of this curve is that at higher pressures it coincides closely with curve corresponding to the extraction of acid-treated fly ash by the same fluid. However, at pressures below 320 atm, it shows significantly slower extraction rates. This indicates that at pressures below 320 atm the removal rate is determined by the desorption process form the active sites present in raw fly ash and absent in acid-treated matrix. A significant increase in extraction rates between 320 and 400 atm suggests that increase in density of the liquid layer, which enhances its desorption and solubilizing properties toward dioxins and furans, is more important than the increase in thickness of the liquid layer in the vicinity of the surface. The thicker layer produces slower transport rates of these toxins from the surface to the bulk of supercritical fluid. This conclusion is also supported by initial temperature and flow rate studies discussed below. Increases in the extraction temperature will significantly reduce the thickness of the liquid layer present in the vicinity of the fly ash surface. This will speed up the transport of the organic material from the surface to the bulk of the fluid. However, experimentally measured rates at 400 atm are smaller when extraction at 50 °C is performed compared to 40 °C. This is likely due to significant loss in density of the fluid. Higher velocity in the bulk of the fluid should increase the mass transfer rate through the liquid film due to the increase in difference of analyte concentration in the bulk of the fluid and the layer. However, increase of the flow rate of the fluid from 120 to 300 mL/min of expanded gas did not improve extraction rates.

There are only a few differences between nitrous oxide and carbon dioxide, which have similar solubility parameters (*28*).

The differences are associated with a small dipole moment in the N_2O molecule and its weak basic and oxidating properties compared to a lack of these features in carbon dioxide. These small differences produce dramatically dissimilar supercritical fluid extraction behavior toward dioxins and furans present in the fly ash matrix. In our research we found no evidence of oxidation of extracted material. Also, replacement of benzene with more basic pyridine in supercritical fluid extraction with CO_2 and Soxhlet extraction did not improve extraction efficiencies.

A small dipole moment is likely to play an important role in desorption of polychlorinated dibenzo-*p*-dioxins and dibenzofurans from the fly ash matrix. However, on the basis of limited experimental data, the way this molecule interacts with the matrix and compounds of interest is difficult to speculate. We are currently conducting more detailed investigations of this interesting phenomenon. Naturally, the extraction properties of the fluid are not related to the size of the dipole moment of its molecules. The presence of methanol added to carbon dioxide did not help remove the toxins. Also, the pollutants are not soluble in water. It is likely that in addition to solubility prerequisite a small dipole, together with appropriate polarizability of the solvent molecules, is required to desorb the dioxins and furans.

Figure 2 shows a rapid increase in extraction rates with an increase in pressure. It can be concluded by extrapolating from this graph, that an increase in pressure should result in faster isolation of the organic material from fly ash.

Poor extraction capabilities of carbon dioxide toward dioxins and furans, as shown in Table II, can be used effectively to cleanup fly ash prior to extraction of the toxins. This step removes weakly bonded organic molecules in the matrix. This step can be followed by removal of compounds in interests with nitrous oxide. Figure 3 summarizes the extraction results reported in this paper by showing ECD chromatograms of each sample mixture. The time windows corresponding to various dioxins and furans are marked on the graph. Figure 3A corresponds to 20-h Soxhlet extraction, which was used in our comparative studies. Extraction with CO_2 removes chlorinated compounds, which elute early (Figure 3B). They are likely to be lower molecular weight or less polar compounds compared to the polychlorinated dioxins and furans. Extractions of acid etched fly ash with CO_2 (Figure 3D) and untreated fly ash with N_2O (Figure 3E) give results similar to those corresponding to Soxhlet extraction with benzene. The N_2O chromatogram is significantly cleaner in the low retention time region since extraction with this fluid is preceded with CO_2 extraction at 325 atm. In the cleanup procedure we dropped the density of carbon dioxide by lowering the pressure of extraction compared to conditions corresponding to quantitative results reported in Table II. This was done to limit the loss of polychlorodibenzofurans (PCDF) to a few percent, since its presence might be of interest to analytical chemists.

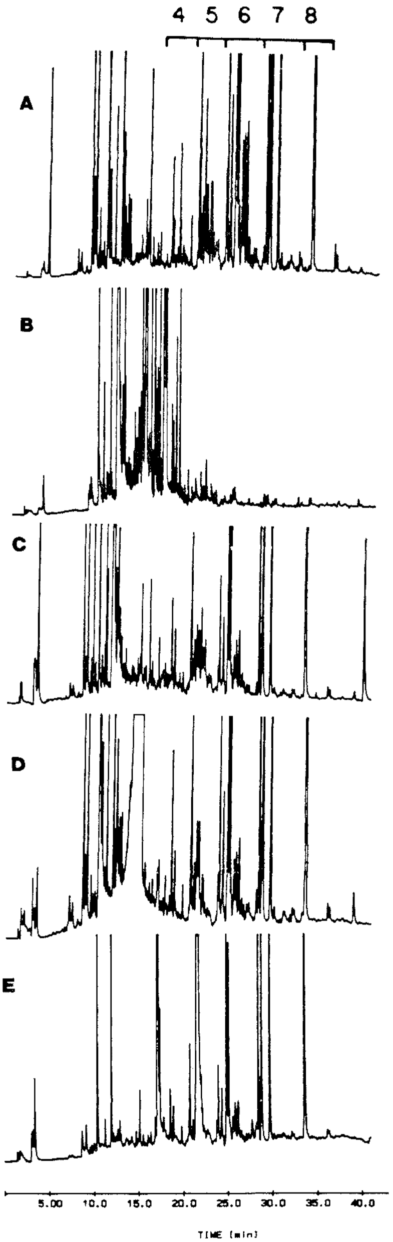

Figure 3. Gas chromatographic separations with ECD detection of various extraction mixtures: (a) 20 h of Soxhlet extraction with benzene; (b) 2 h of SFE with carbon dioxide at 325 atm of untreated fly ash; (c) 2 h of SFE with carbon dioxide and 10% benzene at 400 atm of untreated fly ash; (d) 2 h of SFE with carbon dioxide at 400 atm of acid-treated fly ash; (e) 2 h of extraction with nitrous oxide at 400 atm of fly ash obtained after extraction with carbon dioxide as indicated in (b). Retention time ranges marked by 4, 5, 6, 7, and 8 above Figure 1a correspond to the windows where the tetra-, penta-, hexa-, hepta-, and octachlorodibenzo-*p*-dioxins/dibenzofurans are expected to appear. This figure should be used for qualitative comparison only. Different amounts of furans were extracted in each method.

CONCLUSIONS

The time required to perform the analysis of municipal incinerator fly ash can be reduced substantially by replacing the Soxhlet solvent extraction step with an isolation step based on supercritical fluid extraction. The amount of fly ash required for analysis using supercritical fluid extraction is much smaller when compared to the Soxhlet extraction process and can be decreased even more if direct on-column deposition is performed (*20*, *25*). The initial cost of supercritical fluid extraction instrumentation is significantly reduced if a heated high-pressure vessel is used for delivery of fluids in place of the pumps. Our results indicate that estimation of extraction efficiencies of native dioxins and furans in fly ash using recovery data corresponding to ^{13}C labeled standard should be employed with caution. Good recoveries (within experimental error) were obtained not only for methods which remove the native polutants but also when sample was extracted with pure carbon dioxide.

Precision of determination of polychlorinated dibenzo-*p*-dioxins and dibenzofurans is limited by the high variance of the extraction process $S_T^2 = S_E^2 + S_A^2$, where S_T^2 is a total variance and S_E^2 and S_A^2 are variances associated with the extraction process and analysis, respectively. In our situation $S_E^2 \gg S_A^2$. This is particularly true when Soxhlet extraction is used. In this situation, running a small number of parallel determinations is not an optimum approach to increase precision since the variance is then

$$\frac{S_T^2}{N} = \frac{S_E^2}{N} + \frac{S_A^2}{N} \sim \frac{S_E^2}{N}$$

since $S_E^2 \gg S_A^2$. Similar precision can be obtained by running the same number of extractions, then mixing together the extracts and analyzing the produced mixture. In this case

$$\frac{S_T^2}{N} = \frac{S_E^2}{N} + S_A^2 \sim \frac{S_E^2}{N}$$

since $S_E^2 \gg S_A^2$ and N is small. This approach will save time and expensive GC/MS instrumentation. Supercritical fluid extraction has a smaller variance and therefore the number of extractions needed to be performed to achieve required accuracy is significantly reduced compared to Soxhlet extraction.

ACKNOWLEDGMENT

The authors thank Professor F. W. Karasek for his continuing interest and support during the project. Murray Colquhoun and Mike Lawrence assisted in some of the experiments. Vera Breitung and Bev Ross provided help through their discussions. The high-pressure vessel was constructed by C. Gendron, Science Shops, University of Waterloo. Professor Karasek kindly allowed use of his GC/MS instrumentation. The Ministry of the Environment, Toronto, Canada, supplied municipal incinerator fly ash samples.

Registry No. T_4CDD, 41903-57-5; P_5CDD, 36088-22-9; H_6CDD, 34465-46-8; H_7CDD, 37871-00-4; O_8CDD, 3268-87-9; T_4CDF, 30402-14-3; P_5CDF, 30402-15-4; H_6CDF, 55684-94-1; H_7CDF, 38998-75-3; O_8CDF, 39001-02-0; CO_2, 124-38-9; N_2O, 10024-97-2; HCl, 7647-01-0; benzene, 71-43-2; toluene, 108-88-3.

LITERATURE CITED

(1) Olie, K.; Vermeulen, P. L.; Hutzinger, O. *Chemosphere* **1977**, *8*, 455–479.
(2) Tong, H. Y.; Shore, D. L.; Karasek, F. W. *Anal. Chem.* **1984**, *56*, 2442–2447.
(3) Extraction with Supercritical Gases. *Angew. Chem., Int. Ed. Engl.* **1978**, *17*, 701.
(4) Williams, D. *Chem. Eng. Sci.* **1981**, *36*, 1769.
(5) Paulaitis, M.; et al. *Rev. Chem. Eng.* **1982**, *1*, 179.
(6) McHugh, M.; Krukonis, V. *Supercritical Fluid Extraction*; Butterworth Publishers: Stoneham, MA, 1986.
(7) *Supercritical Fluids*: Squires, T., Paulaitis, M., Eds.; ACS Symposium Series 329: American Chemical Society: Washington, DC, 1987.
(8) Zosel, K. U.S. Patent 3,806,619, 1974.
(9) Coenan, H.; et al. U.S. Patent 4,485,003, 1984.
(10) Modell, M. U.S. Patent 4,061,566, 1977.
(11) Stahl, E.; Schilz, W. *Z. Anal. Chem.* **1976**, *80*, 99.
(12) Sugiyama, K.; Saito, M.; Hondo, T.; Senda, M. *J. Chromatogr.* **1985**, *332*, 107–116.
(13) Lundanes, E.; Greibrokk, T. *J. Chromatogr.* **1985**, *349*, 439–446.
(14) Schantz, M.; Chester, S. *J. Chromatogr.* **1986**, *363*, 397–401.
(15) Hawthorne, S.; Miller, D. *J. Chromatogr. Sci.* **1986**, *24*, 258.
(16) Wright, B.; Wright, C.; Gale, R.; Smith, R. *Anal. Chem.* **1987**, *59*, 38.
(17) Hawthorne, S.; Krieger, M.; Miller, D. *Anal. Chem.* **1989**, *61*, 736.
(18) Hawthorne, S. B.; Miller, D. J. *Anal. Chem.* **1987**, *59*, 1705.
(19) Wright, B. W.; Frye, S. R.; McMinn, D. G.; Smith, R. D. *Anal. Chem.* **1987**, *59*, 640.
(20) Hawthorne, S.; Miller, D. *J. Chromatogr.* **1987**, *403*, 63.
(21) Karasek, F. W.; Dickson, L. *Science* **1987**, *237*, 754.
(22) Submitted for publication in *J. High Resolut. Chromatogr.*
(23) Clement, R.; Viau, P.; Karasek, F. W. *Can. J. Chem.* **1984**, *62*, 2629.
(24) Calcutt, R.; Boddy, R. *Statistics for Analytical Chemists*, Chaplan and Hall: New York, 1983.
(25) Jones, K. *The Chemistry of Nitrogen*; Pergamon Press: Toronto, 1973.
(26) Wright, B.; Fulton, J.; Kopriva, A.; Smith, R. In *Supercritical Fluid Extraction and Chromatography*; Charpentier, B., Sevenants, M., Eds.; ACS Symposium Series 366; American Chemical Society: Washington, DC, 1988.
(27) King, J. In *Supercritical Fluids*; Squires, T., Paulaitis, M., Eds.; ACS Symposium Series 329; American Chemical Society: Washington, DC, 1987.
(28) Giddings, J.; Myers, M.; McLlaren, L.; Keller, R. *Science* **1968**, *162*, 67.

RECEIVED for review July 21, 1989. Accepted September 20, 1989. This work was supported in part by the Natural Sciences and Engineering Research Council of Canada and Imperial Oil of Canada. This work was presented in part at the 1989 Pittsburgh Conference.

Anal. Chem. **1989**, *61*, 2777–2784

Thimble Glass Frit Nebulizer for Atomic Spectrometry

R. H. Clifford and Akbar Montaser*

Department of Chemistry, George Washington University, Washington, D.C. 20052

S. A. Sinex[1] and S. G. Capar

Division of Contaminants Chemistry, Food and Drug Administration, Washington, D.C. 20204

A thimble-shaped glass frit nebulizer has been developed for atomic spectrometry. The thimble glass frit was pressurized internally by gases such as helium (He) or argon (Ar) while the test solution was applied externally to the frit. The pressurized gas exited through the pores of the glass frit and shattered the thin liquid film flowing on the surface of the thimble-shaped device to form small droplets. A small spray chamber surrounded the nebulizer to remove the large droplets. Small droplets were then introduced into inductively coupled plasmas (ICP) sustained in either Ar or He. To reduce the memory effect noted in the frit-type nebulizers, a clean-out system was also devised. Detection limits, signal-to-background ratios (S/B), precision, memory effects, noise power spectra (NPS), and particle size distributions measured with the new nebulizer were compared to those of disk and cylindrical glass frit nebulizers and the commonly used pneumatic nebulizer for Ar ICP atomic emission spectrometry (AES). Analytical performance was also measured for He ICP by using frit-type nebulizers and an ultrasonic nebulizer.

INTRODUCTION

In atomic spectrometry, a nebulizer is used to convert sample solutions into an aerosol. The most commonly used solution nebulizers (*1*) are (a) cross-flow and concentric pneumatic nebulizers, (b) Babington nebulizers, (c) ultrasonic nebulizers, and (d) glass frit nebulizers. In general, pneumatic nebulizers are extremely inefficient because the majority of the solution is directed to the drain. For example, only 1–2% of a solution is transformed into aerosol suitable for atomic and mass spectrometry (*2, 3*). Because very small capillaries are used in the construction of pneumatic nebulizers, these devices are subject to clogging if the test solution is not free from small particles. Although the use of a Babington nebulizer eliminates the clogging problem, this device is inefficient in aerosol production. For ultrasonic nebulizers the efficiency of aerosol transport is improved by a factor of approximately 10 when the test solution consists of a simple matrix. However, such an advantage is eliminated when 10% sulfuric acid solution (commonly used to solubilize food) is nebulized. Moreover, the present ultrasonic nebulizers are much more expensive than the other nebulizers.

To eliminate these problems, two basic types of glass frit nebulizers (see Figure 1A,B) were investigated earlier. Layman and Lichte (*4*) used a porous disk-shaped glass frit as a nebulizer. The nebulizing gas was directed from the top onto the frit and the test solution was introduced on the underside of the disk to generate the aerosol. These and other investigators (*4–10*) concluded that the nebulizer was highly efficient at low uptake rate (e.g., typically 30–150 μL/min) but that it had the following disadvantages: (a) deterioration of concentration detection limits compared with other types of nebulizers, (b) slow equilibration time, (c) memory effects, and (d) the clogging of the pores of the porous glass frit.

Apel and co-workers (*11, 12*) used a cylindrical glass frit, shown in Figure 1B, as the nebulizer instead of a glass frit disk. With this device, called externally pressurized cylindrical glass frit nebulizer (EPCGFN), the test solution was introduced onto the inside surface of the glass frit cylinder while the nebulizing gas pressure was applied externally to the fritted cylinder. In contrast, for the thimble glass frit nebulizer presented in this report, solution was introduced externally while the nebulizing gas was applied to the inside surface of a fritted thimble (Figure 1C). Thus, this new nebulizer will be referred to in this report as internally pressurized thimble glass frit nebulizer (IPTGFN).

Comparison of the geometries of the cylindrical frit with the thimble frit reveals two limitations for the former as a nebulizer. First, the EPCGFN (*11, 12*) is cylindrical and has an inactive nonporous glass at one end. Test solution is introduced internally to the upper surface of the cylinder, and the cylinder acts as both the nebulizer and the spray chamber. For the IPTGFN, no inactive nonporous surface is present, test solution is applied to the external surface of the thimble to form a thin, uniform liquid film, and a small spray chamber surrounds the thimble to remove the large droplets. This arrangement allows the analyst to observe liquid delivery to the nebulizer and the subsequent aerosol generation process and also enhances nebulization efficiency while reducing memory effects associated with frit-type nebulizers, as discussed later in this report.

Another limitation of the EPCGFN is that both upper and lower gas-permeable membranes have surfaces oriented in opposition to one another (*11*). With this configuration, larger droplets deposited on the lower surface may form large pools of solution, thereby reducing the efficiency of the nebulization by a spitting process. In contrast, the IPTGFN uses only one gas permeable membrane and permits the fluid to roll down the thimble to the drain, thus inhibiting production of a supersaturated frit. The IPTGFN is operated vertically, in order to enhance formation of a thin film of solution over the entire surface area, which should lead to more efficient nebulization. Excess solution will not form puddles on the frit surface because gravity ensures smooth drainage of excess solution.

Because of these limitations of the EPCGFN (*11, 12*), an investigation of the analytical potentials of IPTGFN seemed relevant. To reduce or eliminate the memory effect noted in frit-type nebulizers, a clean-out system was also devised. The new nebulizer was compared to disk and cylindrical glass frit nebulizers and the commonly used nebulizer for atomic emission spectroscopy (AES) with respect to detection limits, signal-to-background ratios (S/B), percent relative standard deviation (% RSD) of background, memory effects, particle size distributions, and noise power spectra (NPS). Analytical

---

* To whom correspondence should be addressed.

[1] Present address: Department of Physical Science, Prince George's Community College, Largo, MD 20772-2199.

0003-2700/89/0361-2777$01.50/0 © 1989 American Chemical Society

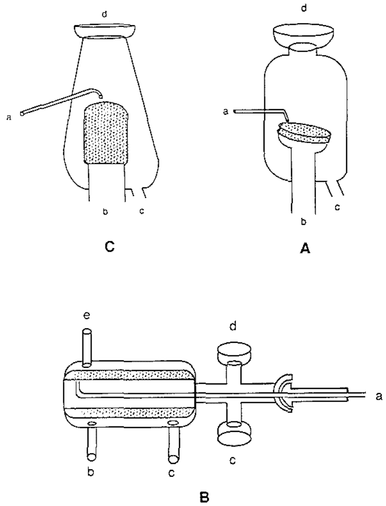

Figure 1. Configuration of the disk-shaped glass frit nebulizer (A), the externally pressurized cylindrical glass frit nebulizer (B), and the internally pressurized thimble glass frit nebulizer (C). The symbols a, b, c, d, and e refer, respectively, to the sample delivery tube, injector gas inlet, drain tube, ball joint for connection to the ICP torch, and backwash inlet tube for the frit.

results were obtained for both the Ar inductively coupled plasma (ICP) (*1*) and the He ICP as developed by Montaser and associates (*13–19*).

EXPERIMENTAL SECTION

Thimble Glass Frit Nebulizer and Other Nebulization Systems. Figure 1C shows a diagram of the thimble glass frit nebulizer surrounded by a small spray chamber. The original glass frit as delivered (part number R-18-12-P5, Witeg Scientific, Garden Grove, CA) was attached to a glass tube, and was in the form of cylinder with a closed end that has been cut with a glass cutting wheel to produce the shape of a thimble 13 o.d. by 25 mm high. The thimble glass frit was placed inside a small spray chamber (total volume 25 cm^3) having an 8 mm i.d. drain tube and a solution delivery tube 5 mm o.d. and 0.4 mm i.d. The top section of the spray chamber was connected to the ICP torches via a female 18/9 ball joint.

Thus far, the pore size of all *effective* frit-type nebulizers has been in the range of 4–10 μm (*4–12*). A pore size of 1–1.6 μm was used for the thimble glass frit to increase the velocity of gas through the pores, thereby producing a more efficient nebulizer.

The disk-shaped glass frit nebulizer (DGFN) was made from a fritted disk (part number 2.350.20, Witeg Scientific) 20 mm diameter by 2 mm thick; 1–1.6 μm pore size. The disk-shaped frit was mounted at an angle of 30°, surrounded by a spray chamber similar to that used for the IPTGFN. For the EPCGFN, the cylindrical frit (special order, ACE Glass, Inc., Vineland, NJ) had an an inside diameter of 1.2 the cm, a length of 5 cm, and a pore size of 4–8 μm. A smaller pore size material for the cylindrical frit was not commercially available. A more complete description of this nebulizer is given elsewhere (*11, 12*).

The pneumatic nebulizer used was the concentric glass nebulizer (Type TR-30-A3, J. Meinhard Associates, Santa Ana, CA) with an ARL conical spray chamber (Applied Research Laboratories, Valencia, CA). An ultrasonic nebulizer and the associated desolvation system (Table I) was used only for the He ICP. A peristaltic pump (Minipulse 2, Gilson Medical Electronics, Middleton, WI) was used to deliver test solution to all nebulizers. A mass flow controller (Model 8200, Matheson Gas Products, East Rutherford, NJ) was used to control the injector gas flow.

Clean-Out System for Frit-Type Nebulizers. In contrast to other nebulizers, the transport efficiency of frit-type nebulizers increases with injector gas flow rate. This principle was used to develop a clean-out system (Figure 2) for reducing the extent of memory effects for frit-type nebulizers. The system consisted of two solenoid valves (Fluorocarbon, Anaheim, CA), a two-way (Model DV2-144-NC-A1) and the other a three-way (Model DV3-234-A1), connected between the nebulizer and the torch for controlling two cycles. The valves were turned on and off electronically from a single switch. During analysis, the nebulized aerosol proceeded directly to the torch while channels for the drain and the supplement gas were closed. During the clean-out cycle, the nebulizer gas flow was switched to the drain, and the gas flow was increased to 3 L/min by the mass flow controller. The supplemental gas was used as injector gas during the switch over. This process allowed the plasma to remain under the same conditions as during measurement, thus preventing the burning of the injector tube, and also reduced the memory effects because the analyte was blown out of the frit pores more rapidly by increasing the nebulizer gas flow.

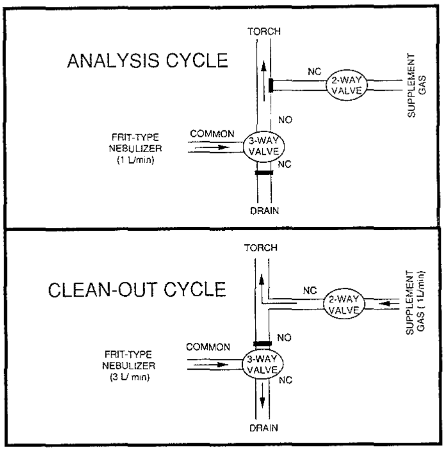

Figure 2. Clean-out system for the frit-type nebulizers. The ports to the valves are either normally closed (NC) or normally open (NO).

Measurement of Transport Efficiency of the Nebulizer. Transport efficiency is defined as the ratio of the amount of analyte converted into the aerosol for injection into the plasma to the amount of analyte aspirated, expressed as percent. Three procedures are used (*2, 3*) to measure transport efficiency: cascade impactor, collection of aerosol on a fiberglass filter of 0.3 μm pore size, and the silica gel procedure. The procedures involving cascade impactor and filter collection measure transport efficiency of analyte with good accuracy and acceptable precision, and with no significant bias between the two. The silica gel method (*2, 3*) measures solvent rather than analyte transport efficiency, and the results have been known to have a positive bias. However, measurement by silica gel collection is quite simple compared to other procedures, and it was adopted for our measurements. The transport efficiency was then used to estimate the mass of aerosol (pure water, not analyte) reaching the plasma per minute.

Transport efficiency was obtained by collecting the aerosol emerging from the spray chamber onto 6–16 mesh silica gel and determing the moisture content through mass difference. Although collection of aerosol at the torch exit could provide more realistic information on transport properties, it was not adopted for our measurements because the sizes of the injector tubes for Ar and He ICP torches were 1.5 and 0.5 mm, respectively, and at high uptake rates, aerosol accumulated at the cold tip of the injector tubes without transfer to the silica gel container.

Because water collected on silica gel results from water aerosol and water vapor, it is important to subtract contribution of water vapor (*23–27*) to measure transport efficiencies and mass transport rates accurately. The data on transport efficiencies and mass transport rates measured in this work could not be corrected for contributions due to water vapor because the extent of water evaporation for our frit nebulizers–spray chambers could not be

Table I. Experimental Facilities and Operating Conditions

	System I
radio frequency generator	2.5-kW, 27.12 MHz crystal-controlled generator (Henry Electronics, Los Angeles, CA) with auto power control. The automatic matching network is described elsewhere (*20*)
Ar ICP torches	Extended tangential flow torch with side arm (Applied Research Laboratories, Valencia, CA). See Table II for operating conditions. A 3.5-turn, shielded load coil was used (*21*)
sample introduction system	See text. For detection limit studies, a multielement solution of the elements (each at 10 μg/mL) shown in Table III was prepared in 1% nitric acid solution. For studies involving the noise power spectra, a 10 μg/mL Mn solution was prepared in 1% nitric acid
spectrometer	1-m focal length direct-reader in a Paschen-Runge mounting (Model 3580, Applied Research Laboratories, Valencia, CA) with a 1080 grooves/mm grating, and 21- and 20-μm entrance and exit slit widths, respectively. Slit height was 10 mm. A 1:1 image of the plasma was formed on the entrance
detection system for NPS measurements	The sequential spectrometer (Model 3580, Applied Research Laboratories, Valencia, CA) was used, 21- and 20-μm entrance and exit slit widths, respectively. Slit height was 10 mm. A 1:1 image of the plasma was formed on the entrance. Current output from the photomultiplier (Type R106 UH, Hamamatsu Corp., Bridgewater, NJ), operated at the same voltage for all measurements, was amplified by a linear current-to-voltage converter (Model 427, Keithley Instrument, Inc., Cleveland, OH). The data acquisition system consisted of a Labmaster ADC (Tecmar, Inc., Cleveland, OH) installed on a IBM-PC-AT microcomputer. ASYSTANT+ (Asyst Software Technologies, Inc., Rochester, NY) was used to acquire the noise power spectra; see ref 21
	System II
radio frequency generator	5-kW, 27.12-MHz crystal-controlled generator (Model HFS-5000D, RF Plasma Products, Kresson, NJ) with auto power control. The automatic matching network is described elsewhere (*20*)
He ICP torch	A low-gas flow torch was used for He ICP (*14*). See Table II for operating conditions. The plasma torch and the matching network were mounted on an X-Y-Z translation stage for moving them with respect to the spectrometer. A 4.5-turn, shielded load coil was used. The top turn of the load coil was grounded (*18*)
sample introduction system	See text. A water-cooled ultrasonic nebulizer (Model UNPS-1, RF Plasma Products, Kresson, NJ) with a desolvation chamber was used for tangential-flow He ICP. The nebulizer was operated at 1.4 MHz with a forward power of 45 W. 1 mL/min analyte solution was nebulized into plasma. The concentrations of Cl, Br, and I were 500 μg/mL for detection limit studies with He ICP
imaging optics	5 cm diameter, 20 cm focal length, spherical plano-convex quartz lens projected a 1:1 image of the plasma onto the entrance slit. The lens aperture was 25 mm
optical filter	A sharp-cut-off, yellow filter (catalog no. CS3-713385, Corning Glass Works, Corning, NY) was used to eliminate possible interferences from second- or third-order spectra
spectrometer	1-m focal length Czerny–Turner monochromator (Model 2061, GCA/McPherson Instrument, Acton, MA) with a 1200 grooves/mm holographic grating blazed at 300 nm, 50 μm entrance slit width and 4 mm slit height. The reciprocal linear dispersion is 0.833 nm/mm
detection system for detection limit measurement	1024-pixel intensified linear photodiode array (Model 1420R, EG&G Princeton Applied Research, Princeton, NJ) with a detector controller (Model 1218) and a system processor (Model 1215-OMA-2). The size of each pixel is 25 μm × 2.5 mm. The detector was cooled to -20 °C
detection system for NPS measurements	Type 9558QB PMT (EMI Electronics, Ltd., Middlesex, England) Cooled to -20 °C and operated at -800 V. Current ouput was amplified by a linear current-to-voltage converter (Model 427, Keithley Instrument, Inc., Cleveland, OH). The data acquisition system consisted of a Labmaster ADC (Tecmar, Inc., Cleveland, OH) installed on an IBM-PC-XT microcomputer. ASYSTANT+ (Asyst Software Technologies, Inc., Rochester, NY) was used to acquire the noise power spectra; see ref 22

ascertained accurately. For example, a typical water loading of 38.5 mg of water per liter of Ar injector gas was measured for an Ar ICP equipped with a Meinhard nebulizer and dual tube Scott spray chamber (*26*). For the same measurement, the mass transports of water vapor and water aerosol were 27.2 and 11.3 mg/L Ar, respectively (*26*). Under such conditions, the Ar injector gas is saturated with water vapor (*23–27*). This observation on saturation of injector gas with water vapor is not necessarily valid for the frit-type nebulizers, especially at very low uptake rate. For these nebulizers, a contribution from water vapor is certain, yet the extent of such a contribution from water vapor is uncertain at this time. Thus, the readers should note that the transport efficiencies and mass transport rates presented in Figures 3 and 4 could not be corrected for the contribution due to water vapor.

Aerosol Particle Counting System. The techniques (*2, 3*) used to estimate droplet diameter include measurement with microscopes, horizontal elutriators and cascade impactors, and devices based on optical scattering. Cascade impactors have often been used in droplet sizing (*3*) but require more time than the optical scattering techniques.

For this work, an aerosol particle couting system (Model 4101 counting system and Model 1100 sensor, Hiac/Royco Instrument Division, Smithtown, NY), developed for airborne particle counting, was used to measure the size and the number of droplets produced by the various nebulizers. In this system, a vacuum pump drew the aerosol into the sensor to measure the number of droplets by near forward scattering. Droplets were drawn into the sensor at a height of 8 mm above the outlet of the spray chamber. Direct connection between the sensor and the spray chamber was not possible because aerosol was drawn by the vacuum system at 28.4 L/min, a much higher rate than the typical gas flow of ICP nebulizers. The additional air sucked into the particle counter should cause solvent to evaporate, similar to the effect with the typical cascade impactors (*2, 3*), resulting in bias toward smaller drop sizes. Relatedly, the background particles drawn with the vacuum system can change droplet size distribution. To minimize the latter, all data reported here have been corrected for the background count in successive measurements. All measurements were the average of three 60-s integrations.

The particle size range of Model 4101 was 0.5 μm and greater, and six user-settable size channels were available. For preliminary studies, the channels were set at 0.5, 1.5, 3, 5, 10, and 15 μm, but the number densities measured above 3 μm were quite low for frit-type nebulizers. Thus, for all results presented in this report, the size channels were set at 0.5, 0.7, 1.1, 1.5, 2.0, and 2.5 μm to compare the relative number of droplets produced by the various nebulizers.

RESULTS AND DISCUSSION

Operational Characteristics of the Thimble Frit Nebulizer vs Other Devices. *Effect of Uptake Rate on Transport Efficiency and Mass Transport Rate.* Frit-type nebulizers are known to posses higher transport efficiencies than the commonly used pneumatic nebulizers (*4–12*). Parts A and B of Figure 3 show percent transport efficiencies

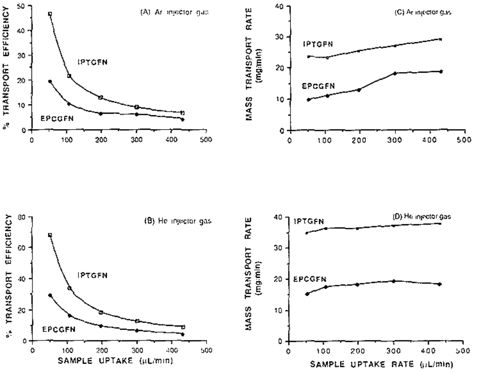

Figure 3. Percent transport efficiencies (A, B) and mass transport rate (C, D) measured with the silica gel procedure for the IPTGFN and EPCGFN using argon and helium injector gas. The injector gas flow rate was 1 L/min. See Experimental Section for contribution due to water vapor.

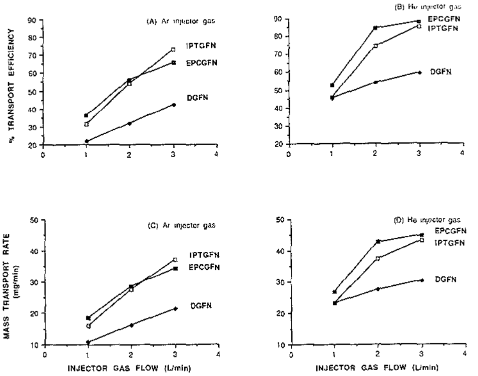

Figure 4. Effect of injector gas flow on transport efficiency (top) and mass transport rate (bottom) for IPTGFN, EPCGFN, and DGFN with (A and C) argon and (B and D) helium injector gas. The uptake rate was 0.05 mL/min. See Experimental Section for contribution due to water vapor.

measured for IPTGFN vs EPCGFN by using Ar and He injector gases at 1 L/min. As discussed in the Experimental Section, these data could not be corrected for contribution due to water vapor (*23–27*). In general, the IPTGFN was more efficient than the EPCGFN in aerosol production, especially when He injector gas and low uptake rate were used. The greater efficiency of the IPTGFN vs the EPCGFN may be partly attributed to the smaller pore size (1–1.6 μm) of the IPTGFN. For an identical EPCGFN at an uptake rate of 0.07 mL/min, Apel and co-workers (*12*) reported efficiencies of 44–50% and 25–33% for Ar and He injector gases, respectively, compared to 15% and 20% measured in this study. Discrepancies between the results may be attributed to the method of measurement. Our measurements were based on aerosol collection for periods ranging from 5 to 60 min for the high and low uptake rates, respectively. No such data were reported by Apel and co-workers (*12*).

Although transport efficiencies decrease at higher uptake rate, it would be more useful to compare the mass of aerosol (solvent in these studies) exiting from the spray chamber per minute. For the EPCGFN, the mass of the aerosol exiting from the spray chamber per minute increased, as shown in Figure 3C,D, by a factor of approximately 1.8 and 1.2 as the uptake rate was changed from 0.05 to 0.45 mL/min, respectively, for Ar and He injector gases. The mass transport rate increased by a factor of approximately 1.2 when the IPTGFN was operated with either Ar or He. These results suggest that the use of uptake rate greater than 0.05 mL/min for the IPTGFN tested in this work should not enhance the sensitivity of determination significantly, and therefore, the IPTGFN can be considered as a low-consumption nebulizer.

Effect of Injector Gas Flow Rate on Transport Efficiency and Mass Transport Rate. The data presented in the previous section were obtained at an injector gas flow of 1 L/min, the rate typically used for Ar and He ICP discharges (*1–19*). Figure 4 presents the effect of the injector gas flow on transport efficiency and mass transport rate measured at the outlet of the spray chamber for IPTGFN, EPCGFN, and DGFN with Ar and He as injector gases. Again, as discussed in the Experimental Section, these data could not be corrected for contribution due to water vapor (*23–27*). In general, higher transport efficiencies were noted at higher injector flow. At 0.05 mL/min, both the transport efficiency and the mass transport rate increased by a factor of approximately 3 as the injector gas flow was increased from 1 to 3 L/min for IPTGFN and EPCGFN. The same variation for DGFN enhanced the mass transport rate by only a factor of 2.

Transport efficiencies and mass transport rates presented in Figure 3 and at 1 L/min and 0.05 mL/min were not the same as those shown in Figure 4 at the same conditions. These variations in the cited properties may be associated with changes in the porosity of the glass frit as the result of partial clogging. The pore sizes for the thimble frit and the cylindrical frit were in the range of 1–1.6 and 4–8 μm, respectively. The data presented in Figure 3 were obtained in the early stage of this study whereas those shown in Figure 4 were acquired toward the end of this work. It is possible that the thimble frit was highly efficient in the earlier experiments because of its small pore size but gradually lost its efficiency due to partial clogging. This gradual clogging could have also occurred for the cylindrical frit, but because pore size decreased from 4–8 μm toward the 1–1.6 μm range, the cylindrical frit became more efficient. Thus far, cleaning in concentrated acids to leach out the minerals causing the blockage has not restored the original performance of the frit-type nebulizers. Scanning electron microscopy on new and old glass frits will be used in future studies to account for the changes in pore size.

The enhancement noted in transport efficiency and mass transport rate with injector gas flow may be used to reduce the extent of memory effect in the frit-type nebulizer.

Effect of Injector Gas Flow Rate on Memory Effect of Frit-Type Nebulizers. To reduce the extent of the memory effect noted in frit-type nebulizers, the clean-out system shown in Figure 2 was used. An evaluation of memory effects for three frit-type nebulizers is presented by the intensity–time profiles shown in Figure 5A–C. The concentration of analyte was 1000 μg/mL Fe. The clean-out cycle was limited to the time shown between points a and b in Figure 5A–C. During the period a–b, which was 60 s, the nebulizer gas flow was increased to 3 L/min to blow out the analyte from the frit into the drain while approximately 1 L/min dry Ar was injected into the axial channel. Without the clean-out system, Fe signal could not be reduced to the 1% level in less than 4 min for most frit nebulizers. Memory effects were the least for DGFN and the most for EPCGFN, probably because the surface areas of the frits were the smallest and the largest, respectively. As shown in Figure 5D, the dependence of the wash-out time (required to reduce the signal to the 1% level) on the surface area of the frit could be minimized when the clean-out system was used. For EPCGFN, the use of the back-wash (at 2.7 mL/min) decreased the extent of memory effect, but it was not as effective as the clean-out system. Even

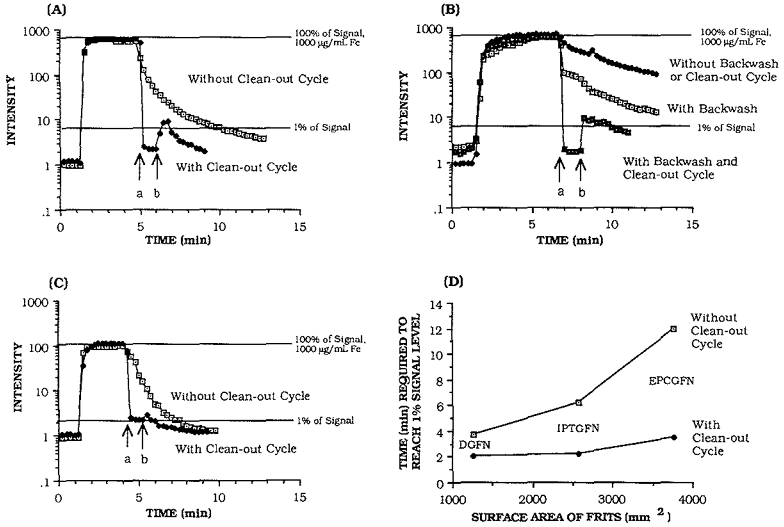

Figure 5. Memory effect of (A) IPTGFN, (B) EPCGFN, and (C) DGFN with and without the use of clean-out system and (D) the influence of surface area of the glass frit on the memory effect. The concentration of Fe was 1000 µg/mL and the uptake rate was 0.4 mL/min. Distilled water was used at 2.7 mL/min to wash the exterior surface of the frit used in EPCGFN.

with the clean-out system, the signal level for EPCGFN did not return to the original background level after approximately 6 min of cleaning. Such a problem was not noted for the IPTGFN and DGFN, yet the wash-out time was still long (approximately 2 min) for IPTGFN and DGFN, compared to 45 s measured for the pneumatic nebulizer equipped with the ARL spray chamber. Optimization of the clean-out period a-b and gas flow may reduce the wash-out time.

Aside from the trend noted for wash-out time, it is necessary to compare signal equilibration time for the frit-type nebulizers. This parameter was also a function of the surface area of the frit. The equilibration times were 83, 105, and 225 s for DGFN, IPTGFN, and EPCGFN, respectively, longer than the 15 s measured for the pneumatic nebulizer equipped with the ARL spray chamber. The duration of the equilibration time for the frit-type nebulizers may be reduced by a faster solution delivery to the nebulizer prior to analytical measurements.

Particle Size Distributions for the Thimble Frit Nebulizer vs Other Nebulization Devices. The most appropriate term to describe droplet distribution of a nebulization device used in analytical spectrometry is the mass median diameter, with a value approximately the same as the Sauter mean diameter (volume-to-surface-area ratio diameter) for pneumatically produced aerosol (*2*, *3*). For the particle counting system available for this study, only the number of droplets of six user-settable sizes could be measured to produce the numerical count distribution. Previous ICP-AES studies (*2*, *3*) have documented that the numerical median diameter has a smaller magnitude than the mass median diameter. Because frit-type nebulizers are known to produce smaller droplets (*4*) than pneumatic nebulizers, numerical count distributions of these devices are compared in Figure 6 for both Ar and He injector gas flows at 1 L/min. The uptake rate was 0.11 and 1 mL/min for the frit-type nebulizers and the pneumatic nebulizer, respectively. For the Ar injector gas, the Meinhard nebulizer-ARL spray chamber produced the largest number of droplets having diameters between 0.5 and 2.5 µm. Among the frit-type nebulizers, the EPCGFN and the DGFN were the most and the least efficient, respectively.

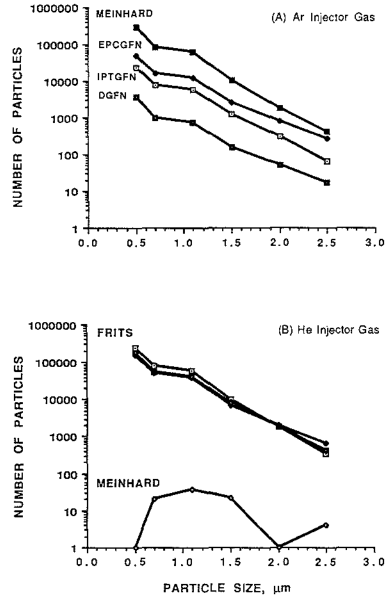

Figure 6. Numerical droplet count distribution of frit-type nebulizers and Meinhard nebulizer using (A) argon and (B) helium injector gas. The injector gas flow rate was 1 L/min. The uptake rate was 0.11 and 1 mL/min, respectively, for the frit-type and the Meinhard nebulizers.

In contrast to the trend noted above, the numerical count distributions for the cited devices were quite different when He was used as the injector gas (Figure 6B). The number of droplets produced by the frit-type nebulizers were 3 orders of magnitude larger, especially for smaller droplets, than those produced by the pneumatic nebulizer. Relatedly, the numerical count distributions for the frit-type nebulizers were

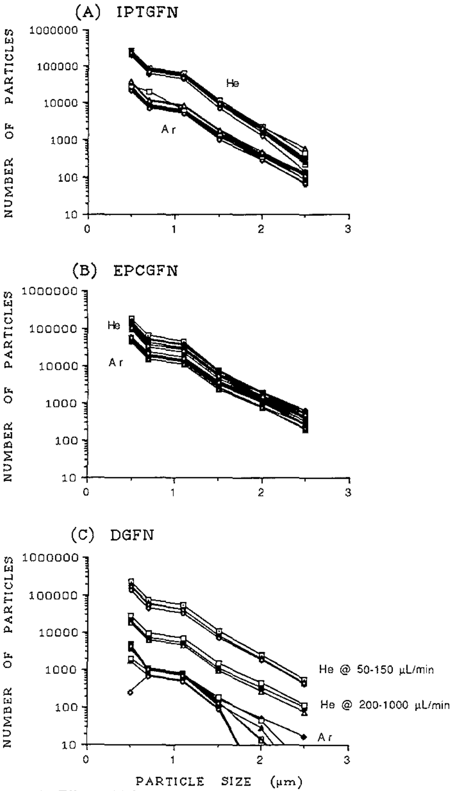

Figure 7. Effect of injector gas type and uptake rate on the numerical droplet count distribution of frit-type nebulizers. The uptake rate (µL/min) was 50 (□), 110 (◆), 160 (◘), 200 (◇), 300 (■), 430 (□), 750 (▲), and 1000 (△).

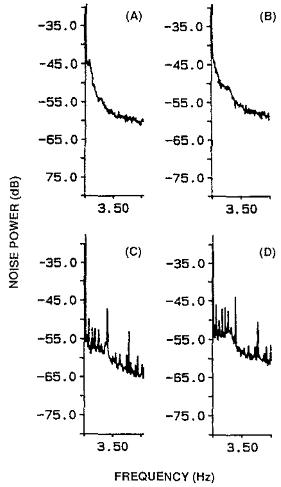

Figure 8. Noise power spectra (0–7 Hz) of Ar ICP using a IPTGFN nebulizer (top) and a Meinhard nebulizer (bottom). Spectra were recorded at Mn II 257.610 nm (A, C) and Ar I 355.431 nm (B, D). A total of 64 scans, each 1024 points long, were averaged. See ref 21 for other details of NPS measurements.

Table II. Plasma Operating Conditions for Ar and He ICP Discharges

parameters	Ar ICP	He ICP
outer flow, L/min	12	7
inter. flow, L/min	1	—
injector flow, L/min	1	1
uptake rate, mL/min	0.05–1	0.05–1
forward power, W	1150	1500
reflected power, W	<5	<5
observation height, mm	15	25

approximately the same. At higher injector gas flows, the pneumatic nebulizer may operate more efficiently (*28*).

Figure 7 shows numerical count distributions for the frit-type nebulizers for the uptake rate of 0.05–1 mL/min. In all cases, larger numbers of droplets were produced with the He injector gas. Except for DGFN, increased sample delivery to the frit did not change the numerical count distribution significantly. These results clearly documented that the IPTGFN was approximately 10 times as efficient in the production of small particles with He as injector gas as with Ar and that the efficiency of small-particle production for the IPTGFN and EPCGFN nebulizers did not change significantly as the uptake rate was increased from 0.05 to 1 mL/min.

Noise Power Spectra of Plasma for the Thimble Frit Nebulizer vs the Meinhard Nebulizer. One major advantage of frit-type nebulizers over the pneumatic nebulizers is their greater efficiency in generation of droplets with diameters in the range of 0.1–1 µm (*4*). The smallest droplet diameter that could be measured with our particle counting system was 0.5 µm. If the fraction of droplets with diameters less than 0.5 µm is significantly larger for the frit-type nebulizers than for the Meinhard nebulizer, it would be reasonable to assume that the noise power spectra of the plasma fed by the former would be less complex. This assumption is partly supported by the noise power spectra shown in Figure 8 for the IPTGFN and the Meinhard nebulizers when Mn II 257.610 and Ar I 355.431 nm spectral lines were monitored. The procedures for acquiring noise power spectra are described elsewhere (*21, 22*). These data clearly revealed that frit-type nebulizers produce less low-frequency noise fluctuation in the Ar plasma than does the Meinhard nebulizer. Similar results are expected for He ICP discharges. The lower white noise level exhibited for the Meinhard nebulizer is associated with cooling of the axial channel as a result of larger uptake rate.

Analytical Performance of the Thimble Frit Nebulizer vs Other Devices. In this section, net analyte emission intensities, S/B ratios, % RSD of background, and detection limits measured with the frit-type nebulizers are reported for Ar and He ICPs. For the Ar ICP, analytical results were obtained simultaneously for 14 elements by a direct-reader spectrometer. Analytical results for He ICP were obtained for three elements by a sequential spectrometer. Detection limit was defined as the analyte concentration giving a signal equivalent to 3 times the noise, calculated from the standard deviation of 11 repetitive 10-s measurements of the background intensities. All analytical conditions are listed in Tables I and II.

Table IIIA shows background intensities, net emission intensities, S/B, % RSD, and detection limits of elements measured with Ar ICP by three frit-type nebulizers and a Meinhard nebulizer. In general, the background intensities measured for the various nebulizers were comparable. Similar trends were noted for the % RSDs of the background.

Among the frit-type nebulizers, IPTGFN yielded the highest net intensities for all elements tested. The results

Table III. Analytical Performance of Frit-Type Nebulizers

A. Frit-Type and Meinhard Nebulizers Used with an Ar ICP[a]

	background intensities[b]				net intensities[b,c]				S/B				% RSD				detection limits[d]			
elements	DGFN	EPC-GFN	IPT-GFN	MEIN	DGFN	EPC-GFN	IPT-GFN	MEIN	DGFN	EPC-GFN	IPT-GFN	MEIN	DGFN	EPC-GFN	IPT-GFN	MEIN	DGFN	EPC-GFN	IPT-GFN	MEIN
As 189.0	0.92	1.23	1.33	1.95	2.13	2.00	9.07	24.3	2.3	1.6	6.8	12.4	0.90	0.94	0.80	0.80	150	170	35	20
Ca 393.4	2.51	1.27	1.24	3.37	111	222	469	986	44.2	175	378	293	3.56	0.28	3.84	1.18	24	1	3	1
Cd 226.5	1.07	1.80	1.66	2.56	13.1	17.3	53.9	193	12.2	9.6	32.5	75.6	1.52	1.42	0.83	0.66	27	44	8	3
Co 228.6	0.63	0.88	0.92	1.34	4.5	4.07	17.1	59.2	7.1	4.6	18.6	44.2	0.94	0.56	0.90	0.61	36	36	14	4
Cr 267.7	1.41	1.89	2.08	2.83	6.46	6.27	22.4	84.7	4.6	3.3	10.8	29.9	1.00	1.18	1.19	0.62	68	110	33	6
Cu 324.8	0.92	1.54	1.65	2.22	9.15	9.27	36.6	70.6	9.9	6.0	22.2	31.8	0.49	0.28	0.42	0.27	18	14	6	3
Fe 259.9	0.75	0.48	1.12	1.65	3.76	1.40	17.6	47.7	5.0	2.9	15.7	28.9	0.49	0.35	0.42	0.39	39	36	8	4
Mn 257.6	0.74	1.11	0.99	1.45	35.2	33.6	116	405	47.6	30.3	117	279	1.15	0.78	0.74	0.92	8	8	2	1
Mo 202.2	0.61	0.97	0.94	1.48	5.21	5.59	20.8	63.3	8.5	5.8	22.1	42.3	0.86	0.60	0.88	0.71	20	31	12	5
Ni 231.6	1.24	1.22	1.49	1.87	2.1	2.18	8.41	29.1	1.7	1.8	5.6	15.6	0.64	0.90	0.82	0.85	110	150	44	17
Pb 220.4	0.85	1.33	1.28	2.02	1.38	1.21	4.02	11.8	1.6	0.9	3.1	5.88	1.07	0.72	0.99	0.59	160	240	95	30
Ti 337.3	0.76	1.31	1.19	1.68	5.27	5.69	21	55.5	6.9	4.3	17.6	33.0	0.46	0.18	0.51	0.28	30	12	9	3
V 292.4	0.59	0.91	0.93	1.42	2.64	2.66	11.9	31.5	4.5	2.9	12.8	22.2	0.38	0.32	0.46	0.40	35	33	11	5
Zn 213.9	0.44	0.63	0.62	1.06	8.74	11.0	45.1	96.8	19.9	17.5	72.7	91.4	2.34	0.75	1.24	0.89	20	13	5	3

B. Frit-type and Ultrasonic Nebulizers Used with a He ICP[a]

	background intensities[e]				net intensities[e,f]				S/B				% RSD				detection limits[g]			
elements	DGFN	EPC-GFN	IPT-GFN	USN	DGFN	EPC-GFN	IPT-GFN	USN	DGFN	EPC-GFN	IPT-GFN	USN	DGFN	EPC-GFN	IPT-GFN	USN	DGFN	EPC-GFN	IPT-GFN	USN
Cl 837.6	1065	1302	1063	1399	1344	1395	1318	5831	1.3	1.1	1.2	4.2	1.50	1.59	1.20	1.54	19	24	15	6
Br 827.2	1096	1242	1138	1464	3041	3102	2961	10683	2.8	2.5	2.6	7.3	1.59	1.68	1.40	1.24	10	11	8	3
I 804.4	1200	1381	1187	1497	624	585	583	2341	0.5	0.4	0.5	1.6	1.47	1.89	1.08	1.34	45	69	33	13

[a] The nebulizers used were disk-shaped glass frit nebulizer (DGFN), externally pressurized cylindrical glass frit nebulizer (EPCGFN), internally pressurized thimble glass frit nebulizer (IPTGFN), the Meinhard nebulizer (MEIN), and the ultrasonic nebulizer (USN). Solution uptake was 0.4 mL/min for all frit-type nebulizers and 1 mL/min for all others. [b] For 10-s integration times. Intensities are expressed in counts/1000. A signal of 1 V is equivalent to 50 kHz. [c] For 10 μg/mL multielement solutions. [d] Detection limits (3σ) in ng/mL. [e] The total integration time for the photodiode array detector was 10 s. [f] For 500 μg/mL multielement solution. [g] Detection limits (3σ) in μg/mL.

shown in Table III for IPTGFN were obtained with the new thimble frit which had a pore size of 1–1.6 μm. The efficiency of the thimble in aerosol production, as shown by the density of fog produced, was reduced after repeated use, indicating partial clogging. For example, the relative net intensities of the Fe 259.9 nm lines were 1.4 and 17.6 when a 10 μg/mL solution was nebulized with the EPCGFN and IPTGFN, respectively. The data shown in Figure 5 indicate that relative net intensities of approximately 600 were obtained when a 1000 μg/mL Fe solution was aspirated with the same nebulizers. If the nebulizer performance is assumed to be linear with concentration, and if no clogging has occurred, net intensities of 140 and 1760 could be expected for EPCGFN and IPTGFN. Thus, it may be argued the pores of both the cylinder and the thimble had gradually become clogged, but in this process, IPTGFN lost its original efficiency because its pore size was quite small (1–1.6 μm) while EPCGFN became more efficient because the original pore size (4–8 μm) was large. The validity of this hypothesis will be investigated by scanning electron microscopy in future studies.

In general, detection limits measured with the IPTGFN were within a factor of 2–5 of the results obtained by the pneumatic nebulizer. In contrast, the use of EPCGFN and DGFN with the ICP-AES technique yielded detection limits that were inferior to those of the pneumatic nebulizer by a factor of 3–24. Apel and co-workers (*12*) reported that detection limits measured for their EPCGFN were inferior to the ICP-AES results obtained with a pneumatic nebulizer by a factor of 3–10.

Table IIIB shows net emission intensities, S/B, % RSD of background, and detection limits of Cl, Br, and I measured with He ICP by three frit-type nebulizers and an ultrasonic nebulizer. Because the pneumatic nebulizer used in this work did not operate efficiently with He as injector gas, analytical performance was compared with an ultrasonic nebulizer equipped with a desolvation chamber. In general, the detection limits measured with the frit-type nebulizers were comparable. Detection limits with the ultrasonic nebulizer were superior to those obtained with the frit-type nebulizers by a factor of 2–4 for He ICP.

CONCLUSIONS

An internally pressurized thimble glass frit nebulizer (IPTGFN) was developed as a new sample introduction system for atomic spectrometry. The thimble was pressurized internally while the test solution was applied to the external surface of the glass frit. The new device was 10 times as efficient in aerosol production (for particle sizes in the ranges 0.5–2.5 μm) when helium rather than argon was used as the nebulizing gas. On concentration basis, detection limits measured with IPTGFN were superior to those obtained with the previous frit-type nebulizers, and were within a factor of 2–5 of the results achieved with a pneumatic nebulizer used in Ar ICP-AES. Detection limits measured for the He ICP with the IPTGFN were inferior to the results obtained with an ultrasonic nebulizer used in conjunction with a desolvation system by a factor of only 2–3 times. Obviously, on absolute basis, the detection limits are comparable because the volume of sample used with IPTGFN is smaller than that of pneumatic and ultrasonic nebulizers.

The extent of the memory effects commonly encountered with frit-type nebulizers was reduced by devising a clean-out system. The wash-out time (required to reduce signal intensity to 1%) was approximately 2 min for the IPTGFN compared to 45 s for a pneumatic nebulizer. At the present time, the most glaring disadvantage of this new glass frit nebulizer is the reduction in aerosol production as a result of repeated usage. If this problem can be eliminated, IPTGFN may be considered as a viable, low cost nebulization system that consumes a microliter quantity of test solution. Conditions leading to the degradation of efficiency of thimble frit are currently being investigated.

ACKNOWLEDGMENT

We thank I. Ishii and H. Tan of GWU, and W. B. Sisson, J. A. Easterling, and W. F. Syner of Food and Drug Administration (FDA) for their assistance during this work. Special thanks are due to C. T. Apel of the Los Alamos National Laboratory, Los Alamos, NM, for providing a copy of the original design for EPCGFN and for his advice on its fabrication. Constructive comments for revising this manuscript were made by R. F. Browner, Georgia Institute of Technology, Atlanta, GA. His assistance is greatly appreciated.

Registry No. As, 7440-38-2; Ca, 7440-70-2; Cd, 7440-43-9; Co, 7440-48-4; Cr, 7440-47-3; Cu, 7440-50-8; Fe, 7439-89-6; Mn, 7439-96-5; Mo, 7439-98-7; Ni, 7440-02-0; Pb, 7439-92-1; Ti, 7440-32-6; V, 7440-62-2; Zn, 7440-66-6; I_2, 7553-56-2; Br_2, 7726-95-6; Cl_2, 7782-50-5.

LITERATURE CITED

(1) *Inductively Coupled Plasma in Analytical Atomic Spectrometry*, Montaser, A., Golightly, D. W., Eds.; VCH: New York, 1987; 660 pp.
(2) Gustavsson, A. In *Inductively Coupled Plasma in Analytical Atomic Spectrometry*, Montaser, A., Golightly, D. W., Eds.; VCH: New York, 1987.
(3) Browner, R. F. In *Inductively Coupled Plasma Emission Spectroscopy*, Part II, Boumans, P. W. J. M., Ed.; Wiley: New York, 1987.
(4) Layman, R. L.; Lichte, F. E. *Anal. Chem.* **1982**, *54*, 638–642.
(5) Nisamaneepong, W.; Haas, D. L.; Caruso, J. A. *Spectrochim. Acta* **1985**, *40B*, 3–10.
(6) Ibrahim, M.; Nisamaneepong, W.; Haas, D. L.; Caruso, J. A. *Spectrochim. Acta* **1985**, *40B*, 367–376.
(7) Ibrahim, M.; Nisamaneepong, W.; Caruso, J. A. *J. Chromatogr. Sci.* **1985**, *23*, 144–150.
(8) Stahl, R. G.; Timmins, K. J. *J. Anal. At. Spectrom.* **1987**, *2*, 557–559.
(9) Michard-Poussel, E.; Mermet, J. M. *Spectrochim. Acta* **1986**, *41B*, 49–61.
(10) Niemczyk, T. M.; Espinosa, D. C. *Appl. Spectrosc.* **1987**, *41*, 26–31.
(11) Apel, C. T.; Layman, L. R.; Gallimore, D. L. US Patent 4,743,407, 1988.
(12) Apel, C. T.; Layman, L. R.; Gallimore, D. L. *ICP Inform. Newsl.* **1989**, *9*, 503–505.
(13) Chan, S.; Montaser, A. *Spectrochim. Acta* **1985**, *40B*, 1467–1472.
(14) Chan, S.; Van Hoven, R. L.; Montaser, A. *Anal. Chem.* **1986**, *58*, 2342–2343.
(15) Chan, S.; Montaser, A. *Spectrochim. Acta* **1987**, *42B*, 591–597.
(16) Montaser, A.; Chan, S.; Koppenaal, D. W. *Anal. Chem.* **1987**, *59*, 1240–1242.
(17) Montaser, A.; Van Hoven, R. L. *CRC Crit. Rev. Anal. Chem.* **1987**, *18*, 45–103.
(18) Chan, S.; Tan, H.; Montaser, A. *Appl. Spectrosc.* **1989**, *43*, 92–95.
(19) Chan, S.; Montaser, A. *Spectrochim. Acta* **1989**, *44B*, 175–184.
(20) Montaser, A.; Ishii, I.; Clifford, R. H.; Sinex, S. A.; Capar, S. G. *Anal. Chem.* **1989**, *61*, 2589–2592.
(21) Montaser, A.; Clifford, R. H.; Sinex, S. A.; Capar, S. G. *J. Anal. At. Spectrom.* **1989**, *4*, 499–503.
(22) Montaser, A.; Ishii, I.; Tan, H.; Clifford, R. H. *Spectrochim. Acta*, in press.
(23) Ripson, P. A. M.; de Galan, L. *Anal. Chem.* **1983**, *55*, 372–373.
(24) Browner, R. F.; Smith, D. D. *Anal. Chem.* **1983**, *55*, 373–374.
(25) Long, S. E.; Browner, R. F. *Spectrochim. Acta* **1986**, *41B*, 639–649.
(27) Long, S. E.; Browner, R. F. *Spectrochim. Acta* **1988**, *43B*, 1461–1471.
(27) Zhu, G.; Browner, R. F. *J. Anal. At. Spectrom.* **1988**, *3*, 781–789.
(28) Cull, K. B.; Carnahan, J. W. *Spectrochim. Acta* **1987**, *42B*, 629–635.

RECEIVED for review July 17, 1989. Accepted September 13, 1989. This research (at GWU) was sponsored in part by the U.S. Department of Energy under Grant No. DE-FG05-87-ER-13659. Partial support for A.M. and R.H.C. was provided by the FDA.

Anal. Chem. **1989**, *61*, 2785-2791

Determination of Chloride and Available Chlorine in Aqueous Samples by Flame Infrared Emission

S. W. Kubala, D. C. Tilotta, M. A. Busch, and K. W. Busch*

Department of Chemistry, Baylor University, Waco, Texas 76798

A specially designed system, using a flame infrared emission (FIRE) detector, was developed to permit the determination of chloride (Cl^-) in water and available chlorine (Cl_2, HOCl, and OCl^-) in liquid bleach. Chloride ion was converted to molecular chlorine (Cl_2) by addition of concentrated sulfuric acid and a saturated solution of potassium permanganate. Bleach samples were treated with sulfuric acid to convert all hypochlorite and hypochlorous acid to Cl_2. After treatment, molecular chlorine was purged from solution with He and introduced into a hydrogen/entrained-air flame. A portion of the HCl emission intensity at 3150–2425 cm^{-1} was monitored by using a lead selenide detector in conjunction with a 3.8-μm optical band-pass filter. Peak emission intensity measurements from repeated injections of aqueous NaCl standards gave a relative standard deviation of 3.34%, and calibration curves were linear up to the maximum concentration of chloride investigated (10 mM NaCl). The average relative standard deviations of the chloride and available chlorine determinations measured with the FIRE system were found to be 4.39% and 1.84%, respectively. The accuracy of the FIRE technique was determined by comparing the available chlorine results with those obtained by iodometric titration for three commercial bleach samples and was found to be 2.97%. The detection limit for chloride and available chlorine was found to be 1.59 ppm (4.49×10^{-2} mM Cl^-) and 1.61 ppm (2.27×10^{-2} mM Cl_2), respectively. Elevated levels of bromide produced a negative interference in the determination of chloride with the FIRE system, but iodide and phosphate did not interfere.

INTRODUCTION

The element chlorine is widely distributed in nature and is used extensively in its various oxidation states (*1*). Aqueous molecular chlorine (Cl_2) and hypochlorite (OCl^-), for example, are employed as bleaching agents (*2*) and as disinfectants to prevent the spread of waterborne diseases (*3*). Because of the reactivity of the higher oxidation states of chlorine, the element occurs in nature primarily as the chloride ion (Cl^-) and is one of the major inorganic constituents of surface waters, groundwaters, and wastewaters. In seawaters, chloride levels, expressed as chlorinity, are approximately related to salinity and can be used to determine the concentrations of all other biounlimited elements present in a sample (*4*). Chloride concentration is also used as an indicator of water condition. For example, elevated chloride concentrations in the sewerage of coastal areas may signal seawater intrusion into the system, while in potable water they are often associated with wastewater contamination (*5*). In process waters, chloride concentrations are monitored regularly since elevated levels are generally associated with increased deterioration of metallic pipes and structures (*5*), while in cooling water, they are used to indicate the cycles of concentration (*6*).

Because of the widespread use and occurrence of the many forms of chlorine, analytical methods for their determination are of great importance. A large number of methods exist for the determination of chloride ion and chlorine in aqueous samples. These include chromatographic (*7–11*), spectrometric (*12–21*), potentiometric (*22–28*), and titrimetric (*29, 30*) procedures, with the most widely used methods involving titration of the sample.

For the titrimetric determination of aqueous chloride, various argentometric methods exist, which use either indicators (*29–31*) or potentiometers (*27, 28*) to detect the endpoint. Alternatively, mercuric nitrate can be used to titrate chloride ion with the use of diphenylcarbazone as an indicator (*5*).

For the determination of chlorine in bleach bath liquors and natural and treated waters in concentrations greater than 1 mg/L (*5*), iodometric titration is the method of choice. For chlorine levels less than this amount, amperometric titrations are preferred (*5*), but require greater operator skill to avoid loss of chlorine through mechanical stirring. Poor endpoints are also a problem unless the electrodes are properly cleaned and conditioned. Alternatively, *N*,*N*-diethyl-*p*-phenylenediamine (DPD) can be used to determine dissolved chlorine colorimetrically or titrimetrically with ferrous ammonium sulfate (*5*).

All of these titrimetric methods suffer severe interference by a variety of species including such anions as bromide, iodide, cyanide, sulfide, and orthophosphate (for chloride) and other oxidizing agents (for chlorine). Because of the problems associated with existing procedures, new analytical methods for the determination of chloride ion and chlorine in aqueous samples could be of great importance in a number of disciplines.

The potential of flame infrared emission (FIRE) spectroscopy as a means of quantitative analysis has only recently become apparent (*32–35*). Previous work in this laboratory has shown that the discrete infrared emission band at 4.42 μm (2262 cm^{-1}) produced by vibrationally excited carbon dioxide is useful analytically as a means of detecting organic materials introduced into the flame (*33, 34*) and also for determining total inorganic carbon (TIC) in aqueous samples (*35*). Spectroscopic studies in this laboratory using Fourier transform techniques have also demonstrated that other discrete infrared emission bands can be observed in a hydrogen–air flame due to the presence of vibrationally excited molecules (*32*). For example, combustion of chlorine-containing compounds in the flame produces HCl, and under high-resolution conditions, the P and R branches of the HCl infrared emission can be easily detected above the flame background in the region 3200–2400 cm^{-1}. Since the HCl emission band lies between the water emission band at 3800–3200 cm^{-1} and the carbon dioxide emission band centered at 2262 cm^{-1} (*32*), the strong, well-resolved infrared emission from HCl should also be useful analytically for the determination of Cl in a variety of chlorine-containing samples.

Since chlorine gas reacts rapidly with hydrogen under flame conditions to form HCl

$$H_2 + Cl_2 \rightarrow 2HCl \tag{1}$$

any reaction that generates molecular chlorine in a quanti-

0003-2700/89/0361-2785$01.50/0 © 1989 American Chemical Society

tative manner could serve as the basis of an analytical procedure employing FIRE as a highly specific means of detection. As one example, samples containing dissolved chloride ion could be oxidized to molecular chlorine according to the following half-cell ($E^0 = -1.36$ V)

$$2Cl^- \rightarrow Cl_2(aq) + 2e^- \qquad (2)$$

using such strong oxidants as permanganate ion ($E^0 = +1.51$ V in acid solution), peroxide ion ($E^0 = +1.77$ V in acid solution), or peroxydisulfate ion ($E^0 = +2.01$ V). The resulting chlorine gas could then be purged from solution by using an inert gas and introduced into a hydrogen/air flame to form excited HCl, which could be detected by means of its infrared emission.

A second example of an analysis that could be carried out in this manner is the determination of available chlorine in bleaches prepared from molecular chlorine and hypochlorite. In solution these species produce hypochlorous acid (pK_a = 7.60 at 25 °C) according to eq 3 and 4, respectively, and the

$$Cl_2 + 2H_2O \rightarrow HOCl + H_3O^+ + Cl^- \qquad (3)$$

$$OCl^- + H_2O \rightarrow HOCl + OH^- \qquad (4)$$

term available chlorine refers to the total oxidizing power of the solution due to chlorine, hypochlorous acid, and hypochlorite ion, expressed in terms of an equivalent quantity of Cl_2 (*36*). (The distribution of Cl between these three species is temperature- and pH-dependent.) Since eq 3 is readily reversible ($K_{eq}^{-1} = 2.2 \times 10^3$ at 24 °C), addition of acid leads to the rapid generation of dissolved molecular chlorine, which can be purged from solution, converted to HCl in the flame, and detected by infrared emission as described previously.

This paper reports the development of a new chlorine-specific method for the direct determination of chloride and available chlorine in aqueous samples based on the principle of flame infared emission (FIRE). The FIRE–chlorine analyzer described in this paper consists of two commercially available purge devices coupled to a FIRE detector. Aqueous chlorine-containing samples are treated chemically to convert the chloride or hypochlorous acid present into molecular chlorine (Cl_2), which is then purged from the sample cell by using an inert carrier gas and introduced into a hydrogen/entrained-air flame to produce vibrationally excited HCl. The FIRE detector consists of a miniature capillary-head burner that supports the hydrogen/entrained-air flame, an optical collection lens, a band-pass filter to isolate the HCl emission band, and a PbSe photoconductive detector.

EXPERIMENTAL SECTION

Apparatus. The FIRE–chlorine instrument shown in Figure 1 consists of two major sections: (A) the chlorine generation and purging apparatus and (B) the FIRE detection system. The purging apparatus has been described previously (*35*) and consists of two demountable purge tubes connected in parallel with polyethylene tubing and two, three-way switching valves. One of the purge tubes serves as the sample chamber while the second serves as the reference chamber.

Each purge device consists of a 5-mL demountable purge tube that can be disconnected for sample introduction and cleaning. A septum located at the top of each purge tube allows the samples and reagents to be introduced by syringe (sulfuric acid syringe: Model No. 2300, Becton-Dickson & Co., Rutherford, NJ; $KMnO_4$ syringe: Model No. 1001, Hamilton Co., Reno, NV; water sample syringe: Model No. 1002, Hamilton Co.).

Helium gas, maintained at a flow rate of 130 mL/min, was used to purge evolved Cl_2 from the aqueous solution into the flame of the FIRE detector. The optimum flow rate of hydrogen in the capillary-head burner was determined to be 324 mL/min with combustion supported only by entrained air. The supply pressures of the helium and hydrogen were regulated at 0.75 atm by using triple-stage regulation (*35*).

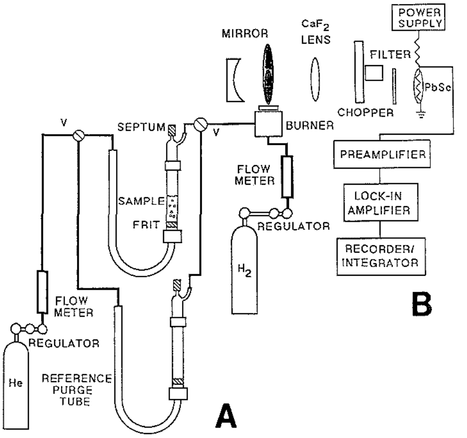

Figure 1. Schematic diagram of FIRE instrument for determination of chloride and available chlorine in aqueous samples, showing (A) purge section and (B) FIRE detector. Key: He, helium cylinder; H_2, hydrogen cylinder; PbSe, lead selenide detector; V, three-way valve.

The optical system of the FIRE detector was modified from that described previously by the addition of a 5-cm-focal-length, *f*/1 concave mirror (Model No. 44340, Oriel Corp., Stratford, CT) installed behind the hydrogen/air flame. This back collection mirror, in conjunction with the CaF_2 lens, directed the infrared emission from the flame onto the PbSe detector.

In addition to the installation of the back collection mirror, the FIRE detector was also modified by replacing the 4.4-μm CO_2 optical band-pass filter with a 3.8-μm optical band-pass filter (Model No. S-902-079, Spectrogon, Secaucus, NJ) to spectrally isolate a portion of the HCl emission consisting of most of the more intense part of the P branch. This optical band-pass filter possessed a full width at half-maximum (fwhm) height of 0.18 μm and was placed immediately in front of the detector.

The flame infrared emission was detected by using a PbSe photoconductive cell operated at room temperature with a bias potential of 45 V. The detector preamplifier circuit, lock-in amplifier, and recorder/integrator have been previously discussed, and except for a slight change in the preamplifier circuit to allow for a larger bias voltage, these components were used without modification (*33, 34*).

Reagents. All chemicals were of ACS reagent grade and were used without further purification. A stock solution of 100 mM NaCl (Mallinckrodt, Inc., St. Louis, MO) was prepared by dissolving NaCl, dried at 120 °C for 24 h, in deionized water. Standard NaCl solutions, having concentrations of 0.1, 0.5, 1.0, 2.0, 5.0, 8.0, and 10 mM, were prepared before use by diluting aliquots of the stock solution to the appropriate volumes.

A saturated solution of $KMnO_4$ (Mallinckrodt) used in conjunction with concentrated H_2SO_4 (Mallinckrodt) served as the oxidizing agent for the aqueous chloride determination. The saturated $KMnO_4$ solution was boiled and filtered to remove any MnO_2 that might be present. Aqueous solutions of $AgNO_3$ (Thorn Smith, Inc., Beulah, MI) and $Na_2S_2O_3$ (Sargent-Welch Scientific Co., Skokie, IL) were used in the titrimetric analyses of aqueous chloride and available chlorine, respectively.

Procedure. Prior to use, the flame in the FIRE system was ignited, and the instrument was allowed to warm up until a stable base line was obtained on the chart recorder. As part of the warmup procedure, He purge gas was directed through the dry reference purge tube and into the flame. When the instrument had stabilized, the analysis for aqueous chloride or available chlorine was carried out according to the appropriate procedure indicated below.

Aqueous Chloride. To construct a calibration curve for chloride by using the FIRE system, the sample purge tube was disconnected, a 1.0-mL volume of an aqueous chloride standard was placed on the glass frit, and a 0.5-mL volume of concentrated

H_2SO_4 was added with a syringe. The purge assembly was then reconnected, and the He flow was switched from the reference purge tube to the sample purge tube by using the dual, three-way valve system. The acidified standard solution was purged for approximately 70 s. A 0.1-mL aliquot of the saturated $KMnO_4$ solution was injected through the septum and into the sample chamber with a syringe. The chlorine gas produced from the resulting oxidation of the aqueous chloride in the sample was purged from the solution and introduced into the flame where it formed vibrationally excited HCl.

After the resulting HCl infrared emission peak had been recorded, the He flow was switched back through the reference purge device. The sample purge tube was then disconnected and rinsed thoroughly with deionized water to remove excess reagents. This process was repeated for all chloride standards to construct a calibration curve of peak intensity versus chloride concentration.

Several natural water samples were collected from sources around the Waco, TX, area and stored according to standard procedures (*5*). One-milliliter volumes of these natural water samples were treated by using the same procedure as outlined for the preparation of the chloride calibration curve, and the resulting infrared emission signal was recorded. Aqueous chloride concentrations in these natural water samples were read from the calibration curve by using measured peak heights. For comparison purposes, aqueous chloride in these samples was also determined by argentometric titration using 0.0136 N $AgNO_3$ with potassium chromate as an indicator according to procedures outlined in ref 5.

Available Chlorine. Calibration curves for available chlorine (Cl_2, HOCl, and OCl^-) were constructed by using aqueous chloride standards as described previously. Bleach sample concentrations were read as chloride concentrations from the chloride calibration curve and converted into available Cl_2 concentration according to the relationship $^1/_2[Cl^-] = [Cl_2]$.

To determine available chlorine in bleach by using the FIRE system, a 0.5-mL aliquot of concentrated H_2SO_4 and a 1.0-mL volume of deionized water were added to the disconnected sample purge tube as described for the aqueous chloride determinations. The sample purge device was then reconnected and the He purge gas flow switched from the reference purge device to the sample purge device. After this acidified deionized water solution was purged for approximately 70 s, a 0.1-mL aliquot of a bleach sample, diluted by a factor of 20 with deionized water, was introduced through the septum with a syringe. The Cl_2 gas generated from the acidification of the bleach sample was purged from the solution into the flame where it formed vibrationally excited HCl. After the HCl infrared emission peak had been recorded, sample cleanup was performed as described previously.

Three commercially available bleach products were selected for the determination of available chlorine. For comparison purposes, available chlorine in these samples was also determined by iodometric titration using 0.151 N $Na_2S_2O_3$ according to the procedure outlined in ref 5.

RESULTS AND DISCUSSION

Instrumental Configuration. The FIRE detection system used in this paper for the determination of chloride and available chlorine is similar to the system that has been previously described for use in total inorganic carbon (TIC) determinations (*35*). However, since the HCl infrared emission band occurs in the 3.17–4.24-μm spectral region of the hydrogen flame (Figure 2B), the 4.4-μm optical band-pass filter used to isolate the CO_2 emission (*35*) was replaced with a 3.8-μm band-pass filter.

The spectra shown in Figure 2 were obtained on a Mattson Cygnus 100 Fourier transform infrared spectrometer under resolution conditions sufficient to reveal the rotational fine structure associated with the P and R branches of the HCl emission band (Figure 2B). As shown in Figure 2A, the 3.8-μm band-pass filter optically isolated the 3.64–4.03-μm portion of the P branch of the HCl emission band. The corresponding flame background spectrum (Figure 2C) shows that this region of the spectrum should be ideal for the detection of hydrogen chloride. A comparison of Figure 2B and Figure 2C also indicates that a filter with a somewhat wider band-pass could have been used and would have been desirable from the standpoint of enhancing the total HCl emission received by the PbSe detector. However, to our knowledge, the filter selected for this study possessed the widest spectral band-pass of any that were commercially available.

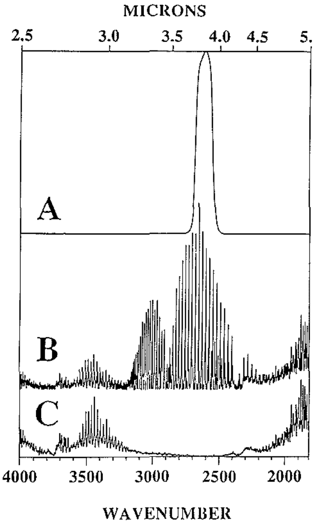

Figure 2. Fourier transform infrared spectra from 4000 to 1800 cm^{-1} plotted on the same relative intensity scale (not corrected for instrument response): (A) transmission spectrum of the band-pass filter used in the FIRE detector (maximum transmission at 3.8 μm 75% *T*, <0.10% elsewhere); (B) flame infrared emission from a hydrogen/entrained-air flame containing hydrogen chloride showing the strong HCl stretching vibration centered at 2900 cm^{-1}; (C) flame infrared emission from a hydrogen/entrained-air flame in the absence of hydrogen chloride showing the background emission from water.

In contrast to the intensity of the water emission bands lying within the band-pass of the 4.4-μm CO_2 filter (*35*), the water emission bands occurring within the band-pass of the 3.8-μm HCl filter are relatively weaker (Figure 2C) and produce a background signal approximately 12 times lower than in the case of CO_2 detection. Since the intensity of the HCl infrared emission band transmitted through the 3.8-μm optical filter is also weaker in comparison to the intensity of the CO_2 infrared emission band transmitted through the 4.4-μm optical filter, a detector-noise-limited situation was encountered; i.e., the noise amplitude was independent of the flame.

In order to increase the signal at the detector and, thus, improve the signal-to-noise ratio (SNR) of the system, two additional instrumental modifications were made. First, the detector bias voltage was increased from 30 to 45 V to enhance the detectivity of the PbSe detector (*37*). Second, a back collection mirror (Figure 1) was added behind the burner to increase the light throughput of the optical system. The location of this mirror was determined experimentally by adjusting the mirror position until the signal from the flame background water emission was maximized at the detector. Use of the mirror enhanced the light throughput by a factor of 2.5. Both of these modifications resulted in improved SNR's and lower detection limits.

Sample Introduction. The purging apparatus (Figure 1) consisted of two separate chambers, one for sample introduction and chlorine generation and a second that served as a reference. Two, three-way valves permitted the He purge gas flow to be switched from one chamber to the other between sample determinations. In the previous study (*35*), degassed water was used in the reference purge tube to maintain a constant flow of He saturated with water vapor to the flame. However, due to the corrosive nature of Cl_2 gas in the presence of water, it was found necessary to flow dry He through the reference chamber and the sample introduction system between sample determinations. This removed residual moisture from the walls of the sample introduction system and reduced corrosion of the burner and plugging of the sample introduction capillary. Therefore, in contrast to the FIRE–TIC procedure (*35*), the FIRE–Cl procedure employed a dry reference purge tube.

Excitation Conditions. Because the FIRE system functions as a mass flow rate detector (*34*), the intensity of the signal arising from the vibrational excitation of HCl in the hydrogen flame is a function of both the He flow rate and the hydrogen/air ratio. Although higher He flow rates resulted in increased peak heights and therefore increased signal-to-noise ratios, a practical upper limit was reached when the sample was forced out of the purge tube. A He flow rate of 130 mL/min was determined to represent the best compromise condition for maximizing the signal-to-noise ratio without sample loss.

Because chlorine gas must be reduced by H_2 at flame temperatures to produce HCl (eq 1), a fuel-rich flame was expected to enhance HCl emission and improve detection limits. As anticipated, a pure H_2 flame, supported only by entrained air, afforded SNR's that were approximately 2.5 times greater than those obtained under fuel-lean flame conditions.

Oxidizing Conditions. To perform chloride determinations using the FIRE system, the chloride ion must first be oxidized to chlorine gas in the sample chamber. The generation of chlorine gas from aqueous chloride samples requires a suitable oxidizing medium. To be satisfactory for use with the FIRE detector, the oxidizing agent must meet two basic requirements. First, it must have a reduction half-cell potential sufficient to oxidize chloride ion to chlorine (in excess of +1.36 V under standard conditions.) Second, the kinetics of the oxidation must be fast. If generation of chlorine gas does not proceed rapidly, broad peaks will be obtained which adversely affect the sensitivity of the system.

Several oxidizing agents were investigated, including concentrated solutions of acidified potassium peroxydisulfate, manganese dioxide, and potassium permanganate. While acidified solutions of both potassium peroxydisulfate and manganese dioxide have suitable half-cell potentials for the reaction, the rate of chlorine production was too slow to be useful for the analysis. By contrast, saturated aqueous $KMnO_4$ and concentrated H_2SO_4 generated chlorine rapidly and quantitatively, permitting analysis by the FIRE system with good detection limits.

More extensive investigations also showed that the sulfuric acid played a role beyond that of supplying hydrogen ions for the reaction, which in excess permanganate is

$$2MnO_4^- + 6Cl^- + 8H_3O^+ \rightarrow 3Cl_2 + 2MnO_2 + 12H_2O \quad (5)$$

By introduction of the chloride-containing solution onto the glass frit of the purge tube and subsequent addition of concentrated sulfuric acid, considerable heat was generated. This heat was found to be critical for promoting the rapid generation of Cl_2 in the next step of the procedure when permanganate was added.

Acidification Conditions. Sulfuric acid and deionized water were first introduced onto the frit, a stable base line was reestablished (about 70 s), and finally the bleach sample was introduced onto the hot, degassed acid. This procedure produced sharp peaks with good reproducibility. Although the reverse procedure (acid added to the degassed bleach) was not tested, degassing the bleach was avoided since the procedure could result in loss of dissolved chlorine (Cl_2) from the sample and degrade the accuracy of the analysis.

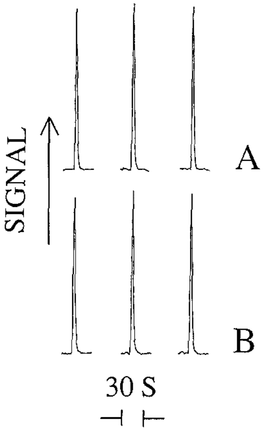

Figure 3. Hydrogen chloride signal profiles obtained by (A) treatment of an acidified 1.0-mL aliquot of 8.00 mM NaCl solution with saturated $KMnO_4$ and (B) treatment of concentrated sulfuric acid with a 0.1-mL aliquot of bleach sample, diluted 20-fold (4.0 μmol of available chlorine).

System Performance. The total time required for signal acquisition from an aqueous sample was approximately 3.5 min (from initial acid injection to purge tube disconnection and cleanup). By judicious selection of the oxidizing medium (for chloride) and proper ordering of reagent addition, good peak profiles were obtained (Figure 3). Since both the oxidation of chloride by permanganate and the formation of chlorine gas from hypochlorite by acidification tend to be slow at room temperature, the heat supplied by the hydration of sulfuric acid is a critical factor in controlling the kinetics of the reactions and, hence, the shape of the peak profiles.

The reproducibility of the FIRE procedure was studied by recording the signals obtained from oxidizing eight 1.0-mL aliquots of a 5 mM NaCl standard. The relative standard deviation (RSD) was determined to be 3.34% for peak height measurements and 5.08% for peak area measurements. The difference in reproducibility between the peak height measurements and the peak area measurements most probably occurs in the trailing edge of the peak profile. Since peak height measurements also gave better reproducibility than peak area measurements in the determination of total inorganic carbon where CO_2 was the emitter (*35*), the origin of tailing in the HCl peaks probably involves the purging step in the analysis, rather than the kinetics of the formation of Cl_2.

Since the peak height measurements were consistently more reproducible for the standards and aqueous samples used in this study, peak height measurements were used exclusively. The root-mean-square signal-to-noise ratio (SNR_{rms}) was approximately 223:1 for the HCl signals obtained from the oxidation of the 5.0 mM NaCl standard.

Calibration curves were prepared by oxidizing 0.10–10 mM NaCl standards and were found to be linear (correlation coefficient of 0.9997). The linear regression equation for a typical calibration curve possessed a slope of 11.46 mm/mM and a y-intercept of −0.09 mm. The detection limit for Cl^- with the FIRE–chlorine system, defined as a concentration of Cl^- producing a signal equivalent to twice the root-mean-square noise, was found to be 1.59 ppm (4.49×10^{-2} mM Cl^-). The detection limit for available Cl_2, based upon the Cl^- calibration curve (and defined at twice the root-mean-square

Table I. Comparison of Chloride Determined by FIRE and by Argentometric Titration for Selected Water and Oil Brine Samples

sample	titration,[a] ppm	FIRE,[a] ppm	% rel error
Hewitt tap	61.4 ± 0.1	60.6 ± 2.5	−1.30
Waco tap	23.4 ± 0.1	25.1 ± 1.8	+7.26
Bosque River	17.1 ± 0.4	15.2 ± 1.2	−11.1
Brazos River	38.2 ± 0.5	35.0 ± 0.5	−8.38
Lake Brazos	32.0 ± 0.2	30.6 ± 1.7	−4.38
Woodbine brine	(41.4 ± 0.1) × 10^3	(43.0 ± 1.2) × 10^3	+3.86
Nacitoch brine	(17.3 ± 2.0) × 10^3	(17.0 ± 0.3) × 10^3	−1.73

[a] Average and standard deviation of four sample determinations.

noise), was found to be 1.61 ppm (2.26 × 10^{-2} mM Cl_2).

Precision and Analytical Accuracy. *Aqueous Chloride.* Natural water and oil brine samples were used to evaluate the analytical performance of the FIRE–chlorine system for the determination of aqueous chloride. The natural water samples included tap water from the Texas cities of Waco and Hewitt, surface waters from Lake Brazos and the Bosque and Brazos Rivers, and brine samples from oil-bearing rock formations. The brine samples were obtained from the Van oil field located in Northeast Texas (Woodbine formation (975 m) and Nacitoch formation (366 m)) and were separated from the associated crude oil by slight heating (80 °C) and centrifugation. A 200-fold dilution of these brine samples was necessary in order to provide a concentration in the linear range of the calibration curve.

Table I compares the chloride values determined by argentometric titration using potassium chromate as an indicator with chloride values obtained with the FIRE detector. Each measurement in the table is an average of four replications. Although the tap water samples used in this study were chlorinated, the concentrations of available chlorine as determined by iodometric titration were below the detection limit of the FIRE detector. As a result, no interference from available chlorine was encountered in the determination of chloride ion for the tap water samples used in this study. However, even if the sensitivity of the FIRE system were improved to the point where available chlorine levels in tap water could be detected along with chloride when the FIRE system is used, interference from available chlorine would be eliminated by the acidification and sample purging step prior to addition of the $KMnO_4$ solution.

As shown in Table I, the precision of the results obtained with the FIRE system is quite good (average relative standard deviation (RSD) 4.39%). The percent difference between the results obtained with the FIRE system and those obtained by argentometric titration (Table I) cannot be ascribed simply to inaccuracies in the FIRE method because the titration method for chloride is subject to interference from such common ions as bromide, iodide, and phosphate. (This will be discussed more fully in the next section.) It is interesting to note that for the three surface water samples (Bosque River, Brazos River, and Lake Brazos) the titration method gave results that were all higher than those obtained by using the FIRE system. High results obtained by argentometric titration may be indicative of interference from such ions as phosphate which are present in these surface waters. From Table I, the average percent relative difference for the seven natural water samples is 5.43%. The agreement between the results obtained with the FIRE detector and those from the titration method is very good, considering that the titration method is not totally error-free.

Available Chlorine. Three commercial bleach products were used to test the performance of the FIRE system for the determination of available chlorine. Bleach samples were diluted 20-fold to give a concentration within the linear range of the FIRE calibration curve.

Table II. Comparison of Available Chlorine Determined by FIRE and by Iodometric Titration for Selected Bleach Samples

bleach sample	titration,[a] ppm	FIRE,[a] ppm	% rel error
Brand X	(57.2 ± 0.9) × 10^3	(60.7 ± 0.8) × 10^3	+6.12
Brand Y	(53.5 ± 0.1) × 10^3	(52.4 ± 0.7) × 10^3	−2.06
Brand Z	(55.5 ± 1.2) × 10^3	(55.9 ± 1.6) × 10^3	+0.72

[a] Average and standard deviation of four sample determinations.

Table II compares the results obtained for available chlorine by iodometric titration with those obtained by using the FIRE detector and shows that the average precision obtained with the FIRE detector is quite good (RSD 1.84%). Taking the iodometric titration as a reference method, the average relative error for the three bleach samples is 2.97%. The close agreement between available chlorine as determined by the FIRE detector and as determined by iodometric titration demonstrates the feasibility of using chloride to prepare the FIRE calibration curve.

Interferences. Interferences with the FIRE–chlorine analyzer can be classified into two major types: chemical and spectral. Spectral interferences in the FIRE detector will occur whenever purgeable contaminants present in the sample are capable of existing as stable molecules or fragments at flame temperatures and emitting infrared radiation within the band-pass of the filter. Because of the specificity of infrared emission and the judicious selection of notch filters, however, the chance of severe spectral interference (i.e., direct overlap) is not particularly likely.

A more subtle form of spectral interference can result from filter imperfections (or filter bleed). Interference filters of the type used in the FIRE–chlorine analyzer have a small, but finite, transmittance at wavelengths well removed from the peak transmission wavelength. The filter used in this study, for example, had a 0.1% transmittance in the vicinity of the 4.42-μm CO_2 emission band. While this transmittance seems small, optical leakage of the CO_2 band can produce measurable signals in the presence of large amounts of carbon-containing interferents.

Chemical interferences can occur with the FIRE–chlorine analyzer in a number of ways, such as altering the oxidation process (in the case of chloride) or retarding the purging of chlorine (Cl_2) from the sample chamber. Thus, any concomitant that produces a volatile chlorine-containing compound that either does not burn readily in the flame or does not form HCl as a combustion product will depress the signal. Chemical interference can also occur if a nonvolatile chlorine-containing compound is produced instead of Cl_2 or if a purgeable contaminant reacts with Cl_2 in the purge gas stream and reduces the amount of Cl_2 reaching the flame.

Anionic Interferences. One commonly employed standard method of chloride determination in neutral or slightly alkaline solution is argentometric titration using potassium chromate as an indicator (the Mohr method (*5*)). Interferences in this method include bromide, iodide, and phosphate, all of which introduce positive errors in the titration. Since these anions can be present in natural waters at concentrations as high as 1 mg/L (Br (*5*)), 0.1 mg/L (I (*5*)), and 0.4 mg/L (P (*38*)), the effect of these species as possible interferences in the determination of aqueous chloride using the FIRE system was investigated.

To determine the extent to which these anions interfere with chloride determinations performed with the FIRE detector, chloride determinations were using 5 mM NaCl standards that had been spiked with concentrations of bromide, iodide, and phosphate equivalent to about 10 times the maximum concentration expected for natural waters (*5*, *38*). The signals obtained from the spiked solutions were then

Table III. Comparison of FIRE Results with Those from Argentometric Titration for Chloride Determination in the Presence of Selected Interferences

sample	FIRE,[a] ppm	titration,[a] ppm
blank[b]	177 ± 7.38	177 ± 1.04
bromide[c]	108 ± 2.60	197 ± 0.628
iodide[d]	176 ± 4.37	196 ± 1.04
phosphate[e]	178 ± 5.00	197 ± 2.72

[a] Average and standard deviation of four sample determinations. [b] 5.00 mM (177 ppm) Cl^-. [c] 5.00 mM Cl^-, 0.595 mM Br^- (equivalent to 21.1 ppm Cl^-). [d] 5.00 mM Cl^-, 0.595 mM I^- (equivalent to 21.1 ppm Cl^-). [e] 5.00 mM Cl^-, 0.223 mM PO_4^{3-} (equivalent to 23.7 ppm Cl^-).

Table IV. Comparison of FIRE Results for Chloride Determination in the Presence of Bromide for Several Sample Pretreatment Methods

sample	FIRE, ppm	% difference[a]
chloride[b]	177 ± 9	0
chloride/IO_3^-[c]	175 ± 10	−1.1
chloride/bromide[d,e]	170 ± 10	−4.0
chloride/bromide[d,f]	168 ± 11	−5.1
chloride/bromide[d,g]	95 ± 7	−46.3

[a] Percent difference compared to chloride (177 ppm) in the absence of bromide. [b] 5.00 mM (177 ppm) Cl^-. [c] 5.00 mM Cl^-, 4.70 mM KIO_3. [d] 5.00 mM Cl^-, 4.70 mM KIO_3, 0.60 mM Br^-. [e] Bromine expelled by boiling the solution prior to analysis. [f] Bromine expelled by purging in the sample chamber prior to analysis. [g] Bromine and chlorine purged together during analysis.

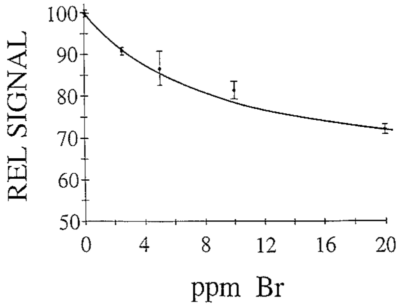

Figure 4. FIRE signal versus bromide concentration for 1.0-mL aliquots of 5.00 mM NaCl spiked with NaBr.

compared to that from an unspiked 5 mM NaCl standard.

Table III shows that the presence of bromide, iodide, or phosphate resulted in a large positive error in the argentometric titration method, with the apparent chloride concentration being given by the sum of the true chloride concentration (177 ppm) and the concentration of the interfering anion, expressed as its chloride equivalent (about 21 ppm). Although no observable difference in peak height occurred in the presence of iodide and phosphate for the FIRE detector (Table III), a 39% suppression of the HCl signal occurred in the presence of bromide. To quantify this effect, 5 mM NaCl solutions having different bromide concentrations were prepared and analyzed. A plot of signal versus bromide concentration (Figure 4), although not linear, did indicate an increasing suppression of the HCl signal as bromide ion concentration was increased.

While no attempt was made to identify the exact mechanism responsible for bromide interference in the chloride determination using the FIRE system, the factors involved are almost certainly chemical in nature. (Direct spectral interference by HBr seems unlikely since HBr emission is not observed under these flame conditions (*32*).) The oxidation chemistry of the halides is complicated by the large number of higher oxidation states available to the halogens, and half-cell potentials provide only an approximate guide because the kinetics of the reactions are often slow (*1*). However, permanganate and bromine half-cell potentials (adjusted for conditions of the analysis, i.e., approximately 11 M acid) indicate that in the presence of excess permanganate, bromide can be oxidized to both Br_2 and BrO_3^-. While bromate would remain in solution, any elemental bromine would be expelled along with elemental chlorine during the purging process. Since the molar solubilities of both Cl_2 and Br_2 are relatively high (9.1×10^{-2} and 0.21 mol/L at 25 °C, respectively (*1*)), both would probably dissolve to some extent in the moisture that condenses between the chlorine generation chamber and the burner. Introduction of chlorine into bromine water under neutral conditions is known (*39*) to result in the formation of bromate ion, BrO_3^-, and chloride ion:

$$Br_2 + 5Cl_2 + 6H_2O \rightarrow 2BrO_3^- + 10Cl^- + 12H^+ \quad (6)$$

Any chloride ion that is not swept out of the condensed moisture as HCl during the 15–20-s period required to record the FIRE signal would contribute to a negative interference.

In the case of iodide, half-cell potentials suggest that reaction with excess permanganate is even more likely to produce higher oxidation states (iodate and possibly periodic acid (*40*)) that would remain in solution. Moreover, any I_2 that might form is also relatively insoluble in water (1.3×10^{-3} M (*1*)) and is much less likely to be purged along with Cl_2 in sufficient quantities to act as an interferent. Further support for the proposed mechanism for bromide interference is the observation that increased corrosion and clogging of the stainless steel capillary tube (used to introduce the sample into the burner) occurred during the analysis of samples containing bromide. The presence of these deposits also resulted in some loss of precision for the chloride results as shown in Table III.

One method of dealing with bromide interference in the determination of chloride by argentometric procedures is to pretreat the sample by using iodate ion in acid solution (*41*). The reaction

$$IO_3^- + 6Br^- + 6H^+ \rightarrow I^- + 3Br_2 + 3H_2O \quad (7)$$

produces bromine, which can be expelled by boiling the solution, and iodide ion, which is not expected to interfere in the FIRE procedure (Table III). The feasibility of using iodate to eliminate bromide interference in the FIRE analyzer was investigated, and the results are shown in Table IV.

As shown in Table IV, pretreatment of 1.0 mL of a 5 mM chloride solution with KIO_3 and permanganate did not alter the FIRE results for chloride within experimental error. However, the presence of both iodate and bromide ion in the sample resulted in a 46.3% suppression of the FIRE signal, compared with chloride solutions containing no bromide. This negative interference is even greater than the 39% suppression observed for bromide-containing samples that were not pretreated with iodate (Table III) and may indicate that Br_2 makes up a greater percentage of the bromide oxidation products when iodate is added prior to treatment by permanganate. In contrast, considerably less suppression of the HCl signal occurred when the bromide-containing solution was pretreated with iodate and then boiled before introduction into the purge tube (−4.0%) or purged directly in the purge tube (−5.1%) to expel bromine prior to addition of permanganate. (Again, precision was somewhat degraded due to deposits that formed in the capillary tube during the analysis.) These results, although preliminary, indicate that aqueous chloride solutions can be successfully pretreated with iodate to remove bromide interference in the FIRE procedure.

Chlorination Species. As discussed previously, the FIRE–chlorine procedure is capable of detecting available Cl_2 in aqueous samples. Since many municipalities add Cl_2 or a chlorine-containing compound (chloroamines) to tap water for disinfection, available chlorine may interfere in the determination of aqueous chloride. Thus, the initial purging step of the acid/sample mixture before oxidation of the aqueous chloride is useful in removing any available Cl_2 that may be present in the water sample.

TIC and Purgeable Organic Compounds. Carbon dioxide can be present in the flame as a result of purging CO_2 from an acidified carbonate-containing solution (*35*) or combusting a purgeable organic compound (*33, 34*). Because the transmission characteristics of the 3.8-μm HCl band-pass filter allow for slight filter bleed in the region of the CO_2 infrared emission band (centered at 4.42 μm (*35*)), carbonates and purgeable organics could act as spectral interferences in the determination of aqueous chloride and available chlorine. To determine if this potential interference is detected by the FIRE–chlorine system, 2-μL injections of cyclopentane were introduced into the purge tube in a manner similar to the procedure outlined for the determination of available chlorine (cyclopentane added to hot acid). Although the results were not quantified, they did indicate that a slight, but detectable, amount of filter bleed from the CO_2 emission band occurred in the transmission of the 3.8-μm HCl optical band-pass filter. Thus, in chloride determination by the FIRE system, the procedure sequence allowing for sample degassing prior to addition of permanganate is important for removing carbonate and volatile organic interferences before the chlorine generation step.

Nonvolatile Inorganics and Organics. Other possible interferences in the FIRE–chlorine method for chloride are those species that are not purged from solution, but are oxidized to CO_2 under the conditions of the FIRE procedure. Permanganate, however, is not a sufficiently strong reagent to oxidize the majority of organic compounds to CO_2 (*42*), and with the exception of a few species such as oxalates and oxalic acids, nonvolatile inorganic or organic species are not expected to produce a chemical interference of this type.

CONCLUSIONS

The FIRE detection system described in this paper has been shown to be a sensitive, reproducible, accurate, and direct means of determining chloride in water and available chlorine in liquid bleach. It is easy to use and requires only a 1-mL sample for each determination. In its present stage of development in this laboratory, the time required for signal acquisition from a sample is 3.5 min from sample injection to purge-tube disconnection and cleanup. The system is easily amenable to automation, however, and a multiple purge-tube version can easily be envisioned.

Although only aqueous chloride and liquid bleach samples were investigated, it should be possible to apply the FIRE method to the determination of chlorine in any sample that can be pretreated to form molecular chlorine or hydrogen chloride gas in the sample chamber or contains purgeable chlorine-containing compounds that can be combusted to hydrogen chloride in the flame. Thus, determination of such species as chlorites, chloroamines, chlorine dioxide, and volatile organic chlorides should be feasible. A special advantage of the FIRE method is its lack of interference from iodide and phosphate, two ions that cause large positive errors in the determination of chloride by argentometric titration. The interference caused by bromide ion in the FIRE method should be amenable to elimination by sample pretreatment using iodate, and we are currently refining this procedure.

ACKNOWLEDGMENT

The authors thank Geoff Hardy (Halliburton Logging Services, Tyler, TX) and Al Rowan (ROCO, Inc., Van, TX) for supplying the oil brine samples.

LITERATURE CITED

(1) Busch, M. A. In *Encyclopedia of Physical Science and Technology*; Academic: New York, 1987; Vol. 6, pp 409–435.
(2) Baum, B. M.; Finley, J. H.; Blumbergs, J. H.; Elliott, E. J.; Scholer, F.; Wooten, H. L. In *Kirk–Othmer Encyclopedia of Chemical Technology*, 3rd ed.; Wiley-Interscience: New York, 1980; Vol. 3, pp 938–958.
(3) Singley, J. E. In *Kirk-Othmer Encyclopedia of Chemical Technology*, 3rd ed.; Wiley-Interscience: New York, 1980; Vol. 24, pp 385–406.
(4) Stumm, W.; Morgan, J. J. *Aquatic Chemistry*; Wiley-Interscience: New York, 1981; Chapter 9, pp 566–582.
(5) *Standard Methods for the Examination of Water and Wastewater*, 16th ed.; Greenberg, A. E.; Trussell, R. R., Clesceri, L. S., Franson, M. A. H., Eds.; American Public Health Association: Washington, DC, 1985; pp 286–294.
(6) *The NALCO Water Handbook*; Kemmer, F. N., McCallion, J., Eds.; McGraw-Hill: New York, 1979; Chapter 38.
(7) Brocco, D.; Tappa, R. *J. Chromatogr.* **1986**, *367*, 240–246.
(8) Moore, W. M. *Anal. Chem.* **1982**, *54*, 602–604.
(9) Takeuchi, T.; Yeung, E. *J. Chromatogr.* **1986**, *370*, 83–92.
(10) MacGee, J.; Allen, K. *Anal. Chem.* **1970**, *42*, 1672–1673.
(11) Ellis, J.; Brown, P. *Anal. Chim. Acta* **1981**, *124*, 431–436.
(12) Alder, J.; Jin, Q.; Snook, R. *Anal. Chim. Acta* **1980**, *120*, 147–154.
(13) Alder, J.; Jin, Q.; Snook, R. *Anal. Chim. Acta* **1981**, *123*, 329–333.
(14) Michlewicz, K.; Carnahan, J. *Anal. Chim. Acta* **1986**, *183*, 275–280.
(15) Cooper, M.; Spurlin, S. *Anal. Lett.* **1986**, *19*, 2221–2230.
(16) Legget, D.; Chen, N.; Mahadevappa, D. *Fresenius' Z. Anal. Chem.* **1983**, *315*, 47–50.
(17) Van Dalen, H.; Kwee, B.; Galan, L. *Anal. Chim. Acta* **1982**, *142*, 159–171.
(18) Aoki, T.; Munemori, M. *Anal. Chem.* **1983**, *55*, 209–212.
(19) Michlewicz, K.; Carnahan, J. *Anal. Chem.* **1985**, *57*, 1092–1095.
(20) Nygaard, D.; Schleicher, R.; Leighty, D. *Am. Lab.* **1985**, *6*, 59–62.
(21) Marino, D.; Ingle, J. *Anal. Chem.* **1981**, *53*, 455–458.
(22) Rigdon, L.; Moody, G.; Frazer, J. *Anal. Chem.* **1978**, *50*, 465–469.
(23) Midgley, D. *Analyst* **1984**, *109*, 439–444.
(24) Midgley, D. *Analyst* **1984**, *109*, 445–452.
(25) Hozumi, K.; Akimoto, N. *Anal. Chem.* **1970**, *42*, 1312–1317.
(26) Barbolani, E.; Piccardi, G.; Pantani, F. *Anal. Chim. Acta* **1981**, *132*, 223–228.
(27) Hulanicki, A.; Jedral, W.; Piotrowska, J.; Tomaszewska, M. *Mikrochim. Acta* **1982**, *I*, 203–212.
(28) Pietrogrande, A.; Zancato, M. *Mikrochim. Acta* **1985**, *II*, 283–288.
(29) Singh, E. *Z. Anal. Chem.* **1977**, *283*, 299–300.
(30) Agarwal, D.; Chaturvedi, G. *J. Indian Chem. Soc.* **1983**, *60*, 311–312.
(31) Garg, S.; Agarwal, D.; Chaturvedi, G. *J. Indian Chem. Soc.* **1981**, *58*, 662–663.
(32) Tilotta, D. C.; Busch, K. W.; Busch, M. A. *Appl. Spectrosc.* **1989**, *43*, 704–709.
(33) Hudson, M. K.; Busch, K. W. *Anal. Chem.* **1987**, *59*, 2603–2609.
(34) Hudson, M. K.; Busch, K. W. *Anal. Chem.* **1988**, *60*, 2110–2115.
(35) Kubala, S. W.; Tilotta, D. C.; Busch, M. A.; Busch, K. W. *Anal. Chem.* **1989**, *61*, 1841–1846.
(36) Faust, S. D.; Aly, O. M. *Chemistry of Water Treatment*; Butterworths: Boston, MA, 1983; Chapter 10, pp 610–632.
(37) *Infrared Detectors*; Hamamatsu Photonics K. K., Solid State Division: 1126 Ichino-cho, Hamamatsu City, 435 Japan, February 1985.
(38) Manahan, S. E. *Environmental Chemistry*, 3rd ed.; Willard Grant Press: Boston, MA, 1979.
(39) Remy, H. *Treatise on Inorganic Chemistry*; Elsevier: New York, 1956; Vol. 1, Chapter 17, p 811.
(40) Jolly, W. L. *Modern Inorganic Chemistry*: McGraw-Hill: New York, 1984; Chapter 8, pp 222–226.
(41) *Standard Methods of Chemical Analysis*, 6th ed.; Furman, N. H., Ed.; Van Nostrand: Princeton, NJ, 1962; Vol. 1, Chapter 9, p 244.
(42) House, H. O. *Modern Synthetic Reactions*, 2nd ed.; Benjamin: Menlo Park, CA, 1972; Chapter 5.

RECEIVED for review July 3, 1989. Accepted September 15, 1989. This work was supported by Baylor University Research Grants 012-S85-URC, 006-S87-URC, 007-F87-URC, and 11.510.

Anal. Chem. 1989, 61, 2792–2800

Structural Features of Aquatic Fulvic Acids. Analytical and Preparative Reversed-Phase High-Performance Liquid Chromatography Separation with Photodiode Array Detection

Farida Y. Saleh* **and Wenching A. Ong**

Institute of Applied Sciences and Department of Chemistry, University of North Texas, Denton, Texas 76203

David Y. Chang

Burlington Research, Inc., Burlington, North Carolina 21215

Stepwise fractionation of aquatic fulvic acids by preparative and analytical high-performance liquid chromatography (HPLC) was successful in separating constituents of the macromolecule. Suwannee River fulvic acids (FA) were separated by preparative reversed-phase HPLC (RP-HPLC) into hydrophilic and hydrophobic fractions. The hydrophilic constituents represent about 40% of the total sample and can be resolved into at least six peaks, all of which exhibit featureless ultraviolet–visible (UV–vis) scans with λ_{max} between 211 and 212 nm. The hydrophobic constituents represent about 30% and can be resolved into 12 peaks as illustrated by the analytical chromatograms. The UV–vis scans of the peaks indicated the presence of repeated peaks with similar UV–vis spectra. The retention and UV–vis spectra of the resolved peaks were characteristic of aliphatic organic acids in the hydrophilic fraction and of conjugated aliphatic ketones and phenols in the hydrophobic fraction. Vanillic acid structures were detected as two minor peaks in the analytical chromatograms of the total sample but not the fractions.

INTRODUCTION

Aquatic fulvic acids (FA) represent up to 80% of the soluble organic carbon and are known to play an important role in several environmental and geochemical reactions. Despite their extensive investigation by spectroscopic and chemical degradation methods, detailed structural information on FA is still largely unknown (*1–5*).

Reversed-phase high performance liquid chromatography (RP-HPLC) has been successful in the separation of many naturally occurring compounds (*6, 7*). However, in fulvic acid research, success in the separation of FA molecular constitutents by any of the HPLC modes has been modest (*8–17*). It is generally accepted that FA is a polymeric material with extensive internal bindings. If this concept is accepted, it should be possible to identify orderly repeated structural units in FA macromolecules. However, to date, the polymeric nature of FA has not been unequivocally verified (*18*).

Two high-efficiency Hypersil ODS and WP-300 ODS microcolumns with single UV wavelength detection were recently applied to the separation of FA (*19, 20*). Chromatograms showed several poorly resolved peaks. The authors implied that better separation could be obtained with high-efficiency columns.

This paper presents the results of an investigation of the semipreparative and analytical separation of aquatic fulvic acid components by RP-HPLC and ultraviolet–visible (UV-vis) DAD detection. The approaches used in the research were to use stepwise fractionation to optimize the separation and to use purified fulvic acids as a starting material in the preparative experiments.

EXPERIMENTAL SECTION

Instrumentation. Waters Model 201 HPLC, equipped with a fixed UV detector (Beckman Model 160) and fluorescence detector (Schoeffel Model 970), was used in the first preparative experiment. A Hewlett-Packard HPLC Model 1090 with Model DR-5 pump and UV-vis photodiode array detector (DAD) was used in all the other experiments.

Samples. The fulvic acids samples were water reference Suwannee River FA prepared by the International Humic Substances Society (*20*).

Reagents and Solvents. All reagents were ACS chemicals of highest purity. Pure HPLC water was obtained from the MilliQ system and the solvents were all HPLC grade. Twelve model compounds were all high-purity ACS reagents and included seven carboxylic acids, two ketones, and two phenols.

Methods. *Preparative RP-HPLC.* Two preparative HPLC experiments were carried out using reference Suwannee River FA. In the first experiment a semipreparative HPLC column of 50 cm × 22.5 mm i.d. dry packed with 25 µm ST/C_{18} (Scientific Technology) was used. A water–methanol binary solvent system was used under stepwise gradient conditions. Solvent A-1 consisted of 1% methanol in water and solvent B-1 consisted of 85% methanol. An aqueous solution of 1 mg/mL Suwannee River reference FA in pure water was used for the separation. The sample capacity of the column was experimentally determined as 1 mL per injection. From each injection, two fractions were collected. The hydrophilic fraction contained solutes eluted with solvent A-1. The hydrophobic fraction contained solutes eluted with solvent B-1. Fractionation was made in batches of 10 mg each. Fractions were freeze-dried to 10 mL solution, centrifuged to remove particulates, decanted, lypholized, and desiccated to a constant weight. A procedure blank for HPLC reinjection involved the collection of the same amounts of solvents A-1 and B-1 concentrated to the original 10-mL volume of the sample. A total of 80 mg of reference SR-FA was fractionated in the first experiment. The efficiency of separation in each batch was checked by reinjecting aqueous or methanolic solution of the fractions into the analytical RP column. Only batches that showed efficient separation were combined for further spectroscopic characterization.

In the second experiment, a custom-made preparative column, NovaPak C_{18} 30 mm × 7.8 mm i.d. was used with solvent program III. The column characteristics and solvent program III are shown in Table I. Methods of sample preparation and fraction collection were similar to the forementioned methods. A total of 40 mg of reference SR-FA was fractionated.

Analytical RP-HPLC Separation. Table I also lists the columns, mobile phases, and the gradient programs used in the analytical separations. Gradient program I consisted of water, acetonitrile, and acetic acid at pH 4. Samples included Suwannee River FA, the two preparative fractions, and 12 model compounds.

0003-2700/89/0361-2792$01.50/0 © 1989 American Chemical Society

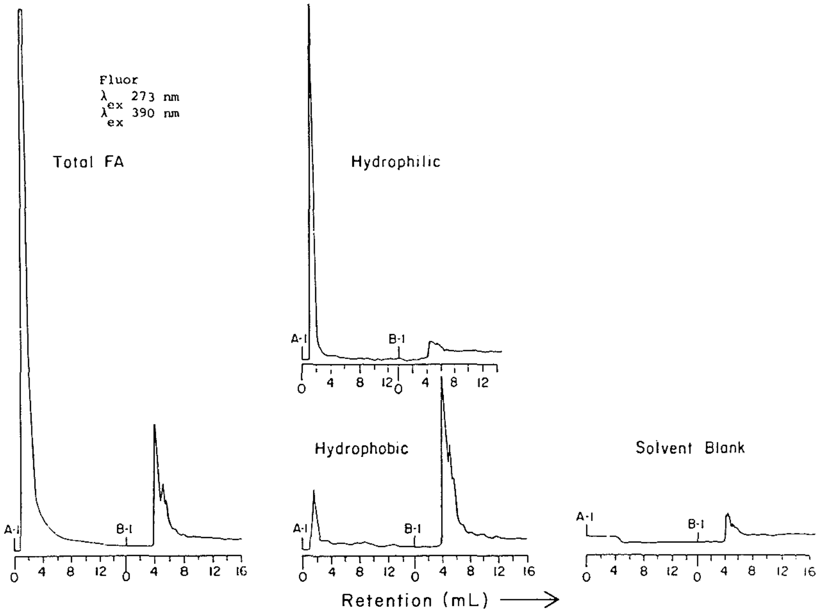

Figure 1. Preparative experiment 1, analytical chromatogram of total SR-FA and HPLC fractions: column, Novapak C-18 5 μm, 15 cm × 4 mm i.d., stepwise gradient; mobile phase, water-methanol; flow rate, 1 mL/min; detector, fluorescence.

Table I. Continuous Gradient Programs and Types of Columns and Samples Used with Each

gradient program	mobile phase	pH at 25 °C	gradient	%A	%B	column types	samples
I	A: H_2O + 0.01% AcH	4.0	t_0 min	99	1	Novapak C18 5 μm, 100 mm length × 3.9 mm i.d.; flow, 0.5 mL/min	SR-FA, HPLC fractions, model compounds
	B: CH_3CN		t_2 min	70	30	Hypersil ODS C18, 200 mm length × 2.1 mm i.d.; flow, 0.3 mL/min	SR-FA, HPLC fractions
			t_{16} min	15	85		
			t_{20} min	15	85		
II	A: H_2O (He purged)	7.0	t_0 min	99	1	Novapak C18 5 μm, 100 mm length × 3.9 mm i.d.; flow, 0.5 mL/min	SR-FA, HPLC fractions, model compounds
	B: CH_3CN		t_2 min	70	30	Hypersil ODS C18, 200 mm length × 2.1 mm i.d.; flow, 0.3 mL/min	SR-FA, HPLC fractions
			t_{16} min	15	85		
			t_{20} min	15	85		
III	A: H_2O (He purged)	7	t_0 min	99	1	custom made Novapak C18 4 μm, 300 mm length × 7.8 mm i.d.; flow, 1.5 mL/min	SR-FA second preparative experiment
	B: CH_3OH		t_{30} min	99	1	Novapak C18 5 μm, 150 mm length × 4 mm i.d.	SR-FA, HPLC fractions
			t_{35}	15	85		
			t_{45} min	15	85		
			t_{50} min	15	85		

Fulvic acid samples were either dissolved in MilliQ water or pH 7 phosphate buffer. Gradient program II consisted of water and acetonitrile at pH 7 and no acetic acid was added for pH adjustment. Because the solvents were purged with He, the pH of the MilliQ water was maintained at 7.00. The 12 model compounds were tested with both gradient programs I and II using a C_{18} Novapak column.

RESULTS AND DISCUSSIONS

Preparative Experiments. Figure 1 shows a typical HPLC chromatogram of the unfractionated FA and the HPLC fractions A-1 and B-1, from the first experiment. Total recovery of FA and contribution of each fraction are shown in Table II. In the first experiment, the combined recoveries of both fractions averaged to 64.5% of the total FA used. In the second experiment, the combined recoveries of both fractions averaged to 69% of the total FA used. It is important to point out that the percentages of B-1 fraction in the first and second experiments are 27 and 31, respectively. Considering that the experiment was run by two different graduate students and on two different columns, the results are very reproducible. The incomplete recovery may be due to irreversible adsorption of some of FA constituents or due to mechanical loss. However a yield of 70% for such biopolymers is excellent compared to the yields by other chemical and thermal degradation methods which do not exceed 25%.

Table II. Preparative Experiments 1 and 2, Percent Recoveries of Fractions

	initial total wt, mg	wt of A-1 fraction, mg	wt of B-1 fraction, mg	% total recovery A + B	% of A-1 recovery from total FA	% of B-1 recovery from total FA
preparative experiment 1						
combined batches (1–5)	50	19.0	11.6	61.2	38.0	23.2
combined batches (6–8)	30	11.20	9.8	70	37.3	32.7
total from experiment 1	80	30.20	21.4	64.5	37.8	26.8
preparative experiment 2						
combined batches (1–2)	20	7.91	6.51	72.1	39.6	32.6
combined batches (3–4)	20	9.29	5.98	76.4	46	29.9
total from experiment 2	40	17.20	12.49	74.2	43.0	31.2
mean recoveries experiments 1 and 2				69.4	40.4	29

The preparative separations of complex solutes are associated with several inherent problems, which can be summarized as follows: (i) chemical changes to the original material during the separation process; (ii) contamination from the mobile phase, solid support, or the instrument components; (iii) loss of resolution due to repeated injections; (iv) irreversible adsorption of some of the sample constituents; (v) the usually small amount of purified fractions. Some of these problems were alleviated by careful selection of the separation conditions and by examination of the retention mechanisms and the possible solvent–solute interactions.

It is important to remember that the mobile-phase composition reflects a wide range of solvent polarities. Such conditions are ideal for FA since the macromolecule is known to contain both hydrophilic and hydrophobic constituents. To allow for the separation of the hydrophobic constituents from the acidic ones, neutral pH was selected for the preparative separation. At pH 7, acidic constituents in FA are dissociated and thus poorly retained on the column. Another advantage of the water/methanol mobile phase is the ability to predict possible interactions with FA constituents. Two reactions are possible. One is hydrolysis and the second is methylation. Indeed both reactions seemed to occur. Hydrolysis was indicated by an increase in the hydrophilic constituents in samples stored in aqueous solutions for about 1 year. Methylation in the hydrophobic fraction was clearly indicated by detection of well-defined gas chromatographic–flame ionization detection (GC–FID) peaks in the B-1 fractions. These peaks could not be detected in the total sample or fraction A-1 but were only detectable in the methylated FA (*21*). These results suggest partial methylation of some of FA constituents, upon elution with 85% methanol.

Trace polyvalent metal ion contamination from the HPLC metallic components has been reported in the literature (*22*). This problem can be minimized by passivating the system by washing the pump with a 0.1 M HNO_3 for 2 h before the separation. Solubilized trace metals are likely to complex with carboxylic and phenolic components of FA and can be detected in the electron spin resonance (ESR) and Fourier transform infrared (FT-IR) spectra (*23*).

Loss of resolution due to repeated injections was not expected to cause major problems in our case since the two fractions were distinctively separated. This problem, however is more serious in the analytical separations of FA. Irreversible adsorption of some FA constituents seemed to occur during the separation, but to a limited extent. The combined recoveries of the fractions in the two preparative experiments were 64.5% and 69.4%, respectively. These are much higher yields than those obtained by chemical or thermal degradation methods.

An additional problem in preparative HPLC is caused by the release of fragments of the packing material. Such a problem was alleviated by using special filters as end columns and by centrifugation of the liquid fractions at high speed followed by decantation.

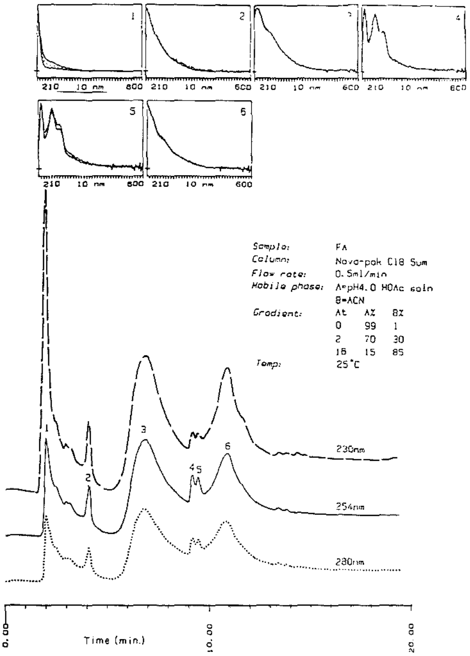

Figure 2. Chromatogram and UV–vis scans of 50 μL 0.02% SR-FA dissolved in MilliQ water: gradient program I, Novapak C_{18} column.

The small amount of purified HPLC fractions continue to pose some limitations to the spectroscopic characterization. However, modern instruments are well adapted to handle small amounts of samples. The approach to analyze total sample, fractions and blanks allowed us to distinguish the original constituents in the sample from the newly formed ones or the artifacts.

Analytical RP-HPLC. In successful chromatograms the UV–vis absorption data points were accumulated and stored in the HP 85-B PC memory. Each separated peak was scanned between λ 200 and 600 nm at three points representing peak maximum, slope upward, and slope downward. Overlap of the spectra collected at these three points is considered as an indication of peak purity and or homogeneity. This approach allowed the development of a UV–vis spectral catalog of FA constituents and several other model compounds, under different gradient programs (*22*).

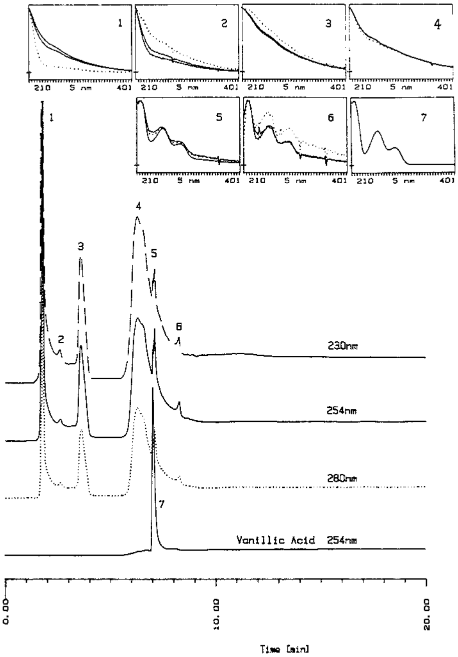

Figure 3. Chromatogram and UV–vis scans of 50 μL 0.02% SR-FA and 50 μL 0.02% vanillic acid in pH 7 buffer: gradient program I; Novapak C_{18} column.

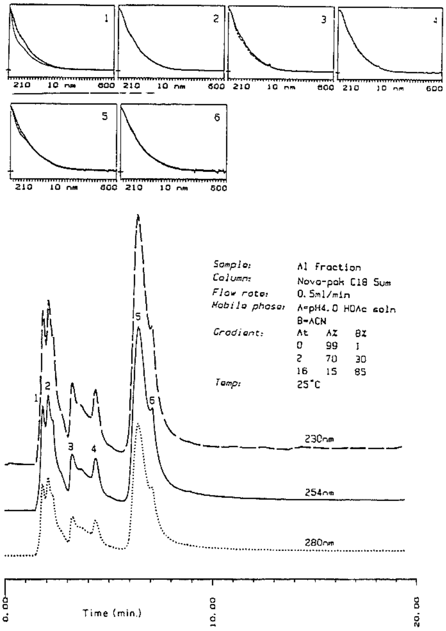

Figure 4. Chromatogram and UV–vis scans of 50 μL 0.02% hydrophilic fraction A-1: gradient program I; Novapak C_{18} column.

Gradient Program I—Novapak C_{18} Column. Figures 2 and 3 show the chromatograms and UV–vis scans of SR FA samples dissolved in MilliQ water or in pH 7 buffer. The experimental conditions in the two chromatograms were exactly the same. Both chromatograms show the resolution of six UV–vis absorption regions. However, peak intensities and elution order are different. In Figure 2, the total elution time in the aqueous sample is about 15 min whereas in the buffered sample, it is only 10 min. This can be attributed to the fast equilibration time in the case of the buffered sample. Also, it is noted that the intensities of the early eluting peaks in the buffered samples in Figure 3 are higher than those in Figure 2. This effect can be attributed to the electrolyte ionization effect on FA components at pH 7, in contrast to the protonated form in the case of the aqueous sample at pH 4.

The scans of the first two peaks in Figure 2 are featureless and showed gradual decrease of absorbance with increase of wavelength. Peak no. 3 in the water-soluble sample is broad and its retention time (t_R) extends from 5.5 to 8.5 min. The UV–vis scans of this peak show several minor shoulders at λ 244, 270, 315, 355, 395, 485, 575, and 590 nm. The scans indicate less purity, suggesting that this peak corresponds to a larger fragment of aquatic FA, which contains both chromophores and auxochrome structures. The UV–vis scans of the fourth and fifth peaks show well-defined features. Both spectra show two distinct absorption lines at λ 260 and 290 nm. These two lines are characteristic of vanillic acid structure. Chromatographic peak 6 in Figure 2 is broad and elutes over a period of 2 min. Its UV–vis scan is similar to peak 3 and is likely due to another large molecular fragment containing chromophores and auxochromes.

In the buffered sample (Figure 3) scans of peaks 1, 2, 3, and 4 are similar to those of peaks 1, 2, 3, and 6 in Figure 2. The last two peaks in Figure 3, i.e. peaks 5 and 6, exhibit the predominant absorption lines of vanillic acid structures noted in peaks 4 and 5 of Figure 2. The t_R and the UV scans of vanillic acid standard solution (peak 7 in Figure 3) has the same t_R as peak 5 of the sample. This may be the first detection of vanillic acid structural units in FA via HPLC analysis. It is important to note that VA structural units occurred in two chromatographic peaks which differ in t_R by 0.4 min in Figure 2 and by 1 min in Figure 3. Detection of additional weak UV and visible absorption lines in the scans suggests that VA structures are not present in the pure acid form.

The analogy between the UV–vis scans of vanillic acid (VA) and those detected in aqueous or in buffered FA solutions leaves little doubt regarding the presence of vanillic acid structure as an integral part of the FA macromolecule. As discussed below, it is interesting to note that the vanillic acid structures were not detected in the chromatograms of either fraction A-1 or B-1. A possible explanation is that vanillic acids are only intermediates formed by the slow degradation from lignin precursors. Once the macromolecule is fractured by the HPLC interactions, VA may undergo further degradation to simpler carboxylic or phenolic compounds.

Figure 4 shows the chromatogram and the UV–vis scans of the hydrophilic fraction A-1. Six regions of UV absorption can be identified. The total elution time is only $7^1/_2$ min. The UV–vis scans of all the six peaks are all similar and all featureless, except for weak shoulders at λ 255 and 365 nm. The scans of the hydrophilic peaks are comparable to the first three peaks in total FA (Figure 2).

Figure 5 shows the chromatogram and UV–vis scans of the hydrophobic fraction of B-1. As may be expected, the total elution time is extended to 19 min. Most of the peaks appear after 6 min, indicating strong hydrophobic interactions. Scans of peaks 1 and 2 are essentially similar except for minor

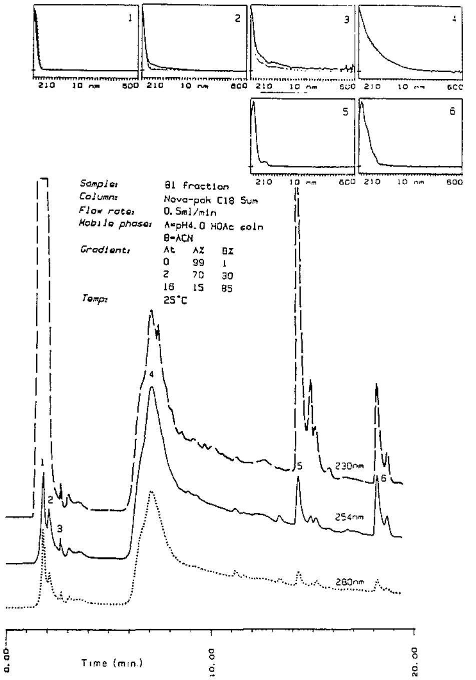

Figure 5. Chromatogram and UV-vis scans of 50 μL 0.02% hydrophobic fraction B-1 dissolved in methanol: gradient program I, Novapak C_{18} column.

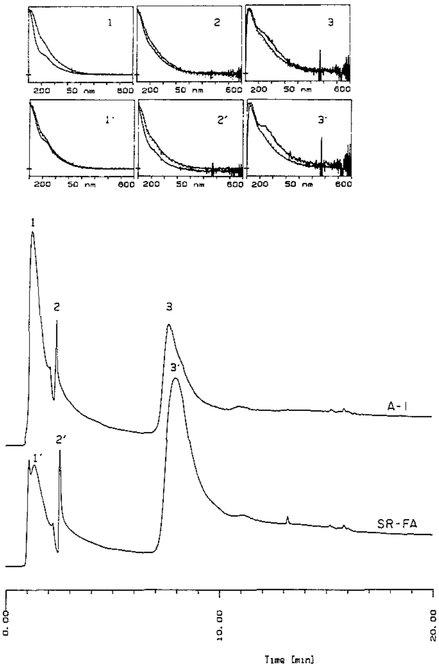

Figure 6. Chromatogram and UV-vis scans of 20 μL of 0.02% SR-FA and 20 μL of 0.02% A-1 fraction dissolved in MilliQ water: gradient program I; Hypersil ODS column.

impurities. Both peaks had λ_{max} at 212 nm and probably correspond to aliphatic structures. The third peak contains more impurities which may be colored. The fourth chromatographic peak is broad and elutes between 6 and 9.5 min. Its scan is featureless and is similar to peaks 3 and 6 detected in total FA in Figure 2. The UV-vis scans of peak 5 have a maximum at λ 220 nm and weak shoulder at λ 265 nm. These absorption features correspond to conjugated ketones (7). Peak 6 shows a characteristic featureless spectrum with minor shoulders at λ 250 and 280 nm.

Gradient Program I—Hypersil C_{18} Column. Figure 6 shows the chromatogram and UV-vis scans of 50 μL of aqueous 0.02% SR-FA and the hydrophilic fraction A-1. The chromatograms show modest resolution of three absorption regions. The first two occurred within the first 3 min. The third peak is broad and extends from 7 to 10 min. The UV-vis scans of the first and second peaks were both featureless and similar to the scans of the early eluting peaks with the Novapak column. Peak 3 is also featureless, but showed some absorption lines in the visible region indicating the presence of chromophores and auxochromes. This scan represents the predominant polymeric structure in FA. It is likely to consist of two or three structural units containing aliphatic and substituted aromatic structures.

Figure 7 shows the chromatogram and scans of the hydrophobic fraction B-1. The chromatogram was monitored at λ = 230 nm. The scans of the early eluting peaks in the first 2 min are similar to those present in the total sample and hydrophilic fractions. Peaks 2–12 occurred between 6 and 18 min with only peak 2 indicating a broad signal with a scan characteristic of the predominant colored fragment of FA. Peaks 3, 5, 6, 7, and 8 showed a distinct absorption line at λ = 226 nm and a weak line at λ 265 nm. The similarities and intensities of these peaks are the first indication of the presence of repeated structural units in FA macromolecular structure. It should be remembered that these peaks occurred between t_R 8.62 and 11.42 min i.e. within 2.8 min in the hydrophobic region. It is suspected that these peaks correspond to a conjugated ketone structure. Peaks 4, 9, and 10 are similar and contain a defined additional absorption line at λ 275 nm; such spectra are characteristic of phenolic compounds. In peak 11 the λ 275 nm line is barely detectable, but a well-defined line at λ 221 nm is noticeable. Peak 12 occurred at 17.2 min and t_R shows several absorption lines at λ 209, 235, 260, 275, and 285 nm. These lines are characteristic of the polynuclear aromatic structures.

The chromatogram of fraction B-1 on a Hypersil column represents one of the most successful chromatographic separations of FA. The UV-vis scans provide the first evidence of the presence of structurally similar units in FA. The effect of storage of the B-1 solution was evaluated by injecting the same sample under the same conditions, after storage at 4 °C for 5 months. Chromatograms showed essentially the same resolution and the UV-vis scans. The only detectable difference was the increase of the magnitude of the phenolic peaks and the decrease in the magnitude of the conjugated ketone peaks.

Gradient Program II—Hypersil C_{18} Column. Because the solvents were purged with He, the pH of the MilliQ water was maintained at 7.00. Figures 8 and 9 show chromatograms and UV-vis scans of the total samples and fractions. In Figure 8 the early eluting peaks (the first 3 min) are stronger than in the case of gradient program I, Figure 7. This can be attributed to secondary chemical equilibrium influencing the retention behavior of organic acids. This behavior was noted

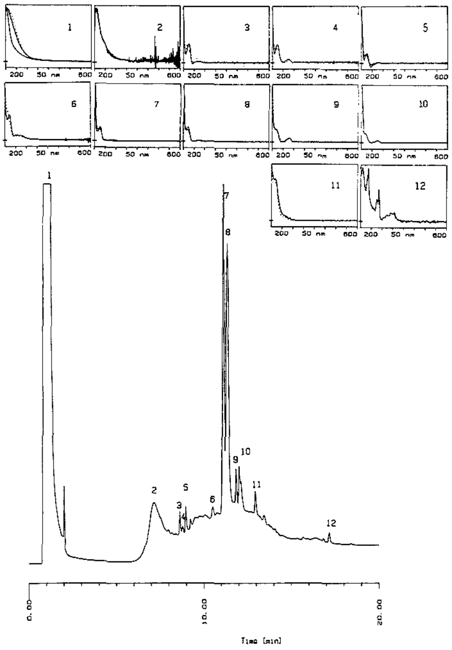

Figure 7. Chromatogram and UV–vis scans of 50 μL of 0.02% aqueous hydrophobic fraction B-1 dissolved in methanol: preparative experiment 1; gradient program I; Hypersil ODS column.

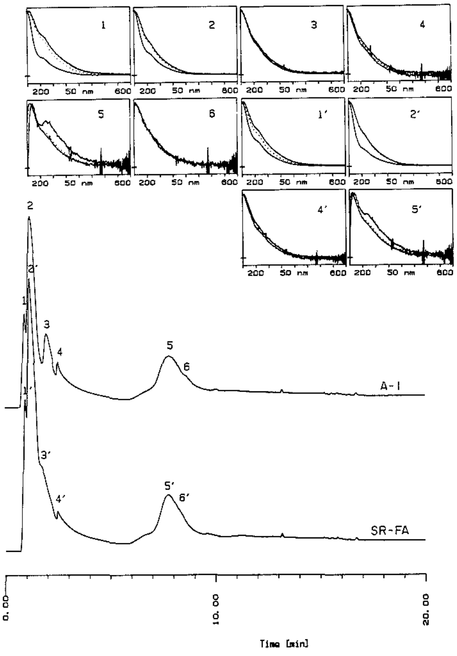

Figure 8. Chromatogram and UV–vis scans of 50 μL of 0.02% SR-FA and 50 μL of 0.02% A-1 fraction dissolved in MilliQ water: gradient program II; Hypersil ODS column.

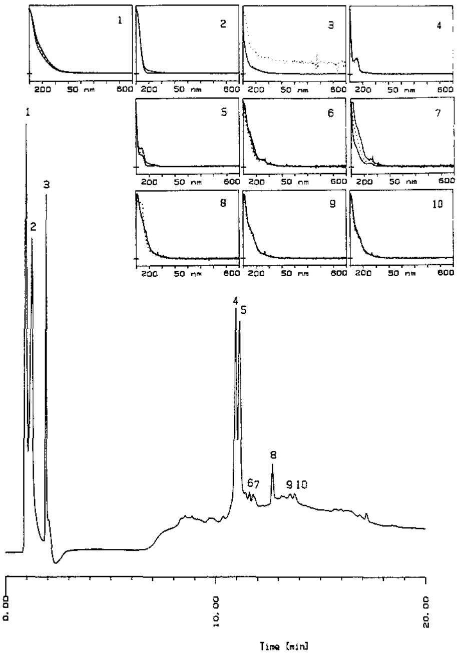

Figure 9. Chromatogram and UV–vis scans of 20 μL of 0.02% hydrophobic fraction B-1 dissolved in methanol: gradient program II; Hypersil ODS column.

earlier under stepwise gradient conditions (*24*). It is interesting to note the similarity between the chromatograms of the hydrophobic fraction in Figure 9 with the one using gradient program I shown in Figure 7. These results can be taken as evidence of the neutral and hydrophobic nature of the constituents in this fraction. The scans of the peaks eluted in the hydrophobic fraction are essentially similar to that obtained at pH 4 with gradient program I.

Model Compounds—Gradient Programs I and II. The retention behavior and the UV–vis scans of 12 model compounds using gradient program I and II are shown in Table III. The reduced UV–vis spectra of all the compounds are shown in Figure 10. Under both gradient conditions, five acidic compounds were eluted in the hydrophilic region and seven in the hydrophobic one. Compounds eluted in the hydrophobic region included methyl vinyl ketone, resorcinol, vanillic acid, crotonaldehyde, and cresol.

As shown in the table, only the retention times of organic acids were shifted toward shorter retention time at pH 7. The retention times of the phenols were slightly shifted. As expected, the retention times of methyl vinyl ketone and crotonaldehyde did not change with a change of pH from 4 to 7.

The model compounds maleic acid, tricarballylic acid, adipic acid, and 1,2,4-benzenetricarboxylic acid all exhibited freatureless spectra and occurred within the same retention times as the hydrophilic fraction. Thus, it can be concluded that the hydrophilic fraction of FA contains several aliphatic carboxylic acids and a few aromatic acids. Results from spectroscopic characterization are supportive of this conclusion. The retention times and UV–vis spectra of the model compounds crotonaldehyde, resorcinol, and *o*-cresol were similar to the separated peaks in the hydrophobic fraction.

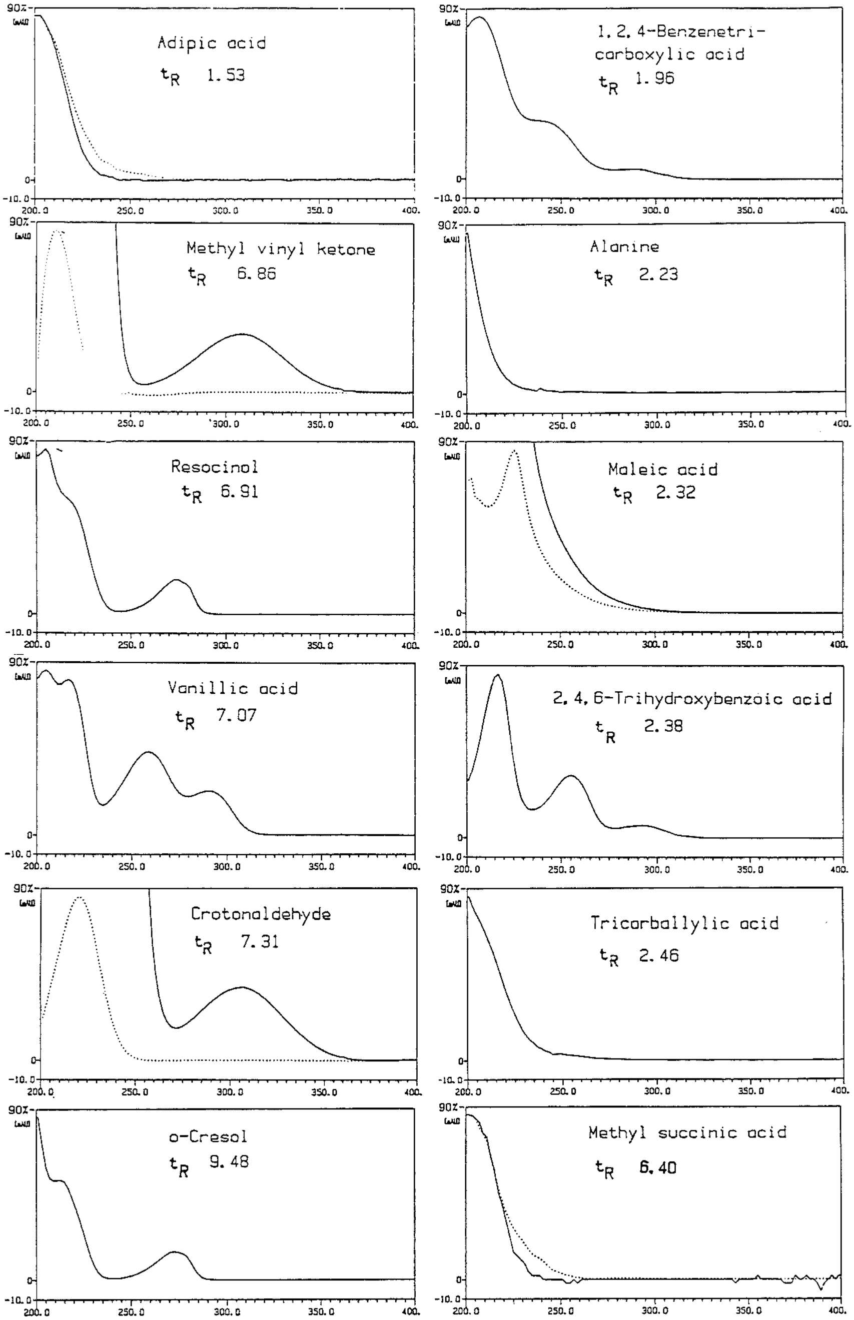

Figure 10. UV–vis scans of 20 μL of 0.02% individual model compounds dissolved in water or methanol.

CONCLUSIONS

The preparative and analytical RP-HPLC separation experiments have shown that the FA macromolecule consists of at least two polymeric fractions, each of which can further be separated into individual constituents. The homogeneity of the major fractions in FA was demonstrated by the peak purity tests using the UV DAD detector. Stepwise fraction-

Table III. List of Model Compounds Structure and Retention on Novapak Column with Gradient Programs I and II

compound	structure	t_R min I Novapak	t_r min II Novapak
1. 1,2,4-benzenetricarboxylic acid, $pk_1{}^a = 2.52$, $pk_2 = 3.84$, $pk_3 = 5.20$	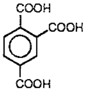	1.95	1.75
2. alanine, $pk_b = 9.87$	$CH_3CH(NH_3)COOH$	2.23	2.00
3. maleic acid, $pk_1 = 1.91$, $pk_2 = 6.33$	$HOOCCH{=}CHCOOH$	2.32	1.70
4. 2,4,6-trihydroxybenzoic acid, $pk_1 = 1.68$	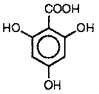	2.38	1.50
5. tricarballylic acid, $pk_1 = 4.42$, $pk_2 = 5.41$	HOCCHCH(COOH)CHCOOH	2.45	2.20
6. methylsuccinic acid, $pk_1 = 4.13$, $pk_2 = 5.62$	$HOOCCH_2CH(CH_3)COOH$	6.40	5.71
7. adipic acid, $pk_1 = 4.418$, $pk_2 = 5.412$	$HOOC(CH2)_4COOH$	6.68	6.05
8. methyl vinyl ketone	$CH_2{=}CHCOCH_3$	6.68	6.8
9. resorcinol, $pk = 5.2$	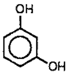	6.91	6.8
10. vanillic acid, $pk = 4.335$	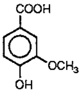	7.07	6.2
11. crotonaldehyde	$CH_3CH{=}CHCHO$	7.31	7.20
12. *o*-cresol, $pk = 10.26$	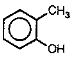	9.48	9.54

[a] pk in H_2O at 25 °C.

ation of FA is a successful approach to unfold the macromolecule into several constituents, as illustrated by the analytical chromatograms of the fractions. The UV–vis scans of the separated peaks indicated the presence of several repeated or similar structures in each of the FA fractions. Vanillic acid structures were detected in chromatograms of total FA but not in the HPLC fractions. This may indicate that these structural units are chemically changed during the separation processes.

The hydrophilic constituents of FA represent about 40% of the total sample and exhibit featureless UV–vis scans. The hydrophobic constituents of FA represent about 30% of the total sample and can be resolved into 12 constituents as illustrated by the analytical chromatograms. The UV–vis scans of the peaks indicated the presence of repeated structurally related units. This is one of the first resolutions of FA individual constituents without chemical or thermal degradation. The UV–vis scans of the repeated units were characteristic of conjugated aliphatic ketones and phenolic compounds.

For years, HS researchers have argued regarding the purity and polymeric nature of FA and HA. The results reported in this paper provide experimental evidence to answer both questions at least in relation to aquatic FA. Using reference Suwannee River aquatic fulvic acids in the preparative HPLC separation allowed a well-defined starting material. Then, obtaining a yield of about 70% of the initial sample after the preparative chromatographic separation provided more representation of the macromolecule than the yields in chemical or thermal degradation methods which do not exceed 25%. Additional evidence of the structural features of FA macromolecule was obtained from the application of ^1H and ^{13}C NMR, FT-IR, and ESR on total sample and fractions (*21*). The detection of several structurally related or repeated units in both of FA fractions can justify the claim that FA is of polymeric nature even though several different monomers may participate in the formation of the macromolecule.

LITERATURE CITED

(1) Thurman, E. M.; Malcolm, R. L. In *Aquatic and Terrestrial Humic Materials*; Christman, R. F., Gjessing, E. T., Eds.; Ann Arbor Science: Ann Arbor, MI, 1983; pp 1–25.

(2) Rook, J. J. In *Water Chlorination: Environmental Impact and Health Effects*; Jolley, R. L., Brungs, W. A., Cummings, R. B., Eds.; Ann Arbor Science: Ann Arbor, MI, 1983; Vol. 3, pp 85–98.

(3) Liao, W.; Christman, R. F.; Johnson, J. D.; Millington, D. S. *Environ. Sci. Technol.* **1982**, *16*, 403–410.

(4) Reuter, J. H.; Ghosal, M.; Chian, E. S. K.; Giabbai, M. In *Aquatic and Terrestrial Humic Materials*; Christman, R. F., Gjessing, E. T., Eds.; Ann Arbor Science: Ann Arbor, MI, 1983; pp 107–141.

(5) Norwood, D. L.; Christman, R. F.; Hatcher, P. G. *Environ. Sci. Technol.* **1987**, *21*, 791–798.

(6) Horvath, C. In *Techniques in Liquid Chromatography*; Simpson, C. F., Ed.; John Wiley and Sons: New York, 1982; pp 229–302.

(7) Larmann, J. P.; Destifano, J. J.; Goldbert, A. P.; Stout, R. W.; Snyder, L. R.; Stadalius, M. A. *J. Chromatogr.* **1983**, *225*, 163–169.

(8) Glaze, W. H.; Peyton, G. R.; Saleh, F. Y.; Huang, F. Y. *Int. J. Environ. Anal. Chem.* **1979**, *7*, 143–160.

(9) Saleh, F. Y.; Mokti, M. M. In *Water Chlorination: Environmental Impact and Health Effects*; Jolley, R. L., Ed.; Ann Arbor Science: Ann Arbor, MI, 1982; Vol. 4, pp 201–217.

(10) Bartle, K. D.; Pomfret, A.; Pappin, M. J.; Mills, D. G. *Org. Geochem.* **1987**, *3*, 139–149.

(11) Glaze, W. H.; Saleh, F. Y.; Kinsley, W. In *Water Chlorination: Environmental Impact and Health Effects*; Jolley, R. L., Ed.; Ann Arbor Science: Ann Arbor, MI, 1980; Vol. 3, pp 99–108.

(12) MacCarthy, P.; Preston, M. J.; Malcolm, R. L.; Thurman, M. E. *Anal. Chem.* **1981**, *53*, 1195–1199.

(13) Curtis, M. A.; Witt, A. F.; Schram, S. B.; Rogers, L. B. *Anal. Chem.* **1981**, *53*, 1195–1199.

(14) Ravichandran, K.; Lewis, J. J.; Yin, I. H.; Koenigbauer, M.; Powley, C. R.; Shah, P.; Rogers, L. B. *J. Chromatogr.* **1988**, *439*, 213-226.
(15) Andres, J. M.; Romero, C.; Gavilan, J. M. *Fuel* **1987**, *66*, 827-830.
(16) Blondeau, R.; Kalinowski, E. *J. Chromatogr.* **1986**, *351*, 585-589.
(17) Hayase, K.; Tsubota, H. *J. Chromatogr.* **1984**, *295*, 530-532.
(18) MacCarthy, P.; Rice, J. A. In *Humic Substances in Soil, Sediment and Water*; Aiken, G. R., McKnight, D. M., Wershaw, R., Eds.; John Wiley and Sons: New York, 1985; pp 527-560.
(19) Hirose, A.; Ishii, D. *HRC CC, J. High Resolut. Chromatogr. Chromatogr. Commun.* **1986**, *9*, 533-534.
(20) International Humic Substances Society (IHSS), Standard and Reference Humic Substances, Golden, CO, 1986, personal communication.
(21) Saleh, F. Y.; Bronnimann, C.; Frye, J., unpublished results.
(22) Saleh, F. Y.; Ong, W.; Kim, I.; Mahmoud, Q. H.; Chang, D. Y. U.S. Geological Survey, Final Report USGS Grant No. 14-08-0001-G1146, NTIS-PB89-193429, 1989; p 332.
(23) Jenke, D. R. *J. Chromatogr.* **1986**, *370*, 419-426.
(24) Saleh, F. Y.; Chang, D. Y. *J. Sci. Total Environ.* **1987**, *62*, 67-74.

RECEIVED for review June 13, 1989. Accepted October 2, 1989. Research was mainly supported by the U.S. Geological Survey, Department of Interior Assistance Award No. 14-08-0001-G1146. Additional support was provided by the University of North Texas Faculty Research Fund. The views and conclusions in this document are those of the authors and should not be interpreted as necessarily representing the official policies either expressed or implied of the U.S. Government.

CORRESPONDENCE

Generation of Chemiluminescence upon Reaction of Iodine with Luminol in Reversed Micelles and Its Analytical Applicability

Sir: Since iodine is often the focus of biomedical and environmental studies, improved analytical methods for the determination of trace amounts of iodine are important. Chemiluminescence (CL) methods are very sensitive for a variety of organic and inorganic analytes (*1*). A first study of the iodine–luminol system in aqueous solutions was reported by Babko et al. (*2*) and the CL reaction was studied quantitatively by Seitz and Hercules (*3*) and then by Lutgens et al. (*4*). In addition, another CL reaction of iodine with a hydrogen peroxide–sodium hypochlorite mixture was reported (*5*). However, the analysis of iodine in aqueous solutions has some handicaps: the pH- and concentration-dependent equilibria of I_2 with IOH, I^-, I_3^-, etc., and the irreversible loss by iodate formation in alkaline solutions (*3, 4*). Moreover, several metal ions in aqueous solutions may interfere with the iodine determination by using the luminol CL reaction (*6*). If so, separation of the interferences would be needed; for example, the technique of solvent extraction or ion chromatographic separation as described in a previous paper could be used (*7*).

Although the analytical applications of CL systems have generally included use of conventional aqueous solutions, considerable attention has been paid in recent years to use of micellar media to enhance CL signals (*8, 9*). Recently, reversed micelles as a medium in CL measurements have been used to amplify the CL of the H_2O_2–luminol system at mild pH in the absence of any catalyst and to determine H_2O_2 (*10*) and glucose or glucose oxidase activity (*11*). In this work, we found that iodine causes CL upon mixing with the reversed-micellar solution of luminol alone: The CL intensity was proportional to iodine concentration and a detection limit (DL) of 2×10^{-10} M iodine was achieved. Further, the CL generation from the iodine luminol reaction performed in the reversed micellar medium allowed us to develop a new method for iodine determination by a coupling of solvent extraction and CL detection. When solvent extraction is used first to separate from some interferences as mentioned above, a technique of subsequent separation from the solvent such as back extraction (*12*) or evaporation of the solvent (*13*) is required usually for CL detection in the conventional aqueous solutions. On the other hand, our approach may have the advantage that such an additional separation scheme is not needed in the analysis. Accordingly, the present method was found potentially useful for the selective CL determination of iodide where oxidation of I^- to I_2 and solvent extraction of I_2 were simultaneously carried out prior to CL analysis; the extraction procedure was effective in separating iodine from the reactants, oxidant, and acid, which could interfere with the iodine determination.

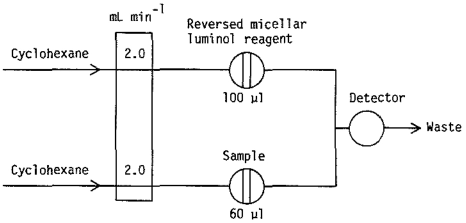

Figure 1. Flow diagram for the determination of iodine with CL detection.

EXPERIMENTAL SECTION

Reagents and Solutions. All reagents were of reagent grade and used without further purification. All aqueous solutions were prepared with water from an Advantec Toyo (Tokyo, Japan) Model GSU-901 water purification system. A 6:5 (v/v) chloroform–cyclohexane (both Wako HPLC grade) mixture containing 0.260 M hexadecyltrimethylammonium chloride, CTAC (Tokyo Kasei), was used as a reversed micellar bulk solvent to prepare reversed-micellar solutions of luminol (Aldrich) according to the literature (*10*), but the reagent conditions were optimized for the iodine determination: A 2.5×10^{-3} M aqueous solution of luminol, prepared daily in a buffer solution of 0.2 M sodium carbonate (pH 11.5), was used (the luminol concentration calculated on a final volume total solution basis was 1.00×10^{-4} M) and a water:surfactant molar ratio, $R = [H_2O]/[CTAC]$, of 10.1 was chosen as optimal.

0003-2700/89/0361-2800$01.50/0 © 1989 American Chemical Society

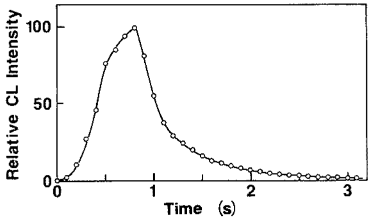

Figure 2. Peak shape for a CL signal observed from the iodine–luminol reaction system in a CTAC reversed micellar medium under the optimum conditions for 100 ng mL^{-1} iodine.

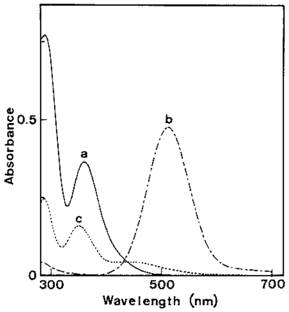

Figure 3. Absorption spectra of iodine species in various media: (a) CTAC reversed micellar solution (R = 10.1) of 0.2 M sodium carbonate buffer ($[I_2] = 1 \times 10^{-4}$ M); (b) 6:5 (v/v) chloroform–cyclohexane mixture ($[I_2] = 1 \times 10^{-4}$ M); (c) aqueous solution of 2×10^{-4} M potassium iodide ($[I_2] = 1 \times 10^{-5}$ M).

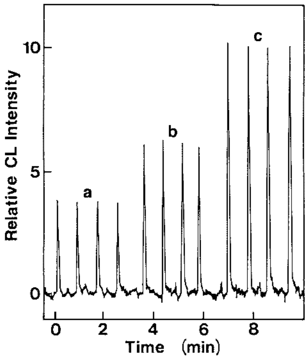

Figure 4. CL–time responses for various concentrations of iodine obtained under the optimum conditions: (a) the blank, 0; (b) 50; (c) 100 pg mL^{-1} iodine.

A 1000 µg mL^{-1} stock solution of iodine was prepared daily by dissolving solid iodine in cyclohexane. Working solutions of iodine were prepared in cyclohexane daily by serial dilutions from the 1000 µg mL^{-1} I_2 solution. All glass sample vessels used for iodine solutions were wrapped with aluminum foil to prevent the solutions from exposure to sunlight or to avoid any photochemical reactions.

Apparatus and Procedures. A Hitachi Model F-2000 fluorescence spectrometer (Tokyo, Japan) with a 1-cm cell was used to obtain the CL intensity as a function of time. With a dispensing syringe, 0.5 mL of the I_2 cyclohexane solution was injected through a rubber septum into the cell in which 0.5 mL of the reversed micellar luminol solution was initially placed. The injection needle had to dip into the reaction mixture near the bottom of the cell, and the I_2 solution had to be injected quickly for optimal mixing of the reactants.

UV–vis absorption measurements for I_2 in the CTAC reversed micellar medium of the carbonate buffer alone, in the chloroform–cyclohexane mixture, and in a normal aqueous solution of 2×10^{-4} M potassium iodide for comparison, were made in the conventional manner on a Hitachi Model 228 A spectrophotometer (Tokyo, Japan) using a 5-cm cell.

Figure 1 shows a manifold of the flow system used for the iodine determination. A Hitachi Model K-1000 flow injection analyzer (Tokyo, Japan), equipped with a 16-port, rotary injection valve which serves as introduction loops of the I_2 sample and the reversed micellar luminol reagent, was used. The programmed automatic injection valve was used to insert slugs of the I_2 sample and the luminol reagent into the respective flow lines of cyclohexane driven continuously by two pumps of the device. After an optimization study of their sizes, the 60- and 100-µL injection loops of the sample and the reagent were chosen, respectively. In this flow system, the sample is mixed with the luminol solution just before entering a spiral flow cell (70 µL) mounted directly in front of the photomultiplier tube in conjunction with a Niti-on Model LF-800 photometer system (Tokyo, Japan) used to detect CL signals. A strip-chart recorder was used to observe peak height and shape. The flow rate of 2 mL min^{-1} for both the streams was determined to be optimal. PTFE tubing (0.5-mm i.d.) was used between all components in the flow system.

RESULTS AND DISCUSSION

When a cyclohexane solution of I_2 was mixed with a reversed-micellar solution of luminol at room temperature, CL was observed for a few seconds, quickly decreasing in intensity as shown in Figure 2. Also, the mixture was found to change in color from violet to brownish yellow immediately upon mixing. As presented in Figure 3, absorption measurements for I_2 dissolved in the three different media show that the visible absorption band at 517 nm for I_2 in the chloroform–cyclohexane mixture alone does not appear on the spectrum in the reversed-micellar solution of the carbonate buffer (pH 11.5), while in the latter medium there is an alternative absorption peak at 352 nm, quite analogous to that in the normal aqueous KI solution, indicating that upon mixing the I_3^- ions were generated under the conditions of the reversed-micellar solution. These results demonstrate that the following reactions upon mixing occur in CTAC reversed micelles containing the basic buffer (or OH^-):

$$I_2 + OH^- \rightleftarrows IOH + I^-, \quad I^- + I_2 \rightleftarrows I_3^-$$

As a result of the reactions, I_2 should enter almost completely into aqueous cores or water pools of the reversed micellar system to form IO^- and I_3^-. On the other hand, I_2 was almost insoluble in normal aqueous solution of the buffer (pH 11.5), and such a change in color was not observed appreciably. This limitation was overcome by the use of the reversed micellar reaction medium, which allowed I_2 to undergo the reactions. Since a decrease in ion hydration number, that is, dehydration has been reported for ions in reversed micelles (*14*), the present effect of reversed micelles on the reactions may be attributed to the dehydration process, which could lead to an increase in activity of the OH^- ion in reversed micelles. Enhanced activity of the water pools appears to contribute to the reactions or the solubilization of I_2 in the CTAC reversed micelles containing luminol. This process permits the reaction of iodine with luminol in the water pools to generate CL upon mixing directly (without any separation of I_2 from the cyclohexane solution), implying that the use of reversed micelles as a medium may be advantageous in CL measurement fol-

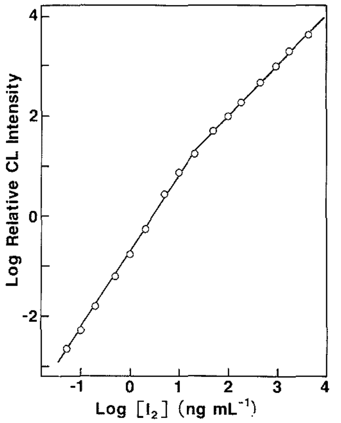

Figure 5. log–log calibration curve for the determination of iodine by using the luminol CL reaction performed in the reversed micellar medium.

lowing solvent extraction separation of I_2 from interferents in aqueous solutions. In addition, I_2 concentration effect can be achieved by entering into a small volume of water pools and thus association of luminol with I_2 or the generated IOH, followed by the CL reaction, seems to be enhanced in reversed micelles.

The CL generation observed in this work may be explained by a mechanism proposed for the iodine–luminol reaction in normal basic aqueous solution (*3*), if it is assumed that in the reversed micelles the IO^- generated by the above reactions of I_2 reacts with luminol to form an azaquinone intermediate necessary for CL. However, at this time we have no obvious evidence supporting such a mechanism and are performing further experiments that, it is hoped, will clarify the situation.

Some CL emission resulted even when pure cyclohexane was used in place of the analyte to determine a blank signal. For luminol CL, it has been noted that the presence of oxygen is required (*6*). Conventionally, solutions were run without deaeration in this work and therefore the solutions contained oxygen from the air. This may make our observation of the spontaneous emission by the luminol reagent alone in the reversed-micellar solution. Figure 4 illustrates typical CL emission intensity vs time profiles obtained for the blank and the I_2 samples under the optimum operating conditions. An analytical signal was taken as the difference in observed peak heights for the analyte and the blank. As shown in Figure 4, the determination of iodine had a DL of 2×10^{-10} M (sample b, 50 pg mL^{-1}); the minimum detectable amount of I_2 was 12 fmol when a 60-μL sample injection volume was used. The DL was given as the concentration for which the analytical signal is 3 times the noise of base line; the magnitude of the typical base-line noise can be also seen in Figure 4. Typical relative standard deviation of the CL signals (four replicate measurements) was 3%. The detection of low iodine concentrations with luminol CL in aqueous alkaline solution alone has been reported (*3*). For comparison, a similar attempt was made to perform the iodine determination by the luminol CL reaction in the aqueous buffer solution used here. However, the blank CL signal of the luminol reagent (1.0×10^{-4} M) alone was observed to be larger by a factor of 10^2 in the aqueous solution alone compared to that in the reversed micellar medium, implying that the background problem associated with using normal aqueous solutions conventionally in CL analysis may be troublesome for obtaining reproducible peak heights over a low iodine concentration range. Although the blank CL generation should be associated with the presence of oxygen in the solutions as mentioned above, the lower blank signal in the reversed micellar system may be explained by assuming the oxygen gas to tend to escape from the water pools, in which the CL reaction occurs, into the disperse medium, that is, the reversed micellar bulk organic solvent, because the solubility of a given gas in water is usually lower than in typical organic solvents (*15*). Figure 5 presents a log–log calibration curve for I_2 obtained with the optimum conditions established here: The plot had a slope of 1.5 from the DL of 50 pg mL^{-1} up to 10 ng mL^{-1} and that of 1.0 above 20 ng mL^{-1}. Also, all preliminary calibration data showed such a discontinuity in the slope around the concentration of 20 ng mL^{-1}. Surfaces of Teflon tubes used here adsorb and desorb iodine readily as noted in the literature (*3*). Thus, the deviations at low I_2 concentrations (below 20 ng mL^{-1}) from the linear first-order response may arise through I_2 loss due to adsorption of I_2 on the Teflon surface which takes place upon each delivering of the sample injected in the flow system. Although several types of adsorption processes have been classified in the literature (*16*), the adsorption described by the Langmuir isotherm applicable to monolayer adsorption seems most likely for the present behavior; if the adsorbed I_2 can occupy only a limited number of the surface sites, a condition of surface saturation is reached at high concentrations of the I_2, which might be more than 20 ng mL^{-1}. At this time we have no evidence of confirmation of the adsorption and hope to clarify this point in later communications.

In connection with the analytical advantage described above, the present CL method was applied to the determination of iodide by using solvent extraction which was carried out simultaneously with oxidation of I^- to I_2 prior to analysis. The oxidation and extraction involved transfer of 10 mL of the I^- sample to a 100-mL separatory funnel which held 10 mL of 0.5 M H_2SO_4 solution of 1.7×10^{-3} M $K_2Cr_2O_7$ and 10 mL of cyclohexane. After the sample was shaken for 30 s, the layers were allowed to separate and the organic layer was analyzed in the same manner as the cyclohexane solution of the I_2 sample described above. A calibration curve, obtained with standard solutions of I^- prepared in pure water from a 1000 μg mL^{-1} standard solution of potassium iodide by serial dilutions, was very similar to that given in Figure 5. The satisfactory results verified that the extraction procedure permits effectively the separation of iodine from the oxidant and acid which could interfere with the iodine determination by the luminol CL method; the present technique should be applicable for such interference problems. In addition, bromide ions may behave in a manner similar to the iodide ions. However, it was confirmed that there was no apparent interference with the determination of iodide at a concentration of bromide in 800-fold excess over that of iodide under the optimum conditions used here.

This CL method also could be applied to the determination of iodate with solvent extraction which would be performed simultaneously with reduction of IO_3^- to I_2 prior to analysis, and further work is currently under way on this possibility. To provide automated, rapid, and reproducible analyses of aqueous samples of iodine, iodide, and iodate, a further investigation is also undertaken to incorporate a membrane phase separator into the manifold of the flow injection analysis.

LITERATURE CITED

(1) Fernandez-Gutierrez, A.; Munoz de la Pena, A. *Molecular Luminescence Spectroscopy. Methods and Applications*: *Part 1*; Schulman, S. G., Ed.; Wiley: New York, 1985; pp 463–546, and references cited therein.
(2) Babko, A. K.; Markova, L. V.; Lukovskaya, N. M. *Zh. Anal. Khim.* **1968**, *23*, 401.

(3) Seitz, W. R.; Hercules, D. M. *J. Am. Chem. Soc.* **1974**, *96*, 4094.
(4) Lutgens, M.; Reiber, H.; Schramm, I. *Bioluminescence* and *Chemiluminescence. New Perspectives*; Scholmerich, J., Andreesen, R., Kapp, A., Ernst, M., Woods, W. G., Eds.; Wiley: New York, 1987; pp 571-574.
(5) Burguera, J. L.; Burguera, M. *An. Quim., Ser. B* **1982**, *78*, 307.
(6) Klopf, L. L.; Nieman, T. A. *Anal. Chem.* **1983**, *55*, 1080.
(7) Sakai, H.; Fujiwara, T.; Yamamoto, M.; Kumamaru, T. *Anal. Chim. Acta*. **1989**, *221*, 249.
(8) Wehry, E. L. *Anal. Chem.* **1986**, *58*, 13R.
(9) Warner, I. M.; McGown, L. B. *Anal. Chem.* **1988**, *60*, 162R.
(10) Hoshino, H.; Hinze, W. L. *Anal. Chem.* **1987**, *59*, 496.
(11) Igarashi, S.; Hinze, W. L. *Anal. Chem.* **1988**, *60*, 446.
(12) Montano, L. A.; Ingle, J. D., Jr. *Anal. Chem.* **1979**, *51*, 926.
(13) Boyle, E. A.; Handy, B.; van Geen, A. *Anal. Chem.* **1987**, *59*, 1499.
(14) Sunamoto, J.; Kondo, H.; Hamada, T.; Yamamoto, S.; Matsuda, Y.; Murakami, Y. *Inorg. Chem.* **1980**, *19*, 3668.
(15) Battino, R.; Clever, H. L. *Chem. Rev.* **1966**, *66*, 395.
(16) Kolthoff, I. M. *J. Phys. Chem.* **1936**, *40*, 1027.

Terufumi Fujiwara
Noriyuki Tanimoto
Jin-Jin Huang
Takahiro Kumamaru*

Department of Chemistry
Faculty of Science
Hiroshima University
1-1-89 Higasisenda-machi, Naka-ku
Hiroshima 730
Japan

RECEIVED for review July 3, 1989. Accepted October 6, 1989. This work was partially supported by a Grant-in-Aid for Scientific Research, No. 63470032, from the Ministry of Education, Science and Culture of Japan.

TECHNICAL NOTES

Small-Volume Electrochemical Cell Designed for Rotating Disk Studies in Bioelectrochemistry

P. N. Bartlett* and R. G. Whitaker[1]

Department of Chemistry, University of Warwick, Coventry CV4 7AL, U.K.

In the electrochemical study of biological redox couples, such as redox proteins, redox enzymes, or coenzymes, it is frequently advantageous to be able to apply rotating disk or ring disk techniques. These enable steady-state measurements to be used to investigate both the heterogeneous and homogeneous kinetics of the biological electron transfer reactions. For such studies the use of small solution volumes is imperative due to the cost and/or difficulty in obtaining purified biological material.

For many bioelectrochemical investigations it is also important to exclude all traces of atmospheric oxygen from the analyte solution. The presence of even low concentrations of molecular oxygen can interfere with the measurements in two ways. Firstly, since oxygen is electroactive below 0 V vs SCE, it will interfere in studies of bioelectrochemical reactions at these potentials. This problem is exacerbated by the high diffusion coefficient for molecular oxygen (*1*) as compared with the low diffusion coefficients for the redox enzymes or proteins. In such a case it may be possible to measure the background current, in the presence of oxygen, and then to subtract this from the current obtained in the presence of the analyte. However, this is frequently an unsatisfactory procedure because it neglects the effects of adsorption of the biological species at the electrode surface upon the oxygen reduction kinetics.

Secondly, molecular oxygen is a natural redox partner for many redox enzymes and so homogeneous reactions with oxygen are also a problem. A great deal of work is in progress to study the reaction of redox enzymes with artificial electron donors/acceptors (*2–4*) with a view to the development of biosensors. In such studies it is essential to exclude oxygen from the electrochemical cell. Failure to do this adequately may result in competition between oxygen and the mediator for the reduced form of the enzyme (*2*).

In this communication we describe a covenient design for a small volume electrochemical cell which is compatible with the requirements of the rotating disk hydrodynamics and the exclusion of oxygen. We present data for the use of such a cell for the determination of diffusion coefficients, for coulometric titrations, and for rotating electrode studies of simple, reversible redox couples.

EXPERIMENTAL SECTION

Cell Design and Construction. The cell is machined from clear Perspex, Figure 1, and has a sample volume of between 3.5 and 4 cm^3. The cell is made in two main parts which screw together. It is designed so that there are no protrusions into the sample compartment to disrupt the rotating disk hydrodynamics. The silver/silver chloride wire reference electrode is retained behind a glass frit sealed into the cell wall. A spiral platinum wire counter electrode is located in a second compartment at the base of the cell, this is separated from the working electrode compartment by a porous glass frit which forms the bottom of the working electrode compartment and defines the sample volume. The counter electrode compartment holds approximately 1.5 cm^3 of electrolyte solution.

The cell is also provided with a detachable cylindrical Perspex sleeve which forms a seal with the top of the cell and the electrode rotator block. This sleeve has inlets/outlets for the passage of oxygen-free nitrogen over the sample solution during the course of an experiment. The sleeve is sealed to the cell and rotator block by tight fitting silicone rubber "O" rings. The sleeve also ensures that the rotating disk is always at the same vertical position within the cell. Although this cell was designed to be used in conjunction with a standard Oxford Electrodes rotating disk system, the same ideas could be adapted for other electrode types.

The internal geometry of the working electrode compartment is shaped in such a way that it is compatible with the flow setup in the cell by the rotating disk. This is achieved by ensuring a smooth contour for the inside of the working electrode compartment and also by cutting the internal walls at an angle of 45° to the glass frit at the bottom of this compartment. Our cell differs in this respect from those described by Miller and Bruckenstein (*5*) and by Eggli (*6*) who both used cylindrical cells.

Equipment and Chemicals. All measurements were made by using purpose built modular instrumentation. Rotating disk electrodes and rotator were purchased from Oxford Electrodes. For the coulometric titrations a large area platinum gauze (12.5

---

[1] Present address: EMS Ltd., Old Fellows House, 2 Queen Victoria Rd., Coventry, U.K.

0003-2700/89/0361-2803$01.50/0 © 1989 American Chemical Society

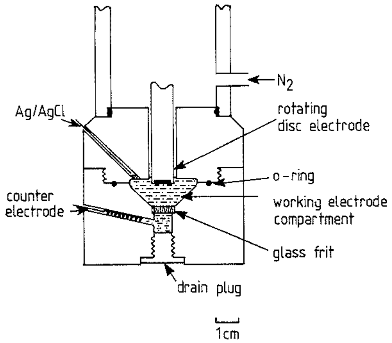

Figure 1. Diagram of the electrochemical cell showing the various components and the details of cell construction.

cm²) was placed in the bottom of the working electrode compartment.

Solutions were deoxygenated with oxygen-free nitrogen produced by passing nitrogen through a train of Dreschel bottles containing a caustic solution of anthraquinone-2-sulfonate. All chemicals were AnalaR grade except where otherwise stated. Ferrocene acetic acid was a gift from MediSense, Inc.

All experiments were carried out at ambient temperature, 22 ± 2 °C.

RESULTS AND DISCUSSION

We begin by considering the rotation speed dependence of the mass transport limited current to determine whether the cell walls perturb the rotating disk hydrodynamics. The mass transport limited current for potassium ferrocyanide (1.00 mmol/L) oxidation in potassium chloride electrolyte (0.25 mol/L) at a platinum rotating disk electrode (area 0.385 cm²) held at 0.5 V vs Ag/AgCl was recorded as a function of rotation speed. A plot of the limiting current as a function of the square root of the rotation speed gives an excellent straight line passing through the origin with a slope of (4.32 ± 0.02) × 10^{-6} A $Hz^{-1/2}$. From the Levich equation (*7*) the slope of this plot is given by

$$\text{slope}_{\text{Lev}} = 1.554nFAD^{2/3}\upsilon^{-1/6}c_{\infty} \qquad (1)$$

where n is the number of electrons transferred, F the Faraday, D the diffusion coefficient, υ the kinematic viscosity, and c_{∞} the bulk concentration. From our measured slope we obtain a value for D, the diffusion coefficient for ferrocyanide in our electrolyte solution, of (6.48 ± 0.05) × 10^{-6} cm² s^{-1}. This is in excellent agreement with the literature value for the same electrolyte of between 6.39 × 10^{-6} and 6.50 × 10^{-6} cm² s^{-1} (*1*). Since the Levich plot is linear and passes through the origin, and since the slope is in excellent agreement with the calculated value, we conclude that the hydrodynamic flow of the rotating disk is not perturbed by wall effects in the working electrode compartment. Miller and Bruckenstein (*5*) found similar behavior for their cylindrical cells, although in their case the rotating disk electrodes used were of much smaller diameter than the cell.

As a further, more stringent, test of the hydrodynamics in the working electrode compartment, and also to determine a suitable cell solution volume for use with the cell, the diffusion coefficient of the ferrocyanide ion was determined by using the method of Albery and Hitchman (*8*). In this experiment the decay of limiting current with time is recorded. A variety of combinations of solution volume and rotation speed were investigated. In each case very similar results for the diffusion coefficient were obtained.

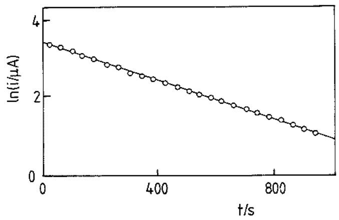

Figure 2. Plot of the logarithm of the limiting current at 25 Hz as a function of time for potassium ferrocyanide 1.0 mmol/L in 0.25 mol/L potassium chloride solution.

Table I. Diffusion Coefficients for Ferrocyanide Determined by the Method of Albery and Hitchman (*8*)

solution vol,[a] cm³	rotation speed, Hz	calcd $D \times 10^6$, cm² s^{-1}
4.0	16	6.60 (±0.10)
3.5	16	6.48 (±0.10)
3.5	25	6.42 (±0.12)

[a] Volume in working electrode compartment only.

Figure 2 shows a typical set of results for the logarithm of the limiting current plotted as a function of electrolysis time at a fixed rotation speed. According to the theory the slope of such a plot is given by

$$\text{slope}_{\text{AH}} = 1.554AW^{1/2}D^{2/3}/(\upsilon^{1/6}V) \qquad (2)$$

where W is the rotation speed of the electrode in Hz and V is the solution volume in cm^{-3}. Values for D obtained in this way are given in Table I; once again the agreement with the literature value is excellent. On the basis of these experiments a solution volume of between 3.5 and 4 cm³ was found to be suitable.

The Albery Hitchman technique has the advantage that D can be determined without knowledge of either n, the number of electrons transferred, or c_{∞} the bulk concentration. Note that the combination of a high rotation speed, a small sample volume, and a large electrode area is an advantage in this experiment since they lead to a faster decay of limiting current with time. Thus this cell design is particularly well suited to this type of measurement.

Finally the cell was tested by carrying out a coulometric titration to ensure that there were no problems with dead volume or mixing between the working and counter electrode compartments. A 3.5-cm³ portion of a deoxygenated solution of ferrocene acetic acid (0.705 mmol/L) in 0.2 mol/L NaCl was placed in the working electrode compartment. The ferrocene derivative was chosen, in preference to the ferri/ferrocyanide couple, because the oxidized form is an intense blue and could therefore be used to observe any dead volume in the cell or any leakage between working and counter compartments.

A large platinum gauze generator electrode poised at 0.35 V (vs Ag/AgCl) was used to oxidize the ferrocene derivative and the current was recorded as a function of time. The total charge passed to oxidize all the ferrocene acetic acid in the cell was found to be 254 mC. This compares with a calculated value of 238 mC based on the number of moles of ferrocene acetic acid present, corresponding to the consumption of 1.06 electrons per molecule of ferrocene acetic acid present in the working electrode compartment. This demonstrates that mixing between the working electrode and counter electrode compartments was minimal over the course of the experiment (130 min).

At a number of points during the titration, polarograms were recorded, using a rotating disk electrode, to monitor the ratio of oxidized to reduced ferrocene acetic acid present.

Using these data, we can construct a Nernst plot showing the progress of the titration. The observed slope of 63 mV/decade is close to that expected for a reversible one-electron couple at 25 °C (59.19 mV).

We have routinely used the cell to study the electrochemistry of biological redox couples in the absence of oxygen, including studies of mediated oxidation of glucose oxidase and diaphorase. Most recently the cell has been used in rotating disk studies of the electrochemistry of glucose oxidase modified by the covalent attachment of ferrocene monocarboxylic acid or ferrocene acetic acid where the combination of low sample volume, exclusion of oxygen, and good rotating disk hydrodynamics is a great advantage (*9*). This work will be reported in a subsequent publication.

CONCLUSIONS

This design of electrochemical cell is convenient and suitable for use with rotating disk electrodes where a small working volume is required and where it is desirable to exclude oxygen. The cell can be used for the determination of diffusion coefficients, either by using the variation of limiting current with rotation speed or by following the decay of current with time at a fixed rotation speed, and for coulometric titrations.

ACKNOWLEDGMENT

We are grateful to Professor W. J. Albery (Imperial College) for initial discussions on the cell shape and to M. Pritchard (Oxford Electrode) for helpful comments on the design and for making the finished cell.

Registry No. O_2, 7782-44-7.

LITERATURE CITED

(1) Adams, R. N. *Electrochemistry at Solid Electrodes*; Marcel Dekker: New York, 1969; p 219.
(2) Cass, A. E. G.; Davis, G.; Francis, G. D.; Hill, H. A. O.; Aston, W. J.; Higgins, I. J.; Plotkin, E. V.; Scott, L. D. L.; Turner, A. P. F. *Anal. Chem.* **1984**, *56*, 667–671.
(3) Crumbliss, A. L.; Hill, H. A. O.; Page, D. J. *J. Electroanal. Chem. Interfacial Electrochem.* **1986**, *206*, 327–331.
(4) Taniguchi, I.; Miyamoto, S.; Tomimura, S.; Hawkridge, F. M. *J. Electroanal. Chem. Interfacial Electrochem.* **1988**, *240*, 333–339.
(5) Miller, B.; Bruckenstein, S. *Anal. Chem.* **1974**, *46*, 2033–2035.
(6) Eggli, R. *Anal. Chim. Acta* **1977**, *91*, 129–138.
(7) Levich, V. G. *Physicochemical Hydrodynamics*; Prentice-Hall, Englewood Cliffs, NJ, 1962; pp 60–72.
(8) Hitchman, M. L.; Albery, W. J. *Electrochim. Acta* **1972**, *17*, 787–790.
(9) Whitaker, R. G. Ph.D. Thesis, University of Warwick, 1989.

RECEIVED for review July 3, 1989. Accepted September 7, 1989. R.G.W. thanks MediSense (UK), Inc., for a research scholarship.

Thin-Layer Microcell for Transmittance Fourier Transform Infrared Spectroelectrochemistry

Chao-Liang Yao, Françoise J. Capdevielle, Karl M. Kadish,* and John L. Bear*

Department of Chemistry, University of Houston, Houston, Texas 77204-5641

Various cells for external reflectance infrared spectroelectrochemistry have been designed to study electrochemical phenomena at the electrode/electrolyte interface (*1–14*). A number of cells have also been designed for monitoring IR spectra of products formed during electrode reactions (*15–19*). These latter thin-layer transmittance cells adopt a "sandwich" configuration originated by Heineman et al. (*15*) and may have two major problems. The first problem is leakage, which is minimized by the use of mechanical spacers and/or O-rings to hold the windows together under pressure. Adhesives may also be used, but these are susceptible to solvent attack. An additional problem with these cells is their fragility because of the weak mechanical strength of most IR window material.

A recently reported Fourier transform infrared (FTIR) cell design eliminated the mechanical spacer by hand-cutting a thin-layer IR chamber directly into a rectangular NaCl window material, which was then attached with Teflon film pressure seal to the bottom of a Teflon compartment (*20*). Another design also eliminated the use of spacers by utilizing a transmittance IR cell with silicon windows, which were directly flame sealed into Pyrex glass (*21*). However, both of these cells, as well as other "simple" cells described in the literature (*15–19*), are somewhat difficult to construct, and their use has therefore been limited mainly to the individual laboratory that designed them.

This note describes the construction and characteristics of a new thin-layer IR transmittance spectroelectrochemical cell that is simple to construct, durable, and completely avoids the problem of leakage. The cell is constructed from a commercially available microcavity IR cell, which has a 34-μL total cell volume. Applications of the spectroelectrochemical microcell are given by monitoring CO or $C{\equiv}CH$ frequencies of the species generated by electrooxidation or electroreduction of $Rh_2(dpf)_4(CO)$, $Rh_2(ap)_4(CO)$, and $Rh_2(ap)_4(C{\equiv}CH)$ in CH_2Cl_2, where ap = 2-anilinopyridinate and dpf = *N,N'*-diphenylformamidinate ion. The thickness limit of the transmittance IR spectroelectrochemical cell is demonstrated by using measured spectra of CH_2Cl_2, 0.1 M TBAP with and without the dirhodium complexes.

EXPERIMENTAL SECTION

Reagents and Instrumentation. $Rh_2(ap)_4(CO)$ and $Rh_2(dpf)_4(CO)$ were generated by bubbling CO into a CH_2Cl_2 solution containing $Rh_2(ap)_4$ or $Rh_2(dpf)_4$ (*22, 23*). $Rh_2(ap)_4(C{\equiv}CH)$ was prepared by reaction of $Rh_2(ap)_4Cl$ with $NaC{\equiv}CH$ in tetrahydrofuran (*24*). Spectroscopic grade CH_2Cl_2 was distilled over CaH_2 under Ar. The supporting electrolyte was tetra-*n*-butylammonium perchlorate (TBAP) and was twice recrystallized from ethanol.

An IBM Model 225 voltammetric analyzer was used for both thin-layer voltammetric measurements and controlled potential electrolysis. IR spectra were recorded with an IBM Model IR/32 FTIR spectrophotometer.

Cell Design and Method. The design of the thin-layer spectroelectrochemical cell is shown in Figure 1. The cell chamber is formed directly from a commercial microcavity IR cell, which was purchased from Aldrich Chemical Co. (No. Z11,229-1). The cell consists of a single block KBr crystal of dimensions 10 × 15 × 25 mm with a snap-in cell holder and spring clip. The cell cavity is formed by ultrasonic machining. KBr and NaCl cells with path lengths of 0.1, 0.2, and 1.0 mm are also available from the manufacturer and can also be utilized. The cell described in this present paper has a path length of 0.2 mm and a volume of 34 μL. The top section of the cell is enlarged slightly by a blade to give a total cell volume of 40 μL as compared to 6 μL for the working electrode compartment volume.

The FTIR cell utilizes a three-electrode configuration. The working electrode is a 52-mesh platinum gauze (120 μm i.d.) (Johnson Matthey, Inc.), which is folded to add mechanical strength and has dimensions of 3 × 10 mm (cells with a path length of 0.1 mm can also be used and in this case a 100-mesh platinum

0003-2700/89/0361-2805$01.50/0 © 1989 American Chemical Society

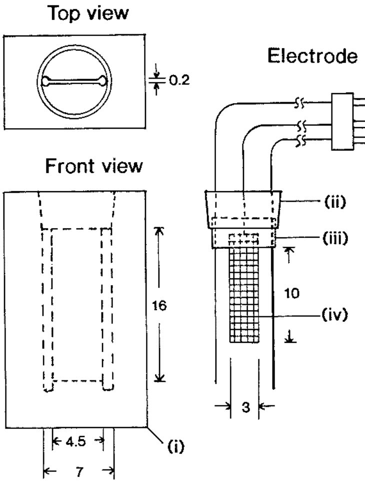

Figure 1. Schematic illustration of KBr cell chamber (top and front views) and the electrode (with the cell cap): (i) KBr cell body, (ii) Teflon cell cap, (iii) Tefzel film, (iv) platinum working electrode gauze; W, working electrode; C, counter electrode; R, silver wire pseudoreference electrode.

gauze would be utilized to reduce the electrode thickness). The transparency of this platinum electrode is about 50% as measured by the intensity of the IR interferogram.

The electrode is inserted into the thin-layer chamber to form a "sandwich" configuration. The working electrode connection is made through a 0.25-mm platinum wire and is insulated from the solution by a welded Tefzel film (E. I. du Pont de Nemours & Co.). The reference electrode is a silver wire. A carefully machined Teflon plug is used as the cell cap and the connection to the copper electrode conducting wire is made through three holes in the cap.

Transfer of deoxygenated solutions into the IR cell is done with a 100 μL syringe using Schlenk techniques. Generally, 64 acquisitions of IR interferograms are recorded for each spectrum and give a resolution of 2 cm^{-1}. The empty cell containing the working electrode is used to obtain the background, and a solution of CH_2Cl_2, 0.1 M TBAP is used as the reference spectrum. IR spectra are displayed in an absorbance or transmittance mode after subtraction of the reference spectrum.

Spectroelectrochemical data can be recorded in either a time-resolved or potential-resolved mode. The former method is commonly used, but the latter method can also be utilized (*16*, *18*). A difference FTIR spectrum is obtained by subtracting spectra at two different potentials in potential-resolved experiments or, alternatively, by subtracting spectra at two different time frames in time-resolved experiments. Both methods are reported in this present paper. A potential was not applied to the working electrode during collection of the FTIR interferograms.

RESULTS AND DISCUSSION

Electrochemical Characterization of the Cell. The thin-layer behavior of the IR cell is demonstrated by the oxidation of ferrocene to ferrocenium ion in CH_2Cl_2, 0.1 M TBAP. A cyclic voltammogram of 1.0 mM ferrocene is shown in Figure 2a. At a scan rate of 7 mV/s, the peak to peak separation is 50 mV, indicating a small solution resistance across the thin-layer chamber. Some edge effects are present as evidenced by the fact that the current does not return to the base line after electrooxidation. The double potential step current–time curve for this solution is shown in Figure 2b. Complete electrolysis of the electroactive species is achieved in less than 40 s. Integration of the current–time curve gives an average 6 μL thin-layer solution volume for five replicate experiments assuming a 100% current efficiency.

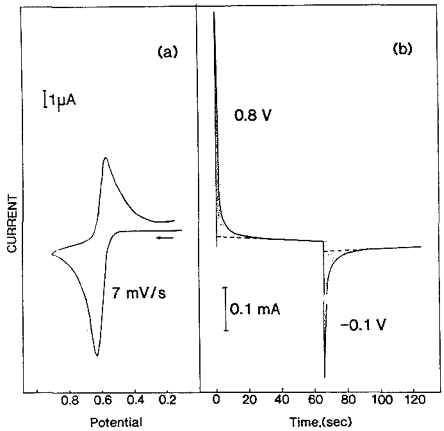

Figure 2. (a) Cyclic voltammogram and (b) current–time curve during controlled potential oxidation and rereduction of 1.0 mM ferrocene in CH_2Cl_2, 0.1 M TBAP in the 0.2 mm path length IR microcell.

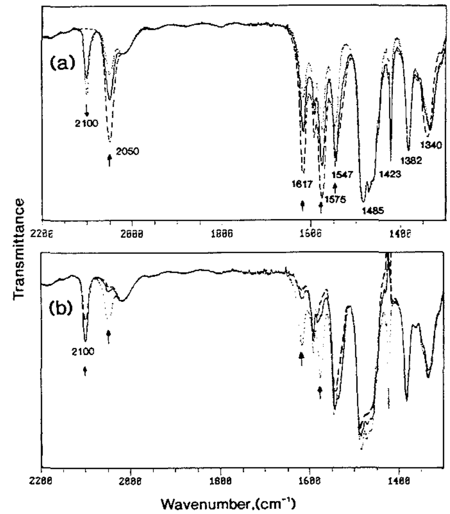

Figure 3. Transmittance IR spectra of $Rh_2(dpf)_4(CO)$ in CH_2Cl_2, 0.1 M TBAP during controlled potential oxidation at 0.90 V for (a) 0 s (---), 10 s (——), and 30 s (···) and for (b) 30 s (···), 60 s (——), and 120 s (---).

Case I: Monitoring the CO Band of a Stable Electrooxidation Product. The oxidation of $Rh_2(dpf)_4(CO)$ in CH_2Cl_2 0.1 M TBAP under 1 atm CO occurs as shown

$$Rh_2(dpf)_4(CO) \rightleftarrows [Rh_2(dpf)_4(CO)]^+ + e^- \qquad (1)$$

The $E_{1/2}$ for the above reaction is 0.37 V and the generated $[Rh_2(dpf)_4(CO)]^+$ is relatively stable in solution (*23*).

The IR spectrum of $Rh_2(dpf)_4(CO)$ in CH_2Cl_2, 0.1 M TBAP is shown in Figure 3a. The bands between 1650 and 1300 cm^{-1} correspond to the bridging dpf ligands, while the intense band at 2050 cm^{-1} corresponds to the axially bound CO stretching frequency of $Rh_2(dpf)_4CO$. This band decreases during electrooxidation at 0.90 V while a new band of $[Rh_2(dpf)_4(CO)]^+$ appears at 2100 cm^{-1}. As the controlled potential electrolysis proceeds, the intensity of this band decreases

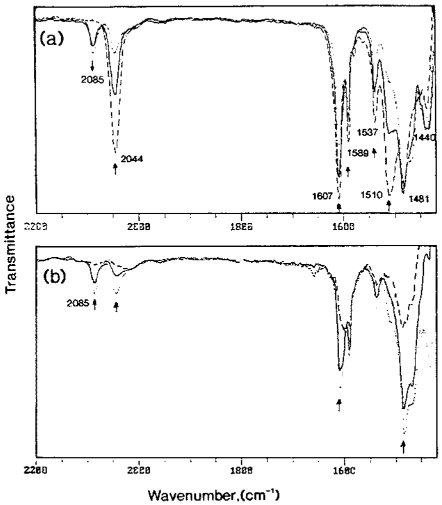

Figure 4. Transmittance IR spectra of $Rh_2(ap)_4(CO)$ in CH_2Cl_2, 0.1 M TBAP during controlled potential oxidation at 0.50 V for (a) 0 s (- - -), 10 s (——), and 30 s (• • •) and for (b) 30 s (• • •), 60 s (——), and 120 s (- - -).

slightly from its maximum value (see Figure 3b), due to a diffusion of electrogenerated $[Rh_2(dpf)_4(CO)]^+$ away from the working electrode chamber. A steady-state value is reached in about 3 min.

Case II: Monitoring the CO Band of an Unstable Electrooxidation Product. The 2,2-trans isomer of $Rh_2(ap)_4$ undergoes two reversible oxidations at $E_{1/2}$ = 0.82 and 0.08 V vs SCE in CH_2Cl_2 under N_2, but under a CO atmosphere, the values of $E_{1/2}$ for these reactions are shifted to 0.80 and 0.25 V (*22*). The large (170 mV) potential shift for the first oxidation and the small (20 mV) shift for the second oxidation provide evidence that CO is lost after formation of the singly oxidized species as shown in eq 2. The ultimate product of eq 2 is $[Rh_2(ap)_4]^+$. However, $[Rh_2(ap)_4(CO)]^+$ is present in solution as a transient intermediate for short time periods and was monitored in this present study.

$$Rh_2(ap)_4(CO) \rightleftharpoons [Rh_2(ap)_4(CO)]^+ + e^- \qquad (2)$$
$$\hookrightarrow [Rh_2(ap)_4]^+ + CO$$

Figure 4a illustrates the FTIR spectra obtained from 0 to 30 s during the controlled potential electrolysis of $Rh_2(ap)_4(CO)$ at 0.50 V. The bands at 1607, 1589, 1537, and 1510 cm⁻¹ are due to the bridging ap ligands and are similar for $Rh_2(ap)_4(CO)$ and $Rh_2(ap)_4$. These bands decrease in intensity upon oxidation while the peak at 1481 cm⁻¹ remains unchanged. The formation of a transient intermediate in reaction 2 was ascertained by monitoring the CO bands of both the reactant and the products formed during electrooxidation. The initial CO band of $Rh_2(ap)_4(CO)$ at 2044 cm⁻¹ decreases in intensity, while a new IR band appears at 2085 cm⁻¹ (see Figure 4a). The 2044-cm⁻¹ band continues to decrease as the electrolysis proceeds. At electrolysis time longer than 30 s, the band at 2085 cm⁻¹ also begins to decrease (Figure 4b), and after 2 min of electrolysis, no bands corresponding to a CO adduct remain.

The transient 2085-cm⁻¹ band corresponds to the ν_{CO} frequency of $[Rh_2(ap)_4(CO)]^+$, which is generated as an intermediate during reaction 2. The concentration of this complex will depend upon both the rate of its formation and the rate of CO dissociation from electrogenerated $[Rh_2(ap)_4(CO)]^+$. When the electrolysis potential was stepped to 0.0 V after complete oxidation, the IR spectrum then corresponded to neutral $Rh_2(ap)_4$, which was formed upon reduction of $[Rh_2(ap)_4]^+$. The short lifetime of $[Rh_2(ap)_4(CO)]^+$ compared to $[Rh_2(dpf)_4(CO)]^+$ is consistent with a faster rate of CO dissociation for the former complex.

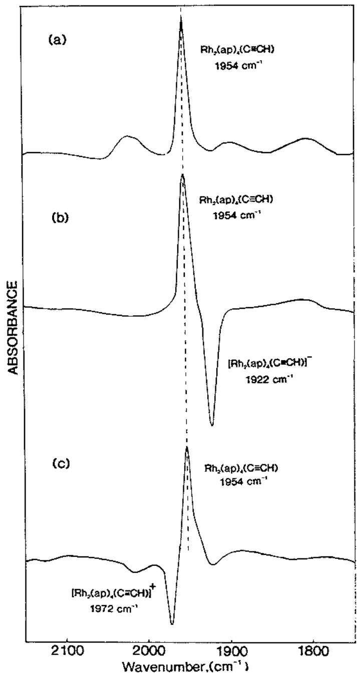

Figure 5. IR spectra of $[Rh_2(ap)_4(C{\equiv}CH)]^n$ (where n = +1, 0, or −1) in CH_2Cl_2, 0.1 M TBAP: (a) initial FTIR spectrum of $Rh_2(ap)_4(C{\equiv}CH)$, (b) difference FTIR spectrum of neutral and singly reduced $Rh_2(ap)_4(C{\equiv}CH)$, and (c) difference FTIR spectrum of neutral and singly oxidized $Rh_2(ap)_4(C{\equiv}CH)$.

Case III: Monitoring the C≡CH Band of a Stable Species during Electrooxidation/Reduction. $Rh_2(ap)_4(C{\equiv}CH)$ undergoes two reversible oxidations at $E_{1/2}$ = 1.03 and 0.38 V and a single reversible reduction at −0.52 V. These reactions are shown by eq 3–5 (*22*). The $\nu_{C{\equiv}CH}$ band of neutral $Rh_2(ap)_4(C{\equiv}CH)$ in CH_2Cl_2, 0.1 M TBAP is located at 1954 cm⁻¹ (see Figure 5a). The difference spectrum of this compound during reduction (reaction 3) is shown in Figure 5b. The positive band at 1954 cm⁻¹ is due to the neutral reactant while the negative one at 1922 cm⁻¹ is due to the $[Rh_2(ap)_4(C{\equiv}CH)]^-$ reduction product. This electroreduction is reversible and the original IR spectrum of $Rh_2(ap)_4(C{\equiv}CH)$ could again be obtained when the applied potential was stepped back to 0.0 V.

$$Rh_2(ap)_4(C{\equiv}CH) + e^- \rightleftharpoons [Rh_2(ap)_4(C{\equiv}CH)]^- \qquad (3)$$

$$Rh_2(ap)_4(C{\equiv}CH) \rightleftharpoons [Rh_2(ap)_4(C{\equiv}CH)]^+ + e^- \qquad (4)$$

$$[Rh_2(ap)_4(C{\equiv}CH)]^+ \rightleftharpoons [Rh_2(ap)_4(C{\equiv}CH)]^{2+} + e^- \qquad (5)$$
$$\hookrightarrow \text{decomposition products}$$

The difference IR spectrum obtained during the first oxidation of $Rh_2(ap)_4(C{\equiv}CH)$ (reaction 4) at 0.70 V is shown in Figure 5c. In this spectrum, the IR absorption band is

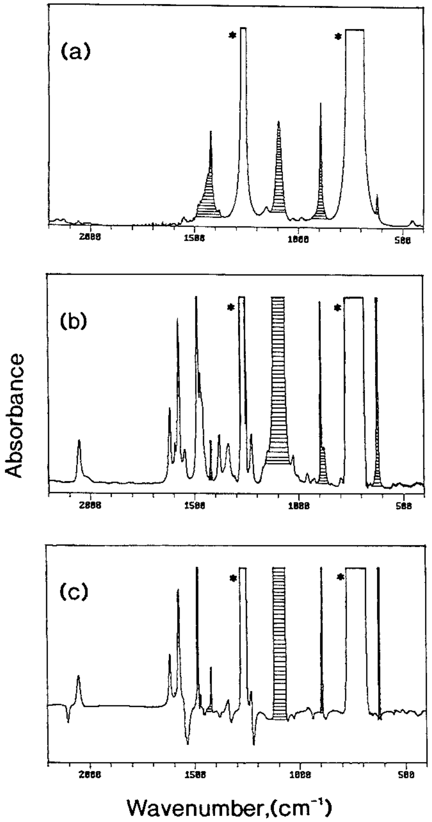

Figure 6. IR spectra (a) of CH_2Cl_2, 0.05 mM TBAP in the cell with 0.1-mm path length, (b) of 2 mM $Rh_2(dpf)_4(CO)$ in CH_2Cl_2, 0.1 M TBAP in a cell with 0.2 mm path length, and (c) difference IR spectrum of neutral and singly oxidized $Rh_2(dpf)_4(CO)$ in a cell with 0.2 mm path length.

shifted from 1954 to 1972 cm^{-1} as $Rh_2(ap)_4(C{\equiv}CH)$ is converted to $[Rh_2(ap)_4(C{\equiv}CH)]^+$. Finally, a further oxidation of $[Rh_2(ap)_4(C{\equiv}CH)]^+$ at 1.2 V (reaction 5) results in the complete disappearance of the C≡CH band as well as most other bands in the spectrum. This is consistent with other electrochemical data which show a multielectron transfer process on the time scale of controlled potential electrolysis where a decomposition of the complex occurs (*24*).

The FTIR spectroelectrochemical cell can be used in this case to monitor the C≡CH stretching frequencies of $[Rh_2(ap)_4(C{\equiv}CH)]^n$, where $n = +1, 0$, or -1. All three species are stable, and their IR spectra can be recorded from the same solution by applying appropriate electrolysis potentials.

Thickness Limit of the Transmittance Spectroelectrochemical Cell. The scaled absorbance subtraction method is commonly used in FTIR spectroelectrochemical experiments (*25*). FTIR spectrophotometers usually have a maximum absorbance at $A = 4.0$ and above this value, data overflow will occur. On the other hand, it has been shown that the maximum absorbance for accurate difference spectrometry should be less than 0.7 unit (*26*). When the maximum absorbance is between 0.7 and 3.5 units, inaccurate subtraction may result in deviation from Beer's law behavior. This is illustrated for the IR spectra of $Rh_2(dpf)_4(CO)$ in CH_2Cl_2, 0.1 M TBAP.

CH_2Cl_2 has two strong absorbance bands at 1264 ($\epsilon = 563$) and 740 ($\epsilon > 600$) cm^{-1} and two weaker bands at 1424 ($\epsilon = 12$) and 896 ($\epsilon = 14$) cm^{-1} (*27, 28*). The ClO_4^- counterion of TBAP has a strong absorbance band at 1100 ($\epsilon = 4000$) cm^{-1}. Molar absorbtivities of the bands at 1264, 1424, 896, and 1100 cm^{-1} were calculated with a 0.1-mm IR cell for a CCl_4 solution containing various concentrations of CH_2Cl_2 and 0.05 M TBAP. All of these bands will determine the thickness limit for an IR cell where one may obtain a satisfactory subtraction of the sample and reference spectra.

The preferred cell thickness for $A \leq 0.7$ at the above absorbance wavelengths would be 3×10^{-2} (896 cm^{-1}), 2×10^{-2} (1424 cm^{-1}), 2×10^{-2} (1100 cm^{-1}) and 8×10^{-4} (1264 cm^{-1}) mm for a solution containing CH_2Cl_2 and 0.1 M TBAP. However, it is virtually impossible to design a transmittance cell with a path length of 10^{-4} mm, and one therefore cannot obtain an accurate subtraction by using the absorbances at 1264 or 740 cm^{-1} (bands with asterisks in Figure 6). There are also problems with the other bands at 896, 1100, and 1424 cm^{-1}. A transmittance cell with a path length of 10^{-2} mm is technically difficult to achieve and, if constructed, would give a large solution resistance. On the other extreme, one can calculate cell thickness values for $A \leq 3.5$ with the same solvent system. These values are 0.2, 0.4, 0.1, and 0.004 mm at the above four wavenumbers.

Most transmittance IR cells reported in the literature have 0.1 to 0.5 mm path lengths. Consequently, the absorbance bands shown as cross-hatched bands in Figure 6a may be subtracted but the final spectrum will almost always contain residual positive or negative components. This is illustrated in Figure 6b for a solution containing 2 mM $Rh_2(dpf)_4(CO)$ in CH_2Cl_2, 0.1 M TBAP after subtraction of the blank solution reference. The cross-hatched bands in this figure result from a failure in Beer's law behavior and are not real bands of the complex. The difference spectrum for neutral and oxidized $Rh_2(dpf)_4(CO)$ (Figure 6c) also shows similar residual components over wavelength ranges where either the solvent or the supporting electrolyte strongly absorb.

Summary. The IR spectroelectrochemical cell reported in this work is constructed from a single block of material and requires neither adhesives, spacers, nor O-ring pressure seals. For this reason the cell is easily reproduced, requires little maintenance, and has no leakage problems. The cell thickness is also reproducible. However, care must be taken to avoid misinterpretation of the resulting IR data in those regions where there are strong absorbances from either the solvent or the supporting electrolyte.

LITERATURE CITED

(1) Hansen, W. N. In *Advances in Electrochemistry and Electrochemical Engineering*; Muller, R. H., Ed.; Wiley; New York, 1973; Vol. 9, pp 1–60.
(2) Neugebauer, H.; Nauer, G.; Neckel, A.; Tourillon, G.; Garnier, F.; Lange, P. *J. Phys. Chem.* **1984**, *88*, 652.
(3) Bewick, A.; Pons, S. In *Advances in Infrared and Raman Spectroscopy*; Hester, R. J. H., Clark, R. E., Eds.; Wiley-Hayden: London, 1985; p 1.
(4) Bewick, A.; Kunimatsu, K.; Pons, S.; Russell, J. W. *J. Electroanal. Chem.* **1984**, *160*, 47.
(5) Pons, S.; Davidson, T.; Bewick, A. *J. Electroanal. Chem.* **1984**, *160*, 63.
(6) Kunimatsu, K.; Golden, W. G.; Seki, H.; Philpott, M. R. *Langmuir* **1985**, *1*, 245.
(7) Pons, S.; Davidson, T.; Bewick, A. *J. Am. Chem. Soc.* **1983**, *105*, 1802.
(8) McDonald, R. S. *Anal. Chem.* **1986**, *58*, 1906.
(9) Habib, M. A.; Bockris, J. O'M. *J. Electrochem. Soc.* **1985**, *132*, 108.
(10) Foley, J. K.; Pons, S. *Anal. Chem.* **1985**, *57*, 945A.
(11) Foley, J. K.; Korzeniewski, C.; Daschbach, J. L.; Pons, S. In *Electroanalytical Chemistry*; Bard, A. J., Ed. Dekker: New York, 1986; Vol. 14, p 309.
(12) Seki, H.; Kunimatsu, K.; Golden, W. G. *Appl. Spectrosc.* **1985**, *39*, 437.
(13) Best, S. P.; Clark, R. J. H.; McQueen, R. C. S.; Cooney, R. P. *Rev. Sci. Instrum.* **1987**, *58*, 2071.
(14) Best, S. P.; Clark, R. J. H.; McQueen, R. C. S.; Joss, S. *J. Am. Chem. Soc.* **1989**, *111*, 548.

(15) Heineman, W. R.; Burnett, J. N.; Murray, R. W. *Anal. Chem.* **1968**, *40*, 1974.
(16) Bullock, J. P.; Boyd, D. C.; Mann, K. R. *Inorg. Chem.* **1987**, *26*, 3084.
(17) DuBois, D. L.; Turner, J. A. *J. Am. Chem. Soc.* **1982**, *104*, 4989.
(18) Nevin, W. A.; Lever, A. B. P. *Anal. Chem.* **1988**, *60*, 727.
(19) DuBois, D. L. *Inorg. Chem.* **1984**, *23*, 2047.
(20) Kadish, K. M.; Mu, X. H.; Lin, X. Q. *Electroanalyst* **1989**, *1*, 35.
(21) Flowers, P. A.; Mamantov, G. *Anal. Chem.* **1989**, *61*, 190.
(22) Bear, J. L.; Yao, C.-L.; Liu, L.-M.; Capdevielle, F. J.; Korp, J. D.; Albright, T. A.; Kang, S.-K.; Kadish, K. M. *Inorg. Chem.* **1989**, *28*, 1254.
(23) Lifsey, R. S. Ph.D. Dissertation, University of Houston, 1987.
(24) Yao, C. L.; Park, K. H.; Khokhar, A. R.; Bear, J. I. *Book of Abstracts*; 197th National Meeting of the American Chemical Society, Dallas, TX; American Chemical Society: Washington, DC, 1989. INOR 363.
(25) Griffiths, P. R.; De Haseth, J. A. Fourier Transform Infrared Spectrometry. In *Chemical Analysis*; Elving, P. J., Winefordner, J. D., Eds.; Wiley-Interscience: New York, 1986; Vol 83; Chapter 10.
(26) Anderson, R. J.; Griffiths, P. R. *Anal. Chem.* **1975**, *47*, 2339.
(27) Palma, F. E.; Piotrowki, E. A.; Sundaram, S.; Clevend, F. F. *J. Mol. Spectrosc.* **1964**, *13*, 119.
(28) Newbound, T. D.; Colsman, M. R.; Miller, M. M.; Wulfsberg, G. P.; Anderson, O. P.; Strauss, S. H. *J. Am. Chem. Soc.* **1989**, *11*, 3762.

RECEIVED for review August 14, 1989. Accepted October 12, 1989. The authors thank the Robert A. Welch Foundation (Grants E-918, J.L.B., and E-680, K.M.K.), the National Science Foundation (Grant CHE-8822881, K.M.K.), and the National Institutes of Health (Grant GM25172, K.M.K.) for financial support.

Highly Stable Voltammetric Measurements of Phenolic Compounds at Poly(3-methylthiophene)-Coated Glassy Carbon Electrodes

Joseph Wang* and Ruiliang Li

Department of Chemistry, New Mexico State University, Las Cruces, New Mexico 88003

The determination of phenolic compounds is of great environmental, industrial, and clinical significance. Since most phenols are oxidized at easily accessible potentials, voltammetry and amperometry may serve as highly sensitive tools for their quantification. Unfortunately, the oxidation of phenolic compounds at solid electrodes produces phenoxy radicals which couple to form a passivating polymeric film on the electrode. A decrease in the response is thus observed upon repetitive scans, the rate of which is concentration dependent (as expected for a dimerization reaction). Consequently, conventional electrodes are usually unsuitable for reliable voltammetric measurements of phenolic compounds. Various strategies have been proposed to address this fouling problem. Anodic polarization in an acidic solution of ferric chloride was employed by Koile and Johnson (*1*) to remove phenolic films from platinum surfaces. Wang and Lin (*2*) described a repetitive electrochemical treatment for renewal in situ of glassy carbon electrodes in the presence of phenolic compounds. Laser activation was explored by Poon and McCreery (*3*) as a means to repeatedly renew solid electrode surfaces in the presence of phenols. Treatment with a flame (*4*) was also suggested to restore the surface activity. Such reactivation schemes are often time-consuming and/or require additional (high cost) instrumentation.

A more attractive avenue for voltammetric measurements of phenols is to eliminate the passivation problem in the first place (rather than exploring means for surface reactivation). A deliberate modification of electrode surfaces may be very advantageous for this purpose. The objective of the research described in this note is to illustrate the unusual stable response of phenolic compounds at poly(3-methylthiophene) (P3MT) coated electrodes. Electroactive conducting polymers have received a great attention in the modification of electrodes because of potential application for energy storage or electrocatalysis and as electrochromic displays or "ion gate" membranes. Among these, films prepared by electropolymerization of thiophene derivatives have attracted considerable interest (*5*). In the course of our work on permselective electropolymerized films, we found that P3MT electrodes exhibit excellent resistance to fouling in the presence of high concentrations of phenolic species. The high stability is accompanied by enhanced sensitivity and selectivity. We wish to report these observations in the following sections.

EXPERIMENTAL SECTION

Apparatus. The 10-mL electrochemical cell (Model MF 1052, Bioanalytical Systems (BAS)) was joined to the working electrode, reference electrode (Ag/AgCl) (3 M NaCl) (Model RE-1, BAS), and the platinum wire auxiliary electrode through holes in its Teflon cover. The three electrodes were connected to an EG&G PAR Model 264A voltammetric analyzer, the output of which was displayed on a Houston Instruments X-Y recorder. Flow experiments employed a glassy carbon thin-layer amperometric detector (Model TL-5, BAS) and a 100-μL injection loop. The flow injection system was described previously (*6*).

Reagents. All aqueous solutions were prepared in double-distilled water. 3-Methylthiophene, acetonitrile (LC grade), *m*-nitrophenol, *p*-chlorophenol (Aldrich), acetaminophen, dopamine (Sigma), phenol (Fisher), *p*-cresol (Kodak), and ascorbic acid (Baker) were used without further purification. The supporting electrolyte was 0.05 M phosphate buffer (pH 7.4).

Procedure. Prior to its coating, the glassy carbon electrode was polished with 0.05-μm alumina slurry, rinsed with double-distilled water, and sonicated in a water bath for 2 min. The electrochemical polymerization was carried out in deaerated acetonitrile solution, containing 0.1 M sodium perchlorate and 0.05 M 3-methylthiophene. For this purpose the potential was cycled three times between 0.0 and 1.7 V (vs Ag/AgCl) at a rate of 20 mV/s; the polymerization was terminated during the third cycle by holding the potential at +0.7 V for 10 min. A film thickness of about 1 μm was estimated. Prior to phenol measurements the modified electrode was pretreated in the phosphate buffer blank solution by repetitively scanning the potential between 0.0 and +0.7 V (10 cycles) until a stable background was obtained.

RESULTS AND DISCUSSION

The unusual stability of P3MT-coated electrodes will be illustrated in the presence of several phenolic compounds that exhibit rapid surface fouling at conventional electrodes. Figure 1 compares repetive cycle voltammograms for 2×10^{-4} M *p*-cresol obtained at 50 mV/s at the P3MT-coated (A) and bare (B) glassy carbon electrodes. An irreversible oxidation process is observed at both electrodes. The inhibitory layer formed at the bare electrode results in disappearance of the peak after the third scan. In contrast, no degraded response is observed for the entire series at the P3MT electrode. Voltammograms of 2×10^{-4} M chlorophenol (Figure 2), phenol, or *m*-nitrophenol (not shown) exhibit similar observations, with complete fouling of the glassy carbon surface within four

0003-2700/89/0361-2809$01.50/0 © 1989 American Chemical Society

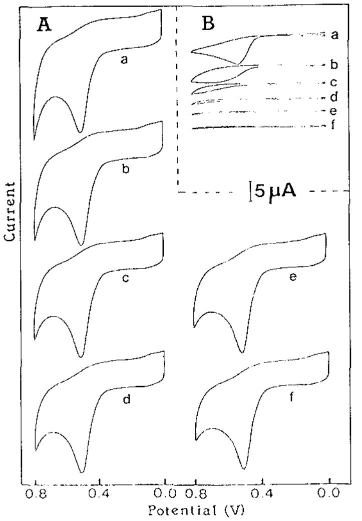

Figure 1. Successive (a–f) cyclic voltammograms for 2 × 10^{-4} M *p*-cresol at P3MT-coated (A) and bare (B) glassy carbon electrodes: scan rate, 50 mV/s; electrolyte, 0.05 M phosphate buffer (pH 7.4).

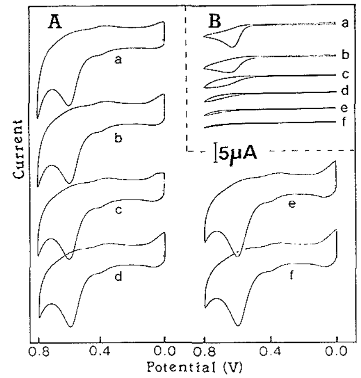

Figure 2. Successive (a–f) cyclic voltammograms for 2 × 10^{-4} M chlorophenol at P3MT-coated (A) and bare (B) glassy carbon electrodes. Other conditions are given in Figure 1.

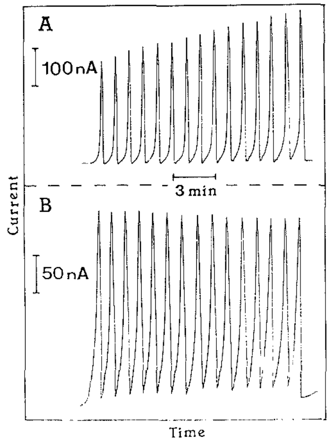

Figure 3. Detection peaks for repetitive injections of a 3 × 10^{-4} M phenol solution at the bare (A) and P3MT-coated (B) electrodes: applied potential, +0.70 V; flow rate, 1.0 mL/min; injections of 100 μL samples. Electrolyte and carrier, 0.05 M phosphate buffer (pH 7.4).

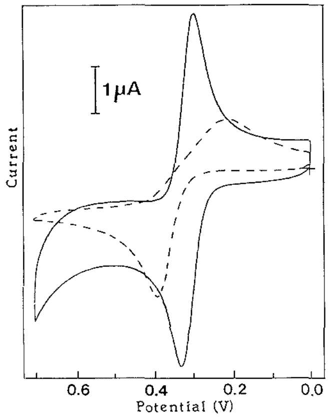

Figure 4. Cyclic voltammograms for 2 × 10^{-4} M acetaminophem at P3MT-coated and bare, glassy carbon electrodes (solid and dotted lines, respectively): scan rate, 10 mV/s; electrolyte 0.05 M phosphate buffer.

scans and a highly stable response at the P3MT surface. The voltammograms of Figure 2A are a part of a series of 140 repetitive runs, that yielded a reproducible chlorophenol peak. The excellent behavior after numerous voltammetric scans implies negligible accumulation of reaction products. Such a high state of surface cleanliness is attributed to the use of a different substrate material (conducting polymer rather than glassy carbon) at which the phenoxy products do not deposit, and thus do not block the surface. It is possible that the microporous structure of the film (discussed in the following section) results in steric hindrance to the dimerization of the phenoxy radicals. The high stability implies that repetitive surface renewal schemes are no longer necessary when voltammetry of phenolic compounds is concerned.

The observation that the P3MT electrode yields a highly stable response in the presence of phenolic compounds can greatly benefit the detection of such compounds by liquid chromatography or flow injection analysis. Amperometric detection has been widely used for monitoring phenols in environmental, industrial, clinical, and food samples. Similar flow measurements have been explored in electrochemical immunoassays (based on the conversion of phenyl phosphate to a detectable phenol) (7). Under flow injection or liquid chromatography conditions, the fouling problem is not as severe (as in voltammetric, batch, experiments), because of the small amount of product that is electrogenerated. This is, in particular, the case for work at low concentrations (10^{-9} to 10^{-5} M). Electrode fouling, however, is evidenced at higher concentrations. For example, for a series of 15 repetitive flow injections of samples containing 3 × 10^{-4} M phenol, an appreciable (37%) loss of electrode activity is observed (Figure 3A). In contrast, a highly stable phenol detection peak is observed when the P3MT detector is used (Figure 3B). Notice, however, that while both electrodes exhibit a fast response time, the recovery time is slower at the P3MT detector (probably due to trapping of the analyte within the surface micropores).

Another observation that accrues from the surface alteration is the overall appearance of the voltammogram. Figure 4

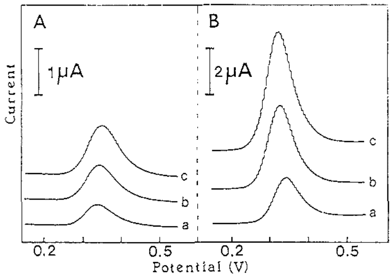

Figure 5. Differential pulse voltammograms for acetaminophen solutions of increasing concentration, (2.5–7.5) × 10^{-5} M (a–c) at bare (A) and P3MT-coated (B) electrodes: scan rate, 10 mV/s; amplitude, 25 mV; electrolyte, 0.05 M phosphate buffer (pH 7.4).

compares cyclic voltammograms for 2 × 10^{-4} M acetaminophen recorded at 10 mV/s at P3MT and ordinary glassy carbon electrodes (solid and dotted lines, respectively). Well-defined symmetrical peaks are observed at the coated electrode; the value of ΔE_p is only 34 mV. Such response is consistent with a thin-layer electrochemical behavior and is attributed to solute depletion within the micropores of the P3MT. The large surface area provided by the three-dimensional porous structure greatly increases the faradaic current (vs the ordinary electrode). Analogous changes in the nonfaradaic residual current are also observed. Note, for example, the marked increase in the cyclic voltammetric background current envelope (e.g., Figures 1 and 2) that reflects the corresponding change in the double layer capacitance. Such changes were observed also in analyte-free electrolyte solutions (not shown). Adsorptive accumulation of acetaminophen may also account for the shape of the voltammogram shown in Figure 4. Analytical advantages accrue from the use of pulse voltammetric procedures aimed at compensating the high background currents. For example, Figure 5 illustrates differential pulse voltammograms, recorded at bare (A) and P3MT (B) electrodes, for successive standard additions of acetaminophen ((2.5–7.5) × 10^{-5} M (a–c)). Significantly larger oxidation peaks are observed at the coated electrode. (Note the different current scales.) The effective correction of the charging current contribution results in similar (flat) base lines. The three peaks of Figure 5 are a part of eight concentration increments, up to 2 × 10^{-4} M. At both electrodes, linearity prevailed over the lower (<1 × 10^{-4} M) concentration range (slopes of 16 (bare) and 71 (P3MT) (μA/mM).

The use of a conductive polymeric surface may benefit also the selectivity of voltammetric measurements. One example of relevance to clinical analysis is the determination of acetaminophen in the presence of ascorbic acid. At the bare glassy carbon electrode these compounds yield partially overlapped oxidation peaks of similar size (Figure 6A); thus, convenient quantitation of the drug in the presence of ascorbic acid is not feasible. The P3MT surface, in contrast, exhibits a diminished response to ascorbic acid and hence greatly enhances the selectivity toward acetaminophen (Figure 6B). Similar selectivity improvements, of relevance to neurochemical studies (*8*), were obtained in measurements of 1 × 10^{-4} M dopamine in the presence of 4 × 10^{-4} M ascorbic acid (not shown). Such behavior is attributed to preferential adsorption of phenolic or catechol compounds.

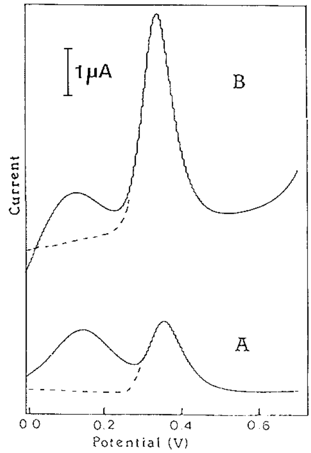

Figure 6. Differential pulse voltammograms for a solution containing 4 × 10^{-4} M ascorbic acid and 1 × 10^{-4} M acetaminophen at bare (A) and P3MT-coated (B) electrodes. Also shown (dotted lines) is the response for acetaminophen alone. Other conditions are given in Figure 5.

In conclusion, the present study illustrates that coverage of glassy carbon electrodes with a P3MT film greatly extends their lifetime for the voltammetry of phenolic species. The resistance to fouling is attributed to the use of a different surface at which phenoxy products do not deposit. This observation represents a new, highly useful, sensing application of conducting polymeric films. The prevention of passivation is accompanied by enhanced sensitivity and selectivity and thus holds great promise for routine sensing applications or flow analysis. P3MT, or other conducting polymers, may be useful for addressing electrode fouling problems in the presence of additional classes of otherwise deactivating organic compounds. Additional work is desired to fully characterize the surface chemistry and redox processes involved in the improved stability reported in this work.

Registry No. P3MT, 84928-92-7; *p*-cresol, 106-44-5; phenol, 108-95-2; *m*-nitrophenol, 554-84-7; acetaminophen, 103-90-2.

LITERATURE CITED

(1) Koile, R. C.; Johnson, D. C. *Anal. Chem.* **1979**, *51*, 741.
(2) Wang, J.; Lin, M. S. *Anal. Chem.* **1988**, *60*, 499.
(3) Poon, M.; McCreery, R. L. *Anal. Chem.* **1987**, *59*, 1615.
(4) Hedenburg, J. F.; Freiser, H. *Anal. Chem.* **1953**, *25*, 1355.
(5) Shi, L. H.; Roncali, J.; Garnier, F. *J. Electroanal. Chem.* **1989**, *263*, 155.
(6) Wang, J.; Hutchins, L. D. *Anal. Chem.* **1985**, *57*, 1536.
(7) Tang, H. T.; Lunte, C. E.; Halsall, H. B.; Heineman, W. R. *Anal. Chim. Acta* **1988**, *214*, 187.
(8) Gerhardt, G. A.; Oke, A. F.; Nagy, F.; Moghaddam, B.; Adams, R. N. *Brain Res.* **1984**, *290*, 390.

RECEIVED for review June 26, 1989. Accepted September 28, 1989. This work was supported by the donors of the Petroleum Research Fund, administrated by the American Chemical Society, and by the National Institutes of Health (Grant No. GM 30913-06).

AUTHOR INDEX

Abbas, N. M. See Singh, R. P.
Abel, K. See Boltinghouse, F.
Abidi, S. L. See Ha, S. T. K.
Abramson, F. P. See Chace, D. H.
Abruna, H. D. See Liu, K. E.
Adley, D. P.
——; Underhill, D. W.
Fundamental factors in the performance of diffusive samplers. 843
Aebli, G. V. See Collison, M. E.
Aggarwal, S. K.
——; Kinter, M.; Wills, M. R.; Savory, J.; Herold, D. A.
Isotope dilution gas chromatography/mass spectrometry for the determination of nickel in biological materials. 1099
Akagi, T. See Hirata, T.
Akatsuka, K.
——; Atsuya, I.
Synthetic reference material for direct analysis of solid biological samples by electrothermal atomic absorption spectrometry. 216
Akitt, J. W. See Wilson, M. A.
Alak, A. M.
——; Vo Dinh Tuan
Silver-coated fumed silica as a substrate material for surface-enhanced Raman scattering. 656
Alam, K. See Singh, R. P.
Albert, K.
——; Kunst, M.; Bayer, E.; De Jong, H. J.; Genissel, P.; Spraul, M.; Bermel, W.
Investigation of a cyclopropyl-containing drug by on-line high-performance liquid chromatography/nuclear magnetic resonance. 772
Alexandrou, N.
——; Pawliszyn, J.
Supercritical fluid extraction for the rapid determination of polychlorinated dibenzo-p-dioxins and dibenzofurans in municipal incinerator fly ash. 2770
Al-Haddad, A. See Creaser, C. S.
Allen, L. See Koropchak, J. A.
Almgren, M. See Staahlberg, J.
Amankwa, L.
——; Cantwell, F. F.
Investigation of fast mass transfer kinetics in solvent extraction using rapid stirring and a porous membrane phase separator 1036
Measurement of the rate of oxidation of iodide by iron(III) using solvent extraction. 2562
Amster, I. J.
——; Land, D. P.; Hemminger, J. C.; McIver, R. T. Jr.
Chemical ionization of laser-desorbed neutrals in a Fourier-transform mass spectrometer. 184
Anderegg, R. J. See Ghosh, A.
Anderson, D. G.
Coatings. 33r
Anderson, J. E.
——; Hopkins, D.; Shadrick, J. W.; Ren, Y.
Apparatus for the fabrication of poly(chlorotrifluoroethylene) composite electrodes. 2330
Anderson, M. A. See Bertsch, P. M.
Andersson-Engels, S.
——; Johansson, J.; Svanberg, S.; Svanberg, K.
Fluorescence diagnosis and photochemical treatment of diseased tissue using lasers: Part I. 1367a
Ando, T. See Terabe, S.
Andreolini, F. See Borra, C.
Angel, S. M.
——; Myrick, M. L.
Near-infrared surface-enhanced Raman spectroscopy using a diode laser. 1648
Anjo, D. M.
——; Kahr, M.; Khodabakhsh, M. M.; Nowinski, S.; Wanger, M.
Electrochemical activation of carbon electrodes in base: minimization of dopamine adsorption and electrode capacitance. 2603
Anson, F. C. See Ugo, P.
Anton, K. See Bruno, A. E.
Aomura, Y. See Ogino, H.
Aoyama, E. See Nakagawa, T.
Appelhans, A. D.
——; Delmore, J. E.
Comparison of polyatomic and atomic primary beams for secondary ion mass spectrometry of organics. 1087
Aras, N. K. See Gokmen, I. G.
Arbogast, B. See Laramee, J. A.
Armstrong, D. W. See Berthod, A.; Bertrand, G. L.
Armstrong, N. R. See Nebesny, K. W.
Arn, D. See Murphy, M. M.
Arnold, D. P.
——; Peachey, R. M.; Petty, J. D.; Sweatman, D. R.
Automated titrations using a discontinuous programmed flow analyzer. 2109
Ashraf-Khorassani, M.
——; Taylor, L. T.
Qualitative supercritical fluid chromatography/Fourier transform infrared spectroscopy study of methylene chloride and supercritical carbon dioxide extracts of double-base propellant. 145
Athanasiou-Malaki, E.
——; Koupparis, M. A.; Hadjiioannou, T. P.
Kinetic determination of primary and secondary amines using a fluoride-selective electrode and based on their reaction with 1-fluoro-2,4-dinitrobenzene. 1358
Athnasios, A. K.
——; Gross, A. F.; Given, P. S. Jr.
Food. 45r
Atsuya, I. See Akatsuka, K.
Ausserer, W. A.
——; Ling, Y. C.; Chandra, S.; Morrison, G. H.
Quantitative imaging of boron, calcium, magnesium, potassium, and sodium distributions in cultured cells with ion microscopy. 2690
Avery, J. P. See Rowlen, K. L.
Azarraga, L. V. See Dobbs, J. C.
Azumi, T. See Terazima, M.

Bachas, L. G. See Daunert, S.; Kjellstrom, T. L.
Bae, I. T.
——; Xing, X.; Yeager, E. B.; Scherson, D.
Ionic transport effects in in situ Fourier-transform infrared reflection adsorption spectroscopy. 1164
Balasanmugam, K. See Miller, J. M.
Baldwin, R. P. See Prabhu, S. V.; Thomsen, K. N.
Ballantine, D. S. Jr.
——; Wohltjen, H.
Surface acoustic wave devices for chemical analysis. 704a
Ballew, R. M.
——; Demas, J. N.
An error analysis of the rapid lifetime determination method for the evaluation of single exponential decays. 30
Bangs, J. D. See Bean, M. F.
Bannister, J. V. See McNeil, C. J.
Barber, A. S.
——; Small, G. W.
Simulation of carbon-13 nuclear magnetic resonance spectra of linear cyclic aromatic compounds. 2658
Barber, T. E. See Johnson, P. A.
Barbour, C. J. See Parcher, J. F.
Bard, A. J. See Kwak, J.
——; Fan, F. R. F.; Kwak, J.; Lev, O.
Scanning electrochemical microscopy. Introduction and principles. 132
Barlow, C. H. See Kelly, J. J.; Phelan, M. K.
Barman, B. N. See Schure, M. R.
Barth, H. G.
——; Sun, S. T.
Particle size analysis. 143r
Bartlett, P. N.
——; Whitaker, R. G.
Small-volume electrochemical cell designed for rotating disk studies in bioelectrochemistry. 2803
Bartsch, R. A. See Olsher, U.
Batie, W. C. See Garbarino, J. R.
Battista, M.
——; Di Corcia, A.; Marchetti, M.
Extraction and isolation of triazine herbicides from water and vegetables by a double trap tandem system. 935
Bayer, E. See Albert, K.
Baykut, G. See McIver, R. T. Jr.
Bean, M. F.
——; Bangs, J. D.; Doering, T. L.; Englund, P. T.; Hart, G. W.; Fenselau, C.; Cotter, R. J.
Assessing heterogeneity of the high-mannose glycopeptide gp432 on the variant surface glycoprotein of trypanosomes: a comparison of plasma desorption mass spectrometry and radiolabeling techniques. 2686
Bear, J. L. See Yao, C. L.
Beary, E. S. See Moody, J. R.; Paulsen, P. J.
Beauchemin, B. T. Jr.
——; Brown, P. R.
Quantitative analysis of diazonaphthoquinones by thin-layer chromatographic/diffuse reflectance infrared Fourier-transform spectrometry. 615
Beauchemin, D.
——; Berman, S. S.
Determination of trace metals in reference water standards by inductively coupled plasma mass spectrometry with on-line preconcentration. 1857
Beaugrand, C.
——; Jaouen, D.; Mestdagh, H.; Rolando, C.
Ion confinement in the collision cell of a multiquadrupole mass spectrometer: access to chemical equilibrium and determination of kinetic and thermodynamic parameters of an ion-molecule reaction. 1447
Beck, K. M. See Ringwelski, A. Z.
Becker, C. H. See Pallix, J. B.
Bello, J. M.
——; Stokes, D. L.; Vo Dinh Tuan
Titanium dioxide based substrate for optical monitors in surface-enhanced Raman scattering analysis. 1779
Bemgaard, A. K.
——; Blomberg, L. G.; Colmsjoe, A. L.
Contribution of interfacial resistance to plate height in open tubular gas chromatography. 2165
Benner, R. L.
——; Stedman, D. H.
Universal sulfur detection by chemiluminescence. 1268
Bennich, H. See Craig, A. G.
Benninghoven, A. See Bletsos, I. V.
Berberich, D. W. See Hail, M. E.
Berger, T. A.
Modeling linear and tapered restrictors in capillary supercritical fluid chromatography. 356
Bergold, A. F.
——; Carr, P. W.
Improved resolution of glycoproteins by chromatography with concanavalin A immobilized on microparticulate silica via temperature-programmed elution. 1117
Berman, S. S. See Beauchemin, D.; Siu, K. W. M.; Sturgeon, R. E.
Bermel, W. See Albert, K.
Bernius, M. T. See Ling, Y. C.
Berthod, A.
——; Armstrong, D. W.; Myers, M. N.; Giddings, J. C.
Use of secondary equilibria for the separation of small solutes by field-flow fractionation (correction). 90

Bertrand, G. L.
——; Armstrong, D. W.
Model for conductometric detection of carbohydrates and alcohols as complexes with boric acid and borate ion in high-performance liquid chromatography. 631
Bertsch, P. M.
——; Anderson, M. A.
Speciation of aluminum in aqueous solutions using ion chromatography. 535
Berube, T. R.
——; Buck, R. P.; Lindner, E.; Gratzl, M.; Pungor, E.
Comparison of proposed response mechanisms of precipitate-based ion-selective electrodes in the presence of interfering ions. 453
Betts, F.
——; Yau, A.
Graphite furnace atomic absorption spectrometric determination of chromium, nickel, cobalt, molybdenum, and manganese in tissues containing particles of a cobalt-chrome alloy. 1235
Beu, S. C. See Laude, D. A. Jr.
Bialkowski, S. E.
Generalized digital smoothing filters made easy by matrix calculations. 1308
Data analysis in the shot noise limit. 1. Single parameter estimation with Poisson and normal probability density functions. 2479
Data analysis in the shot noise limit. 2. Methods for data regression. 2483
Bidlingmeyer, B. A. See Dorschel, C. A.
Bier, M. See Mosher, R. A.
Biggs, W. R.
——; Fetzer, J. C.
Thermal gradient liquid chromatography: application to selective element detection by inductively coupled plasma-atomic emission spectrometry. 236
Bilewicz, R.
——; Wikiel, K.; Osteryoung, R.; Osteryoung, J.
General equivalence of linear scan and staircase voltammetry: experimental results. 965
Bindra, D. S.
——; Wilson, G. S.
Pulsed amperometric detection of glucose in biological fluids at a surface-modified gold electrode. 2566
Birks, J. W. See Poulsen, J. R.; Rowlen, K. L.
Bishop, G. A.
——; Starkey, J. R.; Ihlenfeldt, A.; Williams, W. J.; Stedman, D. H.
IR long-path photometry: a remote sensing tool for automobile emissions. 671a
Bjarnason, A.
——; Taylor, J. W.; Kinsinger, J. A.; Cody, R. B.; Weil, D. A.
Isomer discrimination of disubstituted benzene derivatives through gas-phase iron(I) ion reactions in a Fourier-transform mass spectrometer. 1889
Bjerga, J. M.
——; Small, G. W.
Reconstruction of gas chromatograms from digitally filtered Fourier-transform infrared interferograms. 1073
Blanchard, G. J.
Detection of a transient solvent-solute complex using time-resolved pump-probe spectroscopy. 2394
Blanche, M. S. See Bowen, J. M.
Blanco, R. See Grinberg, N.
Blazewicz, P. R.
——; Whitten, W. B.; Ramsey, J. M.
Low-level detection of metal atoms by multiphoton ionization in a low-pressure flame sampling cell. 1010
Bletsos, I. V.
——; Hercules, D. M.; VanLeyen, D.; Benninghoven, A.; Karakatsanis, C. G.; Rieck, J. N.
Structural characterization of model polyurethanes using time-of-flight secondary ion mass spectrometry. 2142
Blo, G. See Remelli, M.
Blomberg, L. G. See Bemgaard, A. K.
Blyshak, L. A.
——; Dodson, K. Y.; Patonay, G.; Warner, I. M.; May, W. E.
Determination of cyclodextrin formation constants using dynamic coupled-column liquid chromatography. 955
Bobbitt, D. R. See Erskine, S. R.
Bobrowski, A.
Polarographic methods for ultratrace cobalt determination based on adsorption-catalytic effects in cobalt(II)-dioxime-nitrite systems. 2178
Bodenhausen, G. See Eggenberger, U.
Bodor, N. See Prokai, L.
Boehm, R. E.
——; Martire, D. E.
Theory of homopolymer and oligomer separation and its application to gradient elution liquid chromatography. 471
Bohn, P. W. See Stephens, D. A.
Bol'shov, M. A.
——; Boutron, C. F.; Zybin, A. V.
Determination of lead in Antarctic ice at the picogram-per-gram level by laser atomic fluorescence spectrometry. 1758
Boltinghouse, F.
——; Abel, K.
Development of an optical relative humidity sensor. Cobalt chloride optical absorbency sensor study. 1863
Bond, A. M.
——; Majewski, T. P.
Exchange reactions with zinc bis[(2-hydroxyethyl)dithiocarbamate]for automated monitoring of metal ions in industrial effluents by liquid chromatography with electrochemical detection. 1494
Borgerding, M. F.
——; Hinze, W. L.; Stafford, L. D.; Fulp, G. W. Jr.; Hamlin, W. C. Jr.
Investigations of stationary phase modification by the mobile phase surfactant in micellar liquid chromatography. 1353
Bornhop, D. J.
——; Murphy, B. J.; Krieger-Jones, L.
Chemiluminescence sulfur detection in capillary supercritical fluid chromatography. 797
Borra, C.
——; Andreolini, F.; Novotny, M.
Use of capillary supercritical fluid chromatography and microcolumn liquid chromatography for the determination of nonvolatile organics in aqueous environmental samples. 1208
Bos, J.
——; Tijssen, R.; Van Kreveld, M. E.
Determination of the dissociation temperature of organic micelles by microcapillary hydrodynamic chromatography. 1318
Boudreau, S. P.
——; Cooper, W. T.
Analysis of thermally and chemically modified silica gels by heterogeneous gas-solid chromatography and infrared spectroscopy. 41
Boutron, C. F. See Bol'shov, M. A.
Bowen, J. M.
——; Compton, S. V.; Blanche, M. S.
Comparison of sample preparation methods for the Fourier-transform infrared analysis of an organo-clay mineral sorption mechanism. 2047
Bowen, P. See Highfield, J. G.
Bower, N. W. See Gladney, E. S.
Bowling, R. J.
——; McCreery, R. L.; Pharr, C. M.; Engstrom, R. C.
Observation of kinetic heterogeneity on highly ordered pyrolytic graphite using electrogenerated chemiluminescence. 2763
Bragg, N. See Moseley, M. A.
Brajter-Toth, A. See Freund, M. S.; Volk, K. J.
Braman, R. S. See Cobb, G. P.
——; Hendrix, S. A.
Nanogram nitrite and nitrate determination in environmental and biological materials by vanadium(III) reduction with chemiluminescence detection. 2715
Brandt, E. S.
Analysis for spectral sensitizing dyes in photographic films by enhanced Raman scattering spectroscopy. 391
Breiner, S. J. See Lochmuller, C. H.
Brennan, P. J. See Jardine, I.
Brettell, T. A.
——; Saferstein, R.
Forensic science. 95r
Breyer, E. D. See Khaledi, M. G.
Bright, F. V. See Carroll, M. K.; Catena, G. C.
Multifrequency phase fluorescence study of hapten-antibody complexation. 309
Multifrequency phase fluorescence study of hapten-antibody complexation (correction). 1472
——; Litwiler, K. S.
Multicomponent fluorometric analysis using a fiber-optic probe. 1510
Brill, T. B.
Fast thermolysis/FT-IR spectroscopy. 897a
Brindle, I. D.
——; Le, X. C.
Application of signal enhancement by easily ionized elements in hydride generation direct current plasma atomic emission spectrometric determination of arsenic, antimony, germanium, tin, and lead. 1175
Brooks, G. H. See Sutcliffe, C. R.
Brown, M. E.
——; Galwey, A. K.
Arrhenius parameters for solid-state reactions from isothermal rate-time curves. 1136
Brown, P. R. See Beauchemin, B. T. Jr.
Bruening, M. L. See Izatt, R. M.
Bruening, R. L. See Izatt, R. M.
Brumby, S.
Exchange of comments on the simplex algorithm culminating in quadratic convergence and error estimation. 1783
Bruno, A. E.
——; Gassmann, E.; Pericles, N.; Anton, K.
On-column capillary flow cell utilizing optical waveguides for chromatographic applications. 876
Bruntlett, C. S. See Sternitzke, K.
Buch, R. M.
——; Rechnitz, G. A.
Neuronal biosensors. 533a
Buchner, J. D. See Ketkar, S. N.
Buck, R. P. See Berube, T. R.; Sandifer, J. R.
Buddrus, J.
——; Burba, P.; Lambert, J.; Herzog, H.
Quantitation of partial structures of aquatic humic substances by one- and two-dimensional solution ^{13}C nuclear magnetic resonance spectroscopy. 628
Budil, M. See Stingeder, G.
Buehrer, T. See Hu, Z.
Burba, P. See Buddrus, J.
Burdick, D. S. See Tu, X. M.
Burkert, W. G. See Hinze, W. L.
Busch, K. W. See Kubala, S. W.
Busch, M. A. See Kubala, S. W.
Bushee, D. S. See Paulsen, P. J.
Bushey, M. M.
——; Jorgenson, J. W.
Separation of dansylated methylamine and dansylated methyl-d_3-amine by micellar electrokinetic capillary chromatography with methanol-modified mobile phase. 491
Buttry, D. A. See Deakin, M. R.
Byrd, G. D. See Craft, N. E.
Byrd, H. See Deakin, M. R.

Caceci, M. S.
Estimating error limits in parametric curve fitting. 2324
Caldwell, K. A.
——; Gross, M. L.
Nondiscriminatory fast atom bombardment matrix for fatty acid mixture analysis. 494
Callis, J. B. See Kelly, J. J.; Phelan, M. K.
Campiglia, A. D. See Laserna, J. J.; Perry, L. M.
Cantwell, F. F. See Amankwa, L.; Lucy, C. A.
Capar, S. G. See Clifford, R. H.; Montaser, A.
Capdevielle, F. J. See Yao, C. L.
Carey, W. P.
——; DeGrandpre, M. D.; Jorgensen, B. S.
Polymer-coated cylindrical waveguide absorption sensor for high acidities. 1674
——; Wangen, L. E.; Dyke, J. T.
Spectrophotometric method for the analysis of plutonium and nitric acid using partial least-squares regression. 1667
Carlshaf, A. See Joensson, J. A.
Carlson, D. A.
——; Roan, C. S.; Yost, R. A.; Hector, J.
Dimethyl disulfide derivatives of long chain alkenes, alkadienes, and alkatrienes for gas chromatography/mass spectrometry. 1564
Carnahan, J. W. See Gehlhausen, J. M.; Webster, G. K.; Zhang, L.
Carnrick, G. R. See Epstein, M. S.
Caron, F.
——; Kramer, J. R.
Gas chromatographic determination of volatile sulfides at trace levels in natural freshwaters. 114

Carr, P. W. See Bergold, A. F.; Cheong, W. J.; Eikens, D. I.
Carreira, L. A. See Dobbs, J. C.
Carroll, M. K.
——; Bright, F. V.; Hieftje, G. M.
Fiber-optic time-resolved fluorescence sensor for the simultaneous determination of aluminum(3+) and gallium(3+) or indium(3+). 1768
Castles, M. A. See Dobbs, J. C.
——; Moore, B. L.; Ward, S. R.
Measurement of linear alkylbenzenesulfonates in aqueous environmental matrixes by liquid chromatography with fluorescence detection. 2534
Castro, M. E. See Hanson, C. D.; Kerley, E. L.; Tecklenburg, R. E. Jr.
Caswell, K. A.
——; Glass, T. E.; Swann, M.; Dorn, H. C.
Rapid prediction of various physical properties for middle distillate fuels utilizing directly coupled liquid chromatography/proton nuclear magnetic resonance. 206
Cataldi, T. R. I. See Palmisano, F.
Catena, G. C.
——; Bright, F. V.
Thermodynamic study on the effects of β-cyclodextrin inclusion with anilinonaphthalenesulfonates. 905
Caton, J. E. Jr. See Tomkins, B. A.
Chabardes, D. See Pradelles, P.
Chace, D. H.
——; Abramson, F. P.
Selective detection of carbon-13, nitrogen-15, and deuterium labeled metabolites by capillary gas chromatography-chemical reaction interface/mass spectrometry. 2724
Chandra, S. See Ausserer, W. A.
Chang, D. Y. See Saleh, F. Y.
Chang, H. C. K. See Skelton, R. J. Jr.
Chaniotakis, N. A.
——; Park, S. B.; Meyerhoff, M. E.
Salicylate-selective membrane electrode based on tin(IV)-tetraphenylporphyrin. 566
Chao, R. S. See Havel, H. A.
Chastel, O.
——; Kauffmann, J. M.; Patriarche, G. J.; Christian, G. D.
Hydrophobic stripping voltammetry using a lipid-modified glassy carbon electrode. 170
Cheek, G. T.
——; Mowery, R.
Determination of antioxidants in lubricating oils using ultramicroelectrodes. 1467
Chemerika, R. See Shiu, K. K.
Chen, C. Y.
——; Demana, T.; Huang, S. D.; Morris, M. D.
Capillary zone electrophoresis with analyte velocity modulation. Application to refractive index detection. 1590
Chen, J. Y. T. See Mossoba, M. M.
Cheng, H. Y. See VanDyke, D. A.
Cheng, I. F.
——; Whiteley, L. D.; Martin, C. R.
Ultramicroelectrode ensembles. Comparison of experimental and theoretical responses and evaluation of electroanalytical detection limits. 762
Cheng, P. Y. See LaiHing, K.
Cheong, W. J.
——; Carr, P. W.
Limitations of all empirical single-parameter solvent strength scales in reversed-phase liquid chromatography. 1524
Chiarelli, M. P.
——; Gross, M. L.
Amino acid and tripeptide mixture analysis by laser desorption Fourier-transform mass spectrometry. 1895
Chiari, M. See Righetti, P. G.
Chicz, R. M.
——; Regnier, F. E.
Immobilized-metal affinity and hydroxyapatite chromatography of genetically engineered subtilisin. 1742
Single amino acid contributions to protein retention in cation-exchange chromatography: resolution of genetically engineered subtilisin variants. 2059
Chmelik, J.
——; Deml, M.; Janca, J.
Separation of two components of horse myoglobin by isoelectric focusing field-flow fractionation. 912
Separation of two components of horse myoglobin by isoelectric focusing field-flow fractionation (correction). 2224
Chopra, D. R. See Fulghum, J. E.
Chou, T. Y. See Gao, C. X.
——; Gao, C. X.; Grinberg, N.; Krull, I. S.
Chiral polymeric reagents for off-line and on-line derivatizations of enantiomers in high-performance liquid chromatography with ultraviolet and fluorescence detection: an enantiomer recognition approach. 1548
Chourasia, A. R. See Fulghum, J. E.
Chowdhury, A. K.
——; Cooper, J. R.; Wilkins, C. L.
Indium-alkene complex ions as reagents for selective chemical ionization. 86
Christensen, J. J. See Izatt, R. M.
Christensen, P. L.
——; Yeung, E. S.
Fluorescence-detected circular dichroism for on-column detection in capillary electrophoresis. 1344
Christian, G. D. See Chastel, O.; Clark, G. D.
Christopoulos, T. K.
——; Diamandis, E. P.
Potentiometric measurements in air-segmented streams without debubbling. 504
Ci, Y.
——; Lan, Z.
Fluorometric determination of samarium and gadolinium by enhancement of fluorescence of samarium-thenoyltrifluoroacetone-1,10-phenanthroline ternary complex by gadolinium. 1063
Ciszewski, A.
——; Fish, J. R.; Malinski, T.; Sioda, R. E.
Deposition of trace metals on solid electrodes: experimental verification of limits of electrochemical preconcentration. 856
Clark, G. D.
——; Hungerford, J. M.; Christian, G. D.
Optimization of confluent mixing in flow injection analysis. 973
——; Ruzicka, J.; Christian, G. D.
Split zone flow-injection analysis: an approach to automated dilutions. 1773
Clifford, R. H. See Montaser, A.
——; Montaser, A.; Sinex, S. A.; Capar, S. G.
Thimble glass frit nebulizer for atomic spectrometry. 2777
Cobb, G. P.
——; Braman, R. S.; Gilbert, R. A.
Indentification of atmospheric organic sources using the carbon hollow tube-gas chromatography method and factor analysis. 838
Cobb, K. A.
——; Novotny, M.
High-sensitivity peptide mapping by capillary zone electrophoresis and microcolumn liquid chromatography using immobilized trypsin for protein digestion. 2226
Cocco, D. See McNeil, C. J.
Cody, R. B. See Bjarnason, A.
Separation of the reagent ions from the reagent gas in ammonia chemical ionization mass spectrometry. 2511
Coe, C. G. See Maroulis, P. J.
Cohen, L. H.
——; Smith, D. K.
Thin-specimen x-ray fluorescence analysis of major elements in silicate rocks. 1837
Colburn, J. C. See Grossman, P. D.
Colby, S. M. See Wilkerson, C. W. Jr.
Coles, B. A. See Pilkington, M. B. G.
Collin, P. J. See Wilson, M. A.
Collison, M. E.
——; Aebli, G. V.; Petty, J.; Meyerhoff, M. E.
Potentiometric combination ion-carbon dioxide sensors for in vitro and in vivo blood measurements. 2365
Colmsjoe, A. L. See Bemgaard, A. K.
Compton, B. J.
——; Lewis, M.; Whigham, F.; Gerald, J. S.; Countryman, G. E.
Analytical potential of protein A for affinity chromatography of polyclonal and monoclonal antibodies. 1314
Compton, R. G. See Pilkington, M. B. G.
Compton, S. V. See Bowen, J. M.
Connors, K. A.
——; Wright, J. L.
Dependence of surface tension on composition of binary aqueous-organic solutions. 194
Cooper, J. M. See McNeil, C. J.
Cooper, J. R. See Chowdhury, A. K.
——; Wilkins, C. L.
Utilization of spectrometric information in linked gas chromatography-Fourier transform infrared spectroscopy-mass spectrometry. 1571
Cooper, W. T. See Boudreau, S. P.
Cortes, H. J.
——; Jewett, G. L.; Pfeiffer, C. D.; Martin, S.; Smith, C.
Multidimensional chromatography using on-line microcolumn liquid chromatography and pyrolysis gas chromatography for polymer characterization. 961
Cotter, R. J. See Bean, M. F.; Heller, D. N.
Cotton, T. M. See Ni, F.
Countryman, G. E. See Compton, B. J.
Covey, T. R. See Eckerlin, R. H.
Cox, F. O. See Gemperline, P. J.
Cox, J. A.
——; Gray, T. J.
Flow injection amperometric determination of insulin based upon its oxidation at a modified electrode. 2462
——; Jaworski, R. K.
Voltammetric reduction and determination of hydrogen peroxide at an electrode modified with a film containing palladium and iridium. 2176
Coyne, L. B. See Langhorst, M. L.
Craft, N. E.
——; Byrd, G. D.; Hilpert, L. R.
Preparation and certification of standard reference material 1507: 11-nor-Δ^9-tetrahydrocannabinol-9-carboxylic acid in freeze-dried urine. 540
Craig, A. G.
——; Bennich, H.
Influence of sample concentration and adsorption time on the yield of biomolecule ions in plasma desorption mass spectrometry. 375
Crain, J. S.
——; Houk, R. S.; Eckels, D. E.
Noise power spectral characteristics of an inductively coupled plasma-mass spectrometer. 606
Creaser, C. S.
——; Al-Haddad, A.
Fractionation of polychlorinated biphenyls, polychlorinated dibenzo-p-dioxins, and polychlorinated dibenzofurans on porous graphitic carbon. 1300
——; Crosland, S.
Continuous flow fast atom bombardment mass spectrometry using a modified electron impact source. 1310
Creasy, K. E.
——; Shaw, B. R.
Polishable modified carbon fiber composite electrodes containing copolymers of (vinylferrocene) or (vinylpyridine) in a cross-linked polystyrene matrix. 1460
Cretney, W. J. See Yunker, M. B.
Crosland, S. See Creaser, C. S.
Crouch, S. R. See Kim, H.
Cummings, J. G. See Werner, T. C.
Cunningham, L. L. See Harrison, D. J.

DaCunha, A. R. See Stout, S. J.
Dams, R. See Vanhoe, H.
Danielson, N. D.
——; Wangsa, J.; Targove, M. A.
Comparison of paraffin oil and poly(chlorotrifluoroethylene) oil carbon paste electrodes in high organic content solvents. 2585
D'Arcy, J. B. See Xiao, H.
Darnall, D. See Kubiak, W. W.
Dasgupta, P. K. See Genfa, Z.; Lei, W.; Lindgren, P. F.; Okada, T.; Ping, L.; Qi, D.; Strong, D. L.
Daunert, S.
——; Bachas, L. G.
Anion-selective electrodes based on a hydrophobic vitamin B_{12} derivative. 499
——; Payne, B. R.; Bachas, L. G.
Pyruvate carboxylase as a model for oligosubstituted enzyme-ligand conjugates in homogeneous enzyme immunoassays. 2160
David, P. A.
——; Novotny, M.
Characterization of the nitrogen and phosphorus thermionic detector response in capillary supercritical fluid chromatography. 2082
Davis, J. M.
Random-walk theory of nonequilibrium plate height in micellar electrokinetic capillary chromatography. 2455
Davis, K. A.
——; Leary, T. R.
Continuous liquid-phase piezoelectric biosensor for kinetic immunoassays. 1227

Deakin, M. R.
——; Buttry, D. A.
Electrochemical applications of the quartz crystal microbalance. 1147a
——; Byrd, H.
Prussian Blue coated quartz crystal microbalance as a detector for electroinactive cations in aqueous solution. 290
De Andrade, J. F. See Fatibello–Filho, O.
DeGraff, B. A. See Snyder, S. W.
DeGrandpre, M. D. See Carey, W. P.
Deinzer, M. L. See Laramee, J. A.
De Jong, H. J. See Albert, K.
Dekmezian, A. H.
——; Morioka, T.
Interface to eliminate high–boiling gel permeation chromatographic solvents on–line for polymer composition drift studies. 458
De Koning, L. J. See Elling, J. W.
De la Rie, E. R.
Old master paintings: a study of the varnish problem. 1228a
De Leenheer, A. P. See Van Liedekerke, B. M.
Delmore, J. E. See Appelhans, A. D.
Demana, T. See Chen, C. Y.
——; Peterman, D.; Shaffer, J.; Melaragno, P. R.
Flow–through spectroelectrochemical detector based on diffraction at a cylindrical electrode. 1216
Demas, J. N. See Ballew, R. M.; Snyder, S. W.
Deml, M. See Chmelik, J.
Deng, R. C.
——; Williams, P.
Factors affecting precision and accuracy in quantitative analysis by secondary ion mass spectrometry. 1946
DeNiro, M. J.
——; Epstein, S.
Determination of the concentration and stable isotopic composition of oxygen in organic matter containing carbon, hydrogen, oxygen, nitrogen, and sulfur. 1887
Denton, M. B. See Epperson, P. M.
Dessy, R. E.
Waveguides as chemical sensors. 1079a
Deterding, L. J. See Moseley, M. A.
——; Moseley, M. A.; Tomer, K. B.; Jorgenson, J. W.
Coaxial continuous flow fast atom bombardment in conjunction with tandem mass spectrometry for the analysis of biomolecules. 2504
DeVoe, J. R. See Watters, R. L. Jr.
Dewey, D. See Mosher, R. A.
De Wit, J. S. M. See Moseley, M. A.
De Wolf, M. See Vertes, A.
DeZwaan, J. See Hooker, D. B.
Dheandhanoo, S. See Ketkar, S. N.
Diamandis, E. P. See Christopoulos, T. K.
——; Morton, R. C.; Reichstein, E.; Khosravi, M. J.
Multiple fluorescence labeling with europium chelators. Application to time–resolved fluoroimmunoassays. 48
Dickert, F. L.
——; Schreiner, S. K.; Mages, G. R.; Kimmel, H.
A fiber–optic dipping sensor for organic solvents in wastewater. 2306
Di Corcia, A. See Battista, M.
——; Marchetti, M.; Samperi, R.
Extraction and isolation of phenoxy acid herbicides in environmental waters using two adsorbents in one minicartridge. 1363
Dill, K. A. See Ying, P. T.
Diomiguardi, J. P. See Hwang, J. D.
Divis, R. A.
——; White, R. L.
Deconvoluted band representation for infrared spectrum compression. 33
Dix, K. D.
——; Sakkinen, P. A.; Fritz, J. S.
Gas chromatographic determination of water using 2,2–dimethoxypropane and a solid acid catalyst. 1325
Dobashi, A.
——; Ono, T.; Hara, S.; Yamaguchi, J.
Optical resolution of enantiomers with chiral mixed micelles by electrokinetic chromatography. 1984
Dobashi, Y. See Nakamura, K.
Dobbs, J. C.
——; Susetyo, W.; Carreira, L. A.; Azarraga, L. V.
Competitive binding of protons and metal ions in humic substances by lanthanide ion probe spectroscopy. 1519
——; Susetyo, W.; Knight, F. E.; Castles, M. A.; Carreira, L. A.; Azarraga, L. V.
Characterization of metal binding sites in fulvic acids by lanthanide ion probe spectroscopy. 483
Dodson, K. Y. See Blyshak, L. A.
Doering, T. L. See Bean, M. F.
Dondi, F. See Remelli, M.
Dorko, W. D. See Verkouteren, R. M.
Dorn, H. C. See Caswell, K. A.
Dorschel, C. A.
——; Ekmanis, J. L.; Oberholtzer, J. E.; Warren, F. V. Jr.; Bidlingmeyer, B. A.
LC detectors: evaluation and practical implications of linearity. 951a
Dorsey, J. G. See Sentell, K. B.; Ying, P. T.
Dose, E. V.
——; Guiochon, G.
Bias and nonlinearity of ultraviolet calibration curves measured using diode–array detectors. 2571
Douglas, J. G.
Characterization of an ion–selective electrode wall–jet detector for flow injection analysis. 922
Dovichi, N. J. See Yu, M.
Dratz, E. A. See Handelman, G. J.
Drobny, G. P. See Listerud, J. M.
Dubin, P. L.
——; Principi, J. M.
Hydrophobicity parameter for aqueous size exclusion chromatography gels. 780
Duckworth, D. C.
——; Marcus, R. K.
Radio frequency powered glow discharge atomization/ionization source for solids mass spectrometry. 1879
Duell, K. A. See Rowlen, K. L.
Dulak, J. G. See Ketkar, S. N.
Dumke, I.
——; Faber, E.; Poggenburg, J.
Determination of stable carbon and hydrogen isotopes of light hydrocarbons. 2149
Duncan, M. A. See LaiHing, K.
Duncan, M. W. See Wang, T. C. L.
Duncan, W. See Gurka, D. F.
Dyke, J. T. See Carey, W. P.

Eagles, J.
——; Fairweather–Tait, S. J.; Portwood, D. E.; Self, R.; Goetz, A.; Heumann, K. G.
Comparison of fast atom bombardment mass spectrometry and thermal ionization quadrupole mass spectrometry for the measurement of zinc absorption in human nutrition studies. 1023
Ebato, H. See Okahata, Y.
Ebel, J. G. Jr. See Eckerlin, R. H.
Eckels, D. E. See Crain, J. S.
Eckerlin, R. H.
——; Ebel, J. G. Jr.; Henion, J. D.; Covey, T. R.
The case of the tainted dexamethasone. 53a
Eckert, S. E. See Isenhour, T. L.
Edmond, J. M. See Measures, C. I.
Edwards, M. D. See Tomkins, B. A.
Effiong, R.
——; Evilia, R. F.
Determination of nuclear magnetic resonance sample temperatures through measurement of the probe coil ohmic resistance. 1594
Eggenberger, U.
——; Bodenhausen, G.
Analysis of two–dimensional nuclear magnetic resonance spectra with relayed proton–proton–carbon magnetization transfer: a step toward automated structure elucidation. 2298
Egger, K. P. See Krivan, V.
Eiceman, G. A.
——; Shoff, D. B.; Harden, C. S.; Snyder, A. P.; Martinez, P. M.; Fleischer, M. E.; Watkins, M. L.
Ion mobility spectrometry of halothane, enflurane, and isoflurane anesthetics in air and respired gases. 1093
Eikens, D. I.
——; Carr, P. W.
Application of the equation of error propagation to obtaining nonstochastic estimates for the reproducibility of chromatographic peak moments. 1058
Ekmanis, J. L. See Dorschel, C. A.
Ellerbe, P.
——; Meiselman, S.; Sniegoski, L. T.; Welch, M. J.; White, E. V.
Determination of serum cholesterol by a modification of the isotope dilution mass spectrometric definitive method. 1718
Elling, J. W.
——; De Koning, L. J.; Pinkse, F. A.; Nibbering, N. M. M.; Smit, H. C.
Computer–controlled simplex optimization on a Fourier–transform ion cyclotron resonance mass spectrometer. 330
Elnemma, E. M. See Hassan, S. S. M.
El–Rayes, I. See Wang, J.
Engel, M. H.
——; Maynard, R. J.
Preparation of organic matter for stable carbon isotope determination by sealed tube combustion: a cautionary note. 1996
Englund, P. T. See Bean, M. F.
Engstrom, C. E. See Saraceno, R. A.
Engstrom, R. C. See Bowling, R. J.
Epperson, P. M.
——; Denton, M. B.
Binning spectral images in a charge–coupled device. 1513
——; Jalkian, R. D.; Denton, M. B.
Molecular fluorescence measurements with a charge–coupled device detector. 282
Epstein, M. S.
——; Carnrick, G. R.; Slavin, W.; Miller–Ihli, N. J.
Automated slurry sample introduction for analysis of a river sediment by graphite furnace atomic absorption spectrometry. 1414
Epstein, S. See DeNiro, M. J.
Erskine, S. R.
——; Bobbitt, D. R.
Indirect differential thermal lens detection for the reversed–phase separation of underivatized fatty acids. 910
Ettre, L. S.
Laszlo Zechmeister: A pioneer of chromatography. 1315a
Evans, J.
——; Pletcher, D.; Warburton, P. R. G.; Gibbs, T. K.
Amperometric sensor for carbon dioxide: design, characteristics, and performance. 577
Evilia, R. F. See Effiong, R.
Ewing, A. G. See Saraceno, R. A.; Wallingford, R. A.
——; Wallingford, R. A.; Olefirowicz, T. M.
Capillary electrophoresis. 292a
Eyring, E. M. See Phillips, G. R.

Faber, E. See Dumke, I.
Fagan, D. T.
——; Kuwana, T.
Thermal desorption mass analysis of carbon fiber surfaces: surface oxygen complexes. 1017
Fairweather–Tait, S. J. See Eagles, J.
Fajer, R. W. See Roberts, J. M.
Fales, H. M. See Pannell, L. K.
Fan, F. R. F. See Bard, A. J.
Fan, T. W. M.
——; Higashi, R. M.
Reproducible nuclear magnetic resonance surface coil fabrication by combining computer–aided–design and a photoresist process. 636
Farag, H. See Prokai, L.
Farinas, J. C.
Determination of phosphorus in zircons by inductively coupled plasma atomic emission spectrometry. 2696
Farlee, R. D. See Kirkland, J. J.
Farnham, I. See Gurka, D. F.
Farnsworth, P. B. See Skelton, R. J. Jr.
Fasanmade, A. A.
——; Fell, A. F.
Computer–aided time domain differentiation in high–performance liquid chromatography. 720
Fassett, J. D.
——; Paulsen, P. J.
Isotope dilution mass spectrometry for accurate elemental analysis. 643a
Fatibello–Filho, O.
——; De Andrade, J. F.; Suleiman, A. A.; Guilbault, G. G.
Piezoelectric crystal monitor for carbon dioxide in fermentation processes. 746
——; Suleiman, A. A.; Guilbault, G. G.; Lubrano, G. J.
Bienzymatic electrode for the determination of aspartame in dietary products (correction). 1472
Fay, M. J. See Hoffmann, D. P.
Fehl, A. J.
——; Marcott, C.
Capillary gas chromatography/Fourier transform infrared spectroscopy using

an injector/trap and liquid-liquid extraction. 1596
Fell, A. F. See Fasanmade, A. A.
Feng, D.
——; Koch, W. F.; Wu, Y. C.
Second dissociation constant and pH of N-(2-hydroxyethyl)piperazine-N′-2-ethanesulfonic acid from 0 to 50° C. 1400
Fenn, J. B. See Mann, M.
Fenselau, C. See Bean, M. F.
Fernando, A. R.
——; Plambeck, J. A.
Effects of background electrolyte and oxygen on trace analysis for lead and cadmium by anodic stripping voltammetry. 2609
Ferrer-Correia, A. J. V. See Santana-Marques, M. G. O.
Fett, J. W. See Strydom, D. J.
Fetzer, J. C. See Biggs, W. R.
Fielden, P. R.
——; Greenway, G. M.
Diffusion apparatus for trace level vapor generation of tetramethyllead. 1993
Fink, S. W.
——; Freas, R. B.
Enhanced analysis of poly(ethylene glycols) and peptides using thermospray mass spectrometry. 2050
Fish, J. R. See Ciszewski, A.
Fitch, A.
——; Helmke, P. A.
Donnan equilibrium/graphite furnace atomic absorption estimates of soil extract complexation capacities. 1295
Fite, W. L. See Ketkar, S. N.
Fitzpatrick, C. P.
——; Pardue, H. L.
Characteristics of methods for the simultaneous determination of catalysts by first-order inhibition kinetics. 2551
Fleischer, M. E. See Eiceman, G. A.
Fletcher, R. A.
New way to mount particulate material for laser microprobe mass analysis. 914
Flowers, P. A.
——; Mamantov, G.
Thin-layer transmittance cell for infrared spectroelectrochemistry. 190
Foley, R. C. See Haddad, P. R.
Fowler, B. R. See Yunker, M. B.
Fox, A. See Ueda, K.
Fox, D. L.
Air pollution. 1r
Franchini, G.
——; Marchetti, A.; Preti, C.; Tassi, L.; Tosi, G.
Conductometric titrations of polyprotic acids in nonaqueous mixed solvents. Effects of temperature and composition of the solvent mixture. 177
Franko, M.
——; Tran, C. D.
Water as a unique medium for thermal lens measurements. 1660
Freas, R. B. See Fink, S. W.; McLean, M. A.
Freiser, H. See Yu, W. H.
Freund, M. S.
——; Brajter-Toth, A.
Ultramicroelectrode array behavior of one-dimensional organic conductor electrodes. 1048
Fritz, J. S. See Dix, K. D.; Main, M. V.; Plantz, M. R.
Frolow, F. See Olsher, U.
Frommell, E. A. See Schultz, H.
Fu, Z. S. See Hinze, W. L.; Pharr, D. Y.
Fuggerth, E.
Zone gas chromatography. 1478
Fujii, T.
——; Ogura, M.; Jimba, H.
Chemical ionization mass spectrometry with lithium ion attachment to the molecule. 1026
Fujiwara, K.
——; Kanchi, T.; Tsumura, S.; Kumamaru, T.
Phosphine-ozone gas-phase chemiluminescence for determination of phosphate. 2699
Fujiwara, T.
——; Tanimoto, N.; Huang, J. J.; Kumamaru, T.
Generation of chemiluminescence upon reaction of iodine with luminol in reversed micelles and its analytical applicability. 2800
Fulcher, J. N.
——; Howe, G. B.; Jayanty, R. K. M.; Peterson, M. R.; Pau, J. C.; Knoll, J. E.; Midgett, M. R.
Determination of acrylonitrile in stationary source emissions by impinger sampling and gas chromatography with nitrogen-phosphorus detection. 2743
Fulghum, J. E.
——; McGuire, G. E.; Musselman, I. H.; Nemanich, R. J.; White, J. M.; Chopra, D. R.; Chourasia, A. R.
Surface characterization. 243r
Fulp, G. W. Jr. See Borgerding, M. F.
Funazukuri, T.
——; Hachisu, S.; Wakao, N.
Measurement of diffusion coefficients of C_{18} unsaturated fatty acid methyl esters, naphthalene, and benzene in supercritical carbon dioxide by a tracer response technique. 118
Fuoco, R.
——; Pentoney, S. L. Jr.; Griffiths, P. R.
Comparison of sampling techniques for combined supercritical fluid chromatography and Fourier-transform infrared spectrometry with mobile phase elimination. 2212

Gallego, M. See Santelli, R. E.
Galwey, A. K. See Brown, M. E.
Gao, C. X. See Chou, T. Y.
——; Chou, T. Y.; Krull, I. S.
Polymeric activated ester reagents for off-line and on-line derivatizations of amine nucleophiles in high-performance liquid chromatography with ultraviolet and fluorescence detection. 1538
Gara, S. See Stingeder, G.
Garbarino, J. R.
——; Taylor, H. E.; Batie, W. C.
Simultaneous determination of major and trace elements by inductively coupled plasma-mass spectrometry/optical emission spectrometry. 793
Garcia, M. E. See Tomkins, B. A.
Garcia, O. J.
——; Quintela, P. A.; Kaifer, A. E.
Electrodes modified with a film of phosphatidylcholine: electrochemistry inside a lipid layer. 979
Gardella, J. A. Jr.
Recent developments in instrumentation for x-ray photoelectron spectroscopy. 589a
Gardner, G. J. See Siu, K. W. M.
Garland, W. A. See Nadeau, R. W.
Garrell, R. L.
Surface-enhanced Raman spectroscopy. 401a
Gassmann, E. See Bruno, A. E.
Ge, H.
——; Wallace, G. G.
Characterization of novel conducting polymeric stationary phases and electrochemically controlled high-performance liquid chromatography. 2391
Gee, S. J. See Li, Q. X.
Gehlhausen, J. M.
——; Carnahan, J. W.
Determination of aqueous fluoride with a helium microwave-induced plasma and flow injection analysis. 674
Gelfi, C. See Righetti, P. G.
Gemperline, P. J.
——; Hamilton, J. C.
Conditions for detecting overlapped peaks with principal component analysis in hyphenated chromatographic methods. 2240
——; Webber, L. D.; Cox, F. O.
Raw materials testing using soft independent modeling of class analogy analysis of near-infrared reflectance spectra. 138
Genfa, Z.
——; Dasgupta, P. K.
Fluorometric measurement of aqueous ammonium ion in a flow injection system. 408
Genissel, P. See Albert, K.
Gerald, J. S. See Compton, B. J.
Ghosh, A.
——; Anderegg, R. J.
Differential gas chromatographic mass spectrometry. 73
Complex mixture analysis using differential gas chromatographic mass spectrometry. 2118
Gianazza, E. See Righetti, P. G.
Gibbs, T. K. See Evans, J.
Giddings, J. C. See Berthod, A.; Hansen, M. E.; Jones, H. K.; Lee, S.; Schure, M. R.
Gijbels, R. See Vertes, A.
Gil-Av, E. See Watabe, K.
Gilbart, J. See Ueda, K.
Gilbert, R. A. See Cobb, G. P.
Gilpin, R. K. See Hann, C. J.
——; Pachla, L. A.
Pharmaceuticals and related drugs. 191r
Given, P. S. Jr. See Athnasios, A. K.
Gladney, E. S. See Sutcliffe, C. R.
——; Neifert, P. E.; Bower, N. W.
Determination of silicon in National Institute of Standards and Technology biological Standard Reference Materials by instrumental epithermal neutron activation and x-ray fluorescence spectrometry. 1834
Glajch, J. L. See Kirkland, J. J.
Glass, T. E. See Caswell, K. A.
Glavas, S. See Roumelis, N.
Glennon, J. D.
——; Woulfe, M. R.; Senior, A. T.; NiChoileain, N.
Analysis of siderophores and synthetic hydroxamic acids by high-performance liquid chromatography with amperometric detection. 1474
Glick, M. R.
——; Jones, B. T.; Smith, B. W.; Winefordner, J. D.
Fourier-transform flame atomic absorption spectrometry with continuum source excitation. 1694
Goates, S. R. See Raynie, D. E.
Goetz, A. See Eagles, J.
Gokmen, I. G.
——; Aras, N. K.; Gordon, G. E.; Wastney, M. E.; Henkin, R. I.
Radiochemical neutron activation analysis of zinc isotopes in human blood, urine, and feces for in vivo tracer experiments. 2757
Golden, T. See Wang, J.
Golshan-Shirazi, S.
——; Guiochon, G.
Experimental characterization of the elution profiles of high concentration chromatographic bands using the analytical solution of the ideal model. 462
Theory of optimization of the experimental conditions of preparative elution using the ideal model of liquid chromatography. 1276
Theory of optimization of the experimental conditions of preparative elution chromatography: optimization of the column efficiency. 1368
Theoretical study of system peaks and elution profiles of high concentration bands of binary mixtures eluted by a binary eluent containing a strongly retained additive. 2373
Experimental study of the elution profiles of high concentration bands of binary mixtures eluted by a binary eluent containing a strongly retained additive. 2380
Theory of optimization of the experimental conditions of preparative elution chromatography: optimization of the column efficiency (correction). 2464
——; Lin, B.; Guiochon, G.
Influence of the mass transfer kinetics on the separation of a binary mixture in displacement liquid chromatography. 1960
Goodall, D. M. See Lloyd, D. K.
Gordon, B. M. See Jones, K. W.
Gordon, G. E. See Gokmen, I. G.
Gordon, M. J. See Huang, X.
Gordon, R. J. See Ringwelski, A. Z.
Gough, D. S.
——; Hannaford, P.; Lowe, R. M.
Studies of sputtering atomizers for atomic absorption spectroscopy. 1652
Grant, C. L. See Zhang, Z.
Grasserbauer, M. See Stingeder, G.
Grassi, J. See Pradelles, P.
Gratzl, M. See Berube, T. R.
Gray, T. J. See Cox, J. A.
Grayson, M. A. See Morelli, J. J.
Green, J. B. See Yu, S. K. T.
Greenway, G. M. See Fielden, P. R.
Griest, W. H. See Tomkins, B. A.
Griffiths, P. R. See Fuoco, R.
Grimsrud, E. P. See Sears, L. J.
Grinberg, N. See Chou, T. Y.
——; Blanco, R.; Yarmush, D. M.; Karger, B. L.
Protein aggregation in high-performance liquid chromatography: hydrophobic interaction chromatography of β-lactoglobulin A. 514
Grolimund, K. See Mueller, S. R.
Gross, A. F. See Athnasios, A. K.
Gross, M. L. See Caldwell, K. A.; Chiarelli, M. P.; Rempel, D. L.; Santana-Marques, M. G. O.

Grossman, P. D.
——; Colburn, J. C.; Lauer, H. H.; Nielsen, R. G.; Riggin, R. M.; Sittampalam, G. S.; Rickard, E. C.
Application of free-solution capillary electrophoresis to the analytical scale separation of proteins and peptides. 1186
Grushka, E. See Levin, S.
——; McCormick, R. M.; Kirkland, J. J.
Effect of temperature gradients on the efficiency of capillary zone electrophoresis separations. 241
Guenther, G. D. See Hwang, J. D.
Guerrieri, A. See Palmisano, F.
Guilbault, G. G. See Fatibello-Filho, O.; Xu, Y.
Guilbeau, E. J. See Muehlbauer, M. J.
Guiochon, G. See Dose, E. V.; Golshan-Shirazi, S.; Katti, A.; Remelli, M.
Guiso, N. See Pradelles, P.
Gurka, D. F.
——; Farnham, I.; Potter, B. B.; Pyle, S.; Titus, R.; Duncan, W.
Quantitation capability of a directly linked gas chromatography/Fourier transform infrared/mass spectrometry system. 1584

Ha, S. T. K.
——; Wilkins, C. L.; Abidi, S. L.
Analysis of antimycin A by reversed-phase liquid chromatography/nuclear magnetic resonance spectrometry. 404
Hachisu, S. See Funazukuri, T.
Haddad, P. R.
——; Foley, R. C.
Aromatic bases as eluent components for conductivity and indirect ultraviolet absorption detection of inorganic cations in nonsuppressed ion chromatography. 1435
Hadjiioannou, T. P. See Athanasiou-Malaki, E.
Hager, J. W.
Relative elemental responses for laser ablation-inductively coupled plasma mass spectrometry. 1243
Haginaka, J.
——; Yasuda, N.; Wakai, J.; Matsunaga, H.; Yasuda, H.; Kimura, Y.
Internal-surface reversed-phase silica support for direct-injection determination of drugs in biological fluids by liquid chromatography. 2445
Hagman, A.
——; Jacobsson, S.
Theoretical model for quantitative determination of volatile compounds in polymers by dynamic headspace sampling. 1202
Hail, M. E.
——; Berberich, D. W.; Yost, R. A.
Gas chromatographic sample introduction into the collision cell of a triple quadrupole mass spectrometer for mass-selection of reactant ions for charge exchange and chemical ionization. 1874
——; Yost, R. A.
Theoretical and practical aspects of short open tubular columns at subambient pressures in gas chromatography/mass spectrometry. 2402
Compact gas chromatograph probe for gas chromatography/mass spectrometry utilizing resistively heated aluminum-clad capillary columns. 2410
Hailin, G.
——; Wallace, G. G.
Electrosynthesis of chromatographic stationary phases. 198
Hall, P.
——; Selinger, B.
A statistical justification to relating interlaboratory coefficients of variation with concentration levels. 1465
Hamilton, J. C. See Gemperline, P. J.
Hamlin, W. C. Jr. See Borgerding, M. F.
Hammock, B. D. See Li, Q. X.
Hampp, R. See Keil, R.
Hanaoka, N.
Influence of the vessel materials and solvents on the stability of mixtures of bis(2,4,6-trichlorophenyl) oxalate and hydrogen peroxide for peroxyoxalate chemiluminescence. 1298
Handelman, G. J.
——; Kosted, P.; Short, S.; Dratz, E. A.
Determination of selenium in human blood by high-performance liquid chromatography with fluorescence detection. 2244
Hann, C. J.
——; Gilpin, R. K.
Infrared and thermal studies of N-(p-cyanobenzylidene)-p-octyloxyaniline coated on derivatized silica. 1534
Hannaford, P. See Gough, D. S.
Hansen, M. E.
——; Giddings, J. C.
Retention perturbations due to particle-wall interactions in sedimentation field-flow fractionation. 811
Hanson, C. D. See Kerley, E. L.
——; Castro, M. E.; Russell, D. H.
Phase synchronization of an ion ensemble by frequency sweep excitation in Fourier-transform ion cyclotron resonance. 2130
——; Kerley, E. L.; Castro, M. E.; Russell, D. H.
Ion detection by Fourier transform ion cyclotron resonance: the effect of initial radial velocity on the coherent ion packet. 2040
——; Kerley, E. L.; Russell, D. H.
High-resolution ion partitioning technique by phase-specific ion excitation for Fourier-transform ion cyclotron resonance. 83
Hara, S. See Dobashi, A.; Nakamura, K.
Harada, K. See Oka, H.
Harden, C. S. See Eiceman, G. A.
Harrington, P. de B.
——; Street, T. E.; Voorhees, K. J.; Radicati di Brozolo, F.; Odom, R. W.
A rule-building expert system for classification of mass spectra. 715
Harris, J. M. See Weaver, M. R.; Wong, A. L.
Harris, T. D.
——; Schnoes, M. L.; Seibles, L.
High-sensitivity electronic Raman spectroscopy for acceptor determination in gallium arsenide. 994
Harrison, D. J. See Shiu, K. K.
——; Teclemariam, A.; Cunningham, L. L.
Photopolymerization of plasticizer in ion-sensitive membranes on solid-state sensors. 246
Hart, G. W. See Bean, M. F.
Hasegawa, N. See Nakagawa, T.
Haskell, R. J. See Havel, H. A.
Hassan, S. S. M.
——; Elnemma, E. M.
Amphetamine selective electrodes based on dibenzo-18-crown-6 and dibenzo-24-crown-8 liquid membranes. 2189
Hatfield, G. R.
Characterization of single-ply and polylaminate films by nuclear magnetic resonance spectroscopy. 1870
Havel, H. A.
——; Chao, R. S.; Haskell, R. J.; Thamann, T. J.
Investigations of protein structure with optical spectroscopy: bovine growth hormone. 642
Haw, J. F. See Richardson, B. R.
Hawkes, S. J.
Extrapolating gas chromatographic retention indices at two temperatures to a third temperature. 88
Hawthorne, S. B.
——; Krieger, M. S.; Miller, D. J.
Supercritical carbon dioxide extraction of polychlorinated biphenyls, polycyclic aromatic hydrocarbons, heteroatom-containing polycyclic aromatic hydrocarbons, and n-alkanes from polyurethane foam sorbents. 736
Heben, M. J. See Penner, R. M.
Hector, J. See Carlson, D. A.
Hedrick, J.
——; Taylor, L. T.
Quantitative supercritical fluid extraction/supercritical fluid chromatography of a phosphonate from aqueous media. 1986
Heine, C. E.
——; Holland, J. F.; Watson, J. T.
Influence of the ratio of matrix to analyte on the fast atom bombardment mass spectrometric response of peptides sampled from aqueous glycerol. 2674
Heise, H. M. See Janatsch, G.
——; Marbach, R.; Janatsch, G.; Kruse-Jarres, J. D.
Multivariate determination of glucose in whole blood by attenuated total reflection infrared spectroscopy. 2009
Heithmar, E. M. See Henshaw, J. M.
Heller, D. N.
——; Lys, I.; Cotter, R. J.; Uy, O. M.
Laser desorption from a probe in the cavity of a quadrupole ion storage mass spectrometer. 1083
Helmke, P. A. See Fitch, A.
Hemminger, J. C. See Amster, I. J.
Hendrix, S. A. See Braman, R. S.
Henion, J. D. See Eckerlin, R. H.
Henkin, R. I. See Gokmen, I. G.
Henshaw, J. M.
——; Heithmar, E. M.; Hinners, T. A.
Inductively coupled plasma mass spectrometric determination of trace elements in surface waters subject to acidic deposition. 335
Heo, G. S. See Olsher, U.
Hercules, D. M. See Bletsos, I. V.; Hoffmann, D. P.; Kubis, A. J.
Hernandez Mendez, J. See Perez Pavon, J. L.
Herold, D. A. See Aggarwal, S. K.
Herzog, H. See Buddrus, J.
Hess, K. R. See Smith, R. L.
Heumann, K. G. See Eagles, J.
Hieftje, G. M. See Carroll, M. K.
Higashi, R. M. See Fan, T. W. M.
Highfield, J. G.
——; Bowen, P.
Diffuse-reflectance Fourier-transform infrared spectroscopic studies of the stability of aluminum nitride powder in an aqueous environment. 2399
Hill, H. A. O.
——; Klein, N. A.; Psalti, I. S. M.; Walton, N. J.
Enzyme dual-electrode for analyte determination. 2200
Hill, H. H. Jr. See Shumate, C. B.
Hilpert, L. R. See Craft, N. E.
Hinners, T. A. See Henshaw, J. M.
Hinze, W. L. See Borgerding, M. F.; Pharr, D. Y.
——; Pharr, D. Y.; Fu, Z. S.; Burkert, W. G.
Thin-layer chromatography with urea solubilized β-cyclodextrin mobile phases. 422
Hirata, T.
——; Akagi, T.; Shimizu, H.; Masuda, A.
Determination of osmium and osmium isotope ratios by microelectrothermal vaporization inductively coupled plasma mass spectrometry. 2263
Hirokawa, K. See Wagatsuma, K.
Hobo, T. See Watabe, K.; Wu, X. Z.
Hodinar, A.
——; Jyo, A.
Contribution of membrane components to the overall response of anion carrier based solvent polymeric membrane ion-selective electrodes. 1169
Hof, D. E. See Manning, T. J.
Hoffmann, D. P.
——; Proctor, A.; Fay, M. J.; Hercules, D. M.
Application of cross-correlation to quantitative analysis of binary mixtures using extended x-ray absorption fine structure. 1686
——; Proctor, A.; Hercules, D. M.
Improved discrimination of noisy spectra in correlation based spectral analysis. 898
Holcombe, J. A. See Mahan, C. A.; Wang, P.
Holland, J. F. See Heine, C. E.
Homma, M.
——; Oka, K.; Takahashi, N.
Liquid chromatographic determination of theophylline concentration with syringe-type minicolumns for direct plasma injection. 784
Hooker, D. B.
——; DeZwaan, J.
Molecular formula determination of capillary column gas chromatographic effluents using combined microwave-induced plasma emission and mass spectral data. 2207
Hopkins, D. See Anderson, J. E.
Horiguchi, M. See Terazima, M.
Horman, I.
——; Traitler, H.
Pseudo-molecular ions in ion trap detector electron impact mass spectra: practical consequences. 1983
Hough, M. R. See Schultz, H.
Houk, R. S. See Crain, J. S.; Plantz, M. R.
Howe, G. B. See Fulcher, J. N.
Hsu, B. H. See Prokai, L.
Hu, T. See Welch, L. E.
Hu, Z.
——; Buehrer, T.; Mueller, M.; Rusterholz, B.; Rouilly, M.; Simon, W.
Intracellular magnesium ion-selective microelectrode based on a neutral carrier. 574

Huang, J. J. See Fujiwara, T.
Huang, S. D. See Chen, C. Y.
Huang, X.
——; Luckey, J. A.; Gordon, M. J.; Zare, R. N.
Quantitative analysis of low molecular weight carboxylic acids by capillary zone electrophoresis/conductivity detection. 766
Huber, D. M. See Hughes, K. D.
Huestis, D. L. See Pallix, J. B.
Hughes, K. D. See Seitzinger, N. K.
——; Lytle, F. E.; Huber, D. M.
Identification of immobilized bacteria by aminopeptidase profiling. 1656
Huie, C. W.
——; Williams, W. R.
Laser fluorometric detection of porphyrin methyl esters for high-performance thin-layer chromatography. 2288
Hungerford, J. M. See Clark, G. D.
Hunter, R. L. See McIver, R. T. Jr.
Huopalahti, R. See Kallio, H.
Hurtubise, R. J. See Richmond, M. D.
Solid-surface luminescence spectrometry. 889a
Hwang, J. D.
——; Guenther, G. D.; Diomiguardi, J. P.
A hydride generator system for a 1-kW inductively coupled plasma. 285

Ibusuki, T. See Takeuchi, K.
Igaz, S. See Maros, L.
Iglehart, M. L. See Sandifer, J. R.
Ihlenfeldt, A. See Bishop, G. A.
Imasaka, T.
——; Tashiro, K.; Ishibashi, N.
Supersonic jet spectrometry of chemical species laser ablated from organic polymers. 1530
——; Tsukamoto, A.; Ishibashi, N.
Visible semiconductor laser fluorometry. 2285
Ingle, J. D. Jr. See Liu, Y.; Yappert, M. C.
Inoue, H. See Suzuki, K.
Irgum, K. See Tesfalidet, S.
Isenhour, T. L.
——; Eckert, S. E.; Marshall, J. C.
Intelligent robots - the next step in laboratory automation. 805a
Ishibashi, N. See Imasaka, T.
Ishii, I. See Montaser, A.
Isidro Agudo, R. M. See Perez Pavon, J. L.
Ismail, K. Z. See Kuhn, L. S.
Isshiki, K. See Nakayama, E.
Ito, Y. See Oka, H.
Izatt, R. M.
——; Bruening, R. L.; Bruening, M. L.; LindH, G. C.; Christensen, J. J.
Modeling diffusion-limited, neutral-macrocycle-mediated cation transport in supported liquid membranes. 1140

Jackson, L. L.
——; McKown, D. M.; Taggart, J. E. Jr.; Lamothe, P. J.; Lichte, F. E.
Geological and inorganic materials. 109r
Jackson, W. A. See LaCourse, W. R.
Jacobsson, S. See Hagman, A.
Jalkian, R. D. See Epperson, P. M.
Janatsch, G. See Heise, H. M.
——; Kruse-Jarres, J. D.; Marbach, R.; Heise, H. M.
Multivariate calibration for assays in clinical chemistry using attenuated total reflection infrared spectra of human blood plasma. 2016
Janca, J. See Chmelik, J.
Janghorbani, M.
——; Ting, B. T. G.
Comparison of pneumatic nebulization and hydride generation inductively coupled plasma mass spectrometry for isotopic analysis of selenium. 701
Janis, L. J. See Pinkerton, T. C.
——; Regnier, F. E.
Dual-column immunoassays using protein G affinity chromatography. 1901
Jankowiak, R.
——; Small, G. J.
Fluorescence line-narrowing spectroscopy in the study of chemical carcinogenesis. 1023a
Jaouen, D. See Beaugrand, C.
Jardine, I.
——; Scanlan, G.; McNeil, M.; Brennan, P. J.
Plasma desorption mass spectrometric analysis of mycobacterial glycolipids. 416
Jaworski, R. K. See Cox, J. A.
Jayanty, R. K. M. See Fulcher, J. N.
Jayaweera, P.
——; Ramaley, L.
Automated segmented flow electrochemical analyzer. 2102
Jensen, J. N.
——; Johnson, J. D.
Quantitation of interferences under equilibrium conditions with application to free chlorine analysis in the presence of organic chloramines. 991
Jewett, G. L. See Cortes, H. J.
Jimba, H. See Fujii, T.
Jinguji, T. M. See Kelly, J. J.; Phelan, M. K.
Joensson, J. A.
——; Carlshaf, A.
Flow field flow fractionation in hollow cylindrical fibers. 11
Johansson, J. See Andersson-Engels, S.
Johnson, D. C. See LaCourse, W. R.; Welch, L. E.
Johnson, J. D. See Jensen, J. N.
Johnson, J. E. See Wery, J. P.
Johnson, J. T. See Ratzlaff, K. L.
Johnson, P. A.
——; Barber, T. E.; Smith, B. W.; Winefordner, J. D.
Ultra-low detection limits for an organic dye determined by fluorescence spectroscopy with laser diode excitation. 861
Johnson, R. D. See Wade, C. G.
Johnson, R. W.
——; Vo Dinh Tuan
Fumed silica substrates for enhanced fluorescence spot test analysis of benzo[a]pyrene-DNA adduct products. 2766
Jones, B. T. See Glick, M. R.
——; Mullins, N. J.; Winefordner, J. D.
Detection of polycyclic aromatic hydrocarbons by low-temperature phosphorimetry with a moving sample cooling device. 1182
——; Smith, B. W.; Winefordner, J. D.
Continuum source atomic absorption spectrometry in a graphite furnace with photodiode array detection. 1670
Jones, H. K.
——; Giddings, J. C.
Separation and characterization of colloidal materials of variable particle size and composition by coupled column sedimentation field-flow fractionation. 741
Jones, K. W.
——; Gordon, B. M.
Trace element determinations with synchrotron-induced x-ray emission. 341a
Jones, R. W.
——; McClelland, J. F.
Transient infrared emission spectroscopy. 650
Transient infrared emission spectroscopy by pulsed laser excitation. 1810
Jorgensen, B. S. See Carey, W. P.
Jorgenson, J. W. See Bushey, M. M.; Deterding, L. J.; Kennedy, R. T.; Moseley, M. A.; Oates, M. D.
Juhasz, P. See Vertes, A.
Jurs, P. C. See Ranc, M. L.; Stanton, D. T.; Sutton, G. P.
——; Sutton, G. P.; Ranc, M. L.
Carbon-13 NMR spectral simulation. 1115a
Jyo, A. See Hodinar, A.

Kadish, K. M. See Yao, C. L.
Kahr, M. See Anjo, D. M.
Kaifer, A. E. See Garcia, O. J.
Kaldy, M. See Maros, L.
Kalivas, J. H.
——; Roberts, N.; Sutter, J. M.
Global optimization by simulated annealing with wavelength selection for ultraviolet-visible spectrophotometry. 2024
Kallio, H.
——; Laakso, P.; Huopalahti, R.; Linko, R. R.; Oksman, P.
Analysis of butter fat triacylglycerols by supercritical fluid chromatography/electron impact mass spectrometry. 698
Kambara, H. See Sakairi, M.
Kamei, S.
——; Ohkubo, A.; Saito, S.; Takagi, S.
Polyamine detection system for high-performance liquid chromatography involving enzymic and chemiluminescent reactions. 1921
Kanchi, T. See Fujiwara, K.
Kapolos, J. See Katsanos, N. A.
Karakatsanis, C. G. See Bletsos, I. V.
Karatani, H. See Nakayama, E.
Karger, B. L. See Grinberg, N.
Karol, P. J.
A different perspective on the theoretical plate in equilibrium chromatography. 1937
Karpas, Z.
Ion mobility spectrometry of aliphatic and aromatic amines. 684
Karube, I.
——; Sode, K.; Suzuki, M.; Nakahara, T.
Microbial sensor for preliminary screening of mutagens utilizing a phage induction test. 2388
Katsanos, N. A.
——; Kapolos, J.
Diffusion coefficients of gases in liquids and partition coefficients in gas-liquid interphases by reversed-flow gas chromatography. 2231
Katti, A.
——; Guiochon, G.
Optimization of sample size and sample volume in preparative liquid chromatography. 982
Katz, E. D.
——; Lochmuller, C. H.; Scott, R. P. W.
Methanol-water association and its effect on solute retention in liquid chromatography. 349
Kauffmann, J. M. See Chastel, O.
Keil, R.
——; Hampp, R.; Ziegler, H.
Cycling technique for the determination of femtomole amounts of sulfite. 1755
Kelly, J. J. See Phelan, M. K.
——; Barlow, C. H.; Jinguji, T. M.; Callis, J. B.
Prediction of gasoline octane numbers from near-infrared spectral features in the range 660-1215 nm. 313
Kennedy, R. T. See Moseley, M. A.
——; Jorgenson, J. W.
Quantitative analysis of individual neurons by open tubular liquid chromatography with voltammetric detection. 436
Preparation and evaluation of packed capillary liquid chromatography columns with inner diameters from 20 to 50 micrometers. 1128
Kerley, E. L. See Hanson, C. D.
——; Hanson, C. D.; Castro, M. E.; Russell, D. H.
Axial magnetic inhomogeneities and low energy ion injection in Fourier-transform ion cyclotron resonance spectrometry. 2528
——; Russell, D. H.
Mass and energy selective ion partitioning in a two-section Fourier-transform ion cyclotron resonance spectrometer cell. 53
Ketkar, S. N.
——; Dulak, J. G.; Fite, W. L.; Buchner, J. D.; Dheandhanoo, S.
Atmospheric pressure ionization tandem mass spectrometric system for real-time detection of low-level pollutants in air. 260
Ketterer, M. E.
——; Reschl, J. J.; Peters, M. J.
Multivariate calibration in inductively coupled plasma mass spectrometry. 2031
Khaledi, M. G.
——; Breyer, E. D.
Quantitation of hydrophobicity with micellar liquid chromatography. 1040
Khodabakhsh, M. M. See Anjo, D. M.
Khosravi, M. J. See Diamandis, E. P.
Kim, H.
——; Crouch, S. R.; Zabik, M. J.
Room-temperature phosphorescence of compounds in mixed organized media: synthetic enzyme model-surfactant system. 2475
Kim, H. J.
——; Kim, Y. K.
Determination of nitrite in drinking water and environmental samples by ion exclusion chromatography with electrochemical detection. 1485
Kim, Y. K. See Kim, H. J.
Kimmel, H. See Dickert, F. L.
Kimura, Y. See Haginaka, J.
King, A. D. Jr. See Nugara, N. E.
Kinsinger, J. A. See Bjarnason, A.
Kinter, M. See Aggarwal, S. K.
Kirkland, J. J. See Grushka, E.
——; Glajch, J. L.; Farlee, R. D.
Synthesis and characterization of highly stable bonded phases for high-perform-

ance liquid chromatography column packings. 2
Kissinger, P. T. See Sternitzke, K.
Kita, H. See Uosaki, K.
Kjellstrom, T. L.
——; Bachas, L. G.
Potentiometric homogeneous enzyme-linked competitive binding assays using adenosine deaminase as the label. 1728
Klein, N. A. See Hill, H. A. O.
Klusman, R. W. See MacCarthy, P.
Knight, F. E. See Dobbs, J. C.
Knoll, J. E. See Fulcher, J. N.
Kobayashi, N. See Nakagawa, T.
Kobayashi, T. See Ogino, H.
Koch, W. F. See Feng, D.
Koel, M. N. See Lochmuller, C. H.
Kolesar, E. S. Jr.
——; Wiseman, J. M.
Interdigitated gate electrode field effect transistor for the selective detection of nitrogen dioxide and diisopropyl methylphosphonate. 2355
Kolla, P. See Mueller, S. R.
Komi, H. See Nakamura, N.
Komuro, M. See Ogino, H.
Koppenhoefer, B. See Lin, B.
Koropchak, J. A.
——; Allen, L.
Flow-injection Donnan dialysis preconcentration of cations for flame atomic absorption spectrophotometry. 1410
Kosted, P. See Handelman, G. J.
Kounaves, S. P.
——; Young, J. B.
Carbon fiber electrode cell for square wave voltammetric detection of biogenic amines in high-performance liquid chromatography. 1469
Koupparis, M. A. See Athanasiou-Malaki, E.
Koutny, L. B. See Ma, Y.
Kowalski, B. R. See Lorber, A.; Wilson, B. E.
Kowalski, Z. See Kubiak, W. W.
Kramer, J. R. See Caron, F.
Krieger, M. S. See Hawthorne, S. B.
Krieger-Jones, L. See Bornhop, D. J.
Krishen, A.
Rubber. 238r
Krivan, V.
——; Schmid, W.; Egger, K. P.
Radiochemical fast neutron activation analysis of high-purity metals for phosphorus. 2338
Krull, I. S. See Chou, T. Y.; Gao, C. X.
Kruse-Jarres, J. D. See Heise, H. M.; Janatsch, G.
Kuan, S. S. See Xu, Y.
Kubala, S. W.
——; Tilotta, D. C.; Busch, M. A.; Busch, K. W.
Determination of total inorganic carbon in aqueous samples with a flame infrared emission detector. 1841
Determination of chloride and available chlorine in aqueous samples by flame infrared emission. 2785
Kubiak, W. W.
——; Kowalski, Z.
Use of fumed silica to remove surfactant interferences in continuous flow polarographic measurements. 1598
——; Wang, J.; Darnall, D.
Algae columns with anodic stripping voltammetric detection. 468
Kubis, A. J.
——; Somayajula, K. V.; Sharkey, A. G.; Hercules, D. M.
Laser mass spectrometric analysis of compounds separated by thin-layer chromatography. 2516
Kuhn, L. S.
——; Weber, S. G.; Ismail, K. Z.
Control of molecular weight selectivity in electrode modifications based on phase-inversion cellulose acetate membranes. 303
Kumamaru, T. See Fujiwara, K.; Fujiwara, T.
Kunst, M. See Albert, K.
Kuwana, T. See Fagan, D. T.
Kwak, J. See Bard, A. J.
——; Bard, A. J.
Scanning electrochemical microscopy. Theory of the feedback mode. 1221
Scanning electrochemical microscopy. Apparatus and two-dimensional scans of conductive and insulating substrates. 1794

Laakso, P. See Kallio, H.
LaCourse, W. R. See Welch, L. E.
——; Jackson, W. A.; Johnson, D. C.
Pulsed amperometric detection of alkanolamines following ion-pair chromatography. 2466
Lacy, M. J. See Roe, V. D.
Lagesson, V.
——; Newman, J. M.
Microcolumn gas chromatography with ultraviolet detection and identification using a photodiode array spectrophotometer. 1249
LaiHing, K.
——; Cheng, P. Y.; Taylor, T. G.; Willey, K. F.; Peschke, M.; Duncan, M. A.
Photodissociation in a reflectron time-of-flight mass spectrometer: a novel mass spectrometry/mass spectrometry configuration for high-mass systems. 1458
Lambert, J. See Buddrus, J.
Lambert, W. E. See Van Liedekerke, B. M.
Lamothe, P. J. See Jackson, L. L.
Lan, Z. See Ci, Y.
Land, D. P. See Amster, I. J.
Langhorst, M. L.
——; Coyne, L. B.
Industrial hygiene. 128r
LaPack, M. A. See Savickas, P. J.
Laramee, J. A.
——; Arbogast, B.; Deinzer, M. L.
Evidence for radical anion formation during liquid secondary ion mass spectrometry analysis of oligonucleotides and synthetic oligomeric analogs: a deconvolution algorithm for molecular ion region clusters. 2154
Larsson, J. A.
——; Pardue, H. L.
Linearized model for error-compensated kinetic determinations without prior knowledge of reaction order or rate constant. 1949
Larsson, L. See Ueda, K.
Laserna, J. J.
——; Campiglia, A. D.; Winefordner, J. D.
Mixture analysis and quantitative determination of nitrogen-containing organic molecules by surface-enhanced Raman spectrometry. 1697
Lattimer, R. P.
——; Schulten, H. R.
Field ionization and field desorption mass spectrometry: past, present, and future. 1201a
Laude, D. A. Jr.
——; Beu, S. C.
A suspended trapping pulse sequence for simplified mass calibration in Fourier-transform mass spectrometry. 2422
Lauer, H. H. See Grossman, P. D.
Lawrence, A. H.
Characterization of benzodiazepine drugs by ion mobility spectrometry. 343
Le, X. C. See Brindle, I. D.
Leary, T. R. See Davis, K. A.
Ledford, E. B. Jr. See Rempel, D. L.
Lee, M. L. See Raynie, D. E.; Skelton, R. J. Jr.
Lee, S.
——; Myers, M. N.; Giddings, J. C.
Hydrodynamic relaxation using stopless flow injection in split inlet sedimentation field-flow fractionation. 2439
Lei, W.
——; Dasgupta, P. K.; Lopez, J. L.; Olson, D. C.
Sorbent isolation and elution with an immiscible eluent in flow injection analysis. 496
Leone, J. A. See Oquendo, J. N.
Lev, O. See Bard, A. J.
Levin, S.
——; Grushka, E.
Calculation of capacity ratios of the mobile-phase components and column void volumes through system peaks. 2428
Levine, S. P. See Xiao, H.; Ying, L.
Lewis, M. See Compton, B. J.
Lewis, N. S. See Penner, R. M.
Lewis, R. G. See Mulik, J. D.
Li, L.
——; Lubman, D. M.
Resonant two-photon ionization spectroscopic analysis of thin-layer chromatography using pulsed laser desorption/volatilization into supersonic jet expansions 1911
Li, Q. X.
——; Gee, S. J.; McChesney, M. M.; Hammock, B. D.; Seiber, J. N.
Comparison of an enzyme-linked immunosorbent assay and gas chromatographic procedure for the determination of molinate residues. 819
Li, R. See Wang, J.
Liberato, D. J. See Nadeau, R. W.
Lichte, F. E. See Jackson, L. L.
Lin, B. See Golshan-Shirazi, S.; Lin, B.
——; Koppenhoefer, B.; Lin, B.
Overtake phenomena in the movement process of components under temperature programming gas chromatography (correction). 512
Lindgren, P. F.
——; Dasgupta, P. K.
Measurement of atmospheric sulfur dioxide by diffusion scrubber coupled ion chromatography. 19
LindH, G. C. See Izatt, R. M.
Lindner, E. See Berube, T. R.
Ling, Y. C. See Ausserer, W. A.
——; Turner, L. K.; Bernius, M. T.; Morrison, G. H.
Detector discrimination in ion microscopic images: characterization and correction. 65
Linhardt, R. J. See Mallis, L. M.
Linko, R. R. See Kallio, H.
Listerud, J. M.
——; Sinton, S. W.; Drobny, G. P.
NMR imaging of materials. 23a
NMR imaging of materials (correction). 358a
Litwiler, K. S. See Bright, F. V.
Liu, K. E.
——; Abruna, H. D.
Electroanalysis of aromatic aldehydes with modified carbon paste electrodes. 2599
Liu, Y.
——; Ingle, J. D. Jr.
Automated on-line ion-exchange trace enrichment system with flame atomic absorption detection. 520
Automated two-column ion exchange system for determination of the speciation of trace metals in natural waters. 525
Lloyd, D. K.
——; Goodall, D. M.; Scrivener, H.
Diode-laser-based optical rotation detector for high-performance liquid chromatography and on-line polarimetric analysis. 1238
Lochmuller, C. H. See Katz, E. D.
——; Breiner, S. J.; Reese, C. E.; Koel, M. N.
Characterization and prediction of retention behavior in reversed-phase chromatography using factor analytical modeling. 367
——; McGranaghan, M. B.
Isocratic elution of high molecular weight monodisperse polystyrenes. 2449
Loganathan, D. See Mallis, L. M.
Long, J. T.
——; Weber, S. G.
Noise at microelectrodes and microelectrode arrays in amperometry and voltammetry (addition). 288
Loo, J. A. See Udseth, H. R.
Lopez, J. L. See Lei, W.
Lorber, A.
——; Kowalski, B. R.
Numerical and statistical properties of target factor analysis methods. 1168
Lowe, R. M. See Gough, D. S.
Lubman, D. M. See Li, L.; Pang, H. M.
Lubrano, G. J. See Fatibello-Filho, O.
Luckey, J. A. See Huang, X.
Lucy, C. A.
——; Cantwell, F. F.
Kinetics of solvent extraction-flow injection analysis. 101
Mechanism of extraction and band broadening in solvent extraction-flow injection analysis. 107
Luo, S.
——; Walt, D. R.
Fiber-optic sensors based on reagent delivery with controlled-release polymers. 174
Avidin-biotin coupling as a general method for preparing enzyme-based fiber-optic sensors. 1069
Lyne, P. D.
——; O'Neill, R. D.
Selectivity of stearate-modified carbon paste electrodes for dopamine and ascorbic acid. 2323
Lys, I. See Heller, D. N.
Lytle, F. E. See Hughes, K. D.; Seitzinger, N. K.

Ma, W. See Zhang, Z.

Ma, Y.
——; Koutny, L. B.; Yeung, E. S.
Laser–based indirect fluorometric detection and quantification in thin–layer chromatography. 1931
MacCarthy, P.
——; Klusman, R. W.; Rice, J. A.
Water analysis. 269r
McChesney, M. M. See Li, Q. X.
McClelland, J. F. See Jones, R. W.
McClenny, W. A. See Mulik, J. D.
McCormick, R. M. See Grushka, E.
McCreery, R. L. See Bowling, R. J.; Rice, R. J.; Sternitzke, K.; Wang, Y.; Wu, H. P.
——; Packard, R. T.
Raman monitoring of dynamic electrochemical events. 775a
Macdonald, R. W. See Yunker, M. B.
McEnroe, F. J. See Wade, C. G.
McGown, L. B. See Millican, D. W.; Nithipatikom, K.; Tu, X. M.
Fluorescence lifetime filtering. 839a
McGranaghan, M. B. See Lochmuller, C. H.
McGuire, G. E. See Fulghum, J. E.
Maciel, G. E. See Zhang, M.
McIntyre, M. K. See Small, G. W.
McIver, R. T. Jr. See Amster, I. J.
——; Hunter, R. L.; Baykut, G.
Impulse excitation for Fourier–transform mass spectrometry. 489
McKown, D. M. See Jackson, L. L.
McLaren, J. W. See Siu, K. W. M.
McLaughlin, F. A. See Yunker, M. B.
McLean, M. A.
——; Freas, R. B.
Enhanced analysis of sulfonated azo dyes using liquid chromatography/thermospray mass spectrometry. 2054
McManus, T. R.
Petroleum. 165r
McNeil, C. J.
——; Spoors, J. A.; Cocco, D.; Cooper, J. M.; Bannister, J. V.
Thermostable reduced nicotinamide adenine dinucleotide oxidase: application to amperometric enzyme assay. 25
McNeil, M. See Jardine, I.
Magee, L. J. Jr.
——; Osteryoung, J.
Fabrication and characterization of glassy carbon linear array electrodes. 2124
Mages, G. R. See Dickert, F. L.
Mahan, C. A.
——; Majidi, V.; Holcombe, J. A.
Evaluation of the metal uptake of several algae strains in a multicomponent matrix utilizing inductively coupled plasma emission spectrometry. 624
Mahle, N. H. See Smith, C. G.
Main, M. V.
——; Fritz, J. S.
Chromatographic determination of metal ions after complexation with bis(quaternary ammonium hydrazones) of 2,6–diacetylpyridine. 1272
Majewski, T. P. See Bond, A. M.
Majidi, V. See Mahan, C. A.; Wang, P.
Malinski, T. See Ciszewski, A.
Mallis, L. M.
——; Wang, H. M.; Loganathan, D.; Linhardt, R. J.
Sequence analysis of highly sulfated, heparin–derived oligosaccharides using fast atom bombardment mass spectrometry. 1453
Mamantov, G. See Flowers, P. A.
Mann, M.
——; Meing, C. K.; Fenn, J. B.
Interpreting mass spectra of multiply charged ions. 1702
Manning, T. J.
——; Palmer, B. A.; Hof, D. E.
High–Resolution Fourier transform spectrometer to identify the rotational structure of the $B^2\Sigma_u^+–X^2\Sigma_g^+$ transition of $N_2^+(0,0)$ in a helium inductively coupled plasma. 1052
Maple, J. R. See Pace, C. F.
Marbach, R. See Heise, H. M.; Janatsch, G.
Marchetti, A. See Franchini, G.
——; Picchioni, E.; Tassi, L.; Tosi, G.
Ionic equilibria of picric acid in mixed amphiprotic solvents. The 2–methoxyethanol/water solvent system. 1971
Marchetti, M. See Battista, M.; Di Corcia, A.
Marcott, C. See Fehl, A. J.
Marcus, R. K. See Duckworth, D. C.
Marinenko, R. B. See Myklebust, R. L.; Watters, R. L. Jr.
Mark, H.
——; Norris, K.; Williams, P. C.
Methods of determining the true accuracy of analytical methods. 398
Markey, S. P. See Shih, M. C.; Wang, T. C. L.
Markides, K. E. See Raynie, D. E.; Skelton, R. J. Jr.
Marko–Varga, G. A.
Determination of mono– and oligosaccharides in fermentation broths by liquid chromatographic separation and amperometric detection using immobilized enzyme reactors and a chemically modified electrode. 831
Maros, L.
——; Kaldy, M.; Igaz, S.
Simultaneous determination of bromide and iodide as acetone derivatives by gas chromatography and electron capture detection in natural waters and biological fluids. 733
Maroulis, P. J.
——; Coe, C. G.
Calcium chabazite adsorbent for the gas chromatographic separation of trace argon–oxygen mixtures. 1112
Marshall, A. G. See Wang, M.; Williams, C. P.
Marshall, D. B.
Statistical considerations in the analysis of dispersive kinetics data as discrete or continuous distributions of rate constants. 660
Marshall, J. C. See Isenhour, T. L.
Martin, C. R. See Cheng, I. F.
Martin, S. See Cortes, H. J.
Martin, S. J. See Smith, C. G.
Martinez, P. M. See Eiceman, G. A.
Martire, D. E. See Boehm, R. E.
Maschhoff, B. L. See Nebesny, K. W.
Mason, R. T. See Pannell, L. K.
Massart, D. L. See Zupan, J.
Masuda, A. See Hirata, T.
Matsunaga, H. See Haginaka, J.
Matsunaga, T.
——; Shigematsu, A.; Nakamura, N.
Detection of rat basophilic leukemia by cyclic voltammetry for monitoring allergic reaction. 2471
May, W. E. See Blyshak, L. A.
Maynard, R. J. See Engel, M. H.
Mead, D. A. Jr. See Welch, L. E.
Measures, C. I.
——; Edmond, J. M.
Shipboard determination of aluminum in seawater at the nanomolar level by electron capture detection gas chromatography. 544
Megargle, R.
Laboratory information management systems. 612a
Meing, C. K. See Mann, M.
Meiselman, S. See Ellerbe, P.
Melaragno, P. R. See Demana, T.
Menzel, E. R.
Detection of latent fingerprints by laser–excited luminescence. 557a
Merritt, C. M.
——; Winkelman, J. W.
Electrochemical method for measuring C–reactive protein using crown ether–phosphate ester ionophores. 2362
Mestdagh, H. See Beaugrand, C.
Meyerhoff, M. E. See Chaniotakis, N. A.; Collison, M. E.; Trojanowicz, M.
Michael, A. C.
——; Wightman, R. M.
Microelectrodes coated with ionically conducting polymer membranes for voltammetric detection in flowing supercritical carbon dioxide. 270
Voltammetry in supercritical carbon dioxide at platinum microdisk electrodes coated with perfluorinated ion–exchange membranes. 2193
Midgett, M. R. See Fulcher, J. N.
Migneault, D. R.
Enhanced detection of sulfite by inductively coupled plasma atomic emission spectroscopy with high–performance liquid chromatography. 272
Mikkelsen, S. R.
——; Rechnitz, G. A.
Conductometric transducers for enzyme–based biosensors. 1737
Miller, B. See Rosamilia, J. M.
Miller, D. J. See Hawthorne, S. B.
Miller, J. M.
——; Balasanmugam, K.
Fast atom bombardment mass spectrometry of some nonpolar compounds. 1293
Miller, T. D. See Pinkerton, T. C.
Miller–Ihli, N. J. See Epstein, M. S.
Millican, D. W. See Tu, X. M.
——; McGown, L. B.
Fluorescence lifetime selectivity in excitation–emission matrices for qualitative analysis of a two–component system. 580
Misawa, K. See Nakamura, N.
Miyanaga, A. See Sato, H.
Moharir, Y. See Rosenfeld, J. M.
Montaser, A. See Clifford, R. H.
——; Ishii, I.; Clifford, R. H.; Sinex, S. A.; Capar, S. G.
Versatile impedance matching network for inductively coupled plasma spectrometry. 2589
Moody, J. R. See Paulsen, P. J.
——; Wissink, C. E.; Beary, E. S.
Design principles for a large high efficiency sub–boiling still. 823
Moore, B. L. See Castles, M. A.
Morelli, J. J.
——; Grayson, M. A.; Wolf, C. J.
Thermally labile salts for aiding quantitation of reactive decomposition products. 802
Moreno Cordero, B. See Perez Pavon, J. L.
Morgan, S. L. See Ueda, K.
Mori, S.
Secondary effects in aqueous size exclusion chromatography of sodium poly(styrene sulfonate) compounds. 530
Size exclusion chromatography of poly(ethylene terephthalate) using hexafluoro–2–propanol as the mobile phase. 1321
——; Mouri, M.
Separation of styrene–acrylate and styrene–methacrylate copolymers according to composition by liquid adsorption chromatography. 2171
Morioka, T. See Dekmezian, A. H.
Morita, K. See Tokuda, K.
——; Shimizu, Y.
Microhole array for oxygen electrode. 159
Morita, M. See Shibata, Y.
Morris, M. D. See Chen, C. Y.; Treado, P. J.
Morrison, G. H. See Ausserer, W. A.; Ling, Y. C.
Deja Vu (editorial). 15a
Analytical Instrumentation Boom (editorial). 135a
Spatially Resolved Trace Element Analysis (editorial). 337a
Surface Science in Analytical Chemistry (editorial). 465a
NIST and Analytical Chemistry (editorial). 583a
"Harmonization" and Analytical Chemistry (editorial). 697a
Publish or Perish (editorial). 767a
25th Anniversary of a Classic Paper (editorial). 885a
Planetary Rock Analysis (editorial). 945a
Near Field Scanning Optical Microscopy (editorial). 1075a
The "Lost" Supper (editorial). 1197a
Secondary Ion Mass Spectrometry—SIMS VII (editorial). 1311a
Morton, R. C. See Diamandis, E. P.
Moseley, M. A. See Deterding, L. J.
——; Deterding, L. J.; De Wit, J. S. M.; Tomer, K. B.; Kennedy, R. T.; Bragg, N.; Jorgenson, J. W.
Optimization of a coaxial continuous flow fast atom bombardment interface between capillary liquid chromatography and magnetic sector mass spectrometry for the analysis of biomolecules. 1577
Mosher, R. A.
——; Dewey, D.; Thormann, W.; Saville, D. A.; Bier, M.
Computer simulation and experimental validation of the electrophoretic behavior of proteins. 362
Mossoba, M. M.
——; Niemann, R. A.; Chen, J. Y. T.
Picogram level quantitation of 2,3,7,8–tetrachlorodibenzo–p–dioxin in fish extracts by capillary gas chromatography/matrix isolation/Fourier–transform infrared spectrometry. 1678
Mouri, M. See Mori, S.
Mowery, R. See Cheek, G. T.
Muehlbauer, M. J.
——; Guilbeau, E. J.; Towe, B. C.
Model for a thermoelectric enzyme glucose sensor. 77

Mueller, M. See Hu, Z.
Mueller, R. See Schulten, H. R.
Mueller, S. R.
——; Simon, W.; Widmer, H. M.; Grolimund, K.; Schomburg, G.; Kolla, P.
Separation of cations by open-tubular column liquid chromatography. 2747
Mulik, J. D.
——; Lewis, R. G.; Williams, D. D.; McClenny, W. A.
Modification of a high-efficiency passive sampler to determine nitrogen dioxide or formaldehyde in air. 187
Mullins, N. J. See Jones, B. T.
Murphy, B. J. See Bornhop, D. J.
Murphy, M. M.
——; O'Dea, J. J.; Arn, D.; Osteryoung, J. G.
Theory of cyclic staircase voltammetry for electrode kinetics. 2249
Murray, R. W. See Parcher, J. F.
Musselman, I. H. See Fulghum, J. E.
Myers, M. N. See Berthod, A.; Lee, S.
Myklebust, R. L.
——; Newbury, D. E.; Marinenko, R. B.
Strategies for background subtraction in electron probe microanalysis/x-ray compositional mapping. 1612
Myrick, M. L. See Angel, S. M.

Nadeau, R. W.
——; Oldfield, N. F.; Garland, W. A.; Liberato, D. J.
Quantification of recombinant interleukin-2 in human serum by a specific immunobioassay. 1732
Nagamoto, H. See Nakamura, N.
Nagy, D. J.
Density determination of low density polymer latexes by sedimentation field flow fractionation. 1934
Nakagawa, T.
——; Aoyama, E.; Hasegawa, N.; Kobayashi, N.; Tanaka, H.
High-performance liquid chromatography-fluorometric determination of selenium based on selenotrisulfide formation reaction. 233
Nakahara, T. See Karube, I.
Nakamura, K.
——; Hara, S.; Dobashi, Y.
Chiral polysiloxanes derived from (R,R)-tartramide for the gas chromatographic separation of enantiomers. 2121
Nakamura, N. See Matsunaga, T.
——; Yamamoto, K.; Noda, S.; Nishikawa, Y.; Komi, H.; Nagamoto, H.; Nakayama, T.; Misawa, K.
Determination of picogram quantities of rare-earth elements in meteoritic materials by direct-loading thermal ionization mass spectrometry. 755
Nakayama, E.
——; Isshiki, K.; Sohrin, Y.; Karatani, H.
Automated determination of manganese in seawater by electrolytic concentration and chemiluminescence detection. 1392
Nakayama, T. See Nakamura, N.
Nakazawa, H. See Oka, H.
Nebesny, K. W.
——; Maschhoff, B. L.; Armstrong, N. R.
Quantitation of Auger and x-ray photoelectron spectroscopies. 469a
Neifert, P. E. See Gladney, E. S.
Neill, P. H. See Zhang, L.
Nelis, H. J. See Van Liedekerke, B. M.
Nemanich, R. J. See Fulghum, J. E.
Neuburger, G. G.
Detection of ambient hydrogen chloride with a zinc-coated piezoelectric crystal resonator operating in a frequency-time differential mode. 1559
Newbury, D. E. See Myklebust, R. L.
Newman, J. M. See Lagesson, V.
Ni, F.
——; Thomas, L.; Cotton, T. M.
Surface-enhanced resonance Raman spectroscopy as an ancillary high-performance liquid chromatography dectector for nitrophenol compounds. 888
Nibbering, N. M. M. See Elling, J. W.
NiChoileain, N. See Glennon, J. D.
Nicholson, C. See Rice, M. E.
Nielsen, R. G. See Grossman, P. D.
Nielson, K. K.
——; Rogers, V. C.
Statistical estimation of analytical data distributions and censored measurements. 2719
Niemann, R. A. See Mossoba, M. M.
Niessner, R.
——; Robers, W.; Wilbring, P.
Laboratory experiments on the determination of polycyclic aromatic hydrocarbon coverage of submicrometer particles by laser-induced aerosol photoemission. 320
——; Wilbring, P.
Ultrafine particles as trace catchers for polycyclic aromatic hydrocarbons: the photoelectric aerosol sensor as a tool for in situ sorption and desorption studies. 708
Nishi, H.
——; Tsumagari, N.; Terabe, S.
Effect of tetraalkylammonium salts on micellar electrokinetic chromatography of ionic substances. 2434
Nishihama, S. See Suzuki, K.
Nishikawa, Y. See Nakamura, N.
Nithipatikom, K.
——; McGown, L. B.
Fluorescence studies of energy transfer in sodium taurocholate and sodium dodecyl sulfate micellar solutions. 1405
Noda, S. See Nakamura, N.
Nomura, A.
——; Yamada, J.; Tsunoda, K.; Sakaki, K.; Yokochi, T.
Supercritical fluid chromatographic determination of fatty acids and their esters on an ODS-silica gel column. 2076
Norris, K. See Mark, H.
Noszal, B.
——; Sandor, P.
Rota-microspeciation of aspartic acid and asparagine. 2631
Novotny, M. See Borra, C.; Cobb, K. A.; David, P. A.
Nowinski, S. See Anjo, D. M.
Nugara, N. E.
——; King, A. D. Jr.
Light absorption and mixed micelle composition as factors in determining intensities of room-temperature phosphorescence. 1431
Nuwaysir, L. M.
——; Wilkins, C. L.
Photodissociation of laser-desorbed ions as a structure determination tool. 689
Nuwer, M. J.
——; Osteryoung, J.
Electrochemical behavior of N-acetylpenicillamine thionitrite at glassy carbon and carbon fiber electrodes. 1954
Nyquist, R. A. See Smith, C. G.

Oates, M. D.
——; Jorgenson, J. W.
Determination of naphthalene-2,3-dicarboxaldehyde-labeled amino acids by open tubular liquid chromatography with electrochemical detection. 432
Voltammetric detection with gradient elution for open tubular liquid chromatography. 1977
Oberholtzer, J. E. See Dorschel, C. A.
O'Dea, J. J. See Murphy, M. M.; Singleton, S. T.
Odham, G. See Ueda, K.
Odom, R. W. See Harrington, P. de B.
Ogino, H.
——; Aomura, Y.; Komuro, M.; Kobayashi, T.
Determination of trace impurities in high-purity oxygen by gas chromatography with photoionization detection. 2237
Ogura, M. See Fujii, T.
Ohkubo, A. See Kamei, S.
Ohzora, H. See Suzuki, K.
Oka, H.
——; Harada, K.; Suzuki, M.; Nakazawa, H.; Ito, Y.
Foam countercurrent chromatography of bacitracin with nitrogen and additive-free water. 1998
Oka, K. See Homma, M.
Okada, T. See Qi, D.
——; Dasgupta, P. K.
Selective detection approach to ion exclusion chromatography. 548
——; Dasgupta, P. K.; Qi, D.
Identification of ions in anion chromatography by stopped flow chronoamperometry. 1387
Okahata, Y.
——; Ebato, H.
Application of a quartz-crystal microbalance for detection of phase transitions in liquid crystals and lipid multibilayers 2185
Okawa, Y. See Tatsuma, T.
Oksman, P. See Kallio, H.
Oldfield, N. F. See Nadeau, R. W.
Olefirowicz, T. M. See Ewing, A. G.
Olesik, J. W.
——; Smith, L. J.; Williamsen, E. J.
Signal fluctuations due to individual droplets in inductively coupled plasma atomic emission spectrometry. 2002
Olesik, S. V. See Pekay, L. A.
——; Pekay, L. A.; Paliwoda, E. A.
Characterization and optimization of flame photometric detection in supercritical fluid chromatography. 58
Olsher, U.
——; Frolow, F.; Shoham, G.; Heo, G. S.; Bartsch, R. A.
Alkali-metal and alkaline-earth cation and proton selectivities of dibenzo-14-crown-4 and its derivatives in polymeric membranes. 1618
Olson, D. C. See Lei, W.
O'Neill, R. D. See Lyne, P. D.
Ong, W. A. See Saleh, F. Y.
Ono, T. See Dobashi, A.
Oquendo, J. N.
——; Leone, J. A.
On-line dilution scheme for liquid chromatography. 1791
Osteryoung, J. See Bilewicz, R.; Magee, L. J. Jr.; Nuwer, M. J.; Singleton, S. T.; Stojek, Z.; Wechter, C.; Wikiel, K.
Osteryoung, J. G. See Murphy, M. M.
Osteryoung, R. See Bilewicz, R.
Otsuka, K. See Terabe, S.
Otto, M.
——; Wegscheider, W.
Limitations of spectrophotometric multicomponent analysis of metal ions with mixed reagents. 1847
Owens, G. D. See Pinkston, J. D.

Pace, C. F.
——; Maple, J. R.
Laser-induced phosphorescence spectrometry of halogenated naphthalene derivatives prepared in vapor-deposited parent molecule matrices. 872
Pachla, L. A. See Gilpin, R. K.
Packard, R. T. See McCreery, R. L.
Paliwoda, E. A. See Olesik, S. V.
Pallix, J. B.
——; Schuhle, U.; Becker, C. H.; Huestis, D. L.
Advantages of single-photon ionization over multiphoton ionization for mass-spectrometric surface analysis of bulk organic polymers. 805
Palmer, B. A. See Manning, T. J.
Palmisano, F.
——; Guerrieri, A.; Zambonin, P. G.; Cataldi, T. R. I.
Determination of methotrexate in untreated body fluids by micellar liquid chromatography. 946
Pang, H. M.
——; Lubman, D. M.
Supersonic jet spectroscopy of nonvolatiles from pulsed high pressure ammonia expansions. 777
——; Yeung, E. S.
Laser-enhanced ionization as a diagnostic tool in laser-generated plumes. 2546
Pannell, L. K.
——; Pu, Q. L.; Fales, H. M.; Mason, R. T.; Stephenson, J. L.
Intermolecular processes in the ion trap mass spectrometer. 2500
Papadopoulou-Mourkidou, E.
Effect of column temperature on the direct determination of (RS)-α-cyano(3-phenoxyphenyl)methyl (RS)-2-(4-chlorophenyl)-3-methylbutyrate optical isomers by high-performance liquid chromatography/diode array system. 1149
Temperature-dependent solute retention time variations, base-line drifts, and solute peak splits during the analysis of fenvalerate by a high-performance liquid chromatographic/diode array system. 1152
Parcher, J. F. See Strubinger, J. R.
——; Barbour, C. J.; Murray, R. W.
Solid-state voltammetry and polymer electrolyte plasticization as a basis for an electrochemical gas chromatographic detector. 584
Pardue, H. L. See Fitzpatrick, C. P.; Larsson, J. A.
Park, J.
——; Shaw, B. R.
Electrochemical performance of crosslinked poly(styrene)-co-poly(vinylpyridine)

composite electrodes containing carbon black. 848
Park, K. H. See Yao, C. L.
Park, S. B. See Chaniotakis, N. A.
Pasztor, A. J. Jr. See Smith, C. G.
Patonay, G. See Blyshak, L. A.; Unger, E.
Patriarche, G. J. See Chastel, O.
Pau, J. C. See Fulcher, J. N.
Paulsen, P. J. See Fassett, J. D.
——; Beary, E. S.; Bushee, D. S.; Moody, J. R.
Analysis of ultrapure reagents from a large sub-boiling still made of Teflon PFA. 827
Pawliszyn, J. See Alexandrou, N.
Payne, B. R. See Daunert, S.
Peachey, R. M. See Arnold, D. P.
Pekay, L. A. See Olesik, S. V.
——; Olesik, S. V.
Supercritical fluid chromatography/flame photometric detection: determination of high molecular weight compounds. 2616
Penner, R. M.
——; Heben, M. J.; Lewis, N. S.
Preparation and electrochemical characterization of conical and hemispherical ultramicroelectrodes. 1630
Pentoney, S. L. Jr. See Fuoco, R.
——; Zare, R. N.; Quint, J. F.
On-line radioisotope detection for capillary electrophoresis. 1642
Perez Pavon, J. L.
——; Moreno Cordero, B.; Hernandez Mendez, J.; Isidro Agudo, R. M.
Application of a nested-loop system for the simultaneous determination of thorium and uranium by flow-injection analysis. 1789
Pericles, N. See Bruno, A. E.
Perry, K. L. See Swarin, S. J.
Perry, L. M.
——; Campiglia, A. D.; Winefordner, J. D.
Room-temperature phosphorescence of polynuclear aromatic hydrocarbons on matrix-modified solid substrates. 2328
Peschke, M. See LaiHing, K.
Pesek, J. J. See Sandoval, J. E.
——; Siouffi, A. M.
Chemically bonded liquid crystals as stationary phases for high-performance liquid chromatography. Effects of mobile-phase composition. 1928
Peterman, D. See Demana, T.
Peters, M. J. See Ketterer, M. E.
Peterson, M. R. See Fulcher, J. N.
Petit, E. J. See Pinkston, J. D.
Petty, J. See Collison, M. E.
Petty, J. D. See Arnold, D. P.
Pfeiffer, C. D. See Cortes, H. J.
Pharr, C. M. See Bowling, R. J.
Pharr, D. Y. See Hinze, W. L.
——; Fu, Z. S.; Smith, T. K.; Hinze, W. L.
Solubilization of cyclodextrins for analytical applications. 275
Phelan, M. K.
——; Barlow, C. H.; Kelly, J. J.; Jinguji, T. M.; Callis, J. B.
Measurement of caustic and caustic brine solutions by spectroscopic detection of the hydroxide ion in the near-infrared region, 700–1150 nm. 1419
Phillips, G. R.
——; Eyring, E. M.
Comments on the simplex algorithm culminating in quadratic convergence and error estimation. 1786
Philson, S. B. See Wade, C. G.
Picchioni, E. See Marchetti, A.
Pigott, J. D.
Coupled ion-selective electrode measurement of aqueous carbonate and bicarbonate ion activities. 638
Pilkington, M. B. G.
——; Coles, B. A.; Compton, R. G.
Construction of an optically transparent thin-layer-electrode cell for use with oxygen-sensitive species in aqueous and nonaqueous solvents. 1787
Ping, L.
——; Dasgupta, P. K.
Determination of total mercury in water and urine by a gold film sensor following Fenton's reagent digestion. 1230
Pinkerton, T. C.
——; Miller, T. D.; Janis, L. J.
Effect of protein binding on the high-performance liquid chromatography of phenytoin and imirestat in human serum by direct injection onto internal surface reversed-phase columns. 1171
Pinkse, F. A. See Elling, J. W.
Pinkston, J. D.
——; Owens, G. D.; Petit, E. J.
Supercritical fluid injection of polysiloxane solutions for calibration and tuning in supercritical fluid chromatography/mass spectrometry. 775
Piplits, K. See Stingeder, G.
Plambeck, J. A. See Fernando, A. R.
Plantz, M. R.
——; Fritz, J. S.; Smith, F. G.; Houk, R. S.
Separation of trace metal complexes for analysis of samples of high salt content by inductively coupled plasma mass spectrometry. 149
Pletcher, D. See Evans, J.
Poetzl, H. See Stingeder, G.
Poggenburg, J. See Dumke, I.
Poole, C. F.
——; Poole, S. K.
Modern thin-layer chromatography. 1257a
Poole, S. K. See Poole, C. F.
Portwood, D. E. See Eagles, J.
Potter, B. B. See Gurka, D. F.
Poulsen, J. R.
——; Birks, J. W.
Photoreduction fluorescence detection of quinones in high-performance liquid chromatography. 2267
Prabhu, S. V.
——; Baldwin, R. P.
Constant potential amperometric detection of carbohydrates at a copper-based chemically modified electrode. 852
Electrocatalysis and detection of amino sugars, alditols, and acidic sugars at a copper-containing chemically modified electrode. 2258
Pradelles, P.
——; Grassi, J.; Chabardes, D.; Guiso, N.
Enzyme immunoassays of adenosine cyclic 3',5'-monophosphate and guanosine cyclic 3',5'-monophosphate using acetylcholinesterase. 447
Preti, C. See Franchini, G.
Prime, R. B.
——; Shushan, B.
Thermogravimetric analyzer/atmospheric pressure chemical ionization tandem triple quadrupole mass spectrometer system for evolved gas analysis. 1195
Principi, J. M. See Dubin, P. L.
Proctor, A. See Hoffmann, D. P.
Prokai, L.
——; Hsu, B. H.; Farag, H.; Bodor, N.
Desorption chemical ionization, thermospray, and fast atom bombardment mass spectrometry of dihydropyridine ⇌ pyridinium salt-type redox systems. 1723
Psalti, I. S. M. See Hill, H. A. O.
Pu, Q. L. See Pannell, L. K.
Pungor, E. See Berube, T. R.
Purdie, N.
——; Swallows, K. A.
Analytical applications of polarimetry, optical rotatory dispersion, and circular dichroism. 77a
Pyle, S. See Gurka, D. F.

Qi, D. See Okada, T.
——; Okada, T.; Dasgupta, P. K.
Direct current conductivity detection in ion chromatography. 1383
Quilliam, M. A.
——; Wright, J. L. C.
The amnesic shellfish poisoning mystery. 1053a
Quint, J. F. See Pentoney, S. L. Jr.
Quintela, P. A. See Garcia, O. J.

Radicati di Brozolo, F. See Harrington, P. de B.
Ramaley, L. See Jayaweera, P.
Ramsey, J. M. See Blazewicz, P. R.
Ranc, M. L. See Jurs, P. C.
——; Jurs, P. C.
Simulation of carbon-13 nuclear magnetic resonance spectra of piperidines. 2489
Ratzlaff, K. L.
——; Johnson, J. T.
Computation of two-dimensional polynomial least-squares convolution smoothing integers. 1303
Raynie, D. E.
——; Markides, K. E.; Lee, M. L.; Goates, S. R.
Back-pressure regulated restrictor for flow control in capillary supercritical fluid chromatography. 1178
Rechnitz, G. A. See Buch, R. M.; Mikkelsen, S. R.
Redwan, D. S. See Singh, R. P.
Reese, C. E. See Lochmuller, C. H.
Regnier, F. E. See Chicz, R. M.; Janis, L. J.
Reichstein, E. See Diamandis, E. P.
Reid, J. M.
——; Stobaugh, J. F.; Sternson, L. A.
Liquid chromatographic determination of cyclophosphamide enantiomers in plasma by precolumn chiral derivatization. 441
Reilly, J. P. See Wilkerson, C. W. Jr.
Remelli, M.
——; Blo, G.; Dondi, F.; Vidal-Madjar, M. C.; Guiochon, G.
Fluidic and syringe injection study by peak shape analysis. 1489
Rempel, D. L.
——; Ledford, E. B. Jr.; Sack, T. M.; Gross, M. L.
Multichannel heterodyne detection for accurate mass selected ion monitoring in Fourier transform mass spectrometry: implementation and comparison with undersampling. 749
Ren, Y. See Anderson, J. E.
Renn, C. N.
——; Synovec, R. E.
Examination of the automated solute-independent calibration technique. 1915
Reschl, J. J. See Ketterer, M. E.
Rice, J. A. See MacCarthy, P.
Rice, M. E.
——; Nicholson, C.
Measurement of nanomolar dopamine diffusion using low-noise perfluorinated ionomer-coated carbon fiber microelectrodes and high-speed cyclic voltammetry. 1805
Rice, R. J.
——; McCreery, R. L.
Quantitative relationship between electron transfer rate and surface microstructure of laser-modified graphite electrodes. 1637
Richardson, B. R.
——; Haw, J. F.
Spin dynamics in the analysis of carbonaceous deposits on zeolite catalysts by carbon-13 nuclear magnetic resonance with cross polarization and magic-angle spinning. 1821
Richmond, M. D.
——; Hurtubise, R. J.
Analytical characteristics of β-cyclodextrin/salt mixtures in room-temperature solid-surface luminescence analysis. 2643
Rickard, E. C. See Grossman, P. D.
Rieck, J. N. See Bletsos, I. V.
Riggin, R. M. See Grossman, P. D.
Righetti, P. G.
——; Gianazza, E.; Gelfi, C.; Chiari, M.; Sinha, P. K.
Isoelectric focusing in immobilized pH gradients. 1602
Ringwelski, A. Z.
——; Beck, K. M.; Gordon, R. J.
Use of piezoelectric ceramics in detection and measurement of pulsed laser radiation. 796
Riordan, J. F. See Strydom, D. J.
Roan, C. S. See Carlson, D. A.
Robbins, G. A. See Roe, V. D.
Robers, W. See Niessner, R.
Roberts, J. M.
——; Fajer, R. W.; Springston, S. R.
Capillary gas chromatographic separation of alkyl nitrates and peroxycarboxylic nitric anhydrides. 771
Roberts, N. See Kalivas, J. H.
Roe, V. D.
——; Lacy, M. J.; Stuart, J. D.; Robbins, G. A.
Manual headspace method to analyze for the volatile aromatics of gasoline in groundwater and soil samples. 2584
Rogers, V. C. See Nielson, K. K.
Rolando, C. See Beaugrand, C.
Rosamilia, J. M.
——; Miller, B.
Electrochemical probes of oxidation state, product distribution, and redox activity for barium yttrium copper oxide ($Ba_2YCu_3O_{7-x}$) in halide solutions. 1497
Rose, M. See Saraceno, R. A.
Rosenfeld, J. M.
——; Moharir, Y.; Sandler, S. D.
Selective sample preparation for determination of 11-nor-9-carboxy-Δ^9-tetrahydrocannabinol from human urine by gas chromatography with electron capture detection. 925

Rouilly, M. See Hu, Z.
Roumelis, N.
——; Glavas, S.
Decomposition of peroxyacetyl nitrate and peroxypropionyl nitrate during gas chromatographic determination with a wide-bore capillary and two packed columns. 2731
Rowlen, K. L.
——; Duell, K. A.; Avery, J. P.; Birks, J. W.
Whole column detection: application to high-performance liquid chromatography. 2624
Russell, D. H. See Hanson, C. D.; Kerley, E. L.; Tecklenburg, R. E. Jr.
Russell, R. See Zhang, Z.
Rusterholz, B. See Hu, Z.
Ruzicka, J. See Clark, G. D.

Sack, T. M. See Rempel, D. L.
Saferstein, R. See Brettell, T. A.
Saito, S. See Kamei, S.
Sakairi, M.
——; Kambara, H.
Atmospheric pressure spray ionization for liquid chromatography/mass spectrometry. 1159
Sakaki, K. See Nomura, A.
Sakkinen, P. A. See Dix, K. D.
Saleh, F. Y.
——; Ong, W. A.; Chang, D. Y.
Structural features of aquatic fulvic acids. Analytical and preparative reversed-phase high-performance liquid chromatography separation with photodiode array detection. 2792
Salin, E. D. See Sing, R. L. A.
Samperi, R. See Di Corcia, A.
Sander, L. C.
——; Wise, S. A.
Subambient temperature modification of selectivity in reversed-phase liquid chromatography. 1749
Sandifer, J. R.
Implications of ion-exchange kinetics on ion-selective electrode responses and selectivities. 2341
——; Iglehart, M. L.; Buck, R. P.
Analysis of transient currents and interfacial kinetics for neutral carrier membranes. 1624
Sandler, S. D. See Rosenfeld, J. M.
Sandor, P. See Noszal, B.
Sandoval, J. E.
——; Pesek, J. J.
Synthesis and characterization of a hydride-modified porous silica material as an intermediate in the preparation of chemically bonded chromatographic stationary phases. 2067
Santana-Marques, M. G. O.
——; Ferrer-Correia, A. J. V.; Gross, M. L.
Fast-atom-bombardment-induced reduction of aromatic oximes. 1442
Santelli, R. E.
——; Gallego, M.; Valcarcel, M.
Atomic absorption determination of copper in silicate rocks by continuous precipitation preconcentration. 1427
Saraceno, R. A.
——; Engstrom, C. E.; Rose, M.; Ewing, A. G.
Carbon electrodes fabricated by low-temperature pyrolysis of ethylene on nickel. 560
Sato, H.
——; Miyanaga, A.
Background suppression by chelation in the ion-exchange chromatographic separation of anions. 122
Savickas, P. J.
——; LaPack, M. A.; Tou, J. C.
Hollow fiber membrane probes for the in situ spectrometric monitoring of nitrogen trichloride formation during wastewater treatment. 2332
Saville, D. A. See Mosher, R. A.
Savory, J. See Aggarwal, S. K.
Scanlan, G. See Jardine, I.
Schenley, R. L. See Tomkins, B. A.
Scherson, D. See Bae, I. T.
Schmid, W. See Krivan, V.
Schnoes, M. L. See Harris, T. D.
Schomburg, G. See Mueller, S. R.
Schreiner, S. K. See Dickert, F. L.
Schuhle, U. See Pallix, J. B.
Schulten, H. R. See Lattimer, R. P.
——; Simmleit, N.; Mueller, K.
Characterization of plant materials by pyrolysis-field ionization mass spectrometry: high-resolution mass spectrometry, time-resolved high-resolution mass spectrometry, and Curie-point pyrolysis-gas chromatography/mass spectrometry of spruce needles. 221
Schultz, H.
——; Wells, A. W.; Frommell, E. A.; Hough, M. R.
Solid and gaseous fuels. 84r
Schure, M. R.
——; Barman, B. N.; Giddings, J. C.
Deconvolution of nonequilibrium band broadening effects for accurate particle size distributions by sedimentation field-flow fractionation. 2735
Schuyler, M. W. See Yappert, M. C.
Schwartz, L. M.
Calibration of pipets: a statistical view. 1080
Scott, R. P. W. See Katz, E. D.
Scrivener, H. See Lloyd, D. K.
Sears, L. J.
——; Grimsrud, E. P.
Elimination of unexpected ions in electron capture mass spectrometry using carbon dioxide buffer gas. 2523
Seiber, J. N. See Li, Q. X.
Seibles, L. See Harris, T. D.
Seitz, D. M. See Sutcliffe, C. R.
Seitz, W. R. See Shaksher, Z. M.; Werner, T. C.; Zhang, Z.
Seitzinger, N. K.
——; Hughes, K. D.; Lytle, F. E.
Optimization of signal-to-noise ratios in time-filtered fluorescence detection. 2611
Self, R. See Eagles, J.
Selinger, B. See Hall, P.
Senior, A. T. See Glennon, J. D.
Sentell, K. B.
——; Dorsey, J. G.
Retention mechanisms in reversed-phase liquid chromatography. Stationary-phase bonding density and partitioning. 930
Serxner, D. See Smith, R. L.
Shadrick, J. W. See Anderson, J. E.
Shaffer, J. See Demana, T.
Shakhsher, Z. M. See Zhang, Z.
Shaksher, Z. M.
——; Seitz, W. R.
Fluorescence study of organic cation binding to hydrocarbon-bonded silica surfaces. 590
Sharkey, A. G. See Kubis, A. J.
Shaw, B. R. See Creasy, K. E.; Park, J.
Shaw, R. W. See Young, J. P.
——; Young, J. P.; Smith, D. H.
Diode laser initiated resonance ionization mass spectrometry of lanthanum. 695
Shen, F. H. See Watters, R. L. Jr.
Sherma, J.
Pesticides. 153r
Shibata, Y.
——; Morita, M.
Exchange of comments on identification and quantitation of arsenic species in a dogfish muscle reference material for trace elements. 2116
Shigematsu, A. See Matsunaga, T.
Shigematsu, Y. See Uosaki, K.
Shih, M. C. See Wang, T. C. L.
——; Wang, T. C. L.; Markey, S. P.
Evaporation device for continuous flow-liquid secondary-ion mass spectrometry. 2582
Shimizu, H. See Hirata, T.
Shimizu, Y. See Morita, K.; Tokuda, K.
Shirai, T. See Suzuki, K.
Shiu, K. K.
——; Chemerika, R.; Harrison, D. J.
Effects of added plasticizer on redox ion charge transport in quaternized poly(vinylpyridine) films. 570
Shoff, D. B. See Eiceman, G. A.
Shoham, G. See Olsher, U.
Short, S. See Handelman, G. J.
Shumate, C. B.
——; Hill, H. H. Jr.
Coronaspray nebulization and ionization of liquid samples for ion mobility spectrometry. 601
Shushan, B. See Prime, R. B.
Sill, C. W.
Long-term stability of solid standards for radiochemical analysis. 2255
Simmleit, N. See Schulten, H. R.
Simms, J. R. See Strife, R. J.
Simon, W. See Hu, Z.; Mueller, S. R.
Sinex, S. A. See Clifford, R. H.; Montaser, A.
Sing, R. L. A.
——; Salin, E. D.
Introduction of liquid samples into the inductively coupled plasma by direct insertion on a wire loop. 163
Singh, R. P.
——; Alam, K.; Redwan, D. S.; Abbas, N. M.
Determination of chloride in platinum-rhenium alumina-based reforming catalyst by ion chromatography. 1924
Singleton, S. T.
——; O'Dea, J. J.; Osteryoung, J.
Analytical utility of cylindrical microelectrodes. 1211
Sinha, P. K. See Righetti, P. G.
Sinton, S. W. See Listerud, J. M.
Sioda, R. E. See Ciszewski, A.
Siouffi, A. M. See Pesek, J. J.
Sittampalam, G. S. See Grossman, P. D.
Siu, K. W. M.
——; Gardner, G. J.; Berman, S. S.
Ion spray mass spectrometry/mass spectrometry: quantitation of tributyltin in a sediment reference material for trace metals. 2320
——; Sturgeon, R. E.; McLaren, J. W.; Berman, S. S.
Exchange of comments on identification and quantitation of arsenic species in a dogfish muscle reference material for trace elements. Reply to comments. 2118
Skelton, R. J. Jr.
——; Chang, H. C. K.; Farnsworth, P. B.; Markides, K. E.; Lee, M. L.
Radio frequency plasma detector for sulfur selective capillary gas chromatographic analysis of fossil fuels. 2292
——; Farnsworth, P. B.; Markides, K. E.; Lee, M. L.
Element-selective detection after supercritical fluid chromatography using a radio frequency plasma detector. 1815
Slaby, J.
Background illumination filtering in thermal lens spectroscopy. 2496
Slavin, W. See Epstein, M. S.
Small, G. J. See Jankowiak, R.
Small, G. W. See Barber, A. S.; Bjerga, J. M.
——; McIntyre, M. K.
Structure elucidation methodology for disaccharides based on carbon-13 nuclear magnetic resonance spectrum simulation 666
Small, J. A. See Watters, R. L. Jr.
Smit, H. C. See Elling, J. W.
Smith, B. W. See Glick, M. R.; Johnson, P. A.; Jones, B. T.
Smith, C. See Cortes, H. J.
Smith, C. G.
——; Nyquist, R. A.; Martin, S. J.; Mahle, N. H.; Smith, P. B.; Pasztor, A. J. Jr.
Analysis of synthetic polymers. 214r
Smith, D. H. See Shaw, R. W.; Young, J. P.
Smith, D. K. See Cohen, L. H.
Smith, F. G. See Plantz, M. R.
Smith, L. J. See Olesik, J. W.
Smith, P. B. See Smith, C. G.
Smith, R. D. See Udseth, H. R.; Yonker, C. R.
Smith, R. L.
——; Serxner, D.; Hess, K. R.
Assessment of the relative role of Penning ionization in low-pressure glow discharges. 1103
Smith, T. K. See Pharr, D. Y.
Smyth, T. A. See Yunker, M. B.
Sniegoski, L. T. See Ellerbe, P.
Snyder, A. P. See Eiceman, G. A.
Snyder, S. W.
——; Demas, J. N.; DeGraff, B. A.
Single photon counting lifetime measurements of weak, long-lived samples. 2704
Sode, K. See Karube, I.
Sohrin, Y. See Nakayama, E.
Somayajula, K. V. See Kubis, A. J.
Sonesson, A. See Ueda, K.
Souda, R. See Uosaki, K.
Spoors, J. A. See McNeil, C. J.
Spraul, M. See Albert, K.
Springston, S. R. See Roberts, J. M.
Staahlberg, J.
——; Almgren, M.
Theory for system peaks in ion pair chromatography and its application to indirect detection. 1109
Stafford, L. D. See Borgerding, M. F.
Stanton, D. T.
——; Jurs, P. C.
Computer-assisted prediction of gas chromatographic retention indexes of pyrazines. 1328
Starkey, J. R. See Bishop, G. A.
Stedman, D. H. See Benner, R. L.; Bishop, G. A.

Stephens, D. A.
——; Bohn, P. W.
Absorption spectrometry of bound monolayers on integrated optical structures. 386
Stephenson, J. L. See Pannell, L. K.
Sternitzke, K.
——; McCreery, R. L.; Bruntlett, C. S.; Kissinger, P. T.
In situ laser activation of glassy carbon electrochemical detectors for liquid chromatography: demonstration of improved reversibility and detection limits. 1989
Sternson, L. A. See Reid, J. M.
Stingeder, G.
——; Piplits, K.; Gara, S.; Grasserbauer, M.; Budil, M.; Poetzl, H.
Simultaneous quantitative determination of the distribution of dopants in silicon by high mass resolution secondary ion mass spectrometry. 412
Stobaugh, J. F. See Reid, J. M.
Stojek, Z.
——; Osteryoung, J.
Experimental determination of the coefficient in the steady state current equation for spherical segment microelectrodes. 1305
Stokes, D. L. See Bello, J. M.
Stout, S. J.
——; DaCunha, A. R.
Tuning and calibration in thermospray liquid chromatography/mass spectrometry using trifluoroacetic acid cluster ions. 2126
Straub, W. A.
Ferrous analysis. 14r
Street, T. E. See Harrington, P. de B.
Strife, R. J.
——; Simms, J. R.
Ion trap tandem mass spectrometry of tryptamine. Tissue extracts and isotope dilution using combined radio frequency and direct current voltages. 2316
Strong, D. L.
——; Dasgupta, P. K.
Electrodialytic membrane suppressor for ion chromatography. 939
Strouse, J. See Wade, C. G.
Strubinger, J. R.
——; Parcher, J. F.
Surface excess (Gibbs) adsorption isotherms of supercritical carbon dioxide on octadecyl-bonded silica stationary phases. 951
Strydom, D. J.
——; Fett, J. W.; Riordan, J. F.
The odyssey of angiogenin: a protein that induces blood vessel growth. 1173a
Stuart, J. D. See Roe, V. D.
Sturgeon, R. E. See Siu, K. W. M.
——; Willie, S. N.; Berman, S. S.
Atomic absorption determination of lead at picogram per gram levels by ethylation with in-situ concentration in a graphite furnace. 1867
Suleiman, A. A. See Fatibello-Filho, O.
Sun, S. T. See Barth, H. G.
Sundberg, D. C. See Zhang, Z.
Susetyo, W. See Dobbs, J. C.
Sutcliffe, C. R.
——; Gladney, E. S.; Seitz, D. M.; Brooks, G. H.
Comparison of screening techniques for polychlorinated biphenyls in waste oils. 2682
Sutter, J. M. See Kalivas, J. H.
Sutton, G. P. See Jurs, P. C.
——; Jurs, P. C.
Simulation of carbon-13 nuclear magnetic resonance spectra of alkyl-substituted cyclohexanones and decalones. 863
Suzuki, K.
——; Tohda, K.; Tanda, Y.; Ohzora, H.; Nishihama, S.; Inoue, H.; Shirai, T.
Fiber-optic magnesium and calcium ion sensor based on a natural carboxylic polyether antibiotic. 382
Suzuki, M. See Karube, I.; Oka, H.
Suzuki, S. See Watabe, K.; Wu, X. Z.
Svanberg, K. See Andersson-Engels, S.
Svanberg, S. See Andersson-Engels, S.
Swallows, K. A. See Purdie, N.
Swann, M. See Caswell, K. A.
Swarin, S. J.
——; Perry, K. L.
Determination of conjugated dienes in gasoline by differential pulse polarography. 1502
Sweatman, D. R. See Arnold, D. P.
Synovec, R. E. See Renn, C. N.

Taggart, J. E. Jr. See Jackson, L. L.
Takagi, S. See Kamei, S.
Takahashi, N. See Homma, M.
Takeuchi, K.
——; Ibusuki, T.
Quantitative determination of aqueous-phase ozone by chemiluminescence using indigo-5,5'-disulfonate. 619
Tanaka, H. See Nakagawa, T.
Tanda, Y. See Suzuki, K.
Tanimoto, N. See Fujiwara, T.
Targove, M. A. See Danielson, N. D.
Tashiro, K. See Imasaka, T.
Tassi, L. See Franchini, G.; Marchetti, A.
Tatsuma, T.
——; Okawa, Y.; Watanabe, T.
Enzyme monolayer- and bilayer-modified tin oxide electrodes for the determination of hydrogen peroxide and glucose. 2352
Taylor, H. E. See Garbarino, J. R.
Taylor, J. W. See Bjarnason, A.
Taylor, L. T. See Ashraf-Khorassani, M.; Hedrick, J.
Taylor, T. G. See LaiHing, K.
Tecklenburg, R. E. Jr.
——; Castro, M. E.; Russell, D. H.
Evaluation of pulsed fast-atom bombardment ionization for increased sensitivity of tandem mass spectrometry. 153
Teclemariam, A. See Harrison, D. J.
Terabe, S. See Nishi, H.
——; Otsuka, K.; Ando, T.
Band broadening in electrokinetic chromatography with micellar solutions and open-tubular capillaries. 251
Terazima, M.
——; Horiguchi, M.; Azumi, T.
Limitation of absorbance measurements using the thermal lens method. 883
Tesfalidet, S.
——; Irgum, K.
Polymer-bound tetrahydroborate for arsine generation in a flow-injection system. 2079
Thamann, T. J. See Havel, H. A.
Thomas, L. See Ni, F.
Thompson, M.
Robust statistics and functional relationship estimation for comparing the bias of analytical procedures over extended concentration ranges. 1942
Thomsen, K. N.
——; Baldwin, R. P.
Amperometric detection of nonelectroactive cations in flow systems at a cupric hexacyanoferrate electrode. 2594
Thormann, W. See Mosher, R. A.
Tidwell, C. J.
——; Underhill, D. W.
Estimating contaminant concentration from uptake on a diffusive sampler. 917
Tijssen, R. See Bos, J.
Tilotta, D. C. See Kubala, S. W.
Ting, B. T. G. See Janghorbani, M.
Titus, R. See Gurka, D. F.
Tohda, K. See Suzuki, K.
Tokuda, K.
——; Morita, K.; Shimizu, Y.
Cyclic voltammetry at microhole array electrodes. 1763
Tomer, K. B. See Deterding, L. J.; Moseley, M. A.
Tomkins, B. A.
——; Caton, J. E. Jr.; Edwards, M. D.; Garcia, M. E.; Schenley, R. L.; Wachter, L. J.; Griest, W. H.
Determination of regulatory organic compounds in radioactive waste samples. Volatile organics in aqueous liquids. 2751
Tong, W. G. See Wu, Z.
Tosi, G. See Franchini, G.; Marchetti, A.
Tou, J. C. See Savickas, P. J.
Towe, B. C. See Muehlbauer, M. J.
Traitler, H. See Horman, I.
Tran, C. D. See Franko, M.
Simultaneous enhancement of fluorescence and thermal lensing by reversed micelles (correction). 928
——; Van Fleet, T. A.
Micellar induced simultaneous enhancement of fluorescence and thermal lensing (correction). 928
Treado, P. J.
——; Morris, M. D.
A thousand points of light: the Hadamard transform in chemical analysis and instrumentation. 723a
Trojanowicz, M.
——; Meyerhoff, M. E.
Potentiometric pH detection in suppressed ion chromatography. 787
Tsukamoto, A. See Imasaka, T.
Tsumagari, N. See Nishi, H.
Tsumura, S. See Fujiwara, K.
Tsunoda, K. See Nomura, A.
Tu, X. M.
——; Burdick, D. S.; Millican, D. W.; McGown, L. B.
Canonical correlation technique for rank estimation of excitation-emission matrixes. 2219
Turner, L. K. See Ling, Y. C.

Udseth, H. R.
——; Loo, J. A.; Smith, R. D.
Capillary isotachophoresis/mass spectrometry. 228
Ueda, K.
——; Morgan, S. L.; Fox, A.; Gilbart, J.; Sonesson, A.; Larsson, L.; Odham, G.
D-Alanine as a chemical marker for the determination of streptococcal cell wall levels in mammalian tissues by gas chromatography/negative ion chemical ionization mass spectrometry. 265
Ugo, P.
——; Anson, F. C.
Poly(2-vinylpyrazine) as a soluble polymeric ligand and as an electrode coating. Reactions with pentacyanoferrate(II). 1799
Umezawa, Y. See Uosaki, K.
Underhill, D. W. See Adley, D. P.; Tidwell, C. J.
Unger, E.
——; Patonay, G.
Near-infrared laser diode intracavity absorption spectrometry. 1425
Uosaki, K.
——; Shigematsu, Y.; Kita, H.; Umezawa, Y.; Souda, R.
Crystal-face specific response of a single-crystal cadmium sulfide based ion-selective electrode. 1980
Uy, O. M. See Heller, D. N.

Valcarcel, M. See Santelli, R. E.
Vandecasteele, C. See Vanhoe, H.
VanDyke, D. A.
——; Cheng, H. Y.
Electrochemical manipulation of fluorescence and chemiluminescence signals at fiber-optic probes. 633
Van Fleet, T. A. See Tran, C. D.
Vanhoe, H.
——; Vandecasteele, C.; Versieck, J.; Dams, R.
Determination of iron, cobalt, copper, zinc, rubidium, molybdenum, and cesium in human serum by inductively coupled plasma mass spectrometry. 1851
Van Kreveld, M. E. See Bos, J.
VanLeyen, D. See Bletsos, I. V.
Van Liedekerke, B. M.
——; Nelis, H. J.; Lambert, W. E.; De Leenheer, A. P.
High-performance liquid chromatography of quaternary ammonium compounds on a polystyrene-divinylbenzene column. 728
Varughese, K. See Wang, J.
Verkouteren, R. M.
——; Dorko, W. D.
High-accuracy gas analysis via isotope dilution mass spectrometry: carbon dioxide in air. 2416
Versieck, J. See Vanhoe, H.
Vertes, A.
——; De Wolf, M.; Juhasz, P.; Gijbels, R.
Threshold conditions of plasma ignition in laser ionization mass spectrometry of solids. 1029
Vidal-Madjar, M. C. See Remelli, M.
Vo Dinh Tuan See Alak, A. M.; Bello, J. M.; Johnson, R. W.
Volk, K. J.
——; Yost, R. A.; Brajter-Toth, A.
On-line electrochemistry/thermospray/tandem mass spectrometry as a new approach to the study of redox reactions: the oxidation of uric acid. 1709
Voorhees, K. J. See Harrington, P. de B.

Wachter, L. J. See Tomkins, B. A.
Wade, A. P. See Wentzell, P. D.
Wade, C. G.
——; Johnson, R. D.; Philson, S. B.; Strouse, J.; McEnroe, F. J.
Changing views of NMR: automated high-resolution NMR with a sample changer. 107a

Wagatsuma, K.
——; Hirokawa, K.
Quenching mechanisms in argon-nitrogen or neon-nitrogen glow discharge plasmas. 326
Emission spectrometric determination of manganese and chromium in steels with a dual cathode glow discharge lamp. 2137
Wakai, J. See Haginaka, J.
Wakao, N. See Funazukuri, T.
Wallace, G. G. See Ge, H.; Hailin, G.
Wallingford, R. A. See Ewing, A. G.
——; Ewing, A. G.
Separation of serotonin from catechols by capillary zone electrophoresis with electrochemical detection. 98
Walt, D. R. See Luo, S.
Walton, N. J. See Hill, H. A. O.
Wang, H. M. See Mallis, L. M.
Wang, J. See Kubiak, W. W.
——; Golden, T.
Permselectivity and ion-exchange properties of Eastman-AQ polymers on glassy carbon electrodes. 1397
——; Golden, T.; Varughese, K.; El-Rayes, I.
Polishable and robust modified graphite epoxy electrodes. 508
——; Li, R.
Highly stable voltammetric measurements of phenolic compounds at poly(3-methylthiophene)-coated glassy carbon electrodes. 2809
Wang, M.
——; Marshall, A. G.
A "screened" electrostatic ion trap for enhanced mass resolution, mass accuracy, reproducibility, and upper mass limit in Fourier-transform ion cyclotron resonance mass spectrometry. 1288
Wang, P.
——; Majidi, V.; Holcombe, J. A.
Copper atomization mechanisms in graphite furnace atomizers. 2652
Wang, T. C. L. See Shih, M. C.
——; Shih, M. C.; Markey, S. P.; Duncan, M. W.
Quantitative analysis of low-molecular-weight polar compounds by continuous flow liquid secondary ion tandem mass spectrometry. 1013
Wang, Y.
——; McCreery, R. L.
Evaluation of a diode laser/charge coupled device spectrometer for near-infrared Raman spectroscopy. 2647
Wangen, L. E. See Carey, W. P.
Wanger, M. See Anjo, D. M.
Wangsa, J. See Danielson, N. D.
Warburton, P. R. G. See Evans, J.
Ward, S. R. See Castles, M. A.
Warner, A. M.
——; Weber, S. G.
Electrochemical detection of peptides. 2664
Warner, I. M. See Blyshak, L. A.
Warner, M.
Happy 95th birthday, Piet Kolthoff. 287a
Warren, F. V. Jr. See Dorschel, C. A.
Wastney, M. E. See Gokmen, I. G.
Watabe, K.
——; Gil-Av, E.; Hobo, T.; Suzuki, S.
Effect of apolar diluents on the behavior of chiral stationary phases in gas chromatography. Binary mixtures of N-lauroyl-L-valine-tert-butylamide with squalane and n-tetracosane. 126
Effect of apolar diluents on the behavior of chiral stationary phases in gas chromatography. Binary mixtures of N-lauroyl-L-valine-tert-butylamide with squalane and n-tetracosane (correction). 2688
Watanabe, T. See Tatsuma, T.
Watkins, M. L. See Eiceman, G. A.
Watson, J. T. See Heine, C. E.
Watters, R. L. Jr.
——; DeVoe, J. R.; Shen, F. H.; Small, J. A.; Marinenko, R. B.
Characteristics of aerosols produced by the spark discharge. 1826
Weaver, M. R.
——; Harris, J. M.
In-situ fluorescence studies of aluminum ion complexation by 8-hydroxyquinoline covalently bound to silica. 1001
Webber, L. D. See Gemperline, P. J.
Weber, S. G. See Kuhn, L. S.; Long, J. T.; Warner, A. M.
Signal-to-noise ratio in microelectrode-array-based electrochemical detectors. 295
Webster, G. K.
——; Carnahan, J. W.
Nonmetal analyte introduction device for atomic spectrometry. 790
Wechter, C.
——; Osteryoung, J.
Square wave and linear scan anodic stripping voltammetry at iridium-based mercury film electrodes. 2092
Wegscheider, W. See Otto, M.
Weil, D. A. See Bjarnason, A.
Welch, L. E.
——; LaCourse, W. R.; Mead, D. A. Jr.; Johnson, D. C.; Hu, T.
Comparison of pulsed coulometric detection and potential-sweep-pulsed coulometric detection for underivatized amino acids in liquid chromatography. 555
Welch, M. J. See Ellerbe, P.
Wells, A. W. See Schultz, H.
Wentzell, P. D.
——; Wade, A. P.
Chemical acoustic emission analysis in the frequency domain. 2638
Werner, T. C.
——; Cummings, J. G.; Seitz, W. R.
General approach to the development of luminescent cation detectors. 211
Wery, J. P.
——; Johnson, J. E.
Molecular biology at atomic resolution: the 2.8-Å structure of an insect virus and its functional implications. 1341a
Whigham, F. See Compton, B. J.
Whitaker, R. G. See Bartlett, P. N.
White, E. V. See Ellerbe, P.
White, J. M. See Fulghum, J. E.
White, R. L. See Divis, R. A.
Whiteley, L. D. See Cheng, I. F.
Whitten, W. B. See Blazewicz, P. R.
Widmer, H. M. See Mueller, S. R.
Wightman, R. M. See Michael, A. C.
Wikiel, K. See Bilewicz, R.
——; Osteryoung, J.
Square wave voltammetry at a mercury film electrode: experimental results. 2086
Wilbring, P. See Niessner, R.
Wilkerson, C. W. Jr.
——; Colby, S. M.; Reilly, J. P.
Determination of polycyclic aromatic hydrocarbons using gas chromatography/laser ionization mass spectrometry with picosecond and nanosecond light pulses. 2669
Wilkins, C. L. See Chowdhury, A. K.; Cooper, J. R.; Ha, S. T. K.; Nuwaysir, L. M.
Willey, K. F. See LaiHing, K.
Williams, C. P.
——; Marshall, A. G.
Hartley transform ion cyclotron resonance mass spectrometry. 428
Williams, D. D. See Mulik, J. D.
Williams, P. See Deng, R. C.
Williams, P. C. See Mark, H.
Williams, R.
Microcontrollers in the laboratory. 433a
Williams, W. J. See Bishop, G. A.
Williams, W. R. See Huie, C. W.
Williamsen, E. J. See Olesik, J. W.
Willie, S. N. See Sturgeon, R. E.
Wills, M. R. See Aggarwal, S. K.
Wilson, B. E.
——; Kowalski, B. R.
Quantitative analysis in the presence of spectral interferents using second-order nonbilinear data. 2277
Wilson, G. S. See Bindra, D. S.
Wilson, M. A.
——; Collin, P. J.; Akitt, J. W.
Composition of aluminum phosphate solutions. Evidence from aluminum-27 and phosphorus-31 nuclear magnetic resonance spectra. 1253
Winans, R. E. See Zhang, L.
Winefordner, J. D. See Glick, M. R.; Johnson, P. A.; Jones, B. T.; Laserna, J. J.; Perry, L. M.
Winkelman, J. W. See Merritt, C. M.
Wise, S. A. See Sander, L. C.
Wiseman, J. M. See Kolesar, E. S. Jr.
Wissink, C. E. See Moody, J. R.
Wohltjen, H. See Ballantine, D. S. Jr.
Wolf, C. J. See Morelli, J. J.
Wong, A. L.
——; Harris, J. M.
Quantitative estimation of component amplitudes in multiexponential data: application to time-resolved fluorescence spectroscopy. 2310
Woulfe, M. R. See Glennon, J. D.
Wright, J. L. See Connors, K. A.
Wright, J. L. C. See Quilliam, M. A.
Wu, H. P.
——; McCreery, R. L.
Observation of concentration profiles at cylindrical microelectrodes by a combination of spatially resolved absorption spectroscopy and the Abel inversion. 2347
Wu, X. Z.
——; Yamada, M.; Hobo, T.; Suzuki, S.
Uranin sensitized chemiluminescence for alternative determinations of copper(II) and free cyanide by the flow injection method. 1505
Wu, Y. C. See Feng, D.
Wu, Z.
——; Tong, W. G.
Laser analytical spectrometry based on optical phase conjugation by degenerate four-wave mixing in a flowing liquid analyte cell. 998

Xiao, H.
——; Levine, S. P.; D'Arcy, J. B.
Iterative least-squares fit procedures for the identification of organic vapor mixtures by Fourier-transform infrared spectrophotometry. 2708
Xing, X. See Bae, I. T.
Xu, Y.
——; Guilbault, G. G.; Kuan, S. S.
Sucrose enzyme electrode. 782

Yamada, J. See Nomura, A.
Yamada, M. See Wu, X. Z.
Yamada, S.
Ultraviolet and infrared laser excited two-color multiphoton ionization for determination of molecules in solution. 612
Yamaguchi, J. See Dobashi, A.
Yamamoto, K. See Nakamura, N.
Yao, C. L.
——; Capdevielle, F. J.; Kadish, K. M.; Bear, J. L.
Thin-layer microcell for transmittance Fourier transform infrared spectroelectrochemistry. 2805
——; Park, K. H.; Bear, J. L.
Chemically modified carbon paste electrode for chronoamperometric studies. Reduction of oxygen by tetrakis(μ-2-anilinopyridinato)dirhodium(II,III) chloride 279
Yappert, M. C.
——; Schuyler, M. W.; Ingle, J. D. Jr.
Design and evaluation of a dual multichannel detector spectrometer for simultaneous molecular absorption and luminescence measurements. 593
Yarmush, D. M. See Grinberg, N.
Yasuda, H. See Haginaka, J.
Yasuda, N. See Haginaka, J.
Yau, A. See Betts, F.
Yeager, E. B. See Bae, I. T.
Yeung, E. S. See Christensen, P. L.; Ma, Y.; Pang, H. M.; Zhu, J.
Ying, L.
——; Levine, S. P.
Fourier transform infrared least-squares methods for the quantitative analysis of multicomponent mixtures of airborne vapors of industrial hygiene concern. 677
Ying, P. T.
——; Dorsey, J. G.; Dill, K. A.
Retention mechanisms of reversed-phase liquid chromatography: determination of solute-solvent interaction free energies. 2540
Yokochi, T. See Nomura, A.
Yonker, C. R.
——; Smith, R. D.
Stationary phase solvation in capillary supercritical fluid chromatography. 1348
Yost, R. A. See Carlson, D. A.; Hail, M. E.; Volk, K. J.
Young, J. B. See Kounaves, S. P.
Young, J. P. See Shaw, R. W.
——; Shaw, R. W.; Smith, D. H.
Resonance ionization mass spectrometry. 1271a
Yu, M.
——; Dovichi, N. J.
Attomole amino acid determination by capillary zone electrophoresis with thermooptical absorbance detection. 37
Yu, S. K. T.
——; Green, J. B.

Determination of total hydroxyls and carboxyls in petroleum and syncrudes after chemical derivatization by infrared spectroscopy. 1260
Yu, W. H.
——; Freiser, H.
An electrochemical study of the mechanism of cadmium extraction with dithizone. 1621
Yunker, M. B.
——; McLaughlin, F. A.; Macdonald, R. W.; Cretney, W. J.; Fowler, B. R.; Smyth, T. A.
Measurement of natural trace dissolved hydrocarbons by in situ column extraction. An intercomparison of two adsorption resins. 1333

Zabik, M. J. See Kim, H.
Zambonin, P. G. See Palmisano, F.
Zare, R. N. See Huang, X.; Pentoney, S. L. Jr.
Zhang, L.
——; Carnahan, J. W.; Winans, R. E.; Neill, P. H.
Moving wheel liquid chromatography-helium microwave-induced plasma interface 895
Zhang, M.
——; Maciel, G. E.
Built-in carbon-13 intensity reference for solid-state analysis by magic-angle-spinning nuclear magnetic resonance spectrometry. 2579
Zhang, Y. See Zhang, Z.
Zhang, Z.
——; Zhang, Y.; Ma, W.; Russell, R.; Shakhsher, Z. M.; Grant, C. L.; Seitz, W. R.; Sundberg, D. C.
Poly(vinyl alcohol) as a substrate for indicator immobilization for fiber-optic chemical sensors. 202
Zhu, J.
——; Yeung, E. S.
Direct coupling of planar chromatography to gas chromatography by laser desorption. 1906
Elemental analysis based on chemiluminescence in the laser microprobe. 2557
Ziegler, H. See Keil, R.
Zupan, J.
——; Massart, D. L.
Application of the three-distance clustering method in analytical chemistry. 2098
Zybin, A. V. See Bol'shov, M. A.

KEYWORD INDEX

Abel inversion concn profile microelectrode 2347
Ablation laser sampling plasma mass spectrometry 1243
Ablation polystyrene supersonic jet spectrometry 1530
ABS ablation supersonic jet spectrometry 1530
Absorption light phosphorescence 1431
Absorption optical detn thermal lens 883
Absorption reflection FTIR ionic transport 1164
Absorption spectrometry analysis adsorbed monolayer 386
Absorption spectrometry IR laser diode intracavity 1425
Absorption zinc detn intestine nutrition 1023
Acceptor detn gallium arsenide Raman spectroscopy 994
Accuracy chem analysis algorithm 398
Acetaminophen detn voltammetry 2809
Acetate dithizone cadmium mixed complex 1621
Acetone reagent bromide iodide gas chromatog 733
Acetylcholinesterase conjugate cAMP cGMP EIA 447
Acetylpenicillamine thionitrite detn voltammetry 1954
Acetylpyridine hydrazone reagent metal ion chromatog 1272
Acid ascorbic oxidn ferricyanide contg electrocatalyst 848
Acid base reaction chromatog background suppression 122
Acid coronaspray ion mobility spectrometry 601
Acid detn polymer coated waveguide 1674
Acid distn subboiling still 823
Acid pH gradient elution HPLC 2
Acid polyprotic titrn conductometric 177
Acid weak detection ion exclusion chromatog 548
Acidity high polymer coated waveguide sensor 1674
Acoustic emission phys chem change 2638
Acoustic signal normalization chemiluminescence laser microprobe 2557
Acoustic wave device analysis review 704a
Acrylate styrene copolymer chromatog sepn 2171
Acrylonitrile detn waste gas 2743
Activated carbon adsorbent contg diffusive sampler 843
Activation geol inorg analysis review 109r
Activation laser glassy carbon electrode detector 1989
Activity detn aq bicarbonate carbonate detn 638
Additive strongly retained chromatog 2380
Additive strongly retained liq chromatog 2373
Addn noise microelectrode array amperometry voltammetry 288
Adenosine deaminase biotin binding assay 1728
Adipate dihexenyl photopolymn potassium selective membrane 246
Adrenal ext rat analysis methylphenylpyridine SIMS 1013
Adsorbed monolayer analysis absorption spectrometry 386
Adsorbent carbon activated contg diffusive sampler 843
Adsorbent gas chromatog calcium chabazite 1112
Adsorption cadmium sulfide crystal face specific 1980
Adsorption carbon dioxide supercrit silica 951
Adsorption catalytic polarog cobalt ultratrace detn 2178
Adsorption chromatog trace metal preconcn 149
Adsorption desorption model ion selective electrode 453
Adsorption dopamine capacitance electrode 2603
Adsorption polycyclic arom hydrocarbon aerosol 708
Advances in Chromatog, Vol. 28 (book review) 1288a
Advances in Electrophoresis, Vol. 2 (book review) 1377a
Aerosil 200 adsorption polycyclic arom hydrocarbon 708
Aerosol adsorption polycyclic arom hydrocarbon 708
Aerosol airborne analysis review 1r
Aerosol analysis arom hydrocarbon 320
Aerosol spark produced analysis 1826
Affinity chromatog glycoprotein Con A 1117
Affinity chromatog immobilized metal protein 1742
Aggregation protein HPLC 514
Air alkyl peroxyalkanoyl nitrate detn 771
Air analysis anesthetic 1093
Air analysis carbon dioxide amperometry 577
Air analysis org diffusive sampling model 917
Air analysis workplace review 128r
Air carbon dioxide detn 2416
Air carbon monoxide detn exhaust 671a
Air formaldehyde nitrogen dioxide sampler 187
Air hydrogen chloride detection quartz resonator 1559
Air molinate detn ELISA 819
Air org detn FTIR 677
Air org detn supercrit extn 736
Air pollutant detn review 1r
Air present ion mobility spectra amine 684
Air sampling sulfur dioxide detn 19
Air tetramethyllead detn analytical std 1993
Alanine peptidoglycan marker detn liver 265
Alc amino enantiomeric HPLC 1548
Alc HPLC conductometric detection model 631
Alc soly chromatog gel hydrophobicity 780
Aldaric acid detection copper modified electrode 2258
Aldehyde arom detn electrochem 2599
Alditol detection copper modified electrode 2258
Aldonic acid detection copper modified electrode 2258
Algae column metal interference removal 468
Algae metal uptake 624
Algorithm chromatog detector fiber optics 876
Algorithm data processing digital smoothing filter 1308
Algorithm detn reaction kinetics linearized model 1949
Algorithm estg error limit kinetic data 2324
Algorithm oligonucleotide mass spectra 2154
Algorithm protein mass spectra 1702
Algorithm reiterative regression multiexponential data analysis 2310
Algorithm simplex culminating quadratic convergence polemic 1783 1786
Algorithm true accuracy chem analysis 398
Aliph aldehyde detn electrochem 2599
Aliph amine ion mobility spectrometry 684
Alizarine charge transport quaternized polyvinylpyridine 570
Alk earth additive emission spectrometry 1175
Alk earth detn direct mass spectrometry 755
Alk earth detn nonsuppressed ion chromatog 1435
Alk earth detn polymer membrane electrode 1618
Alk earth membrane neutral carrier transport 1140
Alk earth open tubular liq chromatog 2747
Alkadiene identification insect 1564
Alkali metal additive emission spectrometry 1175
Alkali metal detn direct mass spectrometry 755
Alkali metal detn nonsuppressed ion chromatog 1435
Alkali metal detn polymer membrane electrode 1618
Alkali metal membrane neutral carrier transport 1140
Alkali sepn open tubular liq chromatog 2747
Alkane detn water extn resin 1333
Alkanolamine detn chromatog pulsed amperometry 2466
Alkatriene identification insect 1564
Alkene derivatization dimethyl disulfide biochem 1564
Alkene mass spectrometry 86
Alkyl nitrate sepn peroxyalkanoyl nitrate 771
Alkylamine electrokinetic chromatog micellar 491
Alkylbenzene reversed phase liq chromatog 1524
Alkylbenzenesulfonate chromatog detn water 2534
Alkylcyclohexanone NMR carbon simulation 863
Alkyldecalone NMR carbon simulation 863
Alkylmalonamide ligand magnesium selective membrane 574
Allergy detection cyclic voltammetry basophil 2471
Alloy cobalt chromium prosthetic tissue 1235
Allyloxybenzoylmethoxyphenyl bonded silica stationary phase HPLC 1928
Alternating current conductometric transducer biosensor 1737
Alumina adsorption polycyclic arom hydrocarbon 708
Alumina platinum rhenium catalyst analysis chloride 1924
Aluminum aq soln speciation ion chromatog 535
Aluminum clad capillary column resistively heated 2410
Aluminum complexation immobilized ligand fluorescence 1001
Aluminum detn gallium indium present 1768
Aluminum detn laser microprobe chemiluminescence detection 2557
Aluminum detn nonsuppressed ion chromatog 1435
Aluminum nitride powder reaction water 2399
Aluminum phosphato complex soln NMR 1253
Aluminum trace detn seawater 544
Amalgam formation linear scan voltammetry 965
Amalgam forming metal detn stripping voltammetry 2092
Amberlyst A26 tetrahydroborate column arsine generation 2079
Amine alkanol detn chromatog pulsed amperometry 2466
Amine aryl eluent chromatog cation detn 1435
Amine coronaspray ion mobility spectrometry 601
Amine derivatization polymeric activated ester reagent 1538
Amine detn HPLC detector 1469
Amine detn kinetic potentiometry 1358
Amine enantiomeric HPLC 1548
Amine pos ion mobility spectra 684
Amino acid detn electrophoresis thermooptical detection 37
Amino acid detn naphthalenedicarboxaldehyde deriv 432
Amino acid detn single cell 436
Amino acid fluorenylmethyl polymeric chiral reagent 1548

Amino acid isopropyl ester nitrobenzoyl deriv 1984
Amino acid liq chromatog coulometric detection 555
Amino acid present ammonia detn 408
Amino acid resoln chiral diamide diln 126
Amino acid sensor conductometric transducer 1737
Amino acid subtilisin chromatog 2059
Amino alc enantiomeric HPLC 1548
Amino sugar detection copper modified electrode 2258
Aminoacridine detn surface enhanced Raman spectrometry 1697
Aminobenzoic acid contg carbon paste electrode 2599
Aminopeptidase bacteria identification 1656
Aminopyridine iron cyanide carbon paste electrode 2599
Ammonia aq anhyd mass spectrometry 2511
Ammonia detn amino acid present 408
Ammonia detn polymer analysis 802
Ammonia detn wastewater optical sensor 2306
Ammonia high pressure expansion nonvolatile compd 777
Ammonium detn amperometry electrode 2594
Ammonium detn flow injection fluorometry 408
Ammonium detn luminescence detector 211
Ammonium detn nonsuppressed ion chromatog 1435
Ammonium hydrazone acetylpyridine prepn reagent 1272
Ammonium quaternary compd HPLC stationary phase 728
Ammonium sepn open tubular liq chromatog 2747
Ammonolysis uric acid electrooxidn 1709
Amnesic shellfish poisoning review 1053a
Amperometric detection HPLC carbohydrate 852
Amperometric detection hydroxamic acid siderophore HPLC 1474
Amperometric detn air carbon dioxide 577
Amperometric detn insulin electrode oxidn 2462
Amperometric enzymic analysis NADH oxidase 25
Amperometry detection carbohydrate copper modified electrode 2258
Amperometry electrode glassy carbon cupric hexacyanoferrate 2594
Amperometry gold electrode glucose detn 2566
Amperometry immobilized enzyme saccharide detn 831
Amperometry pulsed alkanolamine detn chromatog 2466
Amperometry surfactant interference fumed silica effect 1598
Amphetamine detn urine HPLC 1538
Amphetamine selective electrode dibenzocrown 2189
Amphiphile extn reaction phosphatidylcholine electrode 979
Analysis biochem dual microband electrode 2200
Analysis chem accuracy algorithm 398
Analysis classification computer 2098
Analysis coating review 33r
Analysis crab antennule receptrode review 533a
Analysis data shot noise distribution function 2479
Analysis data shot noise limit 2483
Analysis flow injection carbon paste electrode 2585
Analysis flow injection extn kinetics 101
Analysis flow injection extn mechanism 107
Analysis fluorescence arom hydrocarbon micelle 1405
Analysis fluorometry detection time filtering 2611
Analysis fluoropolymer EGA mass spectrometry 802
Analysis food review 45r
Analysis petroleum coal liq review 165r
Analysis polymer review 214r
Analysis sampling coal review 84r
Analysis spectrochem photodiode array detector 2347
Analysis sulfonated azo dye 2054
Analysis transient IR emission spectroscopy 650
Analysis water review 269r
Analysis—What Analytical Chemists Do (book review) 548a
Analyte introduction device nonmetal atomic spectrometry 790
Analyte velocity modulation capillary zone electrophoresis 1590
Analytical Chem NIST editorial 583a
Analytical Chem term guide 93
Analytical Chem. Principles and Techniques (book review) 418a
Analytical data distribution statistical estn 2719
Analytical Gas Chromatog (book review) 655a
Analytical lab automation intelligent robot review 805a
Analytical method bias detn robust statistics 1942
Analytical std tetramethyllead vapor prepn 1993
Analyzer electrochem automated segmented flow 2102
Anesthetic halogenated detn ion mobility spectrometry 1093
Angiogenin review 1173a
Aniline contg carbon paste electrode 2599
Aniline detn benzene flow injection 496
Anilinonaphthalenesulfonate inclusion complex 905
Anilinonaphthalenesulfonic acid reagent cation detn 211
Anilinopyridine rhodium complex oxidn redn spectroelectrochem 2805
Animal tissue analysis lead atomic absorption 1867
Anion chromatog chelation background suppression 122
Anion radical oligonucleotide mass spectra 2154
Anion selective electrode vitamin B12 based 499
Anion trace detn ion chromatog 939
Anniversary 25th Classic Paper editorial 885a
Announcement Pittsburg Conference Atlanta 139a
Anodic stripping voltammetry cadmium lead detn 2609
Anodic stripping voltammetry copper lead electrodeposition 856
Anodic stripping voltammetry flow metal 468
Anodic stripping voltammetry lead detn 2092
Antennule crab receptrode analysis review 533a
Antibiotic carboxylic polyether optical detector 382
Antibiotic cephalospolin micellar electrokinetic chromatog 2434
Antibiotic detection copper modified electrode 2258
Antibody detn protein G chromatog 1901
Antibody hapten complex phase fluorometry 309
Antidote cholinesterase inhibitor HPLC 728
Antigen detn protein G chromatog 1901
Antimony detn atomic emission spectrometry 1175
Antimycin A chromatog HPLC spectrometry NMR 404
Antioxidant lubricant detn platinum electrode 1467
Apolar diluent chiral stationary phase correction 2688
Apolar diluent effect chiral stationary phase 126
App cell immobilization 1656
App extn flavor juice 1596
App Kel F graphite electrode fabrication 2330
App mixing flow injection analysis 973
App supercrit fluid extn online phosphonate 1986
Aq phase ozone detn chemiluminescence 619
Aq soln aluminum speciation ion chromatog 535
Aqua aluminum complex detn ion chromatog 535
Aquatic fulvic acid structural feature 2792
Aquatic humic substance structure spectroscopy 628
Area surface modified silica gel 41
Argentometric titrn combined programmed flow analysis 2109
Argon bombardment redn arom oxime 1442
Argon detn oxygen gas chromatog 2237
Argon nitrogen quenching discharge plasma 326
Argon sepn oxygen chromatog chabazite adsorbent 1112
Argon sputtering gas atomic absorption spectroscopy 1652
Armstrong pseudophase theory thin layer chromatog 422
Arom aldehyde detn electrochem 2599
Arom amine ion mobility spectrometry 684
Arom compd detn multiphoton ionization 612
Arom hydrocarbon energy transfer micelle 1405
Arom hydrocarbon halogenated phosphorescence spectrometry 872
Arom hydrocarbon mass spectrometry 86
Arom hydrocarbon mol mechanics NMR spectra 2658
Arom hydrocarbon polycyclic thin layer chromatog 422
Arom hydrocarbon polynuclear cyclodextrin complex 955
Arom hydrocarbon polynuclear low temp phosphorimetry 1182
Arom hydrocarbon polynuclear room temp phosphorimetry 2328
Arom hydrocarbon TLC mass spectrometry 2516
Arom oxime redn argon bombardment 1442
Arom polycyclic hydrocarbon adsorption aerosol 708
Arom polycyclic hydrocarbon chromatog subambient temp 1749
Arom polycyclic hydrocarbon detn aerosol 320
Arom polycyclic hydrocarbon detn luminescence 2643
Arom polycyclic hydrocarbon detn water 1333
Arom volatile detn headspace gas chromatog 2584
Array electrode linear glassy carbon 2124
Array microelectrode electrochem detector chromatog 295
Array microhole oxygen electrode 159
Arrhenius parameter detn solid DSC DTG 1136
Arsenic compd dogfish ref material polemic 2116
Arsenic detn atomic absorption spectrometry 2079
Arsenic detn atomic emission spectrometry 1175
Arsenic detn river sediment atomic absorption 1414
Arsenide gallium acceptor detn Raman spectroscopy 994
Arsenocholine dogfish muscle polemic 2118
Arsine generation flow injection system 2079
Aryl amine eluent chromatog cation detn 1435
Ascending water electrode extn study 1621
Ascorbate detn brain electrode 2323
Ascorbate dopamine selectivity fiber electrode 1805
Ascorbic acid chromatog electrochem detector activation 1989
Ascorbic acid detn spectroelectrochem detector 1216
Ascorbic acid oxidn ferricyanide contg electrocatalyst 848
Ash incinerator chlorodibenzodioxin chlorodibenzofuran extn 2770
Asparagine rotamer microspeciation 2631
Aspartame detn food electrode correction 1472
Aspartic acid rotamer microspeciation 2631
Assocn methanol water chromatog retention 349
Atm org source identification gas chromatog 838
Atm pressure spray ionization mass spectrometry 1159
Atom fast bombardment mass spectrometry 153 1293
Atom metal detection multiphoton ionization 1010
Atomic absorption copper detn silicate rock 1427
Atomic absorption ethylation lead detn 1867
Atomic absorption flame spectrometry cation detn 1410
Atomic absorption graphite furnace slurry sample 1414
Atomic absorption spectrometer continuum source 1670
Atomic absorption spectrometry alloy analysis 1235
Atomic absorption spectrometry arsenic detn 2079
Atomic absorption spectrometry copper ligand estn 1295
Atomic absorption spectrometry electrothermal biol ref 216
Atomic absorption spectrometry Fourier transform 1694
Atomic absorption spectroscopy sputtering atomizer 1652

Atomic beam mass spectroscopy drug 1087
Atomic emission droplet signal fluctuation 2002
Atomic emission plasma thermal gradient HPLC 236
Atomic emission sample direct insertion plasma 163
Atomic emission spectrometry analysis hydride generation 1175
Atomic emission spectrometry copper lead electrodeposition 856
Atomic emission spectrometry fluoride detn 674
Atomic emission spectrometry hydride generation online 285
Atomic emission spectrometry sulfite detn 272
Atomic emission sulfite detection HPLC 272
Atomic force microscopy review 243r
Atomic spectrometry inorg analysis review 109r
Atomic spectrometry nonmetal analyte introduction device 790
Atomic spectrometry thimble glass frit nebulizer 2777
Atomization mechanism copper graphite furnace 2652
Atomizer sputtering atomic absorption spectroscopy 1652
Auger electron spectroscopy quantitation review 469a
Auger Electron Spectroscopy (book review) 1164a
Automated diln flow injection technique 1773
Automated discontinuous programmed flow analyzer 2109
Automated online ion exchange trace enrichment 520
Automated segmented flow electrochem analyzer 2102
Automated slurry sample introduction sediment analysis 1414
Automated solute independent calibration chromatog 1915
Automated structure detn NMR 2298
Automatic Methods of Analysis (book review) 547a
Automation analytical lab intelligent robot review 805a
Available chlorine detn flame IR emission 2785
Avidin biotin fiber optic sensor 1069
Azo dye chromatog mass spectra 2054
Bacitracin countercurrent chromatog 1998
Background subtraction electron microprobe analysis 1612
Background suppression chelation anion chromatog 122
Bacteria class identification mass spectrometry 715
Bacteria identification immobilization aminopeptidase 1656
Band broadening flow injection analysis 107
Band profile ideal chromatog model 462
Barium yttrium copper oxide stoichiometry detn 1497
Basalt analysis rare earth mass spectrometry 755
Base acid reaction chromatog background suppression 122
Base solubilizer cyclodextrin 275
Basophilic leukemia cell cyclic voltammetry 2471
Bayes probability data analysis shot noise 2483
Benzaldehyde detn electrochem carbon paste electrode 2599
Benzene alkyl deriv liq chromatog 1524
Benzene analysis aniline flow injection 496
Benzene deriv HPLC retention prediction 367
Benzene deriv isomer mass spectra 1889
Benzene deriv isomer thin layer chromatog 422
Benzene detn near IR Raman spectrometry 2647
Benzil dioxime cobalt complex polarog 2178
Benzo crown ether polymer membrane electrode 1618
Benzocrown immobilized ionophore potassium detn 211
Benzodiazepine ion mobility spectrometry 343
Benzofluoranthene isomer identification fluorometry 580
Benzopyrenetetrol fluorescence silica enhancer 2766
Benzothiazolium dye trace detn 861
Beverage sucrose detn 782
Bias detn analytical method robust statistics 1942
Bias UV calibration curve diode array 2571
Bicarbonate detn ion selective electrode coupled 638
Bidentate silane modified silica packing HPLC 2
Binary diffusion coeff 118
Binary eluent chromatog band profile 2373
Binary eluent retention chromatog 2380
Binary mixt analysis EXAFS 1686
Binding org cation surface fluorescence 590
Binning spectral image CCD 1513
Binuclear anilinopyridine rhodium oxygen electroredn 279
Biog Kolthoff 287a
Biol analysis nitrate nitrite 2715
Biol analysis salicylate membrane electrode 566
Biol analysis selenium HPLC fluorometry 233
Biol surface analysis ESCA review 589a
Biomol capillary electrophoresis review 292a
Biomol electrophoresis fluorescence CD detector 1344
Biomol interface liq chromatog mass spectroscopy 1577
Biomol ion trap mass spectroscopy 2316
Biomol isoelec focusing immobilized gradient review 1602
Biomol mass spectroscopy 2504
Biomol TLC laser desorption detection 1911
Biopolymer capillary electrophoresis review 292a
Biosensor enzyme based conductometric transducer 1737
Biosensor neuronal review 533a
Biosensor piezoelec immunol kinetic immunoassay 1227
Biotin avidin fiber optic sensor 1069
Biotin detn EIA pyruvate carboxylase 2160
Biotin detn enzyme linked binding assay 1728
Biotin europium chelate immunoassay 48
Biphenyl chlorinated HPLC soil 1300
Bitumen characterization review 165r
Biuret reaction peptide electrochem detection 2664
Black beetle virus structure 1341a
Bleach analysis chlorine flame IR emission 2785
Blend polymer analysis review 214r
Blood analysis bromide iodide gas chromatog 733
Blood analysis nitrate nitrite 2715
Blood carbon dioxide potassium detn 2365
Blood cyclophosphamide enantiomer detn HPLC 441
Blood drug detn chromatog silica support 2445
Blood glucose detn 2009
Blood interleukin 2 detn immunobioassay 1732
Blood methotrexate detn HPLC 946
Blood plasma analysis IR spectrometry 2016
Blood protein isoelec focusing review 1602
Blood selenium detn HPLC fluorometry 2244
Blood theophylline detn HPLC 784
Blood trace element mass spectroscopy 1851
Blood vessel growth angiogenin review 1173a
Blood zinc isotope detn 2757
Body fluid cAMP cGMP detn 447
Body fluid glucose detn electrode 2566
Body fluid methotrexate liq chromatog 946
Bombardment fast atom mass spectrometry 153 1293
Bonded phase column packing HPLC 2
Bonding density stationary phase partition 930
Bootstrap algorithm estg error confidence limit 2324
Borate reagent alc carbohydrate conductometric detection 631
Boric acid reagent alc carbohydrate detection 631
Boron implanted silicon wafer analysis SIMS 1946
Brain ascorbate dopamine detn electrode 2323
Brain tryptamine detn 2316
Brine analysis bromide iodide gas chromatog 733
Brine analysis hydroxide ion IR spectrometry 1419
Bromide detn gas chromatog iodide simultaneous 733
Bromocresol green detn spectroelectrochem detector 1216
Bubble segmented stream analysis potentiometry 504
Buffer gas carbon dioxide mass spectrometry 2523
Buffer HEPES dissocn const pH detn 1400
Buffer isoelec focusing biomol review 1602
Butadiene coked zeolite catalyst NMR 1821
Butter glyceride detn 698
Butylamide lauroylvaline chiral phase chromatog 126
Butyltin detn sediment std mass spectrometry 2320
Butyraldehyde detn electrochem carbon paste electrode 2599
C reactive protein detn electrode 2362
Cadmium detn anodic stripping voltammetry 2609
Cadmium detn plasma mass spectrometry 2031
Cadmium detn segmented flow voltammetry 2102
Cadmium dithizone extn mechanism electrochem 1621
Cadmium membrane neutral carrier transport 1140
Cadmium sulfide crystal face specific electrode 1980
Calcium chabazite adsorbent gas chromatog 1112
Calcium detn multiphoton ionization spectrometry 1010
Calcium detn optical fiber detector 382
Calibration automated solute independent chromatog 1915
Calibration curve UV bias nonlinearity 2571
Calibration liq chromatog thermospray mass spectrometry 2126
Calibration multivariate plasma mass spectrometry 2031
Calibration pipet statistics 1080
Calorimeter glucose enzyme sensor model 77
cAMP detn EIA tissue 447
Canonical correlation rank estn emission 2219
Capacitance electrode dopamine adsorption 2603
Capacity factor reversed phase liq chromatog 1524
Capacity ratio calcn liq chromatog 2428
Capillary column aluminum clad resistively heated 2410
Capillary column octylsilyl packed HPLC 1128
Capillary electrophoresis biomol neurochem review 292a
Capillary electrophoresis fluorescence CD biomol 1344
Capillary electrophoresis online radioisotope detector 1642
Capillary electrophoresis peptide protein 1186
Capillary gas chromatog water detn 1325
Capillary isotachophoresis mass spectrometry 228
Capillary microbore chromatog detector fiber optics 876
Capillary supercrit chromatog pressure regulated restrictor 1178
Capillary supercrit fluid chromatog org 1208
Capillary zone electrophoresis amino acid detn 37
Capillary zone electrophoresis carboxylic acid detn 766
Capillary zone electrophoresis ionic compd 2434
Capillary zone electrophoresis peptide mapping 2226
Capillary zone electrophoresis refractive index detection 1590
Capillary zone electrophoresis serotonin catecholamine sepn 98
Capillary zone electrophoresis temp gradient effect 241
Carbohydrate analysis HPLC polarimetry 1238
Carbohydrate detection copper modified electrode 2258
Carbohydrate HPLC amperometric detection 852
Carbohydrate HPLC conductometric detection model 631
Carbon activated adsorbent contg diffusive sampler 843
Carbon adsorption polycyclic arom hydrocarbon 708
Carbon black contg vinylpyridine copolymer electrode 848

Carbon dioxide amperometric detn air 577
Carbon dioxide analysis carbon hydrogen isotope 2149
Carbon dioxide buffer gas mass spectrometry 2523
Carbon dioxide detector fermentor piezoelec crystal 746
Carbon dioxide detn air 2416
Carbon dioxide detn blood 2365
Carbon dioxide doped plasma detector chromatog 1815
Carbon dioxide electrode bicarbonate carbonate 638
Carbon dioxide supercrit adsorption silica 951
Carbon dioxide supercrit extn ash 2770
Carbon dioxide supercrit extn org 736
Carbon dioxide supercrit microdisk electrode voltammetry 2193
Carbon dioxide supercrit voltammetric detection microelectrode 270
Carbon electrode copper coated sugar detection 852
Carbon electrode ethylene pyrolysis nickel 560
Carbon electrode glassy pyrolytic activation 2603
Carbon electrode phosphatidylcholine modified 979
Carbon fiber electrode acetylpenicillamine thionitrite detn 1954
Carbon fiber electrode amine HPLC 1469
Carbon fiber electrode composite copolymer 1460
Carbon fiber epoxy microhole array electrode 1763
Carbon fiber microelectrode fabrication 1805
Carbon fiber microhole oxygen electrode 159
Carbon fiber oxidn product analysis 1017
Carbon glassy amperometry electrode cupric hexacyanoferrate 2594
Carbon glassy electrode detector laser activation 1989
Carbon glassy electrode Eastman AQ 1397
Carbon glassy linear array electrode 2124
Carbon hollow tube gas chromatog org 838
Carbon isotope detn light hydrocarbon 2149
Carbon isotope detn org combustion 1996
Carbon monoxide detn air exhaust 671a
Carbon NMR arom hydrocarbon simulation 2658
Carbon paste electrode modified rhodium complex 279
Carbon paste electrode polychlorotrifluoroethylene mulling oil 2585
Carbon paste modified electrode aldehyde detn 2599
Carbon proton magnetization transfer NMR 2298
Carbon total inorg detn water 1841
Carbon vitreous polypyrrole coated phase HPLC 2391
Carbon vitreous polypyrrole electrochem coated phase 198
Carbon 13 NMR spectral simulation 1115a
Carbon 13 NMR zeolite catalyst 1821
Carbon 13 std internal NMR 2579
Carbonaceous deposit analysis zeolite catalyst NMR 1821
Carbonate detn ion selective electrode coupled 638
Carbowax 20M pyrazine retention index modeling 1328
Carboxylase pyruvate biotin detn EIA 2160
Carboxylic acid detn capillary zone electrophoresis 766
Carboxylic acid detn IR spectroscopy 1260
Carboxylic polyether antibiotic optical detector 382
Carboxymethyldithiocarbamate reagent trace metal sepn 149
Carcinogenesis fluorescence line narrowing spectroscopy review 1023a
Casein peptide mapping 2226
Catalase glucose sensor thermoelec model 77
Catalase immobilized conductometric transducer biosensor 1737
Catalyst Nafion water detn gas chromatog 1325
Catalyst reforming analysis chloride ion chromatog 1924
Catalyst simultaneous detn inhibition kinetic 2551
Catalyst zeolite carbonaceous deposit analysis NMR 1821
Catalytic adsorption polarog cobalt ultratrace detn 2178
Catalytic preceding following chem reaction voltammetry 965
Catechol redox reaction carbon electrode 560
Catechol voltammetry Nafion coated microdisk electrode 2193
Catecholamine sepn serotonin capillary zone electrophoresis 98
Catheter electrode blood analysis 2365
Cathode dual discharge lamp emission spectrometry 2137
Cation detn Donnan dialysis preconcn 1410
Cation detn nonsuppressed ion chromatog 1435
Cation electroinactive detector Prussian Blue 290
Cation exchange liq chromatog protein 2059
Cation exchange resin electrode modification 508
Cation luminescence detector 211
Cation org binding surface fluorescence 590
Cation sepn open tubular liq chromatog 2747
Cation transport macrocycle liq membrane 1140
Caustic analysis hydroxide ion IR spectrometry 1419
CCD binning spectral image 1513
CD analytical application review 77a
CD fluorescence detector electrophoresis biomol 1344
Cell analysis magnesium microelectrode 574
Cell electrochem rotating disk biol 2803
Cell immobilization app 1656
Cell ion cyclotron resonance mass spectrometer 53
Cell potentiometry continuous flow analysis 504
Cell single amino acid detn 436
Cell spectroelectrochem thin layer 1787
Cell spectroelectrochem thin layer transmittance 190
Cell two section ion cyclotron resonance 83
Cell wall streptococcus detn mammal tissue 265
Cellulose acetate membrane electrode biochem 303
Cellulose evapn device liq SIMS 2582
Censored measurement statistical estn 2719
Cephalospolin antibiotic micellar electrokinetic chromatog 2434
Ceramic piezoelec detector laser radiation 796
cGMP detn tissue EIA 447
Chabazite calcium adsorbent gas chromatog 1112
Characterization shale oil review 165r
Charge coupled detector fluorometer 282
Charge coupled device Raman spectrometer 2647
Charge exchange mass spectrometer 1874
Chelation background suppression anion chromatog 122
Chelator europium label fluorescence immunoassay 48
Chelex 100 resin transition metal enrichment 520
Chem analysis accuracy algorithm 398
Chem analysis target factor analysis 1168
Chem bonded liq crystal HPLC phase 1928
Chem change acoustic emission 2638
Chem ionization laser desorption mass spectrometry 184
Chem ionization mass spectrometer 1874
Chem ionization mass spectrometry 86
Chem reaction interface mass spectroscopy 2724
Chem sensor waveguide application review 1079a
Chem Sensors (book review) 92a
Chemiluminescence detection laser microprobe elemental analysis 2557
Chemiluminescence detection organosulfur supercrit fluid chromatog 797
Chemiluminescence detector sulfur universal 1268
Chemiluminescence detn iodine 2800
Chemiluminescence detn polyamine 1921
Chemiluminescence electrogenerated graphite electrode heterogeneity 2763
Chemiluminescence flow injection copper cyanide detn 1505
Chemiluminescence manganese detn seawater 1392
Chemiluminescence measurement dual channel detector 593
Chemiluminescence nitrite nitrate detn 2715
Chemiluminescence ozone detn aq phase 619
Chemiluminescence phosphate detn 2699
Chemisorbed monolayer analysis absorption spectrometry 386
Chemometrics expert system mass spectrometry 715
Chemometrics. A Textbook (book review) 1037a
Chiral diamide diln amino acid resoln 126
Chiral mixed micelle optical resoln 1984
Chiral polysiloxane gas chromatog stationary phase 2121
Chiral reagent polymeric fluorenylmethyl amino acid 1548
Chiral stationary phase apolar diluent effect 126
Chiroptical technique analytical application review 77a
Chloramine interference chlorine detn water 991
Chloride chromatog solute independent calibration 1915
Chloride detn near IR spectrometry 1419
Chloride detn reforming catalyst ion chromatog 1924
Chloride detn water argentometry 2109
Chloride detn water flame IR emission 2785
Chloride effect lead cadmium detn voltammetry 2609
Chloride hydrogen detection zinc quartz resonator 1559
Chlorinated biphenyl dibenzodioxin dibenzofuran HPLC soil 1300
Chlorination wastewater nitrogen chloride detn 2332
Chlorine available detn flame IR emission 2785
Chlorine detection radio frequency plasma chromatog 1815
Chlorine detn water chloramine interference 991
Chlorodibenzodioxin detn fish 1678
Chlorodibenzodioxin extn ash supercrit fluid 2770
Chlorodibenzofuran extn ash supercrit fluid 2770
Chlorophenol detn voltammetry 2809
Chlorophenyl oxalate hydrogen peroxide stability 1298
Cholesterol detn serum 1718
Cholinesterase inhibitor antidote HPLC 728
Chondrule analysis rare earth mass spectrometry 755
Chromatog adsorption trace metal preconcn 149
Chromatog anion chelation background suppression 122
Chromatog automated solute independent calibration 1915
Chromatog biomol detection 1911
Chromatog bonded phase prepn 2067
Chromatog cation exchange liq protein 2059
Chromatog column decompn peroxyacetyl peroxypropionyl nitrate 2731
Chromatog column metal interference removal 468
Chromatog countercurrent bacitracin 1998
Chromatog cyclodextrin complex formation const 955
Chromatog detector capillary microbore fiber optics 876
Chromatog displacement liq mass transfer 1960
Chromatog effluent mol formula detn 2207
Chromatog electrochem gas detector 584
Chromatog electrokinetic band broadening 251
Chromatog electrokinetic capillary micelle 2455
Chromatog electrokinetic micellar ionic compd 2434
Chromatog electrokinetic optical resoln 1984
Chromatog elution particle size review 143r
Chromatog elution profile high concn 462
Chromatog Enantioseparation. Methods and Applications (book review) 1043a
Chromatog equil theor plate model 1937
Chromatog exclusion gel hydrophobicity 780
Chromatog gas alanine cell wall 265
Chromatog gas alkene insect 1564
Chromatog gas alkyl peroxyalkanoyl nitrate 771
Chromatog gas aluminum detn seawater 544
Chromatog gas calcium chabazite adsorbent 1112
Chromatog gas capillary water detn 1325
Chromatog gas carbon hollow tube org 838
Chromatog gas chlorodibenzodioxin 1678
Chromatog gas cholesterol detn 1718
Chromatog gas compact probe 2410

Chromatog gas coupling TLC laser desorption 1906
Chromatog gas detection photodiode array spectrophotometer 1249
Chromatog gas detector sulfur compd 1268
Chromatog gas detn carbon hydrogen isotope 2149
Chromatog gas Fourier IR digital filtering 1073
Chromatog gas Fourier IR mass spectrometry 1584
Chromatog gas glyceride 698
Chromatog gas headspace volatile arom detn 2584
Chromatog gas juice flavor 1596
Chromatog gas linked spectrometry analysis 1571
Chromatog gas mass spectrometry coupling 2402
Chromatog gas mass spectrometry differential 73 2118
Chromatog gas mass spectrometry polyarom hydrocarbon 2669
Chromatog gas mass spectroscopy radiolabeled metabolite 2724
Chromatog gas molinate ELISA 819
Chromatog gas norcarboxytetrahydrocannabinol urine forensic 925
Chromatog gas open tubular 2165
Chromatog gas oxygen analysis impurity 2237
Chromatog gas peak shape injection method 1489
Chromatog gas pyrazine computerized retention prediction 1328
Chromatog gas resoln chiral stationary phase 2121
Chromatog gas resoln stationary phase diln 126
Chromatog gas retention index extrapolation 88
Chromatog gas zone 1478
Chromatog gel microcolumn polymer 961
Chromatog gel polyethylene terephthalate 1321
Chromatog gel polymer solvent elimination 458
Chromatog glycoprotein temp programmed elution 1117
Chromatog HPLC antimycin A 404
Chromatog ion aluminum aq soln speciation 535
Chromatog ion chloride detn reforming catalyst 1924
Chromatog ion direct current cond detector 1383
Chromatog ion electrodialysis membrane suppressor 939
Chromatog ion exclusion nitrite detn 1485
Chromatog ion exclusion weak acid detection 548
Chromatog ion nonsuppressed cation detn 1435
Chromatog ion pair system peak 1109
Chromatog ion stopped flow chronoamperometric detector 1387
Chromatog ion suppressed potentiometric pH detection 787
Chromatog liq alc carbohydrate conductometric detection 631
Chromatog liq amine detn 1469
Chromatog liq amine trace derivatization reagent 1538
Chromatog liq amino acid coulometric detection 555
Chromatog liq amino acid detn 432
Chromatog liq benzene deriv retention 367
Chromatog liq biomol mass spectrometry 2504
Chromatog liq bonded phase column packing 2
Chromatog liq bonded stationary phase 1928
Chromatog liq capacity ratio calcn 2428
Chromatog liq capillary column octylsilyl packed 1128
Chromatog liq carbohydrate amperometric detection 852
Chromatog liq carbohydrate detection modified electrode 2258
Chromatog liq carbon paste electrode 2585
Chromatog liq chiroptical detector review 77a
Chromatog liq chlorinated biphenyl dibenzodioxin dibenzofuran 1300
Chromatog liq cyclophosphamide chiral deriv prepn 441
Chromatog liq detector diode laser polarimeter 1238
Chromatog liq detector linearity evaluation 951a
Chromatog liq electrochem detection peptide detn 2664
Chromatog liq elution profile calcn 2380
Chromatog liq enantiomeric amine amino alc 1548
Chromatog liq fatty acid detection 910
Chromatog liq glassy carbon electrode activator 1989
Chromatog liq gradient elution voltammetric detection 1977
Chromatog liq high concn band 2373
Chromatog liq homopolymer oligomer sepn 471
Chromatog liq hydroxamic acid siderophore detn 1474
Chromatog liq IgG detn protein A 1314
Chromatog liq imirestat phenytoin serum protein 1171
Chromatog liq inorg analysis review 109r
Chromatog liq interface mass spectroscopy biomol 1577
Chromatog liq jet fuel characterization 206
Chromatog liq mass spectrometry spray ionization 1159
Chromatog liq metal ion detn 1272
Chromatog liq methotrexate body fluid 946
Chromatog liq micelle mobile phase 1353
Chromatog liq microelectrode array detector 295
Chromatog liq nerve analysis 436
Chromatog liq NMR cyclopropyl oxazoline 772
Chromatog liq online diln 1791
Chromatog liq open tubular cation sepn 2747
Chromatog liq polyamine 1921
Chromatog liq polymeric stationary phase 198
Chromatog liq polypyrrole stationary phase 2391
Chromatog liq preconcn flow injection analysis 496
Chromatog liq protein aggregation 514
Chromatog liq protein variant 1742
Chromatog liq quaternary ammonium compd 728
Chromatog liq quinone photoredn fluorescence detection 2267
Chromatog liq retention mechanism 930
Chromatog liq reversed phase retention correlation 1524
Chromatog liq selectivity modification subambient temp 1749
Chromatog liq selenium blood 2244
Chromatog liq selenium detn fluorometric detection 233
Chromatog liq silica support drug blood 2445
Chromatog liq silylated silica gel phase 41
Chromatog liq solute partition aq phase 2540
Chromatog liq spectrometry halogen detector 895
Chromatog liq sulfite detn 272
Chromatog liq surface enhanced Raman detection 888
Chromatog liq target factor analysis 1168
Chromatog liq theophylline blood 784
Chromatog liq thermal gradient 236
Chromatog liq thermospray mass spectrometry calibration 2126
Chromatog liq time domain differentiation computer 720
Chromatog liq UV detector bias nonlinearity 2571
Chromatog mass spectra azo dye 2054
Chromatog micellar liq hydrophobicity 1040
Chromatog microcapillary hydrodynamic copolymer micelle 1318
Chromatog mobile phase elimination IR 2212
Chromatog nickel detn urine 1099
Chromatog optimization theory 1276
Chromatog partition gas liq interphase 2231
Chromatog peak moment reproducibility nonstochastic 1058
Chromatog peptide mapping 2226
Chromatog pioneer Laszlo Zechmeister 1315a
Chromatog polynomial least squares smoothing 1303
Chromatog polystyrene elution retention 2449
Chromatog preparative elution optimization 1368
Chromatog preparative liq optimization 982
Chromatog protein G antibody detn 1901
Chromatog pulsed amperometry alkanolamine detn 2466
Chromatog retention methanol water assocn 349
Chromatog sepn styrene acrylate copolymer 2171
Chromatog size exclusion sodium polystyrenesulfonate 530
Chromatog spectrometry overlapped peak detection 2240
Chromatog spruce needle analysis 221
Chromatog sulfur detn coal liq 2292
Chromatog supercrit adsorption stationary phase 951
Chromatog supercrit fluid detector voltammetric 2193
Chromatog supercrit fluid element selective detector 1815
Chromatog supercrit fluid fatty acid detn 2076
Chromatog supercrit fluid flame photometric detection 2616
Chromatog supercrit fluid Fourier IR coupling 2212
Chromatog supercrit fluid mass spectrometry 775
Chromatog supercrit fluid online extn system 1986
Chromatog supercrit fluid organosulfur chemiluminescence detection 797
Chromatog supercrit fluid photometric detection organosulfur 58
Chromatog supercrit fluid restrictor modeling 356
Chromatog supercrit fluid stationary phase solvation 1348
Chromatog supercrit fluid thermionic detector optimization 2082
Chromatog supercrit FTIR propellant 145
Chromatog supercrit pressure regulated restrictor 1178
Chromatog supercrit voltammetric detection microelectrode 270
Chromatog thin layer diazonaphthoquinone detn 615
Chromatog thin layer laser fluorometric detection 1931
Chromatog thin layer mass spectrometry coupling 2516
Chromatog thin layer modern review 1257a
Chromatog thin layer porphyrin methyl ester 2288
Chromatog thin layer urea cyclodextrin phase 422
Chromatograph gas interface mass spectrometer cell 1874
Chromatograph ion online diln 1791
Chrome Azurol S immobilization polymer 1674
Chromium cobalt alloy prosthetic tissue 1235
Chromium detn dual cathode discharge lamp 2137
Chromosorb XAD hydrocarbon detn water 1333
Chronoamperometric detector stopped flow ion chromatog 1387
Chronoamperometry diffusion cyclic voltammetry microelectrode 1630
Chronoamperometry ferrocyanide ferricyanide couple 1211
Chronoamperometry microelectrode array detector 295
Chronoamperometry polychlorotrifluoroethylene graphite composite microelectrode 2330
Cigaret analysis org chromatog factor analysis 838
Citrato aluminum complex detn ion chromatog 535
Citric acid titrn conductometric 177
Classification analysis computer 2098
Classification expert system mass spectra 715
Clay mineral sorption org vapor 2047
Clin application laser review 1367a
Clin chem chiroptical analysis review 77a
Cluster ion calibration chromatog mass spectrometry 2126
Coal liq petroleum analysis review 165r
Coal liq sulfur detn chromatog 2292
Coal sampling analysis review 84r
Coated wire electrode response selectivity 2341
Coating electrode pyrazine deriv polymer ligand 1799
Coaxial continuous flow spectroscopy biomol 2504
Cobalt chloride relative humidity sensor 1863
Cobalt chromium alloy prosthetic tissue 1235
Cobalt phthalocyanine polyvinylpyridine electrode modification 508
Cobalt porphyrin nitrite selective electrode 1169
Cobalt ultratrace detn adsorption catalytic polarog 2178

Coeff current equation spherical segment microelectrode 1305
Coeff variation concn statistical justification 1465
Coil surface fabrication NMR in vivo 636
Coiled straight tube extn kinetics 101
Coke sampling analysis review 84r
Collagen film based conductometric transducer biosensor 1737
Collection mode electrode micro substrate 132
Collision cell mass spectrometer interface chromatograph 1874
Colloid particle size detn sedimentation 741
Colorimetry PCB detn transformer oil 2682
Column capillary aluminum clad resistively heated 2410
Column chromatog metal interference removal 468
Column packing bonded phase HPLC 2
Column polymer bound tetrahydroborate arsine generation 2079
Column short open tubular chromatog spectrometry 2402
Column temp HPLC fenvalerate isomer 1149
Column void vol system peak 2428
Combustion carbon isotope detn org 1996
Compact probe gas chromatog 2410
Complex indium propene reagent chem ionization 86
Complexation capacity soil estn 1295
Complexation metal humic substance model 483
Complexing reagent transition metal elution 520
Composite electrode carbon fiber copolymer 1460
Composite electrode styrene vinylbenzene vinylpyridine copolymer 848
Composite microelectrode polychlorotrifluoroethylene graphite chronoamperometry 2330
Computer aided time domain differentiation HPLC 720
Computer classification analysis 2098
Computer controlled operation mass spectrometer 330
Computer NMR surface coil fabrication 636
Computer program classification mass spectrometry 715
Computer program mass spectrometry identification 73
Computer simulation copper atomization graphite furnace 2652
Computer simulation protein electrophoresis 362
Computerized retention prediction pyrazine gas chromatog 1328
Computer-Enhanced Analytical Spectroscopy (book review) 857a
Con A affinity chromatog glycoprotein 1117
Concn interlab coeff variation statistical justification 1465
Concn profile cylindrical microelectrode spectroscopy 2347
Cond detection anion chromatog background suppression 122
Cond detection chromatog cation detn 1435
Cond detection solute independent calibration 1915
Cond oncolumn detection carboxylic acid detn 766
Conducting insulating substrate feedback mode 132
Conductive insulating sample electrode ultramicro microscopy 1221
Conductometric detection model alc carbohydrate HPLC 631
Conductometric titrn polyprotic acid 177
Conductometric transducer enzyme based biosensor 1737
Conductometry total mercury detn 1230
Conductor org electrode ultramicroelectrode array 1048
Confluent mixing optimization flow injection analysis 973
Conical hemispherical ultramicroelectrode fabrication 1630
Conjugated diene detn gasoline polarog 1502
Contaminant detn diffusive sampling quadratic model 917
Continuous flow analysis potentiometry cell 504
Continuous flow fast atom bombardment spectroscopy 1310
Continuous flow liq SIMS evapn device 2582
Continuous flow liq SIMS polar compd 1013
Continuum source atomic absorption spectrometer 1670
Continuum source Fourier atomic absorption spectrometry 1694
Controlled release fluorescent dye pH sensor 174
Convergence quadratic simplex algorithm culminating polemic 1783 1786
Convolution correlation analysis spectra noise 898
Convolution smoothing polynomial least squares analysis 1303
Cooling device sample moving belt phosphorimetry 1182
Copolymer electrode composite carbon fiber 1460
Copper atomization mechanism graphite furnace 2652
Copper barium yttrium oxide stoichiometry detn 1497
Copper coated carbon electrode sugar detection 852
Copper detn chemiluminescence uranin sensitized 1505
Copper detn iron titanium present spectrophotometry 1847
Copper detn laser microprobe chemiluminescence detection 2557
Copper detn multiphoton ionization spectrometry 1010
Copper detn silicate rock atomic absorption 1427
Copper electrode conductometric transducer biosensor 1737
Copper electroredn ferrocyanide redox reaction 508
Copper emission quenching glow discharge plasma 326
Copper equilibration soil ligand estn 1295
Copper lead preconcn electrodeposition spectrochem analysis 856
Copper modified electrode carbohydrate detection 2258
Copper oxide tube carbon isotope detn 1996
Copper pyridine surface Raman 1648
Copyright transfer Issue 1 95
Coronaspray ion mobility spectrometry liq analysis 601
Correction apolar diluent chiral stationary phase 2688
Correction aspartame detn food electrode 1472
Correction field flow fractionation small solute 90
Correction hapten antibody complex phase fluorometry 1472
Correction isoelec focusing field flow fractionation 2224
Correction micellar enhancement fluorescence thermal lensing 928
Correction optimization preparative elution chromatog 2464
Correction overtake phenomena temp gas chromatog 512
Correction rare earth fluorometry thermal lensing 928
Correction review NMR imaging 358a
Correlation convolution analysis spectra noise 898
Correlation cross EXAFS binary mixt analysis 1686
Coulometric detection amino acid liq chromatog 555
Countercurrent chromatog bacitracin 1998
Countercurrent Chromatog: Theory and Practice (book review) 655a
Counting single photon luminescence lifetime 2704
Coupling supercrit fluid chromatog Fourier IR 2212
Crab antennule receptrode analysis review 533a
Crater erosion spark produced analysis 1826
Cresol detn voltammetry 2809
Cross correlation EXAFS binary mixt analysis 1686
Cross polarization NMR zeolite catalyst 1821
Crosslinked plastic analysis 802
Crown benzo ether polymer membrane electrode 1618
Crown ether phosphate protein detn 2362
Crude oil analysis chromatog IR spectrometry 1584
Crystal face specific cadmium sulfide electrode 1980
Crystal quartz microbalance cation detector soln 290
Culminating simplex algorithm quadratic convergence polemic 1783 1786
Cupric hexacyanoferrate glassy carbon amperometry electrode 2594
Curie point gas chromatog plant 221
Current direct cond detector ion chromatog 1383
Current equation coeff spherical segment microelectrode 1305
Current potential curve kinetics electrode reaction 2249
Current transient neutral carrier membrane 1624
Curve fitting Fourier transform IR spectra 2708
Cyanide detn chemiluminescence uranin sensitized 1505
Cyanide iron aminopyridine carbon paste electrode 2599
Cyanobenzylideneoctyloxyaniline mesophase orientation interaction coated silica 1534
Cyanoferrate charge transport quaternized polyvinylpyridine 570
Cyanoferrate electroredox kinetics laser modified graphite 1637
Cyanoferrate redox microhole array electrode 1763
Cyanuric chloride reagent fiber optic sensor 202
Cyclic staircase voltammetry cylindrical microelectrode 1211
Cyclic staircase voltammetry theory reaction 2249
Cyclic voltammetry basophil allergy detection 2471
Cyclic voltammetry chronoamperometry diffusion microelectrode 1630
Cyclic voltammetry theory electrode microhole array 1763
Cyclindrical electrode diffraction spectroelectrochem detector 1216
Cyclodextrin complex formation const chromatog 955
Cyclodextrin fluorescence probe inclusion complex 905
Cyclodextrin salt matrix luminescence analysis 2643
Cyclodextrin solubilization use analysis 275
Cyclodextrin urea solubilized mobile phase TLC 422
Cyclohexanone alkyl NMR simulation 863
Cyclophosphamide enantiomer detn blood HPLC 441
Cyclopropylmethylaminooxazoline drug detn HPLC NMR 772
Cyclotron ion resonance spectrometry Fourier transform 83
Cyclotron resonance ion Fourier transform 2040
Cyclotron resonance ion mass spectrometer 330 2528
Cyclotron resonance ion mass spectrometry 428
Cyclotron resonance mass spectrometer ion trap 1288
Cylindrical microelectrode concn profile spectroscopy 2347
Cylindrical microelectrode voltammetry analysis 1211
Cysteine penicillamine redox reaction 508
Cysteine stripping reagent transition metal 520
D micellar electrokinetic chromatog methylamine 491
Dansyl methylamine sepn deuteromethylamine chromatog 491
Data acquisition microcomputer master slave arrangement 593
Data analysis shot noise distribution function 2479
Data analysis shot noise limit 2483
Data distribution analytical statistical estn 2719
Data processing algorithm digital smoothing filter 1308
Deaminase adenosine biotin binding assay 1728
Decalone alkyl NMR simulation 863
Decay analysis time resolved fluorescence spectrometry 2310
Decay data kinetics luminescence 660
Decay single exponential rapid lifetime detn 30
Decompn peroxyacetyl peroxypropionyl nitrate chromatog column 2731
Decompn thermal organometallic compd nickel 560
Dehydrogenase substrate detn NADH oxidase 25
Delrin internal std NMR spectrometry 2579
Density polymer latex sedimentation fractionation 1934

Deposit carbonaceous analysis zeolite catalyst NMR 1821
Derivatization dimethyl disulfide alkene biochem 1564
Desorption adsorption model ion selective electrode 453
Desorption cyanobenzylideneoctyloxyaniline silane deriv silica 1534
Desorption kinetics copper graphite furnace 2652
Desorption laser chem ionization mass spectrometry 184
Desorption laser coupling gas chromatog TLC 1906
Desorption laser ionization mass spectrometer 1083
Desorption mass spectrometry review 1201a
Desorption plasma mass spectroscopy protein 375
Desorption polycyclic arom hydrocarbon aerosol 708
Desorption spectroscopy surface characterization review 243r
Detection flame photometric supercrit fluid chromatog 2616
Detection fluorescence photoredn quinone HPLC 2267
Detection HPLC whole column 2624
Detection multichannel heterodyne mass spectrometry 749
Detection plasma atomic emission sulfur 2292
Detection time filtering fluorometry analysis 2611
Detector charge coupled fluorometer 282
Detector chiroptical liq chromatog review 77a
Detector diode array bias nonlinearity 2571
Detector direct current cond ion chromatog 1383
Detector discrimination ion microscopy image quantification 65
Detector dual multichannel mol absorption luminescence 593
Detector electrochem microelectrode array chromatog 295
Detector electrode glassy carbon laser activation 1989
Detector electroinactive cation Prussian Blue 290
Detector flame photometric optimization organosulfur 58
Detector fluorescence CD electrophoresis biomol 1344
Detector gas chromatog electrochem 584
Detector IR photoconductive chloride chlorine detn 2785
Detector laser radiation piezoelec ceramic 796
Detector liq chromatog linearity evaluation 951a
Detector luminescence cation 211
Detector optical fiber magnesium calcium detn 382
Detector optical rotation HPLC online analysis 1238
Detector radio frequency plasma supercrit chromatog 1815
Detector radioisotope capillary electrophoresis 1642
Detector spectroelectrochem flow through 1216
Detector stopped flow chronoamperometric ion chromatog 1387
Detector thermionic optimization supercrit fluid chromatog 2082
Detector trap pseudomol ion mass spectra 1983
Detector voltammetric supercrit fluid chromatog 2193
Detector wall jet flow injection analysis 922
Detn simultaneous catalyst inhibition kinetic 2551
Deuteromethylamine dansyl methylamine sepn chromatog 491
Device evapn continuous flow liq SIMS 2582
Dexamethasone succinylcholine detn forensic 53a
Dialysis Donnan preconcn cation detn 1410
Diamide chiral diln amino acid resoln 126
Diazonaphthoquinone detn TLC IR spectrometry 615
Dibenzocrown amphetamine selective electrode 2189
Dibenzodioxin chlorinated HPLC soil 1300
Dibenzodioxin chloro detn fish 1678
Dibenzofuran chlorinated HPLC soil 1300
Dicarboxylic acid titrn conductometric 177
Dichroism nitrobenzoic acid phthalocyanine monolayer 386
Diene conjugated detn gasoline polarog 1502
Diesel fuel phys property NMR 206
Differential gas chromatog mass spectrometry 73 2118
Differential pulse polarog diene detn gasoline 1502
Differential rate model equil chromatog 1937
Differentiation time domain HPLC computer aided 720
Diffraction cyclindrical electrode spectroelectrochem detector 1216
Diffuse reflectance IR spectrometry diazonaphthoquinone detn 615
Diffusion app tetramethyllead std generation 1993
Diffusion coeff acetylpenicillamine thionitrite 1954
Diffusion coeff binary 118
Diffusion cyclic voltammetry chronoamperometry microelectrode 1630
Diffusion distribution electrogenerated absorber 2347
Diffusion electrode reaction electrochem microscopy 1221
Diffusion ethene propene heptane hexadecane water 2231
Diffusion limited neutral carrier transport 1140
Diffusion mercurous dimeric cation perchloric acid 1305
Diffusion microhole array electrode 1763
Diffusion scrubber sulfur dioxide sampling 19
Diffusive sampler performance fundamental factor 843
Diffusive sampling quadratic model org analysis 917
Digital filtering Fourier IR gas chromatog 1073
Digital smoothing filter algorithm data processing 1308
Dihydropyridine pyridinium system mass spectrometry 1723
Diln automated flow injection technique 1773
Diln online ion chromatograph 1791
Diluent apolar effect chiral stationary phase 126
Dimethyl disulfide derivatization alkene biochem 1564
Dimethyl glyoxime cobalt complex polarog 2178
Diode array detector bias nonlinearity 2571
Diode array detector mol absorption luminescence 593
Diode laser intracavity absorption IR spectrometry 1425
Diode laser near IR Raman spectrometer 2647
Dioxime reagent cobalt detn polarog 2178
Direct current cond detector ion chromatog 1383
Direct current plasma atomic emission spectrometry 1175
Direct loading isotope diln mass spectrometry 755
Disaccharide mol structure detn 666
Discharge atomization ionization source mass spectrometry 1879
Discharge glow Penning ionization 1103
Discharge lamp dual cathode emission spectrometry 2137
Discharge plasma quenching argon neon nitrogen 326
Discontinuous automated programmed flow analyzer 2109
Displacement liq chromatog mass transfer 1960
Dissocn const HEPES buffer detn 1400
Dissocn laser mass spectrometry porphyrin 689
Dissoln geol inorg sample review 109r
Distillate petroleum sulfur detn GC 2292
Distn subboiling still 823
Distribution analytical data statistical estn 2719
Distribution function shot noise data analysis 2479
Dithizone cadmium extn mechanism electrochem 1621
Divinylbenzene copolymer carbon fiber composite electrode 1460
Divinylbenzene polystyrene phase quaternary ammonium HPLC 728
DNA detn fluorometric probe 633
DNA recombinant protein prodn sepn 1742
Dodecanol matrix fatty acid detn 494
Dodecanol valine sodium salt optical resoln 1984
Dodecyl sulfate contg polypyrrole stationary phase 2391
Dodecyl sulfate sodium optical resoln 1984
Dodecyl sulfate surfactant chromatog electrokinetic 491
Dogfish muscle arsenocholine 2118
Dogfish ref material arsenic compd polemic 2116
Domoic acid food poisoning review 1053a
Donnan dialysis preconcn cation detn 1410
Donnan equil soil complexation capacity 1295
Dopamine adsorption capacitance electrode 2603
Dopamine ascorbate selectivity fiber electrode 1805
Dopamine detn brain electrode 2323
Dopamine sepn serotonin capillary zone electrophoresis 98
Dopant depth profile detn silicon SIMS 412
Drinking water analysis lead atomic absorption 1410
Droplet atomic emission signal fluctuation 2002
Drug cyclopropylmethylaminooxazoline detn HPLC NMR 772
Drug detn blood chromatog silica support 2445
Drug hydrochloride salt supercrit fluid extn 1986
Drug mixt thin layer chromatog 422
DSC Arrhenius parameter detn solid 1136
DTG Arrhenius parameter detn solid 1136
Dual cathode discharge lamp emission spectrometry 2137
Dual column immunoassay protein G chromatog 1901
Dual microband electrode biochem analysis 2200
Dual multichannel detector mol absorption luminescence 593
Dubinin Radushkevich isotherm diffusive sampler performance 843
Dye fluorescent controlled release pH sensor 174
Dye laser fluorometry protein detn 2285
Dye thiazine HPLC polystyrene divinylbenzene phase 728
Dye trace detn spectrometry wave mixing 998
Dye triphenylmethane sensor wastewater analysis 2306
Eastman AQ glassy carbon electrode 1397
Editorial Analytical Instrumentation Boom 135a
Editorial Deja Vu 15a
Editorial Harmonization Analytical Chem 697a
Editorial Near Field Scanning Optical Microscopy 1075a
Editorial NIST Analytical Chem 583a
Editorial Planetary Rock Analysis 945a
Editorial Publish Perish 767a
Editorial Secondary Ion Mass Spectrometry 1311a
Editorial Spatially Resolved Trace Element Analysis 337a
Editorial Surface Science Analytical Chem 465a
Editorial The Lost Supper 1197a
Editorial 25th Anniversary Classic Paper 885a
EDTA ruthenium complex vinylpyridine copolymer electrode 848
EDTA stripping reagent transition metal 520
EIA cAMP cGMP detn tissue 447
EIA pyruvate carboxylase biotin detn 2160
Elec conductor substrate electrochem microscopy 1794
Electroanalytical Chem, Vol. 15. A Series of Advances (book review) 1037a
Electroanalytical Techniques in Clin Chem and Lab Medicine (book review) 1043a
Electrocatalysis carbohydrate copper modified electrode 2258
Electrocatalyst ferricyanide contg ascorbic acid oxidn 848
Electrochem analyzer automated segmented flow 2102
Electrochem cell rotating disk biol 2803
Electrochem controlled HPLC polypyrrole phase 2391
Electrochem detection amino acid chromatog 432
Electrochem detection capillary zone electrophoresis 98
Electrochem detection nitrite detn chromatog 1485
Electrochem detection peptide detn liq chromatog 2664
Electrochem detector microelectrode array chromatog 295
Electrochem detn arom aldehyde 2599

Electrochem extn mechanism cadmium dithizone 1621
Electrochem geol inorg analysis review 109r
Electrochem microscopy insulator substrate 1794
Electrochem prepd polymeric stationary phase HPLC 198
Electrochem Raman spectroscopy review 775a
Electrochem use quartz crystal microbalance review 1147a
Electrochemistry (book review) 421a
Electrode amperometry glassy carbon cupric hexacyanoferrate 2594
Electrode amphetamine selective dibenzocrown 2189
Electrode anion selective vitamin B12 based 499
Electrode ascending water extn study 1621
Electrode ascorbate dopamine detn brain 2323
Electrode C reactive protein detn 2362
Electrode cadmium sulfide crystal face specific 1980
Electrode carbon copper coated sugar detection 852
Electrode carbon dioxide potassium detn 2365
Electrode carbon ethylene pyrolysis nickel 560
Electrode carbon fiber acetylpenicillamine thionitrite detn 1954
Electrode carbon fiber amine HPLC 1469
Electrode carbon fiber composite copolymer 1460
Electrode carbon paste modified aldehyde detn 2599
Electrode carbon paste modified rhodium complex 279
Electrode carbon paste polychlorotrifluoroethylene mulling oil 2585
Electrode carbon phosphatidylcholine modified 979
Electrode chem receptor analysis review 533a
Electrode coating pyrazine deriv polymer ligand 1799
Electrode composite styrene vinylbenzene vinylpyridine copolymer 848
Electrode copper modified carbohydrate detection 2258
Electrode cyclindrical diffraction spectroelectrochem detector 1216
Electrode detector glassy carbon laser activation 1989
Electrode dual microband biochem analysis 2200
Electrode enzyme glucose sucrose 782
Electrode fiber optic analysis probe 633
Electrode fluoride selective amine detn 1358
Electrode glassy carbon Eastman AQ 1397
Electrode glassy carbon linear array 2124
Electrode glassy carbon poly methylthiophene coated 2809
Electrode glassy pyrolytic carbon activation 2603
Electrode glucose detn body fluid 2566
Electrode graphite kinetic heterogeneity 2763
Electrode graphite laser modified 1637
Electrode interdigitated gate FET sensor 2355
Electrode ion selective flow injection analysis 922
Electrode ion selective liq membrane effect 1169
Electrode ion selective ppt based mechanism 453
Electrode ion selective response selectivity 2341
Electrode iridium based mercury film voltammetry 2092
Electrode Kel F graphite fabrication app 2330
Electrode lipid glassy pharmaceutical detn voltammetry 170
Electrode magnesium selective micro 574
Electrode membrane salicylate detn 566
Electrode membrane size selectivity biochem 303
Electrode microcylinder voltammetry analysis 1211
Electrode microdisk voltammetry supercrit carbon dioxide 2193
Electrode microhole array cyclic voltammetry theory 1763
Electrode microstructure surface spectroscopy review 775a
Electrode modified graphite epoxy resin 508
Electrode oxidn insulin amperometric detn 2462
Electrode oxygen microhole array 159
Electrode pH suppressed ion chromatog detection 787
Electrode platinum lubricant antioxidant detn 1467
Electrode polymer membrane benzo crown ether 1618
Electrode reaction diffusion electrochem microscopy 1221
Electrode reaction kinetics potential current curve 2249
Electrode reaction quasi reversible voltammetry 965
Electrode reaction Raman spectroscopy review 775a
Electrode solid trace metal preconcn electrodeposition 856
Electrode tin oxide modified horseradish peroxidase 2352
Electrode TTF TCNQ ultramicroelectrode array behavior 1048
Electrode ultramicro ensemble response detection limit 762
Electrode ultramicro microscopy conductive insulating sample 1221
Electrode ultramicro platinum iridium 1630
Electrodeposition solid electrode trace metal preconcn 856
Electrodialysis membrane suppressor ion chromatog 939
Electrogenerated chemiluminescence graphite electrode heterogeneity 2763
Electroinactive cation detector Prussian Blue 290
Electrokinetic capillary chromatog micelle 2455
Electrokinetic chromatog band broadening 251
Electrokinetic chromatog d micellar 491
Electrokinetic chromatog micellar ionic compd 2434
Electrokinetic chromatog optical resoln 1984
Electrolyte polymer chromatog detector 584
Electrolytic cell IR spectroelectrochem 2805
Electron capture bromide iodide gas chromatog 733
Electron capture mass spectrometry ion elimination 2523
Electron impact ion source modified spectroscopy 1310
Electron microprobe analysis background subtraction 1612
Electron spectroscopy Auger quantitation review 469a
Electron spectroscopy surface characterization review 243r
Electron transfer biol electrochem cell 2803
Electron transfer graphite electrode 2763
Electron transfer kinetics acetylpenicillamine thionitrite detn 1954
Electron transfer rate activation carbon electrode 1989
Electron transfer rate laser modified graphite 1637
Electroosmosis isotachophoresis mass spectrometry 228
Electrooxidn fiber optic sensor 633
Electrooxidn kinetics luminol graphite 2763
Electrooxidn rhodium complex IR spectra 2805
Electrooxidn uric acid tandem mass spectrometry 1709
Electrophoresis amino acid detn thermooptical detection 37
Electrophoresis capillary biomol neurochem review 292a
Electrophoresis capillary fluorescence CD biomol 1344
Electrophoresis capillary online radioisotope detector 1642
Electrophoresis capillary peptide protein 1186
Electrophoresis capillary zone ionic compd 2434
Electrophoresis capillary zone refractive index detection 1590
Electrophoresis capillary zone serotonin catecholamine sepn 98
Electrophoresis capillary zone temp gradient effect 241
Electrophoresis peptide mapping 2226
Electrophoresis protein computer simulation 362
Electrophoresis zone capillary carboxylic acid detn 766
Electroplating nickel carbon morphol 560
Electroredn copper ferrocyanide redox reaction 508
Electroredn mercurous dimeric cation silver 1305
Electroredn oxygen rhodium anilinopyridine binuclear 279
Electroredn rhodium complex IR spectra 2805
Electroredn TCNQ spectroelectrochem cell 190
Electroredn thin layer spectroelectrochem cell 1787
Electroredox cyanoferrate kinetics laser modified graphite 1637
Electrostatic ion trap screened mass spectrometer 1288
Electrothermal atomic absorption spectrometry biol ref 216
Element detection thermal gradient HPLC 236
Element selective detector supercrit fluid chromatog 1815
Element Trace Analysis Spatially Resolved editorial 337a
Element trace detn serum 1851
Elemental analysis laser microprobe chemiluminescence detection 2557
Elemental analysis mass spectrometry review 643a
Elemental response relative plasma mass spectrometry 1243
ELISA molinate gas chromatog 819
Eluent compn effect HPLC bonded phase 1928
Elution chromatog preparative optimization 1368
Elution gradient HPLC peptide protein 2
Elution profile calcn liq chromatog 2380
Emission atomic droplet signal fluctuation 2002
Emission atomic spectrometry hydride generation online 285
Emission excitation matrix fluorescence lifetime selectivity 580
Emission IR transient pulsed laser 1810
Emission rank estn canonical correlation 2219
Emission spectrometry analysis hydride generation 1175
Emission spectrometry dual cathode discharge lamp 2137
Emission spectrometry fluoride detn 674
Emission spectrometry mass spectrometry coupling 793
Emission spectrometry nonmetal sample introduction plasma 790
Emission x ray synchrotron induced review 341a
Enantiomer cyclophosphamide detn blood HPLC 441
Enantiomeric amine amino alc HPLC 1548
Enantiomeric purity tryptophan detn polarimetric detection 1238
Enantioselective hydrophobic entanglement optical resoln 1984
Energy dispersive electron microprobe background subtraction 1612
Energy selective ion partition cyclotron cell 53
Energy transfer arom hydrocarbon micelle 1405
Enflurane detn ion mobility spectrometry 1093
Enrichment transition metal Chelex 100 resin 520
Ensemble ultramicroelectrode response detection limit 762
Environmental analysis chromatog IR mass spectrometry 1584
Environmental analysis nitrate nitrite 2715
Environmental analysis nitrite chromatog 1485
Environmental analysis selenium HPLC fluorometry 233
Enzyme based biosensor conductometric transducer 1737
Enzyme based fiber optic sensor 1069
Enzyme electrode glucose detn 2200
Enzyme electrode glucose sucrose 782
Enzyme immobilized saccharide detn fermn broth 831
Enzyme immunoassay oligosubstituted enzyme ligand 2160
Enzyme linked binding assay biotin detn 1728
Enzyme sensor glucose thermoelec model 77
Enzyme synthetic model surfactant phosphorescence 2475
Enzymic analysis amperometric NADH oxidase 25
Enzymic detn polyamine 1921
Eosin B detn spectrometry wave mixing 998
Epoxy composite microhole oxygen electrode 159

Epoxy resin graphite modified electrode 508
Equil ion mol reaction 1447
Erosion crater spark produced analysis 1826
Error estn simplex algorithm polemic 1783 1786
Error limit algorithm estg kinetic data 2324
Error propagation equation chromatog peak moment 1058
Error rapid lifetime detn 30
Error systematic analysis algorithm 398
Erythrocyte selenium detn 2244
ESCA instrumentation surface analysis review 589a
Ester detn enzyme fiber optic sensor 1069
Ester fatty acid supercrit fluid chromatog 2076
Ester fatty unsatd methyl 118
Ester ketone gas chromatog IR detection 1073
Ester polymeric activated reagent amine derivatization 1538
Ethanediol solvent polyprotic acid titrn 177
Ethene diffusion heptane hexadecane water 2231
Ether benzo crown polymer membrane electrode 1618
Ethyl phthalate HPLC polypyrrole phase 2391
Ethylation lead detn atomic absorption 1867
Ethylene propene rubber analysis 458
Ethylene pyrolysis nickel carbon electrode 560
Ethylene vinyl acetate copolymer multilayer 1870
Ethynyl anilinopyridine rhodium spectroelectrochem oxidn redn 2805
Europium chelator label fluorescence immunoassay 48
Europium reagent gadolinium detn fluorometry 1063
Evapn compensation pipet calibration 1080
Evapn device continuous flow liq SIMS 2582
Evolved gas analysis mass spectrometry 802
EXAFS binary mixt analysis cross correlation 1686
Excitation emission matrix fluorescence lifetime selectivity 580
Excitation impulse Fourier transform mass spectrometry 489
Excitation ion phase specific mass spectrometry 83
Excitation rank estn canonical correlation 2219
Exhaust emission carbon monoxide detn 671a
Expert system mass spectra classification 715
Exponential decay single rapid lifetime detn 30
Extn chlorodibenzodioxin chlorodibenzofuran supercrit fluid 2770
Extn geol inorg analysis review 109r
Extn kinetics app rapid stirring 1036
Extn kinetics flow injection analysis 101
Extn mechanism cadmium dithizone electrochem 1621
Extn mechanism flow injection analysis 107
Extn org sorbent supercrit carbon dioxide 736
Extn phenoxy herbicide water detn 1363
Extn reaction amphiphile phosphatidylcholine electrode 979
Extn solvent detn iodide oxidn kinetics 2562
Extn supercrit fluid online app phosphonate 1986
Extractor liq high boiling flavor 1596
Fabrication Kel F graphite electrode app 2330
Factor analysis gas chromatog atm org 838
Factor analysis statistics application 1168
Factor analysis target transform retention prediction 367
Factor fundamental diffusive sampler performance 843
Fast atom bombardment interface spectroscopy 1577
Fast atom bombardment mass spectrometry 153 494 1293
Fast atom bombardment mass spectroscopy 1310 2674
Fast atom bombardment mass spectroscopy biomol 2504
Fast atom bombardment oxime redn 1442
Fast thermolysis Fourier IR spectroscopy review 897a
Fat milk triglyceride detn 698
Fatty acid detn mass spectrometry 494
Fatty acid detn supercrit fluid chromatog 2076
Fatty acid HPLC thermal lens detection 910
Fatty ester unsatd methyl 118
Feces zinc detn mass spectroscopy 1023
Feces zinc isotope detn 2757
Feedback mode insulating conducting substrate 132
Feedback mode scanning electrochem microscopy 1221
Fentons reagent digestion total mercury detn 1230
Fenvalerate artifact chromatog sepn 1152
Fenvalerate isomer HPLC column temp 1149
Fermentor carbon dioxide detector piezoelec crystal 746
Fermn broth saccharide detn immobilized enzyme 831
Ferric ion oxidn iodide kinetics 2562
Ferricyanide detn vinylpyridine copolymer composite electrode 848
Ferricyanide detn voltammetry microelectrode 1211
Ferrocene voltammetry Nafion coated microdisk electrode 2193
Ferrocyanide redox reaction copper electroredn 508
Ferrous analysis review 14r
FET ion selective electrode selectivity 2341
FET ion selective plasticizer photopolymn 246
FET sensor interdigitated gate electrode 2355
Fetoprotein detn serum immunoassay 48
Fiber carbon microelectrode fabrication 1805
Fiber optic electrode analysis probe 633
Fiber optic probe fluorometric analysis 1510
Fiber optic sensor avidin biotin 1069
Fiber optic sensor indicator immobilization 202
Fiber optic sensor pH detn 174
Fiber optic sensor wastewater analysis 2306
Fiber optic time resolved fluorescence sensor 1768
Fiber optic waveguide polymer coated sensor 1674
Fiber optics chromatog detector capillary microbore 876
Fiber quartz filter particulate analysis 914
Fibroblast metal distribution ion microscopy 2690
Field desorption mass spectrometry review 1201a
Field flow fractionation coupled column 741
Field flow fractionation hollow cylinder 11
Field flow fractionation isoelec focusing protein 912
Field flow fractionation sedimentation 811 2735
Field flow fractionation small solute correction 90
Field ionization mass spectrometry review 1201a
Field ionization spectroscopy plant 221
Film monolayer analysis absorption spectrometry 386
Film Nafion platinum microdisk electrode voltammetry 2193
Film probe stability tandem liq SIMS 1013
Film silver based mercury voltammetry 2086
Filter algorithm data processing digital smoothing 1308
Filter paper silver coated substrate 1697
Filter quartz fiber particulate analysis 914
Filtering digital Fourier IR gas chromatog 1073
Filtering lifetime fluorescence review 839a
Filtering spatial thermal lens spectrometer 2496
Filtering time detection fluorometry analysis 2611
Fingerprint detection laser luminescence review 557a
Fish chlorodibenzodioxin detn 1678
Flame atomic absorption detection trace enrichment 520
Flame atomic absorption spectrometry cation detn 1410
Flame Fourier transform atomic absorption spectrometry 1694
Flame IR emission chloride chlorine detn 2785
Flame photometric detection supercrit fluid chromatog 2616
Flame photometric detector optimization organosulfur 58
Flame sampling cell multiphoton ionization spectrometry 1010
Flatband potential cadmium sulfide crystal face 1980
Flavor boiling high liq extractor 1596
Flow analysis laser spectrometry wave mixing 998
Flow analyzer automated discontinuous programmed 2109
Flow automated segmented electrochem analyzer 2102
Flow cell small polarimeter detector 1238
Flow continuous analysis potentiometry cell 504
Flow continuous coaxial spectroscopy biomol 2504
Flow control restrictor supercrit fluid chromatog 1178
Flow diagram error estn simplex polemic 1783
Flow injection analysis carbon paste electrode 2585
Flow injection analysis confluent mixing optimization 973
Flow injection analysis extn kinetics 101
Flow injection analysis extn mechanism 107
Flow injection analysis fluoride detn 674
Flow injection analysis ion exchange preconcn 496
Flow injection analysis wall jet detector 922
Flow injection chemiluminescence copper cyanide detn 1505
Flow injection detection amperometry electrode 2594
Flow injection diln split zone 1773
Flow injection Donnan dialysis preconcn 1410
Flow injection fluorometry ammonium detn 408
Flow injection insulin detn 2462
Flow injection system arsine generation 2079
Flow injection thorium uranium detn 1789
Flow liq analysis ion mobility spectrometry 601
Flow mass restrictor supercrit fluid chromatog 356
Flow polarog surfactant interference silica effect 1598
Flow system ion exchange trace enrichment 520
Flow through spectroelectrochem detector 1216
Flow voltammetry Nafion coated microdisk electrode 2193
Flow voltammetry trace metal monitoring 468
Fluctuation signal atomic emission droplet 2002
Flue gas acrylonitrile detn 2743
Flue gas pollutant mass spectrometer 260
Fluid body cAMP cGMP 447
Fluidic injection chromatog peak shape 1489
Fluorenylmethyl amino acid polymeric chiral reagent 1548
Fluorescein immobilization fiber optic pH sensor 202
Fluorescein labeled enzyme fiber optic sensor 1069
Fluorescence aluminum complexation immobilized ligand 1001
Fluorescence analysis arom hydrocarbon micelle 1405
Fluorescence analysis room temp solid surface 2643
Fluorescence benzopyrenetetrol silica enhancer 2766
Fluorescence CD detector electrophoresis biomol 1344
Fluorescence detection HPLC enantiomeric amine 1548
Fluorescence detection magnesium calcium detn 382
Fluorescence immunoassay europium chelator label 48
Fluorescence immunoassay label rotation detn 309
Fluorescence lifetime filtering review 839a
Fluorescence lifetime selectivity excitation emission matrix 580
Fluorescence line narrowing spectroscopy carcinogenesis review 1023a
Fluorescence measurement dual channel detector 593
Fluorescence org cation binding surface 590
Fluorescence photoredn detection quinone HPLC 2267
Fluorescence probe cyclodextrin inclusion complex 905
Fluorescence sensor fiber optic time resolved 1768

Fluorescence spectrometry time resolved decay analysis 2310
Fluorescence x ray silicate rock analysis 1837
Fluorescence x ray silicon biol 1834
Fluorescent dye controlled release pH sensor 174
Fluoride chromatog solute independent calibration 1915
Fluoride detn atomic emission spectrometry 674
Fluoride selective electrode amine detn 1358
Fluoride selective electrode flow injection analysis 922
Fluorine chemiluminescence reagent laser microprobe 2557
Fluoro aluminum complex detn ion chromatog 535
Fluoroacetic acid cluster ion calibration spectrometry 2126
Fluorodinitrobenzene reagent amine detn potentiometry 1358
Fluoroethyldithiocarbamate nickel detn biol 1099
Fluorometer charge coupled detector 282
Fluorometer laser semiconductor 2285
Fluorometric analysis single frequency phase resolved 1510
Fluorometric detection selenium detn 233
Fluorometric laser detection thin layer chromatog 1931
Fluorometry aminopeptidase bacteria identification 1656
Fluorometry arom hydrocarbon micelle 1405
Fluorometry detection time filtering analysis 2611
Fluorometry flow injection ammonium detn 408
Fluorometry gadolinium samarium detn 1063
Fluorometry laser protein detn dye 2285
Fluorometry laser TLC porphyrin methyl ester 2288
Fluorometry phase hapten antibody complex 309
Fluorometry quinine sulfate detn 593
Fluorometry selenium detn blood 2244
Fluorometry sulfite detn needle wine 1755
Fluorometry two component system qual analysis 580
Fluoronitrobenzooxadiazole reagent selenium detn fluorometry 233
Fluoropolymer analysis EGA mass spectrometry 802
Focus 43a 101a 311a 425a 551a 602a 663a 739a 795a 861a 921a 1001a 1047a 1099a 1167a 1217a 1291a 1329a 1333a 1381a
Following preceding catalytic chem reaction voltammetry 965
Food analysis review 45r
Food analysis triazine herbicide 935
Food liq flavor extn app 1596
Food poisoning domoic acid review 1053a
Food science chiroptical analysis review 77a
Food sucrose detn 782
Forensic amphetamine detn 2189
Forensic benzodiazepine ion mobility spectrometry 343
Forensic fingerprint detection review 557a
Forensic norcarboxytetrahydrocannabinol urine gas chromatog 925
Forensic nortetrahydrocannabinolcarboxylate urine std 540
Forensic science chiroptical analysis review 77a
Forensic science review 95r
Forensic succinylcholine detn dexamethasone 53a
Formal potential redox reaction coating 1799
Formaldehyde detn air passive sampler 187
Formation const cyclodextrin complex chromatog 955
Formation const oxazine 4 methanol complex 2394
Fossil fuel sulfur detn chromatog 2292
Four wave mixing laser spectrometry analysis 998
Fourier IR digital filtering gas chromatog 1073
Fourier IR gas chromatog mass spectrometry 1584
Fourier IR spectroscopy fast thermolysis review 897a
Fourier transform atomic absorption spectrometry 1694
Fourier transform gas chromatog linked analysis 1571
Fourier transform ICR mass spectrometry 2130
Fourier transform ion cyclotron resonance 2040
Fourier transform ion cyclotron resonance spectrometry 53 83
Fourier transform IR ionic transport 1164
Fourier transform IR spectra curve fitting 2708
Fourier transform IR spectrometry blood 2016
Fourier transform IR spectrometry diazonaphthoquinone detn 615
Fourier transform IR spectrometry glucose detn 2009
Fourier transform IR supercrit chromatog coupling 2212
Fourier transform mass spectrometry amino acid 1895
Fourier transform mass spectrometry impulse excitation 489
Fourier transform mass spectrometry laser desorption 184
Fourier transform mass spectrometry mass calibration 2422
Fourier transform spectrometer IR 1052
Fractionation field flow coupled column 741
Fractionation field flow hollow cylinder 11
Fractionation field flow isoelec focusing protein 912
Fractionation sedimentation polymer latex density 1934
Fractionation sedimentation polystyrene latex 2439
Free energy interaction partition liq chromatog 2540
FTIR org detn air 677
FTIR reflection absorption ionic transport 1164
FTIR spectra qual least squares fit 2708
FTIR spectroscopy aluminum nitride water 2399
FTIR supercrit chromatog propellant 145
Fuel diesel phys property NMR 206
Fuel petroleum hydroxyl compd detn 1260
Fulvic acid aquatic structural feature 2792
Fulvic acid metal binding spectroscopy 483
Fumed silica effect surfactant interference polarog 1598
Fumed silica silver substrate SERS 656
Functional relationship analytical method bias detn 1942
Functionalized mixed micelle stationary liq phase 1984
Fundamentals of Analytical Chem, 5th Ed. (book review) 422a
Fungus ext analysis fatty acid ester 2076
Furil dioxime cobalt complex polarog 2178
Gadolinium detn fluorometry 1063
Gallium arsenide acceptor detn Raman spectroscopy 994
Gallium present aluminum detn 1768
Gas analysis anesthetic 1093
Gas and Liq Chromatog in Analytical Chem (book review) 1041a
Gas chromatog alanine cell wall 265
Gas chromatog alkene insect 1564
Gas chromatog alkyl peroxyalkanoyl nitrate 771
Gas chromatog aluminum detn seawater 544
Gas chromatog bromide iodide detn 733
Gas chromatog calcium chabazite adsorbent 1112
Gas chromatog carbon hollow tube org 838
Gas chromatog chiral polysiloxane stationary phase 2121
Gas chromatog chlorodibenzodioxin 1678
Gas chromatog cholesterol detn 1718
Gas chromatog compact probe 2410
Gas chromatog coupling TLC laser desorption 1906
Gas chromatog detection photodiode array spectrophotometer 1249
Gas chromatog detector sulfur compd 1268
Gas chromatog detn carbon hydrogen isotope 2149
Gas chromatog detn org volatile compd 2751
Gas chromatog electrochem detector 584
Gas chromatog Fourier IR digital filtering 1073
Gas chromatog Fourier IR mass spectrometry 1584
Gas chromatog glyceride 698
Gas chromatog headspace volatile arom detn 2584
Gas chromatog juice flavor 1596
Gas chromatog linked spectrometry analysis 1571
Gas chromatog mass spectrometry coupling 2402
Gas chromatog mass spectrometry differential 73 2118
Gas chromatog mass spectrometry polyarom hydrocarbon 2669
Gas chromatog mass spectroscopy radiolabeled metabolite 2724
Gas chromatog modified silica gel 41
Gas chromatog molinate ELISA 819
Gas chromatog nickel detn 1099
Gas chromatog norcarboxytetrahydrocannabinol urine forensic 925
Gas chromatog open tubular 2165
Gas chromatog oxygen analysis impurity 2237
Gas chromatog peak shape injection method 1489
Gas chromatog peroxyacyl nitrate column decompn 2731
Gas chromatog plant analysis 221
Gas chromatog pyrazine computerized retention prediction 1328
Gas chromatog pyrolysis polymer 961
Gas chromatog resoln stationary phase diln 126
Gas chromatog retention index extrapolation 88
Gas chromatog water detn 1325
Gas chromatog zone 1478
Gas chromatograph interface mass spectrometer cell 1874
Gas liq interphase partition chromatog 2231
Gas phase chemiluminescence phosphine ozone reaction 2699
Gasoline analysis conjugated diene polarog 1502
Gasoline analysis mass spectrometry 86
Gasoline analysis thiol flow injection 496
Gasoline arom detn headspace gas chromatog 2584
Gasoline octane number IR spectra 313
GC sulfur detn petroleum distillate 2292
Gel chromatog microcolumn polymer 961
Gel chromatog polyethylene terephthalate 1321
Gel chromatog polymer solvent elimination 458
Gel size exclusion chromatog hydrophobicity 780
Generalized simulated annealing global optimization 2024
Geol inorg material analysis review 109r
Germanium detn atomic emission spectrometry 1175
Germanium detn laser microprobe chemiluminescence detection 2557
Glass frit nebulizer atomic spectrometry 2777
Glass immobilized ionophore cation detn 211
Glassy carbon amperometry electrode cupric hexacyanoferrate 2594
Glassy carbon electrode acetylpenicillamine thionitrite detn 1954
Glassy carbon electrode copper lead electrodeposition 856
Glassy carbon electrode detector laser activation 1989
Glassy carbon electrode Eastman AQ 1397
Glassy carbon electrode poly methylthiophene coated 2809
Glassy carbon linear array electrode 2124
Glassy electrode lipid pharmaceutical detn voltammetry 170
Glassy pyrolytic carbon electrode activation 2603
Global optimization generalized simulated annealing 2024
Glow discharge Penning ionization 1103
Glow discharge plasma quenching 326
Glucose detn amperometry enzyme based sensor 2352
Glucose detn blood 2009
Glucose detn body fluid electrode 2566
Glucose detn enzyme electrode 2200
Glucose enzyme electrode 782
Glucose sensor enzyme thermoelec model 77
Glutaraldehyde reagent polyvinyl alc crosslinking 202
Glutathione liq chromatog electrochem detector activation 1989
Glyceride detn butter 698
Glycerol peptides mass spectroscopy 2674
Glycol polyethylene mass spectra 2050
Glycolipid chromatog mass spectrometry spray ionization 1159
Glycolipid structure detn mycobacteria 416
Glycopeptidolipid structure detn spectroscopy 416
Glycoprotein chromatog temp programmed elution 1117
Glycoprotein variant surface oligosaccharide Trypanosoma 2686

Glycoside chromatog mass spectrometry spray ionization 1159
Gold electrode amperometry glucose detn 2566
Gold film sensor mercury detn 1230
Gradient elution HPLC peptide protein 2
Gradient elution liq chromatog voltammetric detection 1977
Graphite electrode kinetic heterogeneity 2763
Graphite electrode laser modified 1637
Graphite epoxy resin modified electrode 508
Graphite furnace atomic absorption slurry sample 1414
Graphite furnace continuous source spectrometer 1670
Graphite furnace copper atomization mechanism 2652
Graphite Kel F electrode fabrication app 2330
Graphite Nujol paste electrode 279
Group IIB membrane neutral carrier transport 1140
Group IVA detn atomic emission spectrometry 1175
Group VA detn atomic emission spectrometry 1175
Group VA element hydride generation spectrometry 285
Growth hormone structure optical spectroscopy review 642
Guide to Materials Characterization and Chem Analysis (book review) 1162a
Hadamard transform spectrochem analysis review 723a
Halogen detector liq chromatog spectrometry 895
Halogenated anesthetic detn ion mobility spectrometry 1093
Halogenated naphthalene laser induced phosphorescence spectrometry 872
Halothane detn ion mobility spectrometry 1093
Hammett indicator immobilization polymer coated waveguide 1674
Hapten antibody complex phase fluorometry 309
Hapten antibody complex phase fluorometry correction 1472
Hartley transform mass spectrometer 428
Headspace gas chromatog volatile arom detn 2584
Headspace sampling volatile polymer model 1202
Heat pulse scanning zone gas chromatog 1478
Heat sorption propanol SE 54 phase 1348
Heat transfer glucose enzyme sensor 77
Heat transition cyanobenzylideneoctyloxyaniline mesophase coated silica 1534
Helium microwave induced plasma fluoride detn 674
Helium plasma liq chromatog detector 895
Helium plasma transition nitrogen ion 1052
Hemispherical conical ultramicroelectrode fabrication 1630
Heparin oligosaccharide mass spectrometry 1453
HEPES buffer dissocn const pH detn 1400
Heptane ethene propene diffusion 2231
Herbicide phenoxy extn detn water 1363
Herbicide triazine extn isolation method 935
Heroin impurity sepn HPLC 720
Heterodyne multichannel detection mass spectrometry 749
Heterogeneity kinetic graphite electrode 2763
Hexacyanoferrate cupric glassy carbon amperometry electrode 2594
Hexadecane ethene propene diffusion 2231
Hexadecyltrimethylammonium chloride reagent iodine detn chemiluminescence 2800
Hexenyl adipate photopolymn potassium selective membrane 246
High mol wt compd detn 2616
High performance liq chromatog amine trace 1538
High performance liq chromatog detection 2624
High Performance Liq Chromatog (book review) 1161a
High performance TLC diazonaphthoquinone detn 615
High pressure ammonia expansion nonvolatile compd 777
High resoln partition ion cyclotron resonance 83
High salt content sample analysis metal 149
High-Performance Liq Chromatog. Advances and Perspectives, Vol. 5 (book review) 1286a
Hofmeister series relation anion selective electrode 499
Hollow carbon tube gas chromatog org 838
Hollow cathode discharge lamp emission spectrometry 2137
Hollow fiber probe wastewater spectrometry 2332
Honeycomb structure carbon paste electrode 279
Horseradish peroxidase modified tin oxide electrode 2352
HPLC alc carbohydrate conductometric detection model 631
HPLC allyloxybenzoylmethoxyphenyl bonded silica stationary phase 1928
HPLC benzene deriv retention prediction 367
HPLC bonded phase column packing 2
HPLC capillary column octylsilyl packed 1128
HPLC carbohydrate amperometric detection 852
HPLC carbohydrate detection copper modified electrode 2258
HPLC chlorinated biphenyl dibenzodioxin dibenzofuran soil 1300
HPLC chromatog antimycin A 404
HPLC cyclophosphamide enantiomer detn blood 441
HPLC detector amine detn 1469
HPLC detector diode laser polarimeter 1238
HPLC electrochem prepd polymeric stationary phase 198
HPLC enantiomeric amine amino alc 1548
HPLC fatty acid thermal lens detection 910
HPLC fenvalerate isomer column temp 1149
HPLC hydroxamic acid siderophore detn 1474
HPLC imirestat phenytoin serum protein binding 1171
HPLC methotrexate detn blood urine 946
HPLC NMR cyclopropylmethylaminooxazoline drug detn 772
HPLC peptide mapping 2226
HPLC polyamine detn urine 1921
HPLC polypyrrole stationary phase 2391
HPLC protein A IgG detn 1314
HPLC protein aggregation 514
HPLC quaternary ammonium compd stationary phase 728
HPLC quinone photoredn fluorescence detection 2267
HPLC selenium detn 233
HPLC selenium detn blood 2244
HPLC silylated silica gel thermal treatment 41
HPLC subtilisin variant sepn 1742
HPLC sulfite detn 272
HPLC surface enhanced resonance Raman detection 888
HPLC theophylline detn blood 784
HPLC thermal gradient element detection 236
HPLC time domain differentiation computer aided 720
HPLC whole column detection 2624
Humic substance aquatic structure spectroscopy 628
Humic substance metal binding 1519
Humic substance metal complexation model 483
Humidity sensor cobalt chloride 1863
Hydrazine oxalic acid redox reaction 508
Hydrazone acetylpyridine reagent metal ion chromatog 1272
Hydride generation atomic emission spectrometry analysis 1175
Hydride generation online inductively coupled plasma 285
Hydride generation selenium detn biochem 701
Hydrocarbon arom energy transfer micelle 1405
Hydrocarbon arom mol mechanics NMR spectra 2658
Hydrocarbon arom polycyclic detn aerosol 320
Hydrocarbon arom polycyclic thin layer chromatog 422
Hydrocarbon arom polynuclear low temp phosphorimetry 1182
Hydrocarbon arom polynuclear room temp phosphorimetry 2328
Hydrocarbon arom TLC mass spectrometry 2516
Hydrocarbon bonded silica surface fluorescence 590
Hydrocarbon detn water seawater extn 1333
Hydrocarbon light analysis carbon hydrogen isotope 2149
Hydrocarbon mass spectrometry 86
Hydrocarbon polyarom gas chromatog mass spectrometry 2669
Hydrocarbon polycyclic arom adsorption aerosol 708
Hydrocarbon polycyclic arom chromatog subambient temp 1749
Hydrocarbon polycyclic arom detn luminescence 2643
Hydrocarbon unsatd identification insect 1564
Hydrochloric acid detn polymer coated waveguide 1674
Hydrochloric acid reagent polyvinyl alc crosslinking 202
Hydrochloride salt drug supercrit fluid extn 1986
Hydrodynamic microcapillary chromatog copolymer micelle 1318
Hydrogen bonding chiral phase stereoselectivity 126
Hydrogen chloride detection zinc quartz resonator 1559
Hydrogen flame photometric detector optimization organosulfur 58
Hydrogen flow rate optimization thermionic detector 2082
Hydrogen fluoride detn polymer analysis 802
Hydrogen ion detn polymer membrane electrode 1618
Hydrogen isotope detn light hydrocarbon 2149
Hydrogen peroxide chlorophenyl oxalate stability 1298
Hydrogen peroxide detn amperometry enzyme sensor 2352
Hydrogen peroxide detn chemiluminescence probe 633
Hydrogen peroxide detn voltammetry 2176
Hydrolysis uric acid electrooxidn 1709
Hydrophobic chromatog lactoglobulin aggregation 514
Hydrophobic enantioselective entanglement optical resoln 1984
Hydrophobicity micellar liq chromatog 1040
Hydrophobicity size exclusion chromatog gel 780
Hydrophobicity solute surface activity 194
Hydrosilylation silica surface org addn 2067
Hydrosulfide detn cadmium sulfide electrode 1980
Hydroxamic acid detn HPLC 1474
Hydroxide ion detn near IR spectrometry 1419
Hydroxy acid resoln gas chromatog 2121
Hydroxyapatite HPLC subtilisin variant 1742
Hydroxybenzylamine voltammetry Nafion coated microdisk electrode 2193
Hydroxyethyldithiocarbamate zinc complexation water analysis 1494
Hydroxyethylethylenediamine piezoelec crystal detector carbon dioxide 746
Hydroxyl compd detn petroleum fuel 1260
Hydroxyphenylacetic acid chromatog electrochem detector activation 1989
Hydroxypyrenetrisulfonic acid controlled release pH sensor 174
Hygiene industrial air analysis review 128r
Ice lead detn Antarctica 1758
ICR Fourier transform mass spectrometry 2130
Ig binding protein A immunosensor 1227
IgG detn protein A HPLC 1314
Ignition plasma threshold condition mass spectrometry 1029
Image binning spectral CCD 1513
Image quantification ion microscopy detector discrimination 65
Imaging Hadamard transform review 723a
Imaging NMR review 23a
Imirestat phenytoin serum protein binding HPLC 1171
Immobilization bacteria identification 1656
Immobilization indicator fiber optic sensor 202
Immobilized arom primary amine aldehyde detn 2599
Immobilized enzyme saccharide detn fermn broth 831
Immobilized gradient isoelec focusing biomol review 1602
Immobilized ionophore glass cation detn 211
Immobilized metal affinity chromatog protein 1742

Immunoassay dual column protein G chromatog 1901
Immunoassay enzyme amplification oxidase 25
Immunoassay enzyme oligosubstituted enzyme ligand 2160
Immunoassay fluorescence europium chelator label 48
Immunoassay fluorescence label rotation detn 309
Immunoassay kinetic piezoelec immunol biosensor 1227
Immunobioassay interleukin 2 1732
Immunol biosensor piezoelec kinetic immunoassay 1227
Immunosensor protein binding detection piezoelec 1227
Impedance matching inductively coupled plasma 2589
Impulse excitation Fourier transform mass spectrometry 489
In vivo NMR surface coil fabrication 636
Incinerator ash chlorodibenzodioxin chlorodibenzofuran extn 2770
Inclusion complex arom cyclodextrin 955
Inclusion complex cyclodextrin fluorescence probe 905
Indicator Hammett immobilization polymer coated waveguide 1674
Indicator immobilization fiber optic sensor 202
Indigodisulfonate reagent ozone detn 619
Indirect detection ion pair chromatog 1109
Indirect UV detection chromatog cation detn 1435
Indium present aluminum detn 1768
Indium propene complex reagent chem ionization 86
Inductively coupled plasma atomic emission sulfite 272
Inductively coupled plasma direct sample insertion 163
Inductively coupled plasma hydride generation online 285
Inductively coupled plasma impedance matching 2589
Inductively coupled plasma mass spectrometer 606
Inductively coupled plasma mass spectrometry 793 2031 2263
Inductively coupled plasma mass spectrometry metal 149
Inductively coupled plasma mass spectrometry reagent 827
Inductively coupled plasma mass spectrometry solid 1243
Industrial hygiene air analysis review 128r
Industrial wastewater metal detn HPLC 1494
Information management system lab review 612a
Information spectral linked chromatog spectrometry analysis 1571
Inhibition kinetic catalyst simultaneous detn 2551
Inhibitor cholinesterase antidote HPLC 728
Injection method gas chromatog peak shape 1489
Injector trap concentrator flavor compd 1596
Inorg Mass Spectrometry (book review) 547a
Inorg material analysis review 109r
Insect unsatd hydrocarbon identification 1564
Instrumental analysis surface characterization review 243r
Instrumental Analysis, 2nd Ed. (book review) 420a
Instrumental Methods of Analysis, 7th Ed. (book review) 417a
Instrumentation x ray photoelectron spectroscopy review 589a
Insulating conducting substrate feedback mode 132
Insulating conductive sample electrode ultramicro microscopy 1221
Insulator substrate scanning electrochem microscopy 1794
Insulin amperometric detn electrode oxidn 2462
Intelligent robot analytical lab automation review 805a
Interaction free energy partition liq chromatog 2540
Interdigitated gate electrode FET sensor 2355
Interface gas chromatograph mass spectrometer cell 1874
Interface isotachophoresis mass spectrometry 228
Interface liq chromatog mass spectroscopy biomol 1577
Interface liq chromatograph plasma spectrometer 895
Interfacial ion transfer kinetics membrane 1624
Interfacial resistance chromatog plate height 2165
Interference chloramine chlorine detn water 991
Interference isobaric mol ion mass spectrometry 2031
Interference removal metal algae column 468
Interferent ion selective electrode 453
Interferent spectral model nonbilinear rank annihilation 2277
Interferometry digital filtering gas chromatog 1073
Interlab coeff variation concn statistical justification 1465
Interleukin 2 detn blood immunobioassay 1732
Intermol process ion trap mass spectrometer 2500
Internal std Delrin NMR spectrometry 2579
International System unit 94
Interphase gas liq partition chromatog 2231
Intestine zinc absorption detn nutrition 1023
Intracavity absorption IR spectrometry laser diode 1425
Introduction to Computer-Assisted Experimentation (book review) 856a
Iodide detn continuous flow potentiometry 504
Iodide detn gas chromatog bromide simultaneous 733
Iodide oxidn ferric ion kinetics 2562
Iodide selective electrode vitamin B12 based 499
Iodine detn solvent extn chemiluminescence 2800
Ion chromatog aluminum aq soln speciation 535
Ion chromatog automated solute independent calibration 1915
Ion chromatog chloride detn reforming catalyst 1924
Ion chromatog detection amperometry electrode 2594
Ion chromatog direct current cond detector 1383
Ion chromatog electrodialysis membrane suppressor 939
Ion chromatog nonsuppressed cation detn 1435
Ion chromatog stopped flow chronoamperometric detector 1387
Ion chromatog sulfur dioxide air 19
Ion chromatog suppressed potentiometric pH detection 787
Ion chromatograph online diln 1791
Ion cluster calibration chromatog mass spectrometry 2126
Ion cyclotron resonance Fourier transform 2040
Ion cyclotron resonance Fourier transform spectrometry 53
Ion cyclotron resonance mass spectrometer 330 2528
Ion cyclotron resonance mass spectrometry 428
Ion cyclotron resonance spectrometry Fourier transform 83
Ion elimination electron capture mass spectrometry 2523
Ion exchange HPLC polymeric stationary phase 198
Ion exchange kinetics selective electrode characteristic 2341
Ion exchange preconcn flow injection analysis 496
Ion exchange trace enrichment online automated 520
Ion exclusion chromatog nitrite detn 1485
Ion exclusion chromatog weak acid detection 548
Ion interfacial transfer kinetics membrane 1624
Ion microprobe analysis image quantification 65
Ion microscopy image quantification detector discrimination 65
Ion mobility spectrometry amine 684
Ion mobility spectrometry benzodiazepine 343
Ion mobility spectrometry halogenated anesthetic detn 1093
Ion mobility spectrometry liq analysis coronaspray 601
Ion mol reaction kinetics 1447
Ion multiply charged mass spectrometry 1702
Ion pair chromatog amperometry alkanolamine 2466
Ion pair chromatog system peak 1109
Ion partition ion cyclotron resonance cell 53
Ion pseudomol trap detector mass spectra 1983
Ion selective electrode cadmium sulfide 1980
Ion selective electrode flow injection analysis 922
Ion selective electrode liq membrane effect 1169
Ion selective electrode ppt based mechanism 453
Ion selective electrode response selectivity 2341
Ion selective solid state sensor 246
Ion source dual mode mass spectroscopy 1310
Ion spectroscopy surface characterization review 243r
Ion spray tandem mass spectrometry tributyltin 2320
Ion transport quaternized polyvinylpyridine plasticizer 570
Ion trap detector mass spectrometer 1083
Ion trap mass spectrometer intermol process 2500
Ion trap mass spectroscopy biomol 2316
Ion trap screened electrostatic mass spectrometer 1288
Ion yield protein mass spectroscopy 375
Ionic compd micellar electrokinetic chromatog 2434
Ionic transport Fourier transform IR 1164
Ionically conducting polymer membrane microelectrode 270
Ionization atm pressure spray mass spectrometry 1159
Ionization chem lithium attachment mass spectrometry 1026
Ionization chem mass spectrometry 86
Ionization laser desorption mass spectrometer 1083
Ionization laser diagnostic plume vaporization 2546
Ionization laser mass spectrometry polyarom hydrocarbon 2669
Ionization laser mass spectrometry solid 1029
Ionization laser resonance mass spectra lanthanum 695
Ionization laser surface analysis polymer 805
Ionization mass spectrometry polymer 1195
Ionization mass spectrometry review 1201a
Ionization multiphoton metal atom detection 1010
Ionization multiphoton UV IR laser excited 612
Ionization Penning glow discharge 1103
Ionization picric acid amphiprotic mixt 1971
Ionization two photon spectroscopy biomol 1911
Ionophore benzo crown ether polymer membrane 1618
Ionophore C reactive protein detn 2362
Ionophore immobilized glass cation detn 211
IR diffuse reflectance spectrometry diazonaphthoquinone detn 615
IR drug raw material testing 138
IR emission flame chloride chlorine detn 2785
IR emission spectroscopy transient analysis 650
IR emission transient pulsed laser 1810
IR Fourier digital filtering gas chromatog 1073
IR Fourier gas chromatog mass spectrometry 1584
IR Fourier transform ionic transport 1164
IR Fourier transform org air 677
IR Fourier transform spectrometer 1052
IR Fourier transform supercrit chromatog coupling 2212
IR laser diode intracavity absorption spectrometry 1425
IR near diode laser Raman spectrometer 2647
IR near SERS ruthenium pyridine 1648
IR photometry carbon monoxide air 671a
IR sample prepn sorption study 2047
IR spectra cyanobenzylidimethoxyoxyaniline mesophase coated silica 1534
IR spectra Fourier transform curve fitting 2708
IR spectra gasoline octane number 313
IR spectroelectrochem electrolytic cell 2805
IR spectrometry analysis error 398

IR spectrometry blood analysis 2016
IR spectrometry chlorodibenzodioxin 1678
IR spectrometry electrochem cell 190
IR spectrometry gas chromatog linked analysis 1571
IR spectrometry hydroxide ion detn 1419
IR spectrometry reflection glucose detn 2009
IR spectroscopy carboxylic acid detn 1260
IR spectroscopy Fourier fast thermolysis review 897a
IR spectrum compression deconvoluted band 33
IR thermally chem modified silica gel 41
IR UV laser excited multiphoton ionization 612
Iridium based mercury film electrode voltammetry 2092
Iridium platinum electrode ultramicro 1630
Iron cyanide aminopyridine carbon paste electrode 2599
Iron detn copper titanium present spectrophotometry 1847
Iron detn direct loading mass spectrometry 755
Iron detn river sediment atomic absorption 1414
Irreversible isotherm diffusive sampler performance 843
Isobar amine ion mobility spectra 684
Isobaric mol ion interference mass spectrometry 2031
Isoelec focusing field flow fractionation correction 2224
Isoelec focusing field flow fractionation protein 912
Isoelec focusing immobilized gradient biomol review 1602
Isoelec focusing protein simulation 362
Isoflurane detn ion mobility spectrometry 1093
Isomer amine ion mobility spectra 684
Isomer benzene deriv mass spectra 1889
Isomer benzene deriv thin layer chromatog 422
Isomer photodiode array detection gas chromatog 1249
Isomer toluic acid HPLC polypyrrole phase 2391
Isomerization rate quaternary ammonium hydrazone acetylpyridine 1272
Isoprene styrene block copolymer micelle 1318
Isopropyl ester amino acid nitrobenzoyl deriv 1984
Isopropyl methylphosphonate detection FET sensor 2355
Isotachophoresis capillary mass spectrometry 228
Isotachophoresis protein simulation 362
Isotherm sorption diffusive sampler performance 843
Isotope carbon detn org combustion 1996
Isotope diln direct loading mass spectrometry 755
Isotope diln mass spectrometry 2416
Isotope diln mass spectrometry review 643a
Isotope hydrogen carbon detn light hydrocarbon 2149
Isotope oxygen detn org mass spectrometry 1887
Iterative target factor analysis statistics application 1168
Jackknife algorithm estg error confidence limit 2324
Jet fuel liq chromatog characterization 206
Jet supersonic spectroscopy nonvolatile compd 777
Joint prosthetic alloy tissue analysis 1235
Juice flavor gas chromatog 1596
Kamlet scale reversed phase liq chromatog 1524
Kane Kjeldahl data statistical bias 1942
Kel F graphite electrode fabrication app 2330
Kel F oil carbon paste electrode 2585
Ketone ester gas chromatog IR detection 1073
Kinetic Aspects of Analytical Chem (book review) 857a
Kinetic data algorithm estg error limit 2324
Kinetic effect ion selective electrode 2341
Kinetic model ion selective electrode 453
Kinetic potentiometry amine detn 1358
Kinetic reaction amine HPLC derivatization reagent 1538
Kinetics copper compd reaction graphite furnace 2652
Kinetics decay data 660
Kinetics electrode reaction potential current curve 2249
Kinetics electron exchanger laser modified graphite 1637
Kinetics electron transfer acetylpenicillamine thionitrite 1954
Kinetics electron transfer graphite electrode 2763
Kinetics extn app rapid stirring 1036
Kinetics extn flow injection analysis 101
Kinetics interfacial ion transfer membrane 1624
Kinetics iodide oxidn ferric ion 2562
Kinetics ion mol reaction 1447
Kinetics oxygen electroredn rhodium anilinopyridine binuclear 279
Kinetics reaction amine fluorodinitrobenzene 1358
Kinetics reaction detn linearized model 1949
Kinetics solid state reaction DSC DTG 1136
Kjeldahl analysis error 398
Kjeldahl Kane data statistical bias 1942
Kolthoff biog 287a
Krypton detn oxygen gas chromatog 2237
Lab analytical automation intelligent robot review 805a
Lab information management system review 612a
Lab Methods in Vibrational Spectroscopy. 3rd Ed. (book review) 308a
Lab microcontroller 433a
Label rotation detn fluorescence immunoassay 309
Labile photochem compd TLC IR spectrometry 615
Lactoglobulin aggregation hydrophobic chromatog 514
LAMMA particle sample prepn 914
Lamp discharge dual cathode emission spectrometry 2137
Lamp mercury pen source fluorometer analysis 282
Lanthanide ion probe spectroscopy 1519
Lanthanide oxide analysis samarium 1063
Lanthanum laser resonance ionization mass spectra 695
Laser ablation sampling plasma mass spectrometry 1243
Laser activation glassy carbon electrode detector 1989
Laser clin application review 1367a
Laser desorption chem ionization mass spectrometry 184
Laser desorption coupling gas chromatog TLC 1906
Laser desorption detection biomol TLC 1911
Laser desorption ionization mass spectrometer 1083
Laser desorption mass spectrometry amino acid 1895
Laser diode intracavity absorption IR spectrometry 1425
Laser diode near IR Raman spectrometer 2647
Laser dissocn mass spectrometry porphyrin 689
Laser dye detn spectrochem 861
Laser fluorometric detection thin layer chromatog 1931
Laser fluorometry protein detn dye 2285
Laser fluorometry TLC porphyrin methyl ester 2288
Laser induced phosphorescence spectrometry halogenated naphthalene 872
Laser induced photoemission hydrocarbon detn 320
Laser ionization diagnostic plume vaporization 2546
Laser ionization mass spectrometry nonvolatile classification 715
Laser ionization mass spectrometry polyarom hydrocarbon 2669
Laser ionization mass spectrometry solid 1029
Laser ionization surface analysis polymer 805
Laser luminescence fingerprint detection review 557a
Laser mass spectrometry layer chromatog coupling 2516
Laser Micro Analysis (book review) 1376a
Laser microprobe chemiluminescence detection elemental analysis 2557
Laser microprobe mass spectrometry particle analysis 914
Laser modified graphite electrode 1637
Laser photodissocn mass spectrometer 1458
Laser pulsed transient IR 1810
Laser radiation detector piezoelec ceramic 796
Laser Remote Chem Analysis (book review) 660a
Laser resonance ionization mass spectra lanthanum 695
Laser spectrometry analysis four wave mixing 998
Laser thermal lens water media 1660
Laser UV IR excited multiphoton ionization 612
Lasers. Principles and Applications (book review) 658a
Latex polymer density sedimentation fractionation 1934
Latex polystyrene fractionation sedimentation 2439
Lauroylvaline butylamide chiral phase chromatog 126
Lauryl sulfate thallium modified substrate phosphorimetry 2328
Lead copper preconcn electrodeposition spectrochem analysis 856
Lead detn anodic stripping voltammetry 2092 2609
Lead detn atomic emission spectrometry 1175
Lead detn drinking water atomic absorption 1410
Lead detn ethylation atomic absorption 1867
Lead detn ice Antarctica 1758
Lead detn river sediment atomic absorption 1414
Lead detn segmented flow voltammetry 2102
Lead electron diffractor spectroelectrochem detector 1216
Lead membrane neutral carrier transport 1140
Lead voltammetry mercury film electrode 2086
Least square multiexponential data analysis 2310
Least squares fit qual FTIR spectra 2708
Least squares polynomial convolution smoothing analysis 1303
Least squares regression plutonium nitric acid 1667
Lens thermal laser water media 1660
Lens thermal optical absorption detn 883
Lifetime fluorescence filtering review 839a
Lifetime fluorescence selectivity excitation emission matrix 580
Lifetime luminescence single photon counting 2704
Lifetime rapid detn error 30
Ligand estn soil sludge amendment 1295
Ligand immobilized fluorescence aluminum complexation 1001
Ligand oligosubstituted enzyme enzyme immunoassay 2160
Light absorption phosphorescence 1431
Light hydrocarbon analysis carbon hydrogen isotope 2149
Light scattering particle size review 143r
Limit preconcn metal electrodeposition solid electrode 856
Linear array electrode glassy carbon 2124
Linear isotherm diffusive sampler performance 843
Linear restrictor modeling supercrit fluid chromatog 356
Linear scan anodic stripping voltammetry mercury 2092
Linear scan voltammetry amalgam formation 965
Linearity evaluation liq chromatog detector 951a
Linearized model detn reaction kinetics 1949
Linked gas chromatog spectrometry analysis 1571
Lipid glassy electrode pharmaceutical detn voltammetry 170
Lipid layer electrochem 979
Lipid multilayer phase transition 2185
Lipooligosaccharide structure detn spectroscopy 416
Liq analysis coronaspray ion mobility spectrometry 601
Liq cation exchange chromatog protein 2059
Liq chromatog alc carbohydrate conductometric detection 631
Liq chromatog amine detn 1469
Liq chromatog amine trace derivatization reagent 1538
Liq chromatog amino acid coulometric detection 555
Liq chromatog amino acid detn 432
Liq chromatog benzene deriv retention 367
Liq chromatog biomol mass spectrometry 2504
Liq chromatog bonded phase column packing 2
Liq chromatog capillary column octylsilyl packed 1128

Liq chromatog carbohydrate amperometric detection 852
Liq chromatog carbohydrate detection modified electrode 2258
Liq chromatog carbon paste electrode 2585
Liq chromatog chiroptical detector review 77a
Liq chromatog chlorinated biphenyl dibenzodioxin dibenzofuran 1300
Liq chromatog cyclophosphamide chiral deriv prepn 441
Liq chromatog detector diode laser polarimeter 1238
Liq chromatog detector linearity evaluation 951a
Liq chromatog electrochem detection peptide detn 2664
Liq chromatog enantiomeric amine amino alc 1548
Liq chromatog fatty acid detection 910
Liq chromatog glassy carbon electrode activator 1989
Liq chromatog gradient elution voltammetric detection 1977
Liq chromatog high concn band 2373
Liq chromatog homopolymer oligomer sepn 471
Liq chromatog hydroxamic acid siderophore detn 1474
Liq chromatog IgG detn protein A 1314
Liq chromatog imirestat phenytoin serum protein 1171
Liq chromatog inorg analysis review 109r
Liq chromatog interface mass spectroscopy biomol 1577
Liq chromatog mass spectrometry spray ionization 1159
Liq chromatog metal ion detn 1272
Liq chromatog methotrexate body fluid 946
Liq chromatog micellar hydrophobicity 1040
Liq chromatog microelectrode array detector 295
Liq chromatog nerve analysis 436
Liq chromatog online diln 1791
Liq chromatog open tubular cation sepn 2747
Liq chromatog peptide mapping 2226
Liq chromatog polyamine 1921
Liq chromatog polymeric stationary phase 198
Liq chromatog polypyrrole stationary phase 2391
Liq chromatog preconcn flow injection analysis 496
Liq chromatog preparative optimization 982
Liq chromatog protein aggregation 514
Liq chromatog protein variant 1742
Liq chromatog quaternary ammonium compd 728
Liq chromatog quinone photoredn fluorescence detection 2267
Liq chromatog retention mechanism 930
Liq chromatog reversed phase retention correlation 1524
Liq chromatog selectivity modification subambient temp 1749
Liq chromatog selenium blood 2244
Liq chromatog selenium detn fluorometric detection 233
Liq chromatog silica support drug blood 2445
Liq chromatog silylated silica gel phase 41
Liq chromatog solute partition aq phase 2540
Liq chromatog spectrometry halogen detector 895
Liq chromatog sulfite detn 272
Liq chromatog surface enhanced Raman detection 888
Liq chromatog target factor analysis 1168
Liq chromatog theophylline blood 784
Liq chromatog thermal gradient 236
Liq chromatog thermospray mass spectrometry calibration 2126
Liq chromatog time domain differentiation computer 720
Liq chromatog UV detector bias nonlinearity 2571
Liq continuous flow SIMS polar 1013
Liq crystal chem bonded phase HPLC 1928
Liq crystal phase transition 2185
Liq evapn compensation pipet calibration 1080
Liq extractor high boiling flavor 1596
Liq gas interphase partition chromatog 2231
Liq membrane cation transport macrocycle 1140
Liq membrane effect ion selective electrode 1169
Liq secondary ion mass spectra 2154
Liq SIMS continuous flow evapn device 2582
Liq stationary phase functionalized mixed micelle 1984
Lithium attachment chem ionization mass spectrometry 1026
Lithium detn multiphoton ionization spectrometry 1010
Liver peptidoglycan marker alanine detn 265
Loop wire support sample insertion plasma 163
Low mol wt polar compd detn 1013
Low pH gradient elution HPLC 2
Low temp phosphorimetry polynuclear arom hydrocarbon 1182
Lubricant antioxidant detn platinum electrode 1467
Luminescence analysis cyclodextrin salt matrix 2643
Luminescence decay data 660
Luminescence detector cation 211
Luminescence flow injection copper cyanide detn 1505
Luminescence laser fingerprint detection review 557a
Luminescence lifetime single photon counting 2704
Luminescence spectrometry solid surface review 889a
Luminol electrooxidn kinetics graphite 2763
Luminol reagent iodine detn chemiluminescence 2800
Lumogallion immobilized fiber optic fluorescence sensor 1768
Lutidine std ion mobility spectra amine 684
Macrocycle cation transport liq membrane 1140
Magic angle spinning NMR zeolite catalyst 1821
Magnesium detn optical fiber detector 382
Magnesium selective electrode micro 574
Magnetic resonance rotamer microspeciation 2631
Major element detn rock x ray 1837
Mammal tissue streptococcus cell wall detn 265
Management information system lab review 612a
Manganese detn dual cathode discharge lamp 2137
Manganese detn river sediment atomic absorption 1414
Manganese detn seawater chemiluminescence 1392
Manuscript requirement 91
Mapping electron microprobe background subtraction 1612
Mapping peptide trypsin electrophoresis chromatog 2226
Marcellomycin urine voltammetry lipid glassy electrode 170
Mass calibration Fourier transform mass spectrometry 2422
Mass flow restrictor supercrit fluid chromatog 356
Mass selection reactant ion mass spectrometer 1874
Mass selective ion partition cyclotron cell 53
Mass spectra atom oxime redn 1442
Mass spectra benzene deriv isomer 1889
Mass spectra chromatog azo dye 2054
Mass spectra classification expert system 715
Mass spectra ion mol reaction 1447
Mass spectra laser resonance ionization lanthanum 695
Mass spectra liq secondary ion 2154
Mass spectra mol formula detn 2207
Mass spectra polyethylene glycol peptide 2050
Mass spectra pseudomol ion trap detector 1983
Mass spectrometer cell interface gas chromatograph 1874
Mass spectrometer computer controlled operation 330
Mass spectrometer Hartley transform 428
Mass spectrometer ion cyclotron resonance 2528
Mass spectrometer ion trap intermol process 2500
Mass spectrometer laser desorption ionization 1083
Mass spectrometer laser photodissocn 1458
Mass spectrometer plasma noise power spectra 606
Mass spectrometer screened electrostatic ion trap 1288
Mass spectrometer tandem air pollutant 260
Mass spectrometer thermal desorption 1017
Mass spectrometry amino acid tripeptide 1895
Mass spectrometry aq anhyd ammonia 2511
Mass spectrometry atm pressure spray ionization 1159
Mass spectrometry butyltin detn sediment std 2320
Mass spectrometry capillary isotachophoresis 228
Mass spectrometry carbon dioxide air 2416
Mass spectrometry carbon dioxide buffer gas 2523
Mass spectrometry chem ionization 86
Mass spectrometry chem ionization laser desorption 184
Mass spectrometry chem ionization lithium attachment 1026
Mass spectrometry continuous flow liq technique 2582
Mass spectrometry detn carbon hydrogen isotope 2149
Mass spectrometry detn org volatile compd 2751
Mass spectrometry discharge atomization ionization source 1879
Mass spectrometry emission spectrometry coupling 793
Mass spectrometry evolved gas analysis 802
Mass spectrometry fast atom bombardment 153 1293
Mass spectrometry fatty acid detn 494
Mass spectrometry field ionization desorption review 1201a
Mass spectrometry Fourier transform ICR 2130
Mass spectrometry Fourier transform impulse excitation 489
Mass spectrometry gas chromatog compact probe 2410
Mass spectrometry gas chromatog coupling 2402
Mass spectrometry gas chromatog differential 73 2118
Mass spectrometry gas chromatog Fourier IR 1584
Mass spectrometry gas chromatog linked analysis 1571
Mass spectrometry gas chromatog polyarom hydrocarbon 2669
Mass spectrometry heparin oligosaccharide 1453
Mass spectrometry inorg analysis review 109r
Mass spectrometry ion cyclotron resonance 53 2040
Mass spectrometry ion mobility 1093
Mass spectrometry ionization polymer 1195
Mass spectrometry isotope diln direct loading 755
Mass spectrometry isotope diln review 643a
Mass spectrometry laser dissocn porphyrin 689
Mass spectrometry laser ionization solid 1029
Mass spectrometry laser microprobe particle analysis 914
Mass spectrometry mass calibration Fourier transform 2422
Mass spectrometry microelectrothermal vaporization osmium detn 2263
Mass spectrometry multichannel heterodyne detection 749
Mass spectrometry multiply charged ion 1702
Mass spectrometry oxygen isotope detn org 1887
Mass spectrometry phase specific ion excitation 83
Mass spectrometry plasma desorption oligosaccharide analysis 2686
Mass spectrometry plasma laser ablation sampling 1243
Mass spectrometry plasma multivariate calibration 2031
Mass spectrometry plasma reagent analysis 827
Mass spectrometry plasma trace metal detn 149
Mass spectrometry pyridinium dihydropyridine system 1723
Mass spectrometry resonance ionization analysis review 1271a
Mass spectrometry secondary ion image quantification 65
Mass spectrometry secondary ion quant analysis 1946
Mass spectrometry secondary ion silicon analysis 412

Mass spectrometry stationary phase solvation 1348
Mass spectrometry supercrit fluid chromatog 775
Mass spectrometry surface analysis polymer 805
Mass spectrometry tandem polar compd detn 1013
Mass spectrometry tandem spectral interferent model 2277
Mass spectrometry tandem uric acid electrooxidn 1709
Mass spectrometry thermal desorption carbon fiber 1017
Mass spectrometry thermospray liq chromatog calibration 2126
Mass spectrometry thin layer chromatog 2516
Mass spectrometry trace element water 335
Mass Spectrometry/Mass Spectrometry. Techniques and Applications of Tandom Mass Spectrometry (book review) 1286a
Mass spectroscopy alanine cell wall 265
Mass spectroscopy alkene insect 1564
Mass spectroscopy biomol 1911 2504
Mass spectroscopy cholesterol detn 1718
Mass spectroscopy dual mode ion source 1310
Mass spectroscopy gas chromatog radiolabeled metabolite 2724
Mass spectroscopy glycolipid structure detn 416
Mass spectroscopy interface liq chromatog biomol 1577
Mass spectroscopy ion trap biomol 2316
Mass spectroscopy nickel detn 1099
Mass spectroscopy peptides glycerol 2674
Mass spectroscopy plant analysis 221
Mass spectroscopy plasma desorption protein 375
Mass spectroscopy secondary ion drug 1087
Mass spectroscopy selenium detn biochem 701
Mass spectroscopy trace element blood 1851
Mass spectroscopy zinc detn feces 1023
Mass transfer coeff extn kinetics 1036
Mass transfer displacement liq chromatog 1960
Mass transfer glucose enzyme sensor 77
Mass transfer microelectrode array detector 295
Master slave arrangement microcomputer data acquisition 593
Matching impedance inductively coupled plasma 2589
Math model protein electrophoresis 362
Matrix calcn regression analysis digital smoothing 1308
Matrix fluorescence lifetime selectivity excitation emission 580
Mechanics mol disaccharide structure 666
Mechanism copper atomization graphite furnace 2652
Mechanism indigodisulfonate ozone reaction 619
Mechanism ppt based ion selective electrode 453
Membrane electrode salicylate detn 566
Membrane electrode size selectivity biochem 303
Membrane electrodialysis suppressor ion chromatog 939
Membrane liq cation transport macrocycle 1140
Membrane liq effect ion selective electrode 1169
Membrane neutral carrier transient current 1624
Membrane perfluorosulfonate suppressor ion exclusion chromatog 548
Membrane phase separator extn app 1036
Membrane polymer electrode benzo crown ether 1618
Membrane potassium selective dihexenyl adipate photopolymn 246
Mercurous dimeric cation diffusion perchloric acid 1305
Mercury film iridium based electrode voltammetry 2092
Mercury film silver based electrode voltammetry 2086
Mercury pen lamp source fluorometer analysis 282
Mercury total detn digestion conductometry 1230
Merging chamber sample introduction mass spectrometer 2263
Mesophase cyanobenzylideneoctyloxyaniline orientation interaction coated silica 1534
Metabolite detection in vivo NMR 636
Metabolite radiolabeled detection 2724
Metal amalgam forming detn stripping voltammetry 2092
Metal analysis phosphorus radiochem neutron activation 2338
Metal atom detection multiphoton ionization 1010
Metal binding fulvic acid spectroscopy 483
Metal binding humic substance 1519
Metal detn industrial wastewater HPLC 1494
Metal distribution ion microscopy fibroblast 2690
Metal immobilized affinity chromatog protein 1742
Metal interference removal algae column 468
Metal ion detn liq chromatog 1272
Metal ion simultaneous detn spectrophotometry 1847
Metal sampling aerosol spark discharge 1826
Metal trace detn biochem ref 216
Metal trace detn plasma mass spectrometry 149
Metal trace detn water std 1857
Metal trace preconcn electrodeposition solid electrode 856
Metal trace speciation detn water 525
Metal uptake algae 624
Meteorite analysis rare earth mass spectrometry 755
Methacrylate styrene copolymer chromatog sepn 2171
Methane detn oxygen gas chromatog 2237
Methane reagent chem ionization mass spectrometry 184
Methanol complex oxazine 4 formation const 2394
Methanol water assocn chromatog retention 349
Methods in Enzymol. Vol. 158. Metallobiochemistry, Pt. A (book review) 308a
Methotrexate detn blood urine HPLC 946
Methoxyethanol aq elec cond picric acid 1971
Methoxyethanol solvent polyprotic acid titrn 177
Methoxypropane reagent water detn 1325
Methyl methylphosphonate detn air 260
Methyl methylphosphonate sorption montmorillonite 2047
Methyl phthalate HPLC polypyrrole phase 2391
Methyl viologen detn spectroelectrochem detector 1216
Methylamine dansyl sepn deuteromethylamine chromatog 491
Methylaminoalanine detn continuous flow liq SIMS 1013
Methylcatechol voltammetry Nafion coated microdisk electrode 2193
Methylphenylpyridine detn continuous flow liq SIMS 1013
Methylphosphonate isopropyl detection FET sensor 2355
Methylthiophene coated glassy carbon electrode 2809
Micellar d electrokinetic chromatog 491
Micellar electrokinetic chromatog ionic compd 2434
Micellar enhancement fluorescence thermal lensing correction 928
Micellar liq chromatog hydrophobicity 1040
Micelle arom hydrocarbon energy transfer 1405
Micelle chiral mixed optical resoln 1984
Micelle chromatog electrokinetic 251
Micelle compn phosphorescence 1431
Micelle electrokinetic capillary chromatog 2455
Micelle isoprene styrene block copolymer 1318
Micelle mobile phase liq chromatog 1353
Micelle reversed formation iodine detn 2800
Micro electrode magnesium selective 574
Microbalance quartz crystal cation detector soln 290
Microbalance quartz crystal electrochem use review 1147a
Microband electrode dual biochem analysis 2200
Microbial sensor phage mutagen detection 2388
Microcalorimeter glucose enzyme sensor model 77
Microcapillary hydrodynamic chromatog copolymer micelle 1318
Microcell electrolytic IR spectroelectrochem 2805
Microcolumn gas chromatog UV detection 1249
Microcolumn gel chromatog polymer 961
Microcolumn liq chromatog org water 1208
Microcomputer master slave arrangement data acquisition 593
Microcomputers and Lab Instrumentation, 2nd Ed. (book review) 856a
Microcontroller lab 433a
Microdisk electrode voltammetry supercrit carbon dioxide 2193
Microelectrode array electrochem detector chromatog 295
Microelectrode array oxygen sensor 159
Microelectrode carbon fiber fabrication 1805
Microelectrode cylindrical concn profile spectroscopy 2347
Microelectrode cylindrical voltammetry analysis 1211
Microelectrode diffusion cyclic voltammetry chronoamperometry 1630
Microelectrode polychlorotrifluoroethylene graphite composite chronoamperometry 2330
Microelectrode polymer coated voltammetry supercrit fluid 270
Microelectrode spherical segment coeff current equation 1305
Microelectrode ultra ensemble response detection limit 762
Microelectrothermal vaporization mass spectrometry osmium detn 2263
Microheater merging sample introduction mass spectrometry 2263
Microhole array oxygen electrode 159
Microhole electrode array cyclic voltammetry theory 1763
Microprobe electron analysis background subtraction 1612
Microprobe geol inorg analysis review 109r
Microscopy electrochem scanning feedback mode 1221
Microscopy ion image quantification detector discrimination 65
Microscopy ion metal distribution fibroblast 2690
Microscopy review 243r
Microscopy scanning electrochem 132
Microstructure surface electrode spectroscopy review 775a
Microwave induced plasma fluoride detn 674
Microwave induced plasma liq chromatog detector 895
Microwave mol formula detn 2207
Milk analysis bromide iodide gas chromatog 733
Milk fat triglyceride detn 698
Mill tailing std stability radiochem analysis 2255
Mineral analysis rare earth mass spectrometry 755
Mixed reagent metal ion simultaneous detn 1847
Mixing optimization flow injection analysis 973
Mixt analysis gas chromatog mass spectrometry 2118
Mixt analysis single component mass spectrometry 73
Mixt fatty acid analysis 494
Mixt org vapor identification FTIR 2708
Mobile phase elimination IR chromatog coupling 2212
Mobile phase urea solubilized cyclodextrin TLC 422
Model chloramine interference water analysis 991
Model conductometric detection alc carbohydrate HPLC 631
Model headspace sampling volatile polymer 1202
Model metal complexation humic substance 483
Model quadratic diffusive sampling org analysis 917
Model spectral interferent nonbilinear rank annihilation 2277
Modeling pyrazine gas chromatog retention index 1328
Modern thin layer chromatog review 1257a
Modified electrode graphite epoxy resin 508
Modulation analyte velocity capillary zone electrophoresis 1590
Mol absorption measurement dual channel detector 593
Mol formula detn chromatog effluent 2207
Mol ion interference mass spectrometry 2031
Mol ion reaction kinetics 1447
Mol Luminescence Spectroscopy. Methods and Applications. Pt. 2 (book review) 658a

Mol mechanics disaccharide structure 666
Mol mechanics NMR spectra arom hydrocarbon 2658
Mol structure detn disaccharide 666
Mol structure heparin oligosaccharide 1453
Mol wt detn chromatog mass spectrometry 1874
Mol wt polyester gel chromatog 1321
Mol wt selectivity membrane electrode 303
Molasses analysis online polarimetry 1238
Molinate ELISA gas chromatog 819
Moment peak reproducibility chromatog nonstochastic 1058
Monolayer film analysis absorption spectrometry 386
Monosaccharide detn fermn broth immobilized enzyme 831
Morphol bonded phase temp induced selectivity 1749
Morphol carbon nickel electroplating 560
Morphol structure multilayer polymer NMR 1870
Moving belt sample cooling device phosphorimetry 1182
Multichannel heterodyne detection mass spectrometry 749
Multidimensional thin layer chromatog review 1257a
Multiexponential data analysis reiterative regression algorithm 2310
Multilayer polymer morphol structure NMR 1870
Multiligand model metal binding 1519
Multimodal thin layer chromatog review 1257a
Multinuclear NMR (book review) 656a
Multiphoton ionization metal atom detection 1010
Multiphoton ionization UV IR laser excited 612
Multiple linear regression plasma mass spectrometry 2031
Multiply charged ion mass spectrometry 1702
Multivariate analysis hydroxide ion near IR 1419
Multivariate calibration plasma mass spectrometry 2031
Multivariate statistics benzene deriv retention HPLC 367
Muscle dogfish arsenocholine 2118
Muscle relaxant HPLC polystyrene divinylbenzene phase 728
Mutagen detection phage microbial sensor 2388
Mycobacteria glycolipid structure detn 416
Myoglobin sepn isoelec focusing fractionation 912
NADH oxidase amperometric enzymic analysis 25
Nafion catalyst water detn gas chromatog 1325
Nafion coated microelectrode voltammetry 270
Nafion coating fiber electrode 1805
Nafion film platinum microdisk electrode voltammetry 2193
Nafion membrane suppressor ion chromatog 939
Nanosecond pulse laser mass spectrometry hydrocarbon 2669
Naphthalene halogenated laser induced phosphorescence spectrometry 872
Naphthalenedicarboxaldehyde deriv amino acid detn 432
Natural gas analysis carbon hydrogen isotope 2149
Natural Products Isolation. Sepn Methods for Antimicrobials, Antivirals, and Enzyme Inhibitors (book review) 1287a
Near IR diode laser Raman spectrometer 2647
Near IR spectrometry analysis error 398
Near IR spectrometry hydroxide ion detn 1419
Nebulization fluoride detn 674
Nebulization pneumatic selenium detn biochem 701
Nebulizer thimble glass frit atomic spectrometry 2777
Needle spruce analysis chromatog spectroscopy 221
Needle sulfite detn fluorometry 1755
Neon nitrogen quenching discharge plasma 326
Nerve analysis liq chromatog voltammetry 436
Nerve neurotransmitter detn review 292a
Nested loop system thorium uranium detn 1789
Neurochem capillary electrophoresis review 292a
Neuronal biosensor review 533a
Neurotransmitter detn electrode 1397
Neurotransmitter detn nerve review 292a
Neurotransmitter detn single nerve 436
Neutral laser desorption chem ionization spectrometry 184
Neutron activation radiochem phosphorus detn metal 2338
Neutron activation radiochem zinc isotope 2757
Neutron activation silicon detn biol 1834
Neutron scattering particle size review 143r
New Directions in Electrophoretic Methods (book review) 1163a
Nickel detn urine chromatog spectroscopy 1099
Nickel ethylene pyrolysis carbon electrode 560
Nickel present cobalt detn polarog 2178
Niobium noise power spectra mass spectrometry 606
Nioxime reagent cobalt detn polarog 2178
Nitrate detn redn chemiluminescence 2715
Nitric acid detn plutonium present spectrophotometry 1667
Nitric acid detn polymer coated waveguide 1674
Nitride aluminum powder reaction water 2399
Nitrite detn ion exclusion chromatog 1485
Nitrite detn redn chemiluminescence 2715
Nitrite reagent cobalt detn polarog 2178
Nitrite selective electrode pH response 1169
Nitrobenzoic acid chemisorbed monolayer 386
Nitrobenzoyl deriv amino acid isopropyl ester 1984
Nitrocresol HPLC resonance Raman scattering detection 888
Nitrogen argon neon quenching discharge plasma 326
Nitrogen chloride detn wastewater chlorination 2332
Nitrogen compd supercrit chromatog thermionic detector 2082
Nitrogen contg org detn Raman spectrometry 1697
Nitrogen detn oxygen gas chromatog 2237
Nitrogen dioxide air passive sampler 187
Nitrogen dioxide detection FET sensor 2355
Nitrogen fluoride chemiluminescence reagent laser microprobe 2557
Nitrogen ion rotational structure transition 1052
Nitrogen org compd analysis oxygen isotope 1887
Nitrogen oxide doped plasma detector chromatog 1815
Nitrophenol detn voltammetry 2809
Nitrophenol HPLC resonance Raman scattering detection 888
Nitrous oxide supercrit extn ash 2770
NMR aluminum phosphato complex soln 1253
NMR automated high resoln review 107a
NMR carbon alkylcyclohexanone alkyldecalone simulation 863
NMR carbon disaccharide structure 666
NMR carbon piperidine simulation 2489
NMR carbon 13 spectral simulation 1115a
NMR carbonaceous deposit analysis zeolite catalyst 1821
NMR HPLC cyclopropylmethylaminooxazoline drug detn 772
NMR imaging review 23a
NMR in vivo surface coil fabrication 636
NMR multilayer polymer morphol structure 1870
NMR phys property diesel fuel 206
NMR sample temp detn 1594
NMR spectra mol mechanics arom hydrocarbon 2658
NMR spectrometry antimycin A 404
NMR spectrometry internal std Delrin 2579
NMR Spectroscopy (book review) 1162a
NMR two dimensional automated structure 2298
NMR two dimensional spectral interferent model 2277
NMR, Vol. 17 (book review) 1287a
Noise decrease fiber electrode 1805
Noise microelectrode array amperometry voltammetry addn 288
Noise power spectra plasma mass spectrometer 606
Noise shot data analysis distribution function 2479
Noise shot limit data analysis 2483
Noise spectra correlation convolution analysis 898
Nonactin immobilized ionophore ammonium detn 211
Nonaq mixed solvent polyprotic acid titrn 177
Nonbilinear rank annihilation model spectral interferent 2277
Nonequil band broadening deconvolution 2735
Nonequil plate height micelle chromatog 2455
Nonlinear laser spectrometry wave mixing 998
Nonlinearity UV calibration curve diode array 2571
Nonmetal analyte introduction device atomic spectrometry 790
Nonstochastic chromatog peak moment reproducibility 1058
Nonsuppressed ion chromatog cation detn 1435
Nonvolatile compd supersonic jet spectroscopy 777
Norcarboxytetrahydrocannabinol urine gas chromatog forensic 925
Normal distribution shot noise data analysis 2479
Normalization acoustic signal chemiluminescence laser microprobe 2557
Nortetrahydrocannabinolcarboxylate urine std forensic 540
Noscapine sepn papaverine HPLC 720
Nujol graphite paste electrode 279
Nutrition intestine zinc absorption detn 1023
Nylon multilayer film morphol NMR 1870
Octadecyl silica adsorption carbon dioxide 951
Octane number gasoline IR spectra 313
Octyl phthalate plasticizer quaternized polyvinylpyridine 570
Octylsilyl packed capillary column HPLC 1128
ODS silica column fatty acid chromatog 2076
Oil crude analysis chromatog IR spectrometry 1584
Oil transformer PCB detn colorimetry 2682
Oligomer homopolymer sepn liq chromatog 471
Oligonucleotide mass spectra algorithm 2154
Oligosaccharide detn fermn broth immobilized enzyme 831
Oligosaccharide heparin mass spectrometry 1453
Oligosaccharide variant surface glycoprotein Trypanosoma 2686
Oligosubstituted enzyme ligand enzyme immunoassay 2160
Olive oil classification computer 2098
Oncolumn cond detection carboxylic acid detn 766
Online diln ion chromatograph 1791
Online ion exchange trace enrichment automated 520
Online Process Analyzers (book review) 1376a
Online radioisotope detector capillary electrophoresis 1642
Online supercrit fluid extn app phosphonate 1986
Open tubular capillary 251
Open tubular column short chromatog spectrometry 2402
Open tubular gas chromatog 2165
Open tubular liq chromatog cation sepn 2747
Open tubular liq chromatog voltammetric detection 1977
Optic fiber sensor avidin biotin 1069
Optical detection acid ion exclusion chromatog 548
Optical fiber chromatog detector capillary microbore 876
Optical fiber detector magnesium calcium detn 382
Optical fiber mol absorption luminescence measurement 593
Optical monitor substrate surface enhanced Raman 1779
Optical relative humidity sensor 1863
Optical resoln chiral mixed micelle 1984
Optical rotation detector HPLC online analysis 1238
Optical sensor high acidity fiber optics 1674
Optical spectroscopy protein structure review 642
Optical waveguide analysis adsorbed monolayer 386
Optimization confluent mixing flow injection analysis 973

Optimization flame photometric detector organosulfur 58
Optimization global generalized simulated annealing 2024
Optimization preparative elution chromatog 1368
Optimization preparative elution chromatog correction 2464
Optimization preparative liq chromatog 982
Optimization theory preparative liq chromatog 1276
Optimization thermionic detector supercrit fluid chromatog 2082
Optimization wavelength selection simulated annealing 2024
Orange juice flavor analysis 1596
ORD analytical application review 77a
Ore uranium std stability radiochem analysis 2255
Org analysis diffusive sampling quadratic model 917
Org aq solvent surface tension 194
Org cation binding surface fluorescence 590
Org compd detn radioactive liq 2751
Org conductor electrode ultramicroelectrode array 1048
Org detn air FTIR 677
Org detn air supercrit extn 736
Org solvent detn wastewater sensor 2306
Org surface analysis ESCA review 589a
Org trace detn water chromatog 1208
Org vapor mixt identification FTIR 2708
Organometallic compd thermal decompn nickel 560
Organosulfur compd detn chromatog flame detection 2616
Organosulfur supercrit fluid chromatog chemiluminescence detection 797
Organosulfur supercrit fluid chromatog photometric detection 58
Orientation cyanobenzylideneoctyloxyaniline mesophase coated silica 1534
Osmium detn mass spectrometry microelectrothermal vaporization 2263
Osmium 186 187 ratio detn 2263
OV 101 pyrazine retention index modeling 1328
Overlapped peak detection chromatog spectrometry 2240
Overtake phenomena temp gas chromatog correction 512
Oxalate chlorophenyl hydrogen peroxide stability 1298
Oxalato aluminum complex detn ion chromatog 535
Oxalic acid hydrazine redox reaction 508
Oxazine 4 methanol complex formation const 2394
Oxazoline cyclopropyl chromatog liq NMR 772
Oxidase glucose sensor thermoelec model 77
Oxidase glucose tin oxide enzyme electrode 2352
Oxidase NADH amperometric enzymic analysis 25
Oxide barium yttrium copper stoichiometry detn 1497
Oxide nitrogen detection FET sensor 2355
Oxide tin electrode modified horseradish peroxidase 2352
Oxidn ascorbic acid ferricyanide contg electrocatalyst 848
Oxidn electrochem rhodium complex IR spectra 2805
Oxidn electrode insulin amperometric detn 2462
Oxidn iodide ferric ion kinetics 2562
Oxidn state semiconductor superconductor 1497
Oxime immobilized silica gel equil 1001
Oxime redn fast atom bombardment 1442
Oxygen analysis impurity gas chromatog 2237
Oxygen effect glucose enzyme sensor 77
Oxygen effect lead cadmium detn voltammetry 2609
Oxygen electrode microhole array 159
Oxygen electroredn rhodium anilinopyridine binuclear 279
Oxygen flame photometric detector optimization organosulfur 58
Oxygen isotope detn org mass spectrometry 1887
Oxygen org compd mass spectrometry 86
Oxygen sensitive specie spectroelectrochem cell 1787
Oxygen sepn argon chromatog chabazite adsorbent 1112
Ozone chemiluminescence reaction phosphine 2699
Ozone detn aq phase chemiluminescence 619
Painting historic varnish 1228a
Papaverine sepn noscapine HPLC 720
Paraffin oil carbon paste electrode 2585
Particle sample prepn LAMMA 914
Particle size detn colloid sedimentation 741
Particle size detn review 143r
Particle size distribution band deconvolution 2735
Particle submicrometer analysis hydrocarbon 320
Particle wall interaction retention perturbation 811
Particulate airborne analysis review 1r
Partition gas liq interphase chromatog 2231
Partition high resoln ion cyclotron resonance 83
Partition hydrophobicity chromatog correlation 1040
Partition ion cyclotron resonance cell 53
Partition solute aq phase liq chromatog 2540
Partition solute hexadecane aq methane 349
Passive sampler nitrogen dioxide formaldehyde 187
Paste carbon electrode modified rhodium complex 279
Paste carbon modified electrode aldehyde detn 2599
PCB detn transformer oil colorimetry 2682
Peak moment reproducibility chromatog nonstochastic 1058
Peak overlapped detection chromatog spectrometry 2240
Peak shape gas chromatog injection method 1489
Penicillamine cysteine redox reaction 508
Penicillamine reagent selenium detn fluorometry 233
Penicillin detn enzyme fiber optic sensor 1069
Penicillin micellar electrokinetic chromatog 2434
Penning ionization glow discharge 1103
Pentacyanoferrate polyvinylpyrazine complex reaction 1799
Pentadecylacridine Fourier transform mass spectrometry 184
Peptide capillary electrophoresis 1186
Peptide chromatog mass spectrometry spray ionization 1159
Peptide detn liq chromatog electrochem detection 2664
Peptide HPLC silane modified column 2
Peptide mapping trypsin electrophoresis chromatog 2226
Peptide mass spectra 2050
Peptide tri laser desorption mass spectrometry 1895
Peptides glycerol mass spectroscopy 2674
Peptidoglycan marker alanine detn liver 265
Perchloric acid diffusion mercurous dimeric cation 1305
Perfluoroalkoxy resin still purified reagent analysis 827
Perfluorosulfonate membrane suppressor ion exclusion chromatog 548
Permanent gas chromatog calcium chabazite adsorbent 1112
Peroxidase horseradish modified tin oxide electrode 2352
Peroxide detn chemiluminescence probe 633
Peroxide hydrogen chlorophenyl oxalate stability 1298
Peroxide hydrogen detn amperometry enzyme sensor 2352
Peroxide hydrogen detn voltammetry 2176
Peroxyacetyl nitrate detn gas chromatog decompn 2731
Peroxyalkanoyl nitrate sepn alkyl nitrate 771
Peroxyoxalate chemiluminescence reagent stability 1298
Peroxypropionyl nitrate detn gas chromatog decompn 2731
Pesticide analysis chromatog plasma detector 1815
Pesticide analysis method review 153r
Pesticide gas chromatog coupled TLC 1906
Pesticide thin layer chromatog 422
Petroleum coal liq analysis review 165r
Petroleum distillate sulfur detn GC 2292
Petroleum fuel hydroxyl compd detn 1260
pH detection potentiometric suppressed ion chromatog 787
pH detn fiber optic sensor 174
pH detn HEPES buffer 1400
pH electrode bicarbonate carbonate detn 638
pH electrode flow injection analysis 922
pH gradient immobilized isoelec focusing review 1602
pH response nitrite selective electrode 1169
pH sensor fiber optic fluorescein immobilization 202
Phage microbial sensor mutagen detection 2388
Pharmaceutical analysis amine kinetic potentiometry 1358
Pharmaceutical analysis review 191r
Pharmaceutical chem chiroptical analysis review 77a
Pharmaceutical detn voltammetry lipid glassy electrode 170
Phase fluorometry hapten antibody complex 309
Phase resolved fluorescence excitation emission matrix 580
Phase resolved single frequency fluorometric analysis 1510
Phase specific ion excitation mass spectrometry 83
Phase transition liq crystal lipid multilayer 2185
Phenanthroline reagent gadolinium samarium detn 1063
Phenazine std polynuclear arom hydrocarbon phosphorimetry 1182
Phenol detn voltammetry 2809
Phenolic compd detn voltammetry 2809
Phenolic glycolipid structure detn spectroscopy 416
Phenoxy herbicide extn detn water 1363
Phenylformamidine rhodium complex oxidn spectroelectrochem 2805
Phenylporphyrinatotin dichloride membrane salicylate electrode 566
Phenytoin detn fluorescence immunoassay 309
Phenytoin imirestat serum protein binding HPLC 1171
Phenytoin metabolite radiolabeled detection urine 2724
Phosphate crown ether protein detn 2362
Phosphate detn chemiluminescence 2699
Phosphatidylcholine modified carbon electrode 979
Phosphato aluminum complex soln NMR 1253
Phosphine chemiluminescence reaction ozone 2699
Phospholipid chromatog mass spectrometry spray ionization 1159
Phosphonate detn supercrit fluid extn chromatog 1986
Phosphonium isotachophoresis mass spectrometry 228
Phosphorescence analysis room temp solid surface 2643
Phosphorescence light absorption micelle compn 1431
Phosphorescence spectrometry laser induced halogenated naphthalene 872
Phosphorescence synthetic enzyme model surfactant 2475
Phosphorimetry low temp polynuclear arom hydrocarbon 1182
Phosphorimetry room temp polynuclear arom hydrocarbon 2328
Phosphorus compd supercrit chromatog thermionic detector 2082
Phosphorus detn metal radiochem neutron activation 2338
Phosphorus 32 labeled compd electrophoresis detector 1642
Photochem labile compd TLC IR spectrometry 615
Photoconductive IR detector chloride chlorine detn 2785
Photodiode array detection low temp phosphorimetry 1182
Photodiode array detector atomic absorption spectrometer 1670
Photodiode array detector spectrochem analysis 2347
Photodiode array spectrophotometer gas chromatog detection 1249
Photodissocn laser mass spectrometer 1458
Photoelectron spectroscopy x ray quantitation review 469a
Photoelectron x ray spectroscopy instrumentation review 589a
Photoemission laser induced hydrocarbon detn 320
Photoetching NMR surface coil fabrication 636
Photoionization detection oxygen analysis gas chromatog 2237
Photometric detection organosulfur supercrit fluid chromatog 58
Photometric flame detection supercrit fluid chromatog 2616

Photometric flame detector optimization organosulfur 58
Photomultiplier detection luminescence spectrometer 593
Photon ionization spectroscopy resonant 777
Photon single counting luminescence lifetime 2704
Photopolymn dihexenyl adipate potassium selective membrane 246
Photoredn fluorescence detection quinone HPLC 2267
Phthalate HPLC polypyrrole phase 2391
Phthaldialdehyde reaction ammonium detn 408
Phthalic acid titrn conductometric 177
Phthalocyanine adsorbed monolayer 386
Phthalocyanine cobalt polyvinylpyridine electrode modification 508
Phys change acoustic emission 2638
Phys property NMR diesel fuel 206
Picosecond pulse laser mass spectrometry hydrocarbon 2669
Picric acid ionization amphiprotic mixt 1971
Piezoelec ceramic detector laser radiation 796
Piezoelec crystal detector carbon dioxide fermentor 746
Piezoelec immunol biosensor kinetic immunoassay 1227
Pineapple juice flavor analysis 1596
Piperidine carbon NMR simulation 2489
Pipet calibration statistics 1080
Pittsburg Conference Atlanta announcement 139a
Plant analysis gas chromatog mass spectroscopy 221
Plant analysis nitrate nitrite 2715
Plant analysis vitamin K1 2267
Plant ext analysis aminomethylaminopropionic acid SIMS 1013
Plasma analysis IR spectrometry 2016
Plasma atomic emission sulfite detection HPLC 272
Plasma atomic emission thermal gradient HPLC 236
Plasma desorption mass spectrometry oligosaccharide analysis 2686
Plasma desorption mass spectroscopy protein 375
Plasma detection atomic emission sulfur 2292
Plasma direct current atomic emission spectrometry 1175
Plasma discharge quenching argon neon nitrogen 326
Plasma emission spectrometry nonmetal sample introduction 790
Plasma helium transition nitrogen ion 1052
Plasma ignition threshold condition mass spectrometry 1029
Plasma inductively coupled hydride generation online 285
Plasma inductively coupled impedance matching 2589
Plasma mass spectrometer noise power spectra 606
Plasma mass spectrometry emission spectrometry 793
Plasma mass spectrometry laser ablation sampling 1243
Plasma mass spectrometry reagent analysis 827
Plasma mass spectrometry trace metal detn 149
Plasma microwave induced fluoride detn 674
Plasma radio frequency detector supercrit chromatog 1815
Plasma sample insertion wire loop support 163
Plasma spectrometer liq chromatograph interface 895
Plasma spectrometry inorg analysis review 109r
Plasticized membrane nitrite ion selective electrode 1169
Plasticizer photopolymn ion selective FET 246
Plasticizer quaternized polyvinylpyridine ion transport 570
Platinized carbon fiber microhole oxygen electrode 159
Platinum electrode conductometric transducer biosensor 1737
Platinum electrode lubricant antioxidant detn 1467
Platinum iridium electrode ultramicro 1630
Platinum microdisk electrode Nafion film voltammetry 2193
Platinum rhenium alumina catalyst analysis chloride 1924
Plume vaporization laser ionization diagnostic 2546
Plutonium detn nitric acid present spectrophotometry 1667
PMMA surface analysis laser ionization 805
Pneumatic nebulization selenium detn biochem 701
Poisoning amnesic shellfish review 1053a
Poisson distribution shot noise data analysis 2479
Polar compd detn tandem mass 1013
Polarimeter detector small flow cell 1238
Polarimetry analytical application review 77a
Polarity solvent reversed phase liq chromatog 1524
Polarity surface modified silica gel 41
Polarog adsorption catalytic cobalt ultratrace detn 2178
Polarog conjugated diene detn gasoline 1502
Polarog surfactant interference fumed silica effect 1598
Polemic simplex algorithm culminating quadratic convergence 1783
Polishable modified carbon fiber electrode 1460
Pollutant air detn review 1r
Pollutant air tandem mass spectrometer 260
Poly methylthiophene coated glassy carbon electrode 2809
Polyamide plate TLC mass spectrometry detection 2516
Polyamide stationary phase thin layer chromatog 422
Polyamine detn urine HPLC 1921
Polyarom hydrocarbon gas chromatog mass spectrometry 2669
Polybutadienemaleic acid coated column cation chromatog 2747
Polybutadienesulfonic acid coated column cation chromatog 2747
Polycarbonate ablation supersonic jet spectrometry 1530
Polychlorotrifluoroethylene graphite composite microelectrode chronoamperometry 2330
Polychlorotrifluoroethylene mulling oil carbon paste electrode 2585
Polycyclic arom hydrocarbon adsorption aerosol 708
Polycyclic arom hydrocarbon chromatog subambient temp 1749
Polycyclic arom hydrocarbon detn aerosol 320
Polycyclic arom hydrocarbon detn luminescence 2643
Polycyclic arom hydrocarbon detn water 1333
Polycyclic arom hydrocarbon thin layer chromatog 422
Polyester mol wt gel chromatog 1321
Polyether carboxylic antibiotic optical detector 382
Polyethylene glycol mass spectra 2050
Polyethylene multilayer film morphol NMR 1870
Polyethylene oxide polymer detector 584
Polyethylene terephthalate gel chromatog 1321
Polymer bound tetrahydroborate column arsine generation 2079
Polymer coated microelectrode voltammetry supercrit fluid 270
Polymer coated waveguide sensor high acidity 1674
Polymer controlled release dye pH sensor 174
Polymer electrolyte chromatog detector 584
Polymer identification mass spectrometry 715
Polymer ligand pyrazine deriv electrode coating 1799
Polymer membrane electrode benzo crown ether 1618
Polymer membrane ionically conducting microelectrode 270
Polymeric activated ester reagent amine derivatization 1538
Polymeric chiral reagent fluorenylmethyl amino acid 1548
Polymeric stationary phase electrochem prepd HPLC 198
Polymeric surface analysis ESCA review 589a
Polymyxin acylase chromatog support drug detn 2445
Polynomial least squares convolution smoothing analysis 1303
Polynuclear arom hydrocarbon low temp phosphorimetry 1182
Polynuclear arom hydrocarbon room temp phosphorimetry 2328
Polyoxyethylene surface analysis laser ionization 805
Polypropylene volatile detn headspace sampling 1202
Polyprotic acid titrn conductometric 177
Polypyrrole electrochem coated vitreous carbon phase 198
Polypyrrole stationary phase HPLC 2391
Polysiloxane chiral stationary phase gas chromatog 2121
Polystyrene ablation supersonic jet spectrometry 1530
Polystyrene chromatog elution retention 2449
Polystyrene divinylbenzene phase quaternary ammonium HPLC 728
Polystyrene latex fractionation sedimentation 2439
Polystyrene surface analysis laser ionization 805
Polystyrenesulfonate sodium size exclusion chromatog 530
Polyurethane structure SIMS 2142
Polyvinyl alc substrate indicator immobilized sensor 202
Polyvinylpyrazine pentacyanoferrate complex reaction 1799
Polyvinylpyridine cobalt phthalocyanine electrode modification 508
Polyvinylpyridine quaternized ion transport plasticizer 570
Porphyrin cobalt nitrite selective electrode 1169
Porphyrin laser dissocn mass spectrometry 689
Porphyrin methyl ester laser fluorometry TLC 2288
Pos ion mobility spectra amine 684
Postcolumn derivatization Tiron aluminum speciation chromatog 535
Postcolumn reaction anion chromatog background suppression 122
Potassium detection liq 290
Potassium detn amperometry electrode 2594
Potassium detn blood 2365
Potassium detn luminescence detector 211
Potassium membrane neutral carrier transport 1140
Potassium selective solid state sensor 246
Potential current curve kinetics electrode reaction 2249
Potential flatband cadmium sulfide crystal face 1980
Potential formal redox reaction coating 1799
Potential sweep coulometry amino acid chromatog 555
Potentiometric pH detection suppressed ion chromatog 787
Potentiometry anion vitamin B12 membrane electrode 499
Potentiometry bicarbonate carbonate detn 638
Potentiometry biotin detn 1728
Potentiometry cell continuous flow analysis 504
Potentiometry kinetic amine detn 1358
Ppt based ion selective electrode mechanism 453
Pptn preconcn copper silicate rock 1427
Practical HPLC Method Development (book review) 1040a
Preceding following catalytic chem reaction voltammetry 965
Preconcn Donnan dialysis cation detn 1410
Preconcn ion exchange flow injection analysis 496
Preconcn trace metal electrodeposition solid electrode 856
Prediction gasoline octane number IR 313
Preparative elution chromatog optimization 1368
Preparative liq chromatog optimization 982
Preparative-Scale Chromatog (book review) 1161a
Preservation gasoline arom headspace chromatog 2584
Pressure flow relation supercrit fluid chromatog 356
Pressure regulated restrictor supercrit chromatog 1178
Pretreatment electrochem graphite electron exchange 2763
Pretreatment electrochem laser graphite electrode 1637
Primary amine detn kinetic potentiometry 1358
Principal component analysis overlapped peak detection 2240

Principal component regression plasma mass spectrometry 2031
Probability Bayes data analysis shot noise 2483
Probe film stability tandem liq 1013
Problem Solving in Analytical Chem (book review) 420a
Problem Solving with Microbeam Analysis (book review) 858a
Process monitor chromatog solute independent calibration 1915
Programmed automated discontinuous flow analyzer 2109
Propanol sorption stationary phase supercrit chromatog 1348
Propantheline detn continuous flow potentiometry 504
Propene diffusion heptane hexadecane water 2231
Propene ethylene rubber analysis 458
Propene indium complex reagent chem ionization 86
Prosthetic cobalt chromium alloy tissue 1235
Protein A HPLC IgG detn 1314
Protein binding detection piezoelec immunosensor 1227
Protein binding serum imirestat phenytoin HPLC 1171
Protein blood isoelec focusing review 1602
Protein C reactive detn electrode 2362
Protein capillary electrophoresis 1186
Protein cation exchange liq chromatog 2059
Protein detn dye laser fluorometry 2285
Protein detn wheat 398
Protein electrophoresis computer simulation 362
Protein G chromatog antibody detn 1901
Protein HPLC aggregation 514
Protein HPLC silane modified column 2
Protein hydrolyzate analysis amino acid 555
Protein isoelec focusing field flow fractionation 912
Protein mass spectra algorithm 1702
Protein plasma desorption mass spectroscopy 375
Protein structure optical spectroscopy review 642
Protein variant liq chromatog 1742
Proton carbon magnetization transfer NMR 2298
Proton metal competition humic substance 1519
Protonation const rotamer microspeciation 2631
Prussian Blue detector electroinactive cation 290
Pseudomol ion trap detector mass spectra 1983
Pseudomonas fluorescens supernatant analysis siderophore 1474
Pullulan size exclusion chromatog 530
Pulse duration laser mass spectrometry hydrocarbon 2669
Pulse Methods in 1D and 2D Liq-Phase NMR (book review) 92a
Pulse polarog diene detn gasoline 1502
Pulsed amperometry alkanolamine detn chromatog 2466
Pulsed coulometry amino acid liq chromatog 555
Purge trap analysis radioactive liq 2751
Purifn reagent subboiling still comparison 827
Purine TLC mass spectrometry 2516
PVC membrane anion selective electrode 499
PVC membrane nitrite selective electrode 1169
Pyrazine deriv polymer ligand electrode coating 1799
Pyrazine gas chromatog computerized retention prediction 1328
Pyridine deriv eluent chromatog cation detn 1435
Pyridine detn near IR Raman spectrometry 2647
Pyridine ruthenium SERS near IR 1648
Pyridine surface copper silver Raman 1648
Pyridinealdoxime reagent copper iron titanium 1847
Pyridinium dihydropyridine system mass spectrometry 1723
Pyrolysis ethylene nickel carbon electrode 560
Pyrolysis field ionization spectroscopy plant 221
Pyrolysis gas chromatog polymer 961
Pyrolysis mass spectrometry nonvolatile classification 715
Pyrolysis oxygen isotope detn org 1887
Pyrolytic glassy carbon electrode activation 2603
Pyruvate carboxylase biotin detn EIA 2160
QSAR micellar liq chromatog 1040
Quadratic convergence simplex algorithm culminating polemic 1783 1786
Quadratic model diffusive sampling org analysis 917
Quadrupole ion storage mass spectrometer 1083
Quadrupole mass spectrometer interface chromatograph 1874
Quadrupole Storage Mass Spectrometry (book review) 1163a
Qual analysis two component system fluorometry 580
Qual FTIR spectra least squares fit 2708
Quant Analytical Chem, 5th Ed. (book review) 420a
Quant Chem Analysis (book review) 417a
Quant Gas Chromatog for Lab Analyses and Online Process Control (book review) 656a
Quant mapping electron microprobe background subtraction 1612
Quantification ion microscopy detector discrimination 65
Quantitation surface analysis review 469a
Quartz crystal microbalance cation detector soln 290
Quartz crystal microbalance electrochem use review 1147a
Quartz fiber filter particulate analysis 914
Quartz resonator hydrogen chloride detection 1559
Quartz still purified reagent analysis 827
Quasi reversible electrode reaction voltammetry 965
Quaternary ammonium compd HPLC stationary phase 728
Quaternary ammonium hydrazone acetylpyridine prepn reagent 1272
Quaternized polyvinylpyridine ion transport plasticizer 570
Quenching argon neon nitrogen discharge plasma 326
Quinine sulfate detn fluorometry 593
Quinoline hydroxy immobilized ligand 1001
Quinone HPLC photoredn fluorescence detection 2267
Radiation laser detector piezoelec ceramic 796
Radical anion oligonucleotide mass spectra 2154
Radio frequency plasma detector supercrit chromatog 1815
Radioactive liq analysis regulatory org compd 2751
Radiochem analysis solid std stability 2255
Radiochem neutron activation phosphorus detn metal 2338
Radiochem neutron activation zinc isotope 2757
Radioisotope detector capillary electrophoresis 1642
Radiolabeled metabolite detection 2724
Radionuclide detn solid std stability 2255
Radushkevich Dubinin isotherm diffusive sampler performance 843
Rain analysis ammonium fluorometry 408
Raman resonance surface enhanced detection HPLC 888
Raman scattering surface enhanced analysis 1779
Raman spectrometry nitrogen contg org detn 1697
Raman spectroscopy acceptor detn gallium arsenide 994
Raman spectroscopy analysis surface enhanced review 401a
Raman spectroscopy electrochem review 775a
Raman spectrum spectral sensitizer photog 391
Raman substrate silver fumed silica 656
Raman surface pyridine copper silver 1648
Random walk theory plate height 2455
Rank annihilation nonbilinear model spectral interferent 2277
Rank estn canonical correlation emission 2219
Raoults law nonmetal sample soln prepn 790
Rapid lifetime detn error 30
Rare earth detn direct mass spectrometry 755
Rare earth enhancement samarium detn fluorometry 1063
Rare earth fluorometry thermal lensing correction 928
Rat adrenal ext analysis methylphenylpyridine SIMS 1013
Rat basophilic leukemia cell cyclic voltammetry 2471
Rate isomerization quaternary ammonium hydrazone acetylpyridine 1272
Raw material testing drug IR 138
Reactant ion mass selection mass spectrometer 1874
Reaction kinetic amine HPLC derivatization reagent 1538
Reaction kinetics amine fluorodinitrobenzene 1358
Reaction kinetics detn linearized model 1949
Reagent analysis plasma mass spectrometry 827
Receptor based biosensor review 533a
Receptrode review 533a
Recombinant DNA protein prodn sepn 1742
Redn electrochem rhodium complex IR spectra 2805
Redn oxime fast atom bombardment 1442
Redox activity semiconductor superconductor 1497
Redox cyanoferrate microhole array electrode 1763
Redox electrochem amphiphile incorporated phosphatidylcholine 979
Redox reaction catechol carbon electrode 560
Redox reaction coating formal potential 1799
Redox reaction ferrocyanide copper electroredn 508
Redox thin layer spectroelectrochem cell 1787
Ref std biol silicon detn 1834
Ref trace metal detn biochem 216
Reflection absorption FTIR ionic transport 1164
Reflection IR spectrometry blood analysis 2016
Reflection IR spectrometry glucose detn 2009
Reforming catalyst analysis chloride ion chromatog 1924
Refractive index detection capillary zone electrophoresis 1590
Refractive index effect fiber optics detector 876
Refractive index liq chromatog detector linearity 951a
Regression algorithm multiexponential data analysis 2310
Regression analysis matrix calcn digital smoothing 1308
Regression data analysis shot noise limit 2483
Regulatory org compd detn radioactive liq 2751
Reichardt scale reversed phase liq chromatog 1524
Reiterative algorithm multiexponential data analysis 2310
Relative elemental response plasma mass spectrometry 1243
Relative humidity sensor cobalt chloride 1863
Relaxant muscle HPLC polystyrene divinylbenzene phase 728
Relayed magnetization transfer NMR 2298
Resin Chelex 100 transition metal enrichment 520
Resin epoxy graphite modified electrode 508
Resistively heated aluminum clad capillary column 2410
Resoln gas chromatog chiral stationary phase 2121
Resoln gas chromatog stationary phase diln 126
Resoln optical chiral mixed micelle 1984
Resonance cyclotron ion mass spectrometer 2528
Resonance ionization laser mass spectra lanthanum 695
Resonance ionization mass spectrometry analysis review 1271a
Resonance Raman surface enhanced detection HPLC 888
Resonant two photon ionization spectroscopy nonvolatile 777
Respiratory gas analysis anesthetic 1093
Response electrochem TTF TCNQ electrode 1048
Response ion selective electrode 2341
Restrictor modeling supercrit fluid chromatog 356
Restrictor pressure regulated supercrit chromatog 1178
Retention correlation reversed phase liq chromatog 1524

Retention index gas chromatog extrapolation 88
Retention mechanism liq chromatog 930
Retention prediction computerized pyrazine gas chromatog 1328
Reverse phase TLC diazonaphthoquinone detn 615
Reversed micelle formation iodine detn 2800
Reversed phase HPLC benzene deriv 367
Reversed phase HPLC fatty acid 910
Reversed phase HPLC polymeric stationary phase 198
Reversed phase liq chromatog retention 930
Reversed phase liq chromatog retention correlation 1524
Reversed phase liq chromatog subambient temp 1749
Reversed phase packed capillary column HPLC 1128
Reversible electrode reaction voltammetry 965
Review air analysis workplace 128r
Review air pollutant detn 1r
Review amnesic shellfish poisoning 1053a
Review analysis geol inorg material 109r
Review analysis petroleum coal liq 165r
Review analysis polymer 214r
Review angiogenin 1173a
Review capillary electrophoresis biomol neurochem 292a
Review capillary electrophoresis protein 1186
Review carcinogenesis fluorescence line narrowing spectroscopy 1023a
Review chiroptical technique analytical application 77a
Review coal sampling analysis 84r
Review coating analysis 33r
Review electrochem use quartz crystal microbalance 1147a
Review fast thermolysis Fourier IR spectroscopy 897a
Review ferrous analysis 14r
Review fingerprint detection laser luminescence 557a
Review fluorescence lifetime filtering 839a
Review food analysis 45r
Review forensic science 95r
Review Hadamard transform spectrochem analysis 723a
Review intelligent robot analytical lab automation 805a
Review isoelec focusing immobilized gradient biomol 1602
Review isotope diln mass spectrometry 643a
Review lab information management system 612a
Review laser clin application 1367a
Review mass spectrometry field ionization desorption 1201a
Review modern thin layer chromatog 1257a
Review neuronal biosensor receptrode 533a
Review NMR automated high resoln 107a
Review NMR imaging 23a
Review NMR imaging correction 358a
Review particle size detn 143r
Review pesticide analysis method 153r
Review pharmaceutical analysis 191r
Review protein structure optical spectroscopy 642
Review quantitation surface analysis 469a
Review Raman spectroscopy electrochem 775a
Review resonance ionization mass spectrometry analysis 1271a
Review rubber 238r
Review solid surface luminescence spectrometry 889a
Review surface acoustic wave device analysis 704a
Review surface characterization instrumental analysis 243r
Review surface enhanced Raman spectroscopy analysis 401a
Review synchrotron induced x ray emission 341a
Review water analysis 269r
Review waveguide chem sensor application 1079a
Review x ray photoelectron spectroscopy instrumentation 589a
Rhenium platinum alumina catalyst analysis chloride 1924
Rhodamine 6G detn fluorometry 1510
Rhodium anilinopyridine diphenylformamidine electrochem reaction 2805
Rhodium complex modified carbon paste electrode 279
River sediment analysis slurry sample introduction 1414
Robot intelligent analytical lab automation review 805a
Robust statistics analytical method bias detn 1942
Rock silicate analysis copper atomic absorption 1427
Rock silicate analysis x ray fluorescence 1837
Room temp phosphorimetry polynuclear arom hydrocarbon 2328
Room temp solid surface luminescence analysis 2643
Rotamer microspeciation aspartic acid 2631
Rotation label detn fluorescence immunoassay 309
Rotational diffusion oxazine 4 2394
Rotational structure transition nitrogen ion 1052
Rubber ethylene propene analysis 458
Rubeanic acid pptn copper silicate rock 1427
Rubidium noise power spectra mass spectrometry 606
Ruthenium EDTA complex vinylpyridine copolymer electrode 848
Ruthenium pyridine SERS near IR 1648
Saccharide chromatog mass spectrometry spray ionization 1159
Saccharide detection copper modified electrode 2258
Saccharide detn fermn broth immobilized enzyme 831
Safety pyrophoric triethylborane 1867
Salicylate detn selective electrode membrane 566
Salt analysis bromide iodide gas chromatog 733
Salt cyclodextrin matrix luminescence analysis 2643
Salt high content sample analysis metal 149
Samarium detn fluorometry 1063
Sample cooling moving belt device phosphorimetry 1182
Sample dissoln geol inorg review 109r
Sample insertion plasma wire loop support 163
Sample introduction device atomic spectrometry 790
Sample introduction microheater merging mass spectrometry 2263
Sample prepn IR sorption study 2047
Sample prepn particle LAMMA 914
Sample slurry introduction river sediment analysis 1414
Sampler air analysis workplace review 128r
Sampler diffusive performance fundamental factor 843
Sampler passive nitrogen dioxide formaldehyde 187
Sampling analysis coal review 84r
Sampling cell flame multiphoton ionization spectrometry 1010
Sampling diffusive quadratic model org analysis 917
Sampling laser ablation plasma mass spectrometry 1243
Sampling metal aerosol spark discharge 1826
Sampling sulfur dioxide diffusion scrubber 19
Sapphire rod waveguide polymer coated sensor 1674
Savitzky Golay smoothing chromatog spectrochem analysis 1303
Scanning electrochem microscopy characterization 132
Scanning electrochem microscopy feedback mode 1221
Scanning electrochem microscopy insulator substrate 1794
Scanning tunneling microscopy review 243r
Scattering Raman surface enhanced analysis 1779
Science forensic review 95r
Scintillation online radioisotope detector capillary electrophoresis 1642
Screened electrostatic ion trap mass spectrometer 1288
Scrubber diffusion sulfur dioxide sampling 19
SE 54 phase solvation supercrit chromatog 1348
Sealed tube combustion carbon isotope detn 1996
Seawater aluminum trace detn 544
Seawater analysis lead ethylation atomic absorption 1867
Seawater analysis trace metal 149
Seawater manganese detn chemiluminescence 1392
Seawater water hydrocarbon detn extn 1333
Second order nonbilinear rank annihilation model 2277
Secondary amine detn kinetic potentiometry 1358
Secondary ion mass spectra liq 2154
Secondary Ion Mass Spectrometry editorial 1311a
Secondary ion mass spectrometry image quantification 65
Secondary ion mass spectrometry silicon analysis 412
Secondary ion mass spectroscopy drug 1087
Sediment analysis nitrate nitrite 2715
Sediment gas analysis carbon hydrogen isotope 2149
Sediment river analysis slurry sample introduction 1414
Sediment std analysis tributyltin mass spectrometry 2320
Sedimentation colloid particle size detn 741
Sedimentation field flow fractionation 811 2735
Sedimentation fractionation polymer latex density 1934
Sedimentation fractionation polystyrene latex 2439
Segmented bubble stream analysis potentiometry 504
Segmented flow automated electrochem analyzer 2102
Selective electrode membrane salicylate detn 566
Selectivity fluorescence lifetime excitation emission matrix 580
Selectivity ion selective electrode 2341
Selectivity modification liq chromatog subambient temp 1749
Selectivity surface modified silica gel 41
Selenium detn blood HPLC fluorometry 2244
Selenium detn HPLC fluorometric detection 233
Selenium detn hydride generation atomic emission 285
Selenium detn mass spectroscopy biochem 701
Selenotrisulfide formation selenium detn HPLC 233
Semiconductor analysis oxygen electrochem 1497
Semiconductor laser fluorometer 2285
Semiconductor online radioisotope detector capillary electrophoresis 1642
Sensitizer spectral photog Raman spectrum 391
Sensor fiber optic avidin biotin 1069
Sensor fiber optic electrooxidn 633
Sensor fiber optic indicator immobilization 202
Sensor high acidity polymer coated waveguide 1674
Sensor humidity cobalt chloride 1863
Sensor solid state ion selective 246
Sensor transistor nitrogen dioxide DIMP 2355
Sensor wastewater analysis triphenylmethane dye 2306
Sensor waveguide chem application review 1079a
Sepn alkyl nitrate chromatog 771
Serotonin sepn catecholamine capillary zone electrophoresis 98
SERS near IR ruthenium pyridine 1648
SERS substrate silver fumed silica 656
Serum cholesterol detn 1718
Serum fetoprotein detn immunoassay 48
Serum glucose detn 2566
Serum protein binding imirestat phenytoin HPLC 1171
Serum trace element detn 1851
Shale oil characterization review 165r
Shellfish poisoning amnesic review 1053a
Short open tubular column chromatog spectrometry 2402
Shot noise data analysis distribution function 2479
Shot noise limit data analysis 2483
Shpolskii matrix low temp phosphorimetry 1182
SI unit 94
Siderophore detn HPLC 1474
Signal fluctuation atomic emission droplet 2002
Signal instability plasma mass spectrometer 606
Signal noise ratio microelectrode array detector 295
Silane deriv silica desorption cyanobenzylideneoctyloxyaniline 1534
Silane modified silica gel packing HPLC 2
Silanol group modified silica gel 41
Silica allyloxybenzoylmethoxyphenyl bonded stationary phase HPLC 1928

Silica coated cyanobenzylideneoctyloxyaniline mesophase orientation interaction 1534
Silica enhancer benzopyrenetetrol fluorescence 2766
Silica fumed effect surfactant interference polarog 1598
Silica fumed silver substrate SERS 656
Silica gel oxime immobilized equil 1001
Silica gel silane modified packing HPLC 2
Silica gel silylated thermal treatment 41
Silica ODS column fatty acid chromatog 2076
Silica support drug detn blood chromatog 2445
Silica surface hydrosilylation org addn 2067
Silicate rock analysis copper atomic absorption 1427
Silicate rock analysis x ray fluorescence 1837
Silicon analysis dopant depth profile SIMS 412
Silicon detection thermal gradient HPLC 236
Silicon detn biol std ref 1834
Silicon detn laser microprobe chemiluminescence detection 2557
Silicon potassium selective sensor 246
Silicon wafer boron implanted analysis SIMS 1946
Silicone fiber mass spectrometry probe 2332
Siloxane chiral stationary phase gas chromatog 2121
Siloxane supercrit chromatog mass spectrometry 775
Silver based mercury film electrode voltammetry 2086
Silver coated filter paper substrate Raman 1697
Silver coated titania substrate Raman scattering 1779
Silver detn square wave voltammetry 1211
Silver electroredn mercurous dimeric cation 1305
Silver fumed silica substrate SERS 656
Silver pyridine surface Raman 1648
Silylated silica gel thermal treatment 41
Simplex algorithm culminating quadratic convergence polemic 1783 1786
SIMS dopant depth profile detn silicon 412
SIMS polar compd low mol wt 1013
SIMS polyurethane structure 2142
SIMS quant analysis 1946
Simulated annealing global optimization 2024
Simulation computer copper atomization graphite furnace 2652
Simulation computer protein electrophoresis 362
Simulation NMR carbon alkylcyclohexanone alkyldecalone 863
Simulation spectral carbon 13 NMR 1115a
Single component identification mixt mass spectrometry 73
Single exponential decay rapid lifetime detn 30
Single frequency phase resolved fluorometric analysis 1510
Size exclusion chromatog gel hydrophobicity 780
Size exclusion chromatog sodium polystyrenesulfonate 530
Size Exclusion Chromatog (book review) 1285a
Size selectivity membrane electrode biochem 303
Slave master arrangement microcomputer data acquisition 593
Sludge amendment soil ligand estn 1295
Slurry sample introduction river sediment analysis 1414
Small flow cell polarimeter detector 1238
Smoothing filter algorithm data processing digital 1308
Smoothing Savitzky Golay chromatog spectrochem analysis 1303
Sodium chloride adsorption polycyclic arom hydrocarbon 708
Sodium chloride cyclodextrin substrate luminescence analysis 2643
Sodium chloride hydroxide analysis hydroxide ion 1419
Sodium chloride regenerant ion exclusion chromatog 548
Sodium detn Fourier transform atomic absorption 1694
Sodium detn multiphoton ionization spectrometry 1010
Sodium dodecyl sulfate optical resoln 1984
Sodium polystyrenesulfonate size exclusion chromatog 530
Software class identification mass spectrometry 715
Soil analysis gasoline arom headspace chromatog 2584
Soil analysis linked chromatog spectrometry 1571
Soil analysis nitrite chromatog 1485
Soil chlorinated biphenyl dibenzodioxin dibenzofuran HPLC 1300
Soil molinate detn ELISA 819
Soil std stability radiochem analysis 2255
Solid analysis plasma mass spectrometry 1243
Solid Arrhenius parameter detn DSC DTG 1136
Solid electrode electrodeposition trace metal preconcn 856
Solid laser ionization mass spectrometry 1029
Solid state sensor ion selective 246
Solid state voltammetry polymer 584
Solid std stability radiochem analysis 2255
Solid surface luminescence spectrometry review 889a
Solid surface room temp luminescence analysis 2643
Solubilization cyclodextrin use analysis 275
Solute independent calibration automated chromatog 1915
Solute partition aq phase liq chromatog 2540
Solvation stationary phase supercrit fluid chromatog 1348
Solvent effect peroxyoxalate chemiluminescence 1298
Solvent extn detn iodide oxidn kinetics 2562
Solvent extn detn iodine 2800
Solvent org detn wastewater sensor 2306
Solvent polarity reversed phase liq chromatog 1524
Solvent various spectroelectrochem cell 190
Soly alc chromatog gel hydrophobicity 780
Soly complex arom cyclodextrin 955
Somatotropin structure optical spectroscopy review 642
Sorbent org detn air supercrit extn 736
Sorption aluminum ligand immobilized silica 1001
Sorption heat propanol SE 54 phase 1348
Sorption isotherm diffusive sampler performance 843
Sorption polymer gas detection 584
Sorption study IR sample prepn 2047
Source compn optimization thermionic detector 2082
Spark produced aerosol analysis 1826
Spatial filtering thermal lens spectrometer 2496
Speciation aluminum aq soln ion chromatog 535
Speciation trace metal detn water 525
Spectra FTIR qual least squares fit 2708
Spectra IR gasoline octane number 313
Spectra noise power plasma mass spectrometer 606
Spectra pos ion mobility amine 684
Spectral cleanup mass spectrometry computerized 73
Spectral information linked chromatog spectrometry analysis 1571
Spectral interferent model nonbilinear rank annihilation 2277
Spectral sensitizer photog Raman spectrum 391
Spectral simulation carbon 13 NMR 1115a
Spectrochem analysis photodiode array detector 2347
Spectrochem analysis polynomial least squares smoothing 1303
Spectrochem analysis transform Hadamard review 723a
Spectrochem Analysis (book review) 418a
Spectroelectrochem detector flow through 1216
Spectroelectrochem IR electrolytic cell 2805
Spectroelectrochem thin layer cell 1787
Spectroelectrochem thin layer transmittance cell 190
Spectroelectrochemistry. Theory and Practice (book review) 857a
Spectrometer atomic absorption continuum source 1670
Spectrometer IR Fourier transform 1052
Spectrometer mass computer controlled operation 330
Spectrometer mass Hartley transform 428
Spectrometer mass ion cyclotron resonance 2528
Spectrometer mass ion trap intermol process 2500
Spectrometer mass laser photodissocn 1458
Spectrometer mass merging chamber sample introduction 2263
Spectrometer mol absorption luminescence measurement 593
Spectrometer plasma liq chromatograph interface 895
Spectrometer thermal lens spatial filtering 2496
Spectrometer x ray synchrotron source review 341a
Spectrometry analysis adsorbed monolayer 386
Spectrometry atomic absorption alloy analysis 1235
Spectrometry atomic absorption copper ligand estn 1295
Spectrometry atomic absorption Fourier transform 1694
Spectrometry atomic emission hydride generation online 285
Spectrometry atomic thimble glass frit nebulizer 2777
Spectrometry chromatog overlapped peak detection 2240
Spectrometry electrothermal atomic absorption biol ref 216
Spectrometry emission dual cathode discharge lamp 2137
Spectrometry flame atomic absorption cation detn 1410
Spectrometry fluorescence time resolved decay analysis 2310
Spectrometry Fourier transform ion cyclotron resonance 53
Spectrometry inorg analysis review 109r
Spectrometry intracavity absorption IR laser diode 1425
Spectrometry ion mobility benzodiazepine 343
Spectrometry ion mobility halogenated anesthetic detn 1093
Spectrometry ion mobility liq analysis coronaspray 601
Spectrometry IR blood analysis 2016
Spectrometry IR chlorodibenzodioxin 1678
Spectrometry linked gas chromatog analysis 1571
Spectrometry liq chromatog halogen detector 895
Spectrometry luminescence solid surface review 889a
Spectrometry mass amino acid tripeptide 1895
Spectrometry mass continuous flow liq technique 2582
Spectrometry mass detn carbon hydrogen isotope 2149
Spectrometry mass fast atom bombardment 1293
Spectrometry mass multichannel heterodyne detection 749
Spectrometry mass tandem uric acid electrooxidn 1709
Spectrometry multiphoton ionization flame sampling cell 1010
Spectrometry NMR antimycin A 404
Spectrometry phosphorescence laser induced halogenated naphthalene 872
Spectrometry plasma desorption mass oligosaccharide analysis 2686
Spectrometry reflection IR glucose detn 2009
Spectrometry supersonic jet polystyrene ablation 1530
Spectrophotometer photodiode array gas chromatog detection 1249
Spectrophotometry flow injection analysis 496
Spectrophotometry metal ion simultaneous detn 1847
Spectrophotometry plutonium nitric acid detn 1667
Spectroscopy concn profile cylindrical microelectrode 2347
Spectroscopy fluorescence line narrowing carcinogenesis review 1023a
Spectroscopy FTIR aluminum nitride water 2399
Spectroscopy IR emission transient analysis 650
Spectroscopy IR Fourier fast thermolysis review 897a
Spectroscopy mass alanine cell wall 265
Spectroscopy mass alkene insect 1564
Spectroscopy mass biomol 2504
Spectroscopy mass cholesterol detn 1718
Spectroscopy mass gas chromatog radiolabeled metabolite 2724
Spectroscopy mass glycolipid structure detn 416
Spectroscopy mass interface liq chromatog biomol 1577

Spectroscopy mass ion trap biomol 2316
Spectroscopy mass peptides glycerol 2674
Spectroscopy mass plasma desorption protein 375
Spectroscopy mass selenium detn biochem 701
Spectroscopy mass trace element blood 1851
Spectroscopy mass zinc detn feces 1023
Spectroscopy nickel detn urine 1099
Spectroscopy nomenclature 93
Spectroscopy of Surfaces (book review) 1044a
Spectroscopy optical protein structure review 642
Spectroscopy Raman analysis surface enhanced review 401a
Spectroscopy Raman electrochem review 775a
Spectroscopy resonant two photon ionization nonvolatile 777
Spectroscopy secondary ion mass drug 1087
Spectroscopy silane modified silica characterization 2
Spectroscopy spruce needle analysis 221
Spectroscopy two photon ionization biomol 1911
Spectroscopy x ray photoelectron instrumentation review 589a
Spherical segment microelectrode coeff current equation 1305
Spice analysis org chromatog factor analysis 838
Spin dynamics NMR analysis carbonaceous deposit 1821
Split zone flow injection diln 1773
Splitting condition injection chromatog peak shape 1489
Spray atm pressure ionization mass spectrometry 1159
Spruce needle analysis chromatog spectroscopy 221
Sputtering atomizer atomic absorption spectroscopy 1652
Squalane lauroylvaline butylamide chiral phase chromatog 126
Square wave anodic stripping voltammetry mercury 2092
Square wave voltammetry cylindrical microelectrode 1211
Square wave voltammetry mercury film electrode 2086
Stability chlorophenyl oxalate hydrogen peroxide 1298
Stability metal humic substance complex 1519
Stability probe film tandem liq SIMS 1013
Stability silane modified silica packing 2
Stability solid std radiochem analysis 2255
Stable carbon isotope detn org combustion 1996
Staircase cyclic voltammetry theory 2249
Staircase voltammetry theory expt 965
Stationary liq phase functionalized mixed micelle 1984
Stationary phase chiral apolar diluent effect 126
Stationary phase chiral polysiloxane gas chromatog 2121
Stationary phase HPLC allyloxybenzoylmethoxyphenyl bonded silica 1928
Stationary phase modification micelle chromatog 1353
Stationary phase polymeric electrochem prepd HPLC 198
Stationary phase polypyrrole HPLC 2391
Stationary phase quaternary ammonium compd HPLC 728
Stationary phase solvation supercrit fluid chromatog 1348
Statistical estn analytical data distribution 2719
Statistical justification interlab coeff variation concn 1465
Statistics multivariate benzene deriv retention HPLC 367
Statistics pipet calibration 1080
Statistics robust analytical method bias detn 1942
Statistics target factor analysis application 1168
Std analytical tetramethyllead vapor prepn 1993
Std lutidine ion mobility spectra amine 684
Std nortetrahydrocannabinolcarboxylate urine forensic 540
Std ref biol silicon detn 1834
Std ref material geol inorg review 109r
Std sediment analysis tributyltin mass spectrometry 2320
Std solid stability radiochem analysis 2255
Steady state fluorescence excitation emission matrix 580
Stearate modified electrode dopamine detn 2323
Steel analysis chromium manganese 2137
Steel analysis review 14r
Stereoselectivity chiral diamide amino acid resoln 126
Steric effect silane modified silica packing 2
Still subboiling comparison reagent purifn 827
Still subboiling distn acid 823
Stoichiometry detn barium yttrium copper oxide 1497
Stopped flow chronoamperometric detector ion chromatog 1387
Storing vessel material effect peroxyoxalate chemiluminescence 1298
Stream bubble segmented analysis potentiometry 504
Streptavidin europium chelate immunoassay 48
Streptococcus cell wall detn mammal tissue 265
Stripping voltammetry anodic copper lead electrodeposition 856
Stripping voltammetry anodic lead detn 2092
Structure activity micellar liq chromatog 1040
Structure detn disaccharide 666
Structure detn glycolipid mycobacteria 416
Structure IR spectrum compression 33
Structure morphol multilayer polymer NMR 1870
Structure polyurethane SIMS 2142
Structure protein optical spectroscopy review 642
Structure retention relation pyrazine chromatog 1328
Structure TTF TCNQ electrode 1048
Styrene acrylate copolymer chromatog sepn 2171
Styrene copolymer carbon fiber composite electrode 1460
Styrene isoprene block copolymer micelle 1318
Styrene vinylbenzene vinylpyridine copolymer composite electrode 848
Subambient pressure short open tubular column 2402
Subambient temp modification selectivity liq chromatog 1749
Subboiling still acid distn 823
Subboiling still comparison reagent purifn 827
Sublimation enthalpy amino acid mass spectrometry 1895
Submicrometer particle analysis hydrocarbon 320
Substrate characterization ultramicroelectrode movement 132
Substrate SERS silver fumed silica 656
Substrate silver coated filter paper Raman 1697
Substrate thallium lauryl sulfate modified phosphorimetry 2328
Substrate titania surface enhanced Raman scattering 1779
Subtilisin amino acid chromatog 2059
Subtilisin variant sepn HPLC 1742
Succinylcholine detn dexamethasone forensic 53a
Sucrose detn beverage food 782
Sugar amino detection copper modified electrode 2258
Sulfate detn near IR Raman spectrometry 2647
Sulfate dodecyl contg polypyrrole stationary phase 2391
Sulfate lauryl thallium modified substrate phosphorimetry 2328
Sulfate quinine detn fluorometry 593
Sulfide cadmium crystal face specific electrode 1980
Sulfide volatile detn water GC 114
Sulfite detn HPLC atomic spectrometry 272
Sulfite detn needle wine fluorometry 1755
Sulfite reagent ammonium detn 408
Sulfonated azo dye analysis 2054
Sulforhodamine 640 controlled release pH sensor 174
Sulfur detection radio frequency plasma chromatog 1815
Sulfur detection thermal gradient HPLC 236
Sulfur detector chemiluminescence universal 1268
Sulfur detn chromatog coal liq 2292
Sulfur dioxide detn air sampling 19
Sulfur fluoride chemiluminescence reagent laser microprobe 2557
Sulfur org compd analysis oxygen isotope 1887
Sulfur org compd detn supercrit chromatog 2616
Sulfur org flame photometric detection optimization 58
Sulfur org supercrit chromatog chemiluminescence detection 797
Superconductor analysis oxygen electrochem 1497
Supercrit carbon dioxide adsorption silica 951
Supercrit carbon dioxide extn org sorbent 736
Supercrit chromatog FTIR propellant 145
Supercrit chromatog pressure regulated restrictor 1178
Supercrit fluid chromatog detector voltammetric 2193
Supercrit fluid chromatog element selective detector 1815
Supercrit fluid chromatog fatty acid detn 2076
Supercrit fluid chromatog flame photometric detection 2616
Supercrit fluid chromatog Fourier IR coupling 2212
Supercrit fluid chromatog mass spectrometry 775
Supercrit fluid chromatog organosulfur chemiluminescence detection 797
Supercrit fluid chromatog photometric detection organosulfur 58
Supercrit fluid chromatog restrictor modeling 356
Supercrit fluid chromatog stationary phase solvation 1348
Supercrit fluid chromatog thermionic detector optimization 2082
Supercrit fluid extn chlorodibenzodioxin chlorodibenzofuran 2770
Supercrit fluid extn online app phosphonate 1986
Supercrit fluid gas chromatog glyceride 698
Supercrit fluid voltammetry polymer coated microelectrode 270
Supersonic jet spectrometry polystyrene ablation 1530
Supersonic jet spectroscopy nonvolatile compd 777
Support wire loop sample insertion plasma 163
Suppressed ion chromatog potentiometric pH detection 787
Suppression background chelation anion chromatog 122
Suppressor electrodialysis membrane ion chromatog 939
Suppressor perfluorosulfonate membrane ion exclusion chromatog 548
Surface acoustic wave device analysis review 704a
Surface analysis ESCA instrumentation review 589a
Surface analysis laser ionization polymer 805
Surface analysis quantitation review 469a
Surface area carbon paste electrode 2585
Surface area modified silica gel 41
Surface characterization instrumental analysis review 243r
Surface coil fabrication NMR in vivo 636
Surface compn cadmium sulfide 1980
Surface enhanced Raman scattering analysis 1779
Surface enhanced Raman spectrometry nitrogen org 1697
Surface enhanced Raman spectroscopy analysis review 401a
Surface enhanced resonance Raman detection HPLC 888
Surface microstructure electrode spectroscopy review 775a
Surface org cation binding fluorescence 590
Surface potential reactivity immobilized ligand 1001
Surface Raman pyridine copper silver 1648
Surface structure adsorbed monolayer 386
Surface structure graphite electrode reaction kinetics 1637
Surface structure TTF TCNQ electrode 1048
Surface tension compn equation 194
Surfactant chiral optical resoln electrokinetic chromatog 1984
Surfactant effect chromatog stationary phase 1353
Surfactant interference polarog fumed silica effect 1598
Surfactant synthetic enzyme model phosphorescence 2475
Surlyn multilayer film morphol NMR 1870

Synchrotron geol inorg analysis review 109r
Synchrotron induced x ray emission review 341a
Syringe injection chromatog peak shape 1489
System peak analysis liq chromatog 2428
System peak ion pair chromatog 1109
Systematic error analysis algorithm 398
Taft scale reversed phase liq chromatog 1524
Tandem mass spectrometer air pollutant 260
Tandem mass spectrometry fatty acid 494
Tandem mass spectrometry ion spray tributyltin 2320
Tandem mass spectrometry polar compd detn 1013
Tandem mass spectrometry spectral interferent model 2277
Tandem mass spectrometry uric acid electrooxidn 1709
Tandem mass spectroscopy biomol 2316 2504
Tapered restrictor modeling supercrit fluid chromatog 356
Target factor analysis statistics application 1168
Target transform factor analysis retention prediction 367
Tartramide deriv siloxane chiral stationary phase 2121
TCNQ electroredn spectroelectrochem cell 190
TCNQ TTF electrode ultramicroelectrode array behavior 1048
Techniques of Chem. Vol. 20. Techniques of the Study of Ion-Mol Reactions (book review) 1038a
Temp detn NMR sample 1594
Temp effect conductometric titrn polyprotic acid 177
Temp extrapolation gas chromatog retention 88
Temp gradient effect capillary zone electrophoresis 241
Temp programmed elution glycoprotein chromatog 1117
Temp programmed resistively heated capillary column 2410
Temp subambient modification selectivity liq chromatog 1749
Tetraalkylammonium salt effect micellar electrokinetic chromatog 2434
Tetracosane lauroylvaline butylamide chiral phase chromatog 126
Tetracyanofurnodimethane tetrathiafulvalene electrode structure 1048
Tetrafluoroethylene resin still purified reagent analysis 827
Tetrahydroborate polymer bound column arsine generation 2079
Tetramethyllead vapor analytical std prepn 1993
Tetrathiafulvalene tetracyanofurnodimethane electrode structure 1048
Thallium lauryl sulfate modified substrate phosphorimetry 2328
Theophylline detn blood HPLC 784
Thermal Analysis. Techniques and Applications (book review) 1289a
Thermal decompn organometallic compd nickel 560
Thermal desorption mass spectrometry carbon fiber 1017
Thermal gradient liq chromatog 236
Thermal lens detection fatty acid HPLC 910
Thermal lens laser water media 1660
Thermal lens optical absorption detn 883
Thermal lens spectrometer spatial filtering 2496
Thermal treatment silylated silica gel 41
Thermally labile salt plastic analysis 802
Thermionic detector optimization supercrit fluid chromatog 2082
Thermodn effect ion selective electrode selectivity 2341
Thermodn fluorescence probe inclusion complex 905
Thermodn ion mol reaction 1447
Thermoelec enzyme sensor glucose model 77
Thermogravimetry polymer 1195
Thermolysis fast Fourier IR spectroscopy review 897a
Thermooptical detection amino acid detn electrophoresis 37
Thermopile glucose enzyme sensor 77
Thermospray mass spectrometry liq chromatog calibration 2126
Thermospray mass spectrometry uric acid electrooxidn 1709
Thiatricarbocyanine dye trace detn 861
Thiazine dye HPLC polystyrene divinylbenzene phase 728
Thimble glass frit nebulizer atomic spectrometry 2777
Thin layer chromatog coupling gas chromatog 1906
Thin layer chromatog diazonaphthoquinone detn 615
Thin layer chromatog laser fluorometric detection 1931
Thin layer chromatog mass spectrometry coupling 2516
Thin layer chromatog modern review 1257a
Thin layer chromatog urea cyclodextrin phase 422
Thin layer spectroelectrochem cell 1787
Thin layer transmittance spectroelectrochem cell 190
Thin specimen x ray rock analysis 1837
Thiol detn gasoline flow injection 496
Thionitrite acetylpenicillamine detn voltammetry 1954
Thorium detn flow injection 1789
Thorium detn solid std stability 2255
Threshold condition plasma ignition mass spectrometry 1029
Thymidine Fourier transform mass spectrometry 184
Time dependent response ion selective electrode 2341
Time domain differentiation HPLC computer aided 720
Time resolved fiber optic fluorescence sensor 1768
Time resolved fluorescence spectrometry decay analysis 2310
Tin detn atomic emission spectrometry 1175
Tin detn hydride generation atomic emission 285
Tin oxide electrode modified horseradish peroxidase 2352
Tin tetraphenylporphyrin membrane salicylate electrode 566
Tin tributyl detn sediment std spectrometry 2320
Tiron postcolumn derivatization aluminum speciation chromatog 535
Tiron reagent copper iron titanium detn 1847
Tissue analysis magnesium microelectrode 574
Tissue animal analysis lead atomic absorption 1867
Tissue cAMP cGMP detn EIA 447
Tissue cobalt chromium alloy prosthetic 1235
Tissue mammal streptococcus cell wall detn 265
Titania substrate surface enhanced Raman scattering 1779
Titanium detn copper iron present spectrophotometry 1847
Titrn argentometric combined programmed flow analysis 2109
Titrn conductometric polyprotic acid 177
TLC biomol laser desorption detection 1911
TLC laser fluorometry porphyrin methyl ester 2288
Tobacco analysis monosaccharide disaccharide 2258
Tobacco analysis monosaccharide disaccharide detection 2258
Toluic acid isomer HPLC polypyrrole phase 2391
Total inorg carbon detn water 1841
Total mercury detn digestion conductometry 1230
Trace anion detn ion chromatog 939
Trace dye detn spectrometry wave mixing 998
Trace Element Analysis Spatially Resolved editorial 337a
Trace element detn combined spectrometry 793
Trace element detn serum 1851
Trace element detn surface water 335
Trace element detn x ray review 341a
Trace metal detn biochem ref 216
Trace metal detn plasma mass spectrometry 149
Trace metal detn water std 1857
Trace metal monitoring flow voltammetry 468
Trace metal preconcn electrodeposition solid electrode 856
Trace metal speciation detn water 525
Trace org detn water chromatog 1208
Tracer pulse chromatog stationary phase solvation 1348
Transducer conductometric enzyme based biosensor 1737
Transformer oil PCB detn colorimetry 2682
Transient current neutral carrier membrane 1624
Transient IR emission pulsed laser 1810
Transistor field effect ion selectivity electrode 2341
Transistor sensor nitrogen dioxide DIMP 2355
Transition metal enrichment Chelex 100 resin 520
Transition nitrogen ion rotational structure 1052
Transition phase liq crystal lipid multilayer 2185
Transmittance thin layer spectroelectrochem cell 190
Transport cation macrocycle liq membrane 1140
Transport ionic Fourier transform IR 1164
Trap detector pseudomol ion mass spectra 1983
Trap ion mass spectrometer intermol process 2500
Trap purge analysis radioactive liq 2751
Trap screened electrostatic ion mass spectrometer 1288
Triazine herbicide extn isolation method 935
Trifluoroacetate petroleum fuel derivatization detn 1260
Trifluoroethyl ester petroleum fuel derivatization 1260
Trifluorothymidine pyridinium mass spectrometry 1723
Triglyceride detn milk fat 698
Triphenylmethane dye sensor wastewater analysis 2306
Triple quadrupole mass spectrometer interface chromatograph 1874
Triprolidine hydrochloride identification supercrit fluid extn 1986
Triton X100 reagent gadolinium samarium detn 1063
True accuracy chem analysis algorithm 398
Trypanosoma variant surface glycoprotein oligosaccharide 2686
Trypsin peptide mapping 2226
Tryptamine detn brain 2316
Tryptophan detn continuous flow liq SIMS 1013
Tryptophan enantiomeric purity detn polarimetric detection 1238
TTA reagent gadolinium samarium detn 1063
TTF TCNQ electrode ultramicroelectrode array behavior 1048
Tubular open liq chromatog cation sepn 2747
Tunneling microscopy review 243r
Two color multiphoton ionization analysis 612
Two component system qual analysis fluorometry 580
Two dimensional NMR spectral interferent model 2277
Two Dimensional NMR Spectroscopy (book review) 657a
Two photon ionization spectroscopy biomol 1911
Two section cell ion cyclotron resonance 83
Two-Dimensional NMR Methods for Establishing Mol Connectivity (book review) 1038a
Uluramicro electrode microscopy conductive insulating sample 1221
Ultramicroelectrode antioxidant detn lubricating oil 1467
Ultramicroelectrode array behavior TTF TCNQ electrode 1048
Ultramicroelectrode conical hemispherical fabrication 1630
Ultramicroelectrode ensemble response detection limit 762
Ultramicroelectrode movement substrate characterization 132
Ultrasonic nebulization fluoride detn 674
Unsatd fatty ester methyl 118
Unsatd hydrocarbon identification insect 1564
Uranin reagent copper cyanide detn chemiluminescence 1505
Uranium detn flow injection 1789
Uranium ore std stability radiochem analysis 2255
Urea detn enzyme fiber optic sensor 1069
Urea sensor conductometric transducer 1737
Urea solubilized cyclodextrin mobile phase TLC 422
Urea solubilizer cyclodextrin 275

Urease immobilized conductometric transducer biosensor 1737
Uric acid electrooxidn tandem mass spectrometry 1709
Urine amino acid detn electrophoresis 37
Urine analysis amphetamine HPLC 1538
Urine analysis nitrate nitrite 2715
Urine analysis total mercury 1230
Urine analysis trace metal 149
Urine marcellomycin voltammetry lipid glassy electrode 170
Urine methotrexate detn HPLC 946
Urine nickel detn chromatog spectroscopy 1099
Urine norcarboxytetrahydrocannabinol gas chromatog forensic 925
Urine nortetrahydrocannabinolcarboxylate std forensic 540
Urine polyamine detn HPLC 1921
Urine radiolabeled phenytoin metabolite detection 2724
Urine zinc isotope detn 2757
Uronic acid detection copper modified electrode 2258
UV calibration curve bias nonlinearity 2571
UV detection HPLC enantiomeric amine 1548
UV detection microcolumn gas chromatog 1249
UV indirect detection chromatog cation detn 1435
UV IR laser excited multiphoton ionization 612
UV spectrochem analysis wavelength selection model 2024
UV visible chromatog detector linearity evaluation 951a
Valine dodecanol sodium salt optical resoln 1984
Valinomycin contg membrane solid state sensor 246
Valinomycin immobilized ionophore potassium detn 211
Vanadium 3 reductant nitrate nitrite detn 2715
Vapor deposited halogenated naphthalene phosphorescence spectrometry 872
Vapor org mixt identification FTIR 2708
Vaporization microelectrothermal mass spectrometry osmium detn 2263
Vaporization plume laser ionization diagnostic 2546
Variant surface glycoprotein oligosaccharide Trypanosoma 2686
Varnish historic painting 1228a
Velocity modulation capillary zone electrophoresis 1590
Vinyl acetate ethylene copolymer multilayer 1870
Vinylbenzene styrene vinylpyridine copolymer composite electrode 848
Vinylferrocene divinylbenzene styrene polymer composite electrode 1460
Vinylpyridene divinylbenzene styrene polymer composite electrode 1460
Vinylpyridine styrene vinylbenzene copolymer composite electrode 848
Virus black beetle structure 1341a
Viscosity effect flow injection diln 1773
Viscosity effect mixing flow injection analysis 973
Visible spectrochem analysis wavelength selection model 2024
Vitamin B12 based anion selective electrode 499
Vitamin B12 mass spectrometry spray ionization 1159
Vitamin detn multiphoton ionization 612
Vitamin K1 detection photoredn 2267
Vitamin micellar electrokinetic chromatog 2434
Vitreous carbon polypyrrole coated phase HPLC 2391
Vitreous carbon polypyrrole electrochem coated phase 198
Volatile arom detn headspace gas chromatog 2584
Volatile org compd detn radioactive liq 2751
Volatile polymer model headspace sampling 1202
Volatile sulfide detn water GC 114
Volatilization nonvolatile compd supersonic jet 777
Voltammetric detection automated segmented flow analyzer 2102
Voltammetric detection liq chromatog gradient elution 1977
Voltammetry acetylpenicillamine thionitrite detn 1954
Voltammetry analysis cylindrical microelectrode 1211
Voltammetry anodic stripping cadmium lead detn 2609
Voltammetry anodic stripping lead detn 2092
Voltammetry antioxidant detn lubricating oil 1467
Voltammetry carbon black contg polymer electrode 848
Voltammetry cyclic basophil allergy detection 2471
Voltammetry cyclic chronoamperometry diffusion microelectrode 1630
Voltammetry cyclic staircase theory 2249
Voltammetry cyclic theory electrode microhole array 1763
Voltammetry flow trace metal monitoring 468
Voltammetry hydrogen peroxide detn 2176
Voltammetry microdisk electrode supercrit carbon dioxide 2193
Voltammetry nerve analysis 436
Voltammetry pharmaceutical detn lipid glassy electrode 170
Voltammetry phenolic compd detn 2809
Voltammetry silver based mercury film 2086
Voltammetry solid state polymer 584
Voltammetry staircase theory expt 965
Voltammetry stripping anodic copper lead electrodeposition 856
Voltammetry supercrit fluid polymer coated microelectrode 270
Wall jet detector flow injection analysis 922
Waste gas acrylonitrile detn 2743
Waste gas pollutant mass spectrometer 260
Waste radioactive analysis org volatile compd 2751
Wastewater analysis sensor triphenylmethane dye 2306
Wastewater chlorination nitrogen chloride detn 2332
Wastewater industrial metal detn HPLC 1494
Water alkylbenzenesulfonate chromatog detn 2534
Water analysis ammonium fluorometry 408
Water analysis bromide iodide gas chromatog 733
Water analysis calcium magnesium 1435
Water analysis chloride argentometry 2109
Water analysis chloride flame IR emission 2785
Water analysis combined plasma spectrometry 793
Water analysis gasoline arom headspace chromatog 2584
Water analysis lead ethylation atomic absorption 1867
Water analysis nitrate nitrite 2715
Water analysis nitrite chromatog 1485
Water analysis phosphonate supercrit fluid extn 1986
Water analysis review 269r
Water analysis total mercury 1230
Water analysis trace metal 149
Water analysis triazine herbicide 935
Water chlorine detn chloramine interference 991
Water detn capillary gas chromatog 1325
Water drinking analysis lead atomic absorption 1410
Water effect sputtering atomic absorption spectroscopy 1652
Water ethene propene diffusion 2231
Water media laser thermal lens 1660
Water metal detn HPLC 1494
Water methanol assocn chromatog retention 349
Water molinate detn ELISA 819
Water org trace detn chromatog 1208
Water reaction aluminum nitride 2399
Water total inorg carbon detn 1841
Water trace metal speciation detn 525
Water volatile sulfide detn GC 114
Wave acoustic device analysis review 704a
Wave mixing laser spectrometry analysis 998
Waveguide analysis adsorbed monolayer 386
Waveguide chem sensor application review 1079a
Waveguide polymer coated sensor high acidity 1674
Wavelength dispersive electron microprobe background subtraction 1612
Wavelength selection optimization simulated annealing 2024
Weak acid detection ion exclusion chromatog 548
Wheat analysis protein 398
Whole column detection HPLC 2624
Wine sulfite detn fluorometry 1755
Wire coated electrode response selectivity 2341
Wire loop support sample insertion plasma 163
Wire microelectrode concn profile 2347
Workplace air analysis review 128r
X ray analysis binary mixt 1686
X ray analysis surface characterization review 243r
X ray emission synchrotron induced review 341a
X ray fluorescence silicate rock analysis 1837
X ray fluorescence silicon biol 1834
X ray geol inorg analysis review 109r
X ray mapping background subtraction 1612
X ray photoelectron spectroscopy instrumentation review 589a
X ray photoelectron spectroscopy quantitation review 469a
XAD chromosorb hydrocarbon detn water 1333
Xenon detn oxygen gas chromatog 2237
Yttrium barium copper oxide stoichiometry detn 1497
Yttrium oxide analysis samarium 1063
Zechmeister Laszlo chromatog pioneer 1315a
Zeolite catalyst carbonaceous deposit analysis NMR 1821
Zinc absorption detn intestine nutrition 1023
Zinc hydroxyethyldithiocarbamate complexation water analysis 1494
Zinc metab detn 2757
Zinc present cobalt detn polarog 2178
Zinc quartz resonator hydrogen chloride detection 1559
Zircon analysis phosphorus plasma atomic emission 2696
Zone capillary electrophoresis peptide mapping 2226
Zone electrophoresis amino acid detn 37
Zone electrophoresis capillary carboxylic acid detn 766
Zone gas chromatog 1478

"A"-PAGE INDEX

A/C Interface

Carbon-13 NMR Spectral Simulation. Peter C. Jurs, G. Paul Sutton, and Martha L. Ranc. 1115 A
Changing Views of NMR: Automated High-Resolution NMR with a Sample Changer. Charles G. Wade, Robert D. Johnson, Stephen B. Philson, Jane Strouse, and Frank J. McEnroe. 107 A
Intelligent Robots—The Next Step in Laboratory Automation. T. L. Isenhour, S. E. Eckert, and J. C. Marshall. 805 A
Laboratory Information Management Systems. Robert Megargle. 612 A
Microcontrollers in the Laboratory. Ron Williams. 433 A

Analytical Approach

The Amnesic Shellfish Poisoning Mystery. Michael A. Quilliam and Jeffrey L. C. Wright. 1053 A
The Case of the Tainted Dexamethasone. Richard H. Eckerlin, Joseph G. Ebel, Jr., Jack D. Henion, and Thomas R. Covey. 53 A
Detection of Latent Fingerprints by Laser-Excited Luminescence. E. Roland Menzel. 557 A
IR Long-Path Photometry: A Remote Sensing Tool for Automobile Emissions. Gary A. Bishop, John R. Starkey, Anne Ihlenfeldt, Walter J. Williams, and Donald H. Stedman. 671 A
Molecular Biology at Atomic Resolution: The Structure of an Insect Virus and Its Functional Implications. Jean-Pierre Wery and John E. Johnson. 1341 A
The Odyssey of Angiogenin: A Protein That Induces Blood Vessel Growth. Daniel J. Strydom, James W. Fett, and James F. Riordan. 1173 A
Old Master Paintings: A Study of the Varnish Problem. E. René de la Rie. 1228 A

Focus

Chemistry in Miami. Mary Warner. 1291 A
Chemists Warm to Cold Fusion and Chili in Dallas. Alan R. Newman. 739 A
Consortium on Automated Analytical Laboratory Systems. H. M. (Skip) Kingston. 1381 A
Finding a Single Molecule in a Haystack: Optical Detection and Spectroscopy of Single Absorbers in Solids. W. E. Moerner and L. Kador. 1217 A
The First International Symposium on Field-Flow Fractionation. Sharon Kraus. 1329 A
The 40th Pittsburgh Conference and Exposition. Louise Voress. 602 A
Gel Electrophoresis of DNA. Sharon Boots. 551 A
The Great Fruit Scares of 1989. Alan R. Newman. 861 A
A Historic Collaboration. Abraham Savitzky. 921 A
HPCE '89. Mary Warner. 795 A
Instrumental Analysis in Art and History. Ivan Amato. 311 A
Looking at the Environment. Sharon Boots and Mary Warner. 1047 A
Marcel Golay—A Memorial. Georges Guiochon and Leslie Ettre. 922 A
Measuring the Fat of the Land. Alan R. Newman. 663 A
Microelectrodes in Microbal Ecology. Sharon Boots. 425 A
Scanning Electrochemical Microscopy. Royce C. Engstrom and Christine N. Pharr. 1099 A
The Shroud of Turin. Mary Warner. 101 A
The Sound of Photosynthesis. Ivan Amato. 43 A
Surface Science in Analytical Chemistry. Joseph A. Gardella, Jr., and Fred M. Hawkridge. 1333 A
Tracking Genetically Engineered Microorganisms. Alan R. Newman. 1001 A
What Happened to the Ozone Layer? Alan R. Newman. 1167 A

Instrumentation

Capillary Electrophoresis. Andrew G. Ewing, Ross A. Wallingford, and Teresa M. Olefirowicz. 292 A
Fast Thermolysis/FT-IR Spectroscopy: New Dimensions in Combined Thermal Analysis and Spectroscopy. Thomas B. Brill. 897 A
Fluorescence Diagnosis and Photochemical Treatment of Diseased Tissue Using Lasers: Part I. Stefan Andersson-Engels, Jonas Johansson, Sune Svanberg, and Katarina Svanberg. 1367 A
LC Detectors: Evaluation and Practical Implications of Linearity. Craig A. Dorschel, Juris L. Ekmanis, James E. Oberholtzer, F. Vincent Warren, Jr., and Brian A. Bidlingmeyer. 951 A
NMR Imaging of Materials. John M. Listerud, Steven W. Sinton, and Gary P. Drobny. 23 A
Quantitation of Auger and X-ray Photoelectron Spectroscopies. Kenneth W. Nebesney, Brian L. Maschhoff, and Neal R. Armstrong. 469 A
Raman Monitoring of Dynamic Electrochemical Events. Richard L. McCreery and Richard T. Packard. 775 A
Recent Developments in Instrumentation for X-ray Photoelectron Spectroscopy. Joseph A. Gardella, Jr. 589 A
Resonance Ionization Mass Spectrometry. J. P. Young, R. W. Shaw, and D. H. Smith. 1271 A
A Thousand Points of Light: The Hadamard Transform in Chemical Analysis and Instrumentation. Patrick J. Treado and Michael D. Morris. 723 A
Trace Element Determinations with Synchrotron-Induced X-ray Emission. Keith W. Jones and Barry M. Gordon. 341 A
Waveguides as Chemical Sensors. Raymond E. Dessy. 1079 A

Report

Analytical Applications of Polarimetry, Optical Rotatory Dispersion, and Circular Dichroism. Neil Purdie and Kathy A. Swallows. 77 A
Electrochemical Applications of the Quartz Crystal Microbalance. Mark R. Deakin and Daniel A. Buttry. 1147 A
Field Ionization and Field Desorption Mass Spectrometry: Past, Present, and Future. Robert P. Lattimer and Hans-Rolf Schulten. 1201 A
Fluorescence Lifetime Filtering. Linda B. McGown. 839 A
Fluorescence Line-Narrowing Spectroscopy in the Study of Chemical Carcinogenesis. Ryszard Jankowiak and Gerald J. Small. 1023 A
Happy 95th Birthday, Piet Kolthoff. Mary Warner. 287 A
Isotope Dilution Mass Spectrometry for Accurate Elemental Analysis. Jack D. Fassett and Paul J. Paulsen. 643 A
Laszlo Zechmeister: A Pioneer in Chromatography. Leslie S. Ettre. 1315 A
Modern Thin-Layer Chromatography. Colin F. Poole and Salwa K. Poole. 1257 A
Neuronal Biosensors. R. Michael Buch and Garry A. Rechnitz. 533 A
Solid-Surface Luminescence Spectrometry. Robert J. Hurtubise. 889 A
Surface Acoustic Wave Devices for Chemical Analysis. David S. Ballantine, Jr., and Hank Wohltjen. 704 A
Surface-Enhanced Raman Spectroscopy. Robin L. Garrell. 401 A

Analytical CHEMISTRY

VOLUME 61, 1989
January–April
ANCHAM
ISSN 0003-2700

Editor: GEORGE H. MORRISON

Associate Editors: Klaus Biemann, Georges Guiochon, Walter C. Herlihy, Robert A. Osteryoung, Edward S. Yeung

EDITORIAL HEADQUARTERS
1155 Sixteenth St., N.W., Washington, D.C. 20036

Managing Editor: Sharon G. Boots
Associate Editors: Rani A. George, Louise Voress, Mary Warner
Assistant Editors: Grace K. Lee, Alan R. Newman
Editorial Assistant: Felicia Wach
Director, Operational Support: C. Michael Phillippe
Production Manager: Leroy L. Corcoran
Art Director: Alan Kahan
Designer: Amy Meyer Phifer
Production Editor: Elizabeth E. Wood
Circulation: Claud Robinson
Editorial Assistant (*LabGuide*): Joanne Mullican

Journals Department, Columbus, Ohio
Associate Head: Marianne Brogan
Journals Editing Manager: Joseph E. Yurvati
Associate Editor: Rodney L. Temos
Staff Editor: Sharon K. Hatfield

ADVISORY BOARD

Bernard J. Bulkin, Michael S. Epstein, Renaat Gijbels, Peter R. Griffiths, Thomas L. Isenhour, Nobuhiko Ishibashi, James W. Jorgenson, Peter C. Jurs, Mary A. Kaiser, David L. Nelson, Lawrence A. Pachla, Ralph E. Sturgeon, George S. Wilson, Mary J. Wirth, Andrew T. Zander, Richard N. Zare. *Ex Officio:* Sam P. Perone

AMERICAN CHEMICAL SOCIETY PUBLICATIONS DIVISION

Director: Robert H. Marks
Journals Department: Charles R. Bertsch, Head
Special Publications: Randall E. Wedin

Published by the American Chemical Society, 1155 Sixteenth St., N.W., Washington, D.C. 20036

January 1	1–96	1 A–62 A
January 15	97–192	63 A–116 A
February 1	193–288	117 A–270 A
February 15	289–384	271 A–318 A
March 1	385–512	319 A–382 A
March 15	513–640	383 A–442 A
April 1	641–800	443 A–510 A
April 15	801–928	511 A–566 A
May 1	929–1056	567 A–626 A
May 15	1057–1184	627 A–682 A
June 1	1185–1312	683 A–754 A
June 15	Fundamential Reviews 1 R–304 R	
July 1	1313–1472	755 A–818 A
July 15	1473–1600	819 A–870 A
August 1	1601–1792	871 A–930 A
August 15	LabGuide 1 G–294 G	
September 1	1793–2000	931 A–1008 A
September 15	2001–2128	1009 A–1064 A
October 1	2129–2224	1065 A–1124 A
October 15	2225–2336	1125 A–1184 A
November 1	2337–2464	1185 A–1244 A
November 15	2465–2592	1245 A–1300 A
December 1	2593–2688	1301 A–1352 A
December 15	2689–2864	1353 A–1392 A

Analytical CHEMISTRY

VOLUME 61, 1989
May–August
ANCHAM
ISSN 0003-2700

Editor: GEORGE H. MORRISON

Associate Editors: Klaus Biemann, Georges Guiochon, Walter C. Herlihy, Robert A. Osteryoung, Edward S. Yeung

EDITORIAL HEADQUARTERS
1155 Sixteenth St., N.W., Washington, D.C. 20036

Managing Editor: Sharon G. Boots
Associate Editors: Rani A. George, Louise Voress, Mary Warner
Assistant Editors: Grace K. Lee, Alan R. Newman
Editorial Assistant: Felicia Wach
Director, Operational Support: C. Michael Phillippe
Production Manager: Leroy L. Corcoran
Art Director: Alan Kahan
Designer: Amy Meyer Phifer
Production Editor: Elizabeth E. Wood
Circulation: Claud Robinson
Editorial Assistant (*LabGuide*): Joanne Mullican

Journals Department, Columbus, Ohio
Associate Head: Marianne Brogan
Journals Editing Manager: Joseph E. Yurvati
Associate Editor: Rodney L. Temos
Staff Editor: Sharon K. Hatfield

ADVISORY BOARD

Bernard J. Bulkin, Michael S. Epstein, Renaat Gijbels, Peter R. Griffiths, Thomas L. Isenhour, Nobuhiko Ishibashi, James W. Jorgenson, Peter C. Jurs, Mary A. Kaiser, David L. Nelson, Lawrence A. Pachla, Ralph E. Sturgeon, George S. Wilson, Mary J. Wirth, Andrew T. Zander, Richard N. Zare. *Ex Officio:* Sam P. Perone

AMERICAN CHEMICAL SOCIETY PUBLICATIONS DIVISION

Director: Robert H. Marks
Journals Department: Charles R. Bertsch, Head
Special Publications: Randall E. Wedin
Published by the American Chemical Society, 1155 Sixteenth St., N.W., Washington, D.C. 20036

January 1	1–96	1 A–62 A
January 15	97–192	63 A–116 A
February 1	193–288	117 A–270 A
February 15	289–384	271 A–318 A
March 1	385–512	319 A–382 A
March 15	513–640	383 A–442 A
April 1	641–800	443 A–510 A
April 15	801–928	511 A–566 A
May 1	929–1056	567 A–626 A
May 15	1057–1184	627 A–682 A
June 1	1185–1312	683 A–754 A
June 15	Fundamential Reviews 1 R–304 R	
July 1	1313–1472	755 A–818 A
July 15	1473–1600	819 A–870 A
August 1	1601–1792	871 A–930 A
August 15	LabGuide 1 G–294 G	
September 1	1793–2000	931 A–1008 A
September 15	2001–2128	1009 A–1064 A
October 1	2129–2224	1065 A–1124 A
October 15	2225–2336	1125 A–1184 A
November 1	2337–2464	1185 A–1244 A
November 15	2465–2592	1245 A–1300 A
December 1	2593–2688	1301 A–1352 A
December 15	2689–2864	1353 A–1392 A

Analytical CHEMISTRY

VOLUME 61, 1989
September–December
ANCHAM
ISSN 0003-2700

Editor: GEORGE H. MORRISON

Associate Editors: Klaus Biemann, Georges Guiochon, Walter C. Herlihy, Robert A. Osteryoung, Edward S. Yeung

EDITORIAL HEADQUARTERS
1155 Sixteenth St., N.W., Washington, D.C. 20036

Managing Editor: Sharon G. Boots
Associate Editors: Louise Voress, Mary Warner
Assistant Editors: Grace K. Lee, Alan R. Newman
Editorial Assistant: Felicia Wach
Director, Operational Support: C. Michael Phillippe
Production Manager: Leroy L. Corcoran
Art Director: Alan Kahan
Designer: Amy Meyer Phifer
Production Editor: Elizabeth E. Wood
Circulation: Claud Robinson
Editorial Assistant (LabGuide): Joanne Mullican

Journals Department, Columbus, Ohio
Associate Head: Marianne Brogan
Journals Editing Manager: Joseph E. Yurvati
Senior Associate Editor: Rodney L. Temos
Staff Editor: Sharon K. Hatfield

ADVISORY BOARD

Bernard J. Bulkin, Michael S. Epstein, Renaat Gijbels, Peter R. Griffiths, Thomas L. Isenhour, Nobuhiko Ishibashi, James W. Jorgenson, Peter C. Jurs, Mary A. Kaiser, David L. Nelson, Lawrence A. Pachla, Ralph E. Sturgeon, George S. Wilson, Mary J. Wirth, Andrew T. Zander, Richard N. Zare. *Ex Officio:* Sam P. Perone

AMERICAN CHEMICAL SOCIETY PUBLICATIONS DIVISION

Director: Robert H. Marks
Journals Department: Charles R. Bertsch, Head
Special Publications: Randall E. Wedin
Published by the American Chemical Society, 1155 Sixteenth St., N.W., Washington, D.C. 20036

January 1	1–96	1 A–62 A
January 15	97–192	63 A–116 A
February 1	193–288	117 A–270 A
February 15	289–384	271 A–318 A
March 1	385–512	319 A–382 A
March 15	513–640	383 A–442 A
April 1	641–800	443 A–510 A
April 15	801–928	511 A–566 A
May 1	929–1056	567 A–626 A
May 15	1057–1184	627 A–682 A
June 1	1185–1312	683 A–754 A
June 15	Fundamential Reviews 1 R–304 R	
July 1	1313–1472	755 A–818 A
July 15	1473–1600	819 A–870 A
August 1	1601–1792	871 A–930 A
August 15	LabGuide 1 G–294 G	
September 1	1793–2000	931 A–1008 A
September 15	2001–2128	1009 A–1064 A
October 1	2129–2224	1065 A–1124 A
October 15	2225–2336	1125 A–1184 A
November 1	2337–2464	1185 A–1244 A
November 15	2465–2592	1245 A–1300 A
December 1	2593–2688	1301 A–1352 A
December 15	2689–2864	1353 A–1392 A

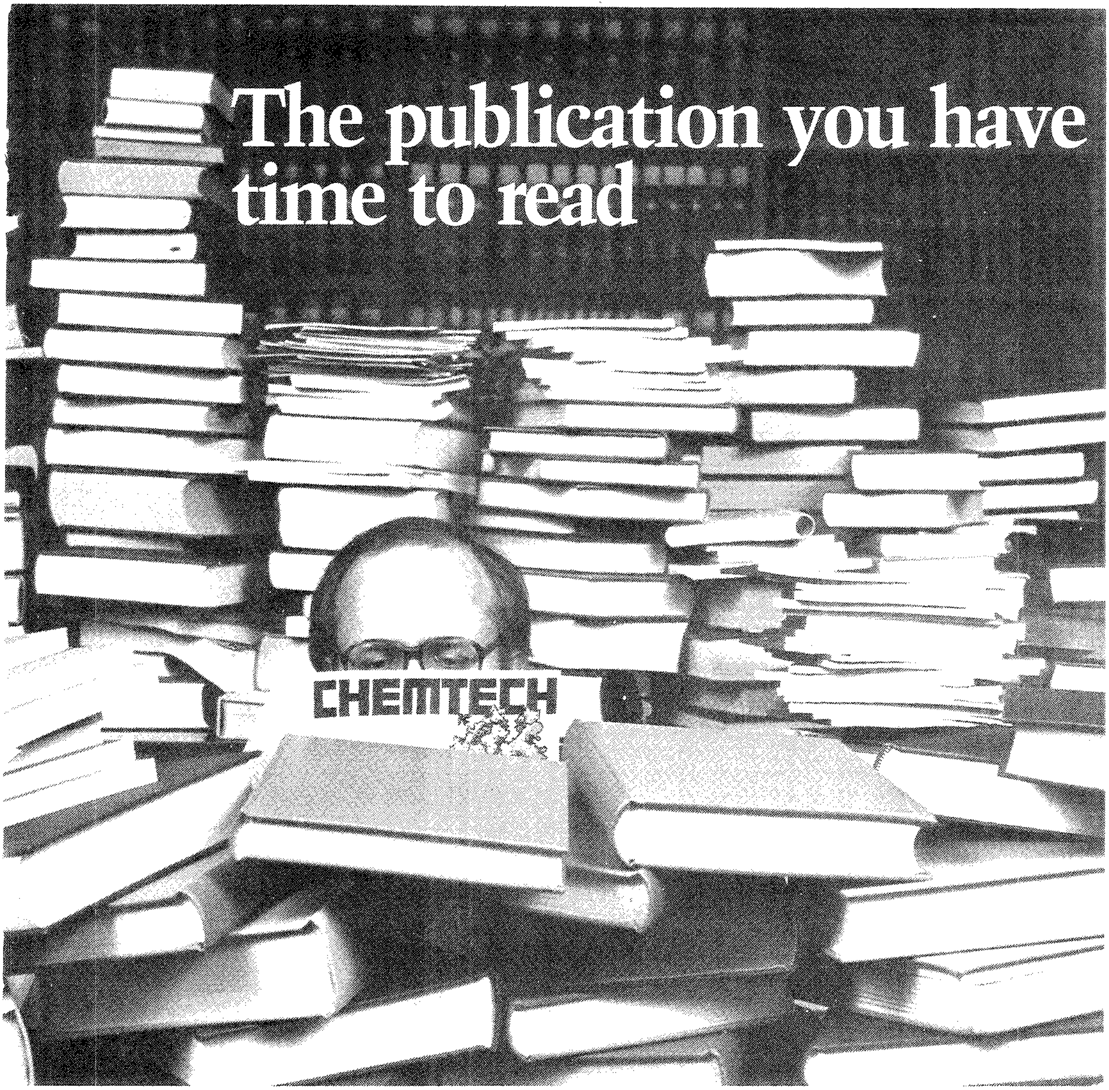
The publication you have time to read
CHEMTECH

. . . To keep up the pace with current changes.

Today, trade publications available to industrial chemists concentrate on either chemistry—or chemical engineering—not both. Even though these fields are interrelated. And even though your work *depends* on your success in knowing what the guy next door is doing. Of course, everyone who wants to keep pace with his own field needs to read the single-discipline journals. But who's got the time to read much more than that?

That's where CHEMTECH comes in.

CHEMTECH is published especially for the busy professional who wants to come up to speed on key developments in the chemical world—up *and* down the line from where he or she is. CHEMTECH helps you solve problems *before* they become red ink at the bottom of the balance sheet.

How does CHEMTECH do it?

- *By bringing you topics vital to your work.* Not just chemical science, but data correlation, economics . . . energy, engineering . . . management, materials, regulations, and more!
- *By bringing concepts to you straight from the experts—articles and abstracts* written by R&D directors, CEO's, distinguished professors, high-level government officials, and by shirt-sleeves lab and plant people who know what's happening—because they're at the forefront making it happen!
- *And by bringing this timely information to you in a dynamic style* that's as entertaining as it is informative. CHEMTECH's scope of coverage will truly stimulate your thinking . . . you'll see.

Keep informed with CHEMTECH
CALL TOLL FREE 800/227-5558
Outside U.S. 202/872-4363
Telex: 440159 ACSP UI 89 2582
ACSPUBS

CHEMTECH

American Chemical Society
1155 16th St., N.W., Washington, D.C. 20036

FOR A BROAD PERSPECTIVE IN THE SCIENCE OF NON- NUCLEAR FUELS . . .

ENERGY & FUELS

Editor John W. Larsen, Lehigh University
Associate Editor Thomas R. Hughes, Chevron Research Company

Ideas . . . Innovations . . . Discoveries . . .

ENERGY & FUELS is the bimonthly journal that delivers an abundance of highly readable reports on topics covering the transformation, utilization, formation, and production of fossil fuels.

Each issue features reports on all aspects of the chemistry of non-nuclear energy sources—including petroleum research, coal chemistry, oil shale, tar sands, C_1 chemistry, organic geochemistry and biomass research.

Plus, ENERGY & FUELS gives you a dynamic vision on how the field is developing. You'll find a wealth of information on . . .

- the formation of, exploration for, and production of fossil fuels
- the properties and structure or molecular composition of both raw fuels and refined products
- the chemistry involved in the processing and utilization of fuels
- the analytical and instrumental techniques used in energy and fuels investigations
- research on non-fuel substances that elucidates aspects of fuel chemistry
- and much more!

ENERGY & FUELS publishes more than research papers. You'll find Communications, Book Reviews, and invited feature essays by major figures in the field. In these, developments in active areas of research are made accessible to chemists involved in other branches of the discipline.

Contributing Authors—
Look to ENERGY & FUELS for Rapid Publication!

The editors are working toward a timely turnaround from submission to publication. For further information on composition and submission of manuscripts write: John Larsen, Editor, ENERGY & FUELS, Department of Chemistry, Lehigh University, Bethlehem, PA 18015. Or call (215) 758-3489.

In a hurry? Call Toll Free 800-ACS-5558 and charge your subscription! (U.S. only.)

Editorial Advisory Board: T. Aczel, Exxon Res. & Eng. Co.; M.M. Boduszynski, Chevron Res. Co.; A.K. Burnham, Lawrence Livermore Natl. Lab.; B. Cecil, U.S. Geological Survey; C.D. Chang, Mobil R & D Corp.; P. Griffiths, Univ. of California, Riverside; C. Horvath, Yale Univ.; J. Howard, Massachusetts Inst. of Tech.; L. Ignasiak, Alberta Res. Council, Canada; M. Lewan, Amoco Production Co.; R. Liotta, Exxon Res. and Eng. Co.; L.J. Lynch, CSIRO, Australia; O. Mahajan, Amoco Res. Center; J. McKay, Western Res. Inst.; H. Meuzelaar, Biomaterials Profiling Ctr.; H.H. Oelert, Technische Universtat Clausthal, W. Germany; M. Poutsma, Oak Ridge Natl. Lab.; Y. Sanada, Hokkaido Univ., Japan; J.H. Shinn, Chevron Res. Co.; M. Siskin, Exxon Res. and Eng. Co.; L. Stock, Univ. of Chicago; I. Wender, Univ. of Pittsburgh; D.D. Whitehurst, Mobil Res. and Tech. Ctr.

1989 Subscription Information
1989 Volume 3 ISSN: 0887-0624 Coden: ENFUEM

	ACS Members*		Non-Member
	One Year	Two Years	One Year
U.S.	$48	$ 86	$289
Canada & Mexico	$58	$106	$299
Europe**	$58	$106	$299
All Other Countries**	$64	$118	$305

*Member rate is for personal use only.
**Air service included.

ENERGY & FUELS is a journal of the American Chemical Society. For information write: American Chemical Society, Marketing Communications Department, 1155 Sixteenth Street, NW, Washington, DC 20036.

Foreign orders must be paid in U.S. currency by international money order, UNESCO coupons, or U.S. bank draft; or order through your subscription agency. For nonmember rates in Japan, contact Maruzen Co., Ltd.

This publication is available on microfilm, microfiche, and online through CJO on STN International.

Here's Why Two Esteemed, Technical Societies Want *Your* Expertise...

The American Chemical Society & American Institute of Chemical Engineers
Announce their 1990 co-publication of

BIOTECHNOLOGY PROGRESS

Editor, Jerome S. Schultz, *University of Pittsburgh*

SUBMIT YOUR PAPERS NOW TO THIS IMPORTANT "NEW" PUBLISHING MEDIUM

Beginning January 1990 BIOTECHNOLOGY PROGRESS, a well-established journal of the American Institute of Chemical Engineers, will become a joint publication of the American Chemical Society and AIChE. As a collaborative effort, several significant changes will occur, ***providing enhanced editorial coverage and expanded readership.*** These include:

- **Accelerated frequency** — from quarterly to bimonthly issues!
- **A redesigned format** which will better meet the needs of both new and current subscribers.
- **A redefined editorial focus** guaranteed to attract:
  1) additional topical papers and primary research findings
  2) an audience comprising the very experts *you* want to reach!

ATTENTION CHEMISTS, LIFE SCIENTISTS, AND ENGINEERS!

In bimonthly issues, BIOTECHNOLOGY PROGRESS will provide the latest concepts — in genetics...microbiology and biochemistry...molecular and cellular biology...chemistry and chemical engineering — as they apply to the development of processes, products, and devices. Emphasis will be placed on the ***application of fundamental engineering principles*** to the ***analysis*** of biological phenomena involved.

BIOTECHNOLOGY PROGRESS will be of particular interest to ***practitioners of R&D in process development, product development, and equipment/instrumentation design for the biotechnology/bioprocess industry.*** Its coverage will encompass food, pharmaceutical, and biomedical arenas.

LOOK FOR HIGHLY TARGETED TOPICS LIKE THESE

- **Applied Biochemistry:** Equilibrium data, protein conformations in solution, mapping of molecular surfaces.
- **Applied Molecular Biology:** Cell physiology, gene expression, protein transport, metabolic engineering.
- **Bioreactor Technology:** Reactor engineering, mechanical engineering, materials science, process control, biosensors.
- **Biocatalytic Processes:** Site specific mutagenesis, enzyme minetics, cofactor regeneration, applied pharmaceutical minetics.
- **Formulation and Product Delivery.**
- **Bioanalysis:** Online monitoring, containment, containment monitoring, offline analysis, statistical analysis (nonlinear regression, multifactor analysis).
- **Bioseparations.**

ADDRESS YOUR MANUSCRIPT SUBMISSIONS & AUTHOR INQUIRIES TO:

Jerome S. Schultz
Editor, BIOTECHNOLOGY PROGRESS
Center for Biotechnology and Bioengineering
University of Pittsburgh
911 William Pitt Union
Pittsburgh, PA 15260
Telephone: 412/648-7956 Fax: 412/624-7145

To receive editorial updates please write:
American Chemical Society, Marketing,
BIOTECHNOLOGY PROGRESS, Room 609,
1155 Sixteenth St., N.W., Washington, D.C. 20036
FAX: 202/872-6005
Telex: 440159 ACSP UI or 89 2582 ACSPUBS

Premiering January/February 1990!
A long-awaited unifying medium for virtually any practitioner of conjugation chemistry

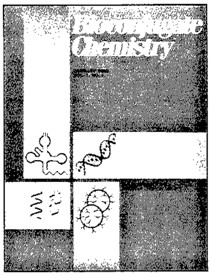

Bioconjugate Chemistry

Editor: Dr. Claude F. Meares
Dept. of Chemistry, Univ. of California, Davis
Davis, CA 95616 (916/752-3360)

Centralized Access Is Here!

In *bimonthly* issues, **Bioconjugate Chemistry** will bring together important research findings in the fast-developing discipline of conjugation chemistry. Now—*in a single, time-saving source*—you'll find information which otherwise might be scattered throughout broader-focus scholarly journals.

The central theme of **Bioconjugate Chemistry** *is the joining of two different molecular functions by chemical or biological means.* This includes:

Conjugation of . . .
antibodies (and their fragments)
nucleic acids and their analogs (α-anomers, phosphonates, . . .)
liposomal components
other biologically active molecules (receptor-binding proteins, hormones, peptides, . . .)

with each other or with any molecular groups that add useful properties . . .
drugs, radionuclides, toxins, fluorophores, photoprobes, inhibitors, enzymes, haptens, ligands, etc.

There is *no* journal with this precise focus published today.

The Leading Edge In Biomedical Advances

Bioconjugate Chemistry will publish research at the core of many biotechnology enterprises, as well as of specific interest to biomedical firms, drug companies, and chemical laboratories.

Topics will emphasize the *chemical* aspects of *conjugate preparation and characterization . . . in vivo* applications of conjugate methodology . . . *molecular biological* aspects of antibodies, genetically engineered fragments, and other immunochemicals . . . and the relationships between conjugation chemistry and the biological properties of conjugates.

Guided by a "Who's Who" in the Field

1990 Editorial Advisory Board

V. Alvarez, *Cytogen Corp.*; L. Arnold, *Genta Inc.*; R. W. Atcher, *Argonne Natl. Labs*; R. W. Baldwin, *Univ. of Nottingham, England*; T. Bumol, *Lilly Corp. Center*; C. H. Chang, *Immunomedics*; G. S. David, *Hybritech, Inc.*; P. B. Dervan, *California Inst. of Tech.*; D. Dolphin, *Univ. of British Columbia, Canada*; T. W. Doyle, *Bristol-Myers Co.*; R. E. Feeney, *Univ. of California, Davis*; D. Fitzgerald, *Natl. Institutes of Health*; J. M. Frincke, *Hybritech, Inc.*; A. Fritzberg, *NeoRx Corp.*; W. F. Goeckler, *The Dow Chemical Co.*; D. Goodwin, *Stanford Univ.*; E. Haber, *The Squibb Inst. for Medical Res.*; T. Hara, *Inst. for Biomedical Res., Japan*; R. Haugland, *Molecular Probes, Inc.*; J. E. Hearst, *Univ. of California, Berkeley*; N. Heindel, *Lehigh Univ.*; C. Helene, *Museum National D'Histoire Naturelle, France*; E. Hurwitz, *Weizmann Inst. of Science, Israel*; D. K. Johnson, *Abbott Laboratories*; D. Kaplan, *The Dow Chemical Co.*; B. A. Khaw, *Massachusetts General Hospital*; K. Krohn, *Univ. of Washington*; P. S. Miller, *The Johns Hopkins Univ.*; H. T. Nagasawa, *Univ. of Minnesota, Minneapolis*; P. Nielsen, *Univ. of Copenhagen, Denmark*; A. Oseroff, *Tufts-New England Medical Ctr.*; M. Ostrow, *The Liposome Co., Inc.*; G. A. Pietersz, *The Univ. of Melbourne, Australia*; R. Reisfeld, *Scripps Clinic & Res. Fnd.*; S. Rocklage, *Salutar, Inc.*; J. Rodwell, *Cytogen Corp.*; P. G. Schultz, *Univ. of California, Berkeley*; P. Senter, *Oncogen*; S. Srivastava, *Brookhaven Natl. Lab.*; P. E. Thorpe, *Imperial Cancer Res. Fund, England*; G. Tolman; A. Tramontano, *Scripps Clinic & Res. Fnd.*; J. Upeslacis, *Lederle Lab.*; R. S. Vickers, *Eastman Kodak Co.*; E. S. Vitetta, *The Univ. of Texas, Dallas*; S. Wilbur, *NeoRx Corp.*; M. Wilchek, *Weizmann Inst. of Science, Israel*; M. Zalutsky, *Duke Univ. Medical Center*

1990 Subscription Rates

	ACS Members *		Nonmember
	One Year	Two Years	One Year
U.S.	$ 29	$ 52	$249
Canada & Mexico	$ 35	$ 64	$255
Europe**	$ 39	$ 72	$259
All Other Countries**	$ 43	$ 80	$263

* Member rate is for personal use only
**Air Service Included

Be a Premier Subscriber—Order Today!

American Chemical Society
Marketing Communications Department
1155 Sixteenth Street, N.W.
Washington, D.C. 20036 U.S.A.
(202) 872-4363
1-800-227-5558
Telex: 440159 ACSP UI or 89 2582 ACSPUBS
FAX: (202) 872-4615
IN JAPAN CONTACT MARUZEN CO., LTD.

Choosing a graduate school?
Need to know who's doing research critical to yours?

New edition just published!

The ACS Directory of Graduate Research 1989

All the information you need on chemical research and researchers at universities in the U.S. and Canada . . . in a single source.

Includes listings for chemistry, chemical engineering, biochemistry, pharmaceutical/medicinal chemistry, clinical chemistry, and polymer science.

Lists universities with names and biographical information for all faculty members, their areas of specialization, titles of all papers published within the last two years, and individual telephone numbers, FAX numbers, and computer addresses.

Provides a statistical summary of academic chemical research—with information by department on numbers of full- and part-time faculty, postdoctoral appointments, graduate students, and M.S. and Ph.D. degrees granted.

What you'll find inside . . .

Information on . . .
- 683 academic departments
- 11,936 faculty members
- 68,276 publication citations

Listings for . . .
- chemistry
- chemical engineering
- biochemistry
- pharmaceutical/medicinal chemistry
- clinical chemistry
- polymer science

1436 pages (1989) Clothbound
Price:
US & Canada **$55.00**
Export **$66.00**

No academic institution or chemically oriented business can afford to be without the ACS Directory of Graduate Research 1989! Order today by calling TOLL FREE (800) 227-5558. In Washington, D.C., call 872-4363. Or use the coupon below.

Please send me ______copy(ies) of the ACS Directory of Graduate Research 1989. Price: US & Canada $55.00 Export $66.00.

☐ Payment enclosed (make checks payable to American Chemical Society).

☐ Purchase order enclosed. P.O.# ____________

Charge my: ☐ MasterCard/VISA ☐ American Express ☐ Diners Club/Carte Blanche

Account # ____________ Expires ____________

Signature ____________

Phone ____________

Ship books to:

Name ____________

Address ____________

City, State, ZIP ____________

ORDERS FROM INDIVIDUALS MUST BE PREPAID. Please allow 4-6 weeks for delivery. Prices are quoted in U.S. dollars. Mail this order form with your payment or purchase order to:
American Chemical Society, Distribution Office Dept. 705,
P.O. Box 57136, West End Station, Washington, D.C. 20037.

705

We'll put all the latest advances in the chemical sciences right in your hands... And you won't need to lift a finger!

AMERICAN CHEMICAL SOCIETY STANDING ORDER PLANS

The ACS has a simple way to ensure that your library always has the chemistry titles your patrons require. It's called the ACS Standing Order Plans.

With ACS Standing Order Plans, you can save the time you'd otherwise spend on literature searches and purchase order details . . . and make certain that your library has the titles your patrons want—when they need them.

AS EASY AS 1-2-3

You can select from three Standing Order Plans—choose one or all or a combination . . . whatever best suits your patrons' needs!

1. **By Series:**
Advances in Chemistry Series
ACS Symposium Series
ACS Monographs
Professional Reference Books
All ACS Series

2. **By Single Title:**
ACS Abstract Books
ACS Directory of Graduate Research
College Chemistry Faculties

3. **By Subject:**
Analytical • Agricultural/Agrochemical • Biological • Biotechnology • Carbohydrate • Cellulose/Paper/Textile • Colloid/Surface • Computers in Chemistry • Electronic Materials • Environmental/Chemical Health and Safety • Food/Flavor • Energy/Fuel/Petroleum/Geochemistry • Industrial/Chemical Engineering • Inorganic • Materials Science • Medicinal/Pharmaceutical • Nuclear • Organic • Polymer/Applied Polymer Science • Physical Chemistry

25 TO CHOOSE FROM!

PLUS FIVE NEW SUBJECT AREAS . . . Chemical Information • Directories • History • Non-Technical • Toxicology!

You tell us which Standing Order Plan (or Plans) you'd like—1, 2, 3, or a combination. Your one-time order assures prompt, automatic delivery of each new title in the plan or plans you've chosen as soon as it's published. We'll send you an invoice with your shipment. You'll have thirty days to examine each new book and (if you decide for any reason) to return it for full credit. And you may modify or cancel your Standing Order Plan at any time. It's that easy!

Make sure your chemistry resources are always complete—don't overlook a single book from the world's most respected publisher in the chemistry field. Enroll in ACS Standing Order Plans today.

Write to American Chemical Society, 1155 Sixteenth Street, N.W., Washington, DC, 20036. Or call us TOLL FREE (800) 227-5558.

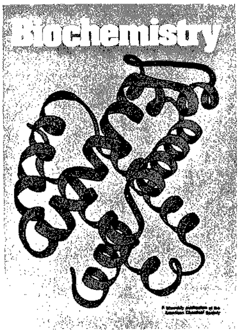

As the frontiers expand...

Biochemistry

reflects the most current results of original research in all areas of biochemistry.

Editor, Hans Neurath, University of Washington

Published biweekly, *Biochemistry* emphasizes the close relationship of chemistry, biochemistry, and molecular and cell biology.

Subject matter covers:

- structure, function and regulation enzymes
- proteins
- carbohydrates
- lipids
- hormones
- receptors
- gene structure and expression
- protein biosynthesis
- viruses
- immunochemistry
- genetics
- bioenergetics
- membrane structure and function
- x-ray crystallography

Over 10,300 pages of original research annually, this internationally renown journal is vital reading for all scientists in this fast-paced field.

1989 Rates	ACS Members*		Non-Member
	1 Year	2 Years	1 Year
U.S.	$ 80	$144	$549
Canada & Mexico	$140	$264	$609
Europe**	$237	$458	$706
All Other Countries**	$342	$668	$811

* Member rate is for personal use only.
** Air Service Included.
Supplementary material is available for this publication.
This publication is available on microfilm, microfiche, and online through CJO on STN International.
For nonmember rates in Japan, contact Maruzen Co., Ltd.

For more information or to subscribe:
American Chemical Society/Marketing Communications Department
1155 Sixteenth Street, NW, Washington, DC 20036

In a hurry?
Call Toll free (800) 227-5558 (U.S. only)
Outside U.S. (202) 872-4363
Telex: 440159 ACSP UI
89 2582 ACSPUBS
FAX: (202) 872-4615

Associate Editors

E. W. Davie; *Univ. of Washington*
E. H. Fischer; *Univ. of Washington*
M. P. Gordon; *Univ. of Washington*
W. W. Parson; *Univ. of Washington*

Editorial Advisory Board

R. H. Abeles; *Brandeis Univ.* • D. S. Auld; *Harvard Medical School* • R. L. Baldwin; *Stanford Univ.* • S. J. Benkovic; *Pennsylvania State Univ.* • G. Blobel; *The Rockefeller Univ.* • T. L. Blundell; *Univ. of London, England* • B. R. Brinkley; *Baylor Coll. of Medicine* • M. J. Coon; *Univ. of Michigan* • D. Davies; *Natl. Inst. of Health* • R. A. Dwek; *Univ. of Oxford, England* • M. Edidin; *Johns Hopkins Univ.* • I. Fridovich; *Duke Univ.* • C. Frieden; *Washington Univ.* • I. H. Goldberg; *Harvard Medical School* • J. Gorski; *Univ. of Wisconsin* • W. F. Harrington; *Johns Hopkins Univ.* • R. Haselkorn; *Univ. of Chicago* • C-H. Heldin; *Ludwig Inst. for Cancer Res., Sweden* • C. Helene; *Museum Natl. d'Histoire Naturelle, France* • J. Hershey; *Univ. of California, Davis* • G. P. Hess; *Cornell Univ.* • P. C. Hinkle; *Cornell Univ.* • F. M. Huennekens; *Scripps Clinic & Res. Foundation* • T. E. Hugli; *Scripps Clinic & Res. Foundation* • R. Jaenicke; *Univ. of Regensburg, W. Germany* • H. Jornvall; *Karolinska Inst., Sweden* • H. R. Kaback; *Roche Inst. of Molecular Biology* • N. R. Kallenbach; *Univ. of Pennsylvania* • Y. Kaziro; *Univ. of Tokyo, Japan* • C. B. Klee; *Natl. Inst. of Health* • G. Kohler; *Max-Planck Inst. for Immunbio., W. Germany* • J. Kraut; *Univ. of California, San Diego* • J. E. Kyte; *Univ. of California, San Diego* • R. J. Lefkowitz; *Duke Univ.* • T. Lindahl; *Imperial Cancer Res. Fund, United Kingdom* • H. Metzger; *Natl. Inst. of Health* • P. L. Modrich; *Duke Univ.* • E. Neufeld; *Univ. of California, Los Angeles* • D. Northrop; *Univ. of Wisconsin* • J. Ofengand; *Roche Inst. of Molecular Biology* • D. Papahadjopoulos; *Univ. of California, San Francisco* • M. L. Pardue; *Massachusetts Inst. of Tech.* • D. C. Phillips; *Univ. of Oxford, England* • J. C. Powers; *Georgia Inst. of Tech.* • J. H. Prestegard; *Yale Univ.* • P. Reichard; *Karolinska Institute, Sweden* • J. F. Riordan; *Harvard Medical School* • C. A. Ryan; *Washington State Univ.* • R. W. Schekman; *Univ. of California, Berkeley* • H. A. Scheraga; *Cornell Univ.* • P. R. Schimmel; *Mass. Inst. of Tech.* • J. Seelig; *Univ. of Basel, Switzerland* • G. G. Shipley; *Boston Univ.* • A. G. So; *Univ. of Miami* • J. Stubbe; *Univ. of Wisconsin* • B. Sykes; *Univ. of Alberta, Canada* • E. W. Taylor; *Univ. of Chicago* • I. Tinoco; *Univ. of California, Berkeley* • C-L Tsou; *Academia Sinica, Beijing* • B. L. Vallee; *Harvard Medical School* • K. E. Van Holde; *Oregon State Univ.* • M. Vaughan; *Natl. Inst. of Health* • S. J. Wakil; *Baylor Coll. of Medicine* • Y-L Wang; *Academia Sinica, Shanghai* • S. Woo; *Baylor Coll. of Medicine* • P. E. Wright; *Scripps Clinic & Res. Foundation*

Now GC detection is more elemental.

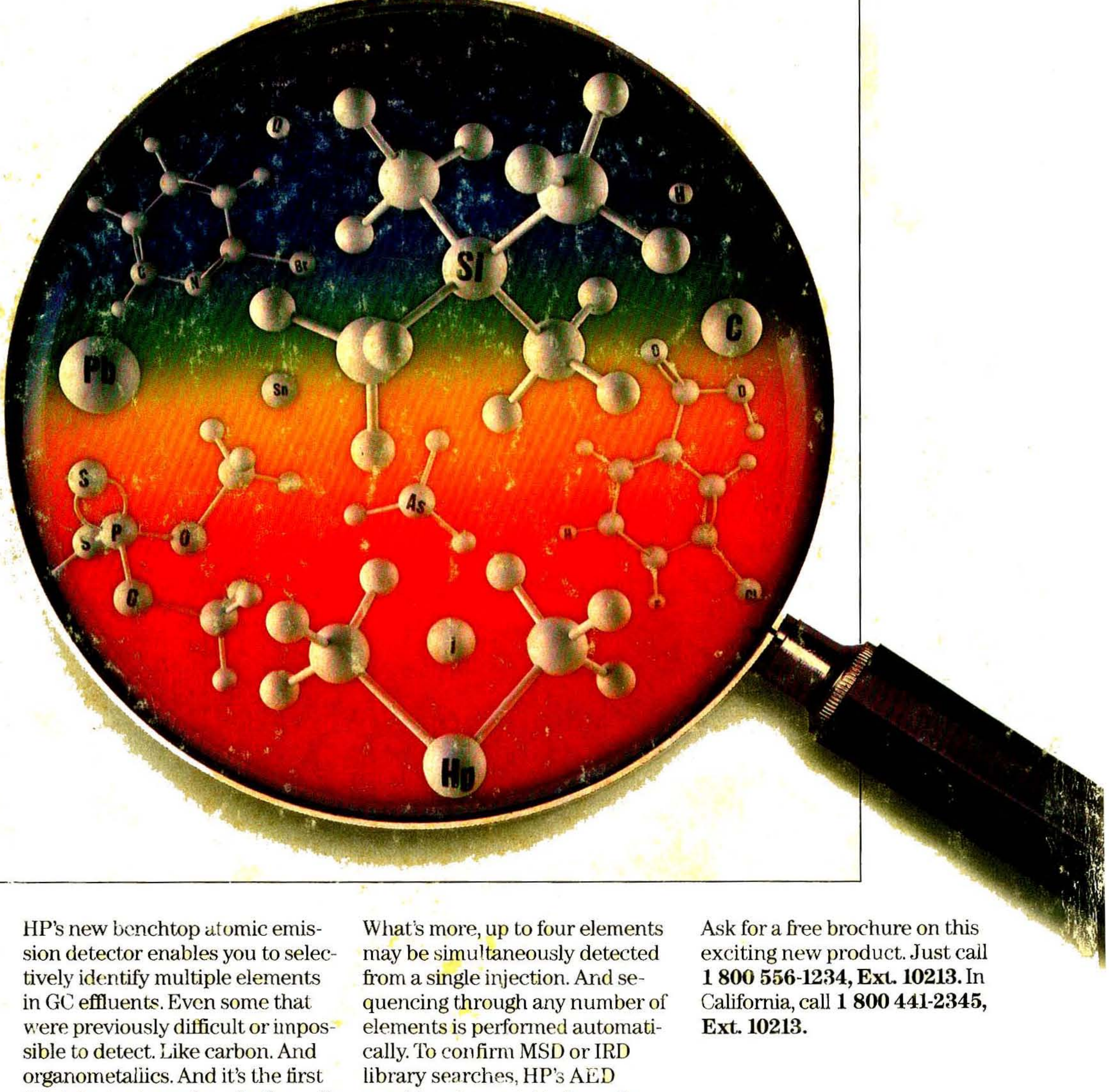

HP's new benchtop atomic emission detector enables you to selectively identify multiple elements in GC effluents. Even some that were previously difficult or impossible to detect. Like carbon. And organometallics. And it's the first GC detector to perform both qualitative *and* quantitative analysis of oxygen.

What's more, up to four elements may be simultaneously detected from a single injection. And sequencing through any number of elements is performed automatically. To confirm MSD or IRD library searches, HP's AED provides elemental information, with the convenience of single-instrument setup.

Ask for a free brochure on this exciting new product. Just call **1 800 556-1234, Ext. 10213.** In California, call **1 800 441-2345, Ext. 10213.**

HEWLETT PACKARD

© 1989 The Hewlett-Packard Company
AG04905

CIRCLE 63 ON READER SERVICE CARD